

Springer Tracts in Civil Engineering

Maria Pina Limongelli
Mehmet Çelebi *Editors*

Seismic Structural Health Monitoring

From Theory to Successful Applications

 Springer

Springer Tracts in Civil Engineering

Series Editors

Giovanni Solari, Wind Engineering and Structural Dynamics Research Group,
University of Genoa, Genova, Italy

Sheng-Hong Chen, School of Water Resources and Hydropower Engineering,
Wuhan University, Wuhan, China

Marco di Prisco, Politecnico di Milano, Milano, Italy

Ioannis Vayas, Institute of Steel Structures, National Technical University of
Athens, Athens, Greece

Springer Tracts in Civil Engineering (STCE) publishes the latest developments in Civil Engineering - quickly, informally and in top quality. The series scope includes monographs, professional books, graduate textbooks and edited volumes, as well as outstanding PhD theses. Its goal is to cover all the main branches of civil engineering, both theoretical and applied, including:

- Construction and Structural Mechanics
- Building Materials
- Concrete, Steel and Timber Structures
- Geotechnical Engineering
- Earthquake Engineering
- Coastal Engineering
- Hydraulics, Hydrology and Water Resources Engineering
- Environmental Engineering and Sustainability
- Structural Health and Monitoring
- Surveying and Geographical Information Systems
- Heating, Ventilation and Air Conditioning (HVAC)
- Transportation and Traffic
- Risk Analysis
- Safety and Security

Indexed by Scopus

To submit a proposal or request further information, please contact: Pierpaolo Riva at Pierpaolo.Riva@springer.com, or Li Shen at Li.Shen@springer.com

More information about this series at <http://www.springer.com/series/15088>

Maria Pina Limongelli ·
Mehmet Çelebi
Editors

Seismic Structural Health Monitoring

From Theory to Successful Applications

 Springer

Editors

Maria Pina Limongelli
Department of Architecture
Built Environment and Construction
Engineering
Politecnico di Milano
Milan, Italy

Mehmet Çelebi
United States Geological Survey
Menlo Park, CA, USA

ISSN 2366-259X

ISSN 2366-2603 (electronic)

Springer Tracts in Civil Engineering

ISBN 978-3-030-13975-9

ISBN 978-3-030-13976-6 (eBook)

<https://doi.org/10.1007/978-3-030-13976-6>

Library of Congress Control Number: 2019932692

© Springer Nature Switzerland AG 2019

This work is subject to copyright. All rights are reserved by the Publisher, whether the whole or part of the material is concerned, specifically the rights of translation, reprinting, reuse of illustrations, recitation, broadcasting, reproduction on microfilms or in any other physical way, and transmission or information storage and retrieval, electronic adaptation, computer software, or by similar or dissimilar methodology now known or hereafter developed.

The use of general descriptive names, registered names, trademarks, service marks, etc. in this publication does not imply, even in the absence of a specific statement, that such names are exempt from the relevant protective laws and regulations and therefore free for general use.

The publisher, the authors and the editors are safe to assume that the advice and information in this book are believed to be true and accurate at the date of publication. Neither the publisher nor the authors or the editors give a warranty, expressed or implied, with respect to the material contained herein or for any errors or omissions that may have been made. The publisher remains neutral with regard to jurisdictional claims in published maps and institutional affiliations.

This Springer imprint is published by the registered company Springer Nature Switzerland AG
The registered company address is: Gewerbestrasse 11, 6330 Cham, Switzerland

Preface

During the last three decades, Seismic Structural Health Monitoring (herein S^2HM) has grown due to the needs of owners, managers, occupants and users as well as great interest by both researchers and professionals. The maturity of this important discipline is also well evidenced by the development of sensing systems that—when deployed, configured and installed properly—enable retrieval of requisite data during significant seismic events. Such data then are post-processed using damage identification algorithms—implemented in structure-specific configured software—to assess serviceability, functionality and/or occupiability of the structure.

One of the main reasons for increased adoption of S^2HM is that it is a superior and significant alternative to other traditional observational and/or intrusive methods which are costly, time-consuming and, due to dependency on the operator, may be subjective and thus associated with large uncertainties.

Several research efforts have been dedicated to these topics, as shown by the ever-increasing number of related journal and conference publications. However, there is a requisite need in the literature for a focused collection of works dedicated to S^2HM .

The primary motivation for this book is to fill this gap by presenting a unified state of the art on theoretical developments and successful applications of S^2HM around the world, compiled by leading researchers and academicians.

The volume is organized in four topical parts. Each part comprises several chapters by authors experienced in different aspects of S^2HM . Part I collects six chapters devoted to the description of the specific requirements of S^2HM systems for different types of civil structures and infrastructures (buildings, bridges, cultural heritage, dams, structures with base isolation devices) and different phenomena to monitor (e.g. soil–structure interaction and excessive drift). Four chapters covering the methods and the computational tools available for the data processing—needed to retrieve information about the structural health from the signals provided by the sensor network—are grouped in Part II. In Part III, hardware and software tools for

S²HM are described in two chapters. Finally, in Part IV, five chapters report on several state-of-the-art applications of S²HM around the world.

The book is aimed to be useful to researchers, practicing engineers and students and to benefit owners and managers from potential applications of S²HM in their properties.

Milan, Italy
Menlo Park, USA

Maria Pina Limongelli
Mehmet Çelebi

Contents

Part I S²HM for Civil Structures

1 S²HM of Buildings in USA	3
Mehmet Çelebi	
1.1 Introduction and Rationale	4
1.2 Historical Background and Requisites	5
1.3 Early Applications	10
1.4 Brief Note on Other U.S. and Non-U.S. Developments Since 2000	25
1.5 Conclusions	26
References	27
2 Seismic Structural Health Monitoring of Bridges in British Columbia, Canada	31
Yavuz Kaya and Carlos Ventura	
2.1 Introduction	32
2.2 BCSIMS Architecture	33
2.3 Conclusion	47
References	48
3 Seismic Structural Health Monitoring of Cultural Heritage Structures	51
Rosario Ceravolo, Giulia de Lucia, Erica Lenticchia and Gaetano Miraglia	
3.1 Introduction	51
3.2 The Role of Structural Health Monitoring in the Analysis and Preservation of Architectural Heritage	54
3.3 Examples of Vibration-Based Investigation of Architectural Heritage	61
3.4 Periodic Dynamic Investigations in Post-earthquake Scenarios	71

3.5	Continuous Monitoring	75
	References	80
4	Seismic and Structural Health Monitoring of Dams in Portugal	87
	Sérgio Oliveira and André Alegre	
4.1	Introduction	87
4.2	Systems for Continuously Monitoring Vibrations in Large Dams	88
4.3	Monitoring and Modelling the Dynamic Behavior of Large Dams	88
4.4	Hardware and Software Components for Continuous Monitoring Vibrations Systems	90
4.5	The Need for Software Development	93
4.6	Numerical Modelling of Dam-Reservoir-Foundation Systems	96
4.7	Cabril Dam Seismic and Structural Health Monitoring System	97
4.8	Measured Seismic Response	103
4.9	Baixo Sabor Dam SSHM System: Main Monitoring Results Under Ambient Excitation and Seismic Loading	106
4.10	Conclusions	110
	References	112
5	Monitored Seismic Behavior of Base Isolated Buildings in Italy	115
	P. Clemente, G. Bongiovanni, G. Buffarini, F. Saitta and F. Scafati	
5.1	Introduction	115
5.2	Seismic Behavior of Isolation Devices	118
5.3	The New Jovine School in San Giuliano di Puglia	121
5.4	The Operative Centre of the Civil Protection Centre at Foligno	123
5.5	The Forestry Building of the Civil Protection Centre at Foligno	127
5.6	Building with Single Curve Surface Sliders	128
5.7	From Short Time to Real Time Monitoring	130
5.8	Conclusions	133
	References	136
6	Identification of Soil-Structure Systems	139
	S. Farid Ghahari, Fariba Abazarsa and Ertugrul Taciroglu	
6.1	Introduction	139
6.2	Identification of SSI Systems	142

6.3	Conclusions	163
	References	165
 Part II Methods and Tools for Data Processing		
7	Structural Health Monitoring: Real-Time Data Analysis and Damage Detection	171
	Yavuz Kaya and Erdal Safak	
7.1	Introduction	172
7.2	Real-Time SHM Data Analysis	173
7.3	Damage Detection Methods	182
7.4	Conclusion	195
	References	196
8	Model Updating Techniques for Structures Under Seismic Excitation	199
	Serdar Soyoz	
8.1	Introduction	199
8.2	Previous Studies	201
8.3	Methods	206
8.4	Case Studies	208
8.5	Conclusions	213
	References	214
9	Damage Localization Through Vibration Based S²HM: A Survey	217
	Maria Pina Limongelli	
9.1	Introduction	218
9.2	Damage Features Based on the Detection of Shape Irregularity	219
9.3	Damage Localization	223
9.4	Damage Indices and Thresholds	227
9.5	Case Studies	228
9.6	The UCLA Factor Building	228
9.7	The 7th Storey Portion of Building at UCSD	231
9.8	Conclusions	233
	References	234
10	Model-Based Methods of Damage Identification of Structures Under Seismic Excitation	237
	Guido De Roeck	
10.1	Introduction	237
10.2	Elimination of Environmental Influences	240
10.3	Model-Based Damage Identification Based on Modal Parameters	241

10.4	Non-Linear System (Damage) Identification	254
10.5	Wave-Based Methods	255
10.6	Conclusions	257
	References	258

Part III Monitoring Tools

11	An Optical Technique for Measuring Transient and Residual Interstory Drift as Seismic Structural Health Monitoring (S^2HM) Observables	263
	David B. McCallen and Floriana Petrone	
11.1	Introduction	263
11.2	Optically-Based Measurements for Interstory Drift	266
11.3	Sensor Testbeds and Experimental Evaluation of DDPS Performance	268
11.4	Model-Based Simulations of Sensor System Performance	273
11.5	Conclusions	274
	References	277
12	Hardware and Software Solutions for Seismic SHM of Hospitals	279
	Carlo Rainieri, Danilo Gargaro and Giovanni Fabbrocino	
12.1	Introduction	279
12.2	Design of Seismic SHM Systems for Health Facilities	281
12.3	Data Processing for Seismic SHM of Hospitals	286
12.4	Seismic SHM of Hospitals: Notes from a Field Experience	289
12.5	Conclusions	297
	References	298

Part IV Applications of S^2 HM Around the World

13	S^2HM in Some European Countries	303
	Maria Pina Limongelli, Mauro Dolce, Daniele Spina, Philippe Guéguen, Mickael Langlais, David Wolinieck, Emeline Maufroy, Christos Z. Karakostas, Vassilios A. Lekidis, Konstantinos Morfidis, Thomas Salonikios, Emmanouil Rovithis, Konstantia Makra, Maria Giovanna Masciotta and Paulo B. Lourenço	
13.1	Introduction	303
13.2	S^2 HM in Italy: The Italian Seismic Observatory of Structures	304
13.3	S^2 HM in France: The French National Building Array Program	313
13.4	S^2 HM in Greece—The ITSAC Experience	321
13.5	Seismic SHM and Testing for Cultural Heritage in Portugal	329

13.6	Conclusions	339
	References	340
14	S²HM Practice and Lessons Learned from the 2011 Tohoku Earthquake in Japan	345
	Toshihide Kashima and Yoshiaki Hisada	
14.1	Introduction	345
14.2	Lessons Learned from the 2011 Tohoku Earthquake	346
14.3	Influence Factors in the Dynamic Characteristics of Buildings	350
14.4	Damage of High-Rise Buildings and Applications of S ² HM to Emergency Management During the 2011 Tohoku Earthquake	354
14.5	Conclusions	359
	References	359
15	Building Structural Health Monitoring Under Earthquake and Blasting Loading: The Chilean Experience	361
	R. Boroschek, P. Villalpando and E. Peña	
15.1	Introduction	362
15.2	Monitoring	362
15.3	Identification and Monitoring System Experience	363
15.4	Conclusions	380
	References	382
16	Developments in Seismic Instrumentation and Health Monitoring of Structures in New Zealand	385
	S. R. Uma and S. Beskhyroun	
16.1	Introduction	385
16.2	Seismic Monitoring Network in New Zealand	387
16.3	Long Term Structural Health Monitoring	391
16.4	Structure and Instrumentation	394
16.5	Results and Discussion	398
16.6	Conclusions	404
	References	405
17	Seismic Monitoring of Seismically Isolated Bridges and Buildings in Japan—Case Studies and Lessons Learned	407
	Yozo Fujino, Dionysius M. Siringoringo, Masaru Kikuchi, Kazuhiko Kasai and Toshihide Kashima	
17.1	Introduction	408
17.2	Seismic Monitoring of Seismically-Isolated Short and Medium Span Bridges	409
17.3	Seismic Monitoring of Seismically-Isolated Long-Span Bridges	417

17.4 Seismic Monitoring of Seismically-Isolated Buildings 424

17.5 Seismic Retrofit of National Museum of Western Art Tokyo
Using Base-Isolation System 434

17.6 Conclusions 444

References 446

Part I
S²HM for Civil Structures

Chapter 1

S²HM of Buildings in USA



Mehmet Çelebi

Abstract The evolution of seismic structural-health monitoring (S²HM) of buildings in the USA is described in this chapter, emphasizing real-time monitoring. Rapid and accurate assessment of post-earthquake building damage is of paramount importance to stakeholders (including owners, occupants, city officials, and rescue teams). Relying merely on rapid visual inspection could result in serious damage being missed because it is hidden by building finishes and fireproofing. Absent visible damage to a building's frame, most steel or reinforced-concrete moment-frame buildings will be green-tagged based on limited visual indications of deformation, such as damage to partitions or glazing. Contrary, uncertainty in judging extent of structural damage may lead an inspector toward a relatively conservative tag, such as a red tag. In such cases, expensive, intrusive, and time-consuming inspections may be recommended to building owners (e.g., following the M_w 6.7 1994 Northridge, Calif., earthquake, approximately 300 buildings were subjected to costly inspection of connections (FEMA 352)). Using real-time data-driven computation of drift ratios as the parametric indicator of structural deformation and damage to a structure could be of great value to minimize potential judgmental errors in such assessments. Recorded sensor data are an indication of performance, and performance-based design standards stipulate that the amplitude of relative displacement of a building's roof (with respect to its base) indicates performance. Establishing sound criteria for performance is the most important issue for S²HM process, and since 2000 (in the USA), using real-time computed drift ratios and acceptable threshold criteria form the basis for almost all applications in S²HM.

Keywords Seismic response · Health monitoring · Drift · Threshold displacements · Performance

M. Çelebi (✉)

U.S. Geological Survey, Earthquake Science Center, 345 Middlefield Rd. (MS977),
Menlo Park, CA 94025, USA
e-mail: celebi@usgs.gov

© Springer Nature Switzerland AG 2019

M. P. Limongelli and M. Çelebi (eds.), *Seismic Structural Health Monitoring*, Springer Tracts in Civil Engineering, https://doi.org/10.1007/978-3-030-13976-6_1

1.1 Introduction and Rationale

Following an earthquake, rapid and accurate assessment of the damage condition and seismic performance of a building is of paramount importance to stakeholders (owners, leasers, permanent and/or temporary occupants, and city officials and rescue teams that are concerned with safety of those in the building and those that may be affected in nearby buildings and infrastructure). Until recently, assessments of damage to buildings following an earthquake were essentially carried out by inspections conducted by city-designated engineers following procedures similar to ATC-20 tagging requirements [1]. Tagging usually involves visual inspection only and is implemented by assigning the colored tags corresponding to the extent of damage the building experienced or absence thereof, indicative of potential hazard to occupants—green tag indicates the building can be occupied (that is the building does not pose a threat to life safety), yellow indicates Restricted Use (that is, hazardous to life safety but not to prevent limited entrance to retrieve possessions), and red indicates entrance prohibited (that is, hazardous to life). However, one of the impediments to accurately assessing the damage level of structures by visual inspection is that some serious damage may not be visible due to the presence of existing building finishes and fireproofing material. In the absence of visible damage to a building's frame, most steel or reinforced concrete moment-frame buildings will be tagged based on visual indications of building deformation, such as damage to partitions or glazing. Lack of certainty regarding the actual deformation that the building experienced may typically lead an inspector toward a relatively conservative tag. In such cases, expensive and time-consuming intrusive detailed structural inspections may be recommended to building owners (e.g., it is known that, following the M_w 6.7 1994 Northridge, Calif., earthquake, approximately 300 buildings ranging in height from 1 to 26 stories were subjected to costly intrusive inspection of connections [2]).

As stated above, much of the discussion presented here related to structural health monitoring is focused on “rapid and accurate assessment of damage of a building” following an earthquake. I distinguish this aspect from those other studies and assessments made months and years after events using recorded data from instrumented buildings. A vast number of other such studies that are performed weeks, months, and years after events have occurred do exist in the literature. See for example, Rojahn and Mork [3], Ventura and Ding [4], Boroschek and Mahin [5], Rahmani and Todorovska [6, 7], Safak and Çelebi [8, 9], Jennings [10], Çelebi and Safak [11, 12], Çelebi et al. [13–22], Çelebi [23–34], and Rodgers and Çelebi [35]. Thus, because of the rapid (and in reality, near real-time) process of obtaining performance indicators, the pioneering developments in early 2000 are distinguished as “near real-time” seismic structural-health monitoring—thus the acronym S²HM.

Over the past few decades, the majority of post-earthquake safety evaluations of buildings have been made through the process of ATC-20 safety-tagging. In this chapter, a new method to evaluate buildings through real-time response of a structure as a health monitoring tool is presented. This alternative advanced method has become established and is also commercially available to owners and their design-

nated engineers. The rationale is that building owners and their designated engineers are expected to use the response data acquired by a real-time structural-health monitoring system to justify a reduced inspection program, compared to that which would otherwise be required by a city government for a similar non-instrumented building in the same area. It is possible that depending on the deformation pattern and associated damage indicators observed in a building, the initial inspections could be directed toward specific locations in the building that experienced large and potentially damage-inducing drifts during an earthquake. A notable program based on this flexibility to use near real-time monitoring in lieu of tagging has been enacted by the City of San Francisco (see the Building Occupancy Resumption Program, BORP)¹ [36], which will be elaborated further in this chapter.

It is important to iterate the reasons why we need real time or near real-time structural health monitoring of a building. These include:

1. Safety of occupants following an earthquake. If there is damage, this information can be used to decide if evacuations are necessary.
2. Deliberations and decision making for occupancy or reoccupancy after evacuations—immediately after an earthquake.
3. Economical aspects: (1) What would be the financial impact of a lengthy shut-down of a building for further inspection and assessment? (2) Should the structure be permanently shut down and/or replaced?
4. If damage is predicted, how severe is it? What is its impact on occupancy, repair, and/or future retrofit?

1.2 Historical Background and Requisites

Almost two decades ago, when it became possible to reliably and quickly transmit digital structural response time-history signal data, programs were developed to acquire near-real time data from instrumented structures. The initial objective of these programs was to develop a method that would enable informed decisions on the performance and occupation resumption of a building within a reasonably short lapse of time (~1 day) following a strong shaking caused by an earthquake (irrespective of near or distant earthquake).

About the year 2000, the recording of streaming data from sensors in an instrumented building became possible, with the most reliable transmittal of data to a remote computer system for studies and/or applications accomplished using telephone lines. The streaming data were then correlated to the performance of each building. Then as now, a key variable to performance studies for reaching perfor-

¹The City of San Francisco, California, has developed a “Building Occupancy Resumption Program” (BORP) [36] whereby a prequalified occupancy decision making process as described in this paper may be proposed to the city as a reduced inspection program but in lieu of detailed inspections by city engineers following a serious earthquake.

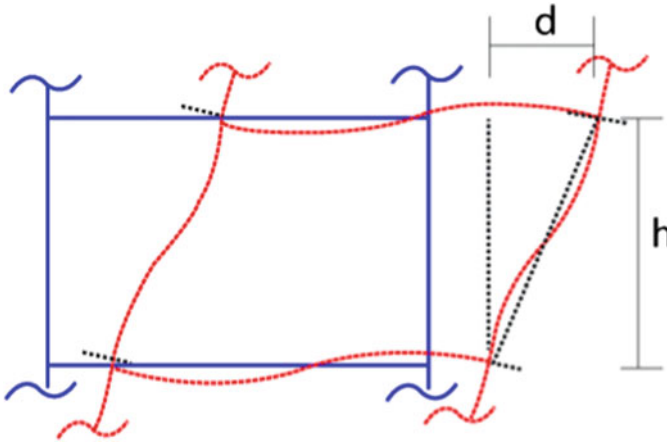


Fig. 1.1 Schematic describing drift ratio computation for a building (d = relative displacement between two consecutive floors, h = floor height)

mance decisions was displacement and, in turn, the drift ratios² of the building. Figure 1.1 displays a schematic of how drift ratios ($DR = d/h$) are computed regardless of whether or not data was sensor based or from mathematical modeling and analyses of the structural system of a building. It is important to note that due to the cost and/or logistical difficulties in deploying sensors on every floor of a building, in most cases, this is not done, thus average drift ratios between a number of floors are also widely used.

About the year 2000, there were two challenges to performing this method: (1) how best to accurately measure or compute displacements in near real-time environment with minimal errors and compute drift ratios and (2) how displacements and/or drift ratios could be related to performance of buildings subjected to earthquake shaking. It was envisioned at the time that once these variables could be reliably acquired using sensors, rational performance-related structural dependent strategies could be developed.

Measuring physical deformation/displacement of a structure subjected to an excitation is very difficult and quite challenging exercise, except for cases of experimental lab-tests conducted in a controlled environment (e.g., using displacement transducers). Real-time measurements of displacement were acquired either directly using GPS or by double integration of accelerometer time-series data. Naturally, both approaches had pros and cons.

For structures with long-period responses, such as tall buildings, displacement measurements using GPS are measured directly only at the roof, so drift ratios are thus an average value for the building. On the other hand, for accelerometer-based systems, the accelerometers must be strategically deployed at specific locations on

²Drift ratio (DR) is defined as relative displacement between any two floors divided by the difference in elevation of the two floors. Usually, this ratio is computed for two consecutive floors.

several floors of a building to facilitate real-time measurement of the actual structural response used to compute displacements and drift ratios.

As stated earlier, GPS technology became the favored method because displacements could be measured without double-integration. It is important to stress that, during about the same period, it was not possible to perform speedy (near real time) retrieval and transmittal and then reliably double-integrate acceleration response data to arrive at displacements [37, 38]. However, the limitations of using GPS were (and mostly still are) (1) the GPS units have to be able to send/receive signals from a minimum number of satellites to minimize the error; (2) because GPS units could only be deployed at the roof of a building, the original computation of drift ratios computed with GPS data are therefore only average drift ratios over the total height of a building; (3) a technically acceptable nearby reference station on either the ground or roof of a 1–2 story stiff building (without interference from taller buildings in an urban setting) is required to compute relative displacements between the roof and the ground level (see the schematic of a typical GPS deployment at a building in Fig. 1.2); and (4) the highest sampling rate of the then commercially available GPS units was 10 Hz,³ which limited the application to buildings of 20 stories or higher due to the corresponding Nyquist frequency ($f_n = 1/(2 \times \Delta t)$) [40] at 5 Hz (0.5 × sample rate), or to periods greater than 2 s.

Thus, if average drift ratios were considered acceptable, then the former approach is preferable and advantageous for taller buildings because direct measurement of displacements is easily converted into drift ratios.

In this schematic, accelerometers (force-balanced accelerometers, FBAs) are also included to facilitate verification of displacements recorded by GPS and vice versa. It is well known that accelerometers have been widely used over decades for seismic monitoring of buildings. Recorded accelerations from accelerometers strategically deployed throughout a building allow double-integration to get displacements. One could deploy as many accelerometers as was economically and physically feasible to improve the computation of drift ratios between two consecutive floors as shown in Fig. 1.1, or the average drift ratios between any two instrumented floors. Furthermore, if configured properly, an exact drift ratio between two consecutive floors of a building can be computed. There remains the possibility of processing errors—from raw data to double integrated displacements. However, with extensive experience in processing raw acceleration data by carefully selecting filters and baseline correction, such errors are minimized. Therefore, with advances in internet-based data transmittal or near real-time remote acquisition of streaming data, it became possible to use classical accelerometer data from deployed structures. As stated earlier, this led to the configuration of accelerometer data based on the establishment of the seismic health monitoring of structures [37, 38, 41].

Whether displacements are acquired using GPS or accelerometers, one must determine what levels of drift ratios are acceptable—to relate the displacement (and there-

³By 2006, as many as 50–100 samples per second (sps) differential GPS systems have been available on the market and have been successfully used [39]. Currently, GPS units with sampling rate of 100 Hz are commercially available.

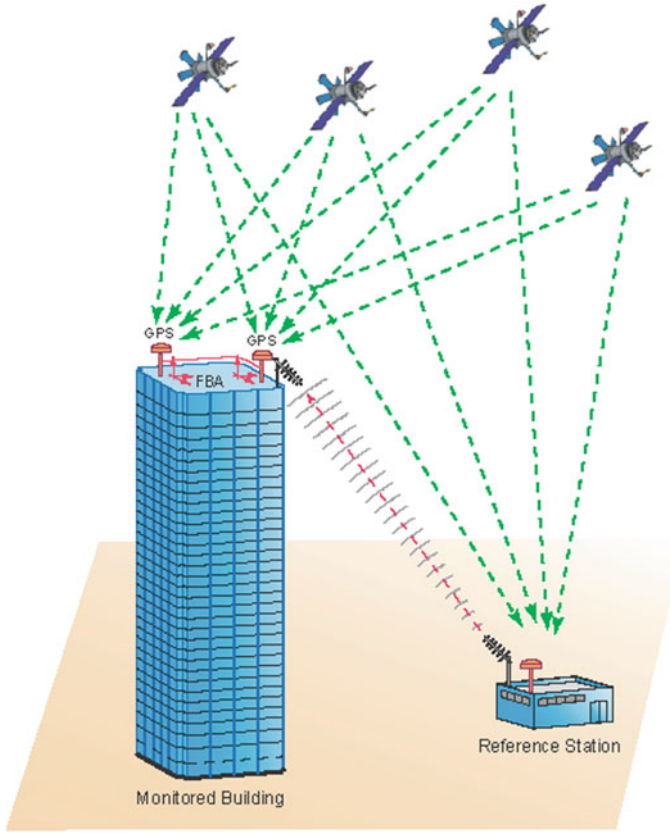


Fig. 1.2 General configuration for GPS acquisition of displacements in 35-story building in San Francisco, Calif. [37]

fore drift ratio data) to the seismic performance of a building. The most relevant parameter to assess performance of a building is the measurement or computation of actual or average story drift ratios. We have not found evidence of reliable applications using other parameters (e.g., mode shape variation, frequency variation). As hypothetically shown in Fig. 1.3 (modified from Figure C2-3 of FEMA 274 [42]), drift ratios are related to the performance-based force-deformation curve [37, 38, 41]. When drift ratios, as computed from relative displacements between consecutive floors, are determined from measured responses of the building, the performance and/or “damage state” of the building can be estimated as in Fig. 1.3. A reasonable number (3–5) of thresholds of levels of relative displacements (or drift ratios) can be established in relation to the desired level of performance. Therefore, structural engineers often determine the requisite level of thresholds in relation to the desired building performance in advance of a seismic event.

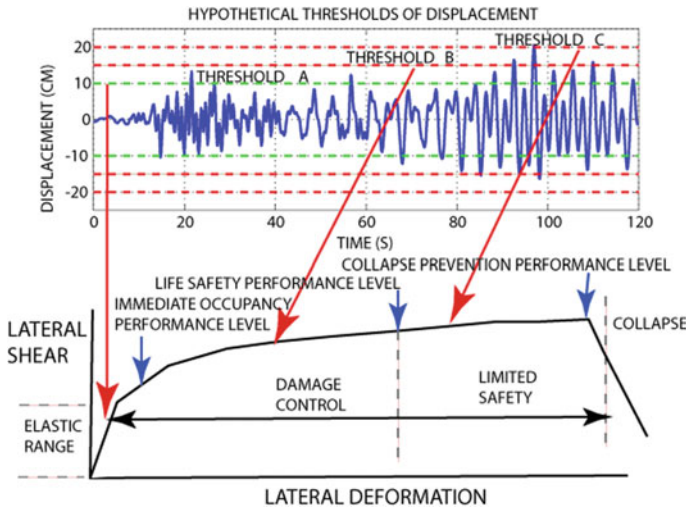


Fig. 1.3 Schematic of hypothetical thresholds of level of displacements related to performance curve as illustrated in FEMA 273 [43] and modified in Çelebi et al. [38]

Table 1.1 Typical threshold stages and ranges of drift ratios

Threshold stage	1	2	3
Suggested typical drift ratios (in percent)	0.2–0.3	0.6–0.8	0.4–2.2

In the final step, recorded sensor data are related to the performance level of a building and therefore to the performance-based design that stipulates the maximum amplitude of relative displacement of the roof of a building (with respect to its base) as an indication of its performance. Establishing sound criteria for performance is the most important step of the S²HM process. As an example, Table 1.1 shows typical drift ratios for steel moment-resisting framed buildings. The table is developed from FEMA 352 [2]. For reinforced-concrete buildings, the lower figures may be more appropriate to adopt.

It is important to state that, as an alternative to FEMA 273 [43] or FEMA 352 [2] suggested values, structural engineers can compute drift ratios through analyses to establish limits related to acceptable performance levels according to Fig. 1.3.

Before these developments in early 2000, there were no other sensor (GPS or accelerometer) data-based performance assessments. As stated by Porter et al. [44, 45]:

[Until now,] sensor information has played little role in PBEE (Performance Based Earthquake Engineering). A notable exception is Çelebi et al. [38] who recently combined sensor information with FEMA 273 (FEMA 1997) [43]. They illustrate the methodology with a 24-story steel-frame building that has been instrumented to compute interstory drift ratios at a few story levels with sensors at adjacent floors. These interstory drift ratios are then compared with drift limits associated with the FEMA-273 performance levels: operational,

immediately occupiable, life-safety, and collapse-prevention. When a drift limit is exceeded, the associated performance level is assumed to be exceeded.

Experience with both types of sensor deployments indicate that they are reliable enough (with acceptable levels of errors) and provide pragmatic alternatives to alert building owners and other authorized parties to make informed decisions and to select choices for predefined actions following significant events. Furthermore, the recent adoption of such methods by financial and industrial enterprises is testimony to their viability.

Thus, the processes advocated in Çelebi and Sanli [37] and Çelebi et al. [38] and Çelebi [41] and based on sensor-based data related to performance-based earthquake engineering (PBEE) are the first near real-time seismic structural-health monitoring (S²HM) developments being used around the world.

1.3 Early Applications

1.3.1 Using GPS for Direct Measurements of Displacements

As stated before, before the year 2000, use of GPS was limited to long-period structures ($T > 1$ s) because differential GPS systems readily available were limited to 10–20 samples per second (sps) capability⁴ with an error of ± 1 cm horizontal and ± 2 cm vertical. Furthermore, with GPS deployed on buildings, measurement of displacement is possible only at the roof [37]. Technology has not yet advanced to detect signals from GPS antennas placed on various floors within a building, as the antennas need to “see” the satellites.

1.3.1.1 Early Testing with GPS

Before going forward with actual utilization of GPS for S²HM of a tall building, we tested GPS capability and reliability with a rather primitive model (Fig. 1.4). Also, prior research provided confidence in the technical feasibility of using GPS technology to measure displacements of civil structures. Aerospace (atmospheric) researchers have accomplished most of the initial work. Studies related to the application of GPS for static or dynamic measurements of displacements of structural systems include but are not limited to those by Hyzak et al. [46], Teague et al. [47], Guo and Ge [48], Kondo and Cannon [49], Lovse et al. [50], Hudnut and Behr [51], Behr et al. [52], and Stein et al. [53]. Temporary deployments to dynamically monitor excessive deflections due to wind, in the decimeter range, of the 1410-m-long Humber Bridge on the east coast of England were successfully carried out [54]. In Japan,

⁴Recently, up to 50 samples per second (sps) differential GPS systems are available on the market and have been successfully used Panagitou et al. [39].

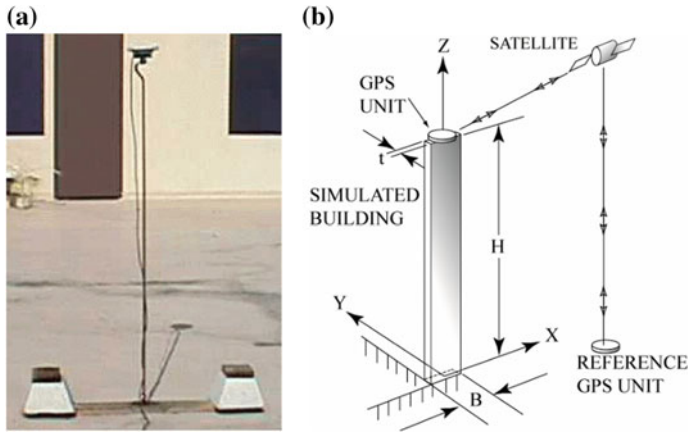


Fig. 1.4 **a** Photograph and **b** schematic of test set-up to simulate using GPS for dynamic monitoring of tall buildings (from [57])

Nakamura [55] cited semistatic displacement measurements (sampling at 1 Hz) of a suspension bridge using temporarily deployed GPS units. Although it is not directly mentioned as to whether permanent and continuous measurements were made, Toriumi et al. [56] depict several meter-level dynamic GPS displacement measurements at the Akashi Bridge, the world's longest span suspension bridge. In the current application, the aim has been actual permanent deployment of GPS units to dynamically obtain displacements during strong-motion events in real or near-real time. More recently, as many as 50 sps differential GPS systems readily available were successfully used on a shaking-table test of a shear-wall building ([39], Jose Restrepo, Univ Calif. San Diego, written communication, 2007)—thus enabling future application of GPS to all types of structures.

To confirm technical feasibility of such an application, before investing a lot of time and fiscal resources on an actual deployment on a building, Çelebi et al. [57] performed tests using a primitive model structure using two bars 1.82 m (6 ft) in length with small thicknesses (0.32 cm [1/8 in.]) and widths of 1.5 in. (3.8 cm) and 2 in. (5 cm), respectively. Figure 1.4 depicts a photo and the overall setup for a simple and inexpensive experiment designed by selecting a standard stock steel bar to simulate a 30- to 40-story flexible building. The authors selected the length, thickness, and width of the two bars to yield a fundamental period of approximately 4 s in the weak direction. For simplicity, the authors purposefully selected the width and thickness of each of the two bars with an extremely weaker axis in one direction. The width was varied to show the sensitivity of measurements during vibration and at a 10-Hz sampling rate. Each bar was fixed at the base, and the GPS unit was attached at its tip. By providing an initial displacement (simply by pulling the top of the bar and releasing), each bar was set into free vibration and its motion was recorded. Results are summarized in Table 1.2. Figure 1.5 shows the particle motion and time-history of one of the tests performed. The axes of the bar were at an angle to

Table 1.2 Results of tests with GPS units (f = frequency, T = period; see Fig. 1.4b for explanation of H, B, and t) (from [57])

Specimen	Length [H] (m (ft))	Width [B] (in. (cm))	Thickness [t] (in. (cm))	Measured [f] (Hz)	Measured [T] (s)	Damping [ξ] (%)
Bar A	1.82 (6)	3.8 (1.5)	0.32 (1/8)	0.245	4.08	~2.0
Bar B	1.82 (6)	5.0 (2.0)	0.32 (1/8)	0.296	3.38	~2.0

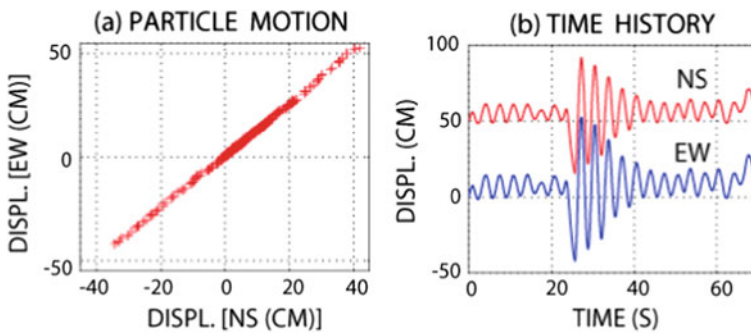


Fig. 1.5 **a** Particle motion and **b** time-history of relative displacements (north-south and east-west components) of simulated test specimen (from [57])

the north-south (N-S) and east-west (E-W) directions. Therefore, the N-S and E-W components of displacements are identical in phase and proportional in amplitude. Also, because the GPS unit is not symmetrically and concentrically mounted in the weak direction (Fig. 1.4a), the amplitudes of positive and negative displacements measured are not the same. The detection of the effect of the eccentric mass adds to the assurance that the measurements are accurate and sensitive. The simple tests and results of Çelebi et al. [57] can be validated easily elsewhere.

Figure 1.6 is a plot of NS components of measured relative displacements and corresponding amplitude spectra of bars A and B. The figure shows the accuracy and sensitivity of GPS monitoring technology at 10 sps. The measurements differentiate between the frequency of the free-vibration response of the two bars with different dynamic characteristics. From the data, the fundamental frequency (period) of the two bars are identified to be 0.245 Hz (4.08 s) and 0.296 Hz (3.38 s), respectively. Also, a damping percentage of approximately 2% is determined. This simple test shows that sampling at 10 Hz with GPS units provides a clear and accurate displacement response history (with high signal-to-noise ratio) from which drift ratios and dynamic characteristics of the specimen can be derived [57].

The tests clearly demonstrate the reliability of GPS measurements from forced vibration. Later Tamura et al. [58] performed similar successful tests before using GPS in larger tall building monitoring projects in Japan.

A schematic of a real-life application using GPS to directly measure displacements was shown earlier in Fig. 1.2, where two GPS units are used to capture both

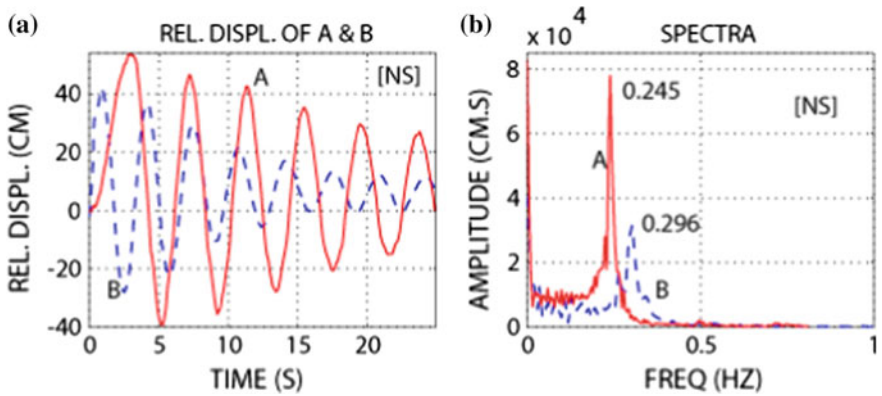


Fig. 1.6 **a** Relative displacements of two test specimens (north-south components only) in free-vibration **(a)** and **b** corresponding amplitude spectra identifying the fundamental frequencies of the test specimens (from [57])

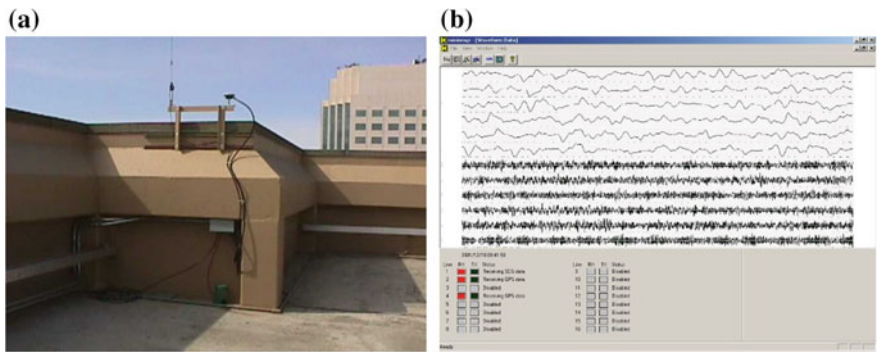


Fig. 1.7 **a** Picture of deployment of GPS antenna at the roof of a 35-story building in San Francisco, Calif. Schematic of the overall system using GPS and accelerometers is shown in Fig. 1.2. **b** Screen capture of streaming acceleration and displacement data in real time (from [57])

the translational and torsional response of the 35-story building in San Francisco, California. Figure 1.7a shows one of the GPS antennas, as well as a triaxial accelerometer deployed to compare the displacements measured by GPS with those obtained by double-integration of the accelerometer records. Figure 1.7b shows screen captured acceleration and displacement data streaming into the monitoring system.

To date, strong shaking data from the deployed system has not been recorded. However, ambient data (Fig. 1.8a–d) obtained from both accelerometers and GPS units are analyzed (Fig. 1.9). Sample cross-spectra (S_{xy}) (Fig. 1.9a–d) and coherency and phase angle plots (Fig. 1.9e–h) of pairs of parallel records N-S component of north deployment [N_N] versus N-S component of south deployment [S_N], from accelerometers are shown in Fig. 1.9e–f. The same is repeated for the differential displacement records from GPS units (Fig. 1.9g–h). Frequency of 0.24–0.25 Hz seen

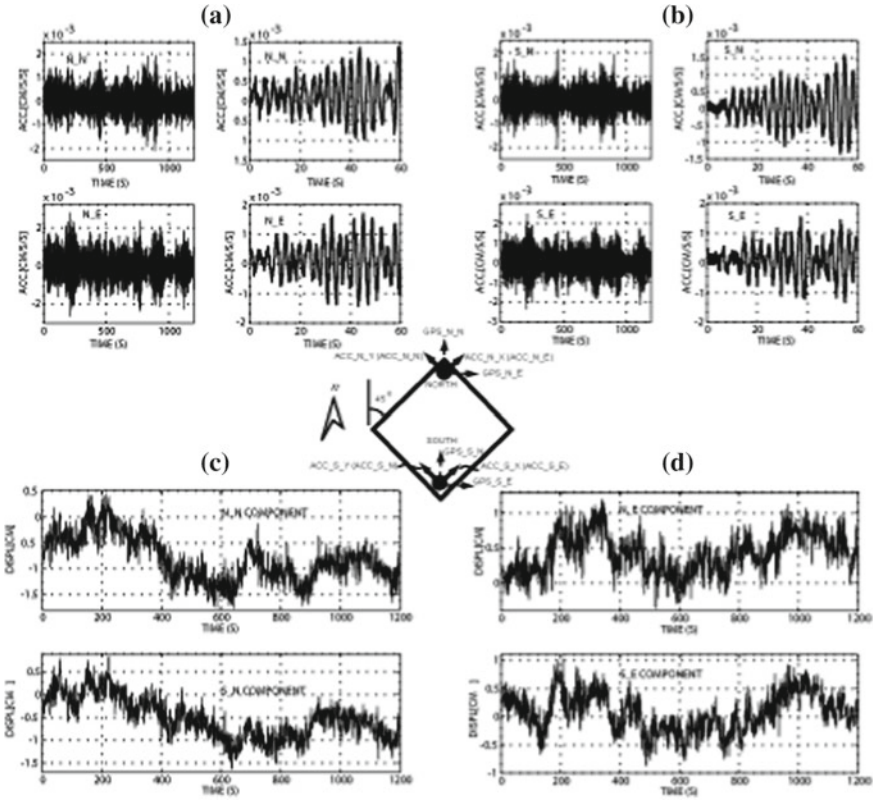


Fig. 1.8 a, b Remotely triggered and recorded (1200 and 60-second windows) accelerations at N (north) and S (south) locations, respectively, and c, d remotely triggered and recorded displacements from GPS at N (north) and S (south) locations, respectively, for a 35-story building in San Francisco, Calif. Locations are defined in the central schematic (from [57])

in Sxy plots from both acceleration and displacement data belong to the expected fundamental frequency for a 35-story building. A second frequency at 0.31 Hz (from acceleration data) Hz is belongs to the torsional mode. Background information on coherency and related spectral relations are found in Bendat and Piersol [59].

At the fundamental frequency at 0.24 Hz, the displacement data exhibits a 0° phase angle; however, the coherencies are lower (~0.6–0.7). The fact that the fundamental frequency (0.24 Hz) can be identified from the GPS displacement data, amplitudes of which are within the manufacturer specified error range, and that it can be confirmed by the acceleration data is an indication of promise of better results when larger displacements can be recorded during strong shaking.

One comment on this is that using GPS monitoring of tall buildings should be a proven option but with the caveat that decision-making on performance is based on average drift ratio.

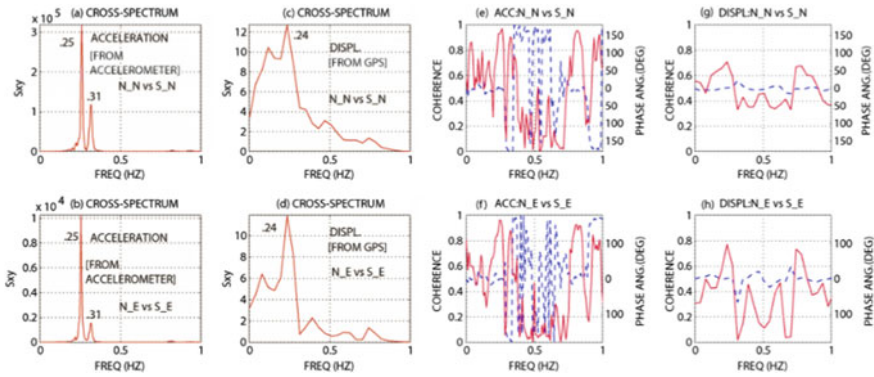


Fig. 1.9 Cross-spectra (S_{xy}) (a, b) of accelerations from accelerometers and (c, d) displacements from GPS and associated coherency and phase angle plots of horizontal and parallel (e, f) accelerations [e, f] and (g, h) from GPS displacements for a 35-story building in San Francisco, Calif. [Note In the coherency-phase angle plots, solid lines are coherency and dashed lines are phase-angle] (from [57])

1.3.2 Early Development—S²HM Use of Displacement Via Real-Time Double Integration of Accelerations

For S²HM purposes, a proven alternative to using GPS technology to acquire displacements is through a strategical configuration of accelerometer-based monitoring of buildings. As mentioned before, about the year 2000, with the advent of real-time streaming of acceleration responses which are double-integrated in near real-time to obtain displacements opened opportunities for an accelerometer-based S²HM capability.

A general flowchart for an alternative strategy based on computing displacements in real-time from signals of accelerometers strategically deployed throughout a building is depicted in Fig. 1.10 and described by Çelebi [41]. Although ideal, generally, deploying multiple accelerometers in every direction on every floor level is not a feasible approach. This is due to installation costs and also being able to robustly (1) stream n number of accelerations from n number of channels, (2) compute and stream displacements and drift ratios after double integration of accelerations, and (3) visually display threshold exceedences, thus fulfilling the objective of timely assessment of performance level and damage conditions.

A schematic of the very first deployed structural-health monitoring system that uses these principles is shown in Fig. 1.11 [38, 41]. The distribution of accelerometers provides data from several pairs of neighboring floors to facilitate drift computations.⁵ The system server at the site (1) digitizes continuous analog data, (2)

⁵The locations of sensors are generally dictated by the desire to obtain optimum response data from different floors and within strategic locations of those floors to compute reliable drift ratios for assessing near real-time performance of a building during an earthquake. Cost also becomes

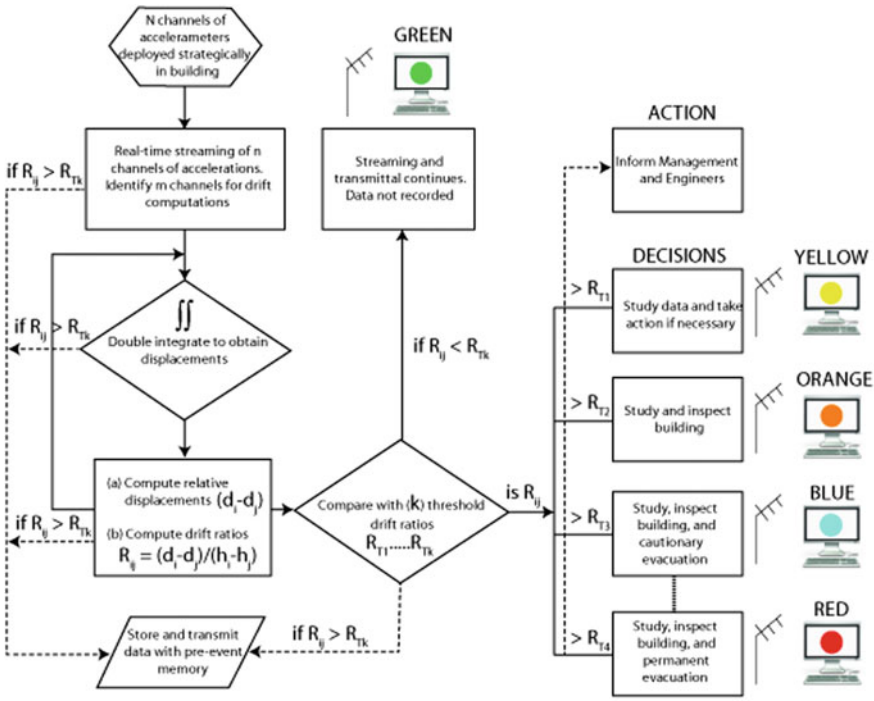


Fig. 1.10 Flow-chart for observation of structural damage levels based on threshold drift ratios as described in Fig. 1.3 (flowchart from [41])

preprocesses the 1000 sps digitized data with low-pass filters, (3) decimates the data to 200 sps and streams it locally, (4) monitors and applies server triggering threshold criteria and locally records the shaking of the building (with a pre-event memory) when prescribed thresholds are exceeded, and (5) broadcasts the data continuously to remote users by high-speed internet. Data can also be recorded on demand to facilitate studies while waiting for strong shaking events.

Whereas Fig. 1.10 depicts the logical process to configure acceleration to displacement dependent S^2HM software, Fig. 1.11a depicts, in general, all elements of this new approach in obtaining structural displacements in near real-time, transmittal of data using the internet, and configuration of performance computations in an onsite or offsite remote server. Figure 1.11b depicts the numbering system and orientations of accelerometers. This schematic actually is representative of the system installed

a consideration. In general, on each instrumented floor, a minimum of three accelerometers are deployed—two parallel at a distance apart to facilitate computation of torsion and the third orthogonal to the other two. A minimum of three verticals are deployed at the basement in ground-level corners to compute rocking, if any [29]. The Los Angeles Tall Buildings Structural Design Council [60] provides guidance also for number of accelerometers according to number of floors of a building (e.g., they recommend 36 channels for buildings taller than 50 stories). However, for S^2HM purposes, the number of accelerometers should be greater.

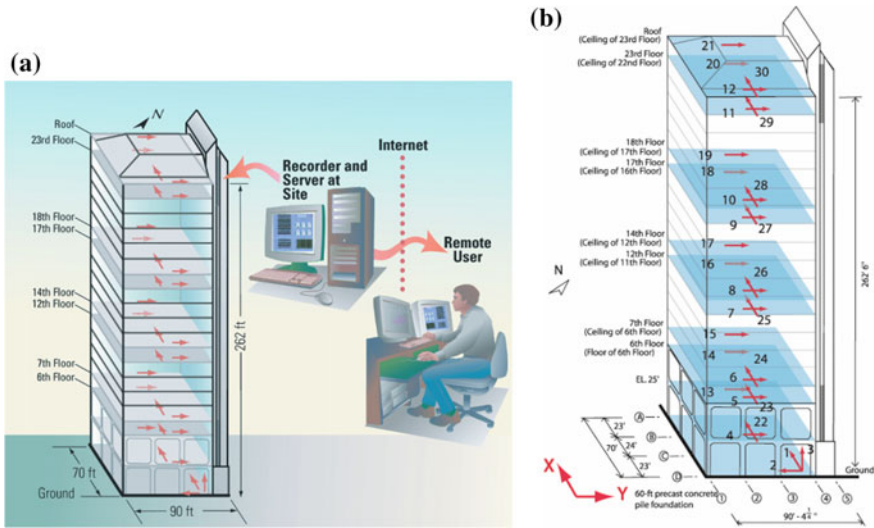


Fig. 1.11 **a** General schematic of data acquisition and transmittal for seismic monitoring of a 24-story building using accelerometers as sensors. **b** Numbering system and orientations (from [38])

in a 24-story building in San Francisco shown in Fig. 1.2. As mentioned earlier, to the best of our knowledge, this actual development is based on the initial project that led to the earliest S²HM development (between 1999 and 2002) in the USA, as well as the world. It is relevant here to state that the project and resulting development was initiated because the building owner and their consultants needed a monitoring system that could be used to make informed decisions about performance and functionality after an earthquake and how soon the building could be re-occupied. By using this technology, the objective of the owners and the consultants was to meet the requirements of San Francisco’s BORP [36], in lieu of tagging as described in the Introduction section of this chapter. Thus, in consideration of financing but without sacrificing reliability, the accelerometer-based array used in the building was designed to provide data from several pairs of neighboring floors to facilitate drift ratio computations.

The broadcast streamed real-time acceleration data were acquired remotely using building-specific S²HM software that was configured to compute velocity, displacement, and drift ratios or average drift ratios as needed. Figure 1.12 shows two computer screenshots of the client software display configured for 12 channels of streaming acceleration, velocity, displacement, or drift-ratio time series. Around the year 2000, at the time of this development, this was the limit of number of channels could be displayed as streaming on a screen. However, computations were made for all combinations to arrive at drift ratios. Each paired set of acceleration response streams was displayed with a different color. The amplitude spectrum for one of the selected channels was periodically recomputed and clearly displayed several identifiable frequencies. In the lower left of Fig. 1.12a, b, time series of drift ratios are

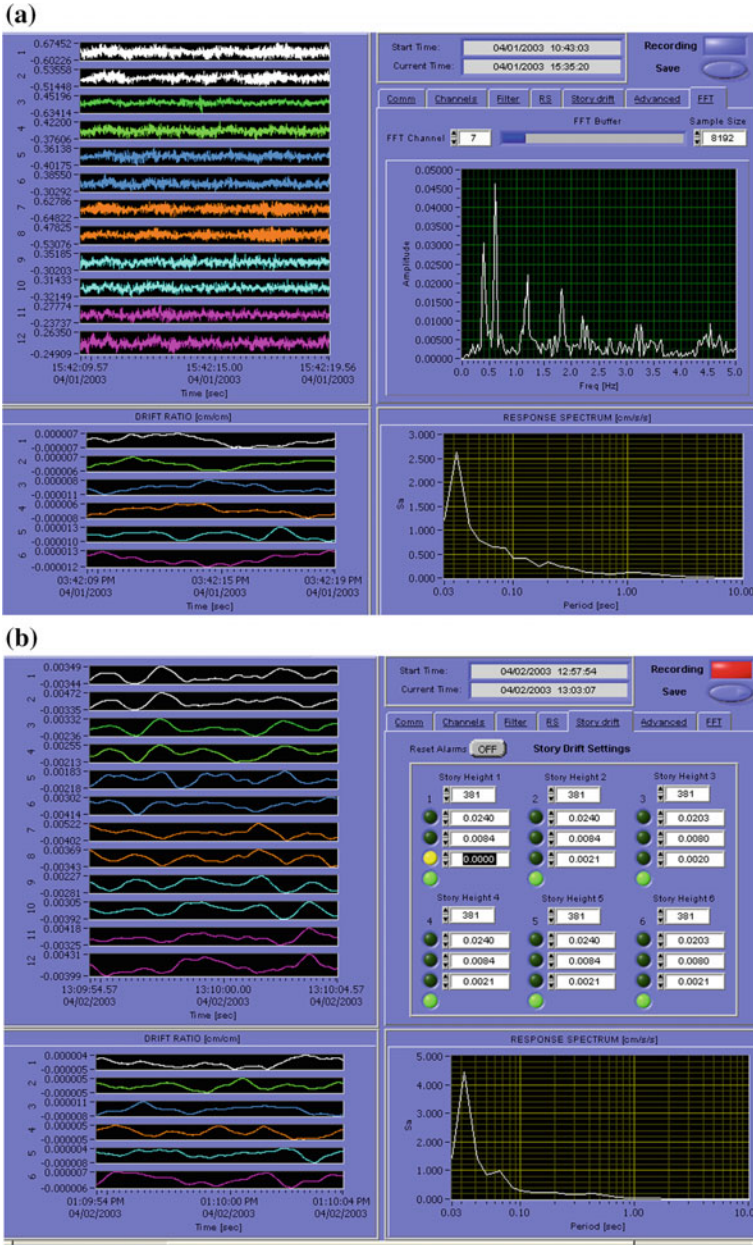


Fig. 1.12 **a** Screenshot of S²HM client software display showing acceleration streams and computed amplitude and response spectra. **b** Screenshot of S²HM client software display showing 12-channel (six pairs with each pair a different color) displacement and corresponding six drift-ratio (each with the same color as the parent displacement) streams. Also shown to the upper right are alarm systems corresponding to thresholds that must be manually input. The first threshold for the first drift ratio is hypothetically exceeded to indicate the starting of the recording and change in the color of the alarm from green to yellow (from [38])

Table 1.3 Summary of threshold stages and corresponding drift ratios for the 24-story building in San Francisco, Calif. (from [38])

Threshold stage	1	2	3
Adopted drift ratio (percent)	0.2	0.8	1.4–2.0

shown for 6 pairs (due to the 12-channel display capability of computer monitors), with each color corresponding to the same pair of acceleration data from the window above.

In the S²HM software, drift ratios are computed using real-time, filtered and double integrated acceleration data. Specific filter options are built into the software for processing of the acceleration data. To compute drift ratios, story heights are entered into the building specific software (Fig. 1.12b). Figure 1.12b also shows the computed pairs of displacements that are used to compute the drift ratios. Corresponding to each drift ratio, there are 4 stages of colored indicators. When only the green color indicator is activated, it indicates that the computed drift ratio is below the first of three specific thresholds (Table 1.3). The thresholds of drift ratios for selected pairs of data must also be manually entered in the boxes. As drift ratios exceed the designated three thresholds, additional indicators are activated having different colors (Fig. 1.12b). The drift ratios are calculated using data from any pair of accelerometer channels oriented in the same direction. The threshold drift ratios for alarming and recording are computed and decided by structural engineers using structural information and are compatible with the performance-based theme, as illustrated in Fig. 1.1 (Fig. C2-3 of FEMA 274 [42]; also see FEMA 273 [43]) and summarized in Table 1.3 for the San Francisco building. Figure 1.12 (right) hypothetically shows that the first level of threshold is exceeded, and the client software is recording data as indicated by the illuminated red button. This information is received by building owner and their consultants for further decision making and action as needed.

1.3.2.1 Testing the System—Ambient Data and Analyses

Sample ambient data recorded on 31 March, 2003, using the S²HM client software are shown in Fig. 1.13. The data are from the two parallel roof channels (CH12 and CH21) and their difference (CH12 minus CH21), as well as the roof orthogonal channel (CH30). The intent of the differential accelerations of parallel channels (CH12 minus CH21) is to illustrate the structural response due to torsion. The recorded peak accelerations are about 0.1–0.2 gals ($\sim 0.1\text{--}0.2\text{ cm/s}^2$). The computed amplitude spectra clearly indicate a peak frequency for the fundamental translational mode (in both directions) at $\sim 0.4\text{ Hz}$ ($\sim 2.5\text{-s}$ period) for all channels and at $\sim 0.6\text{ Hz}$ ($\sim 1.67\text{ s}$) for the torsional motion. Furthermore, the signal to noise ratio is high enough to identify the second translational mode at $\sim 1.2\text{ Hz}$ ($\sim 0.83\text{ s}$). Similarly, the second torsional mode is at $\sim 1.8\text{ Hz}$ (0.56 s). The identified translational frequency is typical of a steel-moment frame building that is 24 stories high. The identified modes and fre-

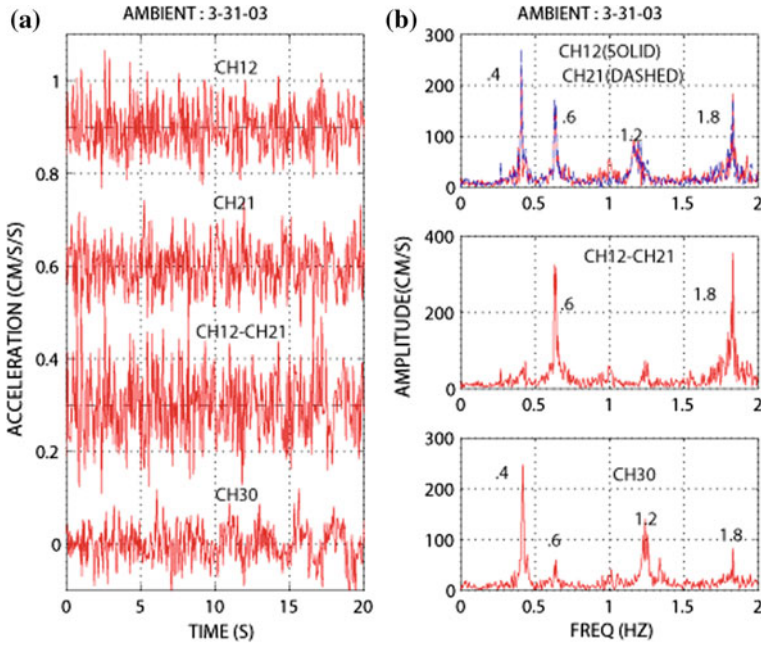


Fig. 1.13 a Twenty seconds of ambient acceleration response data obtained at the roof of a 24-story building in San Francisco, Calif., from parallel channels (CH12 and CH21), their difference (CH12 minus CH21), and from CH30, orthogonal to CH12 and CH21 and b corresponding amplitude spectra (from [38])

quencies are further supported with the cross-spectrum, coherency, and phase angle plots in Fig. 1.14a and b. In Fig. 1.14b the cross spectrum, coherency, and phase angle plots of the motions recorded by CH12 and CH21 (the two parallel accelerometers at the roof level) are shown. The cross spectrum actually exhibits all of the significant frequencies identified in Fig. 1.13 with very high coherency (~1). At 0.4 and 1.2 Hz, the phase angles between the parallel motions are both 0°, which indicate that they are in phase and therefore belong to translational modes. At 0.6 and 1.8 Hz, the phase angles are ~180°, which indicates that they are out of phase and belong to torsional modes. The strong torsional response is further illustrated in Fig. 1.14b that exhibits cross spectrum, coherency, and phase angle plots of the differences of motions recorded by parallel channels (CH12 minus CH21) at the roof and (CH10 minus CH19) at the 18th floor. Again, at ~0.6 Hz, these torsional motions exhibit significant cross-spectral amplitude with very high coherency (~1) and 0° phase angle. Therefore, 0.6 Hz belongs to the first torsional mode, indicating that the ambient data was reliable.

At the level of low-amplitude acceleration response recorded and exhibited in this set of sample data (Fig. 1.13), the signal-to-noise ratio is quite high but is satisfactory to indicate several modal frequencies. It is expected that the coherency of motions

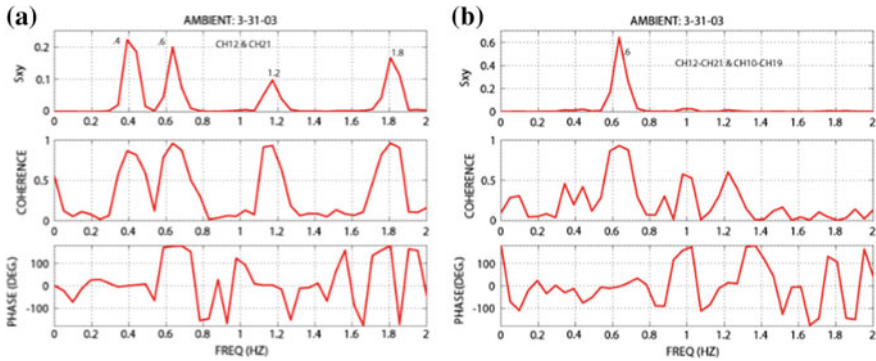


Fig. 1.14 **a** Cross spectrum, coherency, and phase angle plots of ambient acceleration response data obtained from parallel channels (CH12 and CH21) at the roof of a 22-story building in San Francisco, Calif., and **b** cross spectrum, coherency, and phase angle plots of ambient acceleration response data obtained from differences of parallel channels, CH12 minus CH21 at the roof and CH10 minus CH19 at the 18th floor (from [38])

between such pairs of channels will further improve when the signal-to-noise ratio is even higher during strong-shaking events. Further detailed analyses of strong-shaking data are expected to be carried out when such data become available in the future.

1.3.2.2 Sample Low-Amplitude Earthquake Response Data and Analyses

The S²HM system in the 24-story San Francisco building (Fig. 1.2) has recorded responses of the building to several earthquakes since 2003. None of these events were large enough to trigger the alarm system described in the flowchart (Fig. 1.10) or S²HM software (Fig. 1.12). However, the data from small earthquakes was used to confirm the quality of the system as was done for ambient data (from [38]).

December 22, 2003, San Simeon, Calif., Earthquake (M_w 6.4)

During the December 22, 2003, San Simeon, Calif., earthquake (M_w 6.4), at an epicentral distance of 258 km, a complete set of low-amplitude earthquake response data was recorded in the same 24-story monitored building in San Francisco. The largest peak acceleration was approximately 1% of g . Synchronized bandpass-filtered accelerations and corresponding double-integrated displacements are shown in Fig. 1.15 for one side of the building. Figure 1.16 shows computed displacements 20–40 s into the record and reveals the propagation of waves from the ground floor to the roof. The travel time extracted is ~0.5 s. Because the height of the building is

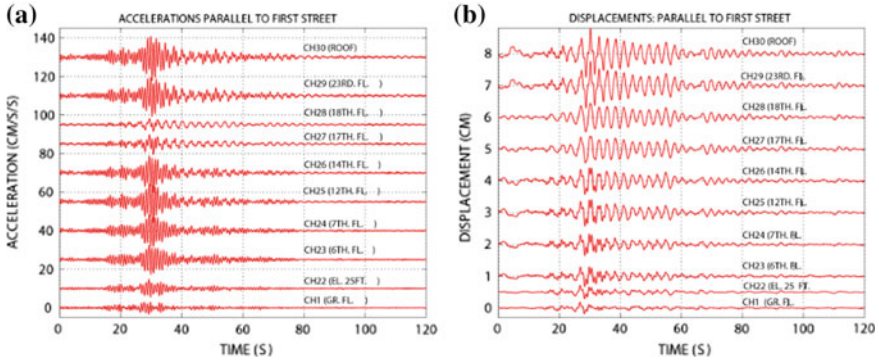


Fig. 1.15 a Bandpass-filtered accelerations and b double-integrated displacements at each instrumented floor (from ground floor to the roof) on one side of a monitored 80-m-tall building in San Francisco, Calif., 258 km from the epicenter of the December 22, 2003, M_w 6.4 San Simeon, Calif., earthquake (from [38])

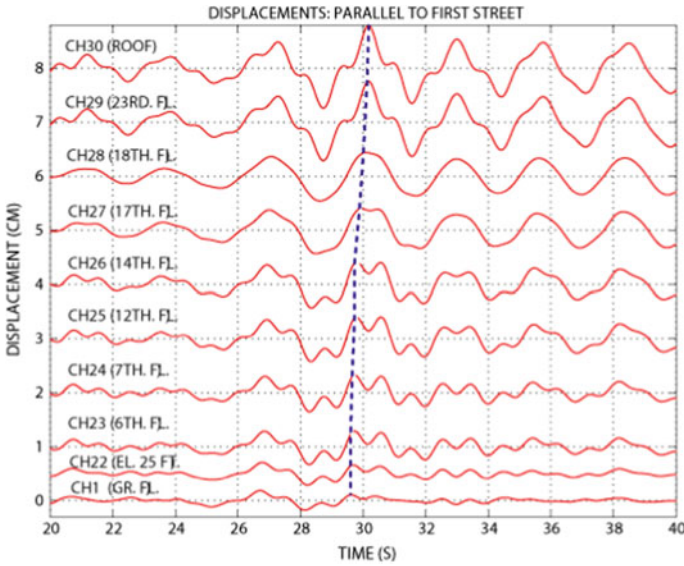


Fig. 1.16 A 20-s window plotted from 20 to 40 s into the record of computed displacements from a monitored 80-m-tall building in San Francisco, Calif., 258 km from the epicenter of the December 22, 2003, M_w 6.4 San Simeon, Calif., earthquake. Travel time of propagating vibrational waves from the ground floor to the roof is approximately 0.5 s (from [38])

known (262.5 ft [80 m]), travel velocity is computed as 160 m/s. One of the possible approaches in detecting potential damage to structures is keeping track of significant changes in the travel time because the travel of waves will be delayed if there are significant cracks in the structural system [61].

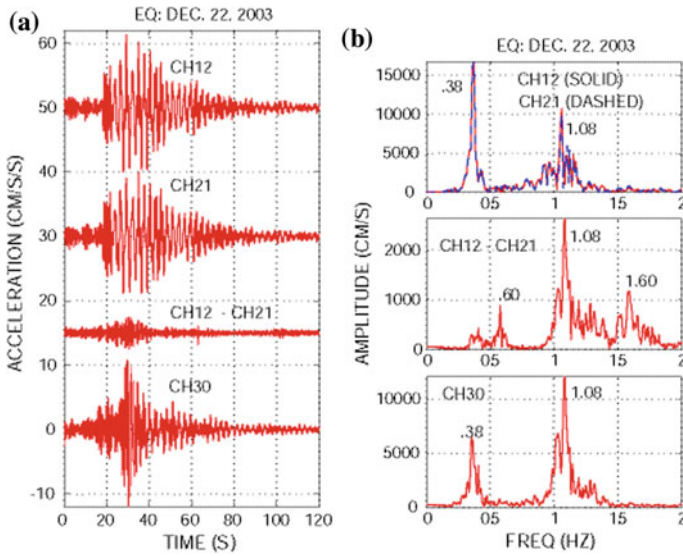


Fig. 1.17 a Acceleration response data obtained at the roof of a monitored 80-m-tall building in San Francisco, Calif., 258 km from the epicenter of the December 22, 2003, M_w 6.4 San Simeon, Calif., earthquake from parallel channels (CH12 and CH21), their difference (CH12 minus CH21), and from CH30, orthogonal to CH12 and CH21 and b corresponding amplitude spectra (from [38])

Similar to Fig. 1.13 using ambient data, Fig. 1.17 depicts the two parallel and orthogonal earthquake motions recorded at the roof of the building and are used to identify the first-mode translational and torsional frequencies as 0.38 Hz and 0.60 Hz, respectively. Also similar to Fig. 1.14, for ambient data, Fig. 1.18a and b shows the cross-spectrum (S_{xy}) and coherency and phase angles at these frequencies using earthquake data. Very small differences in frequencies exist between those computed from ambient motions compared to those computed from earthquake motions.

January 4, 2018, Berkeley, Calif., Earthquake (M_w 4.4)

At an epicentral distance of approximately 16 km, during the January 4, 2018, Berkeley, Calif., Earthquake (<https://strongmotioncenter.org/cgi-bin/CESMD/stationhtml.pl?stationID=CE58480&network=CGS>, accessed May 9, 2018). (M_w 4.4), a complete set of low-amplitude earthquake response data was recorded in the 24-story a monitored building in San Francisco The largest peak acceleration was approximately 3.7% of g at the roof.

Orthogonal set of horizontal accelerations recorded at all instrumented floors are shown for both X and Y directions (see Fig. 1.11) in Fig. 1.19. As in the case of earlier 2003 San Simeon earthquake, the shaking level was not large enough to cause large drift ratios. However, the dominant frequencies are very similar as depicted by

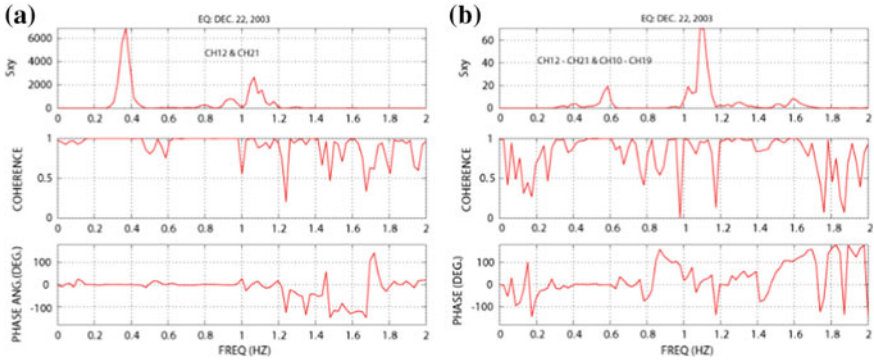


Fig. 1.18 **a** Cross spectrum, coherency, and phase angle plots of ambient acceleration response data obtained from parallel channels (CH12 and CH21) at the roof of a monitored 80-m-tall building in San Francisco, Calif., 258 km from the epicenter of the December 22, 2003, M_w 6.4 San Simeon, Calif., earthquake. **b** Cross spectrum, coherency, and phase angle plots of ambient acceleration response data obtained from differences of parallel channels, CH12 minus CH21, at the roof and CH10 minus CH19 at the 18th floor (from [38])

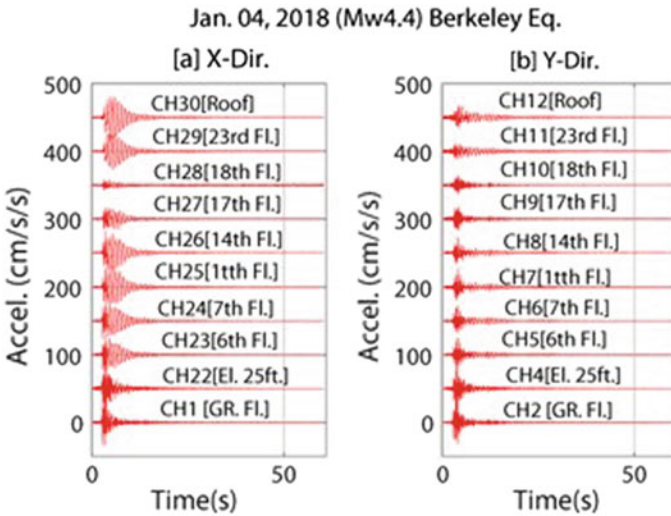
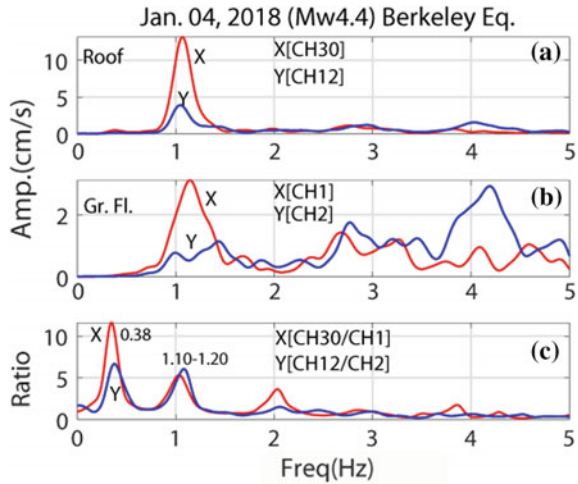


Fig. 1.19 Acceleration time-history plots obtained from two orthogonally deployed accelerometers at all instrumented floors of a monitored 18-story building in San Francisco, Calif., 16 km from the epicenter of the January 22, 2018, M_w 4.4 Berkeley, Calif., earthquake (Fig. 1.11). **a** X-direction; **b** Y-direction

the spectral ratios obtained from smoothed amplitude spectra at the roof and ground floor (Fig. 1.20).

Fig. 1.20 Smoothed amplitude spectra of accelerations at the **a** roof and **b** ground floor of a monitored 18-story building in San Francisco, Calif., 16 km from the epicenter of the January 22, 2018, M_w 4.4 Berkeley, Calif., earthquake and **c** their respective ratios depict the dominant frequencies of the building



1.4 Brief Note on Other U.S. and Non-U.S. Developments Since 2000

In the USA, since 2005, several S²HM projects have evolved. It is significant to note that two companies have begun designing and manufacturing their own S²HM structural monitoring hardware and software—both based on the flowchart in Fig. 1.10. Interestingly, one of the companies now has S²HM-capable monitoring installed in 10 buildings in USA and 14 outside of USA. The second company has 9 monitored structures including 4 buildings in the USA and 5 buildings outside of USA.

Not included in the above inventories is a notable S²HM application in the 828-m tall Burj Khalifa Building in Dubai—currently the tallest building in the world [62]. In addition to an accelerometric array, the S²HM network in the building also includes a GPS array [63]. This system is capable of monitoring for both wind [64] and seismic events. In addition, this building has been recently equipped with a separate S²HM system [65].

The latest widespread use of S²HM arrays in the USA are those installed and being installed in 27 U.S. Department of Veterans Affairs hospitals—mostly short and mid-rise buildings. The most prominent part of the software developed for these buildings is again based on the flowchart in Fig. 1.10. An online search for publications with data analyses for these buildings returned no references.

Kaya and Safak [66] have developed their own Matlab based S²HM software called REC_MIDS. In their paper, they show the essential flowchart of a S²HM system that is similar to Fig. 1.10 in this chapter (Fig. 1.4 in [66]). They have installed and applied their software in 7 buildings in Dubai, as well as in Hagia Sophia Museum in Istanbul, Turkey. The 62-story Sapphire Building is the tallest building in Istanbul, Turkey, and also has a 30-channel real-time capable system (written communication, Erdal Safak, Kandilli Observatory, Istanbul, Turkey, April 2018).

Hisada et al. [67] and Kubo et al. [68], describe S²HM monitoring of Kogakuin University in Tokyo, Japan. The system has two major components—an earthquake early warning system (EEWS) and a real-time strong-motion monitoring system (RSMS). The EEWS system gets its warning from the Japan Meteorological Agency; the RSMS system is based on drift angle (which is same as drift ratio). Two thresholds are used—damage limit as $1/200 = 0.005 = 0.5\%$ drift ratio the safety limit is $1/100 = 1\%$ drift ratio—both limits are adopted from Building Standard Law of Japan [69, 70].

1.5 Conclusions

Capitalizing on advances in GPS, computational and data transmission technology, it is now possible to configure and implement a seismic-monitoring system for a specific building with the objective of rapidly obtaining and evaluating response data during a strong-shaking event in order to help make informed decisions regarding the structural health and occupancy safety of that specific building. Using GPS technology and/or real-time double-integration and related data-acquisition systems, displacements and, in turn, drift ratios, in real-time or near real-time can be obtained. Drift ratios are related to damage condition of the structural system by using relevant parameters of the type of connections and story structural characteristics, including its geometry. Thus, once observed drift ratios are computed in near real-time, technical assessment of the damage condition of a building can be made by comparing the observed with precomputed threshold stages of drift ratios corresponding to preselected damage levels. Both GPS and double-integration applications can be used for performance evaluation of structures and can be considered as building structural-health-monitoring applications.

Benefits in using such real-time systems in either direct measurement of displacements using GPS or real-time computation of displacements by double-integration of accelerations during very strong shaking caused by earthquakes or other extreme events are yet to be recorded and proven. However, analyses of data recorded during smaller events or low-amplitude shaking are promising.

Acknowledgements These developments were funded by PG&E (GPS project) and FDIC (accelerometric S²HM project). Financial supports of these organizations in early development of S²HM configuration are acknowledged. Dr. Ahmet Sanli contributed to both efforts. Any use of trade, firm, or product names is for descriptive purposes only and does not imply endorsement by the U.S. Government.

References

1. Applied Technology Council (1989) Procedures for post-earthquake safety evaluation of buildings. Applied Technology Council ATC-20
2. SAC Joint Venture (2000) Recommended post-earthquake evaluation and repair criteria for welded steel moment-frame buildings. Federal Emergency Management Agency, FEMA-352, Washington, DC
3. Rojahn C, Mork PN (1981) An analysis of strong-motion data from a severely damaged structure, the Imperial County services building, El Centro, California. U.S. geological survey open-file report 81-194
4. Ventura C, Ding Y (2000) Linear and nonlinear seismic response of a 52-storey steel frame building. *J Struct Des Tall Build* 9(1):25–45. [https://doi.org/10.1002/\(SICI\)1099-1794\(200003\)9:1%3c25:AID-TAL140%3e3.0.CO;2-9](https://doi.org/10.1002/(SICI)1099-1794(200003)9:1%3c25:AID-TAL140%3e3.0.CO;2-9)
5. Boroschek RL, Mahin SA (1991) Investigation of the seismic response of a lightly damped torsionally coupled building. Earthquake Engineering Research Center, University of California, Berkeley, UCB/EERC-91/18
6. Rahmani M, Todorovska M (2015) Structural health monitoring of a 54-story steel frame building using wave method and earthquake records. *Earthq Spectra* 31(1):501–525. <https://doi.org/10.1193/112912EQS339M>
7. Rahmani M, Todorovska MI (2014) 1D system identification of a 54-story steel frame building by seismic interferometry. *Earthq Eng Struct Dynam* 43(4):627–640. <https://doi.org/10.1002/eqe.2364>
8. Safak E, Çelebi M (1991) Recorded seismic response of Transamerica building, II: system identification. *J Struct Eng* 117(8):2405–2425. [https://doi.org/10.1061/\(ASCE\)0733-9445\(1991\)117:8\(2405\)](https://doi.org/10.1061/(ASCE)0733-9445(1991)117:8(2405))
9. Safak E, Çelebi M (1992) Recorded seismic response of Pacific Park Plaza, II: system identification. *J Struct Eng* 118(6):1566–1589. [https://doi.org/10.1061/\(ASCE\)0733-9445\(1992\)118:6\(1566\)](https://doi.org/10.1061/(ASCE)0733-9445(1992)118:6(1566))
10. Jennings PC (1997) Use of strong-motion data in earthquake resistant design. In: Proceedings of SMIP97 seminar on utilization of strong-motion data. California Strong Motion Instrumentation Program. Division of Mines and Geology, California Department of Conservation, Sacramento, CA, pp 1–8
11. Çelebi M, Safak E (1991) Recorded seismic response of Transamerica building, I: data and preliminary analysis. *J Struct Eng* 117(8):2389–2404. [https://doi.org/10.1061/\(ASCE\)0733-9445\(1991\)117:8\(2389\)](https://doi.org/10.1061/(ASCE)0733-9445(1991)117:8(2389))
12. Çelebi M, Safak E (1992) Seismic response of Pacific Park Plaza, I: data and preliminary analysis. *J Struct Eng* 118(6):1547–1565. [https://doi.org/10.1061/\(ASCE\)0733-9445\(1992\)118:6\(1547\)](https://doi.org/10.1061/(ASCE)0733-9445(1992)118:6(1547))
13. Çelebi M, Bongiovanni G, Safak E, Brady G (1989) Seismic response of a large-span roof diaphragm. *Earthq Spectra* 5(2):337–350. <https://doi.org/10.1193/1.1585525>
14. Çelebi M, Sereci M, Boroschek R, Carreno R, Bonelli P (2013) Identifying the dynamic characteristics of a dual core-wall and frame building in Chile using aftershocks of the 27 February 2010 (Mw = 8.8) Maule (Chile) earthquake. *Earthq Spectra* 29(4):1233–1254. <https://doi.org/10.1193/011812EQS012M>
15. Çelebi M, Huang M, Shakal A, Hooper J, Klemencic R (2013) Ambient response of a unique performance-based design tall building with dynamic response modification features. *Struct Des Tall Spec Build* 22:816–829. <https://doi.org/10.1002/tal.1093>
16. Çelebi M, Toksöz N, Büyüköztürk O (2014) Rocking behavior of an instrumented unique building on the MIT campus identified from ambient shaking data. *Earthq Spectra* 30(2):705–720. <https://doi.org/10.1193/032112EQS102M>
17. Çelebi M, Okawa I, Kashima T, Koyama S, Iiba M (2014) Response of a tall building far from the epicenter of the March 11 2011 M9.0 Great East Japan earthquake and aftershocks. *Struct Des Tall Spec Build* 23:427–441. <https://doi.org/10.1002/tal.1047>

18. Çelebi M, Kashima T, Ghahari F, Abazarsa F, Taciroglu E (2016) Responses of a tall building with U.S. code-type instrumentation in Tokyo, Japan—to events before, during, and after the Tohoku earthquake of 11 March 2011. *Earthq Spectra* 32(1):497–522. <https://doi.org/10.1193/052114EQS071M>
19. Çelebi M, Hisada Y, Omrani R, Ghahari F, Taciroglu E (2016) Responses of two tall buildings in Tokyo, Japan, before, during, and after the M9.0 Tohoku earthquake of 11 March 2011. *Earthq Spectra* 32(1):463–495. <https://doi.org/10.1193/092713EQS260M>
20. Çelebi M, Ulusoy HS, Nakata N (2016) Responses of a tall building in Los Angeles, California as inferred from local and distant earthquakes. *Earthq Spectra* 32(3):1821–1843. <https://doi.org/10.1193/050515EQS065M>
21. Çelebi M, Hooper J, Klemencic R (2017) Study of responses of 64-story Rincon building to Napa, Fremont, Piedmont, San Ramon earthquakes and ambient motions. *Earthq Spectra* 33(3):1125–1148. <https://doi.org/10.1193/031616EQS041M>
22. Çelebi M, Kashima T, Ghahari SF, Koyama S, Taciroglu E, Okawa I (2017) Before and after retrofit behavior and performance of a 55-story tall building inferred from distant earthquake and ambient vibration data. *Earthq Spectra* 33(4):1599–1626. <https://doi.org/10.1193/122216EQS249M>
23. Çelebi M (1993) Seismic response of an eccentrically braced tall building. *J Struct Eng* 119(4):1188–1205. [https://doi.org/10.1061/\(ASCE\)0733-9445\(1993\)119:4\(1188\)](https://doi.org/10.1061/(ASCE)0733-9445(1993)119:4(1188))
24. Çelebi M (1993) Seismic response of two adjacent buildings with downhole and free-field recordings, I: data and analysis. *J Struct Eng* 119(8):2461–2476. [https://doi.org/10.1061/\(ASCE\)0733-9445\(1993\)119:8\(2461\)](https://doi.org/10.1061/(ASCE)0733-9445(1993)119:8(2461))
25. Çelebi M (1993) Seismic response of two adjacent buildings with downhole and free-field recordings, II: interaction. *J Struct Eng* 119(8):2477–2492. [https://doi.org/10.1061/\(ASCE\)0733-9445\(1993\)119:8\(2477\)](https://doi.org/10.1061/(ASCE)0733-9445(1993)119:8(2477))
26. Çelebi M (1997) Response of Olive View Hospital to Northridge and Whittier earthquakes. *J Struct Eng* 123(4):389–396. [https://doi.org/10.1061/\(ASCE\)0733-9445\(1997\)123:4\(389\)](https://doi.org/10.1061/(ASCE)0733-9445(1997)123:4(389))
27. Çelebi M (1998) GPS and/or strong and weak motion structural response measurements—case studies. In: *Proceedings of structural engineers world congress, CD-ROM, San Francisco, CA, 19–23 July 1998*
28. Çelebi M (1998) Performance of building structures—a summary. In: Çelebi M (ed) *The Loma Prieta, California, earthquake of October 17, 1989—building structures*. U.S. geological survey professional paper 1552–C, c5–c76. <https://pubs.usgs.gov/pp/pp1552/pp1552c/>
29. Çelebi M (2004) Structural monitoring arrays—past, present and future. In: Gulkan P, Anderson J (eds) *Future directions in strong motion instrumentation*. Proceedings of NATO SFP workshop on future directions on strong motion and engineering seismology, Kusadasi, Izmir, Turkey, 17–21 May 2004, NATO science series IV, earth and environmental sciences, vol 58. Kluwer Academic Publishers, pp 157–179
30. Çelebi M (2004) Responses of a 14-story Anchorage, Alaska, building to two close earthquakes and two distant Denali fault earthquakes. *Earthq Spectra* 20(3):693–706. <https://doi.org/10.1193/1.1779291>
31. Çelebi M (2006) Recorded earthquake responses from the integrated seismic monitoring network of the Atwood building, Anchorage, Alaska. *Earthq Spectra* 22(4):847–864. <https://doi.org/10.1193/1.2359702>
32. Çelebi M (2011) Seismic monitoring of structures and new developments. Invited keynote lecture paper. In: *Proceedings of 2011 experimental vibration analyses of civil engineering structures, Varenna, Italy, 3–5 Oct 2011*, pp 15–36
33. Çelebi M (2013) Modern structural monitoring arrays and needs: GPS and other developments, chapter 6. In: Bull JW (ed) *Tall buildings: design advances for construction*. Computational science, engineering and technology series 33. Saxe-Coburn Publications, pp 143–182
34. Çelebi M (2013) Seismic monitoring of structures and new developments, chapter 2. In: Garevski M (ed) *Earthquakes and health monitoring of civil structures*. Springer environmental science and engineering, pp 37–84

35. Rodgers J, Çelebi M (2006) Seismic response and damage detection analyses of an instrumented steel moment-framed building. *J Struct Eng* 132(10):1543–1552. [https://doi.org/10.1061/\(ASCE\)0733-9445\(2006\)132:10\(1543\)](https://doi.org/10.1061/(ASCE)0733-9445(2006)132:10(1543))
36. City and County of San Francisco (2001) Building Occupancy Resumption Program (BORP). City and County of San Francisco, Department of Building Inspection, Emergency Operation Plan (Rev. 2001)
37. Çelebi M, Sanli A (2002) GPS in pioneering dynamic monitoring of long-period structures. *Earthq Spectra* 18(1):47–61. <https://doi.org/10.1193/1.1461375>
38. Çelebi M, Sanli A, Sinclair M, Gallant S, Radulescu D (2004) Real-time seismic monitoring needs of a building owner—and the solution: a cooperative effort. *Earthq Spectra* 20(2):333–346. <https://doi.org/10.1193/1.1735987>
39. Panagitou M, Restrepo JI, Conte JP, Englekirk RE (2006) Seismic response of reinforced concrete wall buildings. In: Proceedings of 8th national conference on earthquake engineering, San Francisco, CA, 18–22 Apr 2006, paper 1494
40. Jerri A (1979) Correction to “The Shannon sampling theorem—its various extensions and applications: a tutorial review”. *Proc IEEE* 67(4):695. <https://doi.org/10.1109/proc.1979.11307>
41. Çelebi M (2008) Real-time monitoring of drift for occupancy resumption. In: Proceedings of 14th world conference on earthquake engineering, Beijing, China, 13–17 Oct 2008 (CD-ROM)
42. Applied Technology Council (1997) NEHRP commentary on the guidelines for the seismic rehabilitation of buildings. Federal Emergency Management Agency FEMA-274, Washington, DC
43. Applied Technology Council (1997) NEHRP guidelines for the seismic rehabilitation of buildings. Federal Emergency Management Agency FEMA-273, Washington, DC
44. Porter KA, Beck JL, Ching JY, Mirani-Reiser J, Miyamura M, Kusaka A, Kudo T, Ikkatai K, Hyoda Y (2004) Real-time loss estimation for instrumented buildings. Caltech EERL report 2004-08. <https://authors.library.caltech.edu/26545/>
45. Porter K, Mitrani-Reiser J, Beck JL, Ching J (2006) Smarter structures: real-time loss estimation for instrumented buildings. In: Proceedings of 8th national conference on earthquake engineering, San Francisco, CA, 18–22 Apr 2006, paper 1236
46. Hyzak M, Leach M, Duff K (1997) Practical application of GPS to bridge deformation monitoring. In: Proceedings of permanent committee meeting and symposium international federation of surveyors, May 1997
47. Teague EH, How JP, Lawson LG, Parkinson BW (1995) GPS as a structural deformation sensor. In: Proceedings of American institute of aeronautics and astronautics guidance, navigation, and control conference, Baltimore, MD, Aug 1995
48. Guo J, Ge S (1997) Research on displacement and frequency of tall buildings under wind loading using GPS. In: Proceedings of institute of navigation conference, Kansas City, MO, Sept 1997
49. Kondo H, Cannon ME (1995) Real-time landslide detection system using precise carrier phase GPS. In: Proceedings of institute of navigation conference, Palm Springs, CA, Sept 1995
50. Lovse JW, Teskey WF, Lachapelle G, Cannon ME (1995) Dynamic deformation monitoring of a tall structure using GPS technology. *J Surv Eng* 121(1):35–40. [https://doi.org/10.1061/\(ASCE\)0733-9453\(1995\)121:1\(35\)](https://doi.org/10.1061/(ASCE)0733-9453(1995)121:1(35))
51. Hudnut KW, Behr J (1998) A continuous GPS monitoring of structural deformation at Pacoima Dam, California. *Seismol Res Lett* 69(4):299–308. <https://doi.org/10.1785/gssrl.69.4.299>
52. Behr JA, Hudnut K, King N (1998) Monitoring structural deformation at Pacoima Dam, California using continuous GPS. In: Proceedings of 11th international technical meeting of the satellite division of the Institute of Navigation [ION GPS-98; Nashville, TN], pp 59–68
53. Stein RS, Hudnut KW, Satalich J, Hodgkinson KM (1997) Monitoring seismic damage to bridges and highways with GPS: insights from the 1994 Northridge earthquake. In: Proceedings of national seismic conference on bridges and highways. Federal Highway Administration and California Department of Transportation, Sacramento, CA, pp 347–360
54. Roberts GW, Dodson AH, Ashkenazi V (1999) Twist & deflect: monitoring motion of the Humber Bridge. *GPS World* 10(10):24–34

55. Nakamura S (2000) GPS measurement of wind-induced suspension bridge girder displacements. *J Struct Eng* 126(1):1413–1419. [https://doi.org/10.1061/\(ASCE\)0733-9445\(2000\)126:12\(1413\)](https://doi.org/10.1061/(ASCE)0733-9445(2000)126:12(1413))
56. Toriumi R, Katsuchi H, Furuya N (2000) A study on spatial correlation of natural wind. *J Wind Eng Ind Aerodyn* 87(2–3):203–216
57. Çelebi M, Prescott W, Stein R, Hudnut K, Behr J, Wilson S (1999) GPS monitoring of dynamic behavior of long-period structures. *Earthq Spectra (J EERI)* 15(1):55–66. <https://doi.org/10.1193/1.1586028>
58. Tamura Y, Matsui M, Pagnin L-C, Yoshida A (2001) Measurement of wind-induced response of buildings using RTK-GPS. In: Proceedings of 5th Asia-Pacific conference on wind engineering, Kyoto, Japan, 21–24 Oct 2001
59. Bendat JS, Piersol AG (2011) *Random data: analysis and measurement procedures*, vol 729. Wiley
60. Los Angeles Tall Buildings Structural Design Council (2017) An alternative procedure for seismic analysis and design of tall buildings in the Los Angeles region—a consensus document. Los Angeles Tall Buildings Structural Design Council. http://www.tallbuildings.org/PDFFiles/2017-LATBSDC-CRITERIA_Final_w_2018_%20Supplements_FINAL_20180320.pdf
61. Safak E (1999) Wave-propagation formulation of seismic response of multistory buildings. *J Struct Eng* 125(4):426–437. [https://doi.org/10.1061/\(ASCE\)0733-9445\(1999\)125:4\(426\)](https://doi.org/10.1061/(ASCE)0733-9445(1999)125:4(426))
62. Abdelrazaq A (2012) Validating the structural behavior and response of Burj Khalifa: synopsis of the full scale structural health monitoring programs. *Int J High-Rise Build* 1:37–51
63. Kijewski-Correa T, Kareem A (2004) The height of precision: new perspectives in structural monitoring. In: Proceedings of 9th biennial conference on engineering, construction and operations challenging environments, Houston, TX, 7–10 Mar 2004. [https://doi.org/10.1061/40722\(153\)28](https://doi.org/10.1061/40722(153)28)
64. Williams S, Bentz A, Kijewski-Correa T (2013) A typology-driven damping model (TD²M) to enhance the prediction of tall building dynamic properties using full-scale wind-induced response data. In: Proceedings of 12th Americas conference on wind engineering, Seattle, WA, 16–20 June 2013
65. Ciudad-Real M, Skolnik D, Swanson D, Bishop E (2017) Earthquake business continuity for United Arab Emirates buildings using structural health monitoring and performance-based earthquake engineering rapid evaluation. In: Proceedings of 16th world conference on earthquake engineering, Santiago, Chile, 9–13 Jan 2017
66. Kaya Y, Safak E (2014) Real-time analysis and interpretation of continuous data from structural health monitoring (SHM) systems. *Bull Earthq Eng* 13(3):917–934. <https://doi.org/10.1007/s1051>
67. Hisada Y, Yamashita T, Murakami M, Kubo T, Arata T, Shindo J, Aizawa K (2012) Seismic response and damage of high-rise buildings in Tokyo, Japan, during the 2011 Tohoku earthquake. In: Proceedings of 15th world conference on earthquake engineering, Lisbon, Portugal, 24–28 Sept 2012
68. Kubo T, Hisada Y, Murakami M, Kosuge F, Hamano K (2011) Application of an earthquake early warning system and a real-time strong motion monitoring system in emergency response in a high-rise building. *Soil Dynam Earthq Eng* 31(2):231–239. <https://doi.org/10.1016/j.soildyn.2010.07.009>
69. The Building Center of Japan (2001) Time-history response analysis of building performance evaluation. The Building Center of Japan, Technical Appraisal Department, Structural Safety Section Report BR KO-02-01, adopted June 1, 2000, amended April 25, 2001
70. The Building Center of Japan (2001) Manual for time history response analysis of building performance evaluation. Technical Appraisal Department, Structural Safety Section Report BR KO-02-01, adopted June 1, 2000, amended April 25, 2001

Chapter 2

Seismic Structural Health Monitoring of Bridges in British Columbia, Canada



Yavuz Kaya and Carlos Ventura

Abstract This paper presents a province-wide seismic monitoring network: the British Columbia Smart Infrastructure Monitoring System (BCSIMS), which encompasses a comprehensive Structural Health Monitoring (SHM) system and a Strong Motion Network (SMN). The SHM network currently involves 14 bridges, 1 tunnel, 1 building and 11 public schools. Real-time readings from these sensors are automatically analyzed: the results are then permanently stored on a data center and can be viewed in the BCSIMS website (www.bcsims.ca). The SHM system then continuously keeps track of the changes in the dynamic characteristics of these structures to detect and locate damage and to make fast decisions on the safety level of structures and the actions that need to be taken. The real-time data analysis includes drift analysis, modal identification, and the calculation of the important statistics of each data channel. Finite element model updating, the damage detection, and structural event reports are other important features that have been developed and implemented in the SHM network. The objective of the SHM network is to provide the British Columbia Ministry of Transportation and Infrastructure with the performance of these structures immediately following a significant event such as strong earthquake or wind. Such information is then used to assess the safety level of these structures and also to help and support the inspection and maintenance program. The entire system has now been automated and tested and validated by an earthquake occurred on December 29th, 2015 in Sidney Island, BC. The SHM system successfully responded to the earthquake and provided the required information to make immediate decisions and expedite to the emergency.

Keywords Structural Health Monitoring · Real-time data analysis · Instrumentation · Emergency response · Damage detection

Y. Kaya (✉)

British Columbia Ministry of Transportation and Infrastructure, 310-1500
Woolridge Street, V3K0B8 Coquitlam, Canada
e-mail: Yavuz.Kaya@gov.bc.ca

C. Ventura

Department of Civil Engineering, University of British Columbia, Vancouver,
Canada

© Springer Nature Switzerland AG 2019

M. P. Limongelli and M. Çelebi (eds.), *Seismic Structural Health Monitoring*, Springer
Tracts in Civil Engineering, https://doi.org/10.1007/978-3-030-13976-6_2

2.1 Introduction

The southwest coast of British Columbia (BC) is located over an active Cascadia Subduction zone, which can produce large earthquakes up to magnitude 9.0 [1, 2]. Strain has been accumulating in the subduction boundary, off the west coast of Vancouver Island [3, 4]. Although Vancouver has not yet experienced a large damaging earthquake, the paleo seismic evidence on the Fraser delta confirms that large earthquakes have occurred in prehistoric time [3]. Such seismic activity, as a result, poses a hazard to the area and the risk to the infrastructure structures built in the area.

To help mitigate this risk, the BC Ministry of Transportation and Infrastructure (MOTI) together with the Geological Survey of Canada (GSC) have maintained an urban strong motion network of over 170 acceleration sensors for more than 15 years. These instruments have been deployed across BC to monitor and report the seismic activity in the region. One of these reports include the generation of shake-maps immediately after a significant seismic event. The MOTI is responsible for 400 km of provincial disaster response routes and maintains over 2500 bridges in BC, some of which are located in the highest seismic zones in BC and are vulnerable to extensive damage in even a moderate quake and to potential collapse in a major earthquake. The automatically generated shake-maps can be used to identify the level of shaking experienced by MOTI's bridges and facilities located in the region affected by the earthquake that are most susceptible to seismic shaking. This process in turn help the decision-makers to effectively implement a risk management program. Fast and accurate field intelligence immediately following an earthquake can ensure the most effective deployment of vital services and mitigate damage to the built environment [5].

In a collaborative effort with the University of British Columbia (UBC), the MOTI has been installing seismic SHM system on bridges and tunnels since early 1990s. The primary purpose of these SHM systems is to monitor the ground motion input and its effect on structures during strong shaking. The MOTI and UBC started a program called the British Columbia Smart Infrastructure Monitoring System (BCSIMS), which integrates data from the instrumented structures (currently 27 in total) and the strong motion network. The BCSIMS program also incorporates a comprehensive structural health monitoring (SHM) system, which processes structural vibration data and delivers results and related reports in real-time to predefined recipients such as bridge inspectors at the MOTI. Consequently, the system is also able to provide immediate notifications after an earthquake event. The goals of the system are: (i) to provide a real-time seismic structural response system to enable rapid deployment and prioritized inspections of the MOTI's bridges and tunnels; (ii) to develop and implement a structural health monitoring program to address the need for safe and cost-effective operation of structures in BC; and (iii) to provide a real-time working platform (www.bcsims.ca) that can integrate many aspects of seismicity in BC [5].

It is very common to see a great number of slight-to-moderately damaged bridges, along with the heavily damaged or undamaged structures following a significant

earthquake. To decide if the damaged structural and if it is safe to use the bridge following an earthquake, a time consuming detailed inspection is required. The SHM systems in the BCSIMS network provide the means to help make such decisions faster, and with more confidence. In other words, the implementation of the BCSIMS has transformed the current practice of inspecting and evaluating all structures after an earthquake to a more rational and practical one that makes effective use of state-of-the-art sensing technology.

2.2 BCSIMS Architecture

The development of the BCSIMS architecture has been a collaborative process between the UBC and MoT that started in early 2009. Figure 2.1 shows an overview of the BCSIMS architecture, and it consists of several sub-systems: hardware and software, data acquisition system, data storage and processing tools, network communications, etc. In general, the BCSIMS network involves two main components: the SMN and the seismic SHM network. They are discussed in detail in the following subsections.

Recorded data from each structure (e.g., bridge, school, dam, tunnel, etc.) is synchronized via Internet in near real-time with the BCSIMS servers, and it is continuously stored on a ring-buffer memory in data repository, which is connected to the Internet. All communication between BCSIMS servers and data repository is over local area network; therefore, the connection lost between servers are minimized due to earthquake. Data recorders located at each structure can store at least one week of

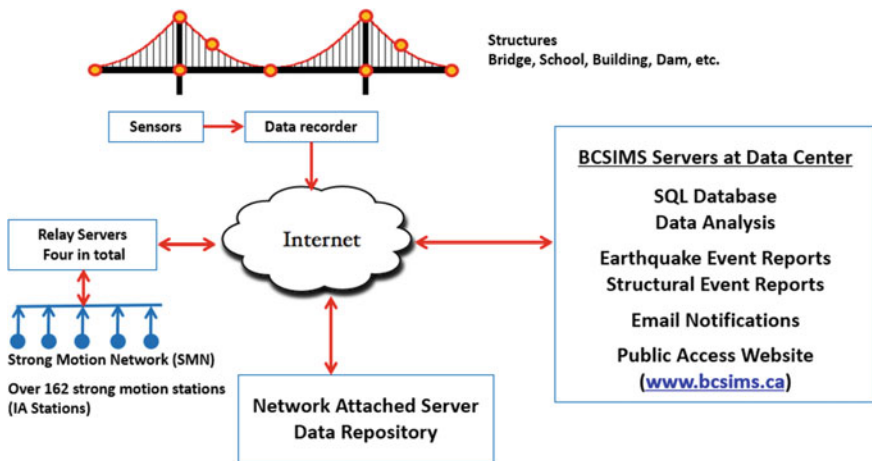


Fig. 2.1 The components of the BCSIMS: servers, hardware and software, data acquisition system, data storage and processing tools, and network communications

data on-site; therefore, this data can be retrieved manually in case of connection lost between BCSIMS servers and data recorder after a significant earthquake.

2.2.1 Strong Motion Network

BCSIMS is a comprehensive seismic monitoring system that involves two sub-networks: Strong Motion Network and Structural Health Monitoring Network. Figure 2.2 shows a screen shot of the most recent version of the homepage of the BCSIMS website (www.bcsims.ca). It includes major fault lines around BC and several structural layers such as bridges, schools, and tunnels. The SMN consists of approximately 170 Internet Accelerometers (IA) stations [6]. The IA stations are designed to detect and measure an earthquake and analyze these data in real-time to calculate important strong motion parameters such as the Peak Ground Acceleration (PGA), Peak Ground Velocity (PGV), Peak Ground Displacement (PGD) and various spectral intensity scales such as Katayama's Spectral Intensity (kSI) [7]. Those parameters along with the recorded earthquake data of each triggered IA sensor are immediately sent to BCSIMS data center in the form of several string messages immediately after the earthquake shaking is over.

Registry of an earthquake metadata (e.g. magnitude, location, hypo-central depth, event date and time, etc.) in BCSIMS is done through an online feed from the United States Geological Survey (USGS). An immediate earthquake notification is sent out

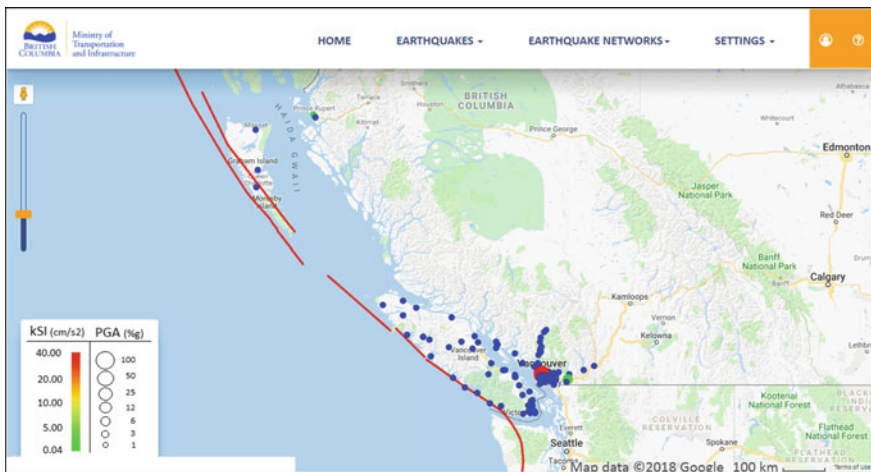


Fig. 2.2 The IA stations (blue circles) are connected to the BCSIMS network in real-time. The size and color of the circles change in real-time based on the reported PGA and kSI values at that SM station. The size of the circle indicates the maximum measured PGA, and the color depicts the maximum calculated kSI value. This feature allows the user to immediately assess the shaking intensity in real-time across the region (www.bcsims.ca) (Color figure online)

by e-mail to a predefined list of recipients, and additional data about the earthquake is made available on the webpage. A service installed on a server in the data center continuously compares the date and time information of the registered earthquakes to that of the string messages received from earthquake sensors. Shake-maps will be created and posted on the website for every earthquake if the following three criteria are met (1) the epicenter of the earthquake is less than 200 km from the nearest IA earthquake station; (2) the magnitude of the earthquake is bigger than 3; and (3) at least one IA station is triggered. An application developed in Matlab automatically produces these shake-maps for urban and regional scale. PGA is determined using the peak horizontal accelerations recorded at each IA station, and peak vertical recordings are not used because they are on average lower than the horizontal amplitudes. Ground Motion Prediction Equations (GMPE) [8–10] are used in order to estimate the PGA in between triggered IA stations.

Shake-maps are immediately posted on the BCSIMS website and can be viewed with many superimposed layers such as bridges, buildings or schools, and they are used by many organizations such as federal, provincial, and local, both public and private, for post-earthquake response and recovery as well as for preparedness exercises and disaster planning. This enables emergency responders and maintenance personnel to quickly assess the shaking intensity across the urban areas and at the location of critical infrastructure. It also allows these agencies to prioritize and maximize the effective use of their scarce resources available.

A recent seismic event in BC is used as an illustration of how the SHM network performs. An earthquake with a magnitude of 4.79 (USGS) occurred near Sidney Island in BC (48.6038 latitude and -123.3068 longitude) on Wednesday December 30th, 2015 at 07:39 A.M. UTC. Fifty strong motion stations were triggered due to this shaking, and the earthquake was felt across the Lower Mainland of BC. The locations of the triggered stations are depicted in Fig. 2.3, and the maximum horizontal acceleration of 0.04 g was recorded at the Brentwood Bay station on Vancouver Island, which is 11.47 km away from the epicenter of the earthquake. Since the magnitude of this earthquake was bigger than 3, more than one internet accelerometer (IA) station was triggered, and the epicenter of the earthquake was less than 200 km from the nearest IA station, the BCSIMS system automatically registered this earthquake on the server, and a shake-map was generated automatically (Fig. 2.3). The entire process was completed within 5 min following the earthquake, and no human interaction was needed.

An earthquake report is automatically generated and e-mailed to predefined list of subscribers such as bridge inspection engineers and bridge area managers of the MOTI. This report is immediately made available on the BCSIMS website, and it includes the following (1) the metadata of the earthquake (e.g., location, magnitude, depth); (2) the snapshot of the earthquake area affected with shake-map and the bridge layer superimposed; (3) tables to show the expected PGA at the location of each structure and their comparison with various seismic hazard values; and (4) list of strong motion stations that are triggered by that earthquake and peak responses. The earthquake data from triggered IA stations is automatically analyzed, and the results are also included in this report [11].

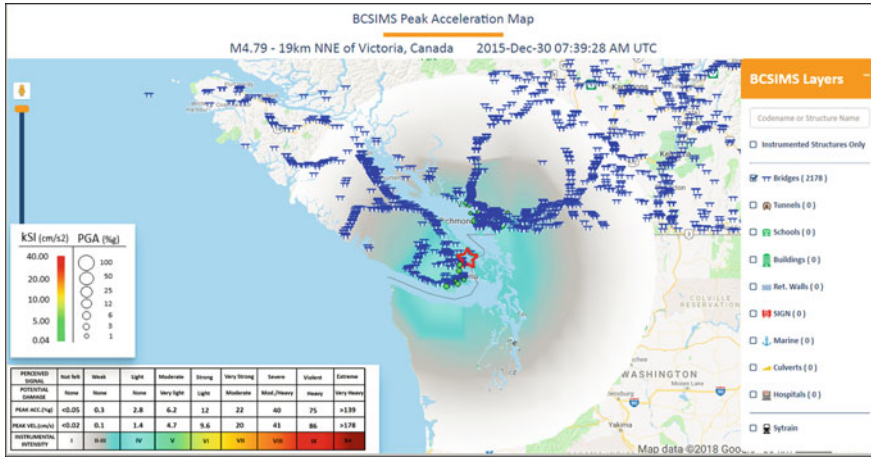


Fig. 2.3 Calculated shake-map for the M_w 4.79 earthquake that occurred near Sidney Island in BC, Canada. The location of the epicenter is indicated by a red star on the map, and the circles (50 in total) on the map show the locations of the triggered IA stations due that shaking (www.bcsims.ca)

Together with the earthquake report, the shake-maps as shown in Fig. 2.3 provide valuable information (e.g., estimated PGA) at or near the bridges that have no seismic SHM system installed. This information is particularly very important because it provides the MOTI personnel (e.g., bridge inspectors and bridge area managers) with additional immediate information on the shaking intensity experienced by the bridges across the earthquake affected area. The shake-map can be viewed with different superimposed layers such as bridges, schools, tunnels, hospitals, etc. Therefore, these shake-map can also be used by different public and private agencies other than MOTI.

2.2.2 Structural Health Monitoring Network

The practical importance of a seismic SHM system cannot be overstated. It is very common to see a large number of slight-to-moderately damaged bridges, along with the heavily damaged or undamaged structures following a large earthquake. Detailed inspection of these damaged structures takes a lot of time to decide if the damage is structural and if it is safe to use it. This process can result in heavy financial losses for the owners of such structure. The SHM system in the BCSIMS provides the means to help make such decisions faster and with more confidence.

A total of 28 structures (14 bridges, 1 tunnel, 2 building, and 11 public schools) in the BCSIMS network are currently installed with a SHM system, which involve continuous monitoring of the dynamic characteristics of structures by digital instruments

(e.g., accelerometers, displacement transducers, environmental sensors, etc.). Both the data collection and the data analysis are done in real-time for these structures. One of the objectives of the SHM systems on these structures is to keep track of the changes in the dynamic characteristics such as modal properties. These changes are then used to detect and locate possible damage, to make fast decisions on the safety level of structure, and the action that needs to be taken.

Table 2.1 shows a list of the structures that have seismic SHM system installed and are currently being monitored in real-time. The type and the number of the sensor used depend on the dynamic characteristics of the structure as well as the intentions of the SHM system installed. It is capable of remote configuration and can automatically upload data to multiple remote servers via the Internet. The SHM network for bridges in BC is growing very fast: there are currently two bridges that are being installed with SHM system in BC (e.g., Lions Gate Bridge and Pattullo Bridge) and several other new bridges and schools are planned to be added to the SHM network in near future.

The collected data from each of these structures is archived and processed in real-time in the data center. The data processing includes drift analysis, modal identification, and the calculation of the important statistics of each data channel such as mean, root-mean-square (RMS) and standard deviation and so on. Finite element model updating, the damage detection, and structural event reports are other important features that have been developed and implemented in BCSIMS. The results of all of these analyses are permanently stored on servers. The SHM data center was originally located at UBC but has been just transferred to MOTI's infrastructure in Kamloops with a back-up server located in Calgary, Canada. As a physical complement, a control room has been established at UBC (Fig. 2.4), which has been developed as a situation-room with all the necessary skilled human resources and enabling technologies available.

No significant large earthquake has been recorded yet that has triggered any of the SHM systems installed on the bridges in BC. Therefore, the recorded ambient vibration data from the Port Mann Bridge will be used in the following subsections to illustrate the performance of the SHM system.

2.2.2.1 Description of the Port Mann Bridge

With a total length of 2020 m and a width of 65 m (10 traffic lanes), the Port Mann Bridge spans the Fraser River and connects the two cities of Surrey and Coquitlam in BC, Canada. Constructed in 2012, the bridge is divided into three sections: an 850 m-long cable-stay and two approach viaducts of 190 m each. The deck structure consists of steel girders and transverse floor beams, which support precast concrete deck panels. The entire cable stay is also divided into two separate decks, which are connected by median struts, as shown in Fig. 2.5d. In total, there are 288 cables installed to connect two 163 m-tall piers to the deck. Each cable has its own properties that vary from one another. The north and south approach bridges, on the other hand, consist of three concrete box girder sections. On many of the approach piers there are

Table 2.1 List of bridges and tunnels that are instrumented with SHM systems and are currently being monitored in real-time in the BCSIMS network

No	Structure name	Total length (m)	Year instrumented	No of channels	Type of sensor
1	French Creek (FC)	200	1997	12	A
2	George Massey Tunnel (GMT)	660	1996	11	A P
3	Queensborough Bridge (QB)	914	1996	12	A P
4	Ironworkers Memorial Second Narrows Crossing (IMSNC)	1290	2011	122	A S W T
5	Pitt River Bridge (PR)	380	2009	46	A W
6	William R. Bennett Bridge (WRB)	1077	2008	12	A
7	Portage Creek Bridge (PCB)	129	1983	41	A S
8	Port Mann Bridge (PM)	850	2013	336	A W D T H P
9	176th Underpass (176B)	75	2013	26	A T H
10	Gaglardi Way Underpass (GWU)	65	2013	22	A T H
11	Kensington Avenue Underpass (KAU)	75	2013	30	A T H
12	Fraser Heights —Wetlands (FHW)	476	2013	20	A T H
13	BNSP Sunbury Bridge	68	2014	36	A H W D
14	BNSF Viaduct East Mill Access	195	2014	84	A H W D
15	Hwy-17 Deltaport Bridge	133	2014	36	A H W D

Note A, acceleration; P, piezometer; S, strain gauge; W, wind; T, temperature; D, displacement; H, humidity

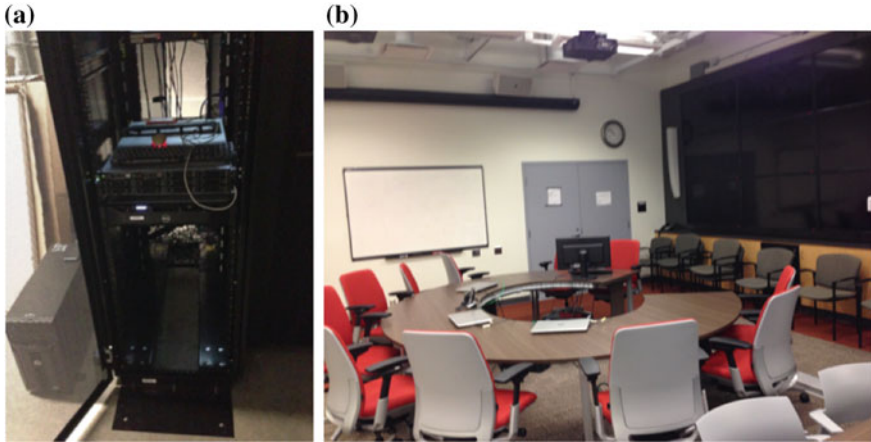


Fig. 2.4 **a** The data processing server at data center, and **b** the situation-room established in the control room at UBC

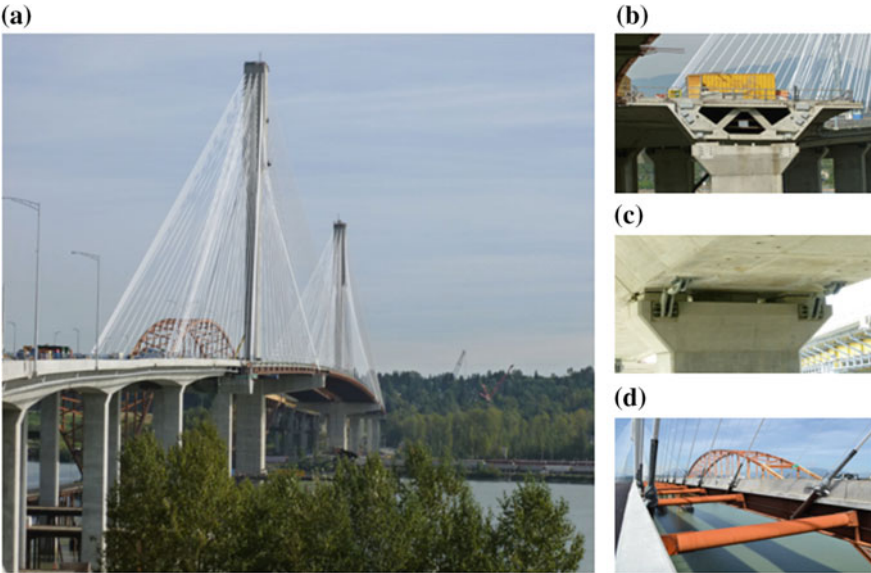


Fig. 2.5 Port Mann Bridge **a** view from North, **b** cross section of approach viaducts, **c** dampers at approach piers, **d** median struts connecting the East and West deck. Photos are taken from Google

viscous dampers installed to prevent excessive longitudinal movement. Foundations for each of the piers consist of steel piles of approximately 100 m with diameters of 1.8 m.

2.2.2.2 Port Mann Bridge Instrumentation

The Port Mann Bridge instrumentation includes a total of 336 measurement channels including displacement transducers at the expansion joints, vibration sensors, and further sensors to record environmental and operational variables. The instrumentation is primarily meant to record structural vibrations under strong motions, and to study the combined effects of the soil and structure interaction. The secondary objective of the instrumentation is to keep track of the modal properties of the bridge (e.g., modal frequency, modal damping ratio and mode shapes) and use them to develop customized damage detection and localization algorithms for the bridge. The instrumentation is distributed across the entire structure, including boreholes, foundations, approach viaducts, and the cable stay.

The cable-supported part of the Port Mann Bridge is instrumented through 34 acceleration sensors (70 channels in different directions), 12 displacement transducers, and 2 weather stations as shown in Fig. 2.6. Weather stations are located at the top of each tower and measure the temperature and humidity, as well as the wind speed and its direction, which sums up to 8 channels per station. The displacement transducers are located at the expansion joints at either side of the cable stay bridge to measure the displacement due to temperature variations, traffic, and external loads. A toll station at the south end of the bridge records both the number and length of vehicles crossing the bridge. This information is used to determine the correlation between calculated modal properties of the bridge (e.g., modal frequency) and the traffic load acting on the bridge deck.

2.2.2.3 SHM Data Archiving

New data archiving and protocols have been developed and implemented in the BCSIMS to be able to integrate the data transmission of different hardware suppliers. This archiving protocol includes the development of new binary file format of Virtual Input Files (VIF), which contains raw data from all of the sensors for each monitored structure. This VIF files are further compressed to minimize the disk space on servers. The default length of VIF files are selected as five minutes because this length currently enables servers to keep up with the post analysis of the data from all of the structures simultaneously. This length can be reduced in the future as more advance technology becomes available. The compressed data is then archived in a ring buffer on the servers in the data center. The length of the ring buffer is scalable based on the available disk space on the servers. The raw data or event data (e.g., earthquake or strong wind) are archived and made available for public and the registered users to download via the BCSIMS website (www.bcsims.ca).

Figure 2.7 includes an archived sample time history record of 5 min long and the corresponding spectrum amplitude calculated for the selected channel #20, which is located at the midspan of the Port Mann Bridge. Spectrum amplitude is based on the Fast Fourier Transform (FFT) of 2 min of data (24,000 data points) with 50% overlap, which results in a 0.0083 Hz in frequency resolution. Spectrum amplitude

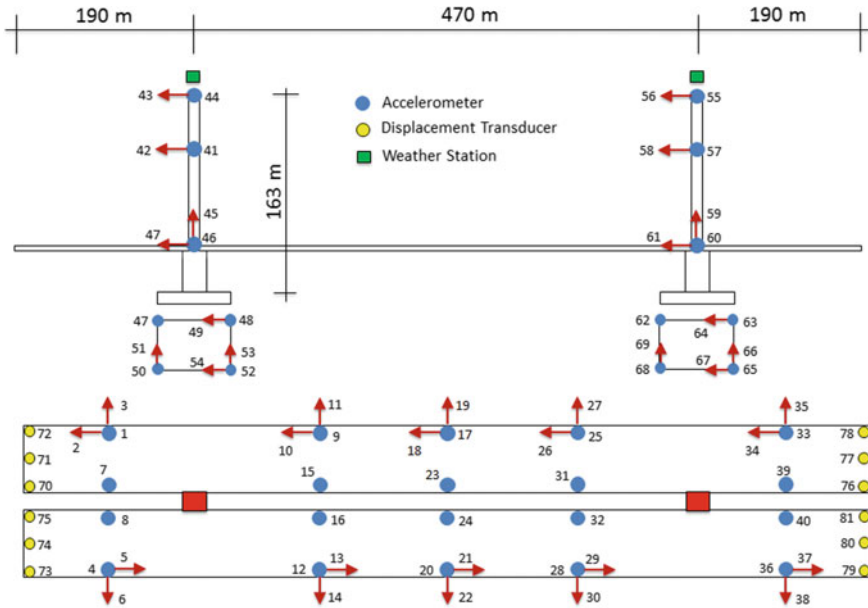


Fig. 2.6 Instrumentation map for Port Mann Bridge (deck, towers and foundation only)

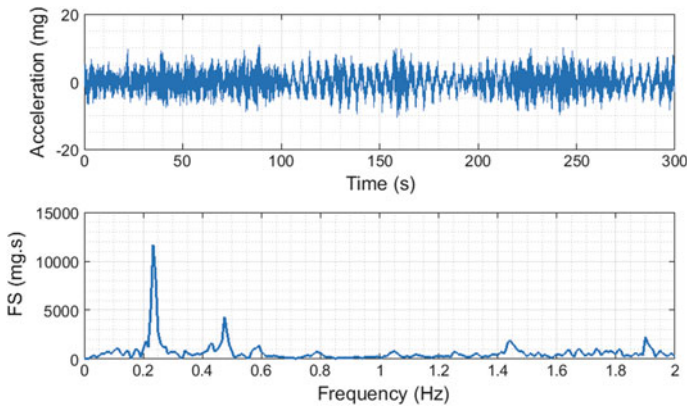


Fig. 2.7 Acceleration time history plot and Fourier Spectrum amplitude of the vertical response from the selected channel #20 located at the mid-span of the Port Mann Bridge (recorded: June 1st, 2018, 04:10 p.m., UTC). The acceleration time history has been base-line corrected

has revealed that the first mode of the bridge (0.233 Hz) dominates the frequency spectrum and is always present in the ambient data; however, higher frequency modes becomes present only when the acceleration amplitudes are higher enough to excite these modes: mainly due to traffic load acting on the bridge or strong wind.

A certain amount of raw data from each structure is permanently stored every day; for example, 75 min of raw data for Port Mann Bridge and 30 min of data for Second Narrows Crossing Bridge. The length of such data is structure specific and determined based on the dynamic characteristics of each structure. They are then used to test the new tools and techniques that are continuously developed as part of the SHM network.

2.2.2.4 Tracking Long Term Statistics

The archived raw data is stored permanently in the data center; however, one of the key requirements in real-time seismic SHM is that recording, processing, and analysis of the data should all be done in real-time. Therefore, the data analysis in the BCSIMS is done in real-time for each measured quantity (e.g., for each channel), including environmental parameters. The seismic SHM system can track slow changes in the characteristics of the structure, such as those due to aging, change of usage, traffic patterns, and other environmental factors (e.g., temperature, wind, rain, etc.). Due to the continuous recording in the SHM, the statistical characteristics of the structural changes and their correlation with the factors that might cause such changes are established using statistical parameters like mean, standard deviation, root-mean-square, etc. These parameters help to better understand the dynamic behaviour of the bridge under different loading conditions, such as seasonal temperature change and daily traffic loads on a bridge, etc. Additionally, many damage detection and localization algorithms require the environmental variables as inputs; therefore, algorithms can be developed and trained to discriminate between normal fluctuation in the system response and structural anomalies, such as damage. This also enables building up a statistical history of the correlation between the dynamic response of the bridge and the environmental factors so that the effect of environment can be adequately accounted for in the recorded data. This information is very helpful to determine whether the identified change in a structural parameter represents damage or not [12, 13].

As an example, Fig. 2.8 shows the time variations of the calculated statistics (e.g., maximum amplitudes and standard deviation) for the selected channel #20, which is located on the mid-span of the Port Mann Bridge and recording the structural vibrations in vertical direction (Fig. 2.6). The calculated statistics are plotted for three months starting from the third week of January 2018 to the end of May 2018. The statistics are calculated at 5 min intervals. The maximum amplitude varies between 0.1 and 3% g while the standard deviation fluctuates between 0.1 and 0.4% g. The SHM system on the Port Mann Bridge automatically calculates the variation of the statistical parameters for each recording channel on the bridge, and they are used to detect abnormal behaviour on the structure. Any calculated statistical parameter that is out of the established boundary limits or pattern would trigger an immediate notification messages being sent to the predefined list of users including the MOTI's bridge engineers.

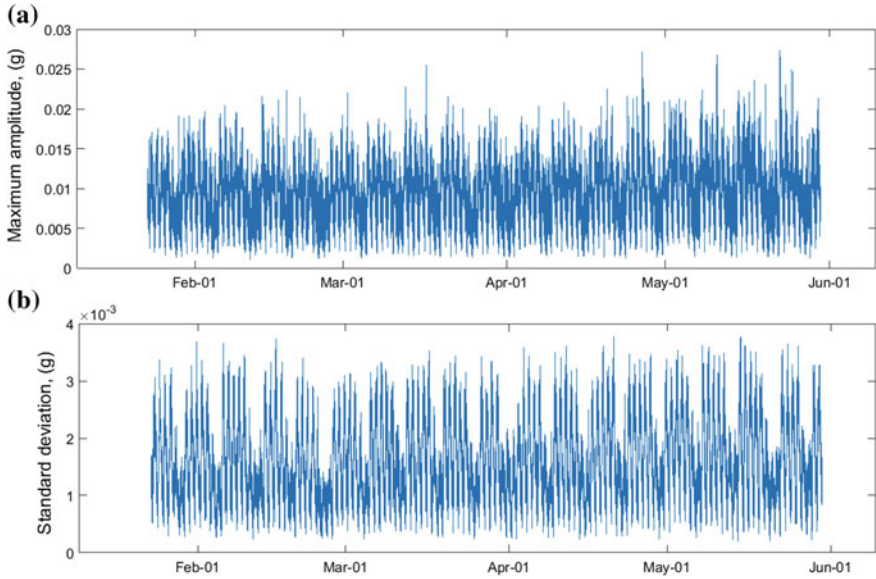


Fig. 2.8 Time variation of statistics parameters for the selected vertical channel #20 on the Port Mann Bridge: recorded for three months from mid January to the end of May in 2018: **a** maximum amplitudes and **b** standard deviation. Statistics are calculated at 5 min intervals

2.2.2.5 Drift Calculation as a Damage Detection Index

One of the decisive control parameters for damage in seismic design is drift, and it is usually controlled in many seismic bridge codes by imposing displacement (or drift) limits on these structural members. Drift is monitored continuously for many structures in the SHM network, and it can be evaluated for bridge piers, bridge towers, or building columns. Drift is defined as the relative displacement of the column top with respect to its base, and it is strongly controlled by the displacement demand. To calculate the drift, the displacements need to be measured or estimated at the top and the base of the column. It is possible to calculate displacements from acceleration data by integrating over the recorded accelerations twice. However, the integration operation on raw data significantly increases the noise amplitudes in the integrated signal and can lead to misleading results [11]. Several tools have been developed in the BCSIMS to minimize such noise increase: the response of a bridge pier at resonant frequency has higher signal-to-noise ratio; therefore, the noise influence during the integration and differentiation is minimal.

The drift pairs for each instrumented structure in the SHM network is defined by engineers and stored on the server. The SHM system then calculates these drifts in real-time from the integrated displacement values. The peak drift values during an event are permanently stored on the server, and any peak drift value exceeding a predefined threshold value may be indicative of possible damage in the structure.

The drift thresholds for each pier have been determined based on the 2014 Canadian Highway Bridge Design Code requirements, and results from detailed nonlinear finite element model analyses. An automated e-mail notification is sent out to a predefined list of users if any of these drift thresholds are exceeded.

2.2.2.6 Tracking Long Term Modal Properties

Dynamic modal properties (e.g., modal frequencies, modal damping ratios, and mode shapes) of the bridges are estimated from output-only data (e.g., recorded bridge ambient vibration data only) and continuously monitored in real-time using the stochastic subspace identification (SSI) method, principal component [14–18, 19]. The method is combined with a hierarchical clustering approach for automated mode selection. The algorithm is semi-automated because two structure-specific parameters must be set a priori (e.g., the minimal distance of adjacent modal frequencies and the number of most dominant modes). The mode tracking is done through an automated mode tracking procedure that compares both frequency and mode shapes [20]. No human interaction is required in this process. The measurement duration (T) for modal identification is structure specific, and it is determined based on both the dynamic characteristics of the structure and the rule of thumb: $T = 1000 \cdot T_1$ where T_1 is the first fundamental period of the structure.

The modal parameters provide very important information about the dynamic characteristics of the structure. As soon as new vibration data from any structure becomes available on the server in the data center, the modal properties of that structure are automatically estimated in near real-time using the SSI method, and the results are permanently stored in the data center. The estimated modal properties of each structure are then incorporated in a control chart, which enables to track them against time (Figs. 2.9 and 2.10). The identified modal properties are further used for finite element model updating and damage detection.

The modal analysis results of the Port Mann Bridge have been validated in comparison to the modal parameters obtained through reference-based field measurements [21]. The fundamental frequency of the bridge varies approximately between 0.225 and 0.245 Hz (4.44 and 4.08 s), and the maximum deviation from the target values does not exceed 0.24% for all considered modes of vibration.

Additionally, the change of modal properties of the structure especially due to environmental conditions can be larger than the change due to the damage; therefore, the effect of environmental conditions on modal properties of structure must be accounted for as they can completely mask the change of modal properties caused by actual damage [12] (Fig. 2.11).

2.2.2.7 Environmental and Operational Variables (EOV)

The environmental and operational variables influence the vibration behavior of bridges significantly [22, 23]. The fundamental frequencies of the Port Mann Bridge

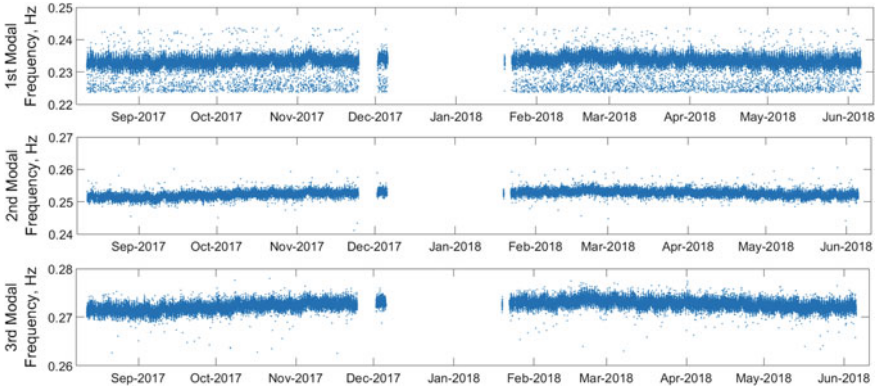


Fig. 2.9 Time variation (control chart) of first three modal frequencies of the Port Mann Bridge between October 2017 and June 2017

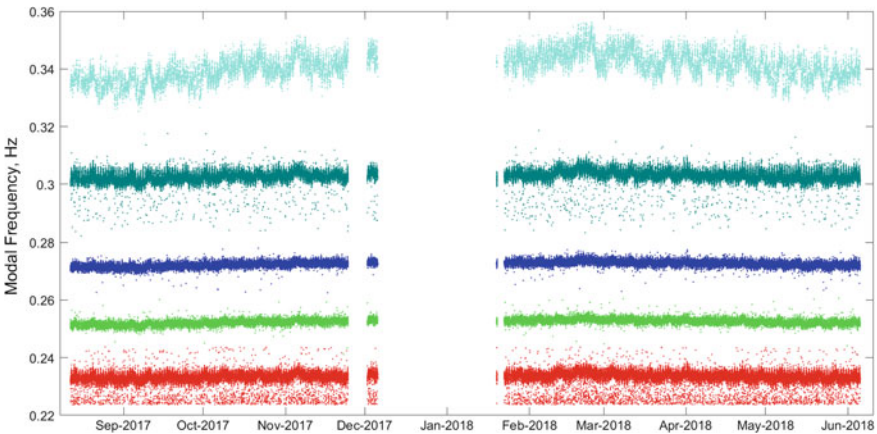


Fig. 2.10 Time variation (control chart) of modal frequencies of the Port Mann Bridge between October 2017 and June 2017

are not particularly sensitive to anomalies in the system response, which is due to the large wave lengths of the corresponding modes of vibration. However, they can be used to show the correlation of the dynamic behaviour and EOVs such as the ambient temperature and mean vibration level. It is observed that the fifth natural mode of the main span is the most sensitive mode to fluctuations in temperature (Fig. 2.12). Fitting a linear line between temperature and modal frequency revealed that the fifth modal frequency decreased by about 18 MHz when the temperature drops from 32 to -5 °C. A very similar trend can be observed for the average acceleration level. The mean vibration level has shown to be a good indicator for the operational loads Δm on the bridge [24], and increased operational modes appear to result in lower natural frequencies. For Mode 5, load-induced fluctuations amount up to 19 MHz.

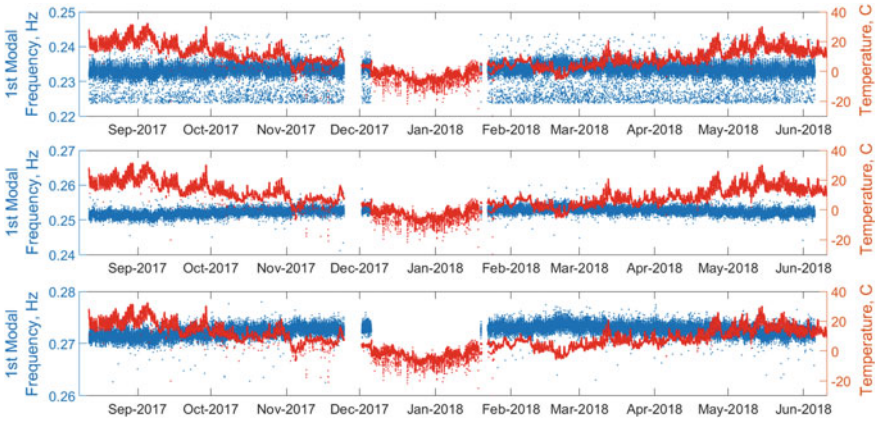


Fig. 2.11 Time variation of first three modal frequencies of the Port Mann Bridge with respect to air temperature between October 2017 and June 2017

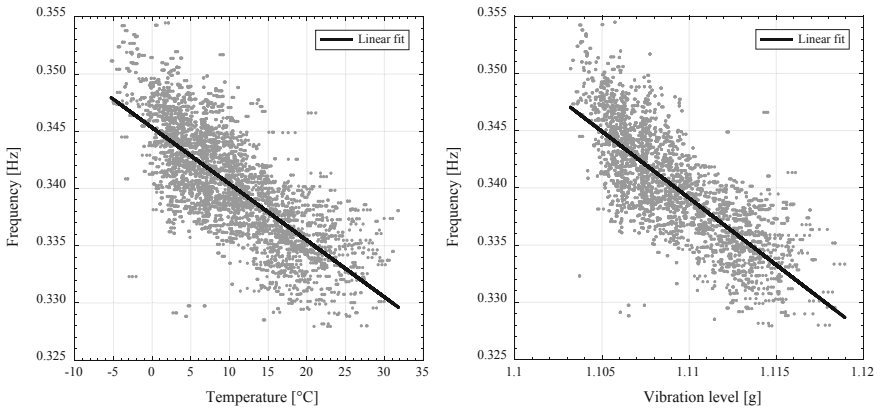


Fig. 2.12 Correlation analysis. Dependency between the fifth natural frequencies and both temperature and mean vibration level

The SHM network has delivered very reliable data for both the vibration behaviour of the bridge and the environmental information. The weather data has been cross-checked with nearby weather stations. The vibration data yields modal parameters that are very close to those estimated from reference-based field measurements. Moreover, the modes of vibration are very consistent over a period of six months. Fluctuation in modal parameters could be attributed to the change in environmental conditions. The traffic volume on the bridge, on the other hand, showed weak correlation with the change in modal frequencies because only the number of vehicles crossing the bridge is recorded on the traffic volume data, and the traffic congestions are misinterpreted, as the largest vehicle loads on the bridge occurs when the traffic

is not moving. To improve the SHM system on the bridge, a bridge weight in motion monitoring system could be considered.

2.2.2.8 SHM Structural Event Reports

As soon as an earthquake with certain characteristics defined in Sect. 2.1 are registered with the BCSIMS network, the SHM network automatically initiates an event recording for each instrumented structure. These recordings are permanently stored on the server and are immediately made available on the BCISMS website for download after the seismic event is over. The event data is then analyzed, and a structural report is generated for each instrumented structure in the SHM network. The entire process takes approximately 10 min after the shaking is over. The structural reports are then e-mailed to a predefined subscribers list and are then published on the website.

This report provides key information on the status of each bridge after an earthquake. One report will be issued for each structure, and it provides bridge inspectors and MOTI engineers with the shaking amplitude at the various locations of the bridge as well as the amplitude of the ground shaking. The calculated structural parameters (e.g., drift ratio of a pier or recorded displacement at bearings) for each structure are automatically compared with user selectable thresholds in the report. Any recorded or calculated structural parameter that exceeds the predefined thresholds is clearly indicated in the report by graphs and figures, and recommendations are also given in the report regarding the actions to be taken. The threshold values are determined in accordance with the code-specified design values or the detailed seismic analysis of the structure. This event report may also be issued for several reasons in addition to seismic events, such as impact, over loading, wind, ship collision with a bridge, or simply for a scheduled health assessment of the structure.

2.3 Conclusion

In collaboration with local, provincial and federal organizations, a comprehensive SHM network has been designed, installed, and maintained since 2009 by UBC for the bridges owned by the BC MOTI, and it is part of a province-wide seismic monitoring system (BCSIMS). The SHM network collects raw vibration data from all instrumented structures and monitors the structural health state of each structure in real-time by evaluating drift values, statistical parameters and modal attributes. The SHM network effectively organizes and processes structural vibration data in an efficient manner and delivers the collected information along with analysis results to the appropriate parties such as bridge engineers in the MOTI.

The SHM data collected from the Port Mann Bridge over the one year has been used in this paper to showcase the SHM tools and methods developed. These tools and techniques have been tested by several small to moderate earthquakes. The

earthquake which occurred on Sidney Island, BC on Wednesday December 30th, 2015 has been used as an example to validate the SHM network and to prove that the SHM network could successfully react to an earthquake as it was designed for and produce required information that the MOTI engineers need to make decisions and respond to the emergencies in an efficient manner. The strong motion event report and the structural event report provide the MOTI and other public and government agencies with additional level information so that they can manage their emergency response resources effectively in the event of an earthquake.

References

1. Rogers GC (1998) Earthquakes and earthquake hazard in the Vancouver area; in geology and natural hazards of the Fraser River delta British Columbia geological survey of Canada. *Geol Surv Can Bull* 525:17–25
2. Goldfinger C, Nelson CH, Morey AE, Johnson JE, Patton JR, Karabanov E, Getierrez-Pastor J, Eriksson AT, Eulalia G, Dunhills G, Enkins R, Dallimore A, Vallier T (2012) Turbidite event history: methods and implications for holocene paleoseismicity of the Cascadia subduction zone, United States Geological Survey Professional Paper
3. Clague JJ, Naesgaard E, Sy A (1992) Liquefaction features on the Fraser delta: evidence for prehistoric earthquakes. *Can J Earth Sci* 29:1734–1745
4. Gragert H, Hyndman RD, Rogers GC, Wank K (1994) Current deformation and the width of the seismogenic zone of the northern Cascadia subduction thrust. *J Geophys Res* 99:653–668
5. Kaya Y, Ventura C, Huffman S, Turek M (2017) British Columbia smart infrastructure monitoring system. *Can J Civil Eng* 44(8):579–588
6. Rosenberger A, Beverley K, Rogers G (2004) The new strong motion seismic network in southern British Columbia, Canada. In: 13th world conference on earthquake engineering Vancouver, B.C., Canada. Paper No. 3373
7. Katayama T, Sato N, Saito K (1998) SI-sensor for the identification of destructive ground motion. In: Proceedings of the ninth world conference of earthquake engineering, vol VII, Tokyo-Kyoto, p 667–672
8. Boore DM, Atkinson GM (2008, February) Ground-motion prediction equations for the average horizontal component of PGA, PGV, and 5%-damped PSA at spectral periods between 0.01 s and 10.0 s. *Earthq Spectra* 24(1):99–138
9. Atkinson GM (2005) Ground motions for earthquakes in Southwestern British Columbia and Northwestern Washington: crustal, in-slab, and offshore events. *Bull Seismol Soc Am* 95(3):1027–1044
10. Atkinson GM, Boore DM (2011) Modifications to existing ground-motion prediction equations in light of new data. *Bull Seismol Soc Am* 101(3):1121–1135
11. Kaya Y, Safak E (2014) Real-time analysis and interpretation of continuous data from structural health monitoring (SHM) systems. *Bull of Earthq Eng*. <https://doi.org/10.1007/s10518-014-9642-9>
12. Kaya Y, Turek M, Ventura C (2013) Temperature and traffic load effects on modal frequency for a permanently monitored bridge. In: Conference Proceedings of the society for experimental mechanics series 38. https://doi.org/10.1007/978-1-4614-6519-5_6
13. Peeters B, Roeck GD (2000) One-year monitoring of the Z24-bridge: environmental effects versus damage events. *Earthq Eng Struct Dynam* 30:149–171
14. Overschee PV, Moor BD (2011) Subspace identification for linear systems: theory, implementation and applications. Kluwer Academic Publishers, Dordrecht, Netherlands

15. Overschee PV, Moor BD (1991) Subspace algorithms for the stochastic identification problem. In: Proceedings of the 30th IEEE conference on decision and control, Brighton, UK, pp 1321–1326
16. Peeters B, Roeck GD (1999) Reference-based stochastic subspace identification for output-only modal analysis. *Mech Syst Signal Process* 13(6):855–878
17. Overschee PV, Moor BD (2012) Subspace identification for linear systems: theory-implementation-application. Springer Science & Business Media, Berlin
18. Ventura C, Laverick B, Brinker R, Andersen P (2003) Comparison of dynamic characteristics of two instrumented tall buildings. In: Proceedings of the XXI international modal analysis conference, Orlando, Florida
19. Ljung L (1999) System identification: theory for the user (2nd edition). Prentice Hall PTR
20. Magalhães F, Cunha Á, Caetano E (2009) Online automatic identification of the modal parameters of a long span arch bridge. *Mech Syst Signal Process* 23(2):316–329
21. McDonald S (2016) Operational modal analysis, model updating, and seismic analysis of a cable-stayed bridge. M.Sc., Department of Civil Engineering, University of British Columbia, Vancouver
22. Cross EJ (2012) On SHM in changing environmental and operational conditions. Ph.D., Faculty of Engineering, University of Sheffield, Sheffield
23. Farrar CR, Doebling SW, Cornwell P, Straser EG (1997) Variability of modal parameters measured on the Alamosa Canyon bridge. In: Proceedings of the XV international modal analysis conference, Orlando, Florida
24. Cross EJ, Koo KY, Brownjohn J, Worden K (2012) Long-term monitoring and data analysis of the Tamar Bridge. *Mech Syst Signal Process* 35(1–2):16–34
25. United States Geological Survey (USGS). <http://earthquake.usgs.gov/earthquakes/feed/v1.0/>
26. MATLAB (2000) Commercial integrating technical computing program. The MathWorks Inc., Natick, MA, USA. www.mathworks.com

Chapter 3

Seismic Structural Health Monitoring of Cultural Heritage Structures



Rosario Ceravolo, Giulia de Lucia, Erica Lenticchia and Gaetano Miraglia

Abstract In the case of heritage buildings, non-invasive techniques are of paramount interest, especially those that can exploit the natural vibration of the structure. Structural Health Monitoring (SHM) can play an important role in the preservation of architectural heritage, especially when it can support a rapid and reliable assessment of structural damage and degradation. More specifically, vibration-based monitoring may help to predict the dynamic response of a structure during seismic events, as well as the damage mechanisms activated by ground motions. This information will in turn allow the selection and development of effective protection strategies. This chapter reports a discussion about the methodological multi-disciplinary approach to SHM, with emphasis on vibration-based SHM techniques, as applied to architectural heritage buildings and structures, along with the description of selected case studies. These examples were chosen in order to cover the various issues connected to design, aims and scopes of the dynamic and seismic SHM, and interpretation of the recorded data.

3.1 Introduction

Historical constructions present a large variety of building technologies, materials, stylistic canons and *rules of art*, which may differ according to the time period and geographical areas. Inspection and diagnosis of structures have been practised for years, and have now established as important tools for the safety assessment of cultural heritage (CH). Indeed, the international deontological guidelines, such as the International Council on Monuments and Sites (ICOMOS) ones [1, 2], define the rehabilitation process of heritage structures similarly to the treatment of a human disease: “the heritage structures require anamnesis, diagnosis, therapy and controls, corresponding respectively to the search for significant data and information, identification of the causes of damage and decay, choice of the remedial measures and

R. Ceravolo (✉) · G. de Lucia · E. Lenticchia · G. Miraglia
Department of Structural, Geotechnical and Building Engineering,
R3 Interdepartmental Centre (R3C), Politecnico di Torino, Corso Duca
Degli Abruzzi 24, 10129 Turin, Italy

control of the efficiency of the interventions”, an operation that calls for a multi-disciplinary approach. In more detail, a CH structure requires a path of knowledge articulated into steps: general identification of the structure and its environment factors; collection of geometric and structural data; identification of the materials and survey of their state of conservation, historical documentation; mechanical characterization of the materials by means of different investigation techniques; soil and foundation analysis, and relevant monitoring activities [3]. The documentation process, in particular, will address aspects such as construction defects, irregularities, deterioration, damage produced by previous seismic events, and in general any factor that makes each of these structures unique and lead to a higher degree of complexity when interpreting the structural behaviour [4]. ICOMOS standards also point to the importance of periodic controls of the construction as the primary tool for preservation.

In the light of the above mentioned concepts, monitoring activities play a fundamental role in both assessment and conservation processes of CH. Indeed, monitoring is not only a method to investigate the past of the structure, but it can have an active role in the conservation of historical buildings and influence decision making [5]. The importance of monitoring is also highlighted by the recent guidelines on the seismic protection of historical buildings, that mention the importance of observation and control of CH buildings. In some recent national codes, the monitoring is described as “a highly desirable practice because it is the main instrument for the conscious conservation” [6].

While realistic evaluations in terms of bearing capacity and ultimate strength normally entail destructive testing, very seldom the extraction of samples is allowed in the case of CH structures. Inspections, by means of endoscopes, thermographs, radar, metal detectors; physical measures, via sonic tomography; or geometric measures by photogrammetry, or other available technologies, can be executed only once or periodically to improve the knowledge level and to reduce the uncertainties. False colour images and spectrometry can reveal the chemical degradation. Unfortunately, all these observations and measures, while increasing the knowledge level, supply only local information.

Modern SHM techniques, that typically apply to the global structural behaviour, try to overcome the limitations of traditional and visual inspections [7], this being especially important when performing a Seismic SHM (SSHM). Whatever the monitoring approach and technique, when conceiving a SHM system, it is necessary to first perform an accurate analysis of the seismic behaviour, in order to capture the most expressive and sensitive parameters [4]. The environmental and operating condition variability must also be taken into account. Vibration-based SHM, which constitutes the main tool for SSHM, has been successfully used for damage detection and quantification in existing structures. Dynamic tests supply information about the whole-body response, and allow to extend to the whole structure the outcomes of the local inspections and measures. In the past, relevant examples of dynamic monitoring included, among others, towers and minarets [7–18], arched structures [19, 20], churches [4, 21–27], or domes and other monumental structures [28–32]. These techniques are particularly appreciated in CH fields because of their usual

non-invasiveness and non-destructiveness, and because provide indirect information about structural integrity. Moreover, the dynamic test setups can be easily installed and removed.

Historical bridges represent a particular example in the SHM of cultural heritage. In fact, they are important not only for their historical and artistic value, but also for their strategical function for the infrastructural system. In fact, in many cases, historical bridges are currently used, even if they are very ancient, or in some cases they become a cultural landmark: such as for the case of many bridges in the U.S.A. An example is the Brooklyn Bridge, that was designated as a National Civil Engineering Landmark by ASCE in 1972, and in that same year, “The Great Bridge: The Epic Story of the Building of the Brooklyn Bridge”, a lengthy account of the construction of the Brooklyn Bridge, was first published [33]. For these reasons, bridges were in most cases the first monitored cultural heritage structure, especially for maintenance reasons. The structural behaviour of historic bridges is generally complex due to the different materials, techniques and shapes used. The dynamic identification and monitoring of masonry bridges are reported in different works: the Rialto bridge was analysed in [34], a Romanesque bridge in Galicia in [35], and the Augustus bridge in Narni was recently analysed in [36]. Other masonry bridges are reported in [37–41], and many others. Some historic iron or steel bridges, instead, are analysed in the works of [42–45] and some examples of historic reinforced concrete bridges are instead reported in [46–48].

The growing use of permanent monitoring systems allows measuring and recording the dynamic response of structures during seismic events, and transmitting these records to seismic network databases for the purposes of damage detection and emergency management. As an example, the Seismic Observatory for Structures (OSS), set up at the end of the 1990s within the Italian Department of Civil Protection, is a nation-wide network for the permanent monitoring of the seismic response of strategic public buildings in Italy [49, 50]. More generally, a SSHM network aims at providing, in the aftermath of an earthquake, a rapid estimation of the seismic damage suffered by the monitored buildings and, plausibly, by similar neighbouring constructions, helping in planning and managing emergency activities.

The availability of simple and direct relationships between modal parameter deviations and presumed damage levels, as determined for different building types, is of the utmost importance for the practical usability of the data collected by SSHM networks during seismic events. Yet, it is well known that even undamaged structures may exhibit significant variations, or ‘wanderings’ [51], of their dynamic characteristics as a consequence of response nonlinearities and/or time-varying environmental conditions, which makes the problem of reliably inferring damage from modal deviations still an open research issue.

In Sect. 3.2, the general issue of applying SHM techniques to CH buildings and monuments is introduced. Section 3.3 is intended to discuss some basic concepts and protocols of vibration-based SHM in the light of their application to CH structures. The architectural heritage consists of a great variety of buildings and monuments, in term of typology, historic period, construction techniques and materials. To give a topical example, industrial heritage and modern architectural heritage in general still

present special issues in term of preservation and related SHM strategies. Therefore, in the second part of the chapter, some significant examples are reported to highlight diverse typologies as well as different scopes of the monitoring programs, e.g.: obtaining an exhaustive depiction of the structural health state and easing the plan of maintenance and restoring intervention; evaluating the efficacy of a strengthening intervention; providing a rapid estimation of the seismic damage possibly suffered by a continuously monitored building.

3.2 The Role of Structural Health Monitoring in the Analysis and Preservation of Architectural Heritage

Historical buildings and monuments are constantly threatened not only by natural hazards, such as earthquakes and floods, but also by scarce maintenance and abandonment. Even improper retrofitting and reinforcement interventions may cause damage or failures to this legacy.

A large part of the issues about the preservation strategies to be used for architectural heritage is related to the intrinsic complexities of these buildings, due to their structural scheme and the uncertainties of their properties.

Moreover, dealing with ancient structures requires a special attention mainly because of factors such as the characteristics of the masonry, the construction defects, the irregularities, the deterioration or failures caused by the external forces: such properties make each of these buildings unique and lead to a higher degree of complexity in interpreting the structural and seismic behaviour [4].

Therefore, the analysis of a historical structure is not a trivial matter, and even its mechanical characterization is often a difficult task. As said, for the analysis and conservation of architectural heritage a multi-disciplinary approach involving historical research, surveys, diagnosis, and structural analysis is mandatory in order to understand the behaviour and the seismic vulnerabilities of these kinds of buildings.

A common feature in the methodologies for the conservation of architectural heritage is represented by the anamnesis stage. In the conservation of historical buildings it is essential to acquire an in-depth knowledge of structures and the materials employed, of their characteristics, and of the possible damage state (and its causes). In fact, the conservation and rehabilitation of heritage buildings can be successfully accomplished only if a diagnosis of the damage to the building has been formulated. This diagnosis should involve a multi-scale approach based on the integration of experimental investigations carried out on-site and in the laboratory. As said in the introduction, vibration-based SHM can provide information about the whole-body response and the overall structural integrity. Because of their non-destructiveness, ambient vibration tests are particularly suited for CH structures. Local inspections, instead, can reveal defects and irregularities in restricted areas whose influence on the global behaviour would be otherwise difficult to appreciate.

Different classifications apply to SHM programs. Based on the scopes of monitoring, three types of SHM programs can be pursued on CH [52].

- Monitoring for understanding the structural behaviour of a building. In this case, the monitoring systems, both dynamic and static, are the basic instruments and give an accurate and reliable knowledge of the historical structure. Indeed, these systems are usually able to capture the phenomena that may influence the structural behaviour of the building such as temperature, wind, dynamic actions [53]. However, in most cases the main purpose of monitoring is to calibrate numerical models that can provide realistic interpretations of the structural and seismic behaviour. While pure numerical modelling procedures can support an appreciable accuracy level in predicting the structural behaviour, especially when the assumption of homogeneous and isotropic materials is acceptable, unfortunately this statement hardly applies to the case of heritage buildings. When models are specifically conceived to assimilate data obtained from monitoring, they can be calibrated to fit some measured static and dynamic properties, and to make a prediction on the real response of the building to external actions.

An exhaustive review of the long term monitoring of the dome of the Santa Maria del Fiore Cathedral has been recently published [54]. An ancient widespread crack pattern, almost symmetric, affected the famous Brunelleschi's dome since the first years of its construction. During centuries, numerous monitoring systems such as *spies* of marble, stone, alloys, iron wedges, up to modern digital deformometers, have been applied in order to control the evolution of cracks over time. The stone or marble *spies*, are a primeval typology of deformometers; in fact they were installed on main cracks and would testify, with their breaking, the crack width evolution. An example of this ancient SHM could be found in the dome of Santa Maria del Fiore and was installed by Gianbattista Nelli in 1694 [54, 55]. The first modern monitoring system (from 1955 to 2009) was installed on the major cracks of the inner dome. The system consists in 22 mechanical deformometers for the measurements of crack width variations four times a year. This is maybe the case of the longest continuously monitoring of a monument (more than 60 years). The second system is more articulated and was put in place in 1987. This system consists of 166 instruments and monitors not only the crack width variations but also the most significant movements of the structures [56]. In the last 20 years, 60 thermometers have monitored both air and masonry temperatures. The total monitoring system installed on the Santa Maria del Fiore's dome is nowadays considered the most significant and complex static monitoring system ever installed on an historical monument, not only for the large quantity of applied sensors but also for the exceptional duration of measurement. In 1987 a dynamic testing campaign was conducted in order to estimate the dynamic parameters of the structure, in terms of modal shapes and frequencies. The results of the identification campaign were used to calibrate a numerical model [57]. At the end of 1990s, a new numerical model was performed. It took advantage of data from the monitoring system [58, 59] and allowed an evaluation of the effects of the thermal loads on the crack opening.

In order to evaluate the structural response of the Arena di Verona to static, dynamic (e.g. shows, concerts) and seismic loads, a permanent SHM system was installed in 2011. Important data are still currently recorded by the monitoring system, in relation both to the static displacements and the dynamic behaviour of the monument. The layout of the Arena's monitoring system is composed by 16 single-axis accelerometers, 20 linear potentiometers (displacement transducer) and 4 integrated sensors of temperature and relative humidity [60]. To choose the optimal positions of sensors, dynamic identification tests, based on ambient vibrations, were firstly performed. The results of modal identification tests have been exploited for the calibration and updating of the FE model of the structure.

In these years of monitoring activities, the system installed in the Arena provided for the assessment of the structural response both under operational conditions and in case of intense shaking events such as earthquakes. The system is designed with a fully automatic process that is able to acquire and analyse monitoring data transmitted to the central server. Using experimental records of the SHM system, behavioural models were accurately tuned and calibrated and can be used in successive steps for simulating the design earthquake expected in Verona, for defining the seismic performance of the monument in case of major events, and then studying the possible safety interventions if a satisfactory performance is not achieved [5].

The church of Santa Caterina in Casale Monferrato is a building completed in 1726 and characterised by an oval dome. In order to assess the structural stability of the church, a series of tests were carried out on the church in 2010, including an experimental modal analysis campaign under ambient vibrations. The testing campaign used specifically designed setups with 18 acquisition channels and monoaxial PCB Piezoelectric capacitive accelerometers. The SHM process followed a scheme that was introduced in the late nineties (e.g. [8]) and that is nowadays a standard for CH structures: after the dynamic tests conducted under ambient vibrations, and the consequent experimental modal analysis, modes were compared with those obtained by a FE model within a recursive model updating process (see model-driven SHM approach in Sect. 2.1). Taking advantage of the predictive model, a seismic assessment was conducted and four factors that may strongly influence the dynamic behaviour were identified: the lantern, the jut of facade, the oval dome and the adjacent structures [4].

- Monitoring for assessing the response to specific events. In this case, local and global parameters such as displacements, stress/strain, modal quantities are measured and compared to typical threshold values. Under such circumstances, monitoring can serve to control the evolution of a damage, e.g. after an event such as an earthquake, in order to support a "symptom-based" decision [61]. The crux of this process is choosing sensitive quantities to be monitored, but also the method of storage.

One of the first and more important example of permanent dynamic monitoring systems is represented by Hagia Sophia. Hagia Sophia is one of the world's most famous cultural heritage sites because of its irreplaceable structural system and significance to multiple religions. Hagia Sophia was built in 532 A.D. in Con-

stantinople (today Istanbul). It is the largest Byzantine structure in the world and in the 15th century it was converted to a mosque [62]. It has been included in the world heritage list of UNESCO since 1985. Hagia Sophia experienced many earthquakes in its history resulting in damages and partial collapses. The monument's history is intimately bound with seismic phenomena that periodically hit the Marmara region with more than 30 seismic events, with magnitudes larger than 7 in the last 2000 years. The "Earthquake Master Plan for Istanbul" has determined the major risk as a large earthquake with 60% probability of occurrence in 30 years. This plan assumes a $M \geq 7.5$ earthquake scenario. In this light, the protection of this monument against the seismic events is an important task in the heritage conservation field. Consequently, several researches have been conducted in order to understand the static and dynamic behaviour of the structure. Among these researches, an ambient vibration survey was conducted in order to determine the low amplitude dynamic response characteristics of the Hagia Sophia monument. A set of 15 instruments was put in place and the modal frequencies and general shapes were identified [63]. Subsequently, in 1991, a strong motion instrumentation was installed in order to identify the dynamic response of the building on the basis of strong motion data records. The system consisted of 9 interconnected Kinematics SSA-2 strong motion accelerometers. The triaxial sensors were fully self-contained with digital recording and storage capabilities. In March 22nd 1992, a 4.8 Mb seismic event hit Istanbul and triggered the strong motion system. Earthquake data from the triaxial accelerometer located at the ground level were applied to the numerical model of the monument in order to evaluate the seismic behaviour of the structure [63]. In November 2008, all sensors and the communication system were renewed and a real-time monitoring system was established. In the six years since 2008, except for a few minor interruptions, the system has been working continuously and about 100 earthquakes have been recorded in Hagia Sophia. An interdisciplinary approach has been applied to the study of dynamic behaviour and earthquake response of Hagia Sophia. Numerical structural analysis was combined with materials and geotechnical investigations, providing important information on the seismic response of Hagia Sophia and establishing its restoration procedures [64, 65].

The church of Santa Maria del Suffragio (or Anime Sante) in L'Aquila (Italy) was heavily damaged during the 2009 L'Aquila earthquake. A post-earthquake monitoring program began in November 2009 in order to check the crack variations and to perform a dynamic characterization of the structure, and ended in February 2013. The SHM was initially composed of 8 displacement transducers and 28 acceleration sensors linked to a 24-bit data logger. The monitoring system was successively modified and optimized in March 2011, however the accelerometers were piezoelectric with nominal sensitivity of 1000 mV/g [66]. Each channel had its own triggering threshold, calibrated on the signal, which is digitalized and pre-elaborated with a high pass digital filter to remove the offset of the sensor due to the instrumental variation of the signal caused by loss of stability in the long term. The signals from the accelerometers were sampled at a frequency of 500 Hz. The monitoring system recorded 120 h of signals, including 50 earth-

quakes with acceleration $\geq 2.5g$. In the last period of the monitoring activity, two velocimeters were installed. Temperature influence on the crack pattern has been investigated by considering two cycles of temperature (December 2009–August 2011). In order to investigate the dynamic parameters of the church, the time history of the earthquake-induced ground motion recorded on March 16th, 2010, was used to detect the first three vibration modes by simple peak picking techniques [31]. Results showed that the variation of crack opening was not directly related to temperature but was linked to structural problems.

A similar application, but related to the monitoring of a bell-tower during seismic events was recently reported by [67]. In this case, the analysis of long-term monitoring data of San Pietro monumental bell-tower located in Perugia, Italy, showed small permanent changes in the structural behaviour after 2016 Central Italy earthquakes.

- Monitoring for assessing the efficacy of structural or seismic interventions. For historical buildings, also in the absence of a significant hazard level, it is highly desirable to check the effectiveness of restoration and strengthening interventions over time [5, 7, 15, 52, 68–70]. Moreover, data from monitoring systems can be crucial in the planning of new strengthening and retrofitting interventions [31].

3.2.1 Vibration-Based Structural Health Monitoring for Cultural Heritage

Vibration-based SHM represents a non-invasive technique that exploits the natural vibration of structures. It is useful to describe the structural conditions of historical buildings and to optimize the plan of maintenance as well as the restoring interventions [4, 7, 71].

In fact, dynamic tests are efficient investigative tool: they allow the detection of the structural behaviour of the building system with non-invasive actions and low expenses, which is crucial when the necessity to preserve the integrity of the materials is particularly significant. Moreover, contrary to other investigation techniques, they provide information on the global behaviour of a structure.

According to [72] vibration-based SHM approaches may be classified into two main groups: the data-driven and the model-driven. Usually, data-driven approaches necessitate a huge amount of information coming from permanent monitoring systems, or from simulations when the structure's dynamic behaviour can be easily identified and reproduced. In data-driven approaches, statistical models of the system are easily defined, and noise levels and environmental variations are established naturally. Conversely, approaches that are driven by high-fidelity models of the structure can potentially work without a validated damage model, but noise and other environmental effects are difficult to incorporate.

System identification is the core of any model-driven SHM approach. Indeed, identification techniques and algorithms are indispensable in order to produce a

realistic model of a structure, especially when dealing with materials and structural schemes that cannot be easily identified. In permanent monitoring systems, varied or anomalous parameters are directly associated to damage, and reliability can be defined as a function of identified quantities that reflect the damage, referred to as symptoms. Alternatively, especially when the analysed buildings present a complex structural scheme, a numerical model can be updated on the grounds of the identified parameters by using model updating techniques, in order to simulate the real behaviour of the structure and to overcome uncertainties and to reduce uncertainty.

Since in typical structural problems safety assessment relies on mechanical models, the engineer is prone to basing any final evaluation, prognosis or decision on results coming from an updated model, rather than on symptoms [4]. Unfortunately, as previously said, CH structures pose many modelling issues.

For instance, in masonry structures the uncertainties translate into great difficulties in defining a modelling method for a generalized application. One can summarize the nature of such uncertainty as follows [7]:

- (i) local variability of the geometric properties and of the masonry internal organization, lack of material continuity, hidden cavities, loss of verticality of walls subject to lateral loads caused by vaults, arches, or roofs;
- (ii) local variability of the material strength and stiffness, due to original defects or electro-chemical degradation;
- (iii) distribution of cracks, subject to thermal path (seasonal width oscillation with basic trend to increase continuously, due to cumulated debris inside the crack);
- (iv) effects of past, non-documented, damage and repairs, architectural changes, local manipulations.

In reinforced concrete CH, infill walls and other non-structural elements may strongly affect the dynamic behaviour of the structure and, consequently, the sensor placement of vibration-based SHM. In this respect, damage-scenario-driven optimal sensor placement strategies can reveal can be an efficient tool an efficient tool [73].

For all these reasons, in CH structures the results of the numerical analysis need to be reconciled with the experimental data coming from dynamical tests, by means of model updating or calibration techniques. The updated model will clarify, downstream the optimization, some less certain aspects of the experimental data. The historical information and the survey documentation are themselves a support to the creation of a finite element model, as well as a comparison term with the calibrated model.

3.2.2 Continuous Monitoring of Cultural Heritage and Wandering of Dynamic Parameters

Modal parameters are the typical outcome of dynamic tests, especially when they are conducted under ambient or natural excitation (in-operation experimental modal analysis). In model-driven SHM approaches, anomalous or varied values of such

parameters can be associated to a damaged state of the model. When a permanent monitoring system is also available (e.g. buildings belonging to a SSHM network) on-line estimates of modal parameters might in principle support a symptom-based diagnosis [61].

As a matter of fact, symptom-based diagnosis is not a trivial task, especially in complex CH buildings. The variation of modal parameters in civil structures under earthquake loading has been the object of several studies [51, 74–77], but the sources of modal wanderings are not completely understood. From observations made during seismic swarms [49], seismic wandering must essentially depend on reversible, amplitude-dependent nonlinearities inherent in the system response, possibly caused by a variety of factors, including (i) soil-structure interaction (SSI), increasingly more pronounced during stronger motions; (ii) nonlinear behaviour of the structure (micro-cracking in concrete, slip in masonry); and (iii) interaction of structural and non-structural elements.

Any SHM approach based on the variation of modal quantities should come to terms with the following feats:

- Conventional linear identification and modelling approaches prove to be effective for the dynamic characterization of reinforced concrete and masonry buildings under small-to-medium ground motions; the resulting equivalent modal model is, however, amplitude dependent, and a significant frequency and damping ‘wandering’ is observed for different shaking amplitudes.
- Repeated under subsequent events, said approaches allow tracking frequency and damping wandering as a function of the seismic response amplitude; if these events are closely spaced in time, such as in the case of earthquake swarms, wandering can be considered substantially independent of environmental effects.
- Even though the investigated cases do not fall into categories typically affected by SSI (tall slender buildings, strong earthquakes, ground amplification, liquefaction etc.), a frequency vs. amplitude relationship is still detectable.
- In the absence of crack patterns, intrinsic system nonlinearities make such amplitude dependence consistently linear in the logarithmic plane, and systematically decreasing for frequencies (with smaller dispersion) while typically increasing for damping ratios (with much larger dispersion). On some vibration modes, equivalent damping ratios is seen to decrease with damage.
- The experimental reconciliation of FE models incorporating SSI effects ensures a significant improvement of model representativeness, both in the modal as well as in the time response domains.
- Structural condition assessment of permanently monitored constructions can highly benefit from the identification of such linear trends, because new data not aligning with previously identified trends are likely to reveal the occurrence of some permanent modification of the structural system.

3.3 Examples of Vibration-Based Investigation of Architectural Heritage

3.3.1 *The Madonnina della Neve Church, an Example of Vibration-Based Structural Health Monitoring Aimed at Designing Seismic Strengthening Interventions*

The scope of a periodic monitoring can be that of obtaining an exhaustive depiction of the structural health state and easing the plan of maintenance and restoring intervention. Under some circumstances, vibration-based SHM can locate weak and damaged elements, loss of connections, or even identify potential collapse mechanisms and seismic vulnerability factors. In this respect, an interesting application of vibration-based SHM is represented by the case of the church “Madonnina della Neve” in Savigliano (Cn), built in 1609. Despite being relatively small, this church presents a considerable amount of morphological complexity due to the multi-level interaction between its different structural elements (Fig. 3.1). In 1763, the church was radically transformed into its current aspect and, in the following decades, service bodies were annexed to the original building. The church, which has a central plan, is surmounted by an oval dome, built without the drum. Visual surveys confirmed a generalized crack pattern, especially located on the oval dome and at the connection between the lateral walls and the facade. In the study of [4] a methodological approach for the application of experimental modal analysis to cultural heritage is presented via three examples, including the case of the “Madonnina della Neve” church.

Firstly, dynamic tests were executed in order to investigate the global behaviour of the structure. Tests were performed to maximize the spatial resolution of experimental modal shapes associated with the main structural response and the number of the modal parameters later used to calibrate the mechanical models. Since the experimental setups depend on the specific aim of the investigations, a FE model of the structure was performed to identify the structural areas and the elements that were mainly affected by each modal component of the dynamic behaviour. Consequently, the setup was defined and 18 sensors were installed on the structure (Fig. 3.1). The sensors used for dynamic test campaign were monoaxial PCB Piezoelectric capacitive accelerometers, with a sensitivity of approximately 1 V/g, a measuring range included between 0 and 3 g, a resolution of 30 μ g and a mass of 17.5 g. The signals were acquired under ambient noise excitation (vehicular traffic, wind, microtremors, etc.). In most masonry structures signal lengths of approximately 20 min, with sampling frequency equal to 400 Hz, can be considered sufficient to perform the experimental modal analysis.

The family of stochastic subspace identification (SSI) methods stems from Ho and Kalman’s classical realisation theory. The identification technique used in this case was the third algorithm considered by the unifying theorem of Van Overschee and De

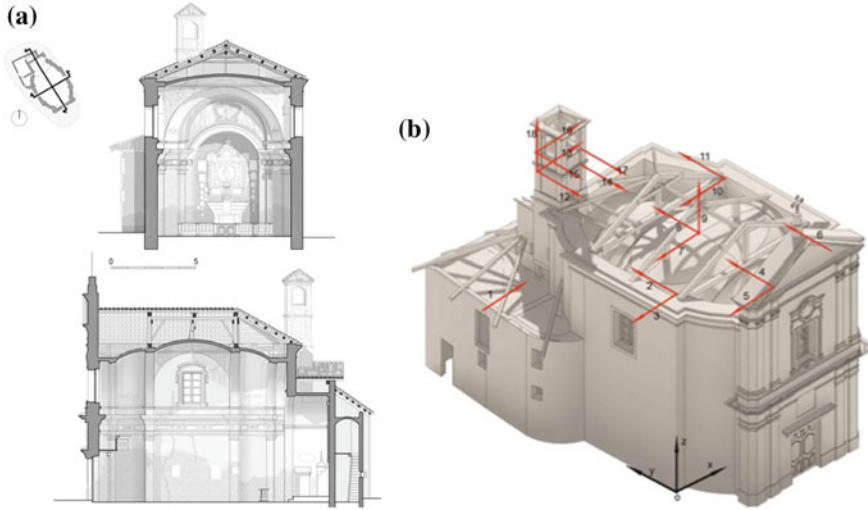


Fig. 3.1 Main sections of the Madonna della Neve (a); the 18 sensors location (b)

Moor [78]. This time-domain method, which is often referred to as “Canonical Variate Analysis” (CVA), was originally developed by Larimore [79]. The signals acquired are conditioned using filters, de-trending and sub-sampling. After a pre-analysis with Welch power spectral representations [80], several time-domain identification sessions were executed. Computational modes are systematically discarded by using the MAC [81]. In greater detail, all signals coming from different acquisitions were segmented and a large number of SSI identification sessions were performed. In order to eliminate spurious eigenmodes, a cleaning criterion was adopted. First, eigenmodes characterized by damping values greater than 0.20 were automatically discarded. Then, both the sets of identified frequencies $\mathbf{F} = [f_1 \ f_2 \ \dots \ f_n]$ and mode shapes $\mathbf{V} = [\mathbf{v}_1 \ \mathbf{v}_2 \ \dots \ \mathbf{v}_n]$ resulting from each acquisition segment were used to compute the Boolean affinity matrix \mathbf{A} defined as:

$$\begin{cases} \mathbf{A}_{i,j} = 1, & \text{if } MAC(\mathbf{v}_i, \mathbf{v}_j) \cdot \exp\left[-\left(\frac{f_i - f_j}{\sigma}\right)^2\right] \geq 0.95 \\ \mathbf{A}_{i,j} = 0, & \text{if } MAC(\mathbf{v}_i, \mathbf{v}_j) \cdot \exp\left[-\left(\frac{f_i - f_j}{\sigma}\right)^2\right] < 0.95 \end{cases} \quad (1)$$

where a frequency threshold σ equal to 0.20 Hz was assumed. An index of recursion C_i relevant to each single i th eigenmode has been defined as follows:

$$C_i = \sum_{j=1}^n \mathbf{A}_{i,j}. \quad (2)$$

Eigenmodes characterized by $C_i > 5$ were kept, whilst the others were discarded as spurious. The threshold value of the index of recursion C_i was proportional to both the segmentation number and to the system order range considered and, in addition, to the noise level of acquired signals.

Stabilization diagrams are used to identify frequencies in each segment (stabilization criterion: maximum frequency deviation: 2%), then additional tolerance criteria are used for MAC (5%) and for damping ($0 \leq \zeta \leq 10\%$). By executing a statistical recurrence of the system's natural frequencies identified by the SSI algorithm and by averaging values, it proves possible to distinguish between the real modes of the structure and modes that appear occasionally, being possibly due to exogenous components [82].

In the case of "Madonnina della Neve" 12 vibration modes of the structure were identified. The two main translational modes were captured at 3.81 and 5.14 Hz, respectively. The third (6.01 Hz) and the fourth (6.66 Hz) mode shapes are characterized by phase opposition between the bell tower and the façade.

Based on the results of the dynamic tests, a model updating was conducted on the numerical model of the church (Fig. 3.2). Vibration-based model updating consists in tuning the preliminary numerical model by using the dynamic parameters obtained through system identification techniques, in particular modal frequencies and shapes (Fig. 3.3). The model updating allows a reliable estimation of the mechanical characteristics of the materials. For instance, the elastic moduli, as related to the different macro elements of the building, provide information about anomalies affecting the structural behaviour such as local weakening, cracking and dislocations, so facilitate damage diagnosis and possible interventions. In the reported application, the equivalent elastic modulus distribution, obtained through the model updating procedure, was used to locate weak regions, associated to damage. To this aim, the model was subdivided in macro elements, so that weaknesses could more accurately defined.

In CH fields, the updating is usually based on local sensitivity approaches, leading to the minimization of a penalty function, in order to exploit the wealth of geometric and mechanical information. The following cost function has been used in the FE model optimization procedure:

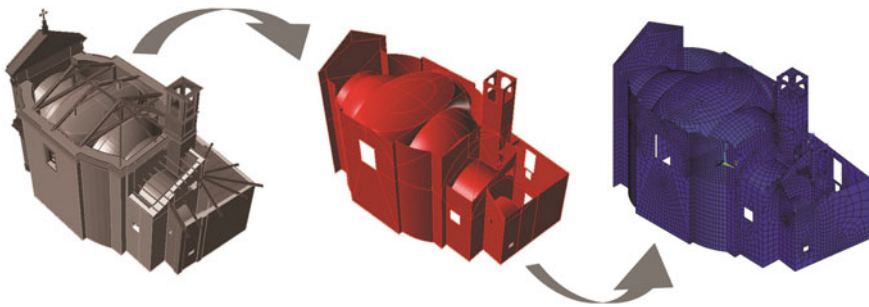


Fig. 3.2 The process of geometrical simplification: from three-dimensional model to finite element model in the case of the church. Based on [4]

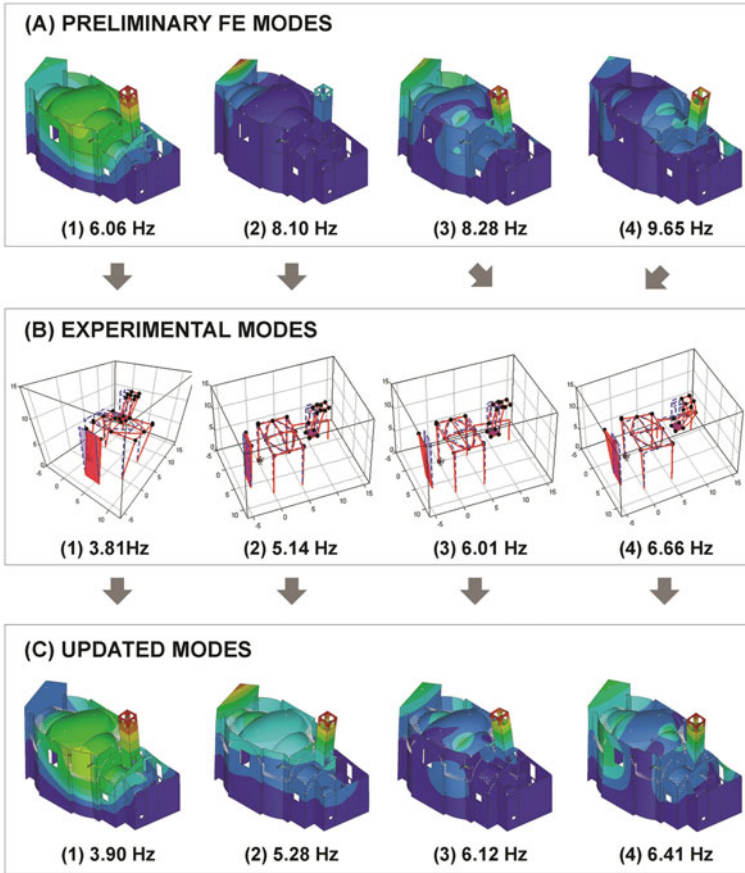


Fig. 3.3 Model updating process performed on the “Madonnina della Neve” FE model

$$f = \sum_{i=1}^m \alpha \left(\frac{f_{Ai} - f_{Ei}}{f_{Ei}} \right)^2 + \beta \left(\frac{1 - \sqrt{MAC_i}}{MAC_i} \right)^2 \quad (3)$$

where f_{Ai} and f_{Ei} represent the i th numerical and experimental mode frequencies, respectively, whilst α and β are two weighting coefficients for frequency and modal shapes [83] respectively, and MAC_i is the modal assurance criterion for the i th mode.

The high geometric complexity of CH heritage structures might sometimes call for more sophisticated updating procedures, [16, 70]. At any rate, the results coming from the optimisation process need to be carefully verified, because success in the optimisation procedure does not entails that the calibrated model is physically meaningful.

In the case of “Madonnina delle Nevi” the outcomes of the model updating process, represented in Fig. 3.4, are confirmed by visible crack pattern in the lateral

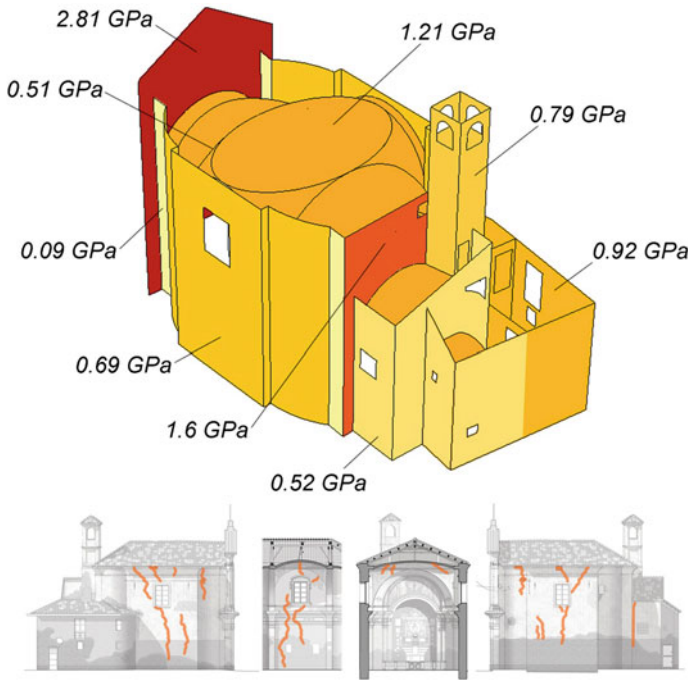


Fig. 3.4 The Young modulus distribution after the calibration process

masonry walls, especially at the connections, and also by historical dating of different bodies.

3.3.2 The Former Clinker Warehouse of Casale Monferrato, a 20th Century Industrial Architectural Heritage

As previously highlighted, architectural heritage consists of a great variety of buildings and monuments, in terms of typology, historic period, construction techniques and materials. Among those, industrial heritage and modern architectural heritage in general still present many issues connected to their preservation or rehabilitations. Presently, much of the world's industrial heritage is unrecognized or undervalued, many buildings are abandoned, or even demolished, and are thus at risk and in need of protection. This situation can be attributed to a variety of factors; in fact, 20th century buildings still struggle to be considered part of an heritage, moreover their original functions have substantially changed, and the materials or technological innovations employed for their construction have not always endured long-term stresses.

An area of conservation that requires attention is seismic provision. In fact, modern architecture buildings were designed and built with no, or very limited, seismic provisions, due to the lack of reference technical standards at the time of their construction. With a view to the restoration and renewal of these buildings, a careful assessment of the performance of their structures is a priority.

The former clinker warehouse, also known as the “Paraboloide” of Casale Monferrato, Italy, is part of this endangered heritage. It was built at the beginning of the past century as part of the Italcementi factory, and it is the only survived building of this larger industrial complex located near the historical city centre. The Paraboloide is the first building in Italy that was built using a thin shell structure in concrete with a parabolic shape. This structural configuration was extremely innovative for the period and it allowed the creation of an unified internal space of considerable height, without any intermediate floors. The scheme, conceived to suit perfectly its industrial use, especially the need for large spaces to stock or produce materials, would spread throughout the country in the following decades, especially for industrial facilities buildings [84].

The Paraboloide presents a rectangular shaped plan of about 23×51 m, a height of 12.6 m; by considering the open gallery placed at the top of the structure, the overall height of the building measures a total of 16.13 m. On the north-east side of the Paraboloide, it is located a 16.82 m high tower in concrete (Fig. 3.5). The main structure consists in a parabolic roofing system in concrete, composed of 8 parabolic arches. A beam system, based on the arches, support the thin shell panels or buttresses, which were built in reinforced concrete with a thickness of 8 cm. The parabolic arches are supported by trapezoidal-concrete panels and their thrust is counter-acted by 6 tie-beams in reinforced concrete. The deflection of the concrete ties is contrasted by reinforced concrete pillars with a square profile of 0.3×0.3 m, which were probably added at a later time (Fig. 3.5).

Two drawings of this innovative construction solution were reported in a popular manual for reinforced concrete structures [85]. Its constructive technology, as well as the structural shape of the thin concrete vault, is comparable to the outstanding



Fig. 3.5 External and internal views of the Paraboloide in Casale Monferrato

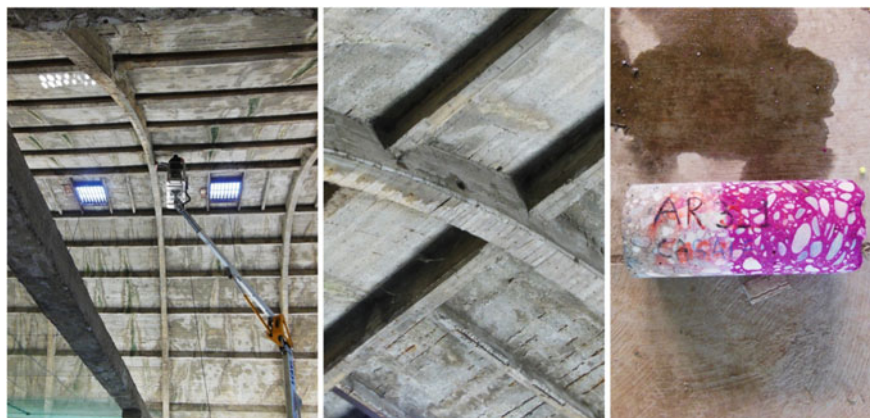


Fig. 3.6 Coring performed on an arch and determination of the carbonatation depth in concrete

constructions of Eduardo Torroja and Pier Luigi Nervi, who also employed this configuration for other industrial facilities in Piedmont [86]. Given the particular configuration of the building and the lack of original documentation (apart from the two drawings reported in [85]), it was considered necessary to carry out an accurate metric survey. The metric survey was carried out by [87, 88] using high resolution terrestrial laser scanning technology (TLS) also known as LiDAR (Laser Imaging Detection and Ranging), in order to obtain an accurate 3D model with uniform level of detail and precision, in addition to continuous metric information for each portions and elements of the structure. This procedure allowed detailed geometric information, which provided a proper reading of the structural typology of the building and the recognition of possible design and construction principles.

In order to evaluate the current state of the structure, the building was investigated by means of both mechanical and dynamic tests. This thorough campaign was intended as the starting point for the preservation and restoration guidelines of this daring structure. In fact, both destructive (Fig. 3.6) and non-destructive test were performed, in order to assess the state of the various structural elements. Given the particular structural configuration of the building, strongly influenced by its geometric complexity, the potential inhomogeneity of the material properties, also in this case, a model-driven approach was employed. All the information gathered from the laser-scanner survey provided the geometric and dimensional characteristics of the structure, as well as the classification of the elements and the materials employed. The simplified geometric model was subsequently used for the construction of the FE model (Fig. 3.7).

The dynamic tests were designed to maximize: (a) the spatial resolution of experimental modal shapes associated with the main structural movements; (b) the number of captured modes, to be successively employed for calibrating the mechanical models. Accordingly, the preliminary FE model was used to identify the structural portions and elements that mainly affects the dynamic behaviour of the structure. Based

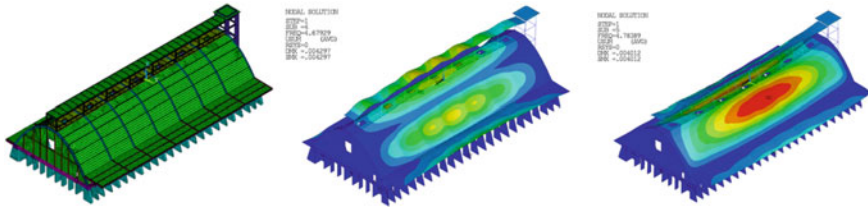


Fig. 3.7 The preliminary FE model of the Paraboloid and the first main modes affecting the vault

on the FE vibration modes (Fig. 3.7), the measuring points (setup) were defined, as well as acquisition settings and parameters. The test design had also to take into account limitations in the number of sensors and the accessibility of the building. In the case of shell and special structures the sensors locations can be particularly difficult to optimize [73, 89]. In the case under analysis, only the central portion of the parabolic vault was instrumented. In fact, based on the results of the preliminary finite element model, it emerged that the most relevant modal components mainly affect the central part of the building along the transversal direction.

The acquisition setup employed was composed of 19 accelerometers: 1 in the X direction, 14 channels in the Y direction, and 4 channels in the Z direction. The sensors have been distributed on different levels and positioned on the main structural elements. The acquisition of the signals was carried out with a sampling frequency equal to 256 Hz, as the main modes were expected in the 0–20 Hz range. Since the acquired signals were generated by ambient excitation, a 30 min acquisition was deemed sufficient.

The dynamic identification, in terms of frequencies, modal shapes and damping, has been carried out in the time domain with SSI. In particular, the Stochastic Subspace Identification (SSI) was used.

Prior to identification, the whole record (30 min) was decimated at 128 Hz to speed up the analysis, with 0–50 Hz useful bandwidth. The signal was then filtered between 0.1 and 25 Hz with a band-pass filter Butterworth of order 4. This operation allows to obtain an estimation of the modes, with a certain reliability, up to about 20 Hz. The filter was applied by removing every type of linear trend present in the signal. Since the dynamic behaviour of the building is mainly characterized by the less inertial direction (direction Y), the identifications were made discarding the channels in the X and Z directions, which would not have added useful information to the identification of the main modes; on the contrary, they could have led to greater problems related to the presence of higher modes within the signals. For this reason, 14 channels were used for the experimental characterization of the modal model of the Paraboloid. Moreover, all the modes with a damping less than 1% and above 8% have been neglected as likely to be spurious. Table 3.1 reports the identified damping and frequency values, while Fig. 3.8 depicts the first vibration mode, limited to the in-plane movements of the arch.

Table 3.1 Identified values for modal damping and frequencies

Mode	1	2	3	4	5	6	7
ζ_{ex} (%)	2.24	3.41	2.65	2.84	2.19	1.15	1.39
f_{ex} (Hz)	3.75	5.61	8.00	8.85	9.25	12.10	15.20

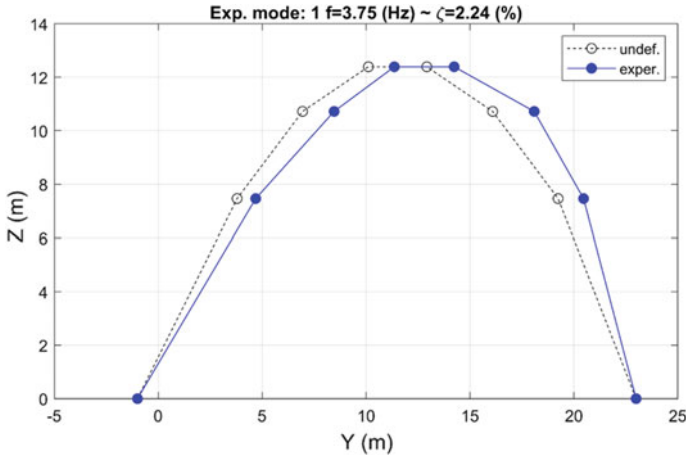


Fig. 3.8 Experimental shape of the first mode, identified at 3.75 Hz

The calibration of the reference FE model is based on the dynamic characteristics extracted in the previous stage, with emphasis on modal frequencies, shapes and Young’s moduli of the materials. Updated models allow to obtain a reliable estimation of the mechanical properties of the materials. In order to take into account the spatial distribution of mass and stiffness, the reference FE model was divided into homogeneous portions, from the point of view of the materials. As a first step, the elastic moduli of the reference FE model were calibrated on the basis of the mechanical tests performed in laboratory on core samples extracted from different structural elements of the building.

After that, the FE model was calibrated by using the identification data of the main vibrating modes of the structure (1, 2, 3, 5). The remaining modes (4, 6 and 7) were used for a posteriori comparison because in first phase of the identification they were considered too uncertain to be used for model updating. The elastic characteristics (Young’s moduli) have been varied in the range between 10 and 50 GPa.

Table 3.2 reports a comparison between the identified frequencies (f_{ex}) and the frequencies of the FE updated model (f_{FEM}).

The updated FE models closely reproduce the real behaviour of the Paraboloid in its current state, and provide a reliable basis for its seismic assessment and the development of more reliable rehabilitation guidelines. Table 3.3 reports the values of each parameter of the FE model, which were updated first with the results of the mechanical tests, and then with the data coming from the dynamic tests. In Fig. 3.9

Table 3.2 Comparison between the identified frequencies (f_{ex}) and the frequencies of the FE updated model (f_{FEM})

Mode	1	2	3	4	5	6	7
f_{ex} (Hz)	3.75	5.61	8.00	8.85	9.25	12.10	15.20
f_{FEM} (Hz)	3.73	5.73	8.02	9.03	9.47	10.91	14.45
Error %	0.534	2.139	0.25	2.033	2.378	9.835	4.935

Table 3.3 Values of the mechanical properties of the materials which have been updated based on the tests results

Element	Parameter number	Model updated with the mechanical tests results		Model updated with the dynamic tests results	
		Elastic modulus [GPa]	Density [kg/m ³]	Elastic modulus [GPa]	Density [kg/m ³]
Buttresses	1	17.5	2300	17.5	2300
Arch-buttress node	2	17.5	2300	12.6	2300
Tie-rod	3	25	2300	31.8	2300
Arch	4	25	2300	40.3	2300
Cantiever roof beam	5	25	2300	32.5	2300
Panels	6	25	2300	34.9	2300
Joist	7	25	2300	27.7	2300
Arched beams	8	17.5	2300	23.0	2300
Tympanums panels	9	25	2300	30.1	2300
Tower	10	17.5	2300	19.8	2300
Pillars	11	25	2300	24.6	2300
Side storage	12	25	2300	19.2	2300

a comparison is reported between the values of the updated parameters, before and after the calibration with the dynamic tests.

As it can be seen in Fig. 3.9, almost all the elastic parameters increase with respect to those obtained from mechanical tests (concrete samples subjected to compressive tests in laboratory) as a result of the model updating. This general increase after the dynamic calibration is in line with expectations, as dynamic moduli are known to exceed of about 15–20% the static ones.

An exception is constituted by the buttress-arch node (material 2), which is reduced by about 30%. This highlights possible weakening at the anchorage of arch rebars, arguably due to carbonatation, and hence the need to act with utmost caution in the operations of strengthening of the concrete tie. Other vulnerability factors are the tower in concrete and overhangs in general. Conversely, the arches demonstrated to be the substantial elements for the static and dynamic behaviour and stability of this stunning structure.

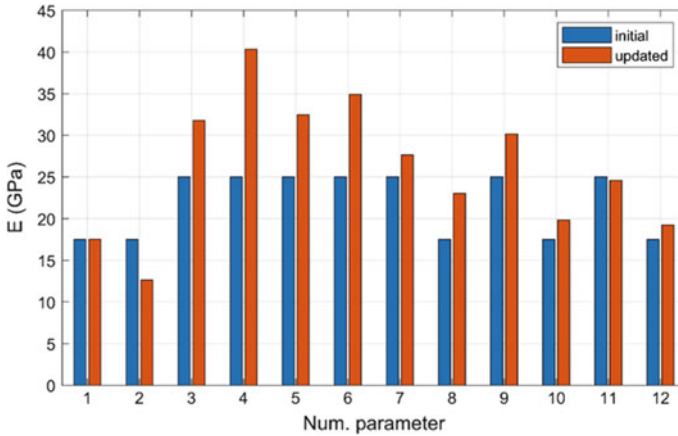


Fig. 3.9 Comparison between the values of the parameters, before and after the calibration with the dynamic tests

3.4 Periodic Dynamic Investigations in Post-earthquake Scenarios

Earthquakes have always represented one of the main causes of damage to and loss of cultural heritage. Typically, architectural heritage buildings are the most vulnerable to the tragic effects of earthquakes. Recent seismic events in Italy, Nepal and Indonesia, caused severe damage to monumental buildings, which has shown once again the high seismic vulnerability of these types of structures, as well as the relevance of this topic in a risk analysis, both from an economic and cultural point of view.

It is not rare that even aftershocks may cause more damage than the main shock itself on this typology (e.g. due to accumulated damage in masonry or due to damage on the structure that exposes vulnerabilities).

Moreover, in the first phase of a post-earthquake emergency, one of the most critical problems is securing damaged structures by employing temporary interventions (e.g. partial demolition, shoring, installation of metal rods, and hoops, etc.). In fact, timely provisional interventions are often necessary to preserve heritage buildings in post-seismic scenarios, especially because they avoid further damage to the structure due to aftershocks or even the full collapse.

However, the choice of the adequate type of temporary intervention for these monumental structures is a complex issue, considering the performance, the costs and the temporary nature of the interventions. Moreover, due to the lack of time and the structural complexity of CH buildings, the real dynamic of the system is usually not considered.

In some cases, vibration-based SHM can be applied in order to understand the sensitivity of structure dynamic measurements to safety interventions and to assess their efficacy, as in the case of the bell-tower of Santa Maria Maggiore Cathedral in

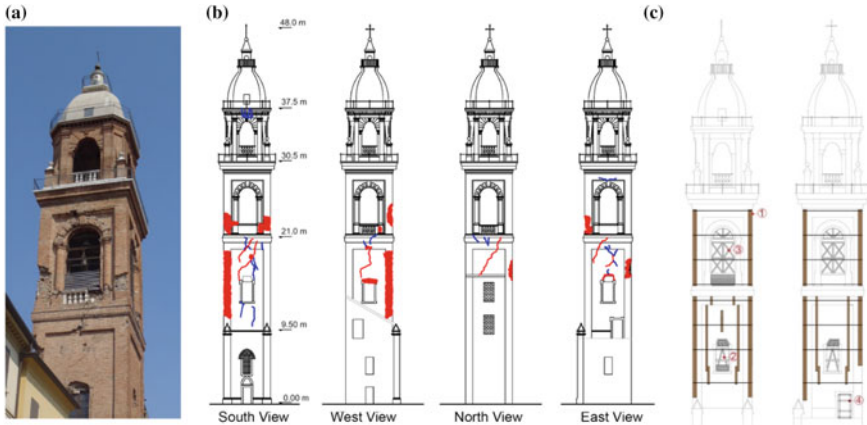


Fig. 3.10 **a** The Mirandola bell-tower after seismic event; **b** Post-earthquake damage survey of the bell-tower; **c** Post-earthquake provisional safety-interventions: metal tie rods (1), wooden falsework in the small opening of the first and second level (2–4), wooden falsework in the large opening of the third level (3)

Mirandola (Italy) heavily damaged by the Emilia (Italy) seismic events of the 20th and 29th May (Fig. 3.10a) [15].

3.4.1 *The Bell-Tower of Santa Maria Maggiore Cathedral in Mirandola, an Example of Dynamic Investigations in Post-earthquake Scenarios*

The bell-tower of Santa Maria Maggiore Cathedral in Mirandola is a 14th century brick masonry bell-tower with a square plan. As is often for historical structures, the tower was subject to several alteration during centuries, as the increasing elevation up to 48 m high, and the modifications and application of reinforcing to withstand the subsequent new loads.

The tower was severely damaged by the Emilia seismic event, that activated a twisting mechanism resulting in the rotation of about a degree of a building portion. The structural damages were mainly located in this portion of the tower, between 20 and 32 m high (Fig. 3.10b).

The after-earthquake dynamic test were carried out in pre-intervention (PR-I) and post-intervention (PS-I) conditions. In fact, provisional safety interventions were put in place by authorities a couple of months after the earthquake in order to prevent the collapse of the cathedral and of the bell-tower immediately after the first emergency phase. The tower was reinforced with eight metal tie-rods located at two levels of the structure. Moreover, the main and large openings were reinforced using wooden false works, together with wooden ribs in the smaller openings (Fig. 3.10c).

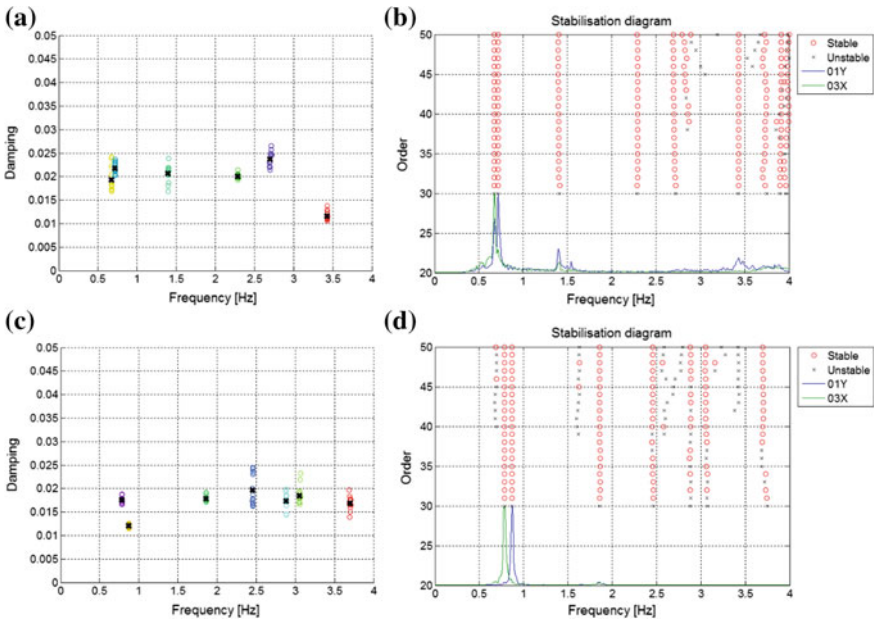


Fig. 3.11 Bell-tower modal identification results (frequency-damping clustering and stabilisation diagram): **a–b** in pre-safety intervention (PS-I), **c–d** in post-safety intervention (PS-I) interventions. The stabilisation parameters chosen for the graph were: $\delta f = 0.005$, $\delta \zeta = 0.1$, $MAC = 0.95$

In order to investigate the dynamic behaviour of the structure after the main seismic event and after the post-earthquake safety interventions, a temporary vibration monitoring system was put in place. It was constituted by eight uniaxial piezoelectric accelerometers (PCB Piezotronics type 393C) with a nominal sensitivity of about 1 V/g, and a measurement range of ± 2.5 g peak. The sensors were placed at different levels of the tower and recorded the dynamic responses to ambient noise. They were installed special metal bases fixed directly on the wall with expansion anchors. In order to simplify the thought execution of further test to assess damage and the long-term efficacy of the reinforcing system, the metal bases were left in place. A total of 8 channels were acquired with a sampling frequency of 192 Hz, for an average signal length of 300 s. Pre-processing and data conditioning involved subsampling (sampling frequency was reduced to 48 Hz), mean removal and de-trending through a polynomial fitting of the signals [4]. The acquisition of the signals was conducted in similar environmental conditions, with a temperature of about 20 °C and 40% of humidity.

Identification of data recorded by sensors was conducted in the time domain using the SSI-CVA algorithm, as described in Sect. 4.1. The several pre-processing operations required for the identification procedures on masonry structures are well described in [4]. Some sample clustering and stabilization diagrams are reported in Fig. 3.11.

Table 3.4 Identified modal frequencies and damping ratios in pre- (PR-I) and post-safety intervention (PS-I) configurations

PR-I		PS-I			
Frequency [Hz]	Damping ratio [%]	Frequency [Hz]	Damping ratio [%]	Δf [%]	$\Delta \zeta$ [%]
0.68	1.6	0.79	1.7	16.2	6.2
0.72	1.5	0.87	0.5	20.8	-66.7
1.41	2.2	1.86	2.6	31.9	18.2
2.30	1.1	2.48	2.3	7.8	109.1
2.71	1.9	3.05	2.2	12.5	15.8
3.68	4.4	4.66	3.1	26.6	-29.5
3.86	0.9	5.48	3.5	42.0	288.9
3.92	0.9	6.26	2.2	59.7	144.4

From the results of identification in terms of modal parameters identified before and after the installation of safety intervention it is possible to notice the mitigation effects provided by the safety interventions on the extensive damage suffered by the bell-tower [7]. From Table 3.4, a comparison between the identification results highlights a general increase in terms of modal frequencies, which can be directly related to the stiffening effects provided by the safety interventions. In fact, the first two bending frequencies increase of about 16 and 21%, respectively; whereas the first torsional mode has seen an increase of about 32%. For what concerns the damping ratios, the trend is not as clear. At any rate, 6 out of the 8 modes show an increase in the damping ratios after the interventions.

In order to better investigate and clarify these results, a comparison can be operated with a similar study conducted on the bell-tower of the S. Annunziata church in Roccaverano [7]. In Roccaverano bell-tower, after the reinforcement through grouting and tie-bars, the bending modes rose from 1.66 and 2.26 to 1.97 and 2.34 Hz, showing an increase of 19 and 4%, respectively. On the other hand, the torsional mode had an 8% reduction, from 4.67 to 4.3 Hz, possibly due to mass added after groutings.

A last comparison was conducted between the first three models of the Mirandola bell-tower with those of about 40 masonry towers or bell-towers from across Europe e.g. [4, 8, 90–97]. This comparison highlighted how the two flexural modal frequencies of the damaged scenario are significantly lower than the typical ones of other bell-towers of comparable height. Then, it can be noted that the torsional mode of Mirandola tower is even more distant from the expected trend of frequency as a function of height represented by the lines in Fig. 3.12. This is most probably related to the presence of a large damage in the structure and the compromised box-like behaviour.

Moreover, this comparison between the case study and literature examples shows how after the earthquake the frequencies of the first three modes were found to be

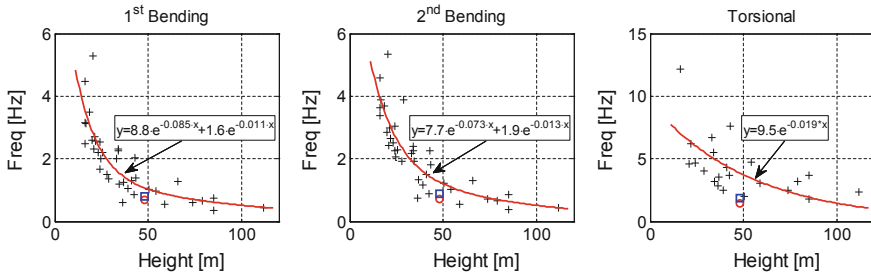


Fig. 3.12 Frequency dependency of the first 2 bending and the torsional mode with respect to height of the building from literature data. The red circle and the blue square represents the Mirandola bell-tower frequencies in the PR-I and PS-I configuration respectively, whilst the regression line is obtained with a generic exponential law

sensibly low. Instead, after the strengthening intervention frequency values are seen to substantially match those expected for undamaged bell towers of similar height.

When the (PR-I) and (PS-I) identification results are available, these can be used to calibrate FE model to assess the intrinsic characteristics of masonry, the structural interaction with adjacent structures and the structural effects of safety measures and strengthening interventions. It is worth to notice that a set of dynamic data of the undamaged structure may strongly improve the quality of the conducted study. In the presented case study, a FE model of the bell-tower was designed starting from geometrical and laser scanner survey data. The FE model updating allowed a significant improving of the calibration of significant number of parameters of the structural portions. Moreover, the observed increase in modal frequency values proves that the confinement provided by safety measures limits the flexural mechanism and the increase of Young modulus in the portion of structure interested by post-earthquake measures implies the increment of global flexural stiffness.

The study conducted on the Mirandola bell-tower confirmed how periodic vibration-based SHM can be an effective tool for investigating the behaviour of structures in complex scenarios as a post-earthquake phase and for assess the structural improving provided by safety interventions, both temporary and permanent.

3.5 Continuous Monitoring

In spite of many successful applications, as described above, long-term SHM is still a critical issue when it comes to historical structures. In fact, the main feature of monumental buildings is its uniqueness, and their monitoring calls for customized systems and protocols.

3.5.1 *The Sanctuary of Vicoforte, an Example of CH Building Subjected to Permanent Static and Seismic Structural Health Monitoring*

The Sanctuary of Vicoforte (Fig. 3.13a) represents an important architectural heritage building for the catholic religiosity. It was built at the end of the 16th century and was designed by the architect Ascanio Vitozzi. The building is very significant in the field of the history of architecture, above all for its dome. The dome was designed by Francesco Gallo after the death of Vitozzi, and the suspension of the construction for several decades, also due to the structural problems related to the soil composition [98]. With the impressive dimension of the main axes (37.23 and 24.89 m), it is the world's largest oval masonry dome (Fig. 3.13b).

After the comprehensive structural survey report made by engineer Martino Garro [99], structural problems of the building prompted the decision to undertake investigations and researches. However, only at the end of the '70 that the scientific community started to systematically investigate the structural health state of the Sanctuary.

At the beginning of the eighties, a strengthening system was installed in order to avoid the expansion of the crack pattern especially located in the dome-drum system. The system consists of four high strength steel bars in each of the 14 tangential directions. Steel frames interconnected the heads of the bars of two adjacent stretches. The tie bars, slightly tensioned at 50 kN by jacks, were re-tensioned in 1997 to compensate the stress losses [98].

Geological and geophysical investigation, conducted between 1976 and 2008, revealed that different materials compose the soil underlying the Sanctuary [100]. A layer of marl slants downward from the north-east to the south-west corner, whilst under the rest of the building there is a clay layer, causing serious crack patterns [98].

Monitoring activities on the Sanctuary of Vicoforte started in 1983 with the installation of instruments to investigate the evolution of the cracks. Since then, the mon-

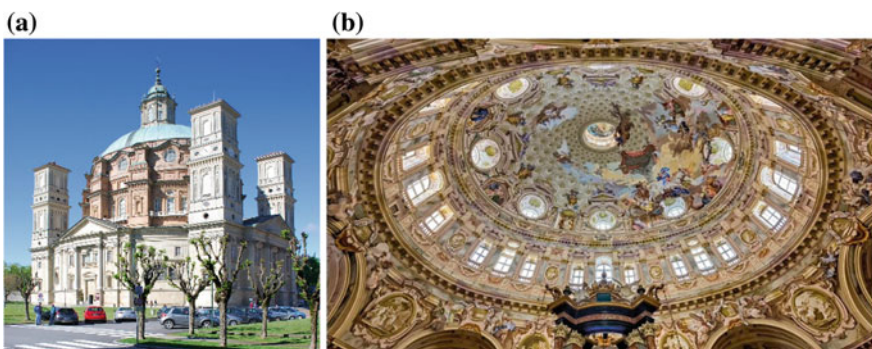


Fig. 3.13 **a** The Sanctuary of Vicoforte, external view; **b** the oval dome of the Sanctuary, internal view

itoring system underwent several upgrading, until the last one in 2004 when the acquisition procedure was automatized. This static monitoring system consists in 133 instruments that are especially located on the dome-drum system. Sensors can be subdivided into two main groups. The first group for the measurement of strains, stresses, and cracks, includes: 12 crack-meters to check the evolution of the cracks; 20 horizontal pressure cells to define the stress in the dome and in the eight pillars; 1 vertical pressure cell near the top of the dome above the main meridian crack (northern side) to determinate the circumferential compression stress; 56 load cells installed on each tie-bars to control its load condition; 2 orthogonal wire gauges measuring the main axes of the dome at its impost to assess the building overall geometry; 12 nails for additional manual measurements of convergence.

The second one for the measurement of the environmental conditions includes: 25 temperature sensors; 3 piezometric electric cells; 1 hydrometer. Recently, data acquired from ten years of monitoring activities (November 2004–November 2014) have been analysed [101]. The aim of these analyses was to check the damage state of the building and to verify the effectiveness of the 1987 strengthening system. From the analysis of the crack openings, ten years of monitoring data show the seasonal influence of the temperature on the structural behaviour of the Sanctuary and the stability of the displacement, demonstrating the efficacy of the tie-bar system.

However, the static monitoring system only provides local information about the health state of the Sanctuary. Consequently, a permanent dynamic monitoring system, designed through a model-based optimal sensor placement procedure [102], was installed in December 2015 to investigate the global phenomena affecting the structure (Fig. 3.14). The positions of the 12 mono-axial piezoelectric accelerometers (PCB Piezotronic, model 393B12, seismic, high sensitivity, ceramic shear ICP® accel., 10 V/g, 0.15–1 k Hz, Resonant Frequency $\geq 10,000$ Hz, Overload Limit ± 5000 g pk, Temperature Range -50 to $+180$ °F) were defined through optimal sensor placement techniques. As shown in Fig. 3.14, three orthogonal accelerometers are located at the base of the crypt to record the ground accelerations (Sag_1, Sag_2, Sag_3).

A set of nine accelerometers are located at different levels of the lantern-dome-drum area, along longitudinal and transverse directions. In more details: (i) two accelerometers are at the base of the dome at 30 m height (T_NOvest_1; T_SOvest_2); (ii) three sensors are on the dome at 45 m height (CB_SOvest_4, CB_SOvest_5, CB_NOvest_6); (iii) one vertical accelerometer is located at the base of the lantern at 50 m height (CA_NOvest_3); and (iv) the last three accelerometers are located at about middle height of the lantern (CB_Ovest_2, C_Nord_0, C_Nord_1).

The acquisition system is designed as a master/slave scheme (see Fig. 3.14) to limit the distortion due to cable length that becomes significant over 50 m length. The data acquired by the accelerometers in the crypt are transmitted to the slave unit, and then to the master unit; the data recorded by all the other instruments converge directly to the master unit. A GPS receiver is used to synchronize the time of all the instruments. The acquired data are transmitted to the Earthquake Engineering and Dynamics lab of the Politecnico di Torino and to OSS [50].

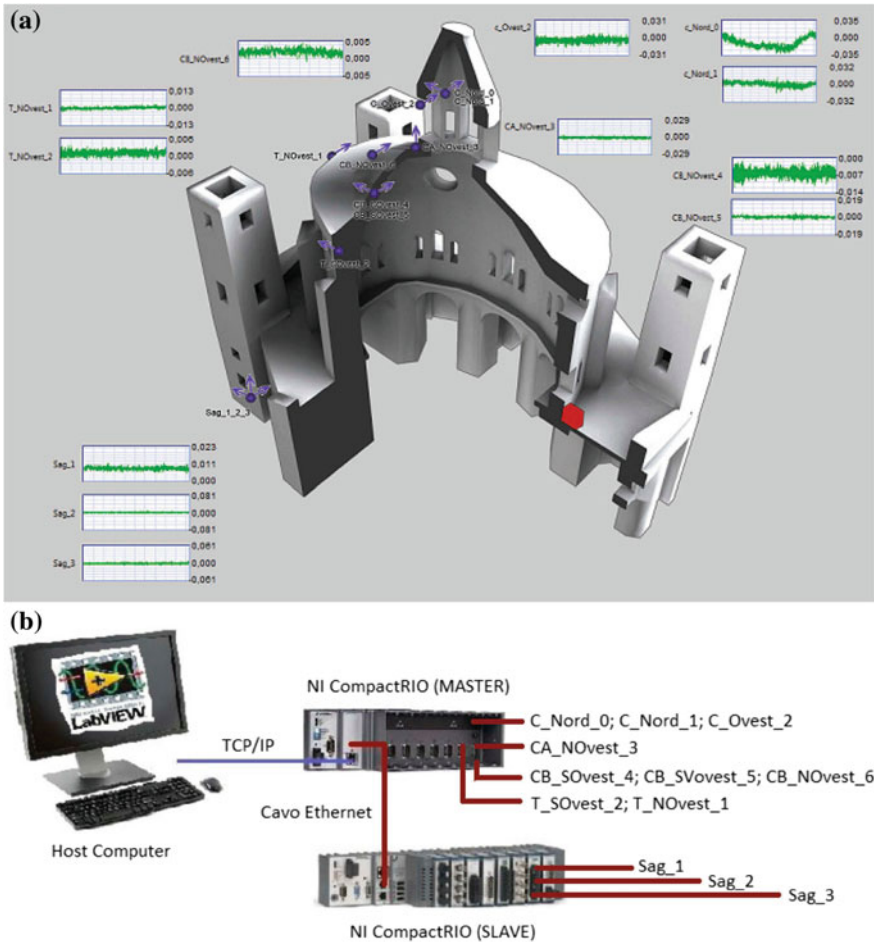


Fig. 3.14 Design of the data acquisition system: **a** sensors and **b** master/slave system

The acquisition system was set to record data according to two criteria: (i) a time criterion and (ii) a threshold criterion. In details, the first criterion implies to record data for 20 min every hour, also in order to limit data storage, whereas the second criterion entails to record the accelerations when the ground horizontal acceleration exceeds a pre-set value (acceleration measured by sensors Sag_2 and Sag_3). This value is set in accordance with the seismic hazard of the area defined by the Italian regulations. More specifically, the pre-set value is 0.042 g, that equals the PGA related with the Damage Limit State and a return period of 50 years. The aim of this last criterion is to record the dynamic response of the Sanctuary during seismic and other dynamic events.

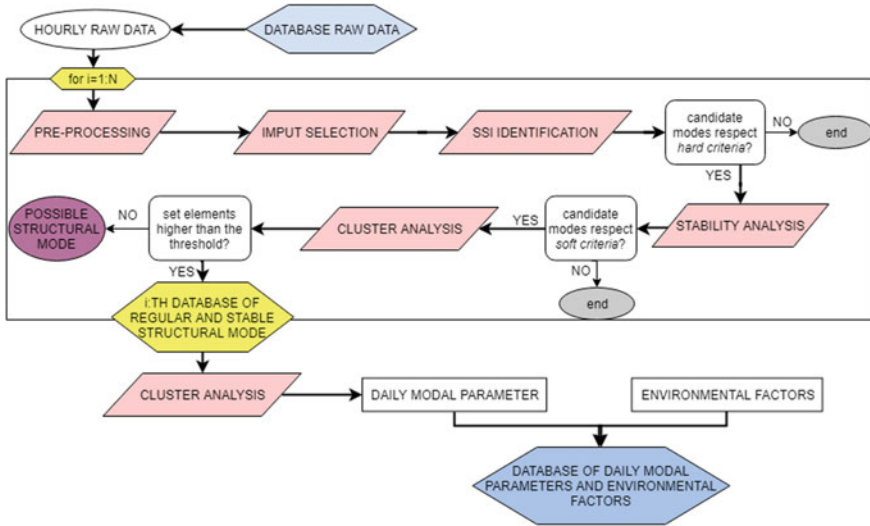


Fig. 3.15 Flowchart of the automatic identification protocol code for the Sanctuary of Vicoforte

The data recorded by the dynamic monitoring system are automatically processed to estimate the main frequencies and modal shapes of the Sanctuary. The code implemented in Matlab® was updated to give the same results of the identification procedure that is performed manually by an expert operator. The flowchart of the Matlab® code is shown in Fig. 3.15 [103], where N is the number of records measured during a single day. In automatic identification procedures, a cluster analysis is used to group the possible physical modes into homogeneous sets representing the same physical mode.

It is worth specifying that signals acquired during earthquakes might be advantageously treated by using the seismic input measured at the foundation, possibly relying on input-output identification procedures. An extended review of the theoretical principles of SSI and its application to support-excited structures has recently been proposed by [104].

The systematic dynamic and seismic monitoring of the lantern-dome-drum system of the Sanctuary started in December 2016 [103]. Some sample data limited to the first two translational modes are reported in Fig. 3.16, together with environmental data [105].

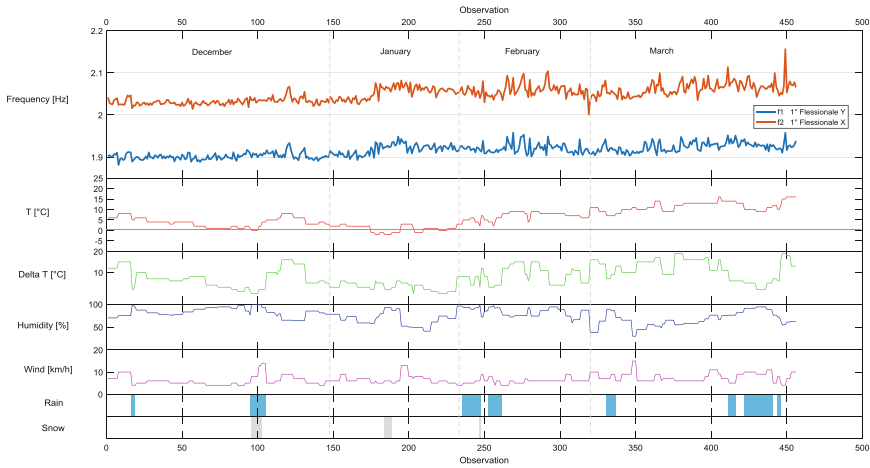


Fig. 3.16 First two frequencies, temperature, ΔT , humidity, wind, rain and snow (from the top to the bottom)

References

1. ICOMOS (2003) Principles for the analysis, conservation and structural restoration of architectural heritage
2. Lourenço P (2006) Recommendations for restoration of ancient buildings and the survival of a masonry chimney. *Constr Build Mater* 20(4):239–251
3. Moro L (2007) Guidelines for evaluation and mitigation of seismic-risk to cultural heritage. Gangemi Editore, Rome (Italy)
4. Ceravolo R, Pistone G, Zanotti Fragonara L, Massetto S, Abbiati G (2016) Vibration-based monitoring and diagnosis of cultural heritage: a methodological discussion in three examples. *Int J Archit Herit* 10(4):375–395
5. Lorenzoni F, Casarin F, Caldon M, Islamia K, Modena C (2016) Uncertainty quantification in structural health monitoring: applications on cultural heritage buildings. *Mech Syst Signal Process* 66–67:268–281
6. Consiglio superiore dei lavori pubblici (2011) Linee Guida per la valutazione e riduzione del rischio sismico del patrimonio culturale - allineamento alle nuove Norme tecniche per le costruzioni
7. De Stefano A, Ceravolo R (2007) Assessing the health state of ancient structures: the role of vibrational tests. *J Intell Mater Syst Struct* 18(8):793–807
8. Bonato P, Ceravolo R, De Stefano A, Molinari F (2000) Cross time-frequency techniques for the identification of masonry buildings. *Mech Syst Signal Process* 14:91–109
9. Bennati S, Nardini L, Salvatore W (2005) Dynamic behavior of a medieval masonry bell tower. II: Experimental measurement and modeling of the tower motion. *J Struct Eng* 131(11):1656–1664
10. Júlio E, Rebelo C, Dias-da-Costa D (2008) Structural assessment of the tower of the University of Coimbra by modal identification. *Eng Struct* 30:3468–3477
11. Bani-Hani K, Zibdeh H, Hamdaoui K (2008) Health monitoring of a historical monument in Jordan based on ambient vibration test. *Smart Struct Syst* 4(2):195–208
12. Bayraktar A, Türker T, Sevim B, Ahmet A, Yildirim F (2009) Modal parameter identification of Hagia Sofia bell-tower via ambient vibration test. *J Nondestr Eval* 28:37–47

13. Lancellotta R, Sabia D (2015) Identification technique for soil-structure analysis of the Ghirlandina Tower. *Int J Archit Herit* 9(4):391–407
14. Ubertini F, Comanducci G, Cavalagli N (2016) Vibration-based structural health monitoring of a historic bell-tower using output-only measurements and multivariate statistical analysis. *Struct Health Monit* 15:438–457
15. Zanotti Fragonara L, Boscato G, Ceravolo R, Russo S, Ientile S, Pecorelli M, Quattrone A (2016) Dynamic investigation on the Mirandola bell-tower in post-earthquake scenarios. *Bull Earthq Eng*. <https://doi.org/10.1007/s10518-016-9970-z>
16. Bassoli E, Vincenzi L, D'Altri A, de Miranda S, Forghieri M, Castellazzi G (2018) Ambient vibration-based finite element model updating of an earthquake-damaged masonry tower. *Struct Control Health Monit*. <https://doi.org/10.1002/stc.2150>
17. Ivorra S, Pallarés F (2006) Dynamic investigation on a masonry bell tower. *Eng Struct* 25(5):660–667
18. Casciati S, Al-Saleh R (2010) Dynamic behavior of a masonry civic belfry under operational conditions. *Acta Mech* 215:211–224
19. Ruocci G, Ceravolo R, De Stefano A (2009) Modal identification of an experimental model of masonry arch bridge. *Key Eng Mater* 413–414:707–714
20. Ramos LF, De Roeck G, Lourenco PB, Campos-Costa A (2010) Damage identification on arched masonry structures using ambient and random impact vibrations. *Eng Struct* 32(1):146–162
21. Turek M, Ventura C (2002) Dynamic evaluation of a 17th century church. In: *Proceedings, annual conference—Canadian society for civil engineering*
22. De Matteis G, Mazzolani F (2010) The Fossanova Church: seismic vulnerability assessment by numeric and physical testing. *Int J Archit Herit* 4(2):222–245
23. Casarin F, Lorenzoni F, Islami K, Modena C (2011) Dynamic identification and monitoring of the churches of St. Biagio and St. Giuseppe in L'Aquila. In: *Proceedings of EVACES 2011, October 3–5, Varenna, Italy*
24. Pau A, Vestroni F (2013) Vibration assessment and structural monitoring of the Basilica of Maxentius in Rome. *Mech Syst Signal Process* 41(1):454–466
25. Pachón PCV, Cámara M, Pinto F (2016) Control of structural intervention by using operational modal analysis. San Juan de los Caballeros church (Cádiz, Spain). In: *Proceedings of the 10th international conference on structural analysis of historical constructions, SAHC 2016*, pp 759–764
26. Elyamani A, Caselles O, Roca P, Clapes J (2017) Dynamic investigation of a large historical cathedral. *Struct Control Health Monit* 24(3)
27. Compan V, Pachón P, Cámara M (2017) Ambient vibration testing and dynamic identification of a historical building. Basilica of the Fourteen Holy Helpers (Germany). *Proc Eng*
28. Meli R, Sánchez-Ramírez R (2007) Criteria and experiences on structural rehabilitation of stone masonry buildings in Mexico City. *Int J Archit Herit*, 3–28
29. Pau A, Vestroni F (2008) Vibration analysis and dynamic characterization of the Colosseum. *Struct Control Health Monit* 15(8):1105–1121
30. Chiorino M, Ceravolo R, Spadafora A, Zanotti Fragonara L, Abbiati G (2011) Dynamic characterization of complex masonry structures: the sanctuary of vicoforte. *Int J Archit Herit* 5(3):296–314
31. Boscato G, Rocchi D, Russo S (2012) Anime Sante Church's Dome after 2009 L'Aquila earthquake: monitoring and strengthening approaches. *Adv Mater Res* 446–449:3467–3485
32. Russo S (2012) On the monitoring of historic Anime Sante church damaged by earthquake in L'Aquila. *Struct Control Health Monit* 20(9):1226–1239
33. McCullough D (1972) *The great bridge: the epic story of the building of the Brooklyn Bridge*
34. Russo S (2016) Integrated assessment of monumental structures through ambient vibrations and ND tests: the case of Rialto Bridge. *J Cult Herit* 19:402–414
35. Pérez-Gracia V, Di Capua D, Caselles O, Rial F, Lorenzo H, González-Drigo R, Armesto J (2011) Characterization of a Romanesque Bridge in Galicia (Spain). *Int J Archit Herit* 5(3):251–263

36. Bertolesi E, Milani G, Lopane F, Acito M (2017) Augustus Bridge in Narni (Italy): seismic vulnerability assessment of the still standing part, possible causes of collapse, and importance of the Roman concrete infill in the seismic-resistant behavior. *Int J Archit Herit* 11(5):717–746
37. Pepi C, Gioffrè M, Comanducci G, Cavalagli N, Bonaca A, Ubertini F (2017) Dynamic characterization of a severely damaged historic masonry bridge. *Proc Eng* 199:3398–3403
38. De Canio G, Mongelli M, Roselli I, Tati A, Addessi D, Nocera M, Liberatore D (2016) Numerical and operational modal analyses of the “Ponte delle Torri”, Spoleto, Italy. In: *Proceedings of the 10th international conference on structural analysis of historical constructions, SAHC 2016*, pp 752–758
39. Olmos B, Jara J, Martínez G, López J (2017) System identification of history Mexican masonry bridges. *Proc Eng* 199:2220–2225
40. Altunišika A, Bayraktar A, Sevima B, Birincia F (2011) Vibration-based operational modal analysis of the mikron historic arch bridge after restoration. *Civ Eng Environ Syst* 28(3):247–259
41. Ataei S, Miri A, Jahangiri M (2017) Assessment of load carrying capacity enhancement of an open spandrel masonry arch bridge by dynamic load testing. *Int J Archit Herit* 11(8):1086–1100
42. Cabboi A, Magalhães F, Gentile C, Cunha Á (2017) Automated modal identification and tracking: application to an iron arch bridge. *Struct Control Health Monit* 24(1)
43. García-Macías E, Castro-Triguero R, Gallego R, Carretero J (2015) Ambient vibration testing of historic steel-composite bridge, the E. Torroja Bridge, for structural identification and finite element model updating. In: *Dynamics of civil structures, 2: proceedings of 33rd IMAC*, pp 147–155
44. Marques F, Moutinho C, Magalhães F, Caetano E, Cunha Á (2014) Analysis of dynamic and fatigue effects in an old metallic riveted bridge. *J Constr Steel Res* 99:85–101
45. Gentile C, Saisi A (2010) Dynamic assessment of the iron bridge at Paderno d’Adda (1889). *Adv Mater Res*, 709–714
46. Gentile C, Gallino N (2007) Operational modal analysis and assessment of an historic RC arch bridge. *WIT Trans Built Environ* 95:95525–95534
47. Ferrari R, Froio D, Chatzi E, Gentile C, Pioldi F, Rizzi E (2015) Experimental and numerical investigations for the structural characterization of a historic RC arch bridge. In: *COMPADYN 2015—5th ECCOMAS thematic conference on computational methods in structural dynamics and earthquake engineering*
48. Van Bogaert P (2017) Refurbishment of a heritage concrete tied arch bridge across river Lys. In: *High tech concrete: where technology and engineering meet—proceedings of the 2017 fib symposium*. <https://doi.org/10.1007/978-3-319-59471-2>
49. Ceravolo R, Matta E, Quattrone A, Zanotti Fragonara L (2017) Amplitude dependence of equivalent modal parameters in monitored buildings during earthquake swarms. *Earthq Eng Struct Dyn* 46(14):2399–2417
50. Dolce M, Nicoletti M, De Sortis A, Marchesini S, Spina D, Talanas F (2017) Osservatorio sismico delle strutture: the Italian structural seismic monitoring network. *Bull Earthq Eng* 15(2):621–641
51. Celebi M (2007) On the variation of fundamental frequency (period) of an undamaged building—a continuing discussion. Porto, Portugal
52. Coisson E, Ottoni F (2013) Monitoring historical structures, from their past to their future
53. Saisi A, Gentile C, Ruccolo A (2018) Continuous monitoring of a challenging heritage tower in Monza, Italy. *J Civ Struct Health Monit* 8(1):77–90
54. Ottoni F, Blasi C (2015) Results of a 60-year monitoring system for Santa Maria del Fiore Dome in Florence. *Int J Archit Herit Conserv Anal Restor* 9(1):7–24. <https://doi.org/10.1080/15583058.2013.815291>
55. Nelli GB (1753) *Discorsi di Architettura del Senator Giovan Battista Nelli e due ragionamenti sopra le cupole di Alessandro Cecchini*, Florence, Italy: Per Gli Eredi Paperini
56. Ottoni F, Coisson E, Blasi C (2010) The crack pattern in Brunelleschi’s Dome in Florence: damage evolution from historical to modern monitoring system analysis. *Adv Mater Res* 133–134:53–64

57. Bartoli G, Betti M, Borri C (2015) Numerical modelling of the structural behavior of Brunelleschi's Dome of Santa Maria del Fiore. *Int J Archit Herit* 9(4):408–429. <https://doi.org/10.1080/15583058.2013.797038>
58. Castoldi A, Anesa F, Imperato F, Gamba F (1989) “Cattedrale di S. Maria del Fiore, Firenze: Sistema di monitoraggio strutturale della Cupola e del suo basamento,” *I Quaderni dell'ISMES*, Bergamo, Italy, vol 262
59. Bartoli G, Chiarugi A, Gusella V (1996) Monitoring systems on historic buildings: The Brunelleschi Dome. *J Struct Eng* 122(6):663–673
60. Lorenzoni F, Casarin F, Modena C, Caldon M (2013) Structural health monitoring of the Roman Arena of Verona, Italy. *J Civ Struct Health Monit* 3(4):227–246
61. Ceravolo R, Pescatore M, De Stefano A (2009) Symptom-based reliability and generalized repairing cost in monitored bridges. *Reliab Eng Syst Saf* 94(8):1331–1339
62. Sasaki J, Koizumi K, Ogura D, Ishizaki T, Hidaka K (2013) Research project on the conservation of Hagia Sophia, Istanbul—the results of environmental monitoring. In: *Built heritage 2013 monitoring conservation management*, Milan-Italy, pp 1084–1091
63. Erdik M, Durukal E, Yiizigullii O, Beyen K, Kadakal U (1993) Strong-motion instrumentation of Aya Sofya and the analysis of response to an earthquake of 4.8 magnitude. *WIT Trans Built Environ* 3:899–914
64. Çakmak A, Moropoulou A, Mullen C (1995) Interdisciplinary study of dynamic behavior and earthquake response of Hagia Sophia. *Soil Dyn Earthq Eng* 14(2):125–133
65. Aoki T, Kato S, Ishikawa K, Hidaka K, Yorulmaz M, Cili F (1997) Principle of structural restoration for Hagia Sophia Dome. *Int Ser Adv Archit* 3:467–476
66. Di Giulio G, Vassallo M, Boscato G, Dal Cin A, Russo S (2014) Seismic monitoring by piezoelectric accelerometers of a damaged historical monument in downtown L'Aquila. *Ann Geophys* 57:1–15
67. Ubertini F, Cavalagli N, Kita A, Comanducci G (2018) Assessment of a monumental masonry bell-tower after 2016 Central Italy seismic sequence by long-term SHM (2017). *Bull Earthq Eng* 16(2):775–801
68. Masciotta M, Ramos L, Lourenço P (2017) The importance of structural monitoring as a diagnosis and control tool in the restoration process of heritage structures: A case study in Portugal. *J Cult Herit* 27:36–47
69. Garziera R, Collini L (2010) A non-destructive technique for the health monitoring of tie-rods in ancient buildings. In *Dynamics of civil structures*, vol 4, conference proceedings of the society for experimental mechanics series 13, pp 7–13
70. Boscato G, Russo S, Ceravolo R, Zanotti Fragonara L (2015) Global sensitivity-based model updating for heritage structures. *Comput Aided Civ Infrastruct Eng* 30(8):620–635
71. De Stefano A, Matta E, Clemente P (2016) Structural health monitoring of historical heritage in Italy: some relevant experiences. *J Civil Struct Health Monit* 6(1):83–106
72. Farrar C, Worden K (2007) An introduction to structural health monitoring. *Phil Trans R Soc A* 15(265):303–315
73. Lenticchia E, Ceravolo R, Chiorino C (2017) Damage scenario-driven strategies for the seismic monitoring of XX century spatial structures with application to Pier Luigi Nervi's Turin Exhibition Centre. *Eng Struct* 137:256–267
74. Clinton J (2006) The observed wander of the natural frequencies in a structure. *Bull Seismol Soc Am* 96:237–257
75. Todorovska M (2009) Soil–structure system identification of Millikan library North–South response during four earthquakes (1970–2002): what caused the observed wandering of the system frequencies? *Bull Seismol Soc Am* 99(2A):626–635
76. Hong A, Betti R, Lin C (2009) Identification of dynamic models of a building structure using multiple earthquake records. *Struct Control Health Monit* 16:178–199
77. Bodin P, Vidale J, Walsh T, Cakir R, Celebi M (2012) Transient and long-term changes in seismic response of the Natural Resource Building, Olympia, Washington, due to earthquake shaking. *J Earthq Eng* 16:607–622

78. Van Overschee P, De Moor B (1996) Subspace identification for linear systems: theory and implementation—applications. Kluwer Academic Press Dordrecht
79. Larimore W (1990) Canonical variate analysis. In: Proceedings of the 29th IEEE conference on decision and control, Honolulu, Hawaii
80. Welch P (1967) The use of fast fourier transform for the estimation of power spectra: a method based on time averaging over short modified periodograms. *IEEE Trans Audio Electro-Acoustic* 15(2):70–73
81. Allemang R (2003) The modal assurance criterion—twenty years of use and abuse. *Sound Vib* 37(8):14–21
82. Carden E, Brownjohn J (2008) Fuzzy clustering of stability diagrams for vibration-based structural health monitoring. *Comput Aided Civ Infrastruct Eng* 23(5):360–372
83. Merce R, Doz G, Vital de Brito J, Macdonald J, Friswell M (2007) Finite element model updating of a suspension bridge. In: Design and optimization symposium, Florida, USA
84. Modica M, Santarella, F (2015) Paraboloidi. Un patrimonio dimenticato dell'architettura moderna, EDI-FIR, Collana Spazi di Architettura
85. Santarella L (1926) Il cemento armato nelle costruzioni civili e industriali, Hoepli, Milano
86. Stella F (2011) Nervi per l'industria. I magazzini del sale di Tortona, Lulu
87. Invernizzi S, Spanò A, Chiabrando F (2018) Survey, assessment and conservation of post-industrial cultural heritage: the case of the thin concrete vault in Casale, Italy. In: Structural analysis of historical constructions
88. Bertolini C, Chiabrando F, Invernizzi S, Marzi T, Spanò A (2014) The thin concrete vault of the Paraboloidi of Casale, Italy. Innovative methodologies for the survey, structural assessment and conservation interventions. In: Structural Faults & Repair, London, UK
89. Lenticchia E, Ceravolo R, Antonaci P (2018) Sensor placement strategies for the seismic monitoring of complex vaulted structures of the modern architectural heritage. *Shock Vib*, art. no. 3739690. <https://doi.org/10.1155/2018/3739690>
90. Foti D, Chorro S, Sabbà M (2012) Dynamic investigation of an ancient masonry Bell Tower with operational modal analysis a non-destructive experimental technique to obtain the dynamic characteristics of a structure. *Open Construct Build Technol J*, 384–391. <https://doi.org/10.2174/18748368012>
91. Ramos L, Marques L, Lourenço P, De Roeck G, Campos-Costa A, Roque J (2010) Monitoring historical masonry structures with operational modal analysis: two case studies. *Mech Syst Signal Process* 24:1291–1305. <https://doi.org/10.1016/j.ymssp.2010.01.011>
92. Russo G, Bergamo O, Damiani L, Lugato D (2010) Experimental analysis of the “Saint Andrea” Masonry Bell Tower in Venice. A new method for the determination of “Tower Global Young’s Modulus E”. *Eng Struct* 32:353–360. <https://doi.org/10.1016/j.engstruct.2009.08.002>
93. Gentile C, Saisi A, Cabboi A (2012) One-year dynamic monitoring of a masonry tower. In: Structural analysis of historical constructions
94. Diaferio M, Foti D, Giannocaro N (2014) Non-destructive characterization and identification of the modal parameters of an old masonry tower. In IEEE workshop on environmental, energy and structural monitoring systems at: Naples, art.n. 6923265, pp 57–62
95. Bassoli E, Vincenzi L, Bovo M, Mazzotti C (2015) Dynamic identification of an ancient masonry bell tower using a MEMS-based acquisition system. In: 2015 IEEE workshop on environmental, energy and structural monitoring systems (EESMS), pp 226–231
96. Pieraccini M, Dei D, Betti M, Bartoli G, Tucci G, Guardini N (2014) Dynamic identification of historic masonry towers through an expeditious and no-contact approach: application to the “Torre del Mangia” in Siena (Italy). *J Cult Herit* 15:275–282
97. Sabia D, Aoki T, Cosentini R, Lancellotta R (2015) Model updating to forecast the dynamic behavior of the Ghirlandina Tower in Modena, Italy. *J Earthq Eng* 19:1–24. <https://doi.org/10.1080/13632469.2014.962668>
98. Chiorino M, Spadafora A, Calderini C, Lagomarsino S (2008) Modeling strategies for the world’s largest elliptical dome at Vicoforte. *Int J Archit Herit* 2(3):274–303

99. Garro M (1962) Opere di consolidamento e restauro. Relazione riassuntiva, Vicoforte di Mondovì
100. Scandella L, Lai C, Spallarossa D, Corigliano M (2011) Ground Shaking scenarios at the town of Vicoforte, Italy. *Soil Dyn Earthq Eng* 21:757–772
101. Ceravolo R, De Marinis A, Pecorelli M, Zanotti Fragonara L (2017) Monitoring of masonry historical constructions: 10 years of static monitoring of the world's largest oval dome. *Struct Control Health Monit* 24(10)
102. Ceravolo R, Pecorelli ML, De Lucia G, Zanotti Fragonara L (2015) Monitoring of historical buildings: project of a dynamic monitoring system for the world's largest elliptical dome. In 2015 IEEE workshop on environmental, energy, and structural monitoring systems (EESMS) proceedings
103. Pecorelli ML, Ceravolo R, Epicoco R (2018) An automatic modal identification procedure for the permanent dynamic monitoring of the sanctuary of Vicoforte. *Int J Archit Herit*. <https://doi.org/10.1080/15583058.2018.155>
104. Kim J, Lynch J (2012) Subspace system identification of support-excited structures—Part I: Theory and black-box system identification. *Earthq Eng Struct Dyn* 41:2235–2251
105. Coletta G, Miraglia G, Pecorelli M, Ceravolo R, Cross E, Surace C, Worden K (2018) Use of the cointegration strategies to remove environmental effects from data acquired on historical buildings. *Eng Struct* (in press)

Chapter 4

Seismic and Structural Health Monitoring of Dams in Portugal



Sérgio Oliveira and André Alegre

Abstract This chapter is focused on the Portuguese experience on the development and exploration of systems for continuously monitoring dam vibrations, using accelerometers. The pioneer system for seismic and structural health monitoring (SSHM) installed in Cabril dam (the highest Portuguese arch dam: 132 m high) is described in detail. The design of this system was the result of a long-term LNEC research program, still ongoing. These monitoring systems should include software developed to automatically perform the analysis of collected data, including the automatic comparison with numerical results from 3DFE models. In view of the good results obtained with the system in operation in Cabril dam since 2008, similar systems have been installed in other large dams in Portugal, particularly in recently built dams. Finally, Baixo Sabor dam is presented as an example of a new Portuguese dam with a complete SSHM system, in operation since 2015. The main experimental results obtained for both dams are shown, namely the evolution of natural frequencies over time, mode shapes and the measured seismic response to earthquake events.

Keywords Modal identification · Concrete dams · Ambient and seismic vibrations

4.1 Introduction

In Portugal, the health monitoring of large dams using systems for continuously measuring the structural vibrations due to ambient excitation and seismic events began in 2008 when LNEC and EDP installed a pioneer system to monitor the dynamic behavior of Cabril dam. This system, designed for seismic and structural health monitoring (SSHM), was the result of a long-term LNEC research program, supported by the Portuguese Company of Electricity (EDP) and Portuguese Foundation for Science and Technology (FCT). The scope of the research project is described in Oliveira [1].

S. Oliveira (✉) · A. Alegre
Department of Concrete Dams, Laboratório Nacional de Engenharia Civil,
Av. do Brasil 101, 1700-066 Lisbon, Portugal
e-mail: soliveira@lnec.pt

© Springer Nature Switzerland AG 2019
M. P. Limongelli and M. Çelebi (eds.), *Seismic Structural Health Monitoring*, Springer
Tracts in Civil Engineering, https://doi.org/10.1007/978-3-030-13976-6_4

As part of the monitoring system, LNEC developed software to automatically perform the analysis of the measured acceleration time series, every hour, in view of the detection of seismic events and identification of the main modal parameters [2]. The time evolution of the identified main natural frequencies, clearly influenced by reservoir water level variations, is automatically compared with the natural frequencies computed numerically using a 3DFE model of the whole dam-reservoir-foundation system, considering the actual recorded water levels [3].

Following the success of the SSHM system of Cabril dam [3–6], EDP group decided to install similar complete systems on other concrete dams, namely in Baixo Sabor dam (2015) [7] and Foz Tua dam (2017). The locations of these dams are shown in Fig. 4.1. Other systems for measuring seismic vibrations in dams are also installed in Alqueva dam, Alto Ceira II dam and Ribeiradio dam.

4.2 Systems for Continuously Monitoring Vibrations in Large Dams

The systems for continuous vibrations monitoring in dams are useful for the safety control studies, mainly because the vibrations of a damaged structure are different from the vibrations of the same structure if it was intact, as shown schematically in Fig. 4.2. So, from the measured dynamic response we can get information about the dynamic parameters and evaluate the structural health [3–6].

The results from the continuous dynamic monitoring systems are essentially used:

- i. to characterize the structural effects under important seismic actions, because eventual induced cracking can be detected through the comparison between the measured dynamic response under ambient excitation, before and after the earthquake;
- ii. to evaluate the influence of deterioration processes (e.g. due to swelling), because an eventual decrease of the global stiffness due to deterioration can be controlled by analyzing the decrease of the natural frequencies over the years (even a small decrease in stiffness, say, of about 1%, can be clearly detected);
- iii. to obtain experimental information about the dynamic response of dam-reservoir-foundation systems during seismic event; this information is very useful for the development and calibration of numerical models used to simulate the seismic response of dams.

4.3 Monitoring and Modelling the Dynamic Behavior of Large Dams

Nowadays, in new large dams, the designers generally propose the installation of systems for continuous monitoring vibrations [8–10]. These monitoring systems

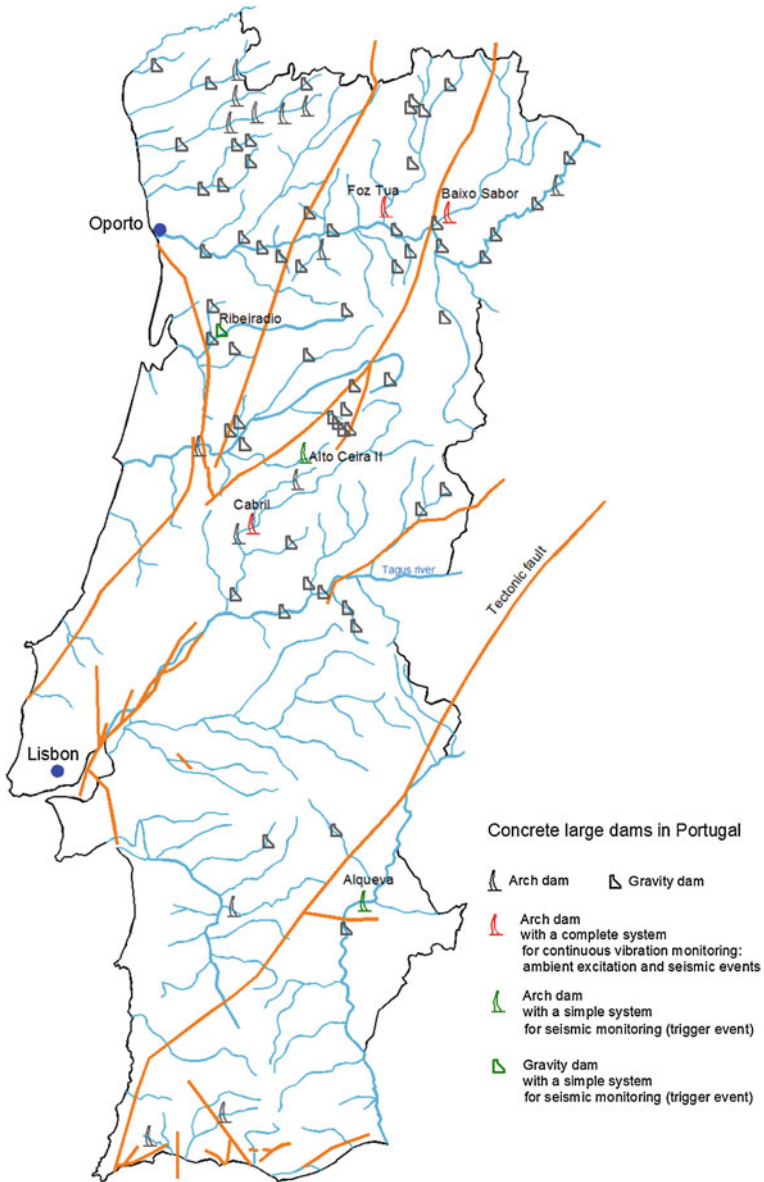


Fig. 4.1 Concrete large dams in Portugal and tectonic faults. Indication of dams with systems for measuring vibrations, under ambient excitation and/or seismic events

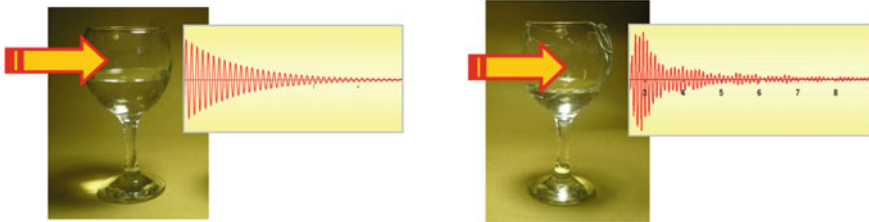


Fig. 4.2 When we measure continuously vibrations in large dams the effect that we want to capture is the same that occurs in a simple glass: if we tap an intact glass, the sound we hear, that is the vibration, is quite different from the sound of a broken glass

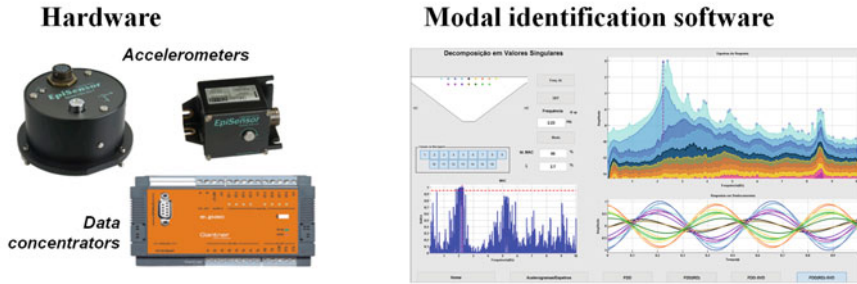
should be prepared for measuring the dynamic response of dams under seismic loading and ambient/operational excitation [2]. It should also be prepared to perform the automatic analysis of collected data and the automatic comparison with numerical data from 3DFE models (Fig. 4.3).

4.4 Hardware and Software Components for Continuous Monitoring Vibrations Systems

A system for continuous monitoring vibrations in large concrete dams includes two types of components: hardware components and software components (Fig. 4.4).

The efficiency of these systems is obviously influenced by the selection of appropriate, high quality hardware components, taking into account the characteristics of the accelerometers and the equipment for digitizing, transmitting and storing data. Nonetheless, said efficiency also depends on the software used for the analysis of collected data [2], namely: software for automatic signal analysis, software for automatic modal identification and software for automatic comparison between measured data or estimated modal parameters and numerical results from finite element models [3].

Monitoring



Modelling

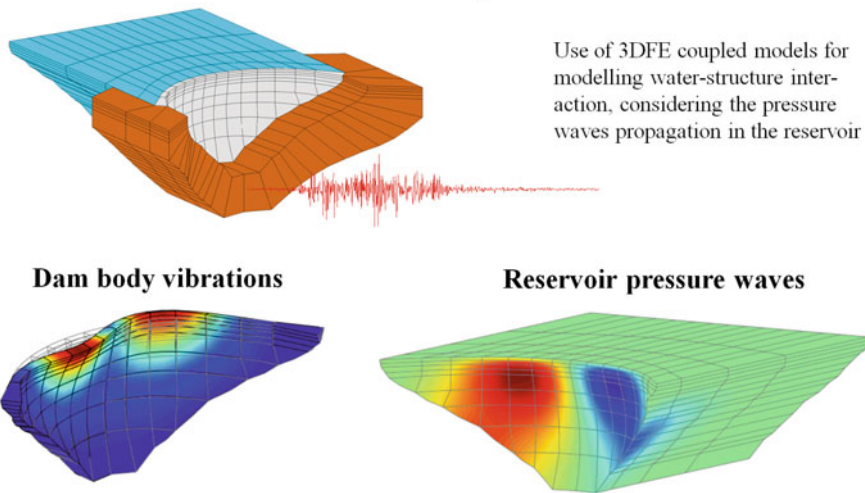


Fig. 4.3 Analysis of the dynamic behavior of large dams. Monitoring and modelling

A system for continuous dynamic monitoring in a large dam should be able

- (i) to automatically estimate, for every hour, the main modal parameters: natural frequencies (as shown in the example of Fig. 4.5, the main natural frequencies of a dam are clearly influenced by the water level), the correspondent mode shapes and modal damping ratios;
- (ii) to automatically gather information about dam deterioration: this information could be extracted through comparison between experimental data and numerical data from reference 3DFE models (Fig. 4.6); as it can be seen in Fig. 4.6a, the natural frequency of the 1st mode increases when the water level in the reservoir falls, and the experimental values identified between 2010 and 2017 are perfectly simulated with the reference numerical model, in which it was assumed

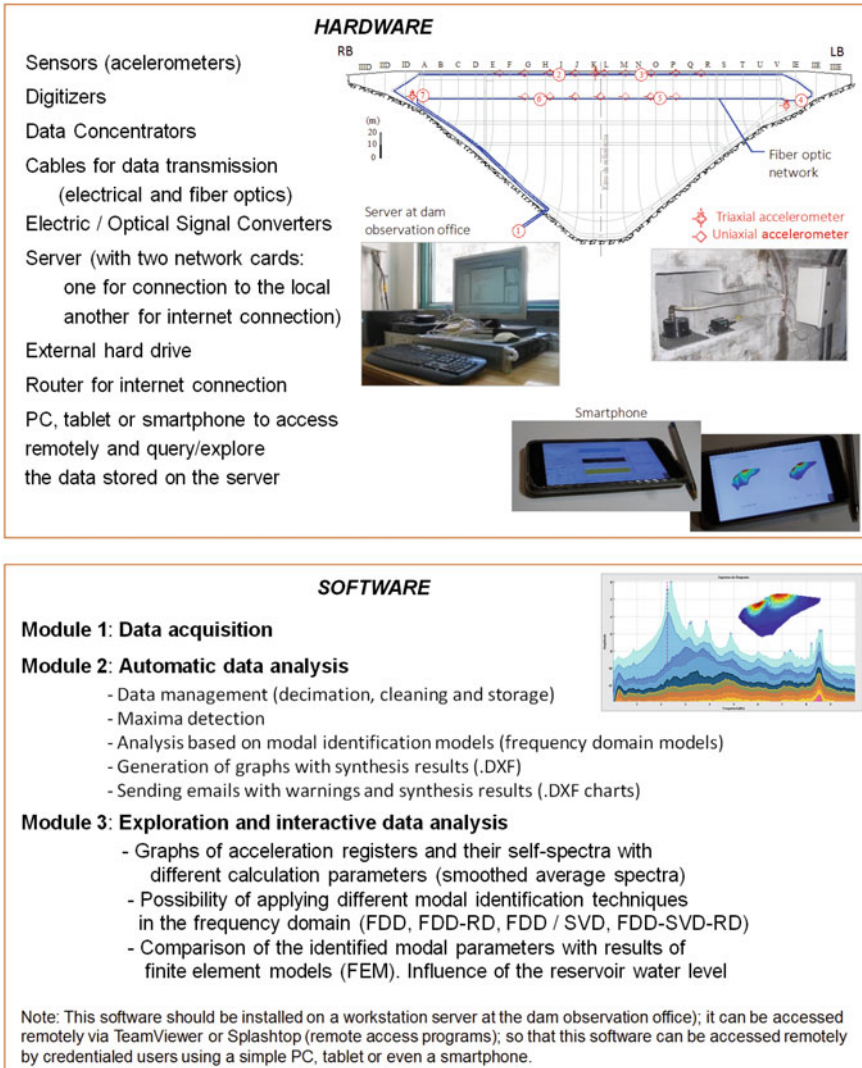


Fig. 4.4 Systems for continuous monitoring vibrations in dams: hardware and software components

a non-damaged elasticity modulus for the concrete, constant over the referred period of about 7 years. The good agreement obtained all over that period, between numerical and experimental values of the 1st natural frequency of the dam, means that the elasticity modulus of the dam concrete has not changed; as shown in Fig. 4.6b, a small decrease in stiffness corresponding, for example, to a damage value of 1% would have been perfectly detected. These results clearly prove the great interest of the continuous monitoring systems installed in large

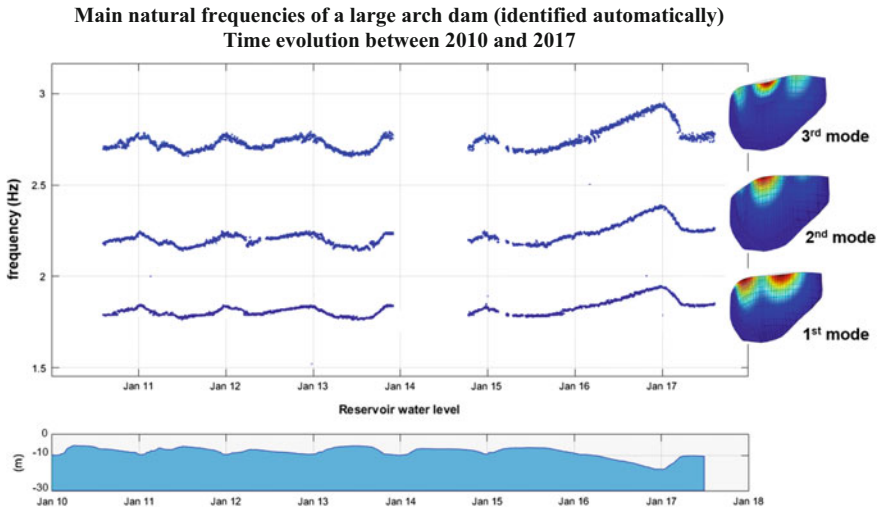


Fig. 4.5 Evolution of the main natural frequencies of a large arch dam (significantly depends on the reservoir water level). Experimental results obtained automatically, between 2010 and 2017, from a system for continuous monitoring vibrations using ten uniaxial accelerometers at the dam crest (for measuring radial accelerations)

dams for the control of eventual progressive deterioration processes associated, for example, with slow swelling processes, or eventual deterioration caused by exceptional events such as strong earthquakes;

- (iii) to automatically identify seismic events and to record the seismic accelerations at the rock mass foundation and at the dam body—for earthquakes of distinct intensity and for different reservoir water levels; using results from the observed behavior under ambient excitation (for several reservoir water levels) and results from the observed behavior under seismic events (for several earthquakes, with different peak accelerations and different frequency contents), the FE models of the system dam reservoir foundation can be calibrated.

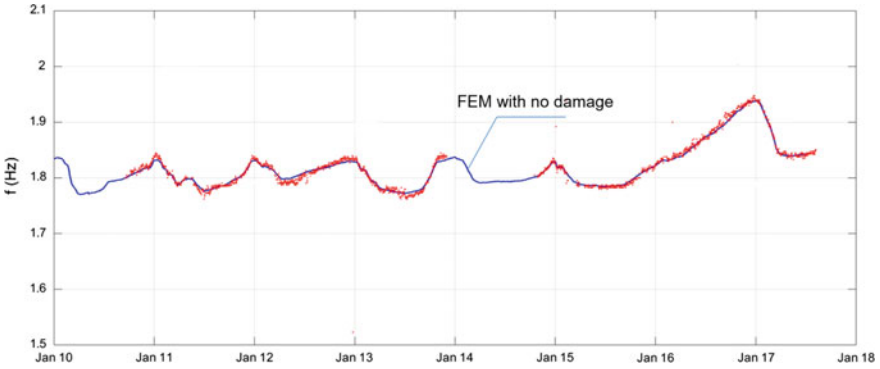
4.5 The Need for Software Development

The main issue on systems for continuously measuring vibrations in dams is related to the fact that the suppliers of equipment for vibration measurement do not provide full solutions that include all the software components required for automatic analysis of the gathered data.

In LNEC, this software to support dynamic monitoring systems is now under development (Fig. 4.7) [2, 3]. The goal is to contribute for the installation of these monitoring systems in the vast majority of large dams, especially in those located on

seismic regions. At LNEC Concrete Dam’s Department, software is being developed to support monitoring systems for dam vibrations control (Fig. 4.7), namely:

- (i) software for automatic modal identification, using the Frequency Domain Decomposition method (FDD) [11, 12] and some sophisticated techniques for automatic identification of the main spectral peaks (Fig. 4.7a);
- (a) Natural frequency of the 1st vibration mode. Comparison between experimental and numerical results from the reference 3DFE model considering no damage (constant elasticity modulus: intact concrete).



- (b) Natural frequency of the 1st vibration mode. Comparison between experimental and numerical results from a 3DFE model considering a linear damage progression from 0 to 3%: $E = E_i (1 - d)$, being $0 < d < 0.03$.

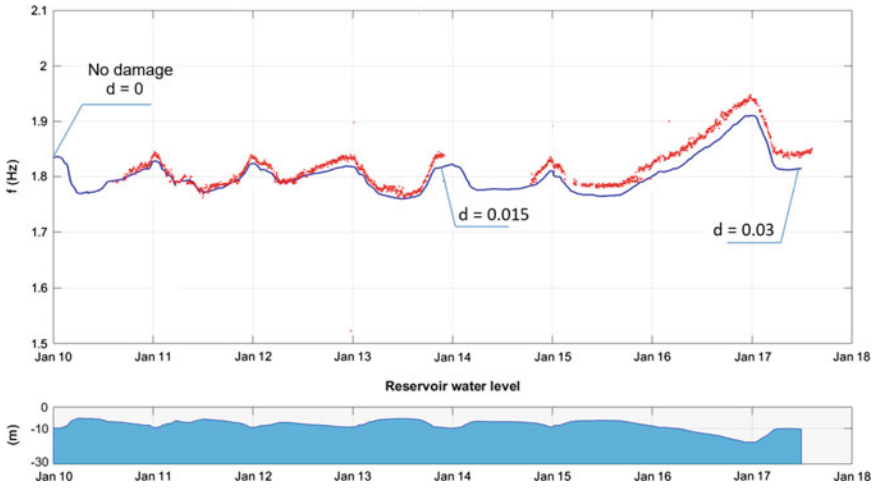
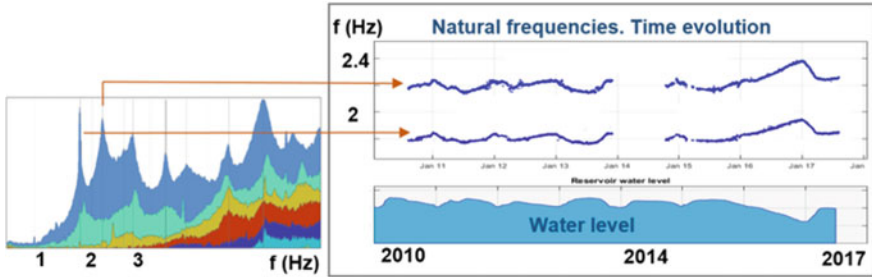


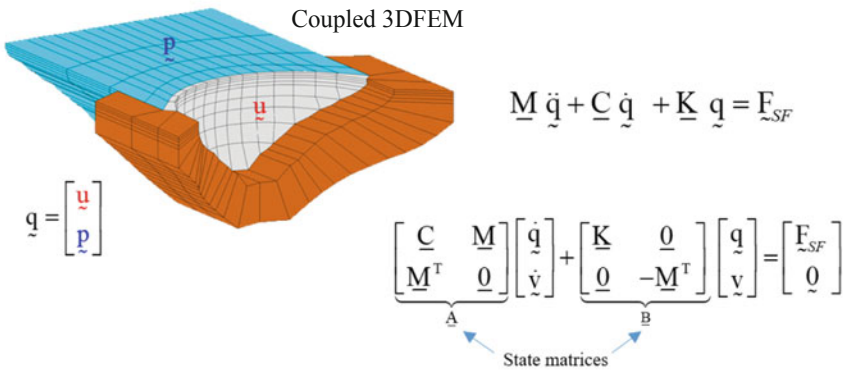
Fig. 4.6 Evolution of the natural frequency of the 1st vibration mode of a large arch dam, between 2010 and 2017

- (ii) software for modelling the dynamic behavior using advanced 3DFE models [13], considering displacements and pressures and an innovative state space formulation solved in modal coordinates using complex global modes of the whole system [14, 15] (Fig. 4.7b); and

(a) Software modules for automatic modal identification, using FDD method



(b) Software modules for modelling the dynamic behaviour using advanced FE models



(c) Software modules for automatic comparison between numerical and experimental

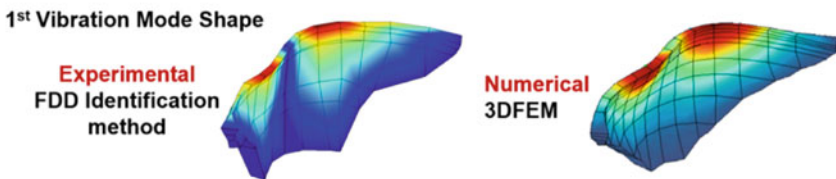


Fig. 4.7 Software development for systems used in continuous monitoring vibrations in dams

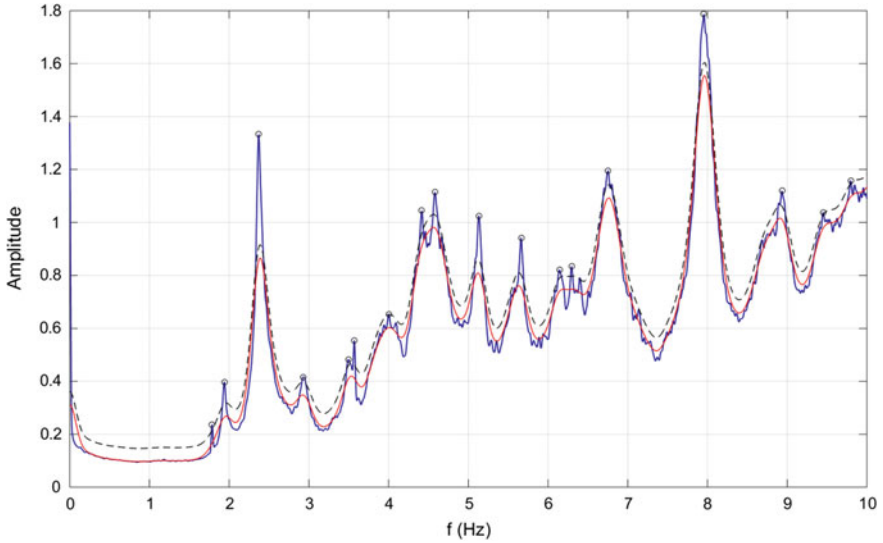


Fig. 4.8 Illustration of the technique used for automatic peak identification: the peaks considered should be above the shifted smoothed spectral line (dashed line) (Color figure online)

- (iii) software for automatic comparison between numerical results from 3DFE models and experimental data from seismic measurements and from modal identification (Fig. 4.7c).

In Fig. 4.8 it is presented the technique used for automatic peak identification. As illustrated, the peaks considered should be above the shifted smoothed spectral line, which is the dashed line (obtained from the smoothed line, in red).

In structural health monitoring of dams, the time evolution graphs of natural frequencies can be used to detect deterioration (induced, for example, by dam swelling).

4.6 Numerical Modelling of Dam-Reservoir-Foundation Systems

The combined use of monitoring systems and numerical models is important for dam safety control [16, 17]. To this end LNEC developed the software DamDySSA2.0 to study the dynamic behavior of dams (Fig. 4.9). This is a 3DFE program for dynamic state space analysis of arch dam-reservoir-foundation systems, based on a 3DFE coupled model that enables to simulate the dynamic dam-reservoir interaction [13], considering linear elastic behavior and generalized damping. The outlined Boundary Values Problem for the discrete coupled system is solved through a FE formulation in displacements (solid) and pressures (fluid), considering the solid-fluid motion coupling at the dam-reservoir interface and the hydrodynamic pressure waves prop-

agation throughout the reservoir, which is a semi-infinite domain terminated by a radiation boundary. The dynamic calculations are performed in time domain based on a novel coupled state space approach with two state matrices using complex modal coordinates [14, 15]. The implemented coupled approach results in the computation of non-stationary vibration modes, which are usually associated to systems with non-proportional damping, as is the case of arch dams, whose dynamic behavior is highly influenced by dynamic water-structure interaction.

4.7 Cabril Dam Seismic and Structural Health Monitoring System

Cabril dam (Fig. 4.10), the highest in Portugal, is located on Zêzere river and has been in operation since 1954. It is a double curvature arch dam, on a granite mass rock foundation, with the particularity of presenting a greater thickness in the crown (see central cantilever in Fig. 4.10). It has 132 m of maximum height above the foundation and a crest length of 290 m.

The central cantilever has a maximum width of 20 m at the base and a minimum width of 4.5 m below the crest. In this dam, a significant horizontal cracking occurred near the crest (between levels 280 and 290 m) during the first filling of the reservoir. Also, a concrete swelling process has been detected since late 90s.

As mentioned previously, in the framework of LNEC research activities regarding monitoring and modelling the dynamic behavior of dams, a dynamic monitoring system (Fig. 4.11) was installed in Cabril dam in 2008.

The outlined configuration for this system was based on experience gathered in LNEC over the years, from both monitoring data and numerical results [18, 19]. The goal was to implement a system with a high dynamic range (Fig. 4.12), capable of a continuous accurate measurement of the dam's response for several dynamic excitations: ambient/operation excitations or earthquakes of various magnitudes. This system was designed to measure accelerations in the upper zone of the dam and near the base, at a sampling rate of 1000 Hz and considering time periods of one hour, and it includes 16 uniaxial and 3 triaxial accelerometers.

The uniaxial accelerometers (measure vibrations in a radial direction) are distributed in the upper part of the dam by two galleries, above and below the cracked zone. As for the triaxial accelerometers, one is located in the central cantilever (upper gallery), while the other two are installed near the insertion of the dam base, in both banks. The accelerometers are connected to a modular system composed by acquisition/digitalization units, which in turn are controlled by 4 data concentrators that receive the recorded data. This data is sent through an optical fiber local network (intranet) to a computer in the observation and control station (OCS), located at the dam power station. In total 25 accelerograms are recorded and stored every hour, continuously. The storage and management of the collected data is carried out at the server located in the OCS using appropriate software developed in LNEC. Regard-

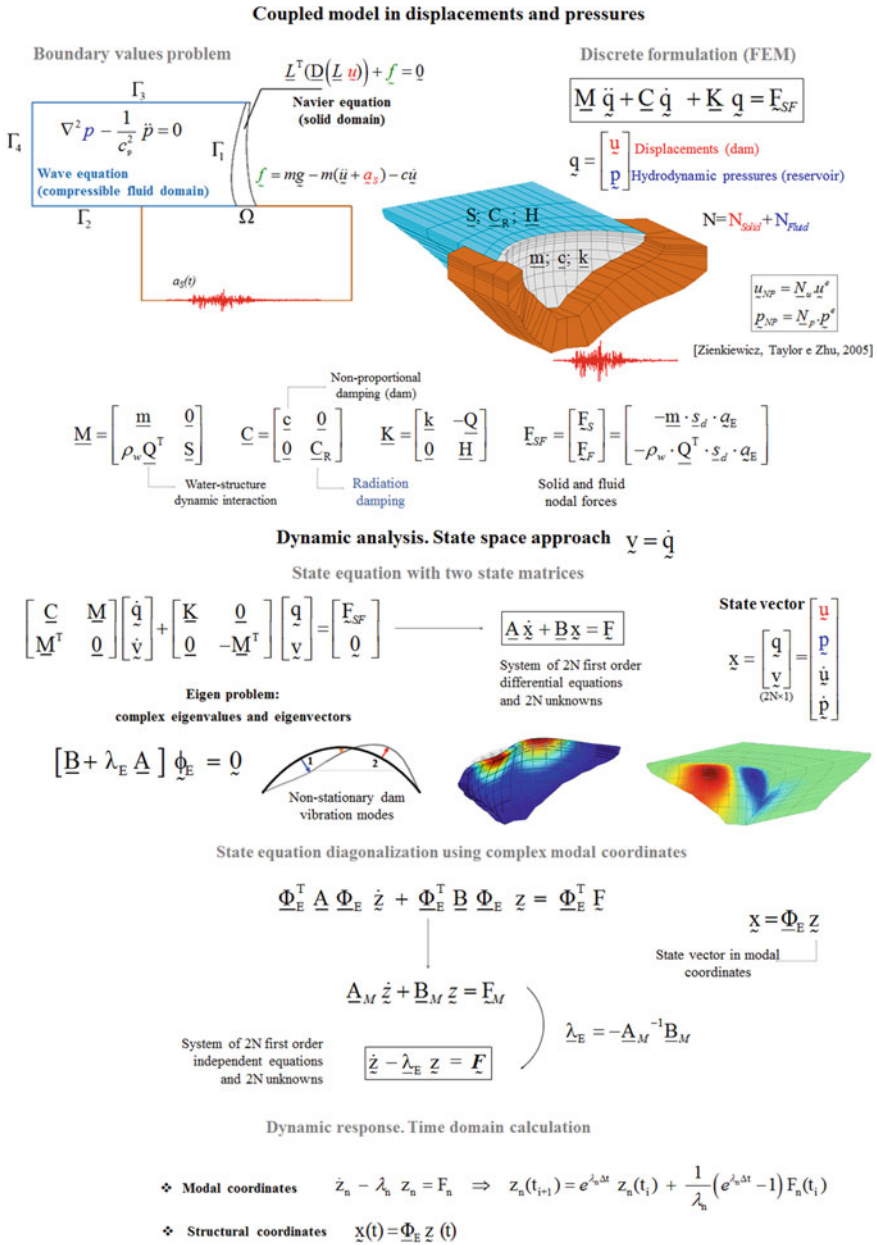


Fig. 4.9 Coupled model and state space approach. Formulation used in DamDySSA2.0 (Dam dynamic state space analysis)

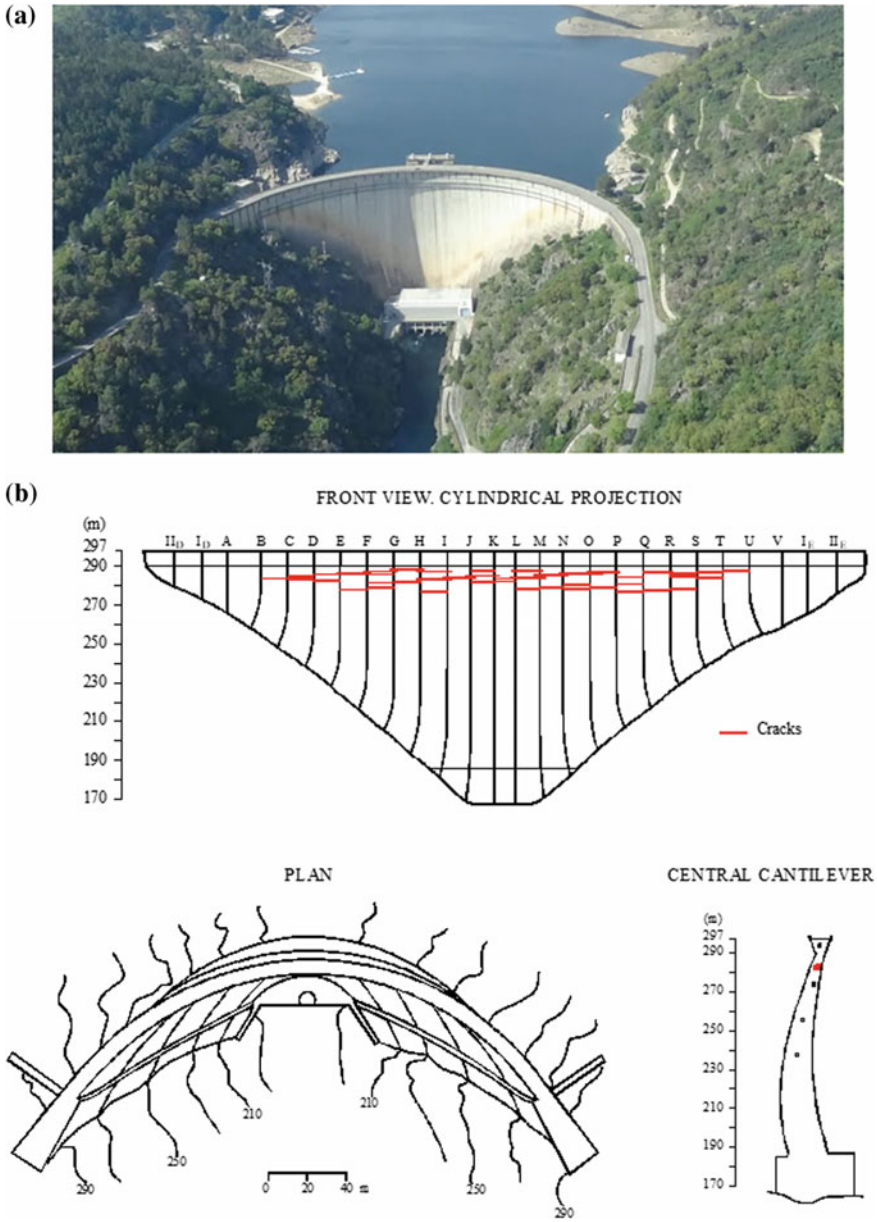
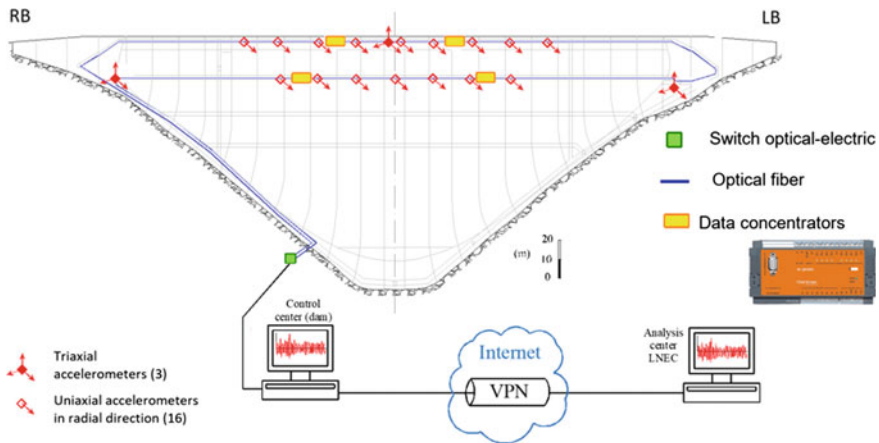


Fig. 4.10 Cabril dam. **a** Aerial view (the intake tower can be seen). **b** Front view, plan and central cantilever



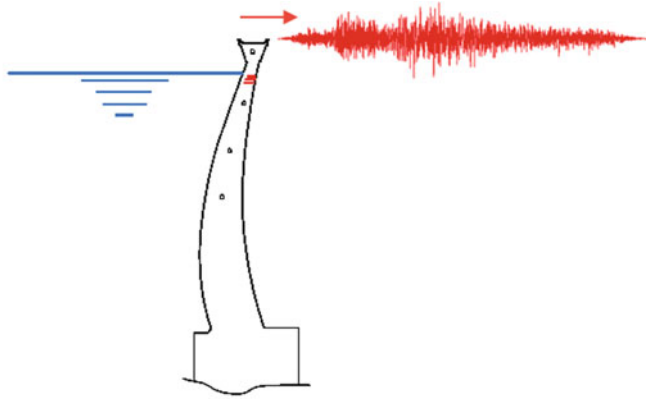
Triaxial and uniaxial accelerometers located at the center of crest gallery



Fig. 4.11 Cabril dam. Vibrations monitoring system—schematic representation and main hardware components

ing the remote control of the system, it is important to refer that the server can be accessed via internet from LNEC by computer or even by smartphone, using suitable software, which is of great relevance given that it allows to control and analyze such important data from a distance.

As mentioned above, the hardware for measuring accelerations and the corresponding data acquisition software must be complemented with suitable software for automatic analysis and management of the collected data, to ensure the efficiency of the dynamic monitoring system and hence accurate results. For the case of Cabril dam, two programs were developed using MATLAB (Fig. 4.13): Modal_ID_auto2.0 and Modal_ID2.0. Modal identification is performed using the frequency domain decomposition method (FDD), based on Singular Value Decomposition (FDD) of the Power Spectral Density (PSD) [11, 12].



VIBRATIONS AMPLITUDE IN CABRIL DAM

Measured and predicted accelerations at top of the central cantilever

■ Ambient excitation	0.001 mg	(10 ⁻⁶ g)
■ Operational excitation	0.1 mg	(10 ⁻⁴ g)
■ Forced vibration tests	1 mg	(10 ⁻³ g)
■ Seismic excitation (T = 10 years)	10 mg	(10 ⁻² g)
■ OBE (T = 145 years) (At the base, 0.02 g ; at the top 5x0.02g = 0.1g)	100 mg	(10 ⁻¹ g)
■ MCE (T = 1000 years) (At the base, 0.2 g ; at the top 5x0.2g = 1g)	1000 mg	(1 g)

Fig. 4.12 Cabril dam. Accelerations at top of the central cantilever for different types of excitation

The software Modal_ID_auto2.0 carries out, automatically, the continuous data analysis providing specific outputs defined in advance (e.g. acceleration records and correspondent Fourier spectra, natural frequencies and mode shapes). Besides the analysis and management of the data, it automatically generates and sends (via e-mail) files with a synthesis of the obtained results, to be analyzed by the engineers and technicians. The continuous analysis of the acceleration records allow to study the evolution of the modal parameters over the years. So, the influence of water level variations and the influence of annual thermal variations can be studied as well as the effects of eventual deterioration processes over the years.

On the other hand, Modal_ID2.0 is an interactive program that performs the modal identification of the main modal parameters for a certain data file, which is associated to the hour-day-year input chosen by the user. Its interactive feature enables

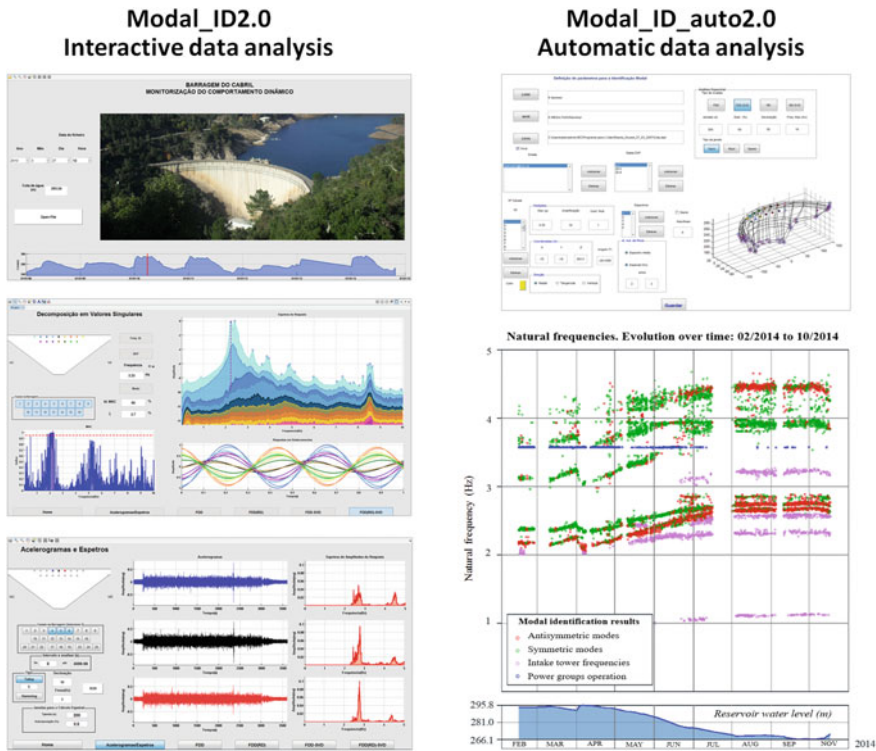


Fig. 4.13 Modal identification software: Modal_ID_auto2.0 and Modal_ID2.0

to carefully observe the records and modal identification outputs for a certain water level, and it facilitates the comparison with numerical results. In terms of the results obtained from the collected data, both programs present as outputs: (a) the acceleration records for each installed accelerometer and the corresponding amplitude spectrum; (b) the medium spectrum, as obtained by applying modal identification techniques; and (c) the natural frequencies, which correspond to the main spectral peaks, and the respective vibration modes, including 3D mode shapes and harmonic waves representing the oscillatory movements in each measuring point, all associated to the measured water level.

4.7.1 Comparison of Experimental Modal Parameters with Numerical Modal Parameters

In this section the modal identification results obtained with ModalID2.0 and ModalID_auto2.0 are compared with results computed using DamDySSA2.0. To

simulate the dynamic response of Cabril dam, the coupled model presented above was used, considering a dynamic elasticity modulus (E_{dyn}) of 32.5 GPa and a Poisson ratio (ν) of 0.2 for the dam. The numerical calculations were carried out for various water levels, assuming a fluid velocity of 1440 m/s.

The goal is to demonstrate the potential of the combined use of monitoring and modelling to study the dynamic behavior of dams, to calibrate and validate the numerical models and to support structural health monitoring.

Figure 4.14 shows the identified modal parameters using the acceleration time histories measured in November 6, 2011, from 10 to 11 a.m. The natural frequencies are estimated from the average singular value spectra and the corresponding mode shapes are obtained from the singular vectors of the PSD matrix. For the case of Cabril dam, it is important to analyze the natural frequencies with care, in order to distinguish between the dam vibration modes and vibrations related to the intake tower motion or the power groups operation. In Fig. 4.15, the evolution of the computed natural frequencies from empty to full reservoir and the mode shapes for a water level of 290 m is shown (colored dashed lines). As for the experimental results, the modal parameters were obtained with ModalID2.0 based on acceleration records measured on April 1, 2014, between 10 and 11 a.m., in which the reservoir water level (H_w) was of 291.45 m. Finally, Fig. 4.16 shows the evolution of the automatically estimated natural frequencies (green and red circles), from February to October 2014, a period during which a water level variation between 266 and 296 m was observed. These are compared with colored lines that represent the evolution of the natural frequencies from numerical modelling.

Based on the presented results, one can note the excellent agreement achieved between modal identification outputs and numerical results obtained with a 3DFE model, for different reservoir water levels, regarding natural frequencies and mode shapes. It is also worth highlighting that the coupled model (displacements and pressures) enables the computation of non-stationary vibration modes, as can be measured in situ. It should also be mentioned that such good agreement was not reached in previous studies using classic added water mass models [4] based on Westergaard's formulation [20].

The obtained results clearly show the utility of the monitoring system installed in Cabril dam for studying the dynamic response of dams and for structural health monitoring, provided that appropriate modal identification software and reliable numerical models (3DFEM) are used.

4.8 Measured Seismic Response

Due to the high dynamic range of Cabril dam's continuous monitoring system, it has been possible to automatically identify and record data series during earthquake events through the measurement of accelerations close to the foundation and in the dam body, thus allowing to study the seismic response of the dam for seismic loading.



The modal identification software, is configured to identify, hourly, the main natural frequencies and mode shapes using the FDD-SVD method.

In Cabril dam it is detected a dynamic interaction between the intake tower and the dam: some of the main natural frequencies of the intake tower are identified by the FDD analysis of the acceleration records measured at the dam body.

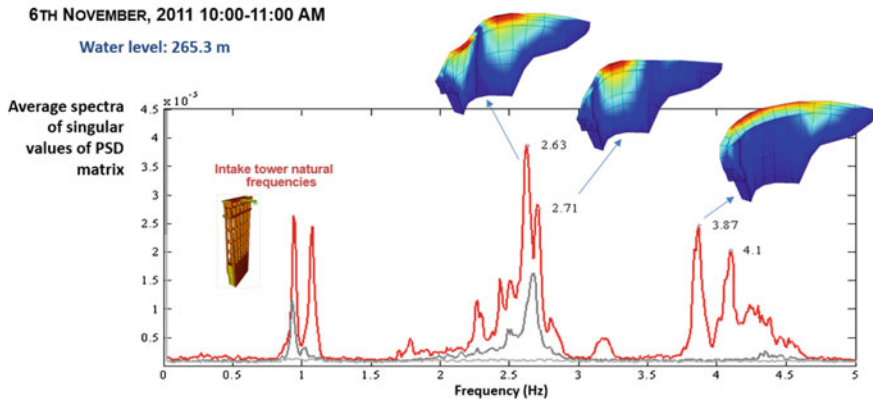


Fig. 4.14 Natural frequencies and mode shapes of Cabril dam identified in November 6, 2011 (10:00–11:00 a.m.) using the Frequency Domain Decomposition Method, with the technique of Singular Value Decomposition of the power spectral density matrix (FDD-SVD method)

In fact, an earthquake of magnitude 4.6 on the Richter scale was measured in Cabril dam quite recently, on September 4, 2018, as shown in Fig. 4.17. The reservoir water level at the time was 281.2 m. The recorded acceleration time histories are shown, particularly in three uniaxial accelerometers at the crest (radial direction) and in the triaxial accelerometer located in the right bank (RB_{xyz}).

This type of results is of great use to analyze the amplification factor of accelerations between the base (insertion interface) and points located in the dam body, most importantly for sensors located at the crest. In the case of Cabril dam, for this specific seismic loading, a maximum amplification factor of about 2 times is determined, corresponding to the sensor located at the top of the central cantilever (KL294). This value decreases for the accelerometer KL275, located in the lower gallery, as well as for the sensors FG294 and PQ294, in the adjacent blocks.

In this scope, a seismic analysis of Cabril dam was carried out with DamDySSA2.0, using the actual recorded acceleration time histories near the insertion interface as the seismic load and considering a water level of 280 m. From the computed seismic response, it was possible to calculate an amplification factor of about 2 between the accelerations at the dam base and the accelerations at the top of the central cantilever, assuming a damping ratio of about 5%. This comparison is of

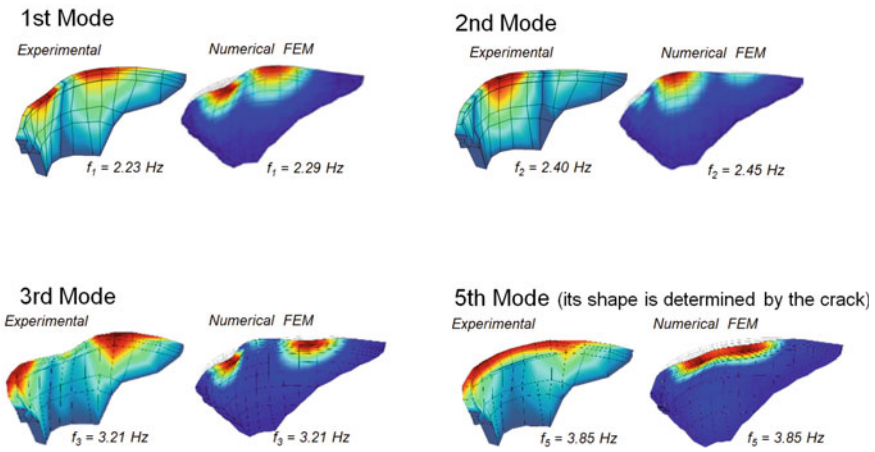
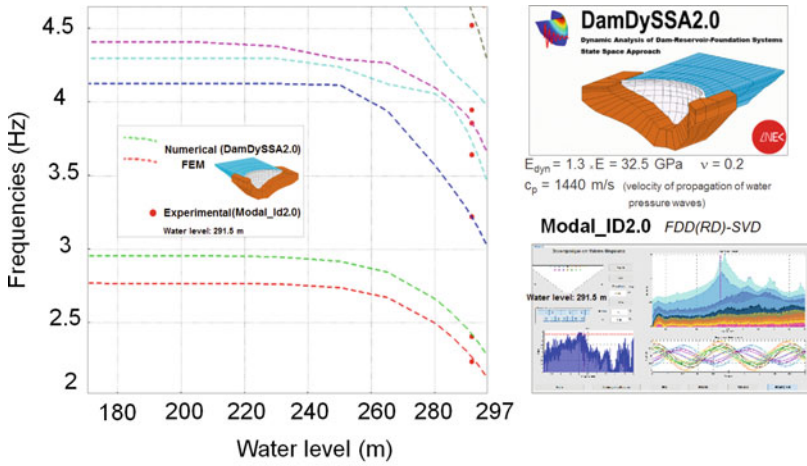


Fig. 4.15 Natural frequencies and mode shapes of Cabril dam. Comparison between modal identification results (analysis of acceleration records from 2014 April 1st, 10:00–11:00 a.m.; water level: 291.5 m) and numerical results from the reference FEM (DamDySSA2.0)

great use not only to further calibrate and validate the numerical model, but also the significance of such studies in the framework of seismic health monitoring.

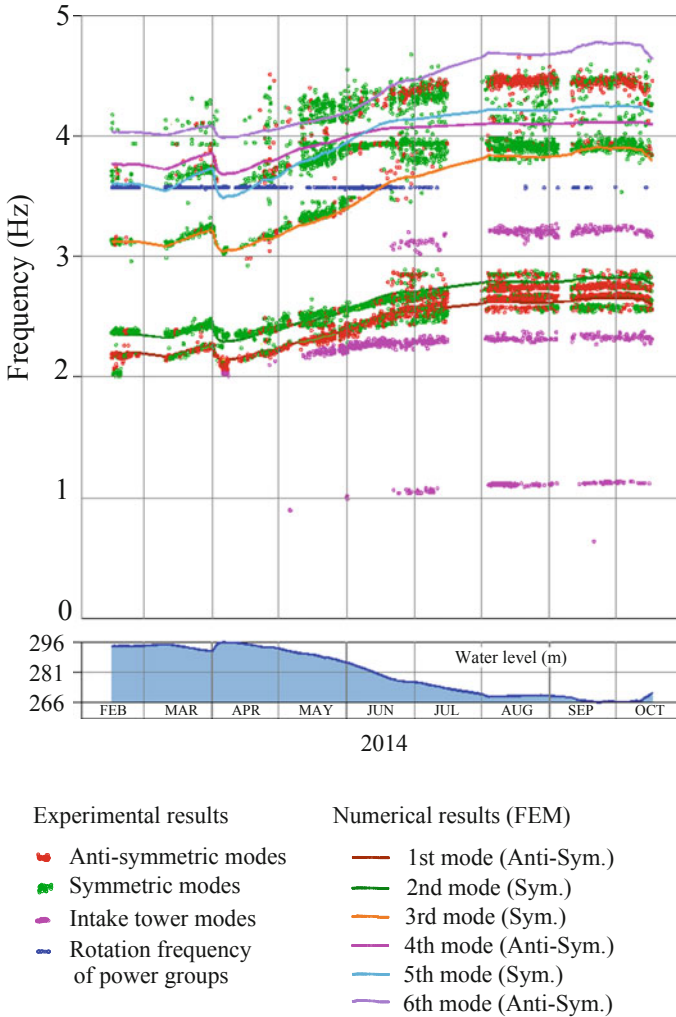


Fig. 4.16 Natural frequencies of Cabril dam. Comparison between automatic modal identification results (analysis of acceleration records collected from February to October, 2014) and numerical FEM results (DamDySSA2.0)

4.9 Baixo Sabor Dam SSHM System: Main Monitoring Results Under Ambient Excitation and Seismic Loading

The Baixo Sabor dam (Fig. 4.18) is located in the north-eastern of Portugal, in the lower part of the Sabor river, which is a tributary of the right bank of the Douro river. The dam, built in late 2015, is a 123 m high arch dam, with a total crest length of 505 m. The dam has a controlled surface spillway at the central part of the crest.

Following the success of the dynamic monitoring system of Cabril dam, a seismic and structural health monitoring system has been installed in Baixo Sabor dam. This monitoring system has been in operation since the beginning of the first filling (Fig. 4.19). The installed monitoring system includes 20 uniaxial accelerometers and

Earthquake September 4th 2018 (M4.6)
Epicenter: Peniche abyssal region, distance to the dam ~200 km
Reservoir water level: 281.2 m

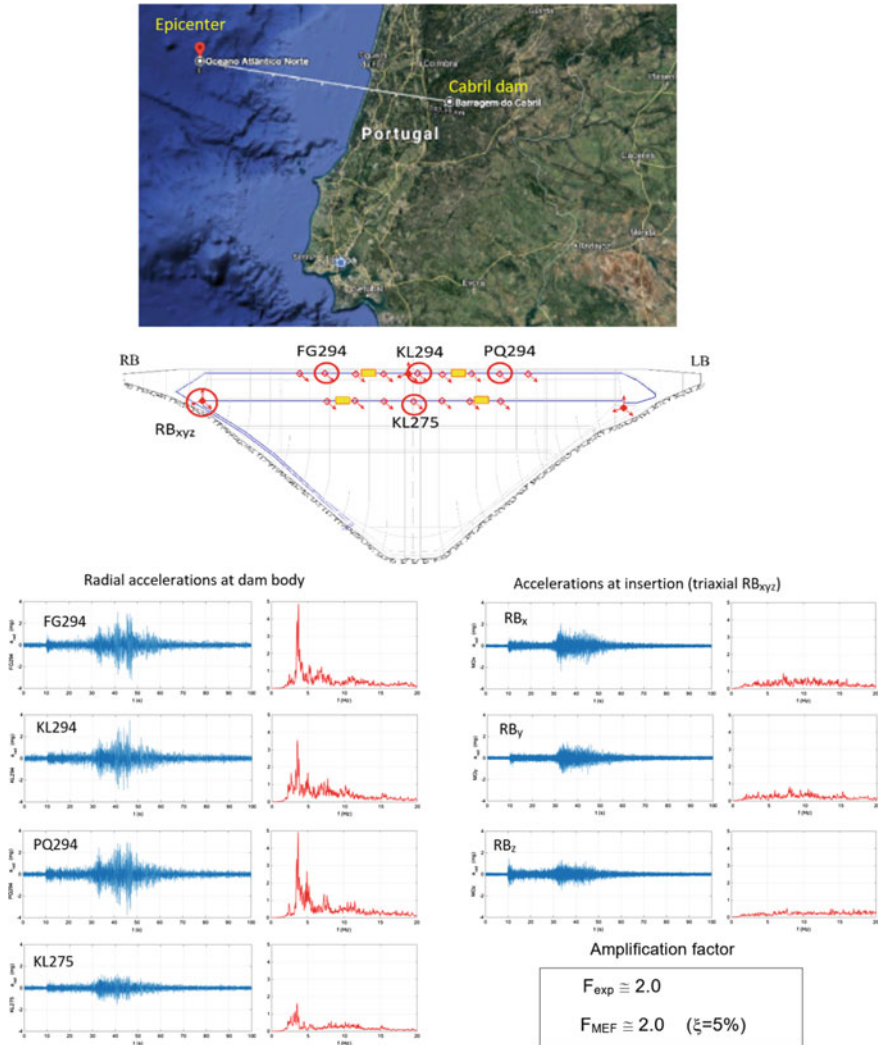


Fig. 4.17 Observation of seismic behavior. Measuring the amplification factor of accelerations from de base (insertion interface) to the dam crest center

6 triaxial accelerometers, aiming to characterize the dynamic behavior of the dam for ambient/operational excitations and the dam’s response when it is subjected to seismic loading [7].

The uniaxial accelerometers were installed in the radial direction along the three upper galleries, to measure accelerations continuously over time, which are connected to an optic fiber network—the system is configured to continuously record

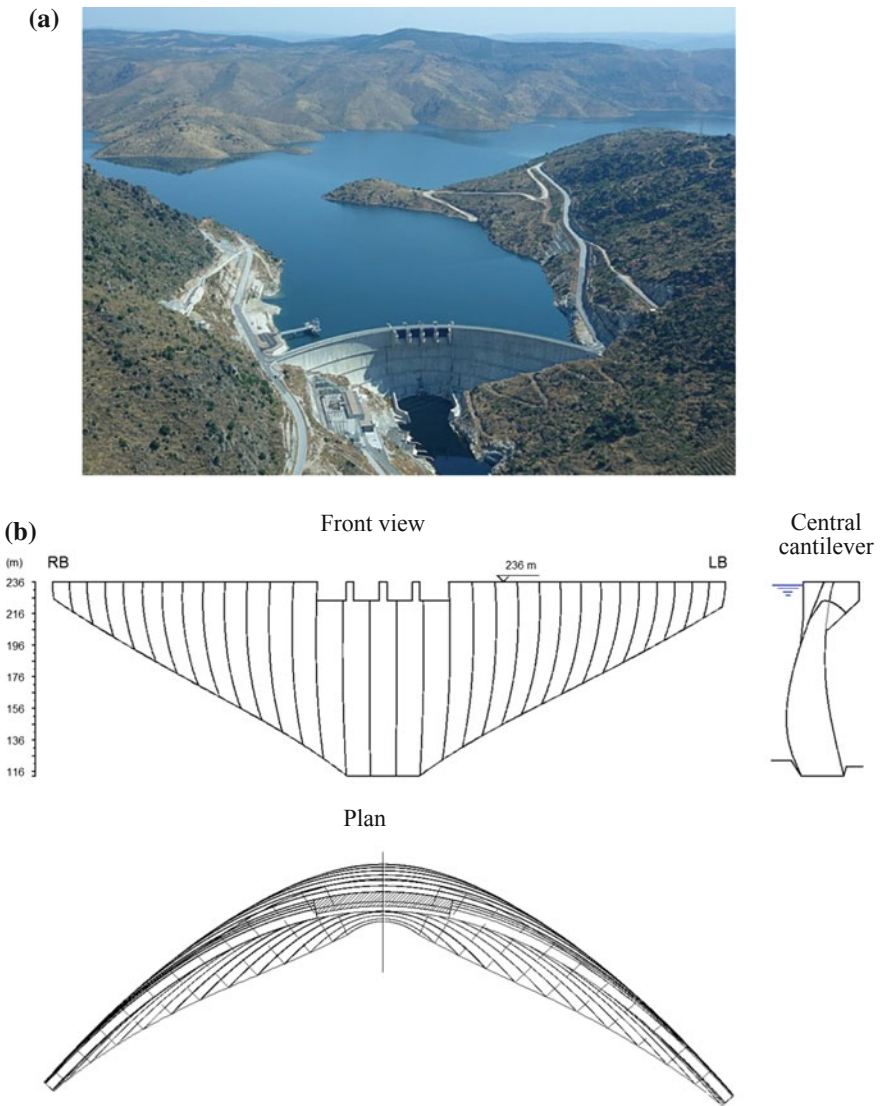


Fig. 4.18 Baixo Sabor dam. **a** Aerial view; **b** Front view, central cantilever and plan

acceleration time series with a sampling rate of 50 Hz and a duration of 30 min at all sensors.

As for the triaxial accelerometers, one is located below the surface spillway, two are located in adjacent points at the upper gallery, and the remaining three are located close to the base, near the dam-foundation interface. These accelerometers were set

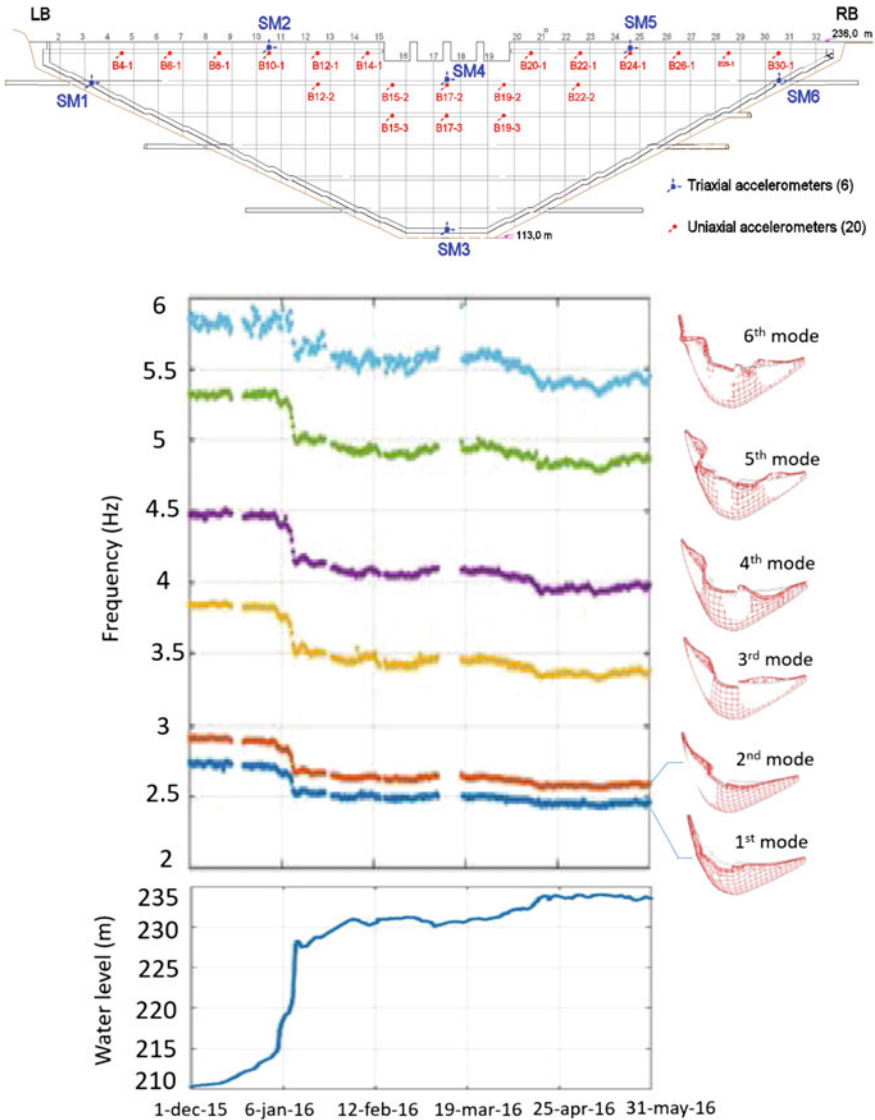


Fig. 4.19 Baixo Sabor dam. Evolution of natural frequencies identified between 1-Dec-2015 and 31-May-2016 and correspondent reservoir water level variation (from [7])

as trigger-event sensors, i.e. each accelerometer is continuously recording and when an earthquake event occurs (automatically identified), an alert is issued and data is automatically stored in local memory, within an interval from a pre event to a post event time, at a given sampling frequency.

Figure 4.19 also shows the evolution of the natural frequencies identified from December 2015 to May 2016 and the corresponding water level variation, as well as the estimated mode shapes for full reservoir. The modal parameters were obtained from the time series recorded with the uniaxial accelerometers. The time period under analysis covers the filling of the reservoir and the first months of operation, clearly showing the influence of the water level variations in the dam's natural frequencies.

Figure 4.20 shows the measured seismic response of the dam. The accelerations were recorded with the triaxial accelerometers during an earthquake of magnitude 2.9 on the Richter scale, on August 3rd 2017. The reservoir water level at the time was 231.08 m. These results are useful to study the seismic behavior of the dam. The dam dynamic response was measured at several points, as well as the seismic accelerograms at the dam-foundation interface. With these measurements it is possible to evaluate the amplification of the accelerations from the base to the top. The time series recorded at the dam-foundation interface can also be used as a seismic input loading in numerical FE models, thus enabling the comparison between experimental and numerical seismic response.

4.10 Conclusions

In Portugal the first studies involving in situ measurements of the dynamic behavior of large dams were carried out by LNEC, and date back to the early 1960s. Since then a research program started at LNEC with the objective of studying the dynamic behavior of dams and related works, involving: (i) the evaluation of the seismic risk; (ii) in situ vibration testing; and (iii) the development of advanced numerical models of finite elements to study the dynamic behavior of dam-reservoir-foundation systems, considering the dynamic water-structure interaction.

In 2008, a first system for continuously monitoring dam vibrations—a Seismic and Structural Health Monitoring (SSHM) system—was installed in Cabril dam, by LNEC and Portuguese Company for Electricity (EDP), with funding from the Portuguese Foundation for Science and Technology (FCT).

The experience acquired by LNEC with the installation and operation of the Cabril dam SSHM system has shown that, with the recent technological developments, in terms of hardware and software components, the installation of this type of systems can effectively contribute to improve the safety control of large dams, especially if used in combination with results from 3DFE models. In fact, these systems provide useful information:

- i. about structural health condition considering that they enable the reliable identification of the evolution over time of the dam's main modal parameters (fre-

Earthquake 2017 august 3rd 9:17 AM (M2.9)
Epicenter: Torre de Moncorvo, distance to the dam ~8 km
Reservoir water level: 231.08 m

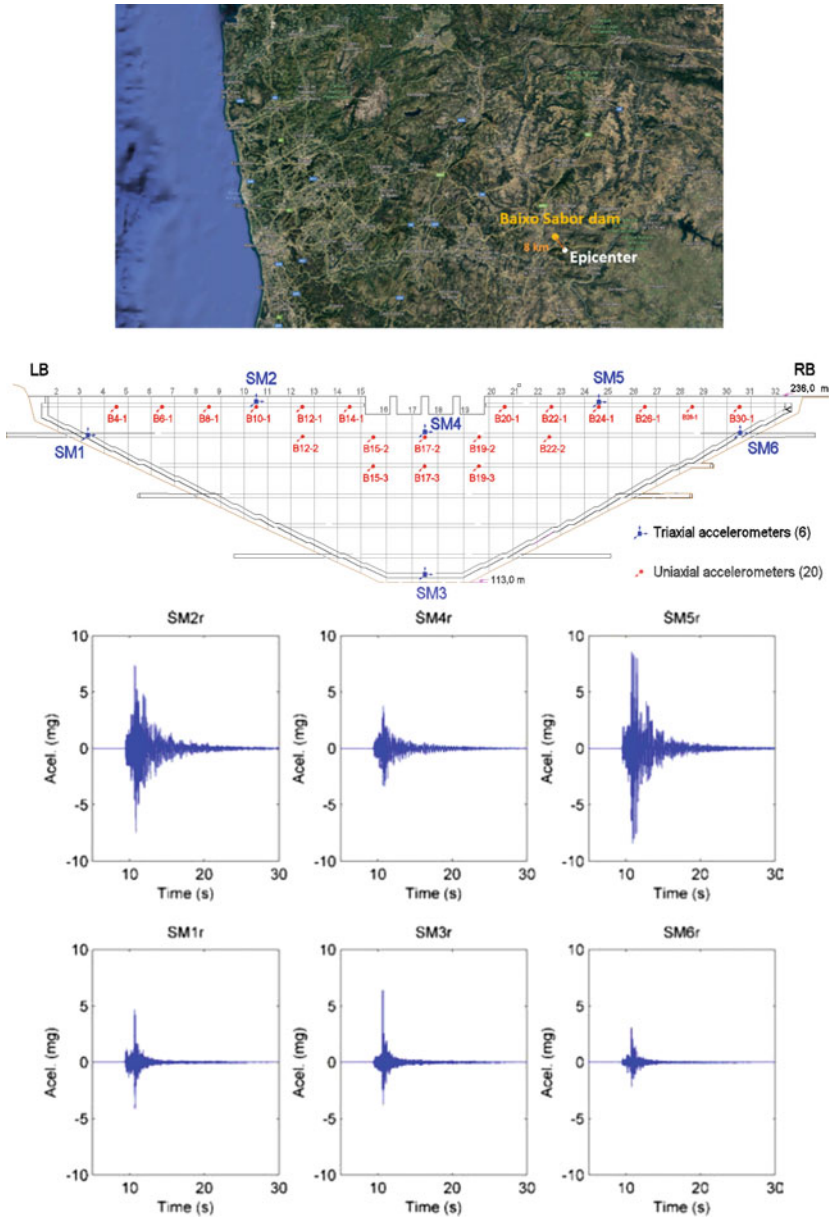


Fig. 4.20 Baixo Sabor dam. Seismic behaviour observation (from [7])

- quencies, damping and configurations of the main modes of vibration), which, as is known, can be directly correlated with the structural health; and
- ii. on the seismic response of dams, which is of great interest for the development of numerical models for simulation/prediction of the dynamic behavior of dams under seismic actions, fundamental in studies to support the design of new dams and in seismic safety review/verification studies of existing dams.

Following the pioneering LNEC research carried out for Cabril dam since 2008, continuous monitoring systems of the type SSHM are currently being installed in several of the new large Portuguese dams, namely in Baixo Sabor dam (2015), Foz Tua dam (2017), Alqueva dam, Alto Ceira II dam and Ribeiradio dam. The results obtained from the SSHM system of Baixo Sabor dam, since 2015, were also presented and showed the effectiveness and capacity of the system for estimating the mode shapes and the evolution of natural frequencies over time and for measuring the seismic response of the dam to earthquake events.

The Portuguese experience with SSHM systems in dams has shown that adequate equipment for continuously monitoring vibrations is currently available. However, the effectiveness of these continuous monitoring systems is still heavily dependent on the software for automatic analysis of collected data. For Portuguese dam engineers, the current challenge is to contribute to increasing the effectiveness of this type of systems through the development of the referred software for automatic analysis of vibration monitoring data, for automatic comparison between experimental data and numerical results from 3DFE models, and the development of web applications that facilitate the internet access to the monitoring data.

Acknowledgements The authors wish to acknowledge the Portuguese Company of Electricity (EDP) and the Portuguese Foundation for Science and Technology for supporting the installation of the Cabril dam vibrations monitoring system (REEQ/815/ECM/2005) and for the Ph.D. grant SFRH/BD/116417/2016.

References

1. Oliveira S (2002) Continuous monitoring system for the dynamic performance assessment of arch dams. Sub-program D. In: Study of evolutive deterioration processes in concrete dams. Safety control over time. National Program for Scientific Re-equipment funded by FCT, REEQ/815/ECM/2005, LNEC-FEUP (in Portuguese)
2. Oliveira S, Silvestre A (2017) Cabril dam system for continuous vibrations monitoring. LNEC Report 205/2017—DBB/NMMR, LNEC (in Portuguese)
3. Oliveira S, Alegre A (2018) Vibrations in large dams. Monitoring and modelling. In: 26th congress and 86th annual meeting, Vienna, Austria, 1–7 July
4. Oliveira S, Espada M, Câmara R (2012) Long-term dynamic monitoring of arch dams. The case of Cabril dam, Portugal. In: 15th world conference on earthquake engineering, Lisbon
5. Oliveira S, Ferreira I, Berberan A, Mendes P, Boavida J, Baptista B (2010) Monitoring the structural integrity of large concrete dams. The case of Cabril dam, Portugal. In: Hydro2010, Lisbon

6. Oliveira S, Mendes P, Garret A, Costa O (2011) Long-term dynamic monitoring systems for the safety control of large concrete dams. The case of Cabril dam, Portugal. In: 6th International conference on dam engineering, LNEC, Lisbon
7. Gomes JP, Palma J, Magalhães F, Pereira S, Monteiro G, Matos D (2018) Seismic monitoring system of Baixo Sabor scheme for structural dynamic behavior monitoring and risk management. In: ICOLD 26th congress and 86th annual meeting, Vienna, Austria, 1–7 July
8. Bukenya P, Moyo P, Oosthuizen C (2014) Long term ambient vibration monitoring of Roode Elsberg Dam—initial results. In: Proceedings of the ICOLD 2014 international symposium on dams in global environmental challenges, Bali, Indonesia, 1–6 June 2014, pp 594–602
9. Bukenya P, Moyo P, Oosthuizen C (2016) Long term integrity monitoring of a concrete arch dam using continuous dynamic measurements and a multiple linear regression model. In: ICOLD 2016
10. Moyo P, Bukenya P (2017) Experiences with continuous monitoring of deformation and modal properties of an arch dam. In: Proceedings of SHMII-8 structural health monitoring of intelligent infrastructure conference, Queensland University of Technology, Brisbane, Australia, 5–8 Dec 2017
11. Brincker R, Ventura C (2015) Introduction to Operational Modal Analysis. Wiley
12. Brincker R, Zhang L, Andersen P (2000) Output-only modal analysis by frequency domain decomposition. In: Proceedings of the ISMA25 noise and vibration engineering, vol 11, Leuven, Belgium, 13–15 Sept, pp 717–723
13. Zienkiewicz O, Taylor R, Zhu J (2005) The finite element method: its basis and fundamentals, 6th ed, Elsevier Butterworth-Heinemann
14. Oliveira S, Alegre A, Silvestre A, Espada M, Câmara R (2015) Seismic safety evaluation of Luzzone dam. Use of a 3DFEM state formulation in pressures and displacements. In: 13th ICOLD international benchmark workshop on numerical analysis of dams, EPFL, Lausanne
15. Oliveira S, Silvestre A, Espada M, Câmara R (2014) Modelling the dynamic behavior of dam-reservoir-foundation systems considering generalized damping. Development of a 3DFEM state formulation. In: 9th International conference on structural dynamics, EURO DYN 2014, Porto
16. Chen H (2014) Seismic safety of high concrete dams. *Earthq Eng Vib* 13:1–16
17. Chopra AK, Wang J (2012) Comparison of recorded and computed earthquake response of arch dams. In: 15th world conference on earthquake engineering, Lisbon
18. Oliveira S, Mendes P (2006) Development of a Cabril dam finite element model for dynamic analysis using ambient vibration test results. In: III ECCSM, LNEC, Lisbon
19. Oliveira S, Rodrigues J, Mendes P, Costa, A (2003) Monitoring and modelling the dynamic behaviour of concrete dams. In: VII congress applied and computational mechanics, University of Évora (in Portuguese)
20. Westergaard HM (1993) Water pressures on dams during earthquakes. *Transactions (ASCE)* 98:418–472

Chapter 5

Monitored Seismic Behavior of Base Isolated Buildings in Italy



P. Clemente, G. Bongiovanni, G. Buffarini, F. Saitta and F. Scafati

Abstract The experimental behavior of four base isolated buildings in Italy under seismic events of low energy at the site are shown. In the buildings with HDRBs the system is put in action also with very low accelerations at the site and the system filters the seismic actions. As a result the acceleration in the superstructure is not amplified and the superstructure is properly protected. This did not happen in the Jovine School at San Giuliano di Puglia, where the seismic action recorded was very low. In the building with CSSs, the accelerations were amplified to the top and the superstructure suffered high seismic actions. This behavior can be related to the static friction of CSSs. In all cases, the importance of an accurate non-linear analysis of their behavior under earthquakes of different magnitudes is pointed out, in order to guarantee that the seismic effects in the superstructure do not exceed those assumed in the design. The importance of the monitoring is evident. It allows a fast check of the seismic performance and so of the suitability of these structures to be kept operational during the emergency phase. A real time monitoring system is advisable.

Keywords Seismic isolation · Seismic monitoring · Experimental seismic analysis

5.1 Introduction

Shun Niitsu of the Shigeru Satoh Laboratory, Japan, said: “In Italy, when you say anti-seismic prevention you always think about something you do after and never before the earthquake happens”. Actually, base isolation in Italy has been used, up to now, mainly in the reconstruction in areas recently hit by earthquakes. As a result we do not have strong motion recordings on seismically isolated buildings but only the experimental response under low energy events.

P. Clemente (✉) · G. Bongiovanni · G. Buffarini · F. Saitta
ENEA, Casaccia Research Centre, Via Anguillarese 301, 00123 Rome, Italy
e-mail: paolo.clemente@enea.it

F. Scafati
University of L'Aquila, Via Giovanni Gronchi 18, 67100 L'Aquila, Italy

© Springer Nature Switzerland AG 2019
M. P. Limongelli and M. Çelebi (eds.), *Seismic Structural Health Monitoring*, Springer Tracts in Civil Engineering, https://doi.org/10.1007/978-3-030-13976-6_5

It is well-known that seismic isolation is based on the increase of the fundamental period of vibration of a building so that accelerations in the superstructure can be reduced significantly. This reduction is offset in terms of displacements, which increase substantially with the period, but these displacements can be concentrated at the base of the building, between the upper and the lower sections of the isolation devices, while the superstructure behaves almost like a rigid body [1, 2]. Therefore, isolation devices are subject to large relative displacements and their nonlinear behavior could be significant.

Base isolated systems are designed with reference to the design earthquake at the site, which is characterized by a certain exceedance probability (usually $\leq 10\%$ in 50 years). Linear analysis is often used and equivalent characteristics, such as stiffness and damping, are used for the check under seismic actions [3].

The suitability of seismic isolation has been demonstrated also during recent earthquakes, when base isolated buildings exhibited an excellent behavior, preserving the structures, the non-structural elements and their contents.

In several countries the extensive adoption of the new anti-seismic systems started after strong earthquakes, in which the already existing base isolated buildings exhibited an excellent behavior [4] and seismic isolation has been used also in the retrofit of existing buildings [5, 6].

In Japan, which is the leader in the application of base isolation, the number of seismic isolated buildings increased very much after the 1995 *Hyogo-ken Nanbu* earthquake ($M = 7.3$), when two isolated buildings in the epicentral area, near Kobe, reported no damage during the quake. One of these was the communication minister in Sanda City (Fig. 5.1a), which was about 30 km far from the epicentre. It had been isolated by means of low damping rubber bearings and elasto-plastic energy dissipators. The monitoring systems allowed to state that the ratio between the acceleration peak at the top and that on the basement was about 1/9, so with a significant reduction of the seismic action.

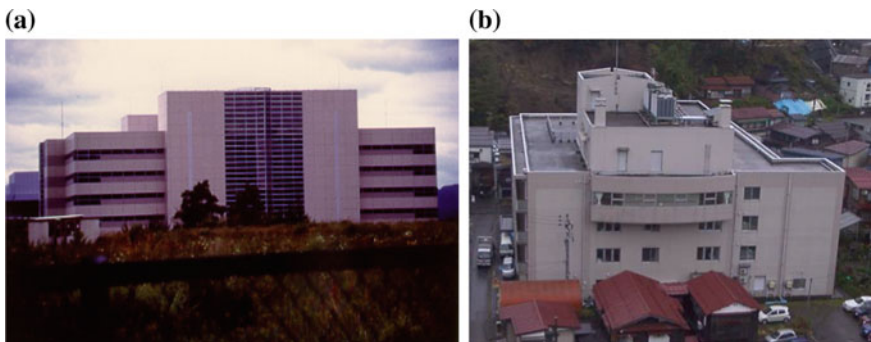


Fig. 5.1 **a** The communication minister in Sanda City and **b** The reinforced concrete building in Ojiya City, Japan

The reinforced concrete building in Ojiya City (Fig. 5.1b), Japan, completed in 1994 and isolated by means of rubber bearings and sliders, supported very well the 2004 Mid Niigata earthquake ($M = 6.8$); the peak acceleration was 0.725 g at the base and 0.194 g at the top, with a reduction ratio of about 1/4.

Most of the 118 isolated buildings affected by the 2011 Tohoku earthquake, located in the Tohoku area or in other Japanese sites, behaved quite well, even though they had been designed to withstand less severe earthquakes [7]. Among these, the 4-storey National Western Art Le Corbusier Museum in Tokyo, retrofitted in 1999 by inserting high damping rubber bearings in a sub-foundation; these isolation system reduced the PGAs in the two horizontal directions from 0.19 to 0.27 g at the base to 0.08 and 0.10 g at the top during the 2011 Tohoku quake. It is worth reminding that also seismic isolated bridges and viaducts, most of those protected by rubber bearings (LRBs and HDRBs), showed an excellent behavior during the quake, but a certain number of them was then destroyed by the subsequent tsunami, due to deck rotation toward the upstream side, resulted from the uplifting force [8].

In China, two concrete seismic isolated buildings and even a 6-storey masonry building showed an excellent behavior during the 2008 Wenchuan earthquake ($M_w = 7.9$).

During the Lushan earthquake ($M_w = 7.0$) of April 20th, 2013, two primary school buildings, one close to the other, showed a quite different behaviour, as demonstrated by the recordings obtained by means of the seismic monitoring systems installed in them. In the first one, which was conventionally founded, the peak ground acceleration value of 0.2 g was amplified to 0.72 g at the top; in the second building, which was protected by means of a base isolation system, the acceleration peak was equal to 0.12 g [9, 10]. The same happened for the county hospital, composed of two buildings with conventional foundations and one with base isolation (Fig. 5.2). The two buildings with conventional foundations suffered damage to partitions, roof and equipment contained, and were unusable after the earthquake; on the contrary, the seismically isolated block was the only hospital building of the county, which remains fully undamaged and operational: this allowed to heal thousands injured people, which was impossible in other hospitals in Lushan.

In California the University of Southern California (USC) hospital in Los Angeles showed a very good behaviour during the 1994 Northridge Earthquake ($M_s = 6.8$). It was about 30 km far from the epicentre and the ratio between the acceleration peak at the top and that at the basement was very low [11].

Very few seismic isolated buildings in Italy are provided with monitoring systems. In this paper, after a general introduction on the seismic behavior of isolation devices, the seismic responses of the following buildings under low energy earthquake are shown [12, 13]:

- the new Jovine school at San Giuliano di Puglia, seismically isolated by means of HDRBs, subject to the December 20th, 2013, earthquake ($M = 3.8$, epicenter distance = 11 km, depth = 25.7 km);



Fig. 5.2 The Lushan county hospital (China) **a** damage suffered by the conventionally founded buildings; **b** full integrity and operability of seismic isolated building

- the Operative Centre of the Civil Protection Centre of Umbria Region at Foligno, seismically isolated by means of HDRBs, subject to the October 30th, 2016, earthquake ($M = 6.5$, epicenter distance = 36 km, depth = 10.0 km);
- the Forestry Building of the Civil Protection Centre at Foligno, seismically isolated by means of HDRBs, subject to the same earthquake of the previous building;
- a building in L’Aquila (realized to temporarily host the homeless residents after the 2009 earthquake), where curved surface sliding devices (CSS) were used; it also was subject to the October 30th, 2016, earthquake ($M = 6.5$, epicenter distance = 63 km, depth = 10.0 km).

Most of these monitoring systems gave results in very short time, allowing a fast check of the seismic performance and so of the suitability of keeping operational these structures during the emergency phase.

5.2 Seismic Behavior of Isolation Devices

The isolation systems are usually designed with reference to the design earthquake at the site. On the other hand, the isolation system should have an adequate stiffness against low horizontal actions, such as wind, traffic or low energy earthquakes, and a good capability of dissipation, re-centering and lateral constraint under service horizontal loads.

To address these requirements, the isolation system must have a suitable stiffness. Therefore, under very low intensity earthquakes the isolation system could not be put in action or could behave in a way different from that assumed in the design [14–16] and the dynamic behavior could be quite different from the expected one. Obviously, different types of isolation devices exhibit different behaviors [17].

In both cases the higher value of the stiffness determines higher accelerations, and so higher seismic effects in the structure. Moreover, in the first case higher modes are activated, in which the superstructure has no displacements at its base.

5.2.1 Behaviour of HDRB Devices

In the case of high damping rubber bearings (HDRB) this nonlinear behavior is mainly related to the rubber non-linear constitutive law; while for sliding devices, with plane or curved surfaces (SD and CSS, respectively), it is mainly related to friction. So the actual behavior of the isolation system depends strongly on the displacements exhibited during the quake [18–20].

Isolation devices have a supporting function, which is expressed in bearing vertical loads in operating conditions and also under seismic actions [21]. They must also have a low horizontal stiffness, which allows a suitable relative displacement between the superstructure and the foundation, in case of seismic events, but also an adequate stiffness against low horizontal actions, such as wind, traffic or low energy earthquakes. Finally they must have a good capability of dissipation, re-centering and lateral constraint under service horizontal loads. These last requirements could also be addressed by means of auxiliary devices. To analyze in detail how the isolation devices can satisfy these requirements, the cases of high damping rubber bearings and of curved surface sliders must be distinguished.

The actual behavior of the rubber bearings seems to be consistent with the mentioned requirements. Relevant studies were carried out, which accounted for the effects of stiffening [22] and of the axial load [21]. In Fig. 5.3a the force-displacement curves relative to a cycle test of a high damping rubber bearing (HDRB) is shown. It is evident that the behavior depends strongly on the maximum displacement reached in each cycle. In Fig. 5.3b typical variability of the shear modulus G_{din} and of the damping ratio ξ are plotted versus the shear strain γ .

It is worth reminding that the design of a base isolated system is usually done by referring to seismic actions that have a low probability of exceedance during the life time of the structure. Furthermore, equivalent characteristics in terms of stiffness and damping, usually those relative to $\gamma = 1$, are chosen and used in the linear analysis [3].

Under earthquakes of lower energy, which cause displacements much lower than the design one, the rubber bearings show a higher stiffness due to the high value of the shear modulus G . As a result, the period of vibration is quite lower than that chosen in the design; anyway, the acceleration is much lower than the design one and so is the total seismic action in the superstructure.

Under very low intensity earthquakes, and also under ambient vibrations, the isolation system could not be put in action and the higher modes of the superstructure can be activated. As a result, some amplification of the response in terms of acceleration could occur.

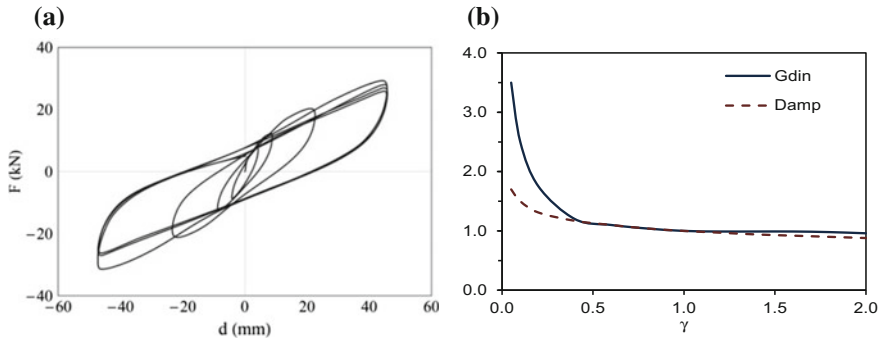


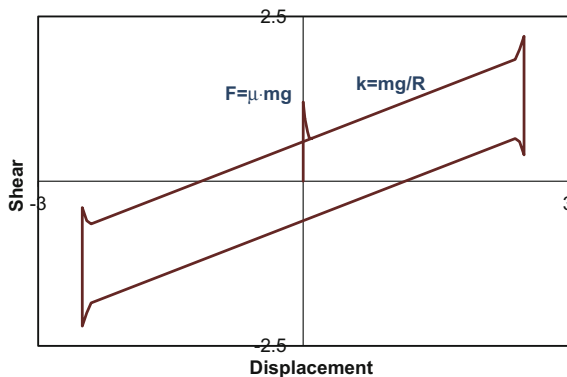
Fig. 5.3 **a** Typical force-displacement diagram for a HDRB; **b** typical variation of the elastic dynamic shear modulus G_{din} and of the equivalent damping factor ξ as ratios of their values at $\gamma = 1$, obtained during dynamic test of a HDRB

5.2.2 Behaviour of CSS Devices

The behavior of CSSs is influenced strongly by the static friction μ_0 at the onset of motion and the static friction μ_1 at the maximum displacement, for each cycle, when the velocity sign changes (Fig. 5.4). Furthermore, the friction μ during the dynamic phase is usually assumed to be constant, but the experimental analysis showed a significant variability [23, 24]. In any case, the dynamic friction is the lowest and the initial static friction the highest. It is $\mu < \mu_1 < \mu_0$.

If μ_0 is very high, then the devices could not be put in action and the system behaves as rigid and there is no decoupling of motion between the superstructure and the soil. Furthermore, if when the devices are put in action the stick-slip phenomenon could occur [25, 26].

Fig. 5.4 Typical force-displacement diagram for a CSS. The three types of friction are apparent as well as their influence on the dynamic behavior of the devices



In the following the recordings obtained during the seismic sequence that affected Central Italy from August 2016 are analyzed. Seismic isolated buildings with HDRBs and CSSs are considered.

5.3 The New Jovine School in San Giuliano di Puglia

The new Francesco Jovine School in San Giuliano di Puglia (Fig. 5.5) was the first school in Italy to be designed with base isolation. It is composed by two buildings rising up from a single base deck, which is seismically isolated by means of 61 HDRBs and 12 SDs (seismic isolation design by P. Clemente, G. Buffarini, M. Dolce and A. Parducci). This solution takes advantage of global symmetry in the construction and respects the architectural design. The isolators were deployed in order to optimize the dynamic behavior of the structure. In fact, in the first two vibration modes the structure just translates along the two main orthogonal directions, respectively, with a period of 2.19 s. The maximum displacement for the design earthquake is 240 mm. The decoupling between the horizontal motion of the structure and that of the soil is guaranteed by the very high stiffness of the elevated structure with respect to the stiffness of the isolation system. The school was opened to activities in 2008. Successive studies demonstrated the suitability of the buildings for being used as strategic ones in case of earthquakes or other natural disasters [27].

The structure was instrumented within the framework of a research project organized by ENEA in collaboration with the Italian National Civil Protection Department and the Municipality of San Giuliano di Puglia and funded by the Office for the reconstruction of San Giuliano di Puglia. The site and the structure were instrumented as shown in Fig. 5.6:



Fig. 5.5 The new Jovine school at San Giuliano di Puglia

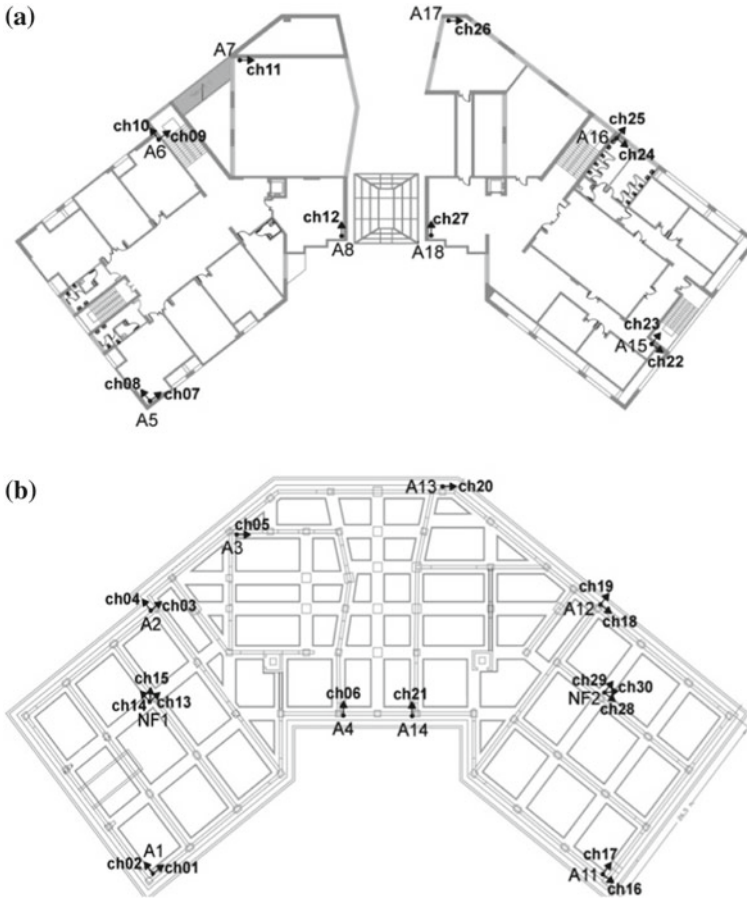


Fig. 5.6 Jovine school: sensor layout **a** on the roofs and **b** on the foundation (NF1 and NF2) and the deck just above the isolation layer

- two triaxial sensors were deployed in the soil quite close to the building, one on the surface and another 30 m below the previous one; these allow measuring the seismic input and the soil amplification;
- two triaxial accelerometer sensors were placed on the foundation, one under the school (NF1) and the other under the university centre (NF2);
- four biaxial accelerometer sensors (two at the school, CH01–CH02 and CH03–CH04, and two at the university centre, CH16–CH17 and CH18–CH19) and four uniaxial accelerometers (two at the school, CH05 and CH06, and two at the university centre, CH20 and CH21), were placed just above the isolation layer;
- four biaxial accelerometer sensors (two at the school, CH07–CH08 and CH09–CH10, and two at the university centre, CH22–CH23 and CH24–CH25) and four uniaxial accelerometers (two at the school, CH11 and CH12, and two

at the university centre, CH26 and CH27), were all placed on the roof of the two buildings.

Up to now, few seismic events of low magnitude have been recorded. The analysis of the dynamic response pointed out that the seismic isolation system was not activated during the earthquake. At any rate, some interesting features of the structure were pointed out. In Fig. 5.7, the acceleration time histories obtained at the foundation (CH13) and on the roof (CH07), respectively, during the earthquake that occurred on December 20th, 2013 (MI = 3.8, epicenter distance = 11 km, depth = 25.7 km) are plotted. The maximum acceleration values were 1.7 cm/s^2 at foundation and about 4.0 cm/s^2 on the roof. The presence of the rubber isolators influenced the wave propagation pattern in the superstructure; furthermore, measurable shifts between the arrival of P waves in the vertical components at the NF1 and NF2 locations at the foundation were found (Fig. 5.8a), as well as a significant shift between the arrival of P waves in the horizontal components at the foundation and the roof (Fig. 5.8b). Three structural resonances were found, equal to 4.0, 4.2 and 5.8 Hz, respectively, all associated with vibration modes of the superstructure. The study of the particle motion at the different sensor locations revealed the deformability of the base deck, which could influence the structural behaviour under strong earthquakes (Fig. 5.9).

5.4 The Operative Centre of the Civil Protection Centre at Foligno

The building that hosts the Operative Centre of the Civil Protection Centre of Umbria Region at Foligno has a very interesting architectural design in the form of a hemispherical shape (Fig. 5.10, structural design by A. Parducci).

It is 22 m high and has four floors above the ground and an underground floor. Its base diameter is about 31 m. The superstructure is formed by ten arch elements

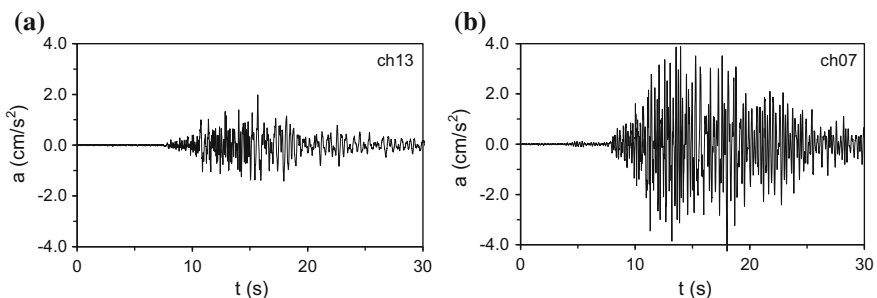


Fig. 5.7 Jovine school: acceleration time histories recorded **a** at the foundation and **b** at the roof in the horizontal direction

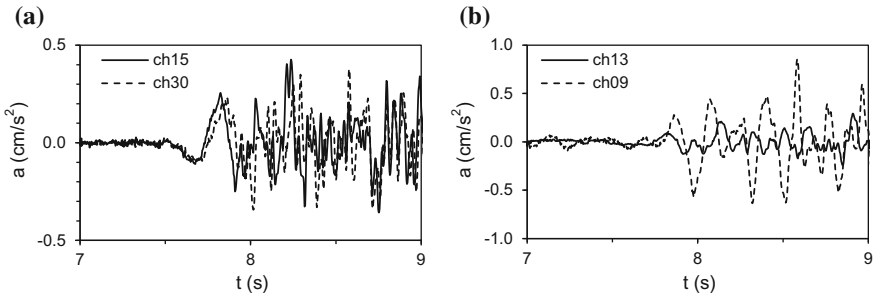


Fig. 5.8 Jovine school: **a** arrival of P waves in the vertical components at the foundation, **b** arrival of P waves in the horizontal components at the foundation and the roof of the school

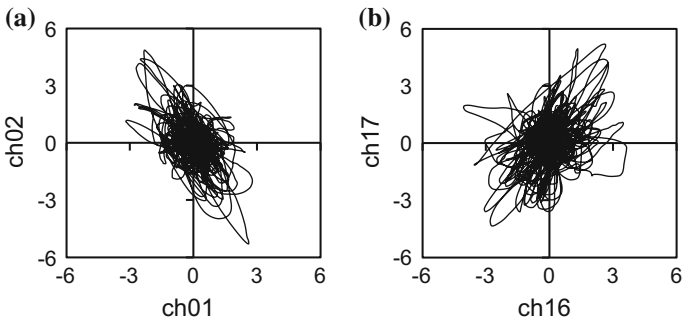


Fig. 5.9 Jovine school: particle acceleration (cm/s²) of the locations **a** CH01–CH02 at the base deck of the school and **b** CH16–CH17 at the base deck of the university



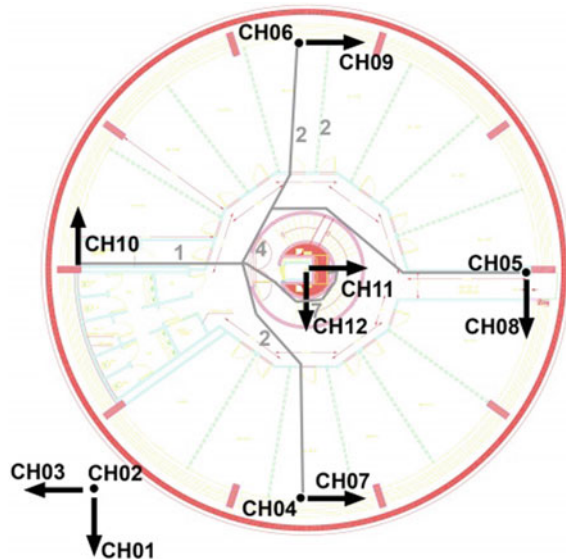
Fig. 5.10 The operative centre of the civil protection centre at Foligno

equally spaced along the perimeter, with the springings at different heights. For all of them, the upper springings are connected to a ring beam at the top of the building; the lower springings are all connected to a ring beam at the first floor. The arches are interconnected by two other ring beams at the intermediate floors. A prestressed concrete cylinder, containing all the building facilities, is suspended to the top ring. It is also connected to the other floors and continues down in the underground floor without other supports. The superstructure is supported by ten HDRBs (diameter = 1000 mm, horizontal stiffness = 1.31 kN/mm, equivalent damping = 10%) deployed along the perimeter, which yield a fundamental frequency of the isolated structure of 0.38 Hz. The isolation devices transfer the loads to the foundations, located under the lower springing of the ten arches and composed by concrete plinths, each supported by four piles.

The building has been equipped with a seismic monitoring system, within the framework of a research project organized by ENEA in collaboration with the Umbria Region [28, 29]. It is composed of twelve accelerometers, deployed in the building as follows (Fig. 5.11):

- three accelerometers (CH01, CH02 and CH03) were placed at the basement, below the isolation system;
- seven accelerometers were placed on the first floor, just above the isolation system: three of them in the vertical direction (CH04, CH05 and CH06), two in *x* direction (CH07 and CH09) and two in *y* direction (CH08 and CH10);
- two accelerometers were placed at the top of the building in the centre of the dome in the horizontal directions (CH11 in *x* direction, CH12 in *y* direction).

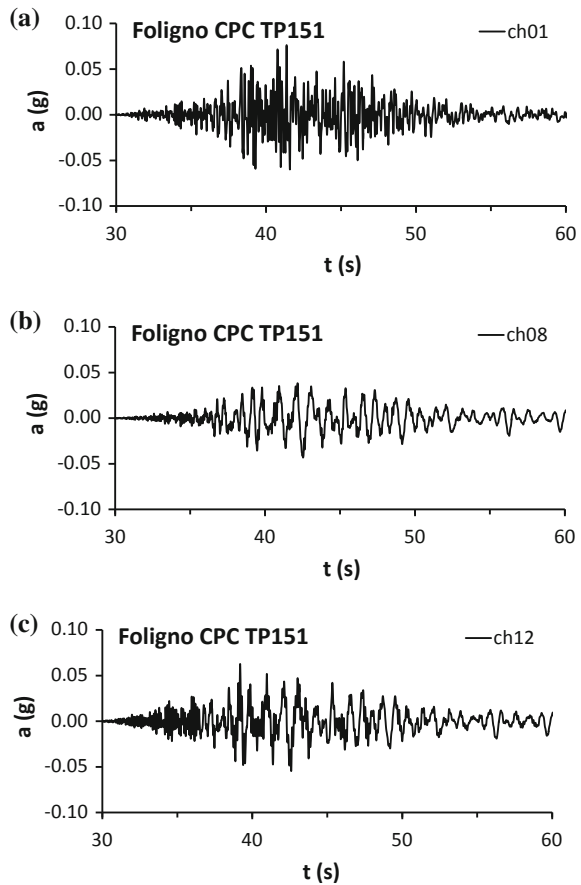
Fig. 5.11 Operative centre: seismic monitoring network



The monitoring system recorded all the events of the Central Italy seismic sequence that started on August 24th, 2016. In Fig. 5.12, the acceleration time histories recorded on the foundation, just above the isolation system and at the top of the building during the earthquake of October 30th, 2016 ($M = 6.5$, distance from epicenter = 36 km), are shown. The absence of any amplification is evident, as well as the presence of a significant change in the frequency content. This is also confirmed by the Fourier spectra (Fig. 5.13), in which a first resonance frequency at about 1 Hz is evident.

From the acceleration time histories, the displacement time histories were obtained by means of double integration. Figure 5.14a shows that the relative displacement between the first floor and the basement was about 10 mm, while the drift between the top and the first floor was less than 5 mm (Fig. 5.14b), which is much lower than the limit value suggested by the code. Taking into account the variabil-

Fig. 5.12 Operative centre: time histories recorded **a** at the basement, **b** just above the isolation system and **c** at the top



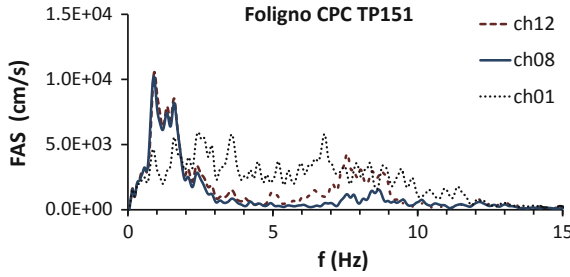


Fig. 5.13 Operative centre: Fourier spectrum amplitude at different level

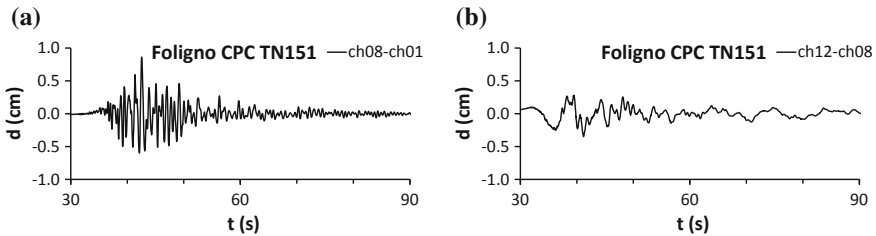


Fig. 5.14 Operative centre: relative displacement **a** between the first floor and the basement and **b** between the top and the first floor

ity of the shear modulus of the rubber with the shear deformation, the resonance frequency value is consistent with the measured relative displacements.

5.5 The Forestry Building of the Civil Protection Centre at Foligno

The Forestry Building of the Civil Protection Centre of Umbria Region in Foligno (Fig. 5.15) has been instrumented by means of twelve accelerometers, deployed in as follows (Figs. 5.16 and 5.17):

- three accelerometers (A01, A02 and A03) were on the basement, under the isolation system;
- six accelerometers were on the first floor, just above the isolation system: three of them in the vertical direction (A06, A07 and A09), one in *x* (longitudinal) direction (A05) and two in *y* (transversal) direction (A04 and A08);
- three accelerometers were at the top of the building: one in *x* (longitudinal) direction (A11) and two in *y* (transversal) direction (A10 and A12).

In Fig. 5.18 the recordings obtained in the transversal direction are shown. It is apparent the absence of amplification to the top and also a significant change in the frequency content. This is confirmed by the Fourier spectra plotted in Fig. 5.19,



Fig. 5.15 The forestry building at the civil protection centre in Foligno, Italy

in which the amplification at a frequency of about 1 Hz is apparent. This value is consistent with the stiffness of the rubber bearings for low displacements [17]. In Fig. 5.20 the drift between the first floor and the basement is plotted.

5.6 Building with Single Curve Surface Sliders

The use of seismic isolation increased rapidly after L'Aquila earthquake of April 6th, 2009, as a consequence of the large damage caused by this event to conventionally founded structures and to cultural heritage structures, but also thanks to the use of such protection system in buildings for temporarily hosting about 15,000 homeless residents. These consisted in wooden, reinforced concrete or steel pre-fabricated houses, each of them placed on a large isolated reinforced concrete slab supported by means of curve surface sliders (CSS), manufactured in Italy, installed at the top of circular columns. In Fig. 5.21 the C4 building is shown.

The building was instrumented by means of ten accelerometers, deployed as follows (Fig. 5.22):

- three accelerometers (CH8x, CH9y and CH10z) were on the foundation, under the isolation system;
- three accelerometers were on the first floor, just above the isolation system: two in x direction (CH3x and CH7x) and one in y direction (CH4y);
- four accelerometers were at the top of the building: two in x direction (CH2x and CH6x) and two in y direction (CH1y and CH5y).

The recordings obtained during the event of 30th October, 2016, along x direction are plotted in Fig. 5.23. The amplification from the basement (CH3x) to the top (CH2x) is apparent.

The absence of the filtering function is confirmed by the Fourier spectra (Fig. 5.24). In Figs. 5.25 and 5.26 the time histories of the relative displacement between the first

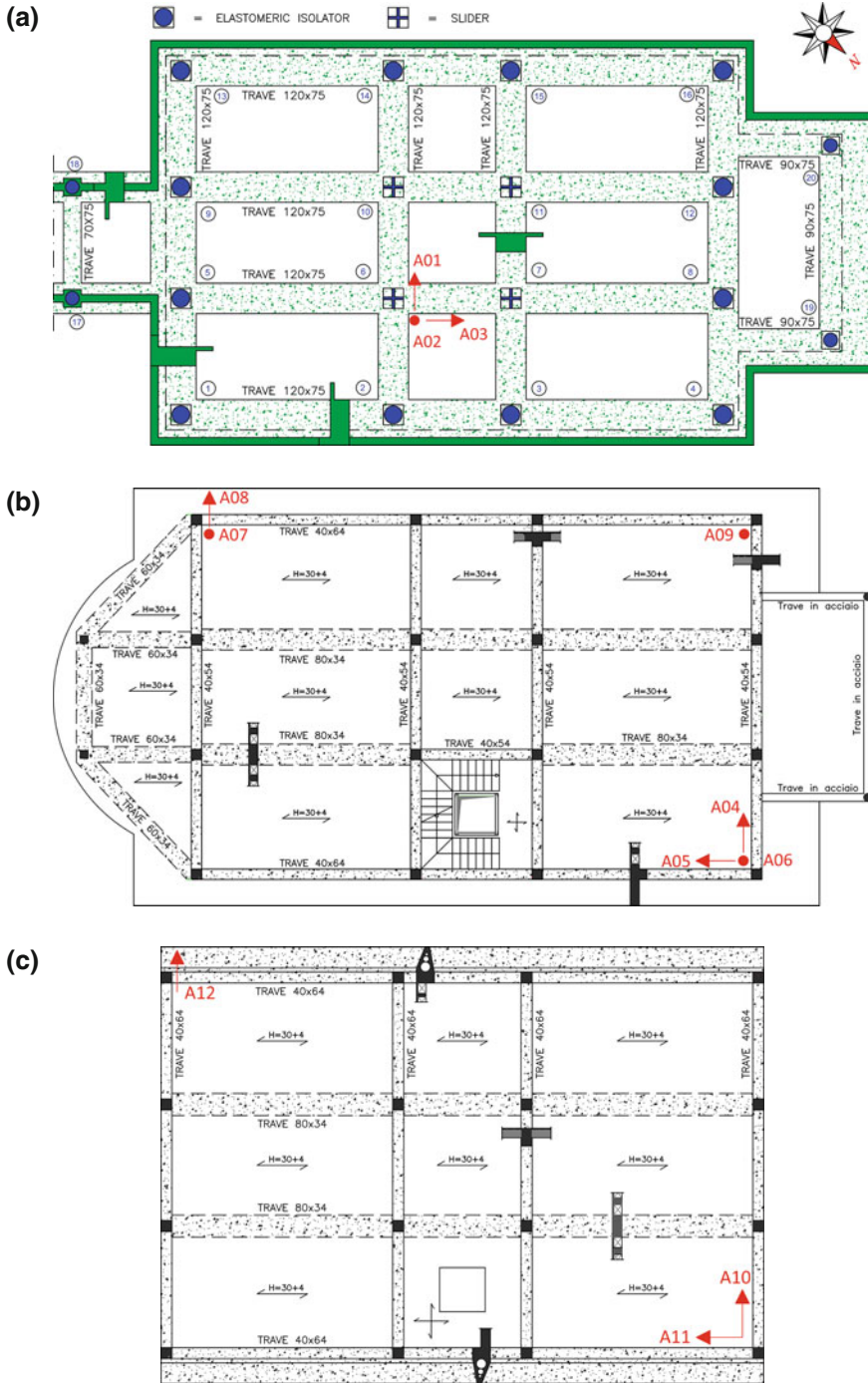


Fig. 5.16 Forestry building: sensor deployment **a** at the basement with the isolation system, **b** at the first floor above the isolation interface, **c** at the top floor

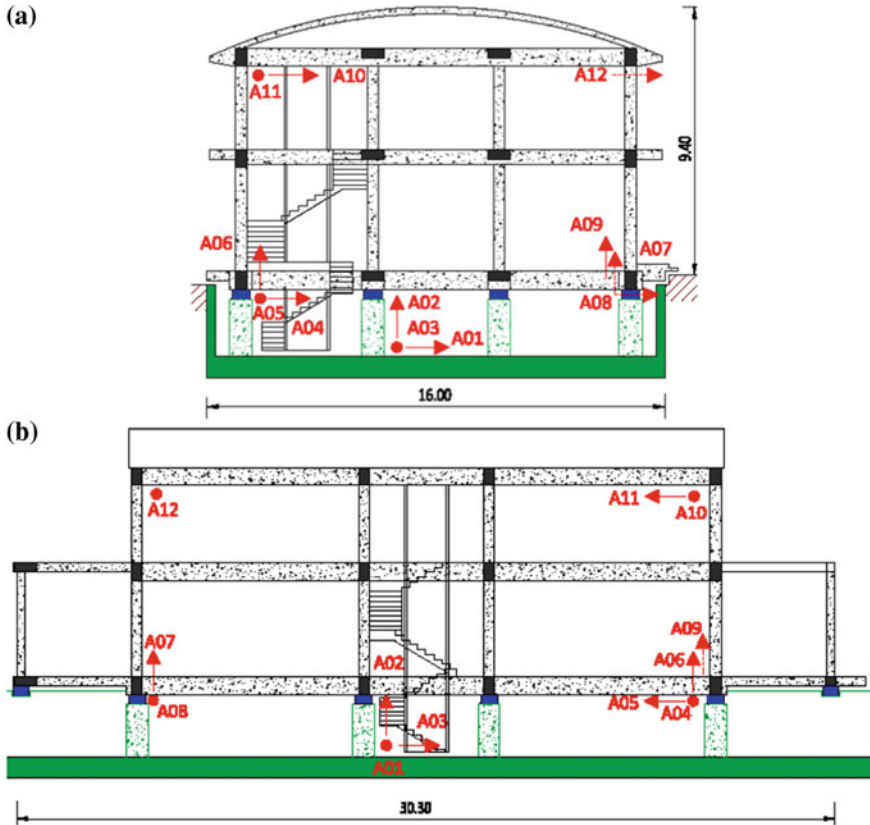


Fig. 5.17 Forestry building: sensor deployment, **a** transversal section, **b** longitudinal section

floor and the foundation, and the drift between the top and the first floor, along x and y direction, respectively, are plotted. The devices worked in x direction but not in y direction, while the drift is significant in y direction but not in x direction. The experimental seismic behavior could be related to the initial static friction and/or to stick-slip phenomenon occurred during oscillations. More detailed analysis is necessary.

5.7 From Short Time to Real Time Monitoring

As already said, most of the monitoring systems installed in Italy gave results in very short time. The seismic performance of the monitored buildings can be checked rapidly and any anomaly in their dynamic behavior can be pointed out. Therefore, the suitability of these structures to be operational can be checked.

Fig. 5.18 Forestry building: accelerometric recordings obtained during the October 30th earthquake ($M = 6.5$) at **a** the basement, **b** on the first floor just above the isolation system and **c** at the top of the building

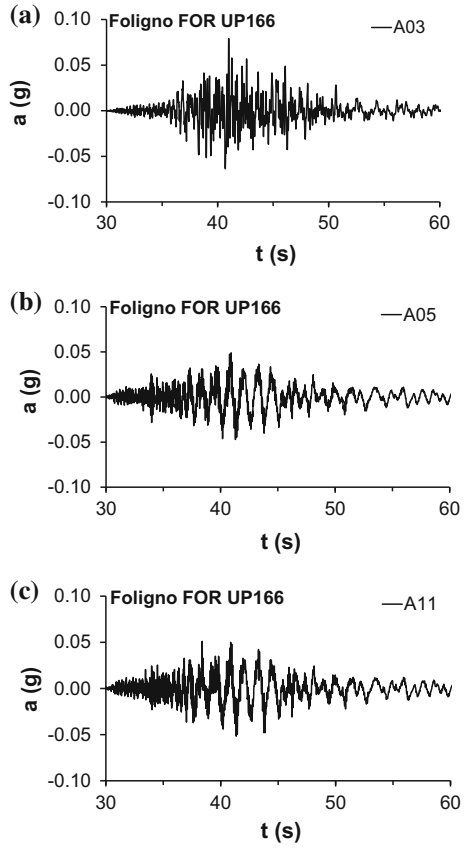
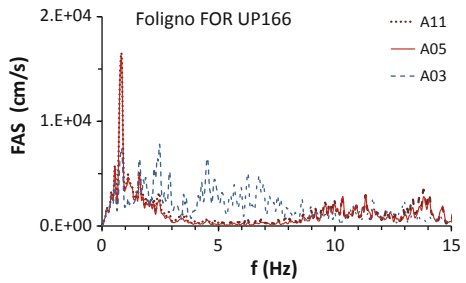


Fig. 5.19 Forestry building: Fourier spectra of recordings in the longitudinal direction



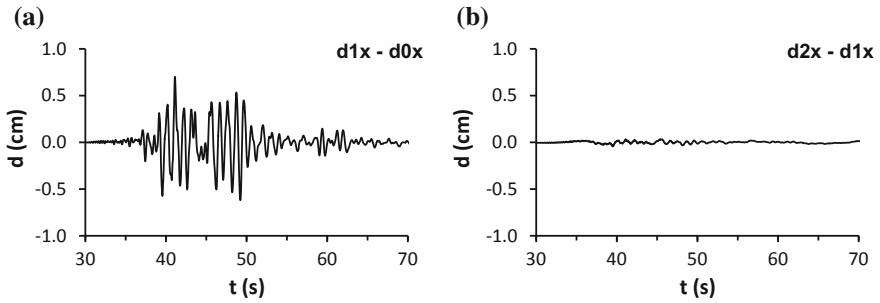


Fig. 5.20 Forestry building: relative displacement **a** between the first floor and the basement and **b** between the top and the first floor



Fig. 5.21 The C4 building, L'Aquila

This is an important feature, especially for the strategic structures, that should be operational also during and after a strong earthquake. This is important also for school buildings, which can be used as strategic structures or for temporarily hosting homeless people in the emergency phase.

The first improvement to be done for all the mentioned systems is the transformation of them in real time systems, i.e., their upgrading with real-time recording capability.

Furthermore, all these monitoring systems are made of accelerometer sensors. The displacements have been deduced by means of a double integration of the acceleration time histories, and the relative displacements are actually evaluated between the first floor and the basement displacements with a certain consume of time.

The use of relative displacement sensors, for example by using optical fibers, between the intrados and the extrados of the devices is advisable.

A real time monitoring system, based on the relative displacements of the isolation devices and supported by a suitable software, could be used as alerting system for

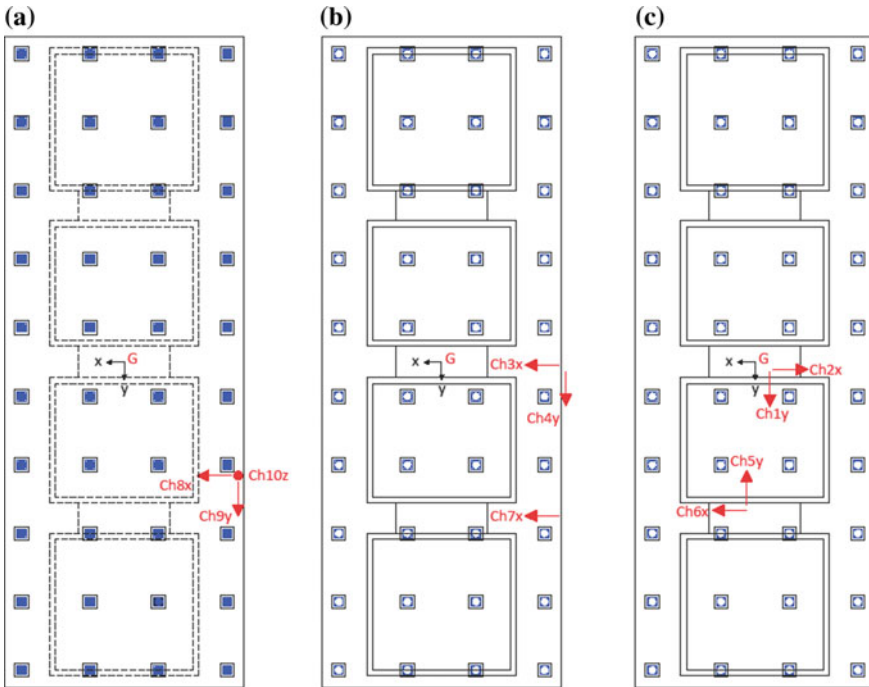


Fig. 5.22 C4 building: location of accelerometers **a** at the foundation, **b** at the first floor and **c** at the top of the building

the buildings. It can also be easily associated to the severity of the earthquake effects in that area and so to the level of the civil protection measures to activate.

5.8 Conclusions

Seismic isolation system could exhibit very different behavior under earthquakes of different energy at the site. In this paper different cases have been considered.

In the first one, the Jovine School at San Giuliano di Puglia, the HDRB isolation system was not activated and the building behaved as a fixed base building. The recorded data showed the importance of the higher modes and of the deformability of the base deck when the isolation system is not put in action.

Also the seismic sequence that occurred in Central Italy since August 2016, gave the opportunity of studying the behavior of isolation systems under low magnitude earthquakes. The behavior of three buildings during the main shock of October 30th, 2016, have been analyzes in detail.

In the first two, seismically isolated by means of HDRBs, the recordings testified the good behavior of HDRBs also under low magnitude events. As a matter of fact,

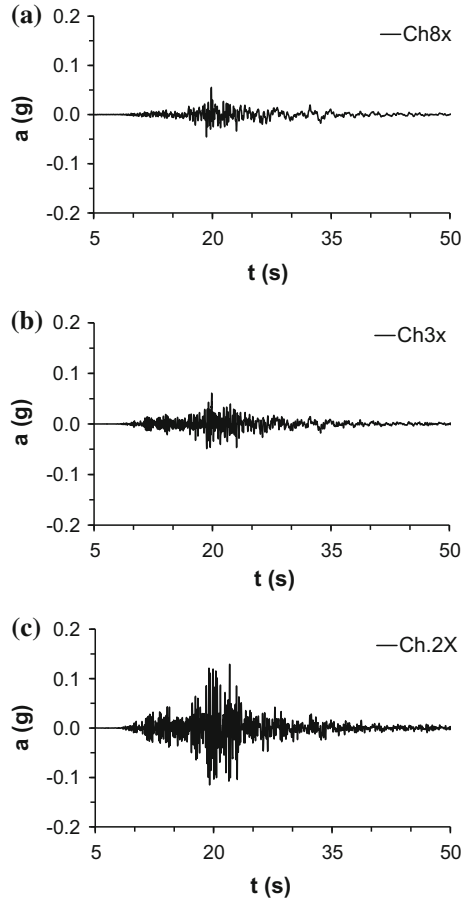


Fig. 5.23 C4 building, L’Aquila: accelerometric recordings obtained during the October 30th, 2016 earthquake ($M = 6.5$) **a** at the basement, **b** at the first floor just above the isolation system and **c** at the top of the building (DPC Osservatorio Sismico delle Strutture—OSS download service, <http://www.mot1.it/ossdownload>)

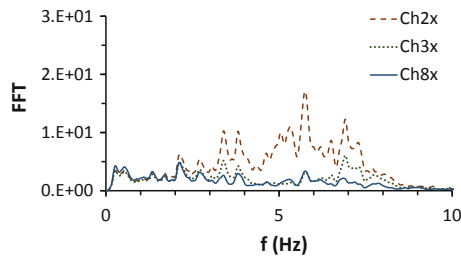


Fig. 5.24 C4 building, L’Aquila: Fourier spectra of recordings obtained during the October 30th, 2016 earthquake ($M = 6.5$) at (CH8x) the basement, (CH3x) at the first floor just above the isolation system and (CH2x) at the top of the building

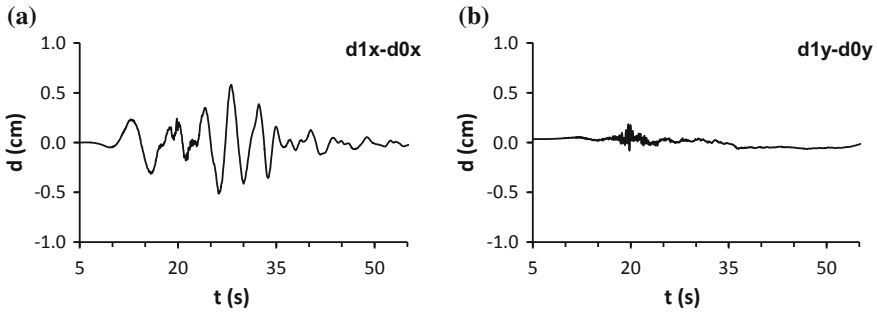


Fig. 5.25 C4 building, L' Aquila: relative displacement between the first floor and the basement

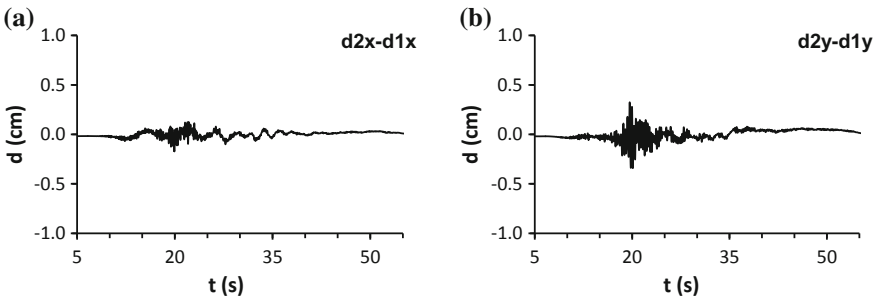


Fig. 5.26 C4 building, L' Aquila: relative displacement between the top and the first floor

the system filtered the seismic waves even though the fundamental period of vibration was significantly lower than that assumed in the structural design and relative to the design earthquake. On the contrary, in the third building, seismically isolated by means of CSSs, the system did not work properly, probably due to a very high static friction.

In all cases, the importance of an accurate non-linear analysis of their behavior under earthquakes of different magnitudes has been pointed out, in order to guarantee that the seismic action in the superstructures do not exceed those assumed in the design.

The importance of the monitoring of seismically isolated buildings is evident to assess the possible dynamic behavior of such structures during earthquakes and to gain experience on the general seismic behavior of such structures to be used in future design and analyses. Furthermore, the importance of a real time monitoring is evident, especially for strategic structures.

Acknowledgements The monitoring of the Jovine School Building in San Giuliano di Puglia is part of a research project organized by ENEA in collaboration with the Italian Department of the Civil Protection and the Municipality of San Giuliano di Puglia. The monitoring of the Civil Protection Centre at Foligno is part of a research project organized by ENEA in collaboration with the Umbria Region. The monitoring of the buildings with CSSs in L' Aquila is part of the Seismic

Observatory of Structures project, organized and managed by the Italian Department of the Civil Protection (DPC Osservatorio Sismico delle Strutture—OSS Download Service, <http://www.motl.it/ossdownload>).

References

1. Naeim F, Kelly JM (1999) Design of seismic isolated structures: from theory to practice. Wiley, New York
2. Skinner RI, Robinson WH, McVerry GH (1993) An introduction to seismic isolation, DSIR Physical Sciences, Wellington, New Zealand. Wiley, New Jersey
3. Clemente P, Buffarini G (2010) Base isolation: design and optimization criteria. *J Seismic Isolation Prot Syst* 1(1):17–40. <https://doi.org/10.2140/siaps.2010.1.17>
4. Clemente P, Martelli A (2019) Seismically isolated buildings in Italy: state-of-the-art review and applications. *Soil Dyn Earthq Eng* 119:471–487. <https://doi.org/10.1016/j.soildyn.2017.12.029>
5. Clemente P, Martelli A (2017) Anti-seismic systems: worldwide application and conditions for their correct use. In: Proceedings of the 16th world conference on earthquake engineering (16WCEE), Santiago del Chile, Keynote lecture, IAEE & ACHISINA, 9–13 Jan
6. Saitta F, Clemente P, Buffarini G, Bongiovanni G (2017) Vulnerability analysis and seismic retrofit of a strategic building. *J Perform Constr Fac* 31(2). [https://doi.org/10.1061/\(ASCE\)CF.1943-5509.0000948](https://doi.org/10.1061/(ASCE)CF.1943-5509.0000948)
7. Matsuda K, Kasai K, Yamagiwa H, Sato D (2012) Responses of base-isolated buildings in Tokyo during the 2011 great east Japan earthquake. In: Proceedings of the 15th world conference on earthquake engineering (15WCEE), Lisbon, IAEE, 24–28 Sept
8. Saito T (2015) Behaviour of response controlled and seismic isolated buildings during severe earthquake in Japan. *Energia, Ambiente e Innovazione* (5):31–37. ENEA, Roma. <https://doi.org/10.12910/EAI2015-078>
9. Zhou FL (2015) Earthquake tragedy and application of seismic isolation, energy dissipation and other seismic control systems to protect structures in China. *Energia, Ambiente e Innovazione* (5):23–30. ENEA, Roma. <https://doi.org/10.12910/EAI2015-077>
10. Zhou FL, Tan P, Heisha W, Huan XY (2015) Progress and application of seismic isolation, energy dissipation and control in civil and industrial structures and design codes in China. In: Proceedings of the 14th world conference on seismic isolation, energy dissipation and active vibration control of structures (14 WCSI), University of California at San Diego, San Diego, CA USA, 9–11 Sept 2015
11. Çelebi M (1996) Successful performance of a base-isolated hospital buildings during the 17 January 1995 Northridge earthquake. In: The structural design of tall buildings, vol 5, pp 95–109
12. Bongiovanni G, Buffarini G, Clemente P, Saitta F, Scafati F (2018) Seismic behaviour of base isolated buildings in Italy. In: Proceedings of the 16th European conference on earthquake engineering (16ECEE), Thessaloniki, 18–21 June 2018. Paper 10376
13. Clemente P (2017) Seismic isolation: past, present and the importance of SHM for the future. *J Civil Struct Health Monit* 7(2):217–231. Springer. <https://doi.org/10.1007/s13349-017-0219-6>
14. Abe M, Yoshida J, Fujino Y (2004) Multiaxial behaviors of laminated rubber bearings and their modeling. I: experimental study. *J Struct Eng* 130:1119–1132
15. Abe M, Yoshida J, Fujino Y (2004) Multiaxial behaviors of laminated rubber bearings and their modeling. II: modeling. *J Struct Eng* 130:1133–1144
16. Clemente P, Bongiovanni G, Buffarini G, Saitta F (2016) Experimental analysis of base isolated buildings under low magnitude vibrations. *Int J Earthq Impact Eng* 1(1–2):199–223. <https://doi.org/10.1504/IJIEI.2016.10000961>

17. Clemente P, Bongiovanni G, Benzoni G (2017) Monitoring of seismic isolated buildings: state of the art and results under high and low energy inputs. In: Proceedings of the New Zealand society for earthquake annual conference and 15th world conference on seismic isolation, energy dissipation and active vibration control of structures (NZSEE2017 and 15WCSI), Wellington, 27–29 April
18. Park YJ, Wen YK, Ang AH-S (1986) Random vibration of hysteretic systems under bi-directional ground motions. *Earthq Eng Struct Dynam* 14:543–557
19. Nagarajaiah S, Reinhorn AM, Constantinou MC (1991) Nonlinear dynamic analysis of 3-D base-isolated structures. *J Struct Eng* 117(7):2035–2054
20. Constantinou MC, Reinhorn AM, Tsopelas P, Nagarajaiah S (1999) Techniques in the nonlinear dynamic analysis of seismic isolated structures. In: Structural dynamic system computational techniques and optimization seismic techniques, vol 12, pp 1–24
21. Yamamoto S, Kikuchi M, Ueda M, Aiken ID (2009) A mechanical model for elastomeric seismic isolation bearings including the influence of axial load. *Earthq Eng Struct Dyn* 38(2):157–180
22. Alhan C, Gazi H, Kurtulus H (2016) Significance of stiffening of high damping rubber bearings on the response of base-isolated buildings under near-fault earthquakes. *Mech Syst Signal Process* 79:297–313
23. Lomiento G, Benzoni G (2016) Testing protocols and acceptance criteria for performance characterization of pendulum isolators. In: Proceedings of the 16th world conference on earthquake engineering, (16WCEE), Santiago del Chile, IAEE & ACHISINA, 9–13 Jan
24. Lomiento G, Bonessio N, Benzoni G (2013) Friction model for sliding bearings under seismic excitation. *J Earthq Eng* 17(8):1162–1191
25. Clemente P, Saitta F, Grossi C, Salvatori A (2015) On the behaviour of buildings with curved surface sliders: consideration and preliminary analyses. In: Proceedings of the 14th world conference on seismic isolation, energy dissipation and active vibration control of structures (San Diego), University of California San Diego, CA USA, 9–11 Sep 2015
26. Saitta F, Clemente P, Bongiovanni G, Buffarini G, Salvatori A, Grossi C (2018) Base isolation of buildings with curved surface sliders: basic design criteria and critical issues. *Adv Civ Eng* 2018:14. Article ID 1569683. <https://doi.org/10.1155/2018/1569683>
27. Bongiovanni G, Buffarini G, Clemente P, Saitta F, De Sortis A, Nicoletti M, Rossi G (2015) Behaviour of the base isolated Jovine School in San Giuliano di Puglia, Italy, under the December 20th 2013 earthquake. In: Proceedings of the 14th world conference on seismic isolation, energy dissipation and active vibration control of structures (14WCSI), University of California San Diego, San Diego, 9–11 Sept
28. Bongiovanni G, Buffarini G, Clemente P, Saitta F, Serafini S, Felici P (2016) Ambient vibration analysis of a strategic base isolated building. In: Proceedings of the 6th international conference on civil structural health monitoring (CSHM-6), Queen's University Belfast, Belfast, 26–27 May
29. Clemente P, Bongiovanni G, Buffarini G, Saitta F, Castellano MG, Scafati F (2019) Effectiveness of HDRB isolation systems under low energy earthquakes. *Soil Dyn Earthq Eng* 118:207–220, Wiley. <https://doi.org/10.1016/j.soildyn.2018.12.018>

Chapter 6

Identification of Soil-Structure Systems



S. Farid Ghahari, Fariba Abazarsa and Ertugrul Taciroglu

Abstract Structures interact with soil under seismic excitations through both inertial and kinematic effects. These soil-structure interaction (SSI) effects are often significant and system identification methods can be used to characterize and quantify them. However, system identification of soil-structure systems is fraught with difficulties. SSI renders it virtually impossible to directly measure the earthquake input motions for a soil-structure system due to kinematic interaction effects, which is the term used for denoting the differences between the soil motions at the free field and the foundation, in the absence of superstructure mass. Moreover, because of disproportional distribution of damping in a soil-structure system, normal modes are no longer able to decompose the overall system's equations of motion. Additionally, while some structures may remain linearly elastic even under high levels of vibration, soil behaves nonlinearly even under weak ground motions. Through work spanning the past decade various new methods of system identification have been devised appropriate for soil-structure systems—some of which, incidentally, are by the authors of the present article. This chapter provides an overview of the said techniques along with several application examples.

Keywords Soil-structure interaction · Blind identification · Output-only identification · Response data

6.1 Introduction

Soil-Structure Interaction (SSI) has been well studied for more than 40 years (e.g., [1–3]). SSI can be classified into two distinct effects—namely, *kinematic* and *inertial* [4]. Even in the absence of a superstructure, a massless foundation experiences different movement during an earthquake—called the Foundation Input Motion (FIM)—from the Free-Field Motion (FFM), which would have been recorded at

S. F. Ghahari · F. Abazarsa · E. Taciroglu (✉)
Civil & Environmental Engineering Department, University
of California, Los Angeles, CA 90095, USA
e-mail: etacir@ucla.edu

© Springer Nature Switzerland AG 2019
M. P. Limongelli and M. Çelebi (eds.), *Seismic Structural Health Monitoring*, Springer
Tracts in Civil Engineering, https://doi.org/10.1007/978-3-030-13976-6_6

139

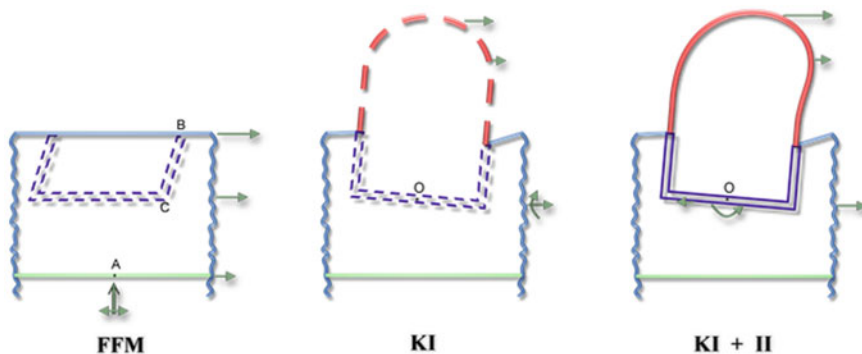


Fig. 6.1 Soil-foundation-structure interaction (courtesy of Mojtaba Mahsuli)

the same site if the foundation was not there (see Fig. 6.1 left and middle). This effect is termed as the Kinematic Interaction (KI), and is due to the stiffness differences between the foundation and its surrounding soil. FIM is dependent on both the foundation and soil properties, and the wave fields. For example, “base-slab averaging” is a major source of KI in surface foundation systems where the foundation slab experiences an average of inclined and incoherent waves [5–7]. For embedded and piled foundations, base-slab averaging is accompanied with embedment effects, which renders FIM to be further different from FFM [8–11]. Dynamic response of the structure inserts force and moments to the base and causes the foundation to have a different response from FIM. This effect is referred to as Inertial Interaction (II) (Fig. 6.1 right). Due to its inertia, the vibrating structure effectively acts as a wave propagating source and alters the wave field around it. Consequently, motions recorded around/near the structure cannot be assumed as the free-field even if KI effects are negligible.

One approach to analyze SFSI effects is to create and analyze a complete Finite Element (FE) model of the full system wherein the soil medium is represented as a semi-infinite domain (see, for example, [12]). In this method of analysis, which is usually referred to as the “direct method,” the region of the soil containing the structure is modeled up to an artificial boundary where special provisions are made in order to avoid reflections of the outbound waves (see, for example, [13]). Because superposition is not required, material nonlinearities in both the soil domain and the structure can be considered; thus, this is a quite general approach to SSI analysis. Nevertheless, the direct method is typically avoided in engineering practice due to the labor-intensive finite element model development, and the high computational cost associated with carrying out successive simulations under multiple input motions. The primary alternative approach is the so-called “substructure method,” wherein the SSI problem is broken down into three distinct parts, which are combined to formulate the complete solution as follows: (i) estimation of FIMs (Fig. 6.2a), (ii) determination of soil-foundation Impedance Functions (IFs) (Fig. 6.2b), and (iii)

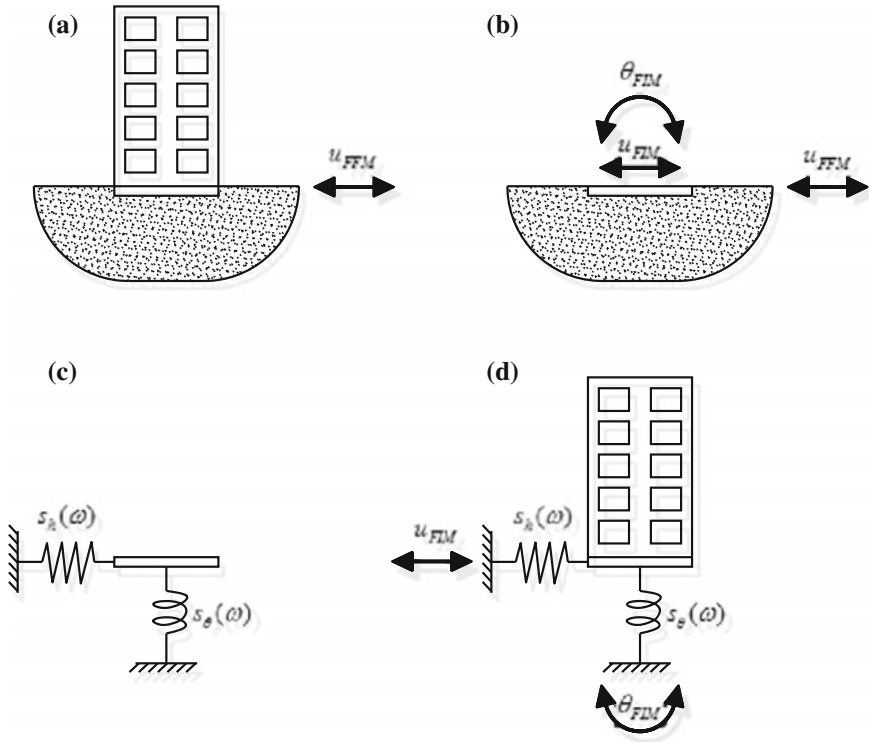


Fig. 6.2 A schematic presentation of the substructure method: **a** soil-structure response problem, **b** evaluation of FIMs, **c** evaluation of impedance function, and **d** analysis of structure on compliant base subjected to FIMs [22]

dynamic analysis of the structure supported on a compliant base represented by the IF and subjected to the FIMs (Fig. 6.2c).

System Identification (SI) is at the heart of Structural Health Monitoring (SHM). Seismic Structural Health Monitoring (S²HM) is more challenging, because traditional Operational Modal Analysis (OMA) techniques (e.g., [14–16]) cannot be used for seismic signals, as they assume various statistical properties on signals, which are not valid for earthquake excitations (see, for example, [17]).

According to the substructure method described above, S²HM becomes even more challenging for SSI systems, because FFMs cannot be used as input excitations anymore, and FIMs are physically unmeasurable. Therefore, Input-Output (IO) identification methods (e.g., [18]) are no longer applicable. Moreover, the IFs are frequency- and amplitude-dependent (see, for example, [19, 20]). IFs also have a (radiation) damping term, which renders the mode shapes of the overall dynamic system complex-valued [21]. Through work spanning the past decade—by the authors, their collaborators and as well as other colleagues—various new methods of system identification have been devised that can handle soil-structure systems. In what

Table 6.1 Input-output pairs for identifying modal properties associated with different conditions of base fixity [28]

System	Input	Output
Flexible base	u_g	$u_g + u_f + h\theta + u$
Pseudo-flexible base	$u_g + u_f$	$u_g + u_f + h\theta + u$
Fixed base	$u_g + u_f + h\theta$	$u_g + u_f + h\theta + u$

follows, the said techniques are reviewed and several application examples are provided.

6.2 Identification of SSI Systems

One of the first well-instrumented structures is the Millikan Library, for which SSI effects were incidentally observed to be quite important. As such, research efforts on identification of soil-foundation systems from their seismic responses (e.g., [23]) are almost contemporary with system identification of buildings (e.g., [24]). A full history of identification studies on this well-known building can be found in [25]. However, the studies initiated by Luco [26] and Safak [27] and later continued by Stewart and Fenves [28] and Safak [29] on identifying and quantifying SSI effects are generally deemed as the pioneering works in this field. They mathematically showed that depending to the type of input motion used in an Input-Output (IO) identification strategy, various idealizations of a soil-structure-foundation system could be identified as presented in Table 6.1. According to their definitions, the “flexible base” system could be identified if KI is negligible and FFM (u_g) is used as input excitation. Otherwise, using various combinations of signals recorded at the foundation (u_f : sway and/or θ : rocking) will result in the identification of systems with fictitious boundary conditions called “pseudo-flexible base” or “fixed base” systems. It is obvious that KI could be present in many cases. Also, the motions recorded close to the buildings could be affected by the waves emitted from the vibrating building—which, in fact, can be detected in the results presented by [28, 30]. Therefore, utilization of IO techniques for identifying soil-foundation-structure systems is rife with potential errors.

6.2.1 Blind Modal Identification (BMID) Techniques

6.2.1.1 Theoretical Background

Because of the unavailability of true input motions that can be used to identify flexible base systems using IO methods, and due to the inherent limitation of classic

Output-Only (OO) identification techniques, Ghahari et al. [31] developed a new OO identification method based on a class of Blind Source Separation (BSS) techniques [32], which can be used for non-stationary seismic data. This method takes advantage of the non-stationarity of seismic signals, indeed, and is based on the assumption that there are points in the time-frequency plane where the modes are disjoint. The details of the method are briefly reviewed next.

The governing equations of motion for a Multi-Degree-Of-Freedom (MDOF) system with n_d DOFs, which is excited by a unidirectional (scalar) FIM, can be expressed as follows

$$\mathbf{M}\ddot{\mathbf{x}}(t) + \mathbf{C}\dot{\mathbf{x}}(t) + \mathbf{K}\mathbf{x}(t) = -\mathbf{M}\mathbf{I}\ddot{x}_g(t) \quad (6.1)$$

where \mathbf{M} , \mathbf{C} , and \mathbf{K} are the constant $n_d \times n_d$ mass, damping, and stiffness matrices of the system, respectively. The vector $\mathbf{x}(t)$ contains relative displacement responses of the system at all DOFs; $\ddot{x}_g(t)$ is a scalar time-signal, which represents the (unknown) FIM; and \mathbf{I} is the influence vector [33]. In practical cases, the absolute acceleration of the structure is recorded, which is

$$\ddot{\mathbf{x}}^t(t) = \ddot{\mathbf{x}}(t) + \mathbf{I}\ddot{x}_g(t). \quad (6.2)$$

By assuming a proportional damping matrix, the absolute acceleration response can be expressed in modal space as

$$\ddot{\mathbf{x}}^t(t) = \Phi\ddot{\mathbf{q}}(t) \quad (6.3)$$

where Φ is an $n_d \times n_d$ real-valued mode shape matrix whose i -th column (ϕ_i) is the i -th mode shape; and $\ddot{\mathbf{q}}(t)$ is a vector that contains the absolute acceleration modal coordinates.

The Cohen-class Spatial Time-Frequency Distribution (STFD) [34] of responses can be calculated as

$$\mathbf{D}_{\ddot{\mathbf{x}}^t\ddot{\mathbf{x}}^t}(t, f) = \int_{-\infty}^{+\infty} h(\tau) \int_{-\infty}^{+\infty} g(s-t) \mathbf{z}\left(s + \frac{\tau}{2}\right) \mathbf{z}^H\left(s - \frac{\tau}{2}\right) ds e^{-2\pi j f \tau} d\tau \quad (6.4)$$

where $\mathbf{z}(t)$ is the analytic associate of $\ddot{\mathbf{x}}^t(t)$, and the functions h and g are smoothing functions that reduce the spurious inference terms [35]. The superscript H denotes a Hermitian transpose. This specific time-frequency distribution is called the smoothed pseudo Wigner-Ville distribution, which is available through a MATLAB [36] toolbox freely available at <http://tftb.nongnu.org/> [37]. Calculating the STFD of both sides of Eq. (6.3) yields

$$\mathbf{D}_{\ddot{\mathbf{x}}^t\ddot{\mathbf{x}}^t}(t, f) = \Phi \mathbf{D}_{\ddot{\mathbf{q}}\ddot{\mathbf{q}}}(t, f) \Phi^T \quad (6.5)$$

Considering the STFD definition provided in Eq. (6.4), and by assuming that it is an ideal time-frequency distribution tool by which the interference-terms are not produced, the Time-Frequency (TF) points can now be classified into three different groups based on the localization of modal coordinates observed in earthquake engineering:

- **Single Auto-Term TF Point (SATFP):** At these points, only one mode is present; thus, $\mathbf{D}_{\ddot{q}\ddot{q}}(t, f)$ matrices are diagonal with only one non-zero diagonal element.
- **Multiple Auto-Term TF Point (MATFP):** At these points, several modes are present; thus, $\mathbf{D}_{\ddot{q}\ddot{q}}(t, f)$ matrices have non-zero diagonal and off-diagonal elements.
- **Cross-Term TF Point (CTTFP):** At these points, the cross-TFDs of modal coordinates are non-zero, while their corresponding auto-TFDs are zero. Thus, $\mathbf{D}_{\ddot{q}\ddot{q}}(t, f)$ matrices are off-diagonal.

As will be discussed in subsequent subsections, SATFPs play an important role in the BMID techniques. While there are various procedures to find these points from $\mathbf{D}_{\ddot{x}\ddot{x}'}(t, f)$ matrices, the proper formula and consequently identification procedure are dependent on the number of available measurements/sensors and the number of contributing modes.

6.2.1.2 Over-determined Case

Let's assume that the number of active modes (n_m) is smaller than the number of sensors (n_r)—i.e., $n_m \leq n_r \leq n_d$. This case is dubbed the over-determined case. For a moment let us assume that we know the SATFPs corresponding to the i -th mode, so we have

$$\mathbf{D}_{\ddot{x}\ddot{x}'}(t_i, f_i) = \boldsymbol{\phi}_i D_{\ddot{q}_i\ddot{q}_i}(t_i, f_i) \boldsymbol{\phi}_i^H \quad (6.6)$$

where $D_{\ddot{q}_i\ddot{q}_i}(t_i, f_i)$ is i -th mode's auto-TFD and the i -th diagonal element of $\mathbf{D}_{\ddot{q}\ddot{q}}(t, f)$. Equation (6.6) shows that an Eigenvalue Decomposition (EVD) can be used to extract $\boldsymbol{\phi}_i$ and $D_{\ddot{q}_i\ddot{q}_i}(t_i, f_i)$ from $\mathbf{D}_{\ddot{x}\ddot{x}'}(t_i, f_i)$. However, $\mathbf{D}_{\ddot{q}\ddot{q}}(t_i, f_i)$ is rank-deficient, and thus, $\boldsymbol{\Phi}$ can't be uniquely determined. Moreover, external criteria are needed to specify the true auto-terms of each source signal and to decide which mode's auto-term should be used for EVD. The difference between the number of modes and the number of sensors poses further difficulties for EVD. Belouchrani and Amin [32] showed that it is necessary and sufficient to use all of the auto-terms simultaneously, without knowing to which source they belong. Hence, a Joint Approximate Diagonalization (JAD) technique is employed instead of EVD [38].

Because the JAD algorithm is restricted to finding a unitary diagonalizing matrix, a preprocessing step called whitening $\ddot{\mathbf{x}}^t(t) = \mathbf{W}\ddot{\mathbf{x}}^t(t)$ is carried out where the whitening matrix is obtained from the correlation matrix of $\ddot{\mathbf{x}}^t(t)$ at zero lag. The whitening process reduces the determination of the $n_r \times n_m$ mode shape matrix $\boldsymbol{\Phi}$ to that of a unitary $n_m \times n_m$ matrix \mathbf{U} , that is

$$\mathbf{D}_{\ddot{\mathbf{x}}\ddot{\mathbf{x}}}(t, f) = \mathbf{U}\mathbf{D}_{\ddot{\mathbf{q}}\ddot{\mathbf{q}}}(t, f)\mathbf{U}^H. \quad (6.7)$$

Now, any whitened STFD-matrix is diagonal when stated in the basis of the columns of the matrix \mathbf{U} . As mentioned previously, this unknown unitary matrix can be identified through a Joint Approximate Diagonalization of $\mathbf{D}_{\ddot{\mathbf{x}}\ddot{\mathbf{x}}}(t, f)$ at the SATFPs. After the identification of \mathbf{U} , the mode shape matrix, and the modal coordinates $\ddot{\mathbf{q}}(t)$, may be recovered as follows

$$\Phi = \mathbf{W}^\# \mathbf{U}, \quad (6.8)$$

$$\ddot{\mathbf{q}}(t) = \mathbf{U}^H \mathbf{W} \ddot{\mathbf{x}}(t) \quad (6.9)$$

where the superscript # denotes a Moore-Penrose pseudo-inverse. Once the modal coordinates are recovered, natural frequencies and damping ratios can be identified by cross-solving for the modal coordinates, as they have the same input excitations and only differ by a factor. Details of this process are omitted here for the sake of brevity and can be found in [31].

There are various criteria that can be used for identifying the SATFPs from $\mathbf{D}_{\ddot{\mathbf{x}}\ddot{\mathbf{x}}}(t, f)$. However, at each SATFP, each STFD matrix is of rank one—or at least, each matrix has one significantly large eigenvalue compared to its other eigenvalues. Therefore, the following criterion may be used to deselect the Non-SATFPs [39],

$$\left| \frac{\lambda_{max}[\mathbf{D}_{\ddot{\mathbf{x}}\ddot{\mathbf{x}}}(t, f)]}{\|\mathbf{D}_{\ddot{\mathbf{x}}\ddot{\mathbf{x}}}(t, f)\|_F} - 1 \right| > \varepsilon \quad (6.10)$$

where $\|\cdot\|_F$ denotes the Frobenius norm, ε is a small positive scalar (typically, 0.001) and $\lambda_{max}[\cdot]$ represents the largest eigenvalue of its argument matrix. Note that in this new criterion, the STFD matrix of the original data (as opposed to that of the whitened data) is used.

To verify the method, a 5-DOF shear building is placed on top of a sway-rocking foundation. Mass-proportional damping with 10% first mode damping is considered for the entire system. The response of the system is simulated under a horizontal accelerogram recorded in El Centro Array #9 during the Imperial Valley earthquake, 1940. As an illustration, TFD of the roof response is shown in Fig. 6.3a. Figure 6.3b displays the time variation of Modal Assurance Criterion (MAC) values between the identified and exact mode shapes in various 10-second time windows. While the method is very successful, this figure shows how the method is able to take advantage of the non-stationary nature of ground motions to identify Mode 4 in a short time window.

The identified natural frequencies and damping ratios are shown in Table 6.2 along with exact values. As seen, neglecting minor errors in damping ratios which are accepted, the method is very successful.

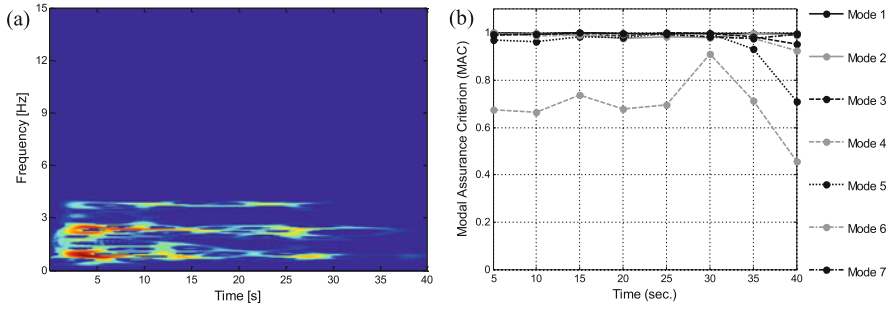


Fig. 6.3 a TFD of the roof response, and b time variation of MAC index

Table 6.2 Comparison of the identified and analytical modal properties

	Mode	1	2	3	4	5	6	7
Exact	f_n (Hz)	0.91	2.45	3.87	4.91	5.43	7.57	10.97
	ξ (%)	10.00	3.70	2.34	1.85	1.67	1.20	0.83
Identified	f_n (Hz)	0.90	2.43	3.86	4.81	5.30	7.59	10.96
	ξ (%)	8.02	3.76	2.29	1.83	1.59	1.21	0.83

6.2.1.3 Torsionally Coupled Buildings

The method presented in the last section can be easily extended to buildings that exhibit lateral-torsional coupling [40] because modal superposition is still valid. However, the identification of natural frequencies and damping ratios from the recovered modal coordinates is more challenging than the unidirectional case. In [40] it was shown that if we use the cross-relation between close modes, we are able to identify modal properties with acceptable accuracy.

To examine the performance of this method, we applied it to the earthquake data recorded at the three-story Hilltop Medical building (CSMIP Station No. 58506) during the 1989 Loma Prieta earthquake. The building’s instrumentation layout is shown in Fig. 6.4. While the building has a symmetrical plan, its torsional movements have been reported in the literature [41]. Here, we apply our identification technique to the first 40 s of the recorded responses of the 2nd, 3rd, and roof floors (ground floor response signals are excluded due to low levels of motion). Table 6.3 displays the identified natural frequencies and damping ratios versus those identified from similar data sets using a completely different method [42]. While we do not expect to see identical results, they are quite similar.

6.2.1.4 Multiple Support Excitation

Along the path towards more complex problems, the BMID method was extended to the analysis of bridge structures under multiple support excitations [43]. Again,

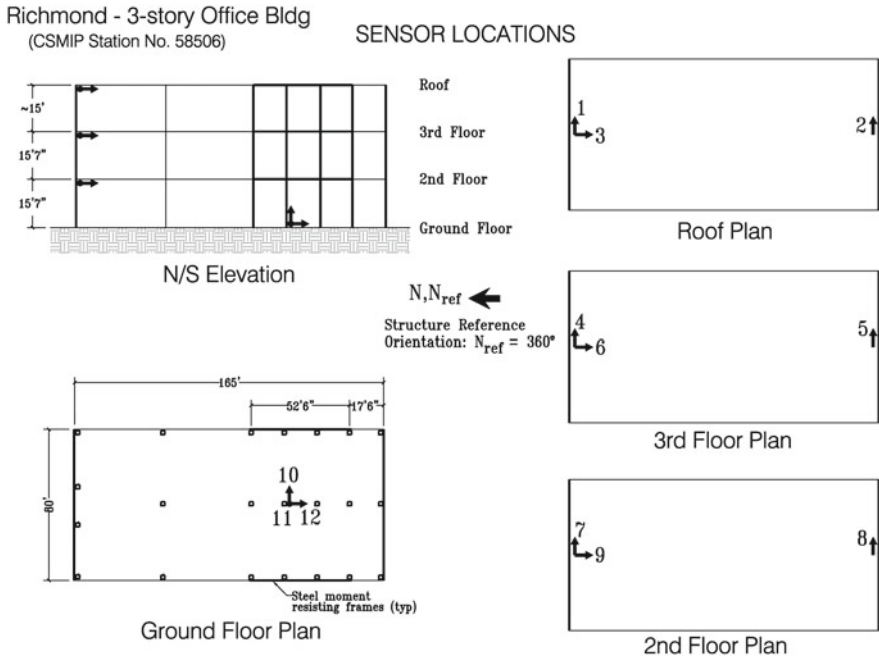


Fig. 6.4 Instrumentation layout of CSMIP station 58506

Table 6.3 Comparison between identified natural frequencies and damping ratios with others' results

	Mode	1	2	3	4	5	6
Exact	f_n (Hz)	1.35	1.64	2.27	3.76	4.75	5.58
	ξ (%)	8.4	4.8	1.4	4.8	5.3	–
[42]	f_n (Hz)	1.30	1.61	2.22	3.83	4.61	5.38
	ξ (%)	8.4	4.5	4.6	7.2	6.2	7.9

the first step—i.e., modal decomposition—is not affected by this extension, but the identification of natural frequencies and damping ratios is a challenging task.

Let's assume that the modal coordinates (in the absolute acceleration sense) are already identified. The i -th modal coordinate can be written as a superposition of i -th modal coordinates under each support excitation, $\ddot{q}_i^t[k] = \sum_{l=1}^{n_g} \ddot{q}_i^{t,l}[k]$, where n_g is the number of support excitations and

$$\ddot{q}_i^{t,l}[k] = A_i \ddot{q}_i^{t,l}[k - 1] + B_i \ddot{q}_i^{t,l}[k - 2] + \beta_i^l C_i \ddot{x}_{g_l}[k] + \beta_i^l D_i \ddot{x}_{g_l}[k - 1] \quad (6.11)$$

where

$$A_i = 2e^{-\xi_i \omega_{ni} \Delta t} \cos(\omega_{di} \Delta t), \quad (6.12)$$

$$B_i = -e^{-2\xi_i\omega_{ni}\Delta t}, \quad (6.13)$$

$$C_i = 2\xi_i\omega_{ni}\Delta t, \quad (6.14)$$

$$D_i = \omega_{ni}\Delta t e^{-\xi_i\omega_{ni}T} \left[\frac{\omega_{ni}}{\omega_{di}} (1 - 2\xi_i^2) \sin(\omega_{di}\Delta t) - 2\xi_i \cos(\omega_{di}\Delta t) \right], \quad (6.15)$$

where Δt is sampling time; and ξ_i , ω_{ni} , and $\omega_{di} = \omega_{ni}\sqrt{1 - \xi_i^2}$ respectively denote the damping ratio, and the undamped and damped natural frequencies of the i -th mode. We can determine the unknown parameters $\mathbf{x} = [\xi_1, \dots, \xi_n, \omega_{n1}, \dots, \omega_{nn}, \beta_1^1, \dots, \beta_n^1, \dots, \beta_n^{n_g}, \ddot{x}_{g1}, \dots, \ddot{x}_{gn_g}]$ by solving the following minimization problem

$$\min_{\mathbf{x}} \|\mathbf{G}(\mathbf{x})\|_2^2 \quad (6.16)$$

where $\mathbf{G}(\mathbf{x})$ is the difference between the recovered modal coordinates and their counterparts calculated using Eq. (6.11) for all times and modes stacked in a single vector. As long as the number of equations ($N \times n_m$) is greater than the number of unknowns ($n_m + n_m + n_g \times n_m + n_g \times N$), the optimization problem will have a solution, but it will be highly non-convex. Based on this reason, we limit our cases to the those in which the input motions experienced by the bridge supports differ only by a time delay.

For validation, the proposed approach was applied to experimental data collected on a 1:50 scale bridge shown in Fig. 6.5 [44]. To excite the test model, an artificially generated time-history displacement was used. For considering the wave passage effects, the input motion was applied with a 7 ms phase-delay at each pier from left to right (there are 5 piers) and the response was recorded at the three middle masses. The identified input excitation is compared with the exact one applied in Fig. 6.6a. As seen, they are very close to each other. To obtain the phase delay, we carried out optimization for a range of delays and determined the one that yields the minimum residual norm, which is shown in Fig. 6.6b. The values of this optimal phase delay is around the 7 ms used by Norman and Crewe.

6.2.1.5 Under-determined Case

As mentioned earlier, the main assumption in BMID is that the number of modes is smaller than the number of measured responses. In this section, we extend the method to the so-called under-determined cases, for which $n_m \geq n_r$ [45].

The first change takes place in the SATFP selection step. We replace EVD with Singular Value Decomposition (SVD) and select points for which the following metric is very close to 1 [46]

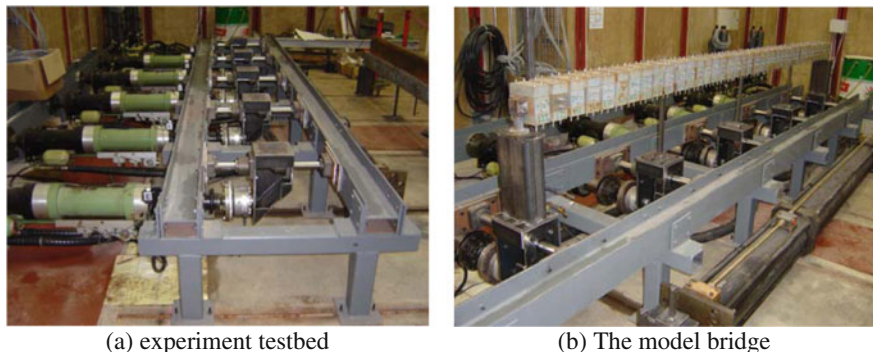


Fig. 6.5 The scaled bridge model under test

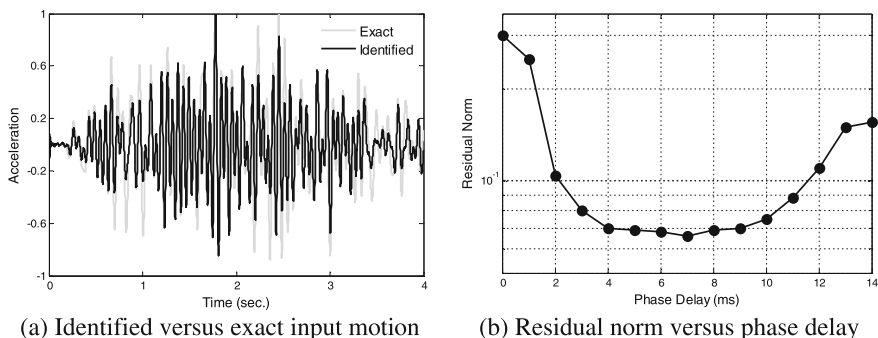


Fig. 6.6 Identification results

$$C(t, f) = \frac{\max_i \{\sigma_i [\mathbf{D}_{\ddot{x}'\ddot{x}'}(t, f)]\}}{\sum_i \{\sigma_i [\mathbf{D}_{\ddot{x}'\ddot{x}'}(t, f)]\}} \tag{6.17}$$

where $\sigma_i[\cdot]$ denotes the singular value of its argument matrix. Now, suppose that there are two SATFPs (t_1, f_1) and (t_2, f_2) that are related to k -th mode. We would then have,

$$\mathbf{D}_{\ddot{x}'\ddot{x}'}(t_1, f_1) = \phi_k D_{\ddot{q}_k\ddot{q}_k}(t_1, f_1) \phi_k^T, \tag{6.18}$$

$$\mathbf{D}_{\ddot{x}'\ddot{x}'}(t_2, f_2) = \phi_k D_{\ddot{q}_k\ddot{q}_k}(t_2, f_2) \phi_k^T. \tag{6.19}$$

As seen, $\mathbf{D}_{\ddot{x}'\ddot{x}'}(t_1, f_1)$ and $\mathbf{D}_{\ddot{x}'\ddot{x}'}(t_2, f_2)$ have the same eigenvectors (corresponding to the largest eigenvalue). That is, the STFD matrices of response signals at all SATFPs corresponding to the same mode have the same eigenvector. Therefore, a clustering approach can be used to categorize the principal eigenvectors of the STFD matrices of the response signals at all SATFPs into n_m groups. For this a “ k -means” clustering can be used. This clustering is a partitioning method through which data

(here, a set of eigenvectors) are grouped into k mutually exclusive clusters. To do so, a distance measure, here MAC, is used and the k -means approach partitions the eigenvectors into clusters in which the vectors within each cluster are both as close to each other as possible *and* as far from those vectors that belong to other clusters as possible.

Once the mode shapes are identified, modal coordinates' TFDs are recovered through the following approach—as mode shape inversion does not work for the under-determined cases.

Assume that there exists a point (t', f') at which p modes are present where $p < n_m$. If these p modes are labeled with indices $\alpha_1, \alpha_2, \dots, \alpha_p$, then Eq. (6.5) can be rewritten at this time-frequency point as

$$\mathbf{D}_{\tilde{\mathbf{x}}\tilde{\mathbf{x}}'}(t', f') = \tilde{\Phi} \mathbf{D}_{\tilde{\mathbf{q}}\tilde{\mathbf{q}}}(t', f') \tilde{\Phi}^T \quad (6.20)$$

where

$$\tilde{\Phi} = [\phi_{\alpha_1}, \dots, \phi_{\alpha_p}], \quad (6.21)$$

$$\tilde{\mathbf{q}}(t) = [\tilde{q}_{\alpha_1}(t), \dots, \tilde{q}_{\alpha_p}(t)]^T. \quad (6.22)$$

Since the matrix $\mathbf{D}_{\tilde{\mathbf{q}}\tilde{\mathbf{q}}}(t', f')$ is full rank, a projector onto the orthogonal complement of $\mathbf{D}_{\tilde{\mathbf{x}}\tilde{\mathbf{x}}'}(t', f')$ can be defined as

$$\mathbf{P} = \mathbf{I} - \mathbf{V}\mathbf{V}^T \quad (6.23)$$

where \mathbf{I} is an $n_r \times n_r$ identity matrix, and \mathbf{V} is an $n_r \times p$ matrix formed by the p principal singular vectors of $\mathbf{D}_{\tilde{\mathbf{x}}\tilde{\mathbf{x}}'}(t', f')$. It can be shown that [47]

$$\mathbf{P}\phi_i = \mathbf{0} \quad \forall i \in \{\alpha_1, \alpha_2, \dots, \alpha_p\}, \quad (6.24)$$

$$\mathbf{P}\phi_i \neq \mathbf{0} \quad \forall i \notin \{\alpha_1, \alpha_2, \dots, \alpha_p\}. \quad (6.25)$$

Thus, by considering the noise effects and the calculation errors, $\{\alpha_1, \alpha_2, \dots, \alpha_p\}$ can be obtained as the p modes that have the smallest $\|\mathbf{P}\phi_i\|$. This process can be employed at all time-frequency points to detect their present modes. Then, the modal coordinates' TFDs can be easily recovered as the diagonal elements of the following matrix,

$$\mathbf{D}_{\tilde{\mathbf{q}}\tilde{\mathbf{q}}}(t', f') = \tilde{\Phi}^\# \mathbf{D}_{\tilde{\mathbf{x}}\tilde{\mathbf{x}}'}(t', f') \tilde{\Phi}^{\#T}. \quad (6.26)$$

By recovering the modal coordinates' TFDs, natural frequencies can be identified as those frequencies that have the highest time-marginal energy, and damping ratios can be identified using the free-vibration portion of the TFD.

To demonstrate the performance of the proposed method, we identify the modal properties of a 10-story shear building from its simulated responses under the horizontal accelerogram recorded at the El Centro Array #9 during the 1940 Imperial Valley earthquake. We carry out identification under incomplete instrumentation in which the responses recorded at the 2nd, 4th, 5th, 6th, and 10th stories are used. Figure 6.7 shows the identified mode shapes (green and red) versus the exact (gray) ones. The figure also displays the mode shapes corresponding to all SATFPs in each cluster. Note that the second estimation is obtained by finding the centroid of the clusters after removing elements with low silhouette indices. As seen, the mode shapes are identified very accurately. By using the proposed recovering technique, the modal coordinates' TFDs are also recovered and are displayed in Fig. 6.8 for two modes. The exact TFDs calculated by using the exact modal coordinates are also shown for comparison, showing almost perfect reconstruction.

6.2.1.6 Extended BMID

Tensor decomposition is a powerful tool, which recently attracted attention in system identification applications [48]. The authors employed Parallel Factor Decom-

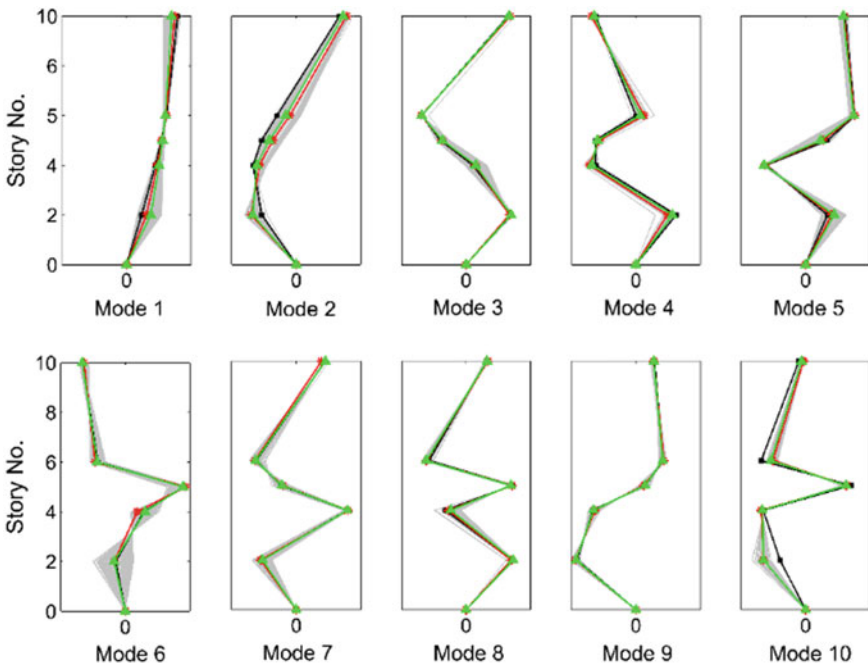


Fig. 6.7 Clustered (gray), exact (black), first estimation (red), and second estimation (green) of the mode shapes (color figure online)

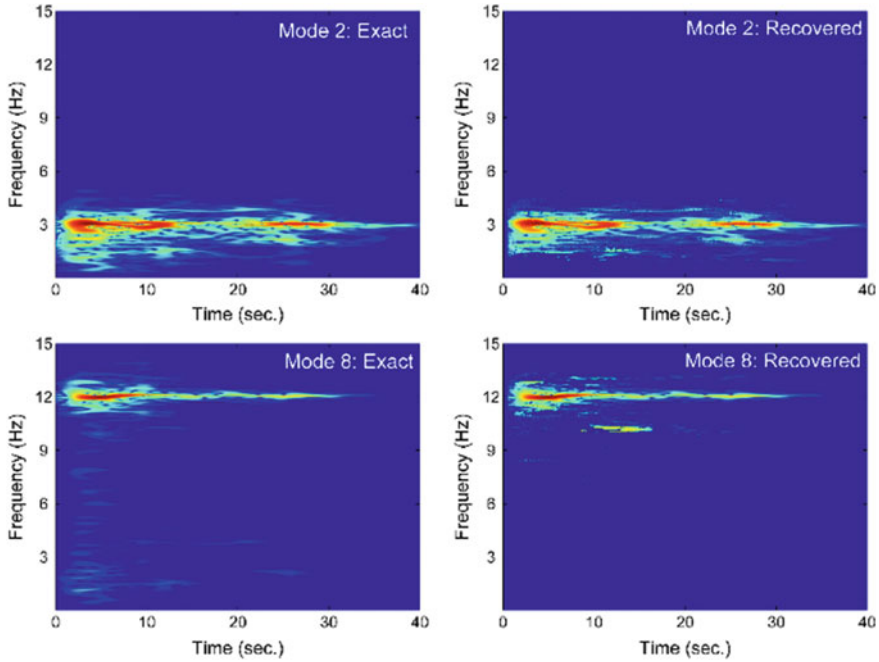


Fig. 6.8 Comparison between the auto-TFDs of the exact and the recovered modal coordinates

position (PARAFAC) [49] to decompose the third-order tensor constructed using STFD matrices selected at SATFPs to identify the mode shapes and modal coordinates' TFDs [50]. The method—dubbed as the eXtended BMID (XB MID)—is able to handle both over-determined and underdetermined cases efficiently. The distinct decomposition procedure as well as the original BMID method are briefly described here.

First, the STFD matrices at selected SATFPs are stacked together to construct a third-order tensor as $[\tilde{\mathbf{D}}_{\ddot{x}'}]_{ijk} = [\mathbf{D}_{\ddot{x}'}(t_k, f_k)]_{ij}$ where $i, j = 1, \dots, n_r$ and $k = 1, \dots, n_K$, where n_K is the total number of SATFPs. Then, a new matrix is defined as $[\mathbf{D}_{\ddot{q}}]_{kr} = [\mathbf{D}_{\ddot{q}\ddot{q}}(t_k, f_k)]_{rr}$ where $r = 1, \dots, n_m$. Per Eq. (6.5), each element of $[\tilde{\mathbf{D}}_{\ddot{x}'}]_{ijk}$ can be expressed as

$$[\tilde{\mathbf{D}}_{\ddot{x}'}]_{ijk} = \sum_{r=1}^{n_m} [\Phi]_{ir} [\Phi]_{jr} [\mathbf{D}_{\ddot{q}}]_{kr}. \quad (6.27)$$

The equation above implies that $\tilde{\mathbf{D}}_{\ddot{x}'}$ can be decomposed into n_m rank-one tensors and that the mode shape matrix can be identified in this manner. To do so, the tensor $\tilde{\mathbf{D}}_{\ddot{x}'}$ can be expressed as a generalized STFD matrix as $[\mathbf{D}_{\ddot{x}'}]_{(i-1)n_r+j,k} = [\tilde{\mathbf{D}}_{\ddot{x}'}]_{ijk}$. The

Khatri-Rao representation of this $n_r^2 \times n_K$ matrix, which is equivalent to Eq. (6.27) is given as

$$\underline{\mathbf{D}}_{\dot{\mathbf{x}}_r} = (\Phi \odot \Phi) \mathbf{D}_{\dot{\mathbf{q}}}^T \quad (6.28)$$

where \odot is the Khatri-Rao product operator. The SVD of $\underline{\mathbf{D}}_{\dot{\mathbf{x}}_r}$ is simply,

$$\underline{\mathbf{D}}_{\dot{\mathbf{x}}_r} \approx \mathbf{U} \mathbf{\Delta} \mathbf{V}^T \quad (6.29)$$

where \mathbf{U} and \mathbf{V} are $n_r^2 \times n_m$ and $n_K \times n_m$ column-wise, respectively; $\mathbf{\Delta}$ is an $n_m \times n_m$ positive-definite diagonal matrix. Equations (6.28) and (6.29) imply that there exist an $n_m \times n_m$ non-singular unknown matrix \mathbf{F} such that

$$\Phi \odot \Phi = \mathbf{U} \mathbf{\Delta} \mathbf{F}, \quad (6.30)$$

$$\mathbf{D}_{\dot{\mathbf{q}}} = \mathbf{V} \mathbf{F}^{-T}. \quad (6.31)$$

By computing the matrix \mathbf{F} —whose details can be found in the paper by [50]—, the mode shape matrix Φ and modal coordinates' TFDs at selected SATFPs, $\mathbf{D}_{\dot{\mathbf{q}}}$, can be easily estimated, while the approach presented in the last section could be also used to recover the modal coordinates' TFDs at all time-frequency points.

The XBMID is the most complete version of the BMID and has been verified, validated, and applied to various real-life case studies (see, for example, [25, 51, 52]). Figure 6.9 shows a scaled 10-story structure, which was constructed and tested at Iran's International Institute of Earthquake Engineering and Seismology (IIIES). Data from those tests are used to validate the XBMID technique. The structure was excited under various types of ground motions (Fig. 6.10) and the identified mode shapes are verified through comparing results with those identified by an IO method, ERA/OKID [18]. As seen in Table 6.4, MAC indices for almost all modes and all shake table tests are close to 1.

6.2.1.7 Non-classical Damping

As mentioned at the beginning of this chapter, non-classical damping is an attribute that is encountered in the identification of SSI systems, due to the concentrated damping source provided by the soil-foundation system that the superstructure interacts with. The studies on modal identification in the presence of non-classical damping are quite limited (see, for example, [53, 54]). This is primarily due to inherent complexities of the problem. Specifically, imperfections and measurement noise could themselves result in complex-valued mode shapes; and modal damping ratios are always highly uncertain due to their low observability in recorded data even for systems with classical damping. Nevertheless, the authors have developed a special version of XBMID that is able to identify modal properties of a system with non-

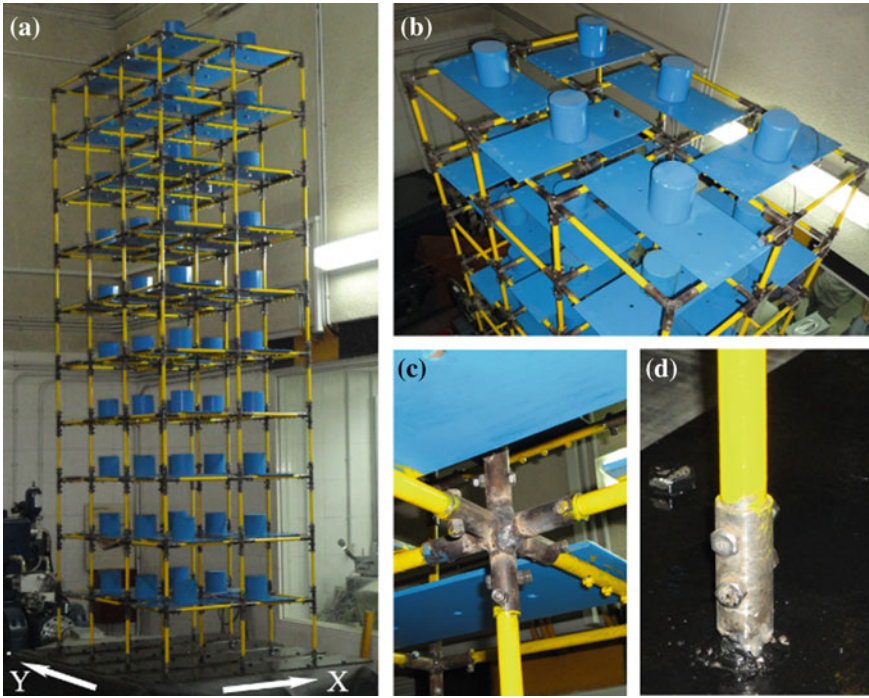


Fig. 6.9 a IIEES test structure; b distribution of additional masses; c beam-column; d column-base connection

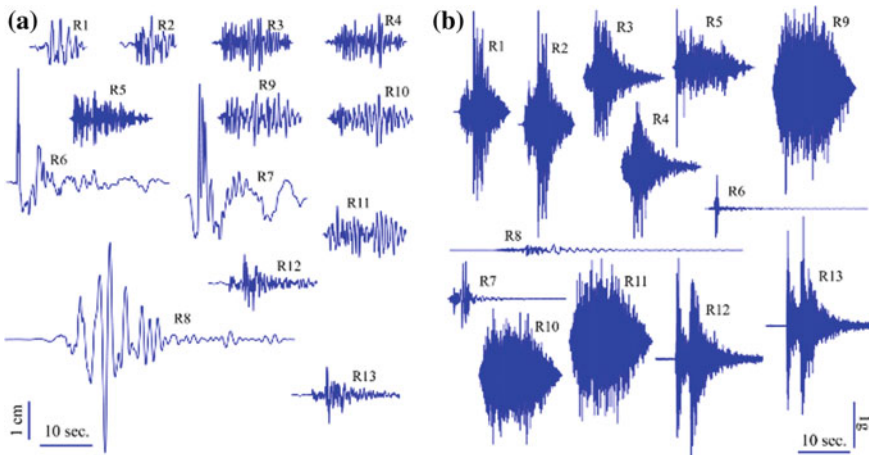


Fig. 6.10 a Displacement and b acceleration time histories of the ground motions

Table 6.4 MAC indices between the identified mode shapes from XB MID and ERA/OKID

Record no. →	1	2	3	4	5	6	7	8	9	10	11	12	13
Mode no. 1	0.95	1.00	1.00	1.00	0.97	0.95	0.94	0.92	0.99	0.99	0.98	1.00	1.00
2	NA *	0.95	0.93	0.98	0.93	NA	NA	0.98	0.93	0.93	0.94	1.00	0.96
3	0.91	0.99	0.96	0.90	0.98	0.91	0.96	1.00	0.97	0.96	0.98	1.00	0.98
4	0.78	1.00	1.00	1.00	0.99	0.98	NA	1.00	0.99	1.00	1.00	1.00	0.98
5	NA	0.93	0.96	0.87	0.99	0.98	0.90	0.85	0.99	0.99	0.95	0.85	1.00
6	0.95	0.91	0.98	0.99	0.94	0.71	0.80	1.00	0.98	0.99	0.99	0.86	0.99
7	0.83	0.96	0.99	0.98	0.99	0.76	0.97	0.95	1.00	0.98	0.95	1.00	1.00
8	0.99	0.99	0.95	1.00	0.99	NA	0.98	0.99	1.00	0.99	0.95	0.99	0.99
9	0.98	0.97	0.99	0.96	0.94	na	na/NA	0.98	1.00	0.98	1.00	1.00	0.99
10	na**	1.00	0.94	0.92	0.69	na/NA	na	0.97	1.00	0.99	0.98	1.00	0.97

*NA: Not identified by ERA/OKID

**na: Not identified by XB MID method

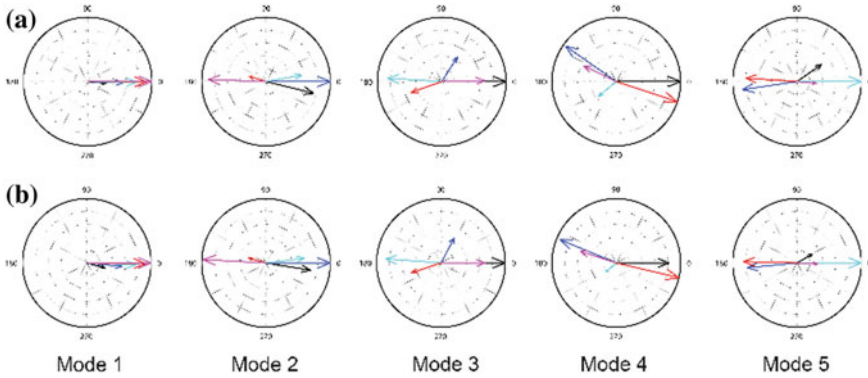


Fig. 6.11 Comparison between exact (a) and identified (b) mode shapes

classical damping from earthquake-induced responses [55]. The main innovation of this improvement is described in what follows.

According to the modal superposition rule, it can be shown that the absolute acceleration of a system with non-classical damping can be expressed as

$$\ddot{\mathbf{x}}^t(t) = \Phi \mathbf{q}(t) + \Phi^* \mathbf{q}^*(t) \tag{6.32}$$

where $\Phi = [\phi_1 \dots \phi_{n_m}]$ and $\ddot{\mathbf{q}}(t) = \ddot{\mathbf{q}}_R(t) + i\ddot{\mathbf{q}}_I(t) = [q_1(t) \dots q_{n_m}(t)]^T$ are the complex-valued mode shape matrix and the modal coordinate vector, respectively. The redundant complex-conjugate term can be eliminated by converting the acceleration response signals to their analytic forms, because modal coordinates are themselves analytic signals. That is,

$$\tilde{\mathbf{x}}^t(t) = \Phi \ddot{\mathbf{q}}(t). \tag{6.33}$$

Now, by calculating the STFD of both sides of the equation above, we have

$$\mathbf{D}_{\tilde{\mathbf{x}}^t \tilde{\mathbf{x}}^t}(t, f) = \Phi \mathbf{D}_{\ddot{\mathbf{q}} \ddot{\mathbf{q}}}(t, f) \Phi^H, \tag{6.34}$$

which is similar to Eq. (6.5), except for the fact that the conventional matrix transpose is replaced with a Hermitian Transpose. So, a complex-valued non-unitary Joint Approximate Diagonalization (JAD) (e.g., [56]) can be employed to identify the mode shapes from $\mathbf{D}_{\tilde{\mathbf{x}}^t \tilde{\mathbf{x}}^t}(t, f)$ at the SATFPs. To verify the proposed method, mode shapes of a 5-story shear-building model that has a non-classical damping source are identified from its responses simulated using ground accelerations. The identified complex-valued mode shapes are displayed in Fig. 6.11 via polar plots along with their exact (analytically computed) counterparts. As seen, the method is able to successfully identify the system’s complex-valued mode shapes.

6.2.2 Model-Based Identification Techniques

Although BMID techniques were shown to be successful in the identification of systems for which input excitation is not available, especially SSI systems, they suffer from various critical issues. First, they are modal methods, and thus, they are limited to linear-elastic systems, whereas soil behavior is typically quite nonlinear even under weak excitations. Second, the performance of BMID techniques (generally all modal identification methods) is highly sensitive to the number of sensors. Model-based identification techniques are appealing alternatives to modal methods, which are especially fruitful for SSI systems. Typically models serve as implicit sources of information and enable reduction of the number of sensors. Model-based techniques, by definition, employ model updating techniques (see, for example, [57]). That is, a preliminary numerical model of a structure/system is created and manipulated such that it exhibits a close response to what is measured in real-life.

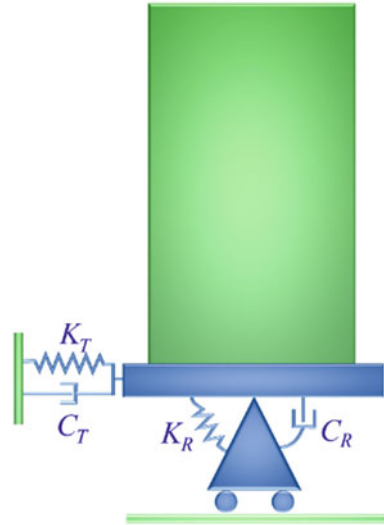
While the identified mode shapes and natural frequencies (i.e., frequency domain data) can be used as input in model updating studies (e.g., [25, 58–60]), the essential benefit of model-based methods in the identification of SSI systems is their ability to work entirely in the time-domain, which enables direct consideration of nonlinear behavior.

6.2.2.1 Simple Models

SSI systems are composed of two substructures, (i) the superstructure, and (ii) the soil-foundation system. The former is manmade, so it could be analytically or numerically modeled with acceptable accuracy, while the latter is not easily modeled due to the complexities of soil nonlinearities and SSI phenomena. As such, and due to the fact that SSI is usually significant in lower vibration modes [26], one idea that has been employed in prior studies is to represent the superstructure with a simple model that has only a few parameters (e.g., [61]), so that the more-complex soil-foundation system and the unknown FIMs can be identified from available data. For example, a Timoshenko beam model has been used to represent the superstructure, which exhibits both shear and flexural deformations as well as rotary inertia (e.g., see [62]). The authors have developed a technique along this line for identification of SSI systems [63], which is summarized next.

Consider a Timoshenko beam on a sway-rocking soil-foundation system as shown in Fig. 6.12, and assume that we have measured the response of the system at three locations, which incidentally is the most common building instrumentation scenario in the US (foundation sway, and horizontal motion at the mid-height, and roof levels). The Fourier amplitude (denoted by an overbar) of the absolute acceleration of this model at the normalized height \tilde{z} under a horizontal FIM is given by

Fig. 6.12 Timoshenko beam model of a soil-structure system



$$\bar{\vec{x}}^t(\tilde{z}, \omega) = \left[\sum_{j=1}^{n_m} W_j(\tilde{z}) \frac{L_j^*}{m_j^*} H_j(\omega) + 1 \right] \bar{\vec{u}}_g(\omega) \quad (6.35)$$

where $W_j(\tilde{z})$ is the j -th translational mode shape, and $\bar{\vec{u}}_g(\omega)$ is the Fourier amplitude of the horizontal FIM. L_j^* and m_j^* are respectively the generalized influence factor and mass, and $H_j(\omega)$ is

$$H_j(\omega) = \frac{-\omega^2}{\omega_j^2 - \omega^2 + 2i\xi_j\omega_j\omega} \quad (6.36)$$

where ξ_j and ω_j are j th flexible-base mode's damping ratio and natural frequency, respectively. Consequently, the absolute acceleration of the mid-height and the roof levels can be predicted by the foundation sway response signal $\bar{\vec{x}}_b^t(\omega)$ as

$$\bar{\vec{x}}^t(\tilde{z}, \omega) = \frac{\left[\sum_{j=1}^n W_j(\tilde{z}) \frac{L_j^*}{m_j^*} H_j(\omega) + 1 \right]}{\left[\sum_{j=1}^n W_j(0) \frac{L_j^*}{m_j^*} H_j(\omega) + 1 \right]} \bar{\vec{x}}_b^t(\omega). \quad (6.37)$$

So, all unknown parameters of both the superstructure and the soil-foundation system can be identified by minimizing the misfit between the predicted and recorded mid-height and roof levels responses in a least-squares sense without the need to measure/record FIMs. The updating parameters are those controlling the behavior of the Timoshenko beam $s = \sqrt{EI/GA_s L^2}$ and $\bar{b} = \rho AL^4/EI$, parameters of the soil-foundation system $k_R = K_R L/EI$ and $k_T = K_T L/GA_s$, and the modal damping ratios ξ_1, \dots, ξ_{n_m} , where L denotes the building's height, ρ is the mass

Fig. 6.13 The Millikan Library



density, A is the cross-sectional area, I is the area moment of inertia, and E and G are the Young's and shear moduli, respectively. $A_s = kA$ is the effective cross-sectional area of the superstructure model with the correction factor being $k = 0.85$ for rectangular sections. K_T and K_R (see, Fig. 6.12) are the sway and rocking soil-foundation stiffnesses.

To verify the proposed identification approach, we use real earthquake data recorded on the Millikan Library (Fig. 6.13) along the North-South (NS) direction during the 2002 Yorba Linda earthquake. Figure 6.14a presents a comparison of the recorded signals at mid-height and roof levels and those predicted by the identified model (Fig. 6.12). As seen, the model is successful in representing a real-life soil-structure system. The blind prediction of other floors' responses that are not used in the identification process, is also very accurate, as seen in Fig. 6.14b.

6.2.2.2 Finite Element Models

Thanks to ever-advancing computational capabilities, Finite Element (FE) analyses of complex large-scale structures are becoming routine tasks. This is crucial for identification purposes, because a given model has to be analyzed many times during iterations of model-based identification procedures. Time-domain output-only FE model updating methods that are based on Bayesian filtering techniques have attracted significant attention recently due to their superior performances (see, for example, [64, 65]). In these techniques, the prior probability distributions of unknown parameters of an FE model, along with the unknown input excitations are updated iteratively through information collected through the measurements (see, Fig. 6.15). The probabilistic framework of these methods makes the possibility to

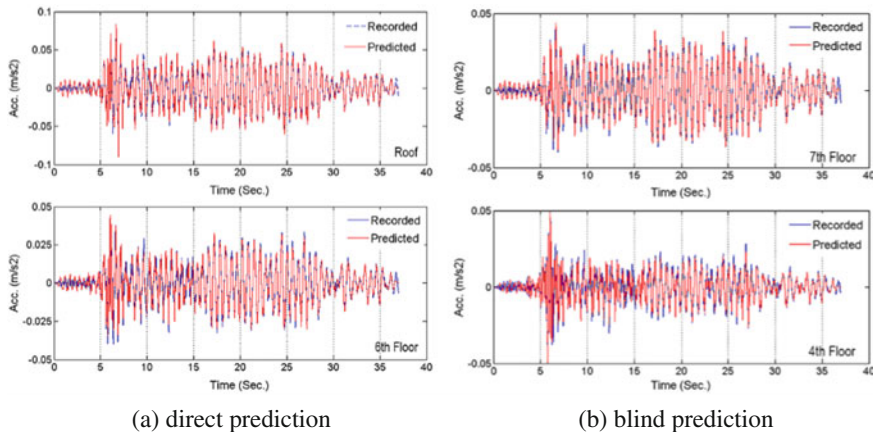


Fig. 6.14 Comparison between recorded (blue) and predicted (red) absolute acceleration (color figure online)

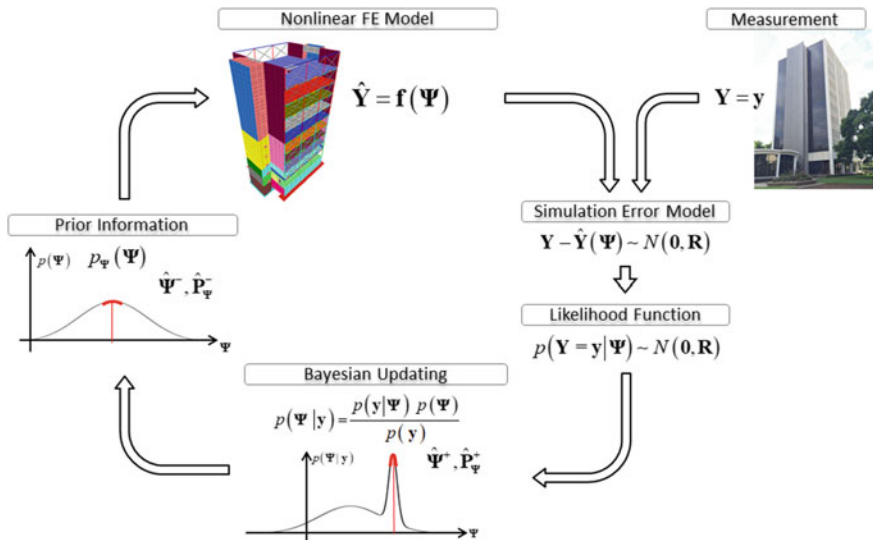


Fig. 6.15 Schematic presentation of the sequential Bayesian FE model updating method [66]

quantify uncertainties associated with the estimation. The details of these methods can be found in the mentioned above references. Herein, we present a few practical applications.

The first example shows the application of the method to the FE model of the Millikan Library [25] and Yorba Linda earthquake [67]. Figure 6.16 displays the predicted (using the identified model parameters and FIM) versus measured responses at two floors. As seen, the predictions are quite accurate.

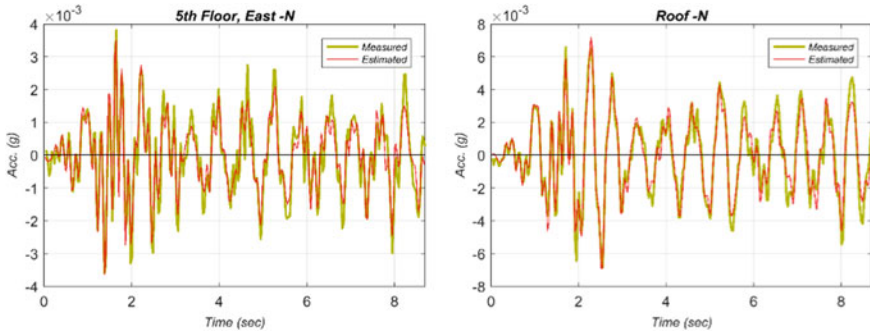


Fig. 6.16 Comparison between recorded (green) and predicted (red) absolute acceleration responses [67] (color figure online)

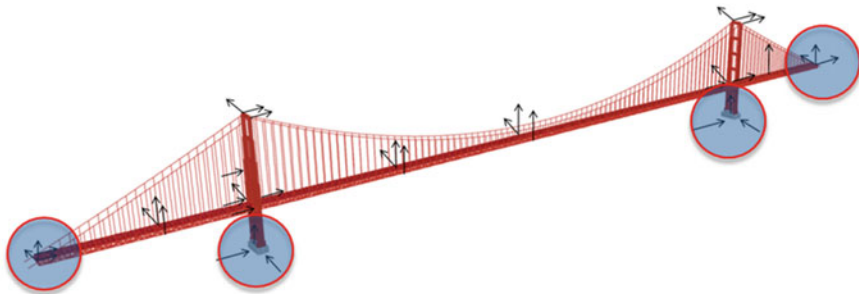


Fig. 6.17 FE model of the Golden Gate Bridge (GGB) with available instrumentation channels indicated by arrows (circles indicate channels considered as input excitations)

The next example is the application of the method to a very large-scale problem involving the Golden Gate Bridge (GGB) under multiple unknown FIMs (Fig. 6.17). We simulated the response of this model using data recorded at the foundation levels (sensors are marked with circles in figure) during the 2014 South Napa earthquake, and subsequently identified various unknown parameters of the model as well as the input excitations. Figure 6.18 displays the exact and the identified FIMs at the base of the two main towers (South tower: CH31, 32, 33; North tower: CH16, 17, 18). The results displayed in this figure indicate that the method works very well. However, it should be kept in mind that these methods are very expensive computationally, because the unknown FIMs are identified along with the system’s parameters, which makes the computational burden extremely high, especially because the superstructure’s geometric nonlinearities were considered.

If the system’s parameters are the main interest, then it is more favorable to utilize an output-only FE model updating method wherein the unknown FIMs do not have to be identified simultaneously, in order to keep the computational expenses low. This can be done using a Cross-Relation (CR) technique [68] provided that we have at least two neighboring instrumented buildings (Fig. 6.19). It is easy to show that following

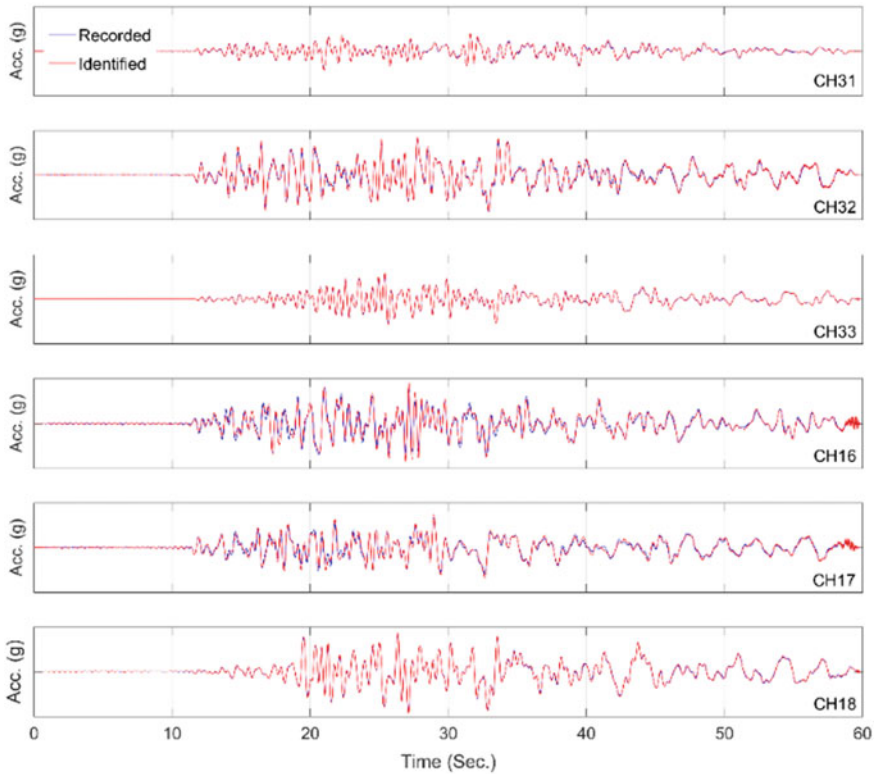


Fig. 6.18 Comparison between the exact and the identified FIMs for GGB

cross-relation can be written between measured responses (e.g., those recorded at the roof levels of the two buildings)

$$\left\{ y_1^{\sin \alpha \ddot{x}_1} + x_1^{\cos \alpha \ddot{y}_1} \right\} * h_2 - \left\{ y_2^{\sin \beta \ddot{x}_2} + x_2^{\cos \beta \ddot{y}_2} \right\} * h_1 \approx 0, \quad (6.38)$$

$$\left\{ y_1^{\cos \alpha \ddot{x}_1} + x_1^{-\sin \alpha \ddot{y}_1} \right\} * h_2 - \left\{ y_2^{\cos \beta \ddot{x}_2} + x_2^{-\sin \beta \ddot{y}_2} \right\} * h_1 \approx 0, \quad (6.39)$$

where, for example, $y_1^{\sin \alpha \ddot{x}_1}$ stands for the response of Building 1 in its local y -direction under the input excitation $\sin \alpha \ddot{x}_1$, in which \ddot{x}_1 , \ddot{y}_1 , \ddot{x}_2 , and \ddot{y}_2 are the recorded responses in local x - and y -directions of Buildings 1 and 2, respectively. Also, $h_1 = h_1^x * h_1^y$ and $h_2 = h_2^x * h_2^y$ where h_i^j is the impulse response function of Building i along the j -direction, and $*$ denotes a linear convolution. The approximate equal sign is used in the equation above to indicate that there is measurement noise. Based on the equations above, we can identify the parameters of two buildings' FE models by minimizing the left-hand sides of Eqs. (6.38) and (6.39).

Fig. 6.19 Two nearby instrumented buildings under a bidirectional seismic excitation

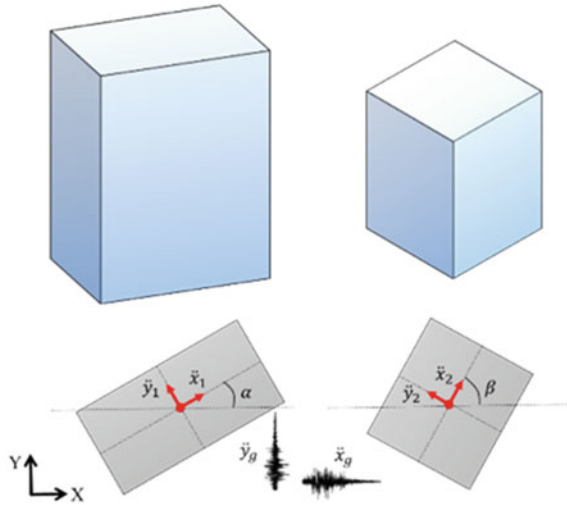


Table 6.5 Identified mean errors and COVs for the cross-relation method verification study

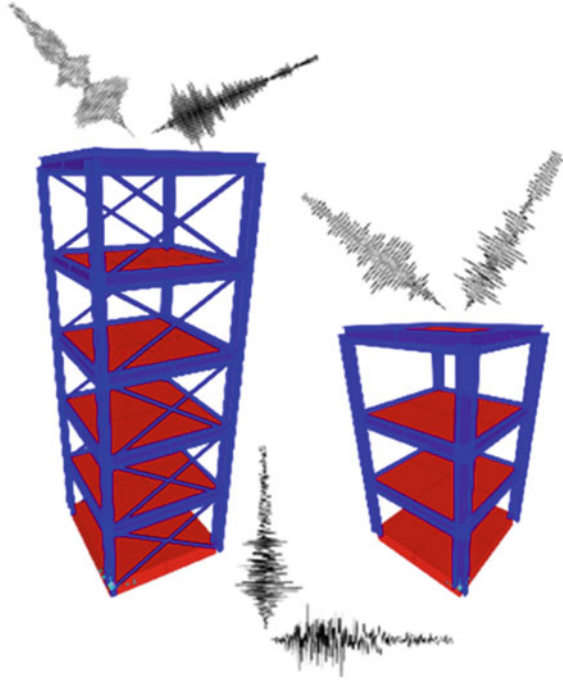
Parameters	$K_y(1)$	$K_x(1)$	$K_y(2)$	$K_x(2)$	$\alpha(1)$	$\beta(1)$	$\alpha(2)$	$\beta(2)$
Final error (%)	0.02	3.65	0.15	0.17	1.61	–	1.85	–
Final COV (%)	0.06	1.75	0.02	0.06	0.48	17.59	0.11	12.74

Figure 6.20 displays the results of a verification study on two buildings whose responses are numerically simulated under bi-directional ground accelerations and polluted by random noise. The stiffnesses of the soil-foundation rocking springs at the bottom of buildings along with the Rayleigh damping ($\alpha\mathbf{M} + \beta\mathbf{K}$) coefficients are attempted to be identified through the proposed cross-relation approach. Table 6.5 presents the final relative errors in the identified values along with their Coefficients-of-Variation (COVs). As seen, while we assumed an initial 50% error in the system parameters at the beginning of the identification, the method yields negligible final errors. Also, the COVs indicate that the estimated values are highly reliable.

6.3 Conclusions

This chapter reviewed the most recent developments in the identification of soil-structure systems from seismic responses. This identification task is a challenging one due to the typically short length of recorded seismic data, the non-stationary nature of input excitations, and the potential nonlinearities of soil-structure systems. More importantly, soil-structure interaction renders it virtually impossible to directly measure the earthquake input motions. So, identification tasks must be carried out

Fig. 6.20 Verification study for the cross-relation method



in an output-only mode, but the classical output-only identification techniques are typically based on specific statistical assumptions regarding the unknown external forces (e.g., white with zero-mean), which are no longer valid for the seismic case. Through work spanning the past decade—by the authors, their collaborators, as well as other colleagues—various new methods of system identification have been devised to tackle these soil-structure identification problems. Within the category of modal methods, a particularly fruitful class of methods comprised Blind Modal Identification (BMID) techniques, which were reviewed from their genesis to their most recent versions. Model-based techniques were also presented through which various limitations of BMID methods are removed or relaxed, albeit by increasing the computational costs and the labor involved in the development of initial models.

Acknowledgements The authors would like to acknowledge M. Ali Ghannad, Mehmet Celebi, Fariborz Nateghi, Anoosh Shamsabadi, Robert Nigbor, Hamed Ebrahimian, Mojtaba Mahsuli, and Nima Shirzad for their contributions to the studies reviewed in this chapter. The authors also acknowledge California Department of Transportation (Caltrans) and California Geological Survey (CGS), which provided financial support for research whose results were presented in this chapter.

References

1. Jennings PC, Kuroiwa JH (1968) Vibration and soil-structure interaction tests of a nine-story reinforced concrete building. *Bull Seismol Soc Am* 58(3):891–916
2. Richart FE Jr. (1975) Some effects of dynamic soil properties on soil-structure interaction. *J Geotech Geoenvironmental Eng* 101(ASCE# 11764 Proceeding)
3. Wolf JP (1976) Soil-structure interaction with separation of base mat from soil (lifting-off). *Nucl Eng Des* 38(2):357–384
4. Wolf JP, Deeks AJ (2004) *Foundation vibration analysis: a strength of materials approach*. Butterworth-Heinemann
5. Luco JE, Mita A (1987) Response of circular foundation to spatially random ground motion. *J Eng Mech* 113(1):1–15
6. Luco JE, Wong HL (1986) Response of a rigid foundation to a spatially random ground motion. *Earthq Eng Struct Dyn* 14(6):891–908
7. Veletsos AS, Prasad AM, Wu WH (1997) Transfer functions for rigid rectangular foundations. *Earthq Eng Struct Dyn* 26(1):5–17
8. Apsel RJ, Luco JE (1976) Torsional response of rigid embedded foundation. *J Eng Mech Div* 102(6):957–970
9. Mita A, Luco JE (1989) Impedance functions and input motions for embedded square foundations. *J Geotech Eng* 115(4):491–503
10. Pais AL, Kausel E (1989) On rigid foundations subjected to seismic waves. *Earthq Eng Struct Dyn* 18(4):475–489
11. Mahsuli M, Ghannad MA (2009) The effect of foundation embedment on inelastic response of structures. *Earthq Eng Struct Dyn* 38(4):423–437
12. Rizos DC, Wang Z (2002) Coupled BEM-FEM solutions for direct time domain soil-structure interaction analysis. *Eng Anal Bound Elem* 26(10):877–888
13. Lysmer J, Kuhlemeyer RL (1969) Finite dynamic model for infinite media. *J Eng Mech Div* 95(4):859–878
14. Juang JN, Pappa RS (1985) An eigensystem realization algorithm for modal parameter identification and model reduction. *J Guid Control Dyn* 8(5):620–627
15. Van Overschee P, De Moor B (1993) Subspace algorithms for the stochastic identification problem. *Automatica* 29(3):649–660
16. Brincker R, Zhang L, Andersen P (2001) Modal identification of output-only systems using frequency domain decomposition. *Smart Mater Struct* 10(3):441–445
17. Pioldi F, Rizzi E (2018) Assessment of frequency versus time domain enhanced technique for response-only modal dynamic identification under seismic excitation. *Bull Earthq Eng* 16(3):1547–1570
18. Lus H, Betti R, Longman RW (1999) Identification of linear structural systems using earthquake-induced vibration data. *Earthq Eng Struct Dyn* 28(11):1449–1467
19. Stewart JP, Fenves GL, Seed RB (1999) Seismic soil-structure interaction in buildings. I: analytical methods. *J Geotech Geoenvironmental Eng* 125(1):26–37
20. Todorovska MI (2009) Soil-structure system identification of Millikan Library North-South response during four earthquakes (1970–2002): what caused the observed wandering of the system frequencies? *Bull Seismol Soc Am* 99(2A):626–635
21. Veletsos AS, Ventura CE (1986) Modal analysis of non-classically damped linear systems. *Earthq Eng Struct Dyn* 14(2):217–243
22. Stewart JP, Seed RB, Fenves GL (1998) Empirical evaluation of inertial soil-structure interaction effects. Pacific Earthquake Engineering Research Center
23. Kuroiwa J (1967) Vibration tests of a multistory building. California Institute of Technology
24. Keightley WO (1963) Vibration tests of structures. Technical report: Caltech EERL.1963.001
25. Ghahari SF, Abazarsa F, Avci O, Çelebi M, Taciroglu E (2016) Blind identification of the Millikan Library from earthquake data considering soil-structure interaction. *Struct Control Heal Monit* 23(4):684–706

26. Luco JE (1980) Soil-structure interaction and identification of structural models. In: Proceedings of 2nd ASCE conference on civil engineering and nuclear power, vol 2, pp 10–11
27. Safak E (1995) Detection and identification of soil-structure interaction in buildings from vibration recordings. *J Struct Eng* 121(5):899–906
28. Stewart JP, Fenves GL (1998) System identification for evaluating soil-structure interaction effects in buildings from strong motion recordings. *Earthq Eng Struct Dyn* 27(8):869–885
29. Safak E (2009) System identification for soil—structure interaction. *Encycl Struct Heal Monit*
30. Stewart JP, Stewart AF (1997) Analysis of soil-structure interaction effects on building response from earthquake strong motion recordings at 58 sites, vol 97, no 1. Earthquake Engineering Research Center
31. Ghahari SF, Abazarsa F, Ghannad MA, Taciroglu E (2013) Response-only modal identification of structures using strong motion data. *Earthq Eng Struct Dyn* 42(8)
32. Belouchrani A, Amin MG (1998) Blind source separation based on time-frequency signal representations. *IEEE Trans Signal Process* 46(11):2888–2897
33. Chopra AK (1995) Dynamics of structures, vol 3. Prentice Hall, New Jersey
34. Boashash B (2003) Time frequency signal analysis and processing: a comprehensive reference
35. Flandrin P (1984) Some features of time-frequency representations of multicomponent signals. *Proc IEEE Int Conf Acoust Speech Signal Process* 3(1):41B.4.1–41B.4.4
36. Mathworks (2014) MATLAB the language of technical computing
37. Flandrin P (1999) Time-frequency/time-scale analysis. *Wavelet Anal Appl* 10:49–182
38. Cardoso J-F, Souloumiac A (1996) Jacobi angles for simultaneous diagonalization. *SIAM J Matrix Anal Appl* 17(1):161–164
39. Nguyen L-T, Belouchrani A, Abed-Meraim K, Boashash B (2005) Separating more sources than sensors using time-frequency distributions. *EURASIP J Appl Signal Process* 17:2005
40. Taciroglu E, Abazarsa F, Ghahari SF (2012) Response-only identification of torsionally coupled buildings using strong motion data. In: 9th international conference on urban earthquake engineering/4th Asia conference on earthquake engineering
41. Chopra AK, la Llera JC (1996) Accidental and natural torsion in earthquake response and design of buildings. In: Eleventh world conference on earthquake engineering
42. Ventura CE, Mirza K (2005) Model calibration of a 3-story steel frame building using earthquake records. In: IMAC-XXIII, conference & exposition on structural dynamics
43. Ghahari SF, Ghannad MA, Norman J, Crewe A, Abazarsa F, Taciroglu E (2013) Considering wave passage effects in blind identification of long-span bridges. In: Conference proceedings of the society for experimental mechanics series, vol 5
44. Norman JAP, Crewe AJ (2008) Development and control of a novel test rig for performing multiple support testing of structures. In: Proceedings of the 14th world conference on earthquake engineering, Beijing, paper, no. 2–2, p 51
45. Ghahari SF, Abazarsa F, Ghannad MA, Celebi M, Taciroglu E (2014) Blind modal identification of structures from spatially sparse seismic response signals. *Struct Control Heal Monit* 21(5)
46. Giulieri L, Ghennioui H, Thirion-Moreau N, Moreau E (2005) Nonorthogonal joint diagonalization of spatial quadratic time-frequency matrices for source separation. *IEEE Signal Process Lett* 12(5):415–418
47. Aïssa-El-Bey A, Linh-Trung N, Abed-Meraim K, Belouchrani A, Grenier Y (2007) Underdetermined blind separation of nondisjoint sources in the time-frequency domain. *IEEE Trans Signal Process* 55(3):897–907
48. Abazarsa F, Ghahari SF, Nateghi F, Taciroglu E (2013) Response-only modal identification of structures using limited sensors. *Struct Control Heal Monit* 20(6)
49. De Lathauwer L, Castaing J (2008) Blind identification of underdetermined mixtures by simultaneous matrix diagonalization. *IEEE Trans Signal Process* 56(3):1096–1105
50. Abazarsa F, Nateghi F, Ghahari SF, Taciroglu E (2016) Extended blind modal identification technique for nonstationary excitations and its verification and validation. *J Eng Mech* 142(2):04015078
51. Çelebi M, Kashima T, Ghahari SF, Abazarsa F, Taciroglu E (2016) Responses of a tall building with US code-type instrumentation in Tokyo, Japan, to events before, during, and after the Tohoku earthquake of 11 March 2011. *Earthq Spectra* 32(1):497–522

52. Taciroglu E, Shamsabadi A, Abazarsa F, Nigbor RL, Ghahari SF (2014) Comparative study of model predictions and data from Caltrans/CSMIP bridge instrumentation program: a case study on the Eureka-Samoa channel bridge
53. Ghahari SF, Ghannad MA, Taciroglu E (2013) Blind identification of soil-structure systems. *Soil Dyn Earthq Eng* 45
54. Abazarsa F, Nateghi F, Ghahari SF, Taciroglu E (2013) Blind modal identification of non-classically damped systems from free or ambient vibration records. *Earthq Spectra* 29(4)
55. Ghahari SF, Abazarsa F, Taciroglu E (2016) Blind modal identification of non-classically damped structures under non-stationary excitations. *Struct Control Heal Monit*
56. Maurandi V, Moreau E (2014) A decoupled jacobi-like algorithm for non-unitary joint diagonalization of complex-valued matrices. *IEEE Signal Process Lett* 21(12):1453–1456
57. Friswell MI, Mottershead JE (1995) Finite element model updating in structural dynamics, vol 38
58. Taciroglu E, Ghahari SF, Abazarsa F (2017) Efficient model updating of a multi-story frame and its foundation stiffness from earthquake records using a Timoshenko beam model. *Soil Dyn Earthq Eng* 92
59. Shirzad-Ghaleroudkhani N, Mahsuli M, Ghahari SF, Taciroglu E (2017) Bayesian identification of soil-foundation stiffness of building structures. *Struct Control Heal Monit*
60. Taciroglu E, Çelebi M, Ghahari SF, Abazarsa F (2016) An investigation of soil-structure interaction effects observed at the MIT green building. *Earthq Spectra* 32(4)
61. Miranda E, Taghavi S (2005) Approximate floor acceleration demands in multistory buildings. I: formulation. *J Struct Eng* 131(2):203–211
62. Cheng MH, Heaton TH (2015) Simulating building motions using the ratios of its natural frequencies and a Timoshenko beam model. *Earthq Spectra* 31(1):403–420
63. Taciroglu E, Ghahari SF (2017) Identification of soil-foundation dynamic stiffness from seismic response signals, no. SP 316. American Concrete Institute, ACI Special Publication
64. Astroza R, Ebrahimian H, Li Y, Conte JP (2017) Bayesian nonlinear structural FE model and seismic input identification for damage assessment of civil structures. *Mech Syst Signal Process* 93:661–687
65. Ebrahimian H, Astroza R, Conte JP, Papadimitriou C (2018) Bayesian optimal estimation for output-only nonlinear system and damage identification of civil structures. *Struct Control Heal Monit*
66. Ebrahimian H, Ghahari SF, Asimaki D, Taciroglu E (2018) A nonlinear model inversion to estimate dynamic soil stiffness of building structures
67. Ebrahimian H, Ghahari SF, Asimaki D, Taciroglu E (2018) A nonlinear model inversion to estimate dynamic soil stiffness of building structures, GSP 292. *Geotechnical Special Publication*
68. Xu G, Liu H, Tong L, Kailath T (1995) A least-squares approach to blind channel identification. *IEEE Trans Signal Process* 43(12):2982–2993

Part II
Methods and Tools for Data Processing

Chapter 7

Structural Health Monitoring: Real-Time Data Analysis and Damage Detection



Yavuz Kaya and Erdal Safak

Abstract Several new tools and techniques on Structural Health Monitoring (SHM) have recently been developed and implemented on various structures, which includes real-time vibration data analysis, damage detection, and warnings for occupants. Running time windows are used to define the statistical characteristics of the changes in structural properties and their correlation with the factors that might cause such changes. Inter-story drifts are commonly used to detect and locate damage on buildings. The classical method to calculate inter-story drifts involves double integration and subtraction of acceleration data, both of which are very sensitive to noise in the records. Therefore, it is extremely difficult to get accurate values of inter-story drifts in real-time SHM systems. It is shown that the fairly accurate drift values can be obtained at non-instrumented stories assuming that the mode shapes of a building can be approximated as a linear combination of the mode shapes of a shear- and bending beam. A new technique based on the interferometric imaging and Transfer Matrix formulation enables the analytical models of multi-story buildings to be uniquely identified and calibrated for each story in real-time using their vibration records. It has been shown that the top-to-bottom spectral ratio of the records at a particular story is dependent only on the properties of that story and the stories above but not the stories below. Both numerical examples and earthquake data from the Factor building at UCLA campus in California are used to validate these tools and methodologies.

Keywords Real-time data processing · Inter-story drifts · Damage detection · FE model calibration

Y. Kaya (✉)

British Columbia Ministry of Transportation and Infrastructure, 310-1500
Woolridge Street, V3K 0B8 Coquitlam, Canada
e-mail: Yavuz.Kaya@gov.bc.ca

E. Safak

Bogazici University, Kandilli Observatory and Earthquake Research Institute,
Istanbul, Turkey

© Springer Nature Switzerland AG 2019

M. P. Limongelli and M. Çelebi (eds.), *Seismic Structural Health Monitoring*, Springer
Tracts in Civil Engineering, https://doi.org/10.1007/978-3-030-13976-6_7

171

7.1 Introduction

Recent developments in sensor and recording technologies enabled large number of structures to be installed with real-time Structural Health Monitoring (SHM) systems, which involves continuous monitoring of the dynamic characteristics of a structure (e.g., modal frequency, mode shape and damping ratio). A good example of a real-time SHM network is the British Columbia Smart Infrastructure Monitoring System (BCSIMS) (www.bcsims.ca) in British Columbia (BC), Canada. This SHM network currently involves 14 bridges, 1 tunnel and 10 public schools [18] and provides BC Ministry of Transportation and Infrastructure (BC-MOTI) with near real-time feedback on the performance of these structures during their normal operation and extreme events such as earthquake or strong wind. The SHM network provides BC-MOTI bridge engineers and inspectors with real-time warnings on the performance of these structures through smart phone applications and public websites.

Extreme loads such as a large earthquake do not occur frequently; therefore, most of the SHM data involve ambient forces such as wind, traffic loads, and microtremors. For most structures, ambient vibration data are sufficient to identify the dynamic properties for linear behavior, such as natural frequencies, damping ratios, and mode shapes, torsion, and soil-structure interaction. Tracking these dynamic characteristics allows detecting and locating damage on structures in real-time and helping to make automatic decisions on the danger level in the structure and on the actions that need to be taken immediately.

Due to the continuous collection of data in real-time SHM systems, the recording, processing, and analysis of these data should also be done in real-time, so that slow changes in the characteristics of the structure, such as aging, change of usage, environmental factors (e.g., temperature, wind, rain, etc.), as well as sudden changes due to an extreme load (e.g., a large earthquake) can be tracked. As the amount of vibration data from instrumented structures are increasing, it is now possible to find sufficient number of structures that have multiple sets of data under different levels of excitations. This allows establishing statistical characteristics of the structural changes and their correlation with the factors that might cause such changes [39]. Decisions whether the identified changes in a structural parameter actually represents damage or not can then be made with ease.

Instantaneous damage detection on a structure is very important in SHM systems. Large numbers of slight-to-moderately damaged or heavily damaged structures are observed after big earthquakes. Time consuming inspections are usually required to decide whether the damage on these structures is structural or not, and if they are safe to re-occupy. Properly installed and operated real-time SHM systems provide the means to make such decisions instantaneously.

This paper presents many tools and methodologies developed over the past several years for processing and analysis of real-time SHM data collected from various structures, such as buildings and bridges. Several time domain and frequency domain techniques are discussed, and real-life examples are provided to illustrate the validity of the techniques. Many spectral analysis methods are presented for modal identi-

fication purposes; additionally, recently developed damage detection methods are presented and discussed with illustrative examples. These tools and methods help to transform the current practice of inspecting and evaluating structures to a more rational and effective ones that use up-to-date sensing technology with fast and efficient analysis algorithms.

7.2 Real-Time SHM Data Analysis

7.2.1 Tracking Time Variations in Signals

A real-time SHM system requires continuous and automated methods that can analyze and process structural vibration data, as well as adapt and account for any changes in signal characteristics. The simplest and most straightforward approach to analyze continuous data is to utilize Running Windows, which are weighting functions that emphasize recent data, while gradually deemphasizing past data. Running Windows ensure that any property calculated from data contains measurements that are relevant to the current state of the structure.

The two widely used running windows are sliding rectangular windows and exponentially decaying windows [11]. Sliding rectangular windows consider only a limited number of past data points with equal weights while the sliding window applies exponentially decaying weights to past data points, and they are defined as

$$w_r(t, i) = \frac{1}{L} \quad \text{for } t - L \leq i \leq t, i = 0, 1, 2, \dots, t \quad \text{and} \quad \sum_{i=1}^t w_r(t, i) = 1 \quad (7.1)$$

$$w_e(t, i) = \frac{1 - \lambda}{1 - \lambda^t} \cdot \lambda^{t-i} \quad (7.2)$$

where $w_r(t, i)$ is the weighting function for sliding window, $w_e(t, i)$ is the weighting function for exponentially decaying window, L is the rectangular window length, and the memory time constant, λ , is known as the forgetting factor with $0.0 < \lambda < 1.0$. When using rectangular windows, it is important that the successive windows overlap by a certain length in order not to have any discontinuity in the analysis. The memory time constant, N_0 , of the sliding window is defined as the number of sampling points over which the characteristics of the structure can be assumed to remain constant, and can be approximated as:

$$N_0 \approx \frac{1}{1 - \lambda} \quad (7.3)$$

Equation (7.3) provides a simple criterion for the selection of λ . Typically $\lambda = 0.900 \sim 0.999$.

7.2.2 Real-Time Data Handling

Real-time SHM systems produce data streams that are infinite in duration; therefore, in order to handle such long data, the continuous data streams are usually divided into segments of equal length using several Running Windows: a larger window to track time variation of signal characteristics and a smaller analysis window to reduce noise by averaging. The analysis of the data within a running window is performed by analyzing the data in each analysis window and then averaging the results. The analysis window moves inside the running window with a predefined overlap ratio. Once the analysis for a running window is finished, it is shifted in time by a predefined overlap ratio and the procedure is repeated. The reason for using analysis windows inside the running window is to reduce the effects of noise by means of averaging. The process is shown schematically in Fig. 7.1. The larger the number of analysis windows the lesser the effect of noise in the results. The length of the analysis window depends on the longest period of the structure: It should be about ten times the longest modal period of the structure. The length of the running window, on the other hand, depends on the signal-to-noise ratio (SNR) in the records. The length should be long enough to allow sufficient number of analysis windows to be fit inside in order to minimize the noise by averaging [14].

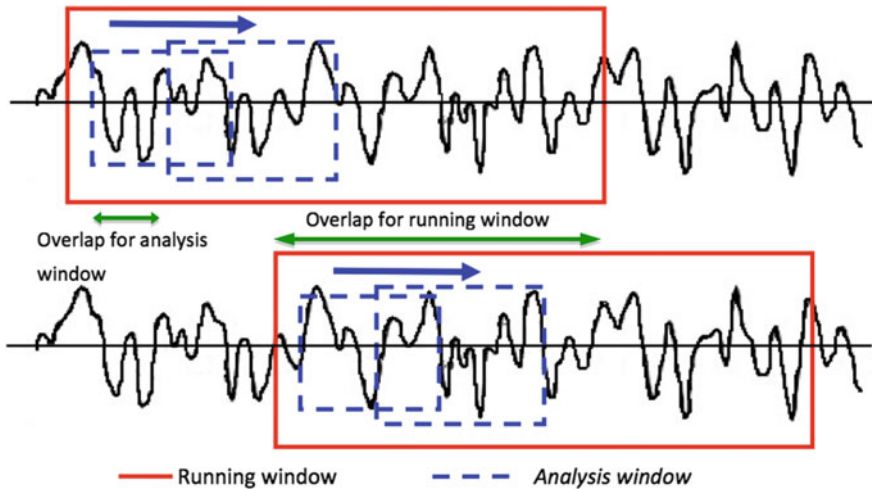


Fig. 7.1 Analysis window moves within the running window by a predefined overlap ratio [17]

7.2.3 Processing of Real-Time Data Using Running Windows

Recorded SHM data contains noise due to environmental factors, flaws in the sensors, installation process, recording instruments, low frequency drifts (e.g., mechanical imperfections in sensors), and possibly outliers (i.e., erroneous isolated peaks). The recorded SHM data is processed to minimize such undesirable effects; it involves removal of mean and linear trends (i.e., baseline correction), windowing, smoothing, instrument correction, decimation, and band-pass filtering.

The mean value of vibration records should be zero; however, it usually fluctuates around zero due to noise, environmental factors (e.g., wind, rain, etc.), natural changes in the structure (e.g., structural modifications, changes in load, aging, etc.), or permanent damage after an extreme event (e.g., structural inelastic deformations during an earthquake). Thus, the change in the mean value of a SHM record is a critical parameter that should be tracked accurately using Running Windows. Baseline correction involves fitting a best straight line to the data and subtracting it from the recorded data. Utilizing the best straight-line fit approach for de-trending is sufficient for the SHM ambient data because the structure remains elastic, and the signals are stationary. However, in case of a sudden extreme loading such as an earthquake, straight-line de-trending may not be sufficient because of sudden baseline shift during earthquakes [1]. In this case, de-trending should be done separately for each segment of the data.

For ambient vibration data, the cutoff frequency of the high-pass filter is increased gradually until the calculated velocities and displacements do not exhibit any trends that increase with time. When dealing with earthquake data, the cutoff frequency of the high-pass filter is selected such that the corresponding velocities and displacements are stable.

Band-pass filtering removes the frequency components in the data that are dominated by noise. Only those frequencies within the specified frequency band are kept in the records. Band-pass filtering eliminates all low frequency components below the lower corner of the band-pass filter, including those of the linear trend. An important point when filtering is that the filter should not alter the phase content of the signal. This requires that, unless the filter is zero-phase, the signal should be filtered twice, first forward and then backward. The commonly used Butterworth filters have non-zero phase, and thus should be used twice. Filtering does not eliminate or reduce the noise in the signal; it merely eliminates the frequency components that are dominated by noise. The noise is still present in the frequency band that is kept, same as in the raw signal (Fig. 7.2a). However, the signal amplitudes in the pass-band are larger than those of the noise.

The signal-to-noise ratios in SHM ambient vibrations are usually very low. On lower floors of multi-story buildings, for example, the noise amplitudes can actually be higher than those of the signal (Fig. 7.2b). In such situations, there is no justification to use band-pass filters; more advanced filtering techniques are required. Although they are low-amplitude and heavily contaminated by noise, the fact that SHM ambient vibrations are stationary and can be considered infinitely long actually

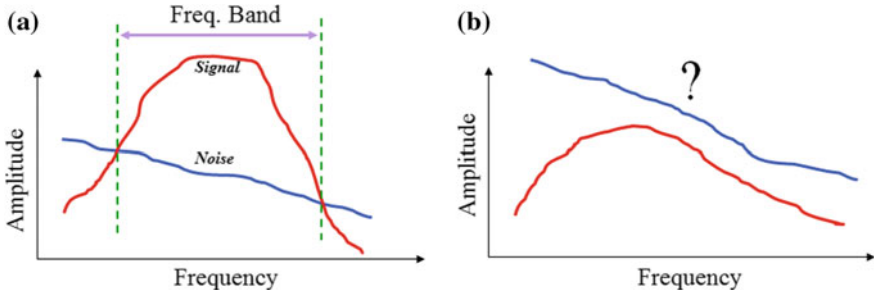


Fig. 7.2 **a** The noise-dominated portion of the spectrum for earthquake-induced vibration records can easily be identified visually using Fourier amplitude spectra, **b** the noise amplitudes for real-time ambient vibration data can be higher than that of the signal [14]

is an advantage, because it allows using statistical filtering techniques for processing. Such filters are superior to band-pass filters because filtering of the noise is done over the entire frequency band. The simplest form of statistical filtering is known as the optimal filtering. Optimal filtering is based on the assumption that the noise is a white-noise random process, and the filter parameters can be obtained by minimizing the error between the record signal and the filtered signal. More on optimal filtering and the related equations can be found in Safak et al. [33].

7.2.4 Segmentation and Averaging

The main problem with spectral analysis of SHM data is the noise in the records. Noise alters the amplitudes and the frequency content of Fourier spectra and introduces spurious resonant peaks. For a typical structure, the SHM data are almost entirely composed of ambient vibrations, induced by wind, traffic, and micro tremors. Therefore, the records are very noisy with very low SNR (signal-to-noise ratio). Unless special processing techniques are used to reduce the effects of noise, Fourier spectral analysis can give misleading results, particularly for records from stiff structures.

We can express a noisy signal as

$$x(t) = s(t) + n(t) \quad \text{with} \quad n(t) = N[0, \sigma] \tag{7.4}$$

where $s(t)$ represents the noise-free real signal, and $n(t)$ the zero-mean Gaussian white noise with standard deviation σ . The discrete Fourier expansions of $s(t)$ and $x(t)$ can be written as:

$$s(t) = \sum_{k=1}^{N/2+1} a_k \cdot \cos(2\pi f_k t) + \sum_{k=1}^{N/2+1} b_k \cdot \sin(2\pi f_k t) \tag{7.5}$$

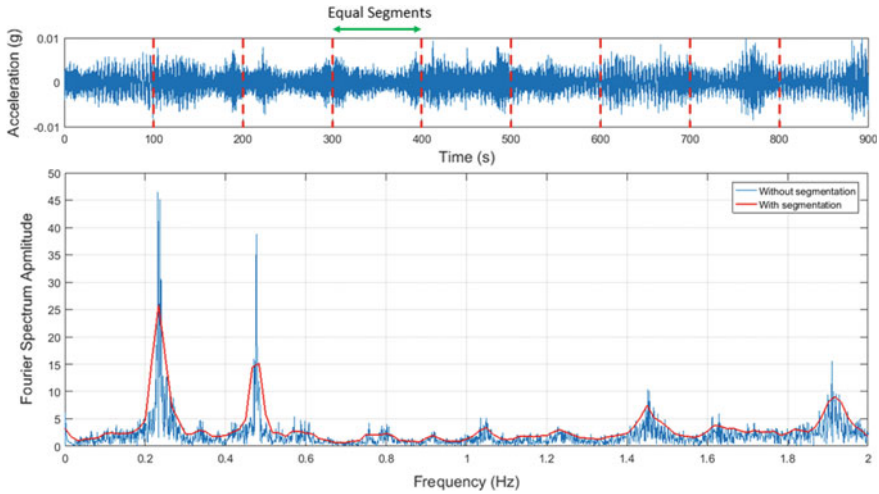


Fig. 7.3 Fourier Spectrum analysis of the SHM ambient vibration data collected on the Port Mann Bridge in Coquitlam, Canada with and without segmentation and averaging

$$x(t) = \sum_{k=1}^{N/2+1} \hat{a}_k \cdot \cos(2\pi f_k t) + \sum_{k=1}^{N/2+1} \hat{b}_k \cdot \sin(2\pi f_k t) \tag{7.6}$$

A simple technique to improve the SNR is the segmentation and averaging. This involves dividing the data into equal-length segments, and calculating the average of the spectral properties of the segments (Fig. 7.3). Assuming that the noise in the records is a random white-noise process, it can be shown that the averaged Fourier coefficients converge to those of the noise-free signal, as the number of segments increase [33]. That is:

$$Mean[\hat{a}_k] = a_k \quad \text{and} \quad Mean[\hat{b}_k] = b_k \tag{7.7}$$

It can also be shown that, the variance of the Fourier coefficients of the noisy signal is inversely proportional to the signal length. That is:

$$Variance[\hat{a}_k] = \frac{2\sigma^2}{N} \quad \text{and} \quad Variance[\hat{b}_k] = \frac{2\sigma^2}{N} \tag{7.8}$$

where σ^2 is the variance of $n(t)$ and N denotes the number of points in the record. The Eq. (7.7) confirms that the mean values of the Fourier coefficients of noisy signal $x(t)$ are equal to those of the noise-free signal, $s(t)$. The Eq. (7.8) shows that the variance of the Fourier coefficients of $x(t)$ is inversely proportional to the record length, that is, the longer the record length the smaller the variance of the Fourier spectrum. This observation suggests that we should consider very long signals when calculating the

Fourier spectra of ambient SHM data, provided that the signal characteristics remain stationary. If the stationary condition is not met, the alternative would be to divide the signal into equal-length of stationary signals, and calculate the Fourier spectrum as the average of the Fourier spectra of these segments.

7.2.5 Least-Square Estimation of Fourier Spectra

For a given signal length and sampling interval, all the sine and cosine terms in the Fourier expansion of the signal are known. The unknowns are the coefficients of these terms (i.e., the Fourier coefficients). Instead of determining the coefficients with standard Fast Fourier transforms, they can be calculated by minimizing the error between the noise-free signal (expressed as the sum of sine-cosine terms with unknown coefficients) and the recorded signal. The minimization results in a linear set of equations for the unknown coefficients of the noise-free signal, which can easily be solved by matrix inversion. The basic equations are given below, and more detail can be found in Safak et al. [33].

For a given signal length, N , and sampling interval, Δt , the discrete frequencies f_k of the Fourier spectra are

$$f_k = \frac{k}{N \cdot \Delta t} \quad \text{where } k = 1, \dots, (N/2 + 1) \quad (7.9)$$

The discrete Fourier expansion of the noise-free signal, $s(t)$, is given by

$$s(t) = \sum_{k=1}^{N/2+1} a_k \cdot \cos(2\pi f_k t) + \sum_{k=1}^{N/2+1} b_k \cdot \sin(2\pi f_k t)$$

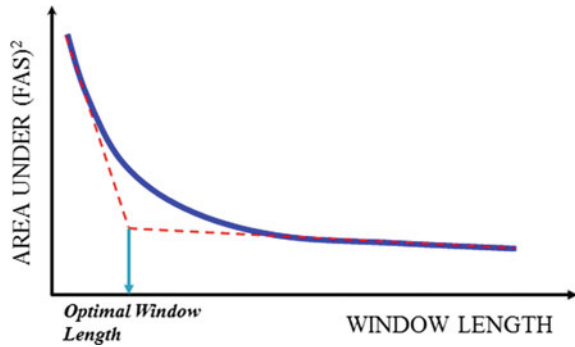
For given f_k (Eq. 7.9), all the sine and cosine terms in the Fourier expansion of $s(t)$ are known. The unknowns are the Fourier coefficients a_k and b_k . Instead of determining a_k and b_k by standard fast Fourier transforms, we can calculate them by minimizing the error V using the Eqs. (7.10) and (7.11) as

$$V = \sum_{t=1}^N [x(t) - s(t)]^2 \quad (7.10)$$

$$\min_{a_k, b_k}(V) \rightarrow \frac{\partial V}{\partial a_k} = 0 \quad \text{and} \quad \frac{\partial V}{\partial b_k} = 0 \quad (7.11)$$

The calculated a_k and b_k represent the least-square estimate of the Fourier coefficients of the noise-free signal.

Fig. 7.4 Selection of optimum windowing length [14]



7.2.6 Selection of Optimal Smoothing Windows

A widely used technique to reduce the influence of noise in Fourier spectra is to apply smoothing windows. There are no straightforward rules on selecting smoothing windows. Too short smoothing windows may not provide sufficient noise reduction, whereas too long smoothing windows may eliminate some of the real peaks. A simple technique for selecting the optimal smoothing window length is suggested in Safak [29]. It involves plotting the area under the squared Fourier amplitude spectrum with increasing window length. The plot shows a decaying curve with increasing window length. Initially, the decay is very fast, but becomes much slower as the window length increases as shown in Fig. 7.4. If it is assumed that the noise-free Fourier amplitude spectrum is a smooth function of frequency, it can be shown that the window length, where the rate of decay in the curve changes from fast to slow, corresponds to the optimal window length.

7.2.7 Statistical Signal Processing

Statistical signal processing accounts for the randomness of the noise in the records, and tries to remove it by using the statistical properties of the signal. The data from SHM systems are of ambient vibrations and mostly stationary (i.e., its temporal and frequency characteristics do not change significantly with time). They are also infinitely long with low SNR. These properties make statistical signal processing tools very appropriate for the analysis of SHM data. Some of the simple statistical signal processing tools is summarized below, and more details are given in Safak et al. [33] and Moon and Stirling [23].

7.2.7.1 Auto-Correlation Functions

Auto-correlation functions provide one of the simple tools for statistical signal processing. The auto-correlation $R(\tau)$ of a signal $x(t)$ is

$$R(\tau) = \frac{1}{N} \sum_{t=1}^N x(t) \cdot x(t - \tau) \quad (7.12)$$

where τ is the time delay and N is the length of the signal. For stationary signals, such as ambient vibrations, the auto-correlation function depends only on the time lag τ . It can be shown that the auto-correlation operation does not alter the frequency content of the signal. For example, for a periodic signal $x(t)$ with added noise $n(t)$:

$$x(t) = A \cdot \cos(\omega t) + n(t) E[R(\tau)] = \frac{A^2}{2} \cdot \cos(\omega t) \quad (7.13)$$

where $E[\cdot]$ denotes the expected value and A is a constant. Taking the autocorrelation does not change the frequency content of the signal. It can also be shown that the autocorrelation improves the SNR, i.e., the SNR in the autocorrelation of a signal is higher than that of the original signal. This is because the autocorrelation operation amplifies (i.e., squares) the amplitudes of any periodic components in the data at times when τ is equal to an integer multiple of the signal's period. Therefore, when calculating Fourier spectra of ambient noise, it is advantageous to use the autocorrelation functions of the records instead of the original records. The Fourier spectrum of the autocorrelation function is commonly known as the power spectral density function. The decay of auto-correlation function with increasing time lag allows calculation of damping in the structure, and is known as the random decrement method.

7.2.7.2 Optimal Filtering

Optimal filtering aims to remove noise by searching periodic components in the record. It is assumed that the periodic components in the record correspond to the noise free signal, and that the remaining components are considered to be the noise. A characteristic of a periodic signal is that its value at any given time can be written as a linear combination of its past values. Therefore, if we were able to separate the record $x(t)$ into its periodic and random components as

$$x(t) = \sum_{k=1}^m a_k \cdot x(t - k) + n(t) \quad (7.14)$$

where the first term on the right-hand side is the periodic component (i.e., the part that can be estimated from the past values). Assume that we know all the values of

$x(t)$ up to time step $(t - 1)$ and want to predict the value at the next time step t . Since the mean value of $n(t)$ is zero, the most likely value of $x(t)$ would be

$$\hat{x}(t) = \sum_{k=1}^m a_k \cdot x(t - k) + n(t) \quad (7.15)$$

The difference between the predicted and the recorded values of $x(t)$ is the error in our estimation. The coefficients a_k in Eq. (7.15) can be selected such that the estimation error V in Eq. (7.16) is minimized.

$$\min_a (V) = \left[x(t) - \sum_{k=1}^m a_k \cdot x(t - k) \right]^2 \rightarrow \frac{\partial V}{\partial a_k} = 0 \quad (7.16)$$

Equation (7.16) results in a set of linear equations to determine the coefficients a_k . These coefficients define the filter to remove noise from the signal. The noise-free signal can be calculated by filtering the record using Eq. (7.15).

The procedure presented above describes the basic idea in optimal filtering. There are numerous variations of the procedure suggested in the literature such as Wiener filtering, Recursive Least Squares, Least Mean Squares, Durbin Algorithm, Burg Algorithm, and Yule-Walker Algorithm. More detail on these methods can be found in textbooks on optimal filtering and linear estimation [12].

7.2.7.3 Eigenvalues of Auto-Correlation Matrix

Another set of powerful tools for spectral estimation, as well as to separate signal from the noise, can be developed based on the eigenvalues and eigenvectors of the autocorrelation matrix. The autocorrelation matrix Q is defined by Eq. (7.17) as

$$Q = \begin{bmatrix} R(0) & \cdots & R(M) \\ \vdots & \ddots & \vdots \\ R(-M) & \cdots & R(0) \end{bmatrix} \quad (7.17)$$

where

$$R = \frac{1}{N} \sum_{t=1}^N x(t) \cdot x(t - \tau) \quad \text{and} \quad \tau = -M, \dots, 0, \dots, M \quad (7.18)$$

Q is a $(M + 1) \cdot (M + 1)$ dimensional matrix that has $(M + 1)$ eigenvalues and eigenvectors. The Karhunen-Loeve expansion states that a stationary signal can be represented in terms of the eigenvectors of its autocorrelation matrix as [13, 22]:

$$x(t) = \sum_{i=0}^M c_i \cdot q_i(t) \quad (7.19)$$

where M is the filter order, $q_i(t)$ denotes the i th eigenvector corresponding i th eigenvalue and c_i is a scalar representing the weighting factor of the i th mode. Equation (7.19) shows that total recorded response can be expressed as a sum of the modal responses of its autocorrelation matrix. It can also be shown that the eigenvalues that correspond to the correlated (i.e., periodic) components of the record are much larger than those that correspond to the uncorrelated (i.e., noise) components in the record. Therefore, the eigenvalues and eigenvectors of the correlation matrix can be used to separate the noise from the signal. The noise-free signal is calculated from Eq. (7.19) by using only those terms that correspond to higher eigenvalues.

An important assumption made in the derivation of Eq. (7.17) is that $x(t)$ is a stationary signal. In other words, the temporal and frequency characteristics of $x(t)$ does not change significantly with time, and therefore the autocorrelation function R is the function of the time lag only between the two components. The assumption of stationarity is appropriate for vibrations under ambient forces and wind loads, but not for vibrations under transient loads such as earthquakes or blast loads.

A key parameter that needs to be selected in the optimal filtering and the eigenvalue approach is the filter order, M . A filter with too small M does not accurately represent the signal, whereas a filter with too large M may try to represent noise as well as the signal. They are several criteria available in the literature to select M (e.g., [36]). A simpler and more straightforward selection of M , proposed by Safak, [32], can be made by plotting the variation of $V = \sum e^2(t)$ with M , where $e(t)$ is the error between the recorded signal and the signal calculated by Eq. (7.19). This sum typically shows a fast drop with increasing M , and then levels off. The M value where the sum starts to level off can be taken as the optimal filter order.

7.3 Damage Detection Methods

7.3.1 *Damage Detection Based on the Changes in Natural Frequencies*

Many methods have been developed over the years to accurately determine the modal frequencies of a structure [2, 5, 25]. Natural frequencies of a structure are the fundamental parameters defining its dynamic response. Natural frequencies are a function of stiffness, and the presence of damage means a reduction in the stiffness. Therefore, it is natural to use the change in natural frequency as a structural damage indicator. However, the dynamic response of a damaged structure is nonlinear and in most cases hysteretic. The stiffness, and consequently the natural frequencies, rapidly changes during the damaging vibrations, and they are hard to track for short-duration transient

loads such as earthquakes. Moreover, data from earthquakes have shown that even though a structure is damaged, the stiffness before and after the damage may not be that much different.

Natural frequencies of a structure can also change due to soil-structure interaction and environmental factors, such as temperature, rain, wind, etc. without any damage. By studying a two-year long continuous data from the Millikan Library building at Caltech, Clinton et al. [7] has shown that the building's natural frequency can change significantly due to environmental factors. Although it is damaged, no changes in the frequency have been observed from the records of a 7-story, reinforced concrete hotel building in Van Nuys, California, which suffered significant damage to the fourth-floor columns during the 1994 Northridge earthquake. Multiple sets of earthquake records from a 40-story steel building in Los Angeles have shown that small nonlinearities, which are always present in buildings, and the variations in damping can also cause changes in the observed frequencies [33].

7.3.2 Damage Detection Based on Permanent Deformations

The structure goes through nonlinear, hysteresis type force-deformation loops when the damage takes place, and the structure does not return to its original configuration when the excitation stops. In other words, the structure shows permanent deformations, such as permanent displacements and/or permanent rotations, after the earthquake. Unlike the trigger-based monitoring, the real-time monitoring can detect permanent deformations. This is accomplished by comparing pre-, during, and post-earthquake records, and it is based on the following two criteria: (1) the dynamic characteristics of the structure change during the earthquake, and (2) the structure exhibits permanent deformations after the earthquake. In other words, the spectral characteristics of the signal (namely, the frequency content and damping) change during the earthquake, and the mean values of the signal before and after the earthquake are different (i.e., the post-earthquake portion of the signal shows permanent DC offset). Such deformations can best be measured by special sensors such as GPS sensors and tiltmeters. Once the presence of permanent displacements and rotations are confirmed, the question becomes whether they represent damage or not. Statistical hypothesis tests can be used to make such decisions (e.g., [20]).

7.3.3 Damage Detection Based on Inter-Story Drift

Drifts can be evaluated for bridge piers, towers, or building columns. Drift is defined as the relative displacement of the column top with respect to its base, and it is mainly controlled by the displacement demand induced by earthquakes. Drift is one of the key design parameters in current seismic codes and has been suggested as damage indicator [3, 4]. To calculate the drift, the displacements need to be measured at the top and the bottom of the column. It is possible to calculate displacements from

acceleration data by double integrating the recorded accelerations twice. However, the integration operation on raw data significantly increases the noise amplitudes in the integrated signal and can lead to misleading results [32]. If the noise in the accelerations is an added white noise, after integration the white noise becomes a Brownian motion whose variance increases linearly with time [24]. The noise amplitudes continuously grow during real-time processing and analysis; therefore, the SNR in the difference of the signals is always much worse than the original signals [32]. However, it can be minimized if only the resonant components of the structure in the signal are considered. These resonant components are located within the narrow frequency bands around the modal frequencies of the structures and have much higher SNR. The noise influence during the integration and differentiation is minimized, if they are done over the band-pass filtered records around the resonant frequencies.

Drift calculations both for bridge piers and building columns can be done in real-time provided that the records at each floor level are synchronized, and that these acceleration records are band-pass filtered bi-directionally: yielding zero-phase shift. In this section, we will only focus on the building type of structures to show how inter-story drifts can be calculated in real-time, but similar approach can be utilized for bridge piers, too.

Relative modal accelerations at each floor level of a multi-story building can be superimposed to yield the relative floor accelerations [6] as

$$x_k(t) = \sum_{j=1}^n x_{j,k}(t) \quad (7.20)$$

where n is number of the degrees-of-freedom of a linearly elastic multi-story building, $x_k(t)$ is time variation of the k th floor's relative displacement, and $x_{j,k}(t)$ is the time variation of the j th mode's relative displacement at k th floor, and it can be calculated as

$$x_{j,k}(t) = \Gamma_j \cdot \phi_{j,k} \cdot q_j(t) \quad (7.21)$$

where Γ_j is the j th modal participation factor; $\phi_{j,k}$ is the amplitude of the j th mode shape at k th floor; and $q_j(t)$ is the time variations of the displacement of the j th mode of a single-degree-of-freedom system. Denoting modal displacement as $D_j(t) = \Gamma_j \cdot q_j(t)$, Eq. (7.21) will lead to

$$x_{j,k}(t) = \phi_{j,k} \cdot D_j(t) \quad (7.22)$$

7.3.4 Estimation of Response at Non-instrumented Floors

Multi-story buildings are usually instrumented at a limited number of floors, and several researchers have developed methods to estimate the response at non-

instrumented floors (e.g., [27]). To calculate the inter-story drifts at stories that are not instrumented, Kaya et al. [15] has proposed a new method called *Mode Shape Based Estimation* (MSBE). It is based on the least-squares algorithm and can approximate the calculated modal displacements at instrumented floors as a linear combination of the mode shapes of a shear beam and a bending beam at every time step. Using different combination at every time step is equivalent to assuming that the shear and bending beams used in the approximation has time varying properties (i.e., they are nonlinear). This allows us to estimate the modal displacements at non-instrumented floors, and hence the inter-story drifts at all stories as shown in Eq. (7.23).

$$\phi_{j,k} = C_{s,j} \cdot \phi_{s,j,k} + C_{b,j} \cdot \phi_{b,j,k} \quad (7.23)$$

where $\phi_{s,j,k}$ and $\phi_{b,j,k}$ are amplitude of the j th mode shapes of a shear beam and a bending beam, respectively, at k th floor; $\phi_{j,k}$ is the amplitude of the j th mode shape of the building at k th floor; $C_{s,j}$ and $C_{b,j}$ are the unknown weighting coefficients for the j th mode. The error in the estimation for the j th mode can be expressed as the square sum of the differences over the instrumented floors between the recorded modal acceleration, $\ddot{z}_{j,k}(t)$ and the calculated modal acceleration, $\ddot{x}_{j,k}(t)$.

$$\varepsilon_j(t) = \sum_{i=1}^{NIF} [\ddot{z}_{j,k}(t) - \ddot{x}_{j,k}(t)]^2 \quad (7.24)$$

where $\varepsilon_j(t)$ is the error function for the j th mode and NIF is the number of instrumented floors. In order to calculate the recorded modal displacements, $\ddot{z}_{j,k}(t)$ first the modal frequencies of the building are identified by using Fourier/spectral analysis. Next, the recorded accelerations at each instrumented floor are band-pass filtered around each modal frequency of the building, and then double integrated [14]. The summation in the error function is only over the instrumented floors; therefore, the coefficients of $C_{s,j}$ and $C_{b,j}$ can be estimated by minimizing the error function as

$$\frac{\partial \varepsilon_j}{\partial C_{s,j}} = 0, \quad \frac{\partial \varepsilon_j}{\partial C_{b,j}} = 0. \quad (7.25)$$

which will lead to (7.26) and (7.27)

$$\begin{aligned} \frac{\partial \varepsilon_j}{\partial C_{s,j}} &= \sum_{j=1}^{NIF} -2\phi_{s,j,k} y_{j,k}(t) D_j(t) + 2C_{s,j} \phi_{s,j,k}^2 D_j^2(t) + 2C_{b,j} \phi_{s,j,k} \phi_{b,j,k} D_j^2(t) \\ \frac{\partial \varepsilon_j}{\partial C_{b,j}} &= \sum_{j=1}^{NIF} -2\phi_{b,j,k} y_{j,k}(t) D_j(t) + 2C_{b,j} \phi_{b,j,k}^2 D_j^2(t) + 2C_{s,j} \phi_{s,j,k} \phi_{b,j,k} D_j^2(t) \end{aligned} \quad (7.26)$$

$$\begin{bmatrix} \sum_{j=1}^{NIF} \phi_{s,j,k}^2 & \sum_{j=1}^{NIF} \phi_{s,j,k} \cdot \phi_{b,j,k} \\ \sum_{j=1}^{NIF} \phi_{s,j,k} \cdot \phi_{b,j,k} & \sum_{j=1}^{NIF} \phi_{b,j,k}^2 \end{bmatrix} \cdot \begin{pmatrix} C_{s,j} \cdot D_j(t) \\ C_{b,j} \cdot D_j(t) \end{pmatrix} = \begin{bmatrix} \sum_{j=1}^{NIF} \phi_{s,j,k} \cdot y_{j,k}(t) \\ \sum_{j=1}^{NIF} \phi_{b,j,k} \cdot y_{j,k}(t) \end{bmatrix} \quad (7.27)$$

Equation (7.27) is time-dependent and must be calculated at every time step, t . Note that the $C_{s,j} \cdot D_j(t)$ and $C_{b,j} \cdot D_j(t)$ can be calculated in real-time; therefore, using Eqs. (7.20) and (7.27), the k th floor displacements of the multi-story building can then be calculated in real-time as

$$x_k(t) = \sum_{j=1}^{NIM} \left([\phi_{s,j,k} \ \phi_{b,j,k}] \cdot \begin{bmatrix} C_{s,j} \cdot D_j(t) \\ C_{b,j} \cdot D_j(t) \end{bmatrix} \right) \quad (7.28)$$

The total displacements at any floor can then be calculated as

$$x_k^T(t) = x_k(t) + x_g(t) \quad (7.29)$$

where $x_g(t)$ is the displacement at the base of the building that can be calculated by double integrating the base accelerations. For multi-story buildings, using only first a few modes is sufficient to get accurate displacement values. Modes that are buried in noise should not be considered in the calculation of inter-story drifts since their contribution to total drift would be negligible, and they will be more influenced by noise.

The amplitudes of the shear- and bending-beam ($\phi_{s,j,k}$ and $\phi_{b,j,k}$) in Eq. (7.23) are determined based on the assumption that both the amount of the mass and the stiffness of the shear and bending beams are uniformly distributed. Theoretically, the MSBE method can only be applied to those structures whose mass and stiffness is uniformly disturbed along the height of the structure. Most high-rise buildings can be approximated to meet this requirement. Kaya and Dowling [16] have used the Timoshenko beam to calculate the mode shape of the beam, and slightly better results have been obtained.

7.3.4.1 Factor Building as an Example

Factor building is located at the UCLA's campus in California and is instrumented after the 1994 Northridge earthquake by the US Geological Survey. The instrumentation includes 72-channel accelerometer network distributed at each floor level. The instrumentation layout is given in Fig. 7.5, and additional information about the building is provided in Kohler et al. [19]. Building has experienced several earthquakes since the instrumentation was completed. Kaya et al. [15] has used the M4.7 West

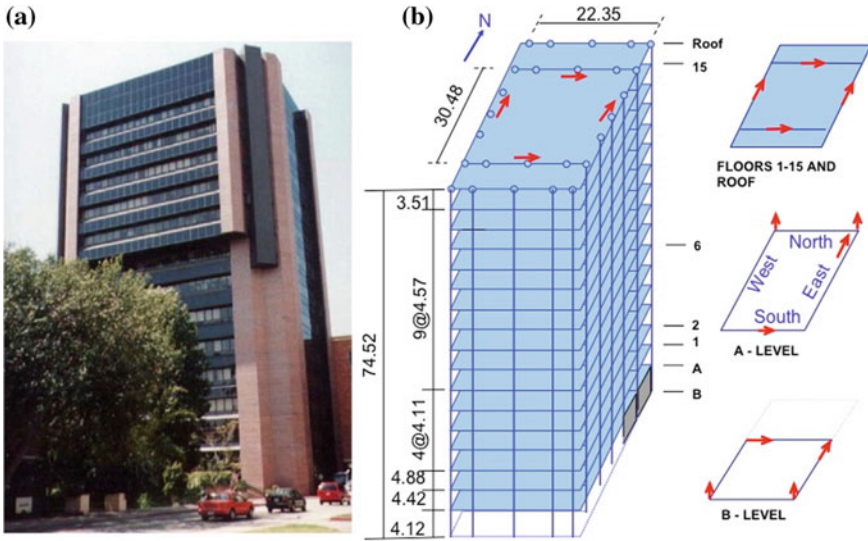


Fig. 7.5 **a** Photo of the Factor building taken from the northeast side of the building, **b** the sensor layout of the Factor building. Arrows show the polarities of the sensors on each floor, and all dimensions are in meter [19]

Hollywood earthquake of October 30th, 2004 in California to validate the MSBE method.

Using three different methods, the modal response and the total relative response of the building at each floor level were calculated assuming that the acceleration recordings were available at three floor levels only (1st, 8th and roof floor levels). The results at the non-instrumented floors are compared with the recorded response of the building at each floor level. Figure 7.6 shows the estimated first four mode shapes of the building, and it was concluded that the interpolation methods require a sensor at each floor level where the sign of the slope of the mode shape changes due to linear segments of the mode shape. However, this was not the case for MSBE method because the MSBE method does not interpolate the amplitudes of the recorded data over the height of the building. It instead provides the best-fit mode shapes to the recorded data in least-square sense. As shown in Fig. 7.6, the performance of the MSBE methods becomes more clear and important for higher modes especially when the modal participation factor for those higher modes are significant such as the case in tall buildings. Figure 7.7 shows the comparison of the recorded and estimated relative floor accelerations at 13th floor level, and it proved that the MSBE method would always provide more reliable results than interpolation methods, which usually overestimate the building response.

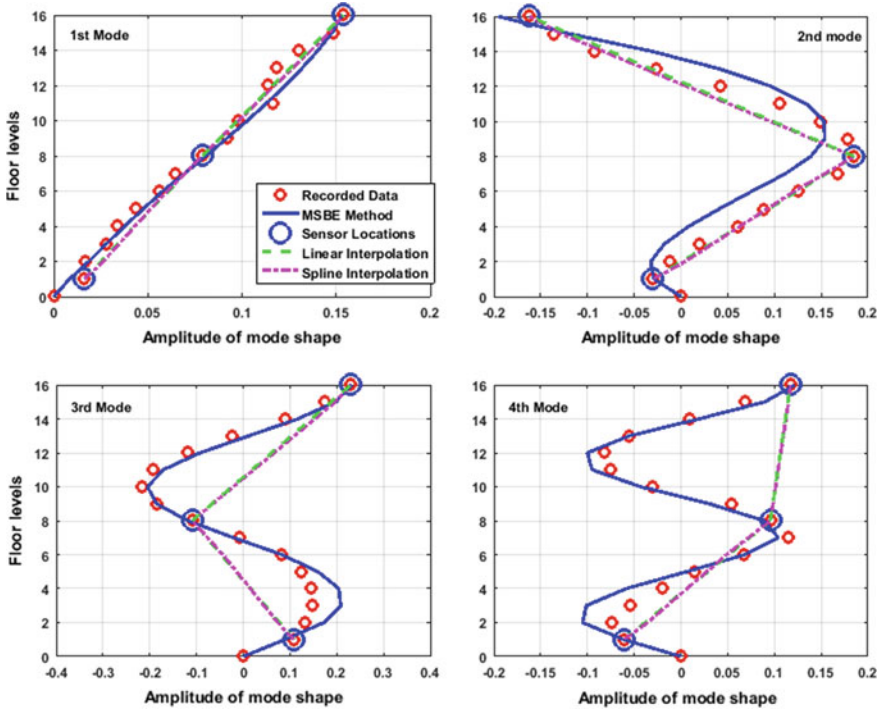


Fig. 7.6 The first four-mode shapes of the Factor building: the red circles are the relative displacement amplitudes (calculated from the recorded accelerations) of the building at each floor level; the blue circles show the location of the sensors of configuration C1; the dashed green line, dashed magenta line, and the solid blue line show the calculated mode shapes (calculated modal displacement amplitudes at each floor level) using the linear interpolation, cubic spline interpolation, and the MSBE methods, respectively [15] (Color figure online)

7.3.5 Damage Detection Based on Wave Propagation and Interferometric Imaging

The vibrations of structures can be characterized in terms of wave propagation parameters: wave velocities, attenuation of wave amplitudes, and the wave reflections and transmission coefficients [31]. The incoming seismic waves travel upward in the building until it reaches to the roof. It is then reflected by the free surface on the roof and propagates downward and again is reflected back upwards by the ground. Vibrations in the building are caused by these up and down bouncing waves, and they last until they damped out and the earthquake stops. For system identification and damage detection, it has been shown that, when compared to modal parameters (e.g., modal frequency, mode shape and damping ratio), the wave propagation parameters are more reliable and robust, and also more sensitive to damage [30].

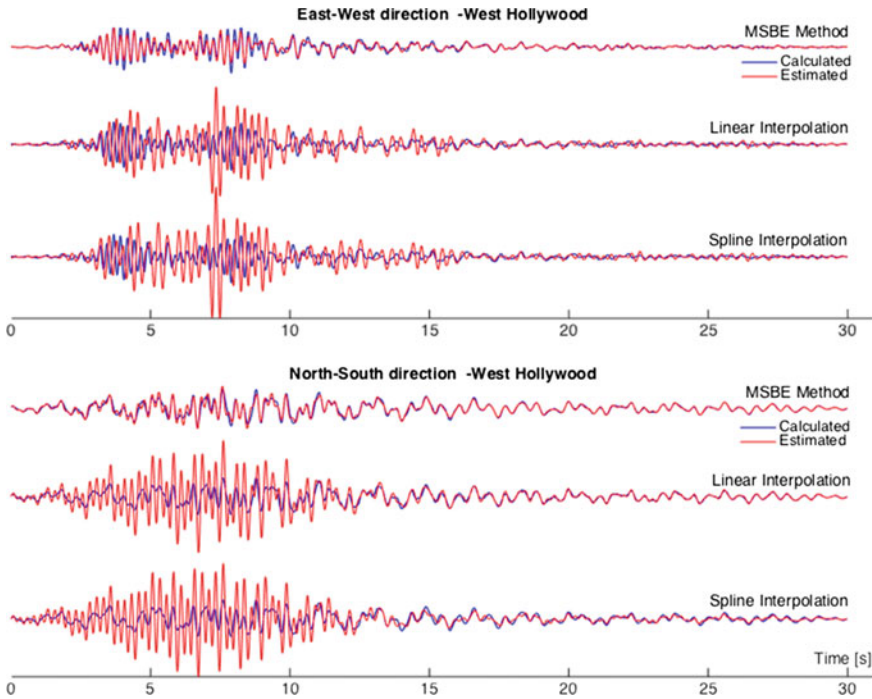


Fig. 7.7 The comparison of the calculated (blue line) and the estimated relative accelerations (red lines) of the 13th floor for West Hollywood earthquake [15] (Color figure online)

For earthquake-induced vibrations, total accelerations recorded on multi-story buildings are the sum of accelerations of the building plus the ground accelerations. They may also include the coupling effects of the building to its subsurface (i.e., soil-structure interaction) and are not independent of the excitation of the building [35]. Furthermore, the wave propagation of a building on a flexible soil is dispersive when foundation rocking is present [26]. These effects can be eliminated from the recorded total acceleration data using the interferometric imaging method.

Interferometry utilizes the correlations among the synchronized records collected from different locations, and these correlations can be shown to lead to the Green's functions that account for the wave propagation between different receivers in the structure [8, 21, 28, 34, 38]. The properties of the waves can be investigated without knowing the seismic input that generated the waves. It can be shown that when de-convolved by the roof record (acceleration data recorded at the roof level of the building), the floor accelerations in multi-story buildings become a sum of attenuating up-going and down-going waves along the height of the building [35]. The deconvolution by the roof record is done in frequency domain by using the following equations, Eqs. (7.30) and (7.31):

$$T_n(z, \omega) = \frac{u_n(z, \omega) \cdot u_N^*(z = H, \omega)}{|u_N(z = H, \omega)|^2 + \varepsilon} \tag{7.30}$$

$$T_n(z, \omega) = \frac{1}{2} [e^{ik(z-H)} \cdot e^{-\gamma|k|(z-H)} + e^{ik(H-z)} \cdot e^{-\gamma|k|(H-z)}] \tag{7.31}$$

where $u_n(z, \omega)$ and $u_N(z = H, \omega)$ are the signals recorded at height z and H of the building, respectively; the superscript (*) denotes the complex conjugate; H is the total height of the building; ω is the circular frequency; ε is the stabilization parameter, which can be taken as 10% of the average spectral power of $u_N(\omega)$, and $k = \omega/c$ is the wavenumber. $T_n(z, \omega)$ is the deconvolution of $u_n(z, \omega)$ out of $u_N(z = H, \omega)$ at height z (the n th floor).

An example of this for the Factor Building in UCLA campus in California is given in Fig. 7.8. Figure shows two-second segment of the floor accelerations after they are de-convolved by the roof accelerations. The horizontal axes denote the time and the floor level, and the vertical axis is the accelerations de-convolved by the recorded roof accelerations. The accelerations are color-coded based on their amplitudes. As clearly seen in Fig. 7.8, when de-convolved by the roof accelerations, the accelerations in the building become simple up- and down-going waves along the height of the building. Furthermore, the roof-deconvolved records do not show any sign of reflection along the height of the building, which are free of the coupling of the building to its subsurface and independent of the excitation of the building [35]. If there was a reflection at any floor level, the up-going or the down-going propagating wave would have changed its propagation direction. For example, an up-going wave would have reflected at floor levels, some portion travelling downwards and the rest going upwards. This is clearly not the case in Fig. 7.8, since the up-going waves reflect from the top floor only. This is the result of deconvolution by the roof record. Deconvolution by the base record would give reflections at floor levels.

This property of the roof-deconvolved records indicate that any structural change in a story would only change the de-convolved records at the floors below that story.

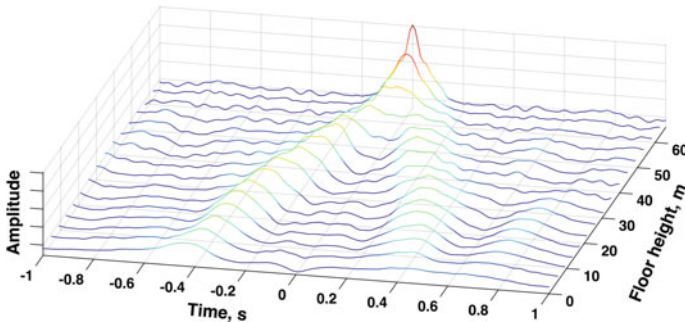
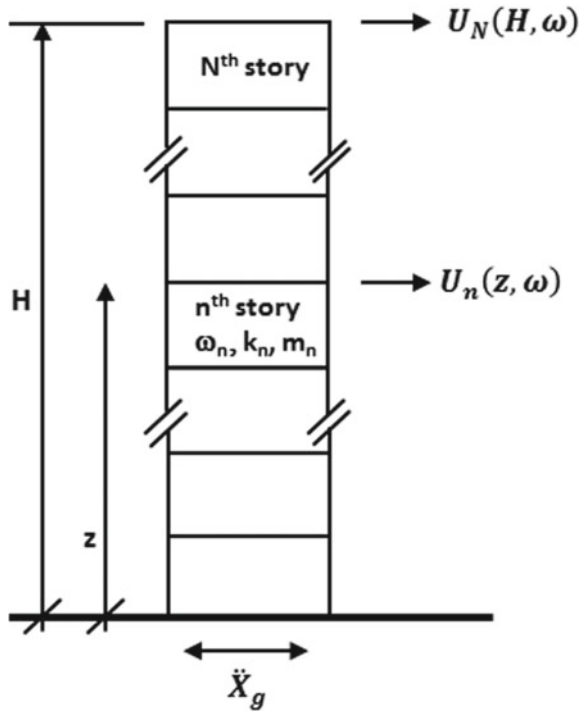


Fig. 7.8 Two-second segment of roof-deconvolved acceleration time histories of the Factor Building. Neither the up-going waves nor the down-going wave shows any sign of reflection along the height of the building [17]

Fig. 7.9 Multi-story building under base excitation of \ddot{X}_g acceleration



In other words, the roof-deconvolved record at a floor depends only on the properties of the stories above. This is not valid for the raw records since they are formed by the combination of both up-going and down-going waves. Therefore, we can then take the ratio of the Fourier amplitude spectra of the deconvolved records at two adjacent floor levels to calculate the spectral ratio, $SR_n(\omega)$ for n^{th} story as seen in Eq. (7.32) (Fig. 7.9).

$$SR_n(\omega) = \frac{T_n(z_t, \omega)}{T_n(z_b, \omega)} \tag{7.32}$$

where $T_n(z_t, \omega)$ and $T_n(z_b, \omega)$ are the Fourier amplitude spectra of the accelerations calculated at the top and bottom of the n^{th} story, respectively; $SR_n(\omega)$ is the spectral ratio of n^{th} story. Note that using the Running Windows presented in Sect. 7.2, the spectral ratio for each story of a building in Eq. (7.32) can now be calculated in real-time.

Using the transfer matrix formulation [15], it can be shown that the top/bottom spectral ratio of any floor will depend only on the physical properties of that story and the stories above that floor. For an N -story building, the spectral ratios for the top two stories are defined by the following equations, Eqs. (7.33) and (7.34):

$$SR_N(\omega) = \frac{\omega_N^2}{\omega_N^2 - \omega^2} \tag{7.33}$$

$$SR_{N-1}(\omega) = \frac{\omega_{N-1}^2 \cdot (m_{N-1}/m_N) \cdot (\omega^2 - \omega_N^2)}{\omega^2 \cdot \omega_N^2 + (m_{N-1}/m_N) \cdot (\omega^2 - \omega_N^2)(\omega_{N-1}^2 - \omega^2)} \tag{7.34}$$

where m_N is the mass of the N th story and ω_N is the fixed-based frequency of the N th story.

Transfer matrix formulation basically defines the relationship between the forces and displacements of any adjacent stories in a multi-story building [10, 37]. $SR_n(\omega)$ is a function of the physical properties of the story n and the stories above it. By studying the transfer function of a simple 2-DOF model, for small damping ratios (e.g., $\xi_n < 0.20$), it was shown that the spectral ratio of the transfer function of the upper-floor acceleration to that of the lower floor acceleration always peaks at or near the predominant frequency of the fixed-based frequency (i.e., $\omega_n^2 = k_n/m_n$) of that story (i.e., as if that story were a fixed-based one-story building) [28].

The spectral ratio $SR_N(\omega)$ in Eq. (7.33) is a function of the individual frequency ω_N of the top story (i.e., $\omega_N^2 = k_N/m_N$), and it peaks at $\omega = \omega_N$. The spectral ratio $SR_N(\omega)$ is not influenced by the dynamic characteristics of the stories below or by the excitation; therefore, the natural frequency of the top story and consequently the stiffness of the top story can be determined uniquely assuming that the mass of the top floor is known or estimated.

As stated earlier, the spectral ratio $SR_n(\omega)$ is a function of the properties of story n and stories above (i.e., $(n + 1)$, $(n + 2)$). This ratio does not depend on the properties of the stories below. We start calculating the spectral ratios from the top story, and continue downward. For story n , since ω_{n+1} and k_{n+1} have already been determined earlier from the spectral ratio $SR_{n+1}(\omega)$, the ω_n and the k_n can now be determined from the spectral ratio of $SR_n(\omega)$ assuming that the mass of m_n is known

Table 7.1 Mass and stiffness distribution of 10-story shear-beam building

Building story	Story mass (10^{-6} ton)	Story Stiffness (10^{-2} kN/m)		
		Undamaged	Damaged (1)	Damaged (2)
Story 1	5.625	0.5	0.5	0.5
Story 2	5.625	0.5	0.5	0.5
Story 3	5.625	0.5	0.5	0.5
Story 4	5.625	0.5	0.5	0.5
Story 5	5.625	0.5	0.5	0.5
Story 6	5.625	0.5	0.5	0.4
Story 7	5.625	0.5	0.5	0.5
Story 8	5.625	0.5	0.5	0.5
Story 9	5.625	0.5	0.4	0.4
Story 10	5.625	0.5	0.5	0.5

or estimated. Determination of ω_n and k_n does not change ω_{n+1} and k_{n+1} , which are already determined from the previous step. Thus, starting from the top story and taking the SR of each story below consecutively, the individual frequencies of each story can be calculated. This approach also provides a simple tool to calibrate Finite Element (FE) models of buildings from vibration records [15].

As an example, we consider the simulated response of an elastic 10-story building with 4% viscous damping for all modes, excited by the $M_w = 7.3$ Kocaeli, Turkey earthquake of 1999 [9]. To make it more realistic, we added 10% noise to the simulated response.

The distribution of the stiffness and mass for the building is given in Table 7.1: the damage is simulated at the 6th and 9th stories by reducing the stiffness of these stories by 20%. Calculated spectral ratios for each story are depicted in Figs. 7.10, 7.11, and 7.12 for the damaged and the undamaged structures.

For the damage at the 9th story level, the spectral ratios both for the damaged and the undamaged structure at the 10th story exhibit the same predominant frequency of 4.79 Hz (no frequency shift) (Fig. 7.10). However, the predominant frequency of the 9th story for the damaged structure is shifted by 13% from 2.93 to 2.57 Hz, and all of the stories below 9th story experience similar frequency shifts. This frequency shift at the 9th story indicates a structural change (e.g., damage) because it is the highest story at which such frequency shift exists. The frequency shifts at the stories below the 9th story do not necessarily indicate a structural change at that story because such shifts may also stem from the structural changes that may exist on upper stories. The FE model of the building is then calibrated only on the 9th story (Damaged (1) state

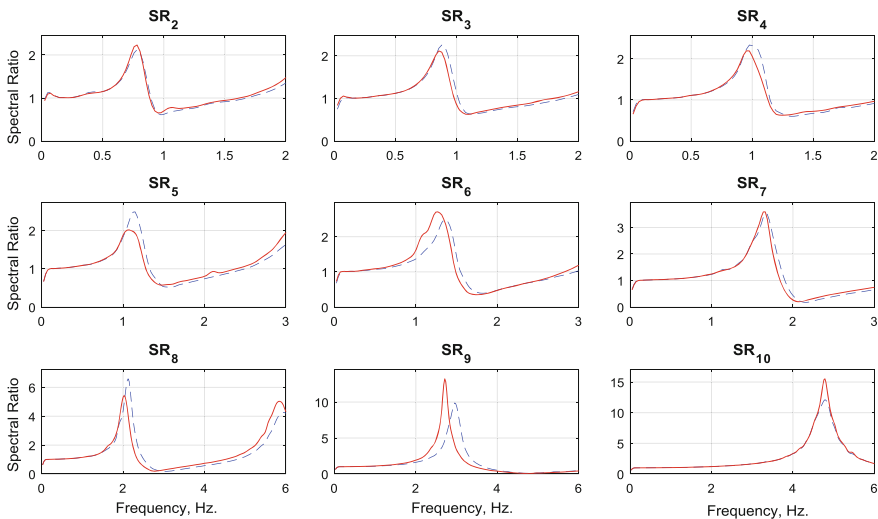


Fig. 7.10 Spectral ratio graphs of each story of the linear elastic 10-story building. The dashed blue line indicates the damaged structure and the solid red line indicates the intact structure [17] (Color figure online)

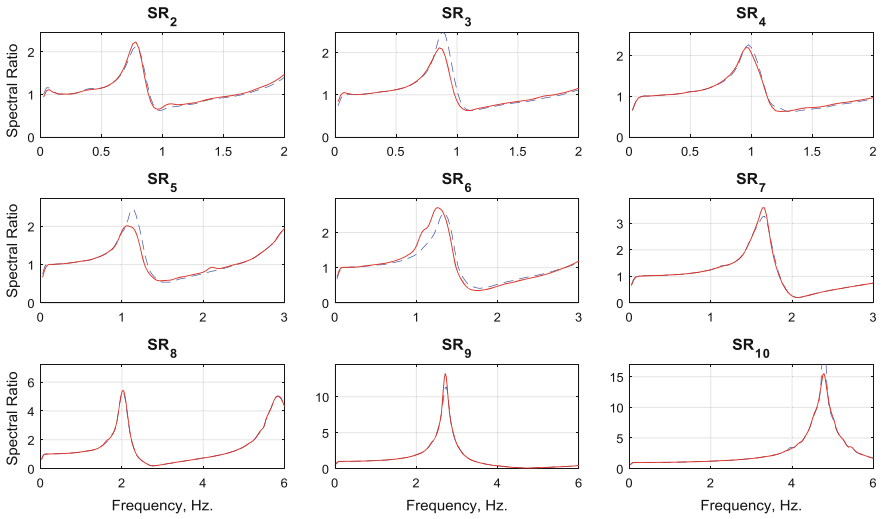


Fig. 7.11 Spectral ratio graphs of each story of the linear elastic 10-story building after the finite element model of the building is calibrated at the 9th story. The dashed blue line indicates the damaged structure and the solid red line indicates the intact structure [17] (Color figure online)

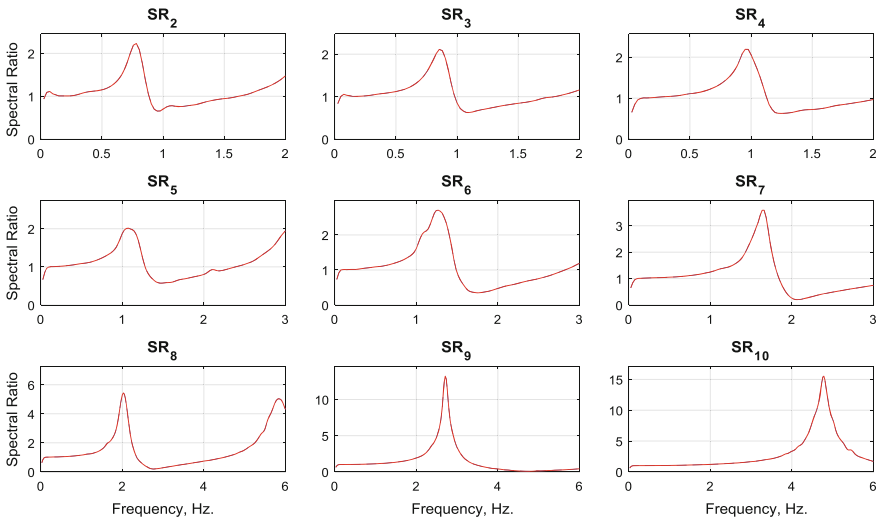


Fig. 7.12 Spectral ratio graphs of each story of the linear elastic 10-story building after the finite element model of the building is further calibrated at the 6th story. The dashed blue line indicates the damaged structure and the solid red line indicates the intact structure [17] (Color figure online)

in Table 7.1) by reducing the 9th story stiffness until the predominant frequencies matches (Fig. 7.11).

5% frequency shift at the 6th story SR is observed from 1.34 to 1.27 Hz, but no frequency shift (e.g., no damage) is experienced for the 7th and 8th stories because the FE model of the building was already calibrated at the 9th story level. The stories below 6th experience similar frequency shifts in their SR graphs (Fig. 7.11). Thus the building FE model is calibrated at the 6th story level (Damaged (2) state in Table 7.1). Finally, Fig. 7.12 shows the SRs both for the damaged and undamaged building, and no frequency shift is observed in any of the SRs. Thus, this indicates that no further calibration on the FE model is required, and that the FE model of the building is fully calibrated at all stories of the building. The calibrated FE model can now be used to detect the location and the extent of the damage to the building by comparing its initial and calibrated FE models (Table 7.1).

7.4 Conclusion

One of the key requirements in modern SHM systems is that the recording, processing, and analysis of the structural data should be done in real-time. This paper presents tools and methodologies for real-time processing and analysis of SHM data, as well as for real-time system identification and damage detection. System identification is accomplished by utilizing several user-selectable time-varying spectral analysis techniques, whereas the damage detection is achieved based on inter-story drifts, interferometric imaging and Transfer Matrix formulation of structural response.

Equal-length and overlapping sliding Running Windows are presented to keep track of time varying characteristics of signals. The data in each segment is analyzed separately, and the sequential analysis results are averaged to form the overall output and minimize the effect of noise.

Calculation of inter-story drifts requires (1) double integration and subtraction of ambient vibration data, which usually result in erroneous drift ratios, and (2) that the vibration time histories are known at every floor level of a building. To minimize such errors, band-pass filters are used to calculate the modal response of the structure and then combine them to form the displacements at the instrumented floors. Vibration time histories at the non-instrumented floors are estimated using the calculated modal response of the structure based on the fact that the mode shape of a building can be approximated as the linear combination of a shear- and bending-beams with time varying properties. The calculated inter-story drifts are then compared to threshold values that correspond to different structural damage and performance levels. Earthquake records from the Factor Building at UCLA campus in California are utilized to validate these new tools and methodologies.

Interferometric imaging and Transfer Matrix formulation shows that, for multi-story buildings, the top-to-bottom spectral ratio of the records at a particular story depends only on the structural properties of that story and the stories above; any structural change at the stories below does not affect the spectral ratio of the stories

above. This observation allows the identification of the individual natural frequency each story uniquely (also, the stiffness if the story if story mass is known). The FE models of buildings can be calibrated for each story, and the detection and location of damage can be made by observing the changes in spectral ratios. Numerical example on the 10-story linear elastic shear-beam building is used to validate the methods.

References

1. Boore DM (2001) Effect of baseline corrections on displacement and response spectra for several recordings of the 1999 Chi-Chi, Taiwan, Earthquake. *Bull Seismol Soc Am* 91:119–1211
2. Brincker R, Ventura C (2015) Introduction to operational modal analysis. Wiley
3. Celebi M, Sanli A, Sinclair M, Gallant S, Radulescu D (2004) Real-time seismic monitoring needs of a building owner-and the solution: a cooperative effort. *Earthq Spectra* 20(2):333–346
4. Celebi M (2008) Real-time monitoring of drift for occupancy resumption. In: The 14th world conference on earthquake engineering, Beijing, China, 12–17 Oct 2008
5. Cole HA (1968) On-the-line analysis of random vibrations. AIAA paper no. 68–288
6. Chopra AK (2007) Dynamics of structures: theory and applications to earthquake engineering. Prentice-Hall, Upper Saddle River, USA
7. Clinton JF, Bradford SC, Heaton TH, Favela J (2004) The observed wandering of natural frequencies in a structure. *Bull Seismol Soc Am* 96(1):237–257
8. Derode A, Larose E, Campillo M, Fink M (2003) How to estimate the Green's function for a heterogeneous medium between two passive sensors? Application to acoustic waves. *Appl Phys Lett* 83:3054–3056. <https://doi.org/10.1063/1.1617373>
9. Erdik M (2001) Report on 1999 Kocaeli and Duzce (Turkey) earthquakes. In: Casciati F, Magonette G (eds) Proceedings of the 3rd international workshop on structural control, structural control for civil and infrastructure engineering. World Scientific
10. Holzer H (1921) Die Berechnung der Drehschwingungen. Springer, Berlin, Germany
11. Ljung L, Söderstrom T (1983) Theory and practice of recursive identification. MIT press, MA
12. Kailath T, Sayed AH, Hassibi B (2000) Linear estimation. Prentice Hall, Upper River Saddle, New Jersey
13. Karhunen KK (1947) Über lineare Methoden in der Wahrscheinlichkeitsrechnung. *Ann Acad Sci Fennicae Ser A. I. Math Phys* 1947, 37:1–79
14. Kaya Y, Safak E (2014) Real-time analysis and interpretation of continuous data from structural health monitoring (SHM) systems. *Bull Earthq Eng*. <https://doi.org/10.1007/s10518-014-9642-9>
15. Kaya Y, Kocakaptan S, Safak E (2015) Estimation of vibration time histories at the non-instrumented floors of multi-story buildings using the recorded vibrations at the instrumented floors and calibration of analytical models. *Bull Earthq Eng*. <https://doi.org/10.1007/s10518-015-9774-6>
16. Kaya Y, Dowling J (2016) Application of Timoshenko beam theory to the estimation of structural response. *Eng Struct* 123:71–76. <https://doi.org/10.1016/j.engstruct.2016.05.026>
17. Kaya Y (2016) Finite element model calibration of multi-story buildings through interferometric imaging and spectral ratio method. *Can J Civ Eng* 43:320–325. <https://doi.org/10.1139/cjce-2015-0467>
18. Kaya Y, Ventura C, Huffman S, Turek M (2017) British Columbia smart infrastructure monitoring system. *Can J Civ Eng* 44(8):579–588. <https://doi.org/10.1139/cjce-2016-0577>
19. Kohler MD, Davis PM, Safak E (2005) Earthquake and ambient vibration monitoring of the steel-frame UCLA factor building. *Earthq Spectra* 21(3):715–736
20. Lehmann EL (1959) Testing statistical hypotheses. Wiley, New York, NY

21. Lobkis OI, Weaver RL (2001) On the emergence of the Green's function in the correlations of a diffuse field. *J Acoust Soc Am* 110:3011–3017. <https://doi.org/10.1121/1.1417528>
22. Loève M (1978) Probability theory, vol II, 4th ed. Graduate texts in mathematics, vol 46, Springer
23. Moon TK, Stirling WC (2000) Mathematical methods and algorithms for signal processing. Prentice Hall, Upper River Saddle, New Jersey, USA
24. Morters, Peres (2010) Brownian motion. Cambridge University Press. ISBN: 978-0-521-76018-8
25. Overschee PV, Moor BD (2012) Subspace identification for linear systems: theory-implementation-application. Springer Science & Business Media
26. Rahmani M, Ebrahimian M, Todorovska M (2015) Wave dispersion in high-rise buildings due to soil-structure interaction. *Earthq Eng Struct Dyn* 44(2):317–323. <https://doi.org/10.1002/eqe.2454>
27. Azam SE, Chatzi E, Papadimitriou C, Smyth A (2015) Experimental validation of the Kalman-type filters for online and real-time state and input estimation. *J Vib Control* 23(15):2494–2519. <https://doi.org/10.1177/1077546315617672>
28. Safak E (1995) Detection and identification of soil-structure interaction in buildings from vibration recordings. *J Struct Eng ASCE* 121(5):899–906
29. Safak E (1997) Models and methods to characterize site amplification from a pair of records. *Earthq Spectra EERI* 13(1):97–129
30. Safak E (1998) Detection of seismic damage in multi-story buildings by using wave-propagation analysis. In: Proceedings (in CD-ROM) of the sixth U.S. national conference on earthquake engineering, Seattle, Washington, 31 May–4 June 1998. Elsevier Science Inc., New York, NY
31. Safak E (1999) Wave propagation formulation of seismic response of multistory buildings. *J Struct Eng ASCE* 125(4):426–437
32. Safak E (2004) Analysis of real-time data from instrumented structures. In: Proceedings (CD ROM), the 13th world conference on earthquake engineering, paper no. 2193, Vancouver, B.C., Canada, 1–6 Aug 2004
33. Safak E, Cakti E, Kaya Y (2010) Recent developments in Structural Health Monitoring and data analysis. In: Garevski M, Ansal A (eds) *Earthquake engineering in Europe*, Chapter 14, Springer, London, pp 331–355
34. Snieder R (2004) Extracting the Green's function from the correlation of coda waves: a derivation based on stationary phase. *Phys Rev E* 69:046610. <https://doi.org/10.1103/PhysRevE.69.046610>
35. Snieder R, Safak E (2006) Extracting the building response using seismic interferometry: theory and application to the Millikan Library in Pasadena, California. *Bull Seismol Soc Am* 96(2):586–598. <https://doi.org/10.1785/0120050109>
36. Soderstrom T (1987) Model structure determination. In: Singh M (ed) *Encyclopedia of systems and control*, Pergamon Press, Elmsford, NY
37. Thomas WT (2003) *Theory of vibration with applications*, 4th edn. Nelson Thornes Ltd., Cheltenham, UK, p 387
38. Wapenaar K, Thorbecke J, Draganov D (2004) Relations between reflection and transmission responses of three-dimensional inhomogeneous media. *Geophys J Int* 156:179–194. <https://doi.org/10.1111/j.1365-246X.2003.02152.x>
39. Zhang Y, Kurata M, Lynch JP (2017) Long-term modal analysis of wireless structural monitoring data from a suspension bridge under varying environmental and operational conditions: system design and automated modal analysis. *J Eng Mech* 143(4)

Chapter 8

Model Updating Techniques for Structures Under Seismic Excitation



Serdar Soyoz

Abstract Vibration-based system identification of structures has become a well-established way of condition assessment with the main steps of modal analyses and tracking any change in the identified modal parameters. In addition, Finite Element Model (FEM) updating is crucial especially for damage detection and reliability estimation under seismic excitation. In literature, it was shown that seismic reliability of structures with and without FEM updating turned out to be different. The main idea behind FEM updating is minimizing the difference between modal parameters obtained from FEM and system identification by changing values of parameters such as Young's modulus of materials and soils springs constants. Real-world examples of FEM updating cover bridges, tall buildings and historical structures.

Keywords System identification · FEM updating · Seismic excitation

8.1 Introduction

In Structural Health Monitoring (SHM) field, mainly four objectives; namely, determination of damage existence, location, severity and consequences exist. The first steps have been investigated extensively and related research outcome can be found in literature; however, little research exists on the estimation of damage consequences. The main reason for this gap is due to need of FEM and verification of results obtained from FEM and system identification.

FEM updating allows both validation of FEM representing intact structure without any damage and obtaining damage levels and locations during a seismic event. Validation of FEM of intact structure is important because using validated FEM, engineers can perform more reliable assessments under future earthquake scenarios. On the other hand, FEM updating under a seismic event allows determination of

S. Soyoz (✉)
Department of Civil Engineering, Bogazici University, Bebek,
34342 Istanbul, Turkey
e-mail: serdar.soyoz@boun.edu.tr

damage on the structure. After obtaining FEM of the damaged structures, seismic reliability estimation can also be performed to estimate remaining life of structures.

Although there are more detailed methods as explained in following sections, FEM updating is performed mainly by minimizing the difference between the identified modal frequencies and shapes and the corresponding ones obtained from FEM. The minimization is achieved by changing structural parameters in the model. Selection of structural parameters to be changed plays a crucial role in FEM updating. The first step in the updating procedure should be the construction of a detailed model which especially includes elements for soil domain. This can be the whole soil medium or soil springs representing the medium. There are two reasons to include soil springs in the model. The first reason is that without the soil springs; FEM updating procedure would artificially soften the structure to minimize difference between experimentally and analytically obtained modal properties. The other reason is that without soil springs, higher seismic demands would occur on structural members especially at foundation level artificially.

After obtaining a representative FEM, the main structural parameter to be changed can be considered as Young's modulus of structural material. Under ambient vibration and seismic excitation, structural stiffness would be different. This difference is important if linear models are used for seismic performance assessment because effective stiffness values obtained from system identification during seismic excitation should be used in FEM. However; current practice of seismic performance assessment is based on nonlinear analyses; therefore, updating stiffness values based on ambient vibration survey and let nonlinear modeling take care of the damage progress leads to accurate results.

The other parameter which can change modal frequencies is structural mass. It is considered to be known (or determined) exactly; therefore, it is not treated as a structural parameter to be changed in FEM updating process. However, in the seismic analysis of special structures such as offshore platforms, one should be careful with marine growth effects which changes structural mass significantly.

Therefore, Young's modulus and soil stiffness values are mostly used as parameters to be changed so that error between identified and analytical modal values is minimized. Theoretically, different combinations of structural and soil stiffness values would give the same modal frequencies; however, utilization of mode shapes in addition to modal frequencies in FEM updating process would solve this uniqueness problem. Also, one should pay attention to the ranges of soil and structure stiffness values i.e. they should be within reasonable ranges in terms of engineering judgment and existing literature.

In FEM updating, mostly modal frequencies and shapes are chosen as parameters for which error is minimized. On the other hand, identification of actual damping and assigning it in the model is important to obtain a representative FEM. Identified damping ratios based on seismic and ambient vibration measurements would be different; however, similar to discussion related with stiffness values, ambient vibration-based identified damping values would be representative in a nonlinear seismic performance assessment because hysteretic damping would already be taken care of by nonlinear modeling itself.

In the following sections; first, summary of previous studies on FEM updating is presented. Here, the focus is on FEM updating of real-world structures or large scale models in conjugation with seismic excitations. Afterwards, different FEM updating methods are discussed. Finally, case studies on FEM updating of a tall building and a stone arch bridge are presented.

8.2 Previous Studies

Most of the studies in literature demonstrate that dynamic characteristics obtained from FEM and vibration data exhibit remarkable differences. The assumptions made in development of FEM due the uncertainties in structures are one of the main reasons of these differences. By the virtue of vibration-based system identification, these differences can be minimized and more reliable seismic assessments at design stage become possible through FEM updating procedures.

There is significant amount of FEM updating studies in literature especially related with mechanical and aerospace engineering which mainly considers small scale models. Comprehensive background on FEM updating can be found in Friswell and Motershead [1] from mechanical engineering perspective. Doebeling et al. [2] and Carden and Fanning [3] summarizes vibration-based condition monitoring methodologies including FEM updating techniques.

There are studies on FEM updating such as Ghanem and Shinozuka [4] and Beck and Katafygiotis [5] which mainly establishes theoretical framework. There are other significant studies which deal only with calibration or validation of FEM using ambient vibration such as Brownjohn et al. [6], Caetano et al. [7]. Also, studies such as Boroschek and Yanez [8] validate modeling assumptions by comparing dynamic properties obtained analytically and experimentally. In addition, these procedures can also be developed for damage detection by correlating FEM's with the results of vibration measurements acquired from damaged or deteriorated structures such as Teughels and De Roeck [9] and Soyoz and Feng [10].

Following literature focuses on civil engineering related examples which especially considers realistic models and seismic inputs. Literature summary and the following sections mainly present studies on

- FEM updating with linear models for seismic performance assessment.
- FEM updating with linear models for damage detection.
- FEM updating using nonlinear models.

8.2.1 FEM Updating with Linear Models for Seismic Performance Assessment

Venture and Ding [11] presents FEM updating of a 52 story steel frame tall building using seismic measurements from Sierra Madre and Northridge earthquakes. They both compare the modal frequencies and shapes obtained from FEM and identification and also time history response of the structure and sensor readings. In the second phase of the study, they perform nonlinear time history and pushover analyses for seismic performance assessment of the building.

Skolnik et al. [12] investigated 15-story steel building which suffered damage to exterior brick veneer during 1994 Northridge event and afterwards was instrumented with permanent monitoring system by USGS. Authors identified modal properties based on ambient vibration and low level seismic response and then, they updated FEM by considering a fictitious stick element which adds flexural rigidity to the structure. Afterwards, they carried out performance assessment of the updated model under Northridge earthquake.

Casarin and Modena [13] carried out both non-destructive testing and ambient vibration survey to determine to physical and global dynamic values of Reggio Emilia Cathedral. They also calibrated FEM and estimated seismic vulnerability of the structure.

Ntotsis et al. [14] developed a methodology for FEM updating based on Bayesian framework and applied it to two existing bridges in Greece for the purpose of condition monitoring. They used ambient vibration and low-level seismic input data to verify their methodology. Structural parameters to be updated were chosen as Young's modulus and moment of inertia of the deck and pier.

Pela et al. [15] investigated the seismic performance of two masonry arch bridges, a stone masonry bridge with brick-made vaults and a stone masonry bridge with concrete made vaults. The structural capacity, which was obtained through pushover analysis, was compared with the demand of the earthquake ground motion described by an inelastic response spectrum. In the study, core tests allowed the determination of stone and mortar characteristics. Additionally, based on ambient vibration test results, Young's modulus, unit weight and Poisson's ratio of masonry materials were further tuned.

Ramos et al. [16] carried out modal and structural identification of two historical structures. They presented the relation between the identified frequency and environmental conditions such as temperature and humidity. They modeled the structure in DIANA with solid elements which have the same Young's modulus values for different portions of the tower in the initial model but different values after model updating. A minor earthquake occurred and response of the structure was collected by permanent monitoring system but no change on the identified modal frequencies was observed.

De Matteis and Mazzolani [17] presented ambient vibration test results and FEM of a masonry structure. Based on identified modal values, a refined FEM was developed. Afterwards, they carried out limit analysis to identify the most vulnerable parts

of the structure providing an estimation of its actual seismic vulnerability. Finally, a shaking-table test on a 1/5.5-scale model was carried out both to investigate the dynamic response of the structure and to validate FEM of the test model.

Soyoz et al. [18] extended their previous study on the identification of stiffness values of a bridge model and obtained failure probabilities under severe earthquake inputs. They obtained failure probabilities at different level of damage states and examined the effects of identification on reliability estimation.

Butt and Omenzetter [19] presented system identification and modeling of a three story RC building monitored for two years. Modal identification was conducted for 50 earthquake response records considering soil-structure interaction. Afterwards, FEM of the building was developed to investigate the influence of various structural and non-structural components such as cladding and partitions, as well as soil underneath the foundation and around the building, on the building dynamics. FEM was then calibrated using a sensitivity based technique by tuning the stiffness of structural concrete, soil and cladding.

Ozer and Soyoz [20] performed a study which presents FEM updating using linear systems based on error minimization. In the same study, reliability estimation at each damage level was carried out for non-updated and updated model using fragility curves. To obtain fragility curves, nonlinear analyses under input motions with increasing intensities for each damage state were performed.

Karmakar et al. [21] studied seismic vulnerability of Vincent Thomas suspension bridge. FEM of the bridge was developed and verified by identified modal values obtained from ambient vibration and a moderate earthquake response data. In addition, FEM was further validated by simulating the dynamic response of the Northridge earthquake and comparing with the recorded response. Finally, nonlinear time history analyses were performed and the ductility demands of critical sections were presented in terms of fragility curves.

Costa et al. [22] carried out modal updating of three masonry arch bridges based on the modal parameters obtained from operational modal analysis. The material properties of the initial FEM were obtained from material tests and results of previous similar studies. Even though significant amount of material tests was conducted, there were still differences between the analytical and identified modal properties. Therefore, at the final step, each FEM was tuned by adjusting the material properties and soil conditions based on the modal values obtained from dynamic tests.

Sevim et al. [23] investigated near and far fault ground motion effects on a masonry arch bridge in terms of displacement and stress values. Dynamic properties of the bridge were inferred from ambient vibration test by using Frequency Domain Decomposition method. Researchers preferred linear FEM of the structure due to high uncertainties associated with the nonlinear modeling of masonry. FEM was calibrated according to identified modal parameters by changing only boundary conditions.

8.2.2 *FEM Updating with Linear Models for Damage Detection*

Yu et al. [24] determine an updated FEM of a reinforced concrete building which was damaged during 1994 Northridge earthquake. They used frequency response functions and modal frequencies for FEM updating. The building was excited using a linear inertial shaker located at the roof. Flexural stiffness values of structural members, modal damping ratios, and translational and rotational mass values were chosen as the updating parameters. They validated the updated FEM by comparing the predicted and measured dynamic responses under sine-sweep vibration test. These results indicate that the updated model replicates the dynamic behaviour of the building reasonably well. Furthermore, the updated stiffness factors correlate well with the observed building damage patterns.

Gentile and Saisi [25] identified modal values of a masonry bell tower with the presence of major cracks. They carried out ambient vibration test on a 74 m high masonry tower and assigned different material properties for damaged and undamaged zones. Calibration of FEM was achieved by changing the material properties of the tower and they show that material properties of damaged zones after FEM updating process are significantly lower than other parts of the tower as expected.

Soyoz and Feng [26] developed an extended Kalman filtering (EKF) method and applied it to instantaneously identify elemental stiffness values of a structure during damaging seismic events based on vibration measurement. Identification of the structural elemental stiffness enables location as well as quantification of structural damage. The elemental stiffness values of the structure were instantaneously identified in real time during the damaging earthquake excitations using the EKF method. The identified stiffness degradations and their locations agreed well with the structural damage observed by visual inspection and strain measurements. More importantly, the seismic response accelerations analytically simulated using the instantaneous stiffness values thus identified agreed well with the measured accelerations, demonstrating the accuracy of the identified stiffness.

Weng et al. [27] presented a methodology for FEM updating of structural parameters including connection rigidities using non-linear least-square technique. The proposed method was verified through a shaking table test of a 1/4-scale six-story steel frame structure by loosening the connection bolts for damage simulations and a two-story RC frame subject to different levels of ground excitations back to back.

Moaveni et al. [28] tested a full-scale seven-story reinforced concrete building section on the UCSD-NEES shake table such that the building experienced progressive damage. Ambient vibration tests and low-amplitude white noise base excitations were applied to the building at each level of damage to identify modal parameters of the building. Afterwards, sensitivity-based FEM updating strategy was used to detect, localize and quantify damage. Damage in the building was identified based on the change in Young's modulus. Identified damage correlated well with the observed damage at the bottom two stories of the building. It was noted that the assumption

of linear systems used for identification purposes was progressively violated with increasing level of excitation.

Ji et al. [29] presented full-scale shaking table test study which considers realistic seismic damage on a model of a high-rise steel building. Damage to concrete slabs, beam-column connections, and nonstructural walls were generated by three levels of ground motion. Dynamic properties of the model were obtained using white noise response and change in these properties before and after damage were estimated. A numerical study was also conducted to validate the vibration-based identification studies.

Binda et al. [30] identified the modal values of Spanish Fortress after L'Aquila Earthquake using ambient vibration data and indicated that the structure had the unitary vibration mode in spite of high level of damage probably due to provisional emergency steel cables.

Cimellaro et al. [31] identified modal values of a tower and a damaged palace after L'Aquila Earthquake using different output identification methods such as frequency domain decomposition, random decrement, eigensystem realization algorithm. They also updated FEM by changing material properties.

Moaveni et al. [32] identified progressive damage, using an equivalent linear finite-element model updating strategy, on a two-thirds-scale, 3-story, 2-bay, infilled RC frame was tested on the UCSD-NEES shake table. The building experienced progressive damage and ambient vibration tests and low-amplitude white noise base excitations were applied to the building at each level of damage to identify modal parameters of the building. A sensitivity-based FEM updating strategy was employed to detect, locate, and quantify damage (as a loss of effective local stiffness) based on the changes in the identified effective modal parameters. The results indicated that proposed method could reliably identify the location and severity of damage observed in the tests.

Belleri et al. [33] investigated the damage assessment of a three-story half-scale precast concrete building tested on the UCSD-NEES shake table. Modal parameters of the structure at different damage states have been identified from white-noise and earthquake response with the assumption that the structure was in linear range. The changes in the identified modal parameters were correlated with the observed damage.

Bassoli et al. [34] presented FEM updating procedure for a masonry tower that suffered seismic damage. Mechanical properties of the tower in its current damaged state were investigated. Different material properties have been assigned corresponding to the regions where damaged masonry existed.

Ubertini et al. [35] presented the change in identified modal frequencies of a historical bell tower located in Italy due to 2016 Central Italy earthquakes. They predicted and compared the nonlinear response of the structure using a calibrated FEM and observed that decrease in identified modal frequencies agreed well with the ones obtained from non-linear FEM.

8.2.3 *FEM Updating with Non-linear Models*

Asgarieh et al. [36] proposed a methodology to update hysteretic behavior of structural elements by minimizing an error function which was defined as the difference between experimentally identified time-varying modal parameters and those obtained from FEM at selected time instances. The proposed methodology was applied on a three-story RC frame with masonry infill tested on a shaking table with increasing intensities of input motions. Asgarieh et al. [37] applied the same methodology to a different test model, a seven story shear wall building. In addition to proposed method, they applied unscented Kalman filter approach and validated that both approach predicted the nonlinear behavior satisfactorily.

Chatzis et al. [38] developed a methodology to transform time domain identification results into physical parameters and compared them with the ones obtained from Unscented Kalman Filter. They also verified their method on the small-scale shaking table model where input was different earthquake motions and damage was simulated by removing structural elements.

8.3 Methods

FEM updating can be performed based on pre and post event measurements and a linear system or seismic measurement and a non-linear system. In this chapter, only FEM updating methods using linear methods are covered.

The first method is based on error minimization and second method is sensitivity-based updating. These two methods are principally the same; mainly, the first one searches the minimum error for a given set of parameters whereas the second approach updates the search domain itself. The first method is more robust and more applicable to real-world structures if the boundaries of the parameters to be changed for FEM updating purposes are estimated confidently.

Although FEM updating has the potential of improving knowledge in structural parameters, problems which may be encountered during updating process should be tackled with care. For instance, local minima, difficulties in mode matching, low sensitivity of global modes to local structural features and high uncertainty on identified parameters are some of the possible problems in FEM updating.

8.3.1 *Error Minimization-Based FEM Updating*

In this method, an error function as given in Eq. (8.1), compares similarity between modal frequencies and mode shapes obtained from identification and FEM.

$$E(\alpha) = \sum \left(k_i \cdot \left[\frac{(f_i^* - f_i)}{f_i^*} \right]^2 + h_i \cdot [1 - MAC_i]^2 \right) \quad (8.1)$$

α is stiffness correction coefficient,

i is mode number,

k_i is the weighting coefficient for i th modal frequency,

h_i is the weighing coefficient for i th modal assurance criteria,

f_i^* is the measured modal frequency of i th mode,

f_i is the simulated modal frequency of i th mode,

MAC_i is the modal assurance criteria for i th mode shape.

Weighing coefficients can be determined by considering contribution (e.g. mass participation ratio) of different modes to dynamic behavior of the structure. For the purpose of FEM updating, a Matlab code, which automatically creates FEM by changing the values of the chosen structural parameters within pre-determined limits, can be utilized. This code will obtain the modal parameters of different non-updated models and obtain the error based on Eq. (8.1), and the FEM resulting in minimum error will be chosen as the updated model.

8.3.2 Sensitivity-Based FEM Updating

Sensitivity-based methods update structural parameters by minimizing an error function expressing the difference between FEM predicted and experimentally identified dynamic properties such as natural frequencies and mode shapes. Optimum solutions of the problem are reached through sensitivity-based constrained optimization algorithms. Main steps of this method are given in Eqs. (8.2–8.6).

$$z_{ID} = (\omega_{ID}^1, \phi_{ID}^1, \omega_{ID}^2, \phi_{ID}^2, \dots, \omega_{ID}^r, \phi_{ID}^r) \quad (8.2)$$

$$z_{FEM} = (\omega_{FEM}^1, \phi_{FEM}^1, \omega_{FEM}^2, \phi_{FEM}^2, \dots, \omega_{FEM}^r, \phi_{FEM}^r) \quad (8.3)$$

$$\delta z = S \delta \theta \quad (8.4)$$

$$\delta z = z_{ID} - z_{FEM} \quad (8.5)$$

$$\delta \theta = \theta_a - \theta \quad (8.6)$$

where

S is the sensitivity matrix

$\delta \theta$ is the perturbation in structural parameters

δz is the error in the measured output

θ_a is the actual structural parameters that reproduce z_{ID} .

Sensitivity matrix is the first derivative of the eigenvalues and mode shapes with respect to the parameters evaluated at the current parameter estimate. Calculation of sensitivity matrix can be formulated as follows:

$$\left[K - w_j^2 M \right] \phi_j = 0 \Rightarrow \frac{\partial}{\partial \theta} \frac{\partial K}{\partial \theta} \phi_j + \frac{\partial \phi_j}{\partial \theta} K = \frac{\partial w_j^2}{\partial \theta} M \phi_j + \frac{\partial M}{\partial \theta} w_j^2 \phi_j + \frac{\partial \phi_j}{\partial \theta} w_j^2 M \quad (8.7)$$

$$\Rightarrow \left[K - w_j^2 M \right] \frac{\partial \phi_j}{\partial \theta} = - \left[\frac{\partial K}{\partial \theta} - w_j^2 \frac{\partial M}{\partial \theta} - M \frac{\partial w_j^2}{\partial \theta} \right] \phi_j \quad (8.8)$$

Premultiplying Eq. (8.7) with θ_j^T , we obtain

$$\frac{\partial w_j^2}{\partial \theta} = \phi_j^T \left[\frac{\partial K}{\partial \theta} - w_j^2 \frac{\partial M}{\partial \theta} \right] \phi_j \quad (8.9)$$

Equations (8.8) and (8.9) give derivatives of frequency and mode shape with respect to structural parameters.

The ultimate objective in sensitivity based FEM updating is to minimize $J = \varepsilon^T \varepsilon$.

$$\varepsilon = \delta z - S \delta \theta \quad (8.10)$$

$$\Rightarrow J = (\delta z - S \delta \theta)^T (\delta z - S \delta \theta) \quad (8.11)$$

$$= \delta z^T \delta z - 2 \delta \theta^T S^T \delta z + \delta \theta^T S^T S \delta \theta \quad (8.12)$$

$$\frac{\partial J}{\partial \delta \theta} = 0 \text{ gives } \delta \theta = [S^T S]^{-1} S^T \delta z \quad (8.13)$$

$$\theta_{j+1} = \theta_j + \delta \theta \quad (8.14)$$

8.4 Case Studies

In this section, two case studies are presented. The first one is related with a tall building for which modal identification, FEM updating and seismic analysis under predicted earthquake motions are discussed. In the second case study, similar framework is presented for a stone arch bridge.

For these two examples, FEM updating is performed based on ambient vibration measurements. The motivation of such a study is to estimate seismic performance of structures based on updated FEM.

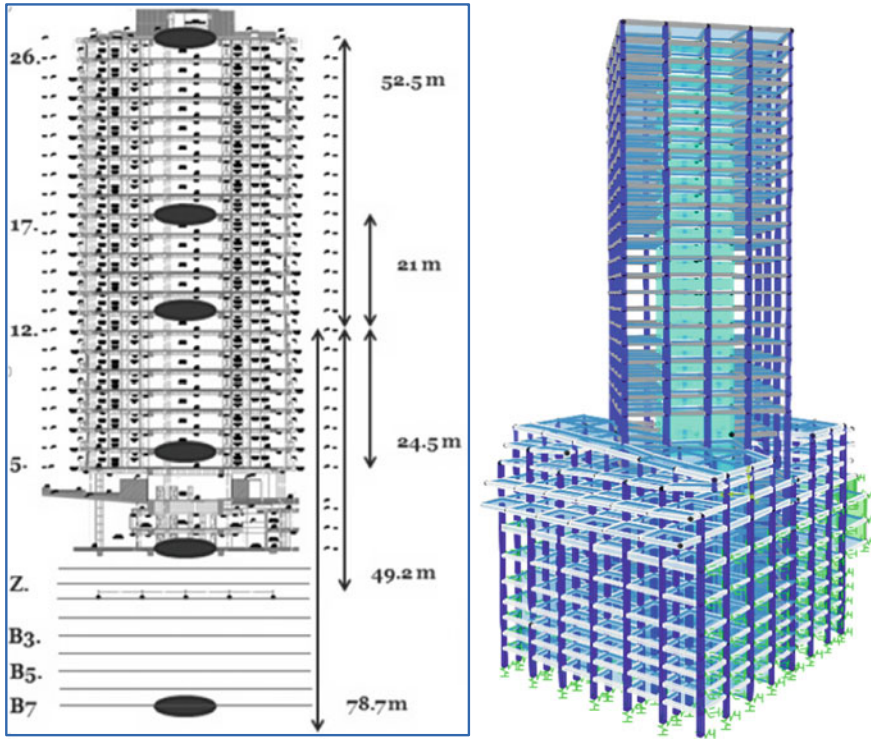


Fig. 8.1 Sensor layout and FEM of the building

Table 8.1 Identified and analytical frequencies

Mode	Identification (Hz)	Updated FEM (Hz)	Non-updated FEM (Hz)
1	0.59	0.59	0.50
2	2.15	2.03	1.77
3	3.18	3.18	2.62

8.4.1 Case1-Tall Building

Kaynardag and Soyoz [39] demonstrated the importance of FEM updating based on system identification on the seismic performance of a tall building. For this purpose, a twenty-six story, core-wall tall building in Istanbul was instrumented with thirteen accelerometers (Fig. 8.1). Modal values were identified using EFDD algorithm. FEM of the building was updated based on the identified modal shapes and frequencies by changing structural parameters such as Young’s modulus of the building, soil spring values and interaction with the adjacent buildings. Table 8.1 and Fig. 8.2 compare the results obtained from identification and updated and non-updated FEMs.

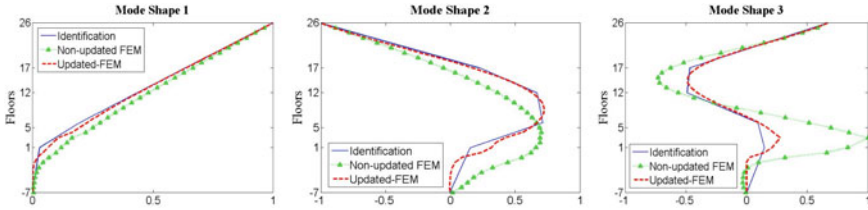


Fig. 8.2 Identified and analytical mode shapes

Table 8.2 Change in structural parameters

Model definition	Fundamental frequency (Hz)
Initial model	0.50
Initial model + Interaction with adjacent building	0.56
Updated FEM	0.59

FEM of the building was created in SAP2000 software platform based on the design drawings and site investigations. The shear walls, columns and beams were modeled as beam elements and the slabs were explicitly modeled.

Decoupling of modes in linear analyses demonstrate that the first three modes produce significant portion of seismic demand on the structure. Therefore, only the first three modes are considered in the updating process and weighing coefficients are determined as 0.60, 0.25 and 0.15 respectively.

Table 8.2 presents the change in fundamental frequency of the building due to calibration of the model. Here, the important point is that before starting updating process a very detailed FEM was established. For example, interaction with adjacent structures were taken into account which was not a common practice both in engineering and research; however, it shows that it has a significant effect on fundamental frequency and exclusion of such an effect would lead to wrong updating results. After completion of FEM updating, Young’s modulus, horizontal spring and vertical spring values were changed to 1.15, 3 and 5 times of their initial values respectively.

Afterwards, NLTH analyses were performed with the updated and the non-updated FEM to observe the influence of the identified modal frequencies and shapes. In order to observe the performance of the building in a possible earthquake caused by the North Anatolian Fault, probability density functions in terms of inter-story drift ratios were established (Fig. 8.3). And by setting a threshold value failure probabilities for the updated and non-updated models were obtained. This kind of probabilistic assessment of seismic performance of tall building with the integration of vibration-based identified modal values comprises a unique approach. In addition, the investigation of the results of this study reveals the importance of the detailed modeling and selecting an appropriate viscous damping ratio for tall buildings.

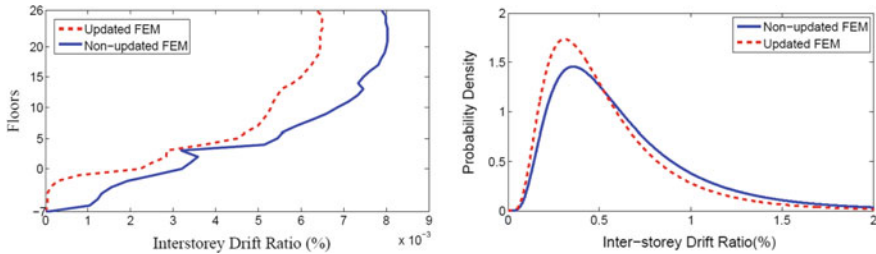


Fig. 8.3 Drift ratios for updated and non-updated models

8.4.2 Case 2-Stone Arch Bridge

Aytulun et al. [40] presented system identification and seismic performance assessment of a masonry arch bridge located on the railway route which is on the northeastern part of Turkey (Fig. 8.4). 41 masonry arch bridges were registered as historical and needed to be preserved on the route. On the other hand, the railway line passes through North Anatolian Fault, resulting in high seismic demand on bridges. Therefore, seismic assessment of the bridges was carried out by finite element analysis; however, masonry structures such as stone arch bridges have significant uncertainties in terms of material properties, boundary conditions and modeling assumptions. As a result, it becomes almost unavoidable to perform dynamic identification tests to validate FEM.

Modal properties of twelve bridges such as modal frequencies, mode shapes and modal damping ratios were identified through vibration measurements collected under ambient conditions, impact loading and train passage. Figure 8.5 shows one representative bridge and its sensor layout. Based on identified modal parameters, FEM of the bridges were updated to obtain actual values of Young's modulus of masonry and soil. FEM updating procedure was performed by minimizing the difference between experimental and analytical modal properties.

In the process of FEM updating procedure, initial FEM of the bridge was established using ANSYS software. Studies in literature verified that changes in frictional coefficient did not affect modal parameters of the stone arch bridge. Therefore, modal calibration was conducted by changing only Young's modulus of masonry and soil. Table 8.3 presents identified, non-updated, and updated modal frequencies of the bridge. Elasticity modulus of masonry was changed from 7.80 to 14.05 GPa and Elasticity modulus of soil was changed from 20 to 30 GPa (soil formation was identified as rock formation in soil investigation reports)

Afterwards, seismic performance assessment of a representative bridge was carried out using ANSYS software. In the analyses, macro modeling approach was followed to develop homogenized behavior of stone and mortar. Seismic performance of the bridge was obtained by nonlinear time history analyses. It was also observed that tensile strength capacity was reached on spandrel walls which may result in a probable local failure (Fig. 8.6).

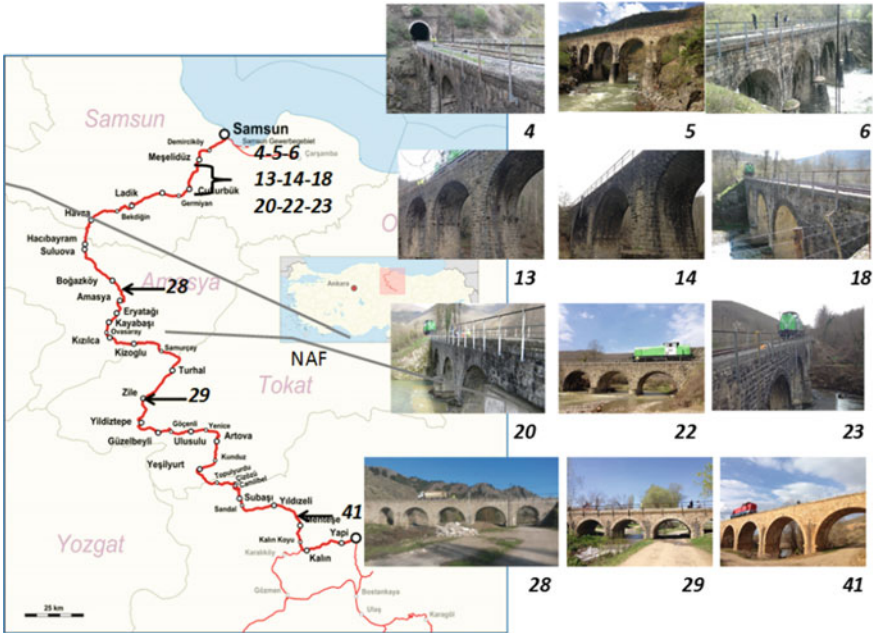


Fig. 8.4 Bridges on the railway

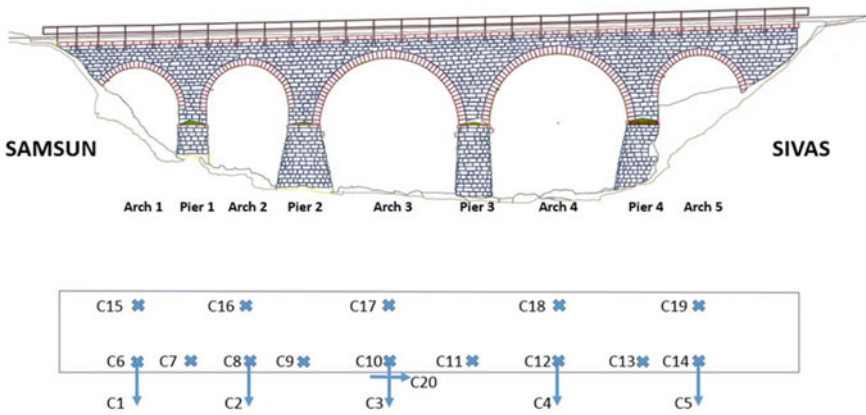


Fig. 8.5 Sensor layout on the bridge

Table 8.3 Identified and analytical frequencies

Mode	Identification (Hz)	Updated FEM (Hz)	Non-updated FEM (Hz)
1. Trans	8.31	7.17	5.37
2. Trans	10.84	10.83	8.11
3. Trans	13.18	15.65	11.72
1. Vert	20.02	22.90	17.15
2. Vert	24.32	25.05	18.77

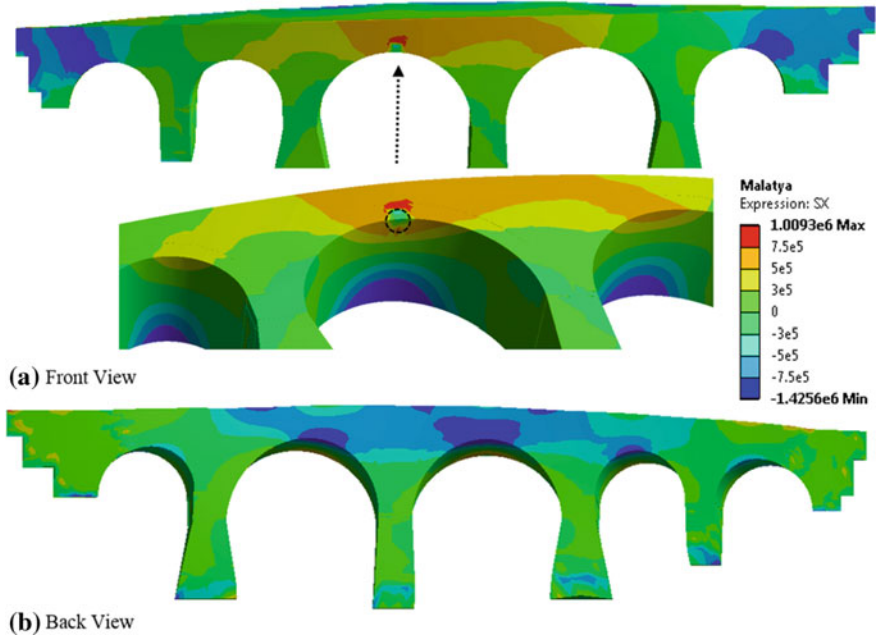


Fig. 8.6 Stress distribution (Pa) in longitudinal direction

8.5 Conclusions

In this chapter, summary of FEM updating of civil structures under seismic excitation is given. FEM updating can be used both for damage detection or validation of intact model to perform more reliable seismic performance assessment. It was shown that estimated reliability of structures for updated and non-updated cases would be different.

FEM updating is performed mainly by minimizing the difference between the identified modal frequencies and shapes and the corresponding ones obtained from FEM. The minimization is achieved by changing structural parameters in the model. The main difference between civil engineering and other engineering field in terms of FEM updating is that civil structures have significantly more degrees-of-freedom

and relation with soil medium which imposes an important boundary condition; therefore, FEM updating methodologies should be chosen properly.

Along this line, detailed localization and detection of damage can be achieved only for some types of structures such as reinforced concrete highway bridges which have less number of degrees-of-freedom. On the other hand, FEM updating of structures such as tall buildings may only deal with the validation of FEM in terms of modal values. Even this level of validation will lead to obtaining a more representative FEM and therefore more reliable seismic performance assessment would be possible.

Acknowledgements Case studies presented in the chapters were possible with contributions of Mr. Korkut Kaynardag and Mr. Emre Aytulun.

References

1. Friswell MI, Mottershead JE (1995) Finite element model updating in structural dynamics. Kluwer Academic Publishers, Boston
2. Doebling SW, Farrar CR, Prime MB, Shevitz DW (1996) Damage identification and health monitoring of structural and mechanical systems from changes in their vibration characteristics: a literature review. Los Alamos National Laboratory, LA-13070-MS
3. Carden EP, Fanning P (2004) Vibration-based condition monitoring: a review. *Struct Health Monit* 355–377
4. Ghanem R, Shinozuka M (1995) Structural system identification. *J Eng Mech* 121(2):255–273
5. Beck JL, Katafygiotis LS (1998) Updating models and their uncertainties. *J Eng Mech* 124(4):455–467
6. Brownjohn JMW, Pan TC, Deng XY (2000) Correlating dynamic characteristics from field measurements and numerical analysis of a high-rise building. *Earthq Eng Struct Dyn* 29:523–543
7. Caetano E, Cunha A, Gattulli V, Lepidi M (2008) Cable-deck dynamic interactions at the International Gadiana Bridge: on-site measurements and finite element modeling. *Struct Control Health Monit* 15:237–264
8. Boroschek LR, Yanez FV (2000) Experimental verification of basic analytical assumptions used in the analysis of structural wall buildings. *Eng Struct* 22:657–669
9. Teughels A, De Roeck G (2004) Structural damage identification of the highway bridge Z24 by FE model updating. *J Sound Vib* 278:589–610
10. Soyoz S, Feng MQ (2009) Long-term monitoring and identification of bridge structural parameters. *Comput-Aid Civ Infrastruct Eng* 24:82–92
11. Ventura CE, Ding Y (2000) Linear and nonlinear seismic response of a 52-storey steel frame building. *Struct Des Tall Build* 9:25–45
12. Skolnik D, Lei Y, Yu E, Wallace JW (2006) Identification, model updating, and response prediction of an instrumented 15-story steel-frame building. *Earthq Spectra* 22(3):781–802
13. Casarin F, Modena C (2008) Seismic assessment of complex historical buildings: application to Reggio Emilia Cathedral, Italy. *Int J Archit Heritage* 2:304–327
14. Ntotsis E, Karakostas C, Lekidis V, Panetsos P, Nikolaou I, Papadimitriou C, Salonikos T (2009) Structural identification of Egnatia Odos bridges based on ambient and earthquake induced vibrations. *Bull Earthq Eng* 7:485–501
15. Pela L, Aprile A, Benedett A (2009) Seismic assessment of masonry arch bridges. *Eng Struct* 31:1777–1788
16. Ramos LF, Marques L, Lourenco PB, De Roeck G, Campos-Costa A, Roque J (2010) Monitoring historical masonry structures with operational modal analysis: two case studies. *Mech Syst Signal Process* 24:1291–1305

17. De Matteis G, Mazzolani FM (2010) The Fossanova Church: seismic vulnerability assessment by numeric and physical testing. *Int J Archit Heritage* 4:222–245
18. Soyoz S, Feng MQ, Shinozuka M (2010) Remaining capacity estimation based on structural identification results. *J Eng Mech* 136(1):100–106
19. Butt F, Omenzetter P (2014) Seismic response trends evaluation and finite element model calibration of an instrumented RC building considering soil–structure interaction and non-structural components. *Eng Struct* 65:111–123
20. Ozer E, Soyoz S (2015) Vibration-based damage detection and seismic performance assessment of bridges. *Earthq Spectra* 31(1):137–157
21. Karmakar D, Ray Chaudhuri S, Shinozuka M (2015) Finite element model development, validation and probabilistic seismic performance evaluation of Vincent Thomas suspension bridge. *Struct Infrastruct Eng* 11(2):223–237
22. Costa C, Arede A, Costa A, Caetano E, Cunha A, Magalhaes F (2015) Updating numerical models of masonry arch bridges by operational modal analysis. *Int J Archit Heritage* 9:760–774
23. Sevim B, Atamturktur S, Altunışık AC, Bayraktar A (2016) Ambient testing and seismic behavior of historical arch bridges under near and far fault ground motions. *Bull Earthq Eng* 14:241–259
24. Yu E, Taciroglu E, Wallace JW (2007) Parameter identification of framed structures using an improved finite element model-updating method. *Earthquake Eng Struct Dyn* 36:619–660
25. Gentile C, Saisi A (2007) Ambient vibration testing of historic masonry towers for structural identification and damage assessment. *Constr Build Mater* 21:1311–1321
26. Soyoz S, Feng MQ (2008) Instantaneous damage detection of bridge structures and experimental verification. *Struct Control Health Monit* 15(7):958–973
27. Weng JH, Loh CH, Yang JN (2009) Experimental study of damage detection by data-driven subspace identification and finite-element model updating. *J Struct Eng* 135(12):1533–1544
28. Moaveni B, He X, Conte JP, Restrepo JI (2010) Damage identification study of a seven-story full-scale building slice tested on the UCSD-NEES shake table. *J Struct Eng* 32:347–356
29. Ji X, Fenves GL, Kajiwara K, Nakashima M (2011) Seismic damage detection of a full-scale shaking table test structure. *J Struct Eng* 137:14–21
30. Binda L, Modena C, Casarin F, Lorenzoni F, Cantini L, Munda S (2011) Emergency actions and investigations on cultural heritage after the L’Aquila earthquake: the case of the Spanish Fortress. *Bull Earthq Eng* 9:105–138
31. Cimellaro GP, Pianta S, De Stefano A (2012) Output modal identification of ancient L’Aquila city hall and civic tower. *J Struct Eng ASCE* 138:481–491
32. Moaveni B, Stavridis A, Lombaert G, Conte JP, Shing PB (2013) Finite element model updating for assessment of progressive damage in a 3-story infilled RC frame. *J Struct Eng* 139(10):1665–1674
33. Belleri A, Moaveni B, Restrepo JI (2014) Damage assessment through structural identification of a three-story large-scale precast concrete structure. *Earthq Eng Struct Dyn* 43:61–76
34. Bassoli E, Vincenzi L, D’Altri AM, Miranda S, Forghieri M, Castellazzi G (2017) Ambient vibration-based finite element model updating of an earthquake-damaged masonry tower. *Struct Control Health Monit* [online]
35. Ubertini F, Cavalagli N, Kita A, Comanducci G (2018) Assessment of a monumental masonry bell-tower after 2016 Central Italy seismic sequence by long-term SHM. *Bull Earthq Eng* 16:775–801
36. Asgariéh E, Moaveni B, Stavridis A (2014) Nonlinear finite element model updating of an infilled frame based on identified time-varying modal parameters. *J Sound Vib* 333:6057–6073
37. Asgariéh E, Moaveni B, Barbosa AR, Chatzi E (2017) Nonlinear model calibration of a shear wall building using time and frequency data features. *Mech Syst Signal Process* 85:236–251

38. Chatzis MN, Chatzi EN, Smyth AW (2015) An experimental validation of time domain system identification methods with fusion of heterogeneous data. *Earthq Eng Struct Dyn* 44:523–547
39. Kaynardag K, Soyoz S (2017) Effect of identification on seismic performance assessment of a tall building. *Bull Earthq Eng* 15:3227–3243
40. Aytulun E, Soyoz S, Karcioğlu E (2018) Comparison of nonlinear time history and pushover analyses for the assessment of stone arch bridges. In: 16th European conference on earthquake engineering, Thessaloniki, Greece, 17–21 June

Chapter 9

Damage Localization Through Vibration Based S²HM: A Survey



Maria Pina Limongelli

Abstract Several methods proposed in literature for the localization of stiffness losses rely on the detection of irregularities in the deflected shape of the structure. This requires accurate description of the deflected shape achievable through a high spatial resolution of sensors, high quality or measures and accounting for the approximations introduced by signal processing. In the first part of this paper a survey of vibration-based damage localization algorithms based on the detection of (changes of) irregularities in the deflected structural shape is reported. Most of these methods rely on damage parameters defined in terms of the local variations of curvature due to the direct relationship of this parameter with the variations of stiffness. Due to some drawbacks related to the estimation of curvature from noisy recorded responses, other methods have been proposed to detect local variations of the deformed shape without directly computing the curvature. Also, many of the methods proposed in literature have been validated only on numerical models, due to the scarce availability of experimental data recorded on damaged structures. Recently data recorded on benchmark structures have become available giving the opportunity to verify the capability of these methods for damage localization in real-world conditions. In the last part of the paper, a method for damage localization based on the detection of localized changes in the structural deformed shapes, the Interpolation Method, is applied to two benchmark structures. The first is the UCLA Factor Building whose response to several non-destructive earthquakes has been recorded by a dense network of sensors. The second is the 7th storey portion of building tested to collapse, using base inputs of increasing severities, on the USDS shaking table.

Keywords Vibration-based · Damage · Localization · Shape irregularity · Interpolation method

M. P. Limongelli (✉)
Department of Architecture, Built Environment and Construction
Engineering (ABC), Politecnico di Milano, Piazza Leonardo da
Vinci, 32, Milan, Italy
e-mail: mariagiuseppina.limongelli@polimi.it

© Springer Nature Switzerland AG 2019
M. P. Limongelli and M. Çelebi (eds.), *Seismic Structural Health Monitoring*, Springer
Tracts in Civil Engineering, https://doi.org/10.1007/978-3-030-13976-6_9

217

9.1 Introduction

Vibration-based damage identification methods allow assessing structural damage states mainly induced by stiffness losses. One of the major advantages of these methods is the possibility to detect damage at a global level, using sensors not necessarily deployed close to the—unknown—location of damage. Different levels of refinement in the identification of damage are possible depending on the amount of information provided by the recorded responses. Detection, that is the identification of the existence of damage, might be possible based on a single sensor able to capture meaningful characteristics of the structural response, e.g. the natural modes more sensitive to damage. Localization requires a higher number of sensors deployed at several locations along the structure. The assessment of damage, that is the estimation of its severity, usually requires a finite element model that allows to map the responses recorded on the structure to different damage types and scenarios through the physical model of the real structure.

This paper is limited to response-based methods that do not make use of a physical (e.g. Finite Element) model of the structure. Model-based methods have usually a considerable computational cost, due to the need to update the model parameters through iterative optimization processes. This makes them less suitable for real-time structure damage identification. It must be said that when damage assessment is concerned, response-based methods fail to provide both the type and the severity of damage, whereby model-based methods become a useful option.

Several vibration-based methods that rely only on recorded responses have been proposed in literature [1–15]. This paper will focus on methods that perform localization of damage through the detection of irregularities in the deflected shape of the structure. Most of these methods exploit the relationship between a local loss of stiffness and the corresponding local variation of curvature. The damage feature is therefore defined in terms of this latter parameter.

One of the drawbacks related to the choice of curvature as damage feature consists in the fact that the double differentiation needed for its computation is highly sensitive to noise in recorded responses. Furthermore, a high spatial resolution, meaning a high number of sensors, and high-quality measures, that usually require more expensive sensors, are needed to obtain accurate estimates of the deformed shapes from which curvatures are computed. Due to this, in literature have been proposed methods to identify variations of curvature without explicitly computing curvatures. Some of them will be described in the next sections.

One of the main issues in the research field related to damage identification, even more challenging when damage induced by earthquakes is involved, is the validation on real structures of the algorithms proposed by researchers. The number of monitored structures in seismic prone areas is still quite low and usually, due to economic constraints, a small number of sensors is deployed on them. Beside this, many of the instrumented structures have never experienced damage during an earthquake and in some cases, even if data exist, they are not freely available for research purposes. Due to all these facts, the algorithms proposed in literature for

damage identification are often verified using data simulated using number models or obtained through shaking table tests of scaled laboratory specimens.

In the last years, several vibration tests have been performed on full scale structures artificially damaged for research purposes. Data have been recorded using quite dense networks of sensors and made available to the scientific community. The last section of this paper reports the application of an algorithm for damage localization, the Interpolation Method, to two benchmark structures. The first is the UCLA Factor Building (see reference USGS [16]) whose response to several earthquakes of low to medium intensity has been recorded by a dense network of sensors permanently installed. The second case study is the experimental model of a portion of a 7-storey building tested on shaking table at UCSD, through the George E. Brown Jr. Network for Earthquake Engineering Simulation (NEES) program [17, 18].

9.2 Damage Features Based on the Detection of Shape Irregularity

9.2.1 *Modal and Operational Shapes*

Modal and operational shapes inherently describe the geometry of a structural system, a localized reduction of stiffness produces a corresponding increase of curvature that alters the deformed structural shape. This allows to localize damage by processing the geometric changes of this shape. The irregularity induced by a stiffness loss affects the global deformed shape therefore, considering its decomposition in the frequency domain, not only the modal shapes are affected by damage but, in principle, all the operational shapes. An ‘operational deflected shape’ is the deflection shape of a structure subjected to harmonic excitation. If the frequency of the excitation is close to a modal one, the ODS is dominated by the corresponding mode shape; for other values of the frequency of excitation, the ODS derives from the combination of several modes. The modal or operational shapes most useful for damage identification are usually those corresponding to the highest frequency shifts induced by damage. Therefore, low or high modes can be both equally useful to damage identification purposes depending on the location of damage and on the sensitivity of modes to damage at that location. This means that all the available modes or of operational shapes should be included in the damage localization procedure in order to have accurate results.

Several damage localization algorithms based on the detection of shape irregularities have been proposed in literature [3, 4, 5, 8, 10, 11, 12, 13, 15]. Most of them rely on modal shapes, others on operational deflected shapes retrieved from Frequency Response Functions [19–21]. Both families of methods present advantages and drawbacks. The estimation of modal shapes is today quite reliable thanks to the developments of the experimental and operational modal analysis techniques. The computation of operational shapes from Frequency Response Functions (Fig. 9.1) is

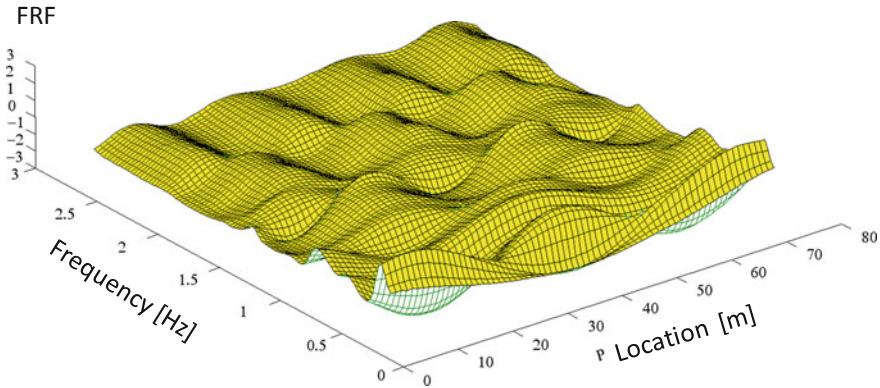


Fig. 9.1 Operational shapes

more straightforward therefore more feasible to online algorithms for real-time identification of damage.

At resonance the effect of noise is usually lower with respect to other frequency values therefore the modal shapes are estimated with higher accuracy with respect to the generic ODS. On the other side, the number of modal shapes that can be identified in the frequency range excited by the input (forced or ambient vibrations) is always much lower than the number of operational shapes in the same frequency range. Therefore, in a certain sense, the amount of information contained in the complete set of ODS in a certain frequency range, is higher with respect to the one contained in the modal shapes. The *quality* of these information depends on the uncertainties related to the retrieval of the ODS. These can be due to e.g. noise in recorded sensors, non-linear behavior of the structure, round off in signal processing. Large set of data, obtained measuring the response of the structure to vibrations for long periods of time, can help reducing the effect of uncertainties but this is possible only if permanent monitoring systems are installed on the structure. If the acquisition of data is limited to short periods of time—as is the case for forced vibration tests—a high quality of recorded data should be sought in order to accurately identify the location of damage. In the latter case modal shapes can be more useful with respect to ODS. In reference [21] a comparison between results obtained ODS or modal shapes is presented.

In the past, permanent monitoring systems were much less diffused with respect to short term monitoring and this is probably one of the reasons why most of the damage localization algorithms have been formulated in terms of modal shapes. Nowadays, with large amount of data available, the possibility to use operational shapes is becoming more and more appealing due to the lower interaction they require with an operator. This last feature makes them more feasible for the implementation in autonomous SHM systems.

The components of the deflected shapes are measured at a discrete number of points corresponding to the sensor's locations. The higher is the number of sensors

and the more uniform their distribution, the higher is the spatial resolution of the deformed shapes, hence the accuracy of damage localization.

In the following section an overview of some methods for damage localization based on the detection of irregularities in the deflected shapes is reported. All methods will be generically described with reference to a generic ‘deflected shape’ meaning that they can be applied considering both modal and operational shapes.

9.2.2 Shape Variation Due to a Loss of Stiffness

The effect on the deformed shape of a localized stiffness loss can be schematically explained with reference the simple cantilever beam represented in Fig. 9.2. Two configurations are represented: the reference and the damaged ones. Damage is intended as a reduction of the sectional bending stiffness in a small portion of the beam. In the circle is reported the enlarged detail of the damaged portion.

As clearly shown by the comparison inside the circle, a sharp variation of the deflected shape occurs at the location of damage whilst, at all the other sections, the two deflected shapes can be almost perfectly superimposed with a simple vertical shift.

Therefore a feature able to describe the shape of the beam and to detect the local difference between two shapes is needed to identify the correct location of damage. It has been shown that for ‘beam-like’ structures like buildings or bridges a very good approximation of the deformed shape can be obtained through cubic spline functions [5, 22]. Comparison of shapes is a very important topic widely studied in several different fields. One technique, commonly used for example in the field of Computer vision, is to define the shape of a curve through its curvature. A major reason for this is that small variations of shapes are hardly detectable through the comparison of the shapes themselves [23–25] while they sensibly affect curvatures. Furthermore,

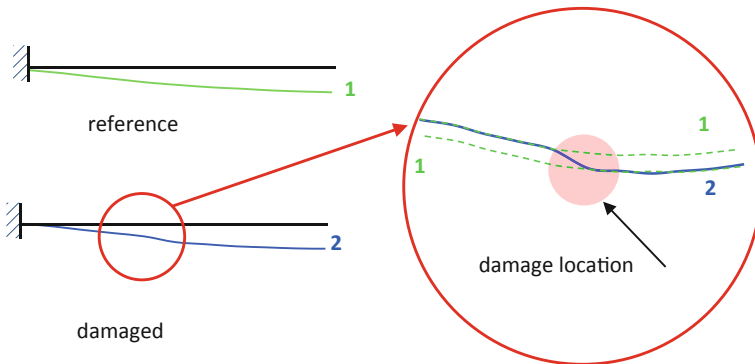


Fig. 9.2 Shape variation due to stiffness loss

curvatures are invariant to rigid transformations that are independent on the spatial translation or rotation of the curve.

Finally, for the detection of stiffness losses, curvature is the most straightforward feature being directly linked to the bending stiffness.

For a simple Eulero-Bernoulli beam, the curvature and the flexural stiffness are related by the expression:

$$v'' = \frac{M}{EI} \quad (9.1)$$

where v'' , M and EI are respectively the curvature, the bending moment and the bending stiffness of the same section. Damage entailing a reduction of the bending stiffness at one location of the beam determines an increase in the magnitude of curvature in the same section. Therefore, changes in the curvature can be used to detect and locate damage.

A totally different and quite challenging point is the accurate curvature estimation from the available data. The relationship between the curvature $1/r$ and the second derivative of a function $v(x)$ is the following:

$$\frac{1}{r} = \frac{|v''(x)|}{|1 + v'(x)^2|^{\frac{3}{2}}} \quad (9.2)$$

If the function $v(x)$ represents a deflected shape (as is the case herein), $v'(x)$ is first derivative. For small values of the rotations, the square of the rotation can be neglected with respect to unity and it can be assumed that the curvature $1/r$ is equal to the modulus of the second derivative of the function $v''(x)$. A discontinuity in the curvature ($1/r$) in this case has a direct effect on the second derivative of the function.

In real applications, data from accelerometers or displacement transducers provide few components of the deflected shape of the structure that is a discrete representation of a continuous function. Therefore, the computation of curvature requires the use of a numerical algorithm, such as for example the central difference approximation to the second derivative. The curvature v''_i at the i -th location is given as a function of the values of the function at the neighboring locations:

$$v''_i = \frac{v_{i+1} - 2v_i + v_{i-1}}{h^2} \quad (9.3)$$

where v_i is the component of the deflected shape at location i and h is the distance between the locations where structural responses are measured, that is the distance between the sensors.

Two practical drawbacks affect the computation of the curvature for discrete functions. The first is related to the spatial resolution of the available deflected shapes. This depends on the location and number of sensors that is usually limited due to economic constraints therefore is related to the 'quantity' of available data. Some authors [11] proposed to tackle the problem by interpolating the deflected shape

using a smooth function such as a cubic spline. The interpolation allows to refine the location of damage in the identified region but does not introduce new ‘information’ therefore is not able to reduce the uncertainty about the correct damaged portion of the structure. The second drawback is related to the ‘*quality*’ of available data: estimators of curvature, like the one reported in Eq. (9.3), are very sensitive to the noise introduced by the acquisition process [3]. Noise is further amplified by the double differentiation which, behaving as high-pass filters in the Fourier-domain, can mask the damage hampering its correct localization. A common approach to tackle this problem is to smooth the data—prior or after to curvature calculation—but this might as well remove the effect of damage, thus rendering the data less informative for damage identification purposes. A more effective approach is to apply methods that detect variations in the curvature profile without a direct estimation of this parameter. A number of these will be described in one of the following sections.

9.3 Damage Localization

This section reports a short, not exhaustive, description of a number of methods proposed in literature to localize stiffness losses through the detection of variations of local curvature. Many of them require the direct estimation of this parameter whereas other methods use feature that do not require the direct computation of curvature to detect its changes.

All the methods can be applied to a generic ‘shape’, be it a modal or an operational one. However, each of the method was originally proposed for one of the two families, usually for modal shapes. In the following reference will be made to the original version.

9.3.1 *Methods Based on Curvature*

Pandey et al. [8] showed that the absolute change in *modal curvature* can be an efficient indicator of stiffness losses. The damage index is defined at each location i as the sum of the curvature variation between a reference (U) and possibly damaged (D) configuration, over all the identified modal shapes:

$$\Delta c_i = \sum_{k=1}^{n_{modes}} \left| \phi_{k,i,D}'' - \phi_{k,i,U}'' \right| \quad (9.4)$$

Stubbs et al. [11] proposed to use the variation of the *modal strain energy* stored in each portion (sub-element) of a beam as a damage feature. The basic idea is that damage does not change the fractional modal strain energy $F_{k,i}$ that is the ratio between the strain energy stored in the i -th element and total strain energy for the

k -th mode. Based on this assumption, the ratio between the bending stiffness in the damaged and undamaged states can be written as a function of the modal curvature and, summing over all the modes, the following expression is obtained for the damage index:

$$\beta_i = \frac{\sum_{k=1}^{n_{modes}} (EI)_{i,k}^U}{\sum_{k=1}^{n_{modes}} (EI)_{i,k}^D} = \sum_{k=1}^{n_{modes}} \left[\frac{(\phi''_{k,i})_D^2}{\sum_{i=1}^L (\phi''_{k,i})_D^2} \right] / \sum_{k=1}^{n_{modes}} \left[\frac{(\phi''_{k,i})_U^2}{\sum_{i=1}^L (\phi''_{k,i})_U^2} \right] \quad (9.5)$$

β_i is defined as the sum, over all identified modes, of the elements bending stiffness in the damaged and in the reference configurations. The damage index β_i assumes values higher than 1 at a damaged location.

Another index was proposed by Zhang and Aktan in 1998 [14] based on the curvature of the **Uniform Load Surface** (ULS). The ULS is the deflection vector due to a unit load applied at each of the p DOF (uniform load). The deflection f_{ij} at location i due to a unit load at location j is approximated by the sum of the contributions of the identified n_{modes} , the deflection f_i due to a uniform unit load distribution is the sum of the contributions due to the single unit loads.

$$f_{i,j} \cong \sum_{k=1}^{n_{modes}} \frac{\phi_i^k \phi_j^k}{\omega_k^2} \quad f_i \cong \sum_{k=1}^{n_{modes}} \frac{\phi_i^k \sum_{j=1}^p \phi_j^k}{\omega_k^2} \quad (9.6)$$

The flexibility is sensitive to the number of modes, to the load location and to the boundary conditions. The curvature of the deflection f_i can be obtained through a central difference approximation as in Eq. (9.3) and the damage index at each location is defined as the variation of curvature of the deflection between the damaged and the reference states:

$$f_i'' = f_{i,D}'' - f_{i,U}'' \quad (9.7)$$

Due to the low values of flexibility close to supports, this index may not allow a correct localization when damage is located at these regions due the masking effect of numerical errors [26].

All the previous methods require the computation of the variation of curvature from signals recorded in the reference and in the—possibly—damaged state.

The knowledge of the reference condition apparently is not needed by the **Gapped smoothing method** proposed by Ratcliffe [10]. A smooth cubic polynomial function is used to interpolate the curvature of the modal shape and the damage index at the i -th location is calculated as:

$$\delta_i = \left[(p_0 + p_1x_i + p_2x_i^2 + p_3x_i^3) - C_i \right]^2 \quad (9.8)$$

C_i is the curvature computed at location i from recorded responses and the coefficients p_0 ; p_1 ; p_2 , and p_3 are determined interpolating the values of curvature C_{i-2}

C_{i-1} , C_{i+1} , C_{i+2} and skipping C_i . The locations corresponding to the maximum values of the damage index are assumed as the damaged ones. The idea underlying the method is that the error between the curvature calculated from data and the value interpolated through a smooth (polynomial) function, is higher at locations with an irregularity. Therefore, the damaged location is identified as the one corresponding to the maximum value of the interpolation error. Even if the computation of the curvature in the reference condition is not explicitly required by this method, the underlying assumption is that a discontinuity in the curvature profile is necessarily related to damage. This is not necessarily true since a discontinuity in the curvature profile may be due to an intrinsic irregular distribution of stiffness: due for example to a change of the transversal section along the axis of a beam, or to the local change of the vertical bearing elements along the height of a building. This may lead to false alarms in the identification of damage locations. Damage is a change with respect to a reference conditions therefore its identification requires the comparison of the current state with a reference one. The assumption that an irregularity in the deformed profile corresponds to a damage, implies that in the reference state the deformed shape was regular, meaning that in the original configuration there was a regular distribution of stiffness. If the stiffness distribution is already irregular at the ‘birth’ of the structure or generally in the reference state, the simple detection of an irregularity in the deflected shapes does not necessarily correspond to a damage. In this cases Eq. (9.8) might give false indications of damaged locations.

Beside this last drawback, inherent in methods that do not compare the inspection to the reference value of the damage feature, all the damage identification algorithms described so far, need the direct identification of the curvature values and this may introduce large uncertainties in case of noisy signals. To overcome this problem, methods have been developed to detect curvature changes without directly estimating curvature. Some of them are described in the next section.

9.3.2 *Methods Based on the Indirect Detection of Curvature Changes*

Several proposals have been formulated for robust estimators of curvature from noisy signals. Most of them have been applied in the field of image processing (e.g. [27]) but a final solution of the problem is still a research topic.

A completely different approach consist in the use of methods able to detect changes in curvature without actually computing the curvature itself.

Methods based on the use of *wavelet functions* treat the deflected shape as a signal in the spatial domain, and use the wavelet transform to detect the signal irregularity caused by damage. The use of these functions for damage detection purposes has been investigated by several authors. In the paper by Fan and Qiao [28] a comprehensive survey is given. Herein reference is made to the work of Gentile and Messina [3] focused on the detection of cracks simulated through a local reduction of the elastic

modulus inducing a local loss of stiffness. In this paper an interesting and clear physical interpretation of the damage localization capability of wavelets is proposed. It can be proved that these functions, if properly chosen, are a good approximation of the derivatives of the deflected shape.

Specifically, if a wavelet function has m vanishing moments, the following equation holds:

$$\lim_{s \rightarrow 0} \frac{Y(x; s)}{s^{m+1/2}} = K \frac{d^m y(x)}{dx^m} \quad (9.9)$$

where $y(x)$ is the recorded signal, $Y(x; s)$ is the signal transformed using the wavelet and s is a real positive number called ‘dilation parameter’ of the wavelet function. A specific derivative can be approached through a wavelet transform, by choosing appropriately the number of vanishing moments of a Gaussian wavelet [3]. As Eq. (9.9) shows, the signal transformed using the wavelet is proportional to the m -th derivative of the function: for $m = 2$ the transformed signal is proportional to the curvature. Therefore a discontinuity in the proper wavelet transform corresponds to a discontinuity in the corresponding derivative that can be used to identify the location of damage. In their paper Gentile and Messina apply this technique to the detection of open cracks that are modelled through a local reduction of the elastic modulus.

A second approach is based on the use of *smooth functions* to interpolate the deflected shapes. The Interpolation method [20, 21, 29] is based on the use of a cubic spline to interpolate the deflected shapes retrieved from recorded responses. Interpolation is performed at the i -th location considering all the measured components of the deflected shapes $v_1, v_2, \dots, v_{i-1}, v_{i+1}, \dots, v_n$ except v_i . The interpolation error is defined as follows:

$$E_i = \left| (c_{0,i} + c_{1,i}(x_i - x_{i-1}) + c_{2,i}(x_i - x_{i-1})^2 + c_{3,i}(x_i - x_{i-1})^3) - v_i \right| = \left| \hat{v}_i - v_i \right| \quad (9.10)$$

The coefficients $c_{0,i}$, $c_{1,i}$, $c_{2,i}$ and $c_{3,i}$ of the cubic spline function are computed imposing interpolation and continuity conditions at all the instrumented locations. More details on the interpolation procedure can be found in reference [5]. Due to the so-called ‘Gibbs phenomenon for splines [20], a sharp increase of the interpolation error occurs at the locations with a curvature discontinuities and this can be used to detect the damaged location as the one where the highest value of the interpolation error is found’.

The curvature discontinuity affects both modal and operational shapes. In order to enhance the value of the interpolation error at the damaged location with respect to all the others, the sum of the interpolation error computed for all the n_{shapes} shapes—modal or operational—is considered:

$$E_i = \sqrt{\sum_{k=1}^{n_{shapes}} E_i^2} = \sqrt{\sum_{k=1}^{n_{shapes}} |\hat{v}_{k,i} - v_{k,i}|^2} \quad (9.11)$$

Changes of interpolation error between two different states (reference and potentially damaged) highlight the onset of a curvature discontinuity therefore the following difference δE_i is assumed as the damage feature at location i :

$$\delta E_i = E_i^D - E_i^U \tag{9.12}$$

This definition of the damage feature allows to overcome the shortcoming intrinsic in the Gapped smoothing method and related to the assumption of a regular distribution of stiffness in the reference configuration.

A further improvement of the Interpolation Method, currently under investigation, is related to its possible use for the estimation of damage severity beyond for damage localization. A linear relationship exists and has been proven [20] between the value of the interpolation error at the damaged location and the curvature discontinuity. Currently the application of this relationship to identify the severity of real damage scenarios is being studied.

9.4 Damage Indices and Thresholds

In real world conditions, due to several sources of variability influencing recorded responses the damage features described in the previous section can exhibit changes even if no damage occurs or, viceversa, they can exhibit no change when damage exists. This leads to false or missing detection of damage. This problem could be tackled through statistical analyses if the distributions of the damage feature are known. This is possible if large set of data are available to identify these distributions.

Assuming this is the case, in Fig. 9.3 the distribution of the damage feature in the reference configuration $f_{I,ref}$ at one instrumented location is compared to the distribution in the inspection (damaged) state $f_{I,isp}$. In the figure it is assumed that the damage feature increases with damage (e.g. the modal period increases with the loss of stiffness). The comparison of the two distributions allows to investigate the onset of damage.

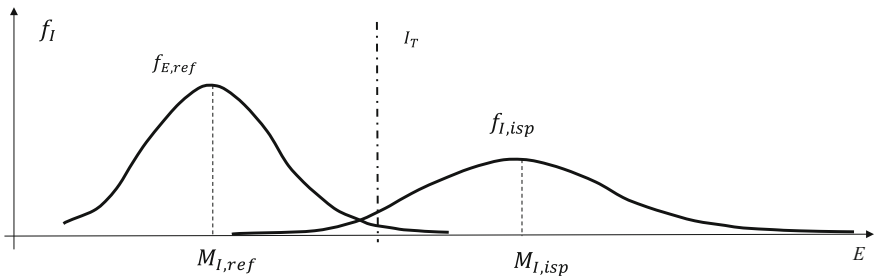


Fig. 9.3 Distributions in the undamaged ($f_{I,ref}$) and in the damaged ($f_{I,isp}$) states

If one, or both distributions cannot be determined reference can be done to the distribution of values of the damage feature computed at all the instrumented locations [29–31]. The values of the sample mean and standard deviation are obtained from the available set of damage features at all the instrumented location. In order to differentiate the intact from the damage states a threshold value has to be defined. This can be done in terms of an ‘*accepted probability of false alarms*’ in the undamaged configuration. Assuming a normal distribution the threshold can be computed as [29]:

$$I_T = M_I + \nu \cdot \sigma_I \quad (9.13)$$

where M_I and σ_I are respectively the sample mean and the sample standard deviation of the sample population of the damage index in the reference state. The value ν is defined in the standard normal distribution as the α -percentile that defines the accepted probability of false alarm.

The classification of a certain location i as “damaged” is carried out basing on the comparison of the current value of the damage feature I_i with the threshold at the same location $I_{i,T}$.

if $I_i - I_{i,T} > 0$ damage at location i
 if $I_i - I_{i,T} < 0$ no damage at location i .

9.5 Case Studies

In the following the application of the Interpolation Method, recalled in Sect. 9.3.2 to the case of two multistory building under seismic excitation, is reported.

In the first case, the UCLA Factor Building, responses recorded during or after a severe earthquake, able to damage the building, are not available. For this reason, the responses recorded by the monitoring system have been used to calibrate a finite element model and damage has been simulated reducing the stiffness of several elements of the model. In the second case, for the 7th storey building responses have been recorded in several damage states of increasing severity ad used to verify the capability of the Interpolation Method to correctly localize damage.

9.6 The UCLA Factor Building

The UCLA Factor Building (see Fig. 9.4) is a 17-storey moment-resisting steel frame structure consisting of two stories below grade and 15 above grade. The building houses laboratories, faculty offices, administrative offices, the School of Nursing, School of Medicine, auditoriums, and classrooms. The building is permanently instrumented with an embedded 72-channel accelerometer array recording

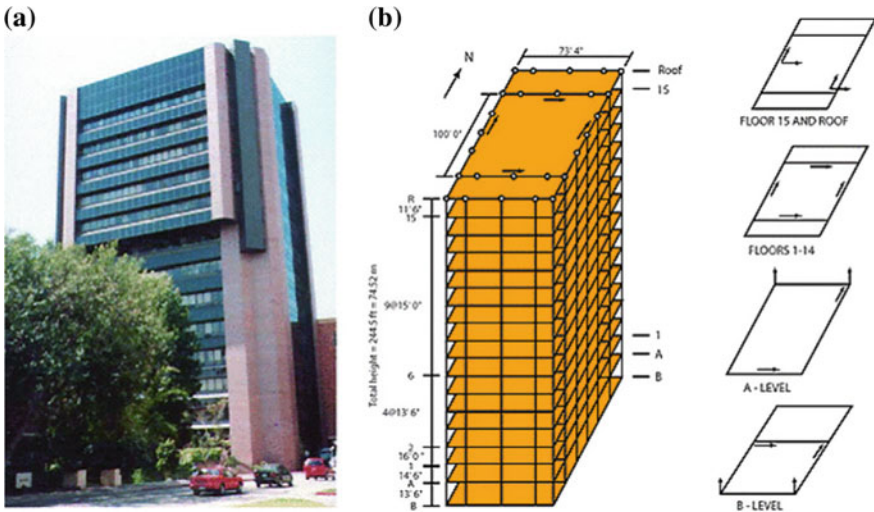


Fig. 9.4 The Factor Building. **a** East face; **b** sensors location (from Ref. USGS [16])

both ambient vibrations of the building and motions from local earthquakes. The sensors array is composed by four horizontal channels per floor: two in North-South direction and two in East-West direction. The two floors below grade are also equipped with two vertical channels. The array continuously records ambient vibrations as well as motions from local earthquakes. More details on the Factor Building and on the recording network can be found on reference (USGS [16]).

In reference [32] the Interpolation Method has been applied to the Factor Building. Specifically, data recorded on the building during several seismic events in 2004 have been used to retrieve the probability distributions of the Interpolation Error at all the stories of the building. Results show that a lognormal distribution fits correctly the statistical variation of the damage feature, the Interpolation Error, in the undamaged configuration. At the time being, only responses recorded during events that did not severely damage the Factor Building are available. In order to test the performance of the IM, a numerical model of the building has been used to simulate several damage scenarios. A reduction of the storey stiffness was simulated in the numerical model by removing a number of columns at one or more storeys. A selection of results is reported in Fig. 9.5 for damage scenarios corresponding to 2 damage columns at 2 or 4 storeys in the transversal (x) or in the longitudinal (y) direction of the building. The name of the scenario describes the location of the damaged columns: for example $Dx_{04_12_2c}$ means 2 damaged columns (2c) along the x (transversal) direction, located at storeys 4 and 12. In the figures the blue bars indicates the correct location of damage. The black curve joins the values of the Interpolation Damage Index (IDI) at all the storeys. A value equal to $v = 2$ corresponding to probability of false alarms of about 2% has been assumed in all these cases. For all scenarios the IDI attains the highest values at the damaged locations, allowing a correct localization.

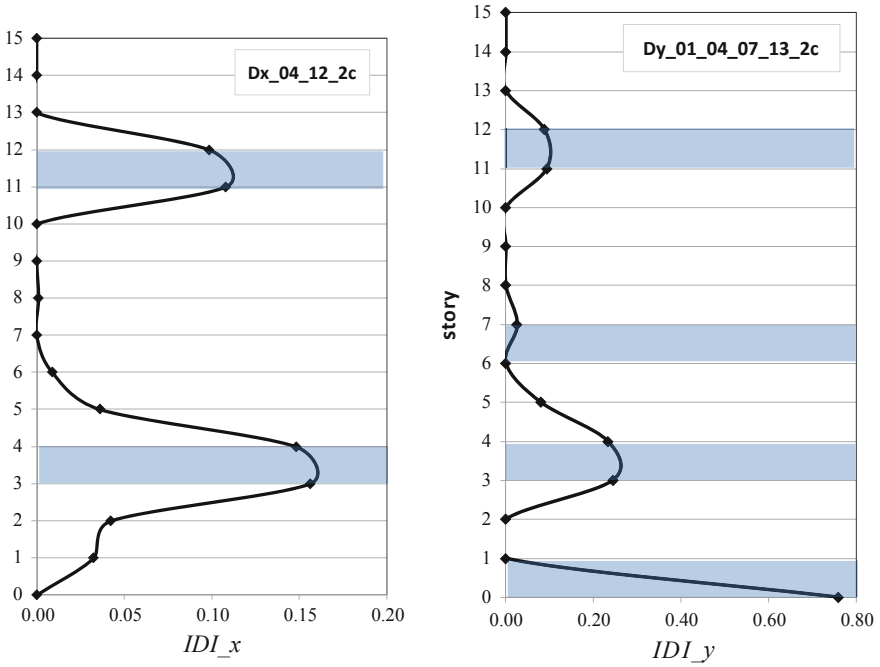
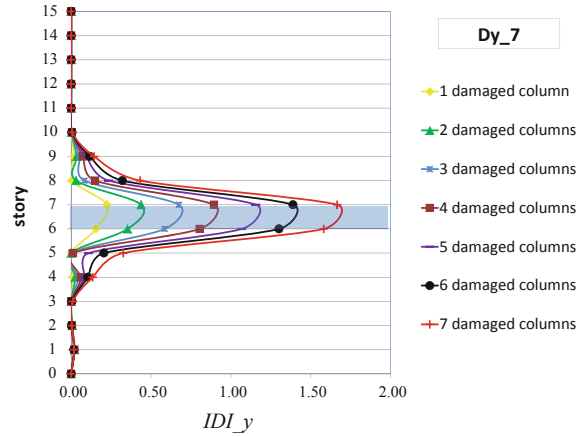


Fig. 9.5 Results for two and four damaged columns per story along respectively the transversal (x) and the longitudinal (y) direction

Fig. 9.6 Increase of damage index with the severity of damage (from Limongelli [32])



In Fig. 9.6 the values of the IDI at all the stories of the building for different severities of damage are reported. The value of the damage index increases with damage showing the direct correlation, mentioned in Sect. 9.3.2 with the loss of stiffness.

9.7 The 7th Storey Portion of Building at UCSD

This structure, that represents a slice of a full-scale reinforced concrete shear wall building, is 20 m in height and 275 tons in weight. It consists of a main shear wall (web wall), a back wall perpendicular to the main wall (flange wall) for transversal stability, a concrete slab at each floor level, an auxiliary post-tensioned column to provide torsional stability, and four gravity columns to transfer the weight of the slabs to the shake table. Figure 9.7 shows the test building on the shake table (NEES).

The tests on the specimen were performed at the UCSD-NEES shake table located at the Englekirk Structural Engineering Center, 15 km east of the main campus of the University of California–San Diego (UCSD). The building was progressively damaged through several historical seismic motions (M_W from 6.6 to 6.7) reproduced on the shake-table. Before and between the seismic shake-table tests, the building was subjected to long-duration (8 min) ambient vibration tests and to long-duration (3 min) low-amplitude white-noise (WN) excitation tests. The test structure was instrumented with a dense array of sensors including accelerometers, strain gauges, potentiometers, and linear variable displacement transducers (LVDTs). Herein data from 8 longitudinal acceleration channels (located at each floor level) were used to apply the Interpolation Evolution Method [33]. This is an extended version of the IM that can be applied using the nonlinear responses recorded during a damaging

Fig. 9.7 Test structure (NEES)



event. The IEM is based on the idea of repeating the application of the IM at each time instant during the strong motion therefore retrieving the location of the damage at each time instant. At the end of the motion, the histogram of the damage locations throughout the entire shaking is obtained and the damage location can be selected, for example, as that corresponding to the highest frequency of detection.

9.7.1 Damage Scenarios

As described in Panagiotou et al. [34] and Moaveni et al. [17, 18], after the 4 seismic tests, damage was concentrated at the first and second storeys. Flexural cracks occurred at the base and at the first story. During the last test EQ4 a large split crack appeared and extended up to one-third of the height of the second level. Figure 9.8 shows the structural damage at the bottom of the structure and at the first storey after at the end of the tests.

Results obtained from the application of the IEM to the 7th storey specimen are shown in Fig. 9.9 for the different excitations. In all cases, the correct location of damage at storeys 1 and 2 is found except for the case of EQ3 where damage is found between storeys 2 and 3. This circumstance is due to the interpolation process performed for the computation of the damage feature that, as discussed in reference [29], may somehow ‘spread’ the effect of damage to the locations nearby the damaged one.

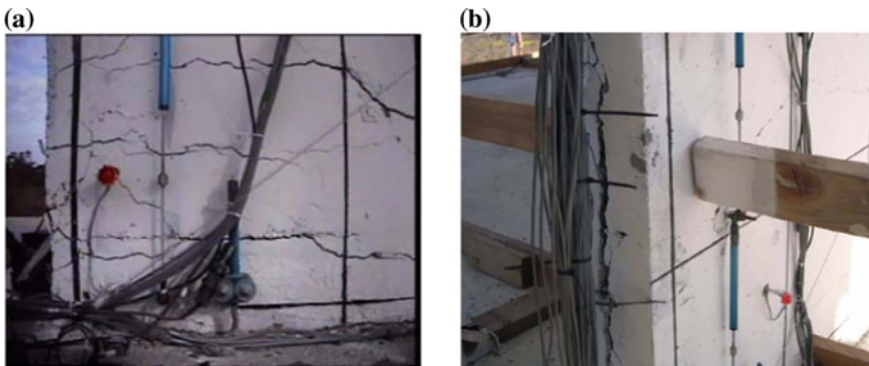


Fig. 9.8 **a** Extent of flexure-shear cracking in the first storey at the bottom corner of the first story of the web wall during EQ4; **b** splitting crack due to lap-splice failure at the bottom of the second story of the web wall on the west side after EQ4 [34]

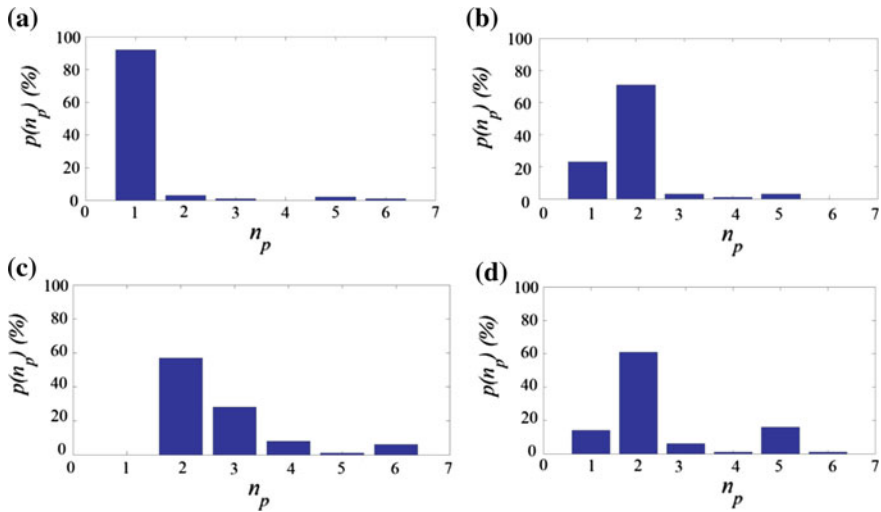


Fig. 9.9 7th story shear wall building at UCSD. Histograms of the identified damaged storey: **a** EQ1, **b** EQ2, **c** EQ3, **d** EQ4

9.8 Conclusions

In this paper, response-based methods for damage localization in structures under seismic excitation are presented. Damage is intended as a loss of stiffness. Thanks to the low computational efforts they require, these methods can be more feasible for online real-time damage identification purposes with respect to model-based approaches. A large majority of these method are based on the detection of localized variations of curvature performed though a direct computation of this parameter or using techniques based on interpolation or on wavelet functions to identify losses of regularity in the deformed shape. A short survey of these methods is reported in the paper.

In order to tackle the problem of false or missing alarms—caused by the several sources of uncertainties that affect the identification of damage features from responses to vibrations (sensor’s noise, signal processing assumptions and truncation, low spatial resolution)—the distribution of the damage feature should be retrieved and a threshold values should be fixed to distinguish damaged from undamaged states.

Response-based methods are usually not able to identify the type and severity of damage. This usually requires the use of a physical model. However, several damage features obtained though response-based approaches exhibit a strong correlation with the severity of damage and this appears promising for the definition of a damage feature requiring a low computational effort—so that it can be efficiently used for on-line damage identification—but enabling a more refined description of damage through the estimation of its severity beyond its existence and location.

Acknowledgements The authors would like to thank the USGS ANSS program and the NSF Center for Embedded Networked Sensing at UCLA for the availability of data recorded on the Factor Building and the NEES for the availability of the 7th storey building data. This work was partially funded by the Italian Civil Protection Department within project DPC-RELUIS 2017–2018.

References

1. Corrado N, Gherlone M, Surace C, Hensman J, Durrande N (2015) Damage localisation in delaminated composite plates using a Gaussian process approach. *Meccanica* 50(10):2537–2546
2. Dutta A, Talukdar S (2004) Damage detection in bridges using accurate modal parameters. *Finite Elem Anal Des* 40(3):287–304
3. Gentile A, Messina A (2003) On the continuous wavelet transforms applied to discrete vibrational data for detecting open cracks in damaged beams. *Int J Solid Struct* 40:295–315
4. Ho YK, Ewins DJ (2000) On the structural damage identification with mode shapes. In: International conference on system identification and structural health monitoring, pp 677–686
5. Limongelli MP (2003) Optimal location of sensors for reconstruction of seismic responses through spline function interpolation. *Earthq Eng Struct Dyn* 32:1055–1074
6. Lu Q, Ren G, Zhao Y (2002) Multiple damage location with flexibility curvature and relative frequency change for beam structures. *J Sound Vib* 253(5):1101–1114
7. Pai PF, Jin S (2000) Locating structural damage by detecting boundary effects. *J Sound Vib* 231(4):1079–1110
8. Pandey AK, Biswas M, Samman MM (1991) Damage detection from changes in curvature mode shapes. *J Sound Vib* 145(2):321–332
9. Parloo E, Guillaume P, Van Overmeire M (2003) Damage assessment using mode shape sensitivities. *Mech Syst Signal Process* 17(3):499–518
10. Ratcliffe CP (1997) Damage detection using a modified Laplacian operator on mode shape data. *J Sound Vib* 204(3):505–517
11. Stubbs N, Kim JT, Topole K (1992) An efficient and robust algorithm for damage localization in offshore structures. In: 10th ASCE structures conference. American Society of Civil Engineers, New York, NY, pp 543–546
12. Surace C, Saxena R, Gherlone M, Darwich H (2014) Damage localisation in plate like-structures using the two-dimensional polynomial annihilation edge detection method. *J Sound Vib* 333(2014):5412–5426
13. Wahab MA, De Roeck G (1999) Damage detection in bridges using modal curvatures: application to a real damage scenario. *J Sound Vib* 226(2):217–235
14. Zhang Z, Aktan AE (1998) Application of modal flexibility and its derivatives in structural identification. *J Res Nondestr Eval* 10(1):43–61. <https://doi.org/10.1080/09349849809409622>
15. Zhang Y, Lie ST, Xiang Z (2013) Damage detection method based on operating deflection shape curvature extracted from dynamic response of a passing vehicle. *Mech Syst Signal Process* 35(2013):238–254
16. USGS (2013) Earthquake hazard program. UCLA Factor Seismic Array. Available from: <http://factor.gps.caltech.edu/node/61>. Last visited Oct 2013
17. Moaveni B, He X, Conte JP, Restrepo JI (2010) Damage identification study of a seven-story full-scale building slice tested on the UCSD-NEES shake table. *Struct Saf* 32(5):347–356
18. Moaveni B, He X, Conte JP, Restrepo JI, Panagiotou M (2011) System identification study of a seven-story full-scale building slice tested on the UCSD-NEES shake table. *J Struct Eng ASCE* 137(6). NEES Network for Earthquake Engineering Simulation Project. <http://nees.ucsd.edu/7story.html>

19. Domaneschi M, Limongelli MP, Martinelli L (2012) Damage detection in a suspension bridge model using the interpolation damage detection method. In: Biondini F, Frangopol DM (eds) *Bridge maintenance, safety, management, resilience and sustainability*. Taylor & Francis Group, London, ISBN 978-0-415-62124-3
20. Limongelli MP (2019) The surface interpolation method for damage localization in plates. *Mech Syst Signal Process* 118(2019):171–194. <https://doi.org/10.1016/j.ymssp.2018.08.032>
21. Limongelli MP (2016) Damage localization using the modal interpolation method. In: 8th European workshop on structural health monitoring, EWSHM 2016, 3, pp 1648–1657
22. Limongelli MP (2005) Performance evaluation of instrumented buildings. *ISET J Earthq Technol* 42:47–62
23. Huth O, Feltrin G, Maeck J, Kilic N, Motavalli M (2005) Damage identification using modal data: experiences on a prestressed concrete bridge. *J Struct Eng ASCE* 131:1898–1910
24. Khan AZ, Stanbridge AB, Ewins DJ (1999) Detecting damage in vibrating structures with a scanning LDV. *Opt Lasers Eng* 32:583–592
25. Salawu OS, Williams C (1994) Damage location using vibration mode shapes. In: *International modal analysis conference*, pp 933–939
26. Yan AM, Golinval JC (2006) Null subspace-based damage detection of structures using vibration measurements. *Mech Syst Signal Process* 20(3):611–626
27. Page DL, Sun Y, Koschan AF, Paik J, Abidi MA (2002) Normal vector voting: crease detection and curvature estimation on large, noisy meshes. *Graph Mod* 64(3–4):199–229. ISSN 1524-0703. <https://doi.org/10.1006/gmod.2002.0574>
28. Fan W, Qiao P (2011) Vibration-based damage identification methods: a review and comparative study. *Struct Heal Monit* 10(1):83–111
29. Limongelli MP (2010) Frequency response function interpolation for damage detection under changing environment. *Mech Syst Signal Process*. <https://doi.org/10.1016/j.ymssp.2010.03.004>
30. Domaneschi M, Limongelli MP, Martinelli L (2013) Multi-site damage localization in a suspension bridge via aftershock monitoring. *Int J Earthq Eng* 3:56–72
31. Stubbs N, Kim JT (1995) Model-uncertainty impact and damage-detection accuracy in plate girders. *J Struct Eng* 121(10). [https://doi.org/10.1061/\(ASCE\)0733-9445\(1995\)121:10\(1409\)](https://doi.org/10.1061/(ASCE)0733-9445(1995)121:10(1409))
32. Limongelli MP (2014) Seismic health monitoring of an instrumented multistorey building using the interpolation method. *Earthq Eng Struct Dyn* 43:1581–1602. <https://doi.org/10.1002/eqe.2411>
33. Iacovino C, Ditommaso R, Limongelli MP, Ponzo FC (2018) The interpolation evolution method for damage localization in structures under seismic excitation. *Earthq Eng Struct Dyn* 47(10):2117–2136. <https://doi.org/10.1002/eqe.3062>
34. Panagiotou M, Restrepo J, Conte J (2011) Shake-table test of a full-scale 7-story building slice. Phase I: rectangular wall. *J Struct Eng* 691–704. [https://doi.org/10.1061/\(asce\)st.1943-541x.0000332](https://doi.org/10.1061/(asce)st.1943-541x.0000332)
35. Limongelli MP, Chatzi E, Döhler M, Lombaert G, Reynders E (2016) Towards extraction of vibration-based damage indicators. In: 8th European workshop on structural health monitoring, EWSHM 2016, 1, pp 546–555

Chapter 10

Model–Based Methods of Damage Identification of Structures Under Seismic Excitation



Guido De Roeck

Abstract Vibration-based Structural Identification has become an increasingly popular experimental technique, e.g. for model calibration, control of structural behavior during construction, assessment of the efficiency of structural repair, ... Main breakthrough was the development of operational modal analysis (OMA), avoiding the use of artificial vibration sources. Vibration-based Structural Health Monitoring is based on the principle that modal parameters of a structure are stiffness dependent. Changes in natural frequencies, damping ratios, mode shapes or combinations can therefore be used as features to detect and to identify damage. Non model-based methods try to identify damage from a comparison of pure measurements (or features directly derived from them) before and after a seismic event without relying on a (numerical) model. In most cases only the first (alarm) level of damage can be reached. The advantage of model-based methods is that they can go further in the damage identification process. They intend to localize and to quantify the damage. Disadvantage is the need to construct a reliable model. Mostly, linear models are used representing the quasi-linear state at small ambient vibrations before and after an earthquake, although there is an interest to use non-linear models for simulating the structural behavior during the earthquake.

Keywords Damage identification · Model-based methods · Seismic excitation

10.1 Introduction

Vibration-based damage identification is based on the principle that modal parameters of a structure are stiffness dependent. Changes in natural frequencies, damping ratios, and mode shapes can therefore be used as features to detect and to identify damage. Compared to other approaches for structural damage identification, vibration-based damage identification has the advantages of (1) being nondestructive, (2) being able

G. De Roeck (✉)

Department of Civil Engineering, University of Leuven, Kasteelpark
Arenberg 40 Bus 2448, B 3001 Louvain, Belgium
e-mail: guido.deroeck@kuleuven.be

© Springer Nature Switzerland AG 2019

M. P. Limongelli and M. Çelebi (eds.), *Seismic Structural Health Monitoring*, Springer
Tracts in Civil Engineering, https://doi.org/10.1007/978-3-030-13976-6_10

237

to identify damage that is invisible at the surface, (3) being ‘global’ because no a priori location of the damage needs to be assumed as opposed to local methods such as ultrasonic testing.

Output-only or operational modal analysis became very popular as no artificial vibration source is needed which is anyhow impossible in many cases. Powerful time domain system identification algorithms like Stochastic Subspace Iteration (SSI) have replaced the obsolete “peak-picking” method [1, 2]. Although theoretically a white noise (unmeasured) excitation is assumed, in practice these algorithms provide accurate lower modes and good damping estimates, even in case of (moderately) “colored” excitation.

In the context of checking the healthy state of structures, operational modal analysis can be used for permanent monitoring. In this case automated system identification (i.e. automatic treatment of response data with minimum or zero user intervention) is mandatory [3]. Moreover, as environmental fluctuations also have an impact on modal properties (at least the natural frequencies), a training period that covers the range of environmental changes, is needed to filter their influence [4–8]. For temperature variations it means about one year.

In general four levels are discriminated in damage assessment. The first level provides an alarm that something has changed in structural behavior, e.g. due to a past earthquake. At levels two and three, an attempt is made to localize and quantify the damage. A probabilistic approach is necessary to account not only for the remaining uncertainty after filtering the environmental influence, but also the imperfections of the assumed numerical model [9, 10]. So far, mostly quasi-linear behavior of the damaged structure under small vibrations is assumed.

Non-model based methods try to extract damage sensitive features from the pure response measurements without resorting to a (numerical) model of the structure. This is clearly an advantage while their drawback is that localization is rarely achieved and quantification is not possible. This class of vibration based methods is the most widespread.

On the other hand, there is the group of methods that try to assess damage by means of a model representing the structure before and after damage. The most powerful methodology is based on updating FE-model, allowing in general localization and quantification of damage. By an optimization process, differences between measured and calculated modal parameters are minimized, taking parameterized damage patterns as updating variables.

As part of the optimization, sensitivities of the modal parameters to the damage pattern have to be calculated by finite differences or the classic Fox-Kapoor equations.

A particular problem is the choice of input values for the unknown damage representation. The optimization process can be entrapped in a local minimum. This can be avoided by using global optimization methods like Particle Swarm Optimization (PSO) [11], Genetic Algorithm (GA) [12] or the Coupled Local Minimizers (CLM) method [13]. As an alternative, several statistics-based parameter selection approaches were proposed as well. Among these methods, global sensitivity analysis (GSA) is the most widely used. In contrast to local sensitivity analysis, such methods consider the whole variation range of the inputs and are therefore referred

to as 'global'. An interesting application is presented [14]: conclusion was that GSA is better suited than local sensitivity based methods to complex structures, such as historical buildings with high uncertainty.

An effective seismic assessment of historical constructions (e.g. masonry towers) can be achieved only through nonlinear static and dynamic analyses with properly defined finite element models. Historical structures cannot be investigated through invasive tests due to their preservation needs. Therefore ambient vibration testing represents a valid tool to calibrate (linear) numerical models. In [15] it is investigated how the seismic assessment of historical masonry towers is influenced by the level of refinement of the adopted models and by the type of the performed analyses. A typical problem in case of towers is the interaction with adjacent constructions, which is difficult to model in a simple, suitable way.

Whenever possible, the use of simplified, yet physical models is recommended as it is beneficial for the updating process. A good example is given in [16], in which a series of tests are reported about the effects of seismic damage on a specimen representative of a high-rise building. The specimen had realistic full-scale dimensions (8 m × 12 m × 21.9 m) and it included concrete floor slabs, beam-to-column connections, and nonstructural walls. Simplified models were adopted to represent the specimen for the purpose of examining the experimentally observed trends in modal properties. First a shear spring model with lumped mass was considered. The shear spring elements were calibrated to the apparent story stiffness measured from the tests. The modal analysis of the shear spring model gave natural frequencies that were quite different from those obtained from the system identification of the test specimen. Therefore, in a second attempt, a so-called fishbone model [17] was used because it can simulate both shear and bending behavior of structural frames. The modal analysis of this fishbone model provided a reasonable correspondence with the dynamic properties observed in the tests. The seismic damage in the test specimen was simulated by decreasing the element stiffnesses of the numerical model.

Recently, there is an interest in updating nonlinear models of the damaged structure [18], which might be a step closer to level four. In [19], signal processing methodologies and nonlinear identification are used to analyze the occurred damage in reinforced concrete (RC) structures during a shaking table test. Both signal-based and model-based quantifications of damage are considered. Different from the more common model-based approach that considers modal parameters before and after an earthquake, the damage identification is based on the nonlinear behavior during the seismic event. The modified Bouc-Wen hysteretic model is used to evaluate the physical parameters, including the stiffness degradation, the strength deterioration and the pinching hysteresis. The proposed method allows to identify the relationship between the seismic excitation and the severity of structural damage.

Level four, prediction of the remaining life time, is still an unresolved issue as changes in the dynamic behavior are basically related to stiffness degradation and not directly to strength reduction. Anyhow, in many cases there is at least some relation between the two. In fatigue assessment, vibration monitoring can deliver the true fatigue load. This load can be introduced in a (calibrated) FE-model to predict the remaining capacity by applying standard procedures for fatigue analysis. This is

of growing importance for bridges because the dynamic loading due to traffic has increased severely during the past decades.

A particular challenge for all four levels is the discovery of small local damage. Not only natural frequencies and mode shapes will hardly be affected but also its influence hidden in the uncertainty blur. Therefore, the development of a distributed strain sensor network able to cope with the very low strain intensities during ambient excitation is a challenge for future developments. Optical fiber sensors with Bragg grating technology permanently attached to the structure could be a good choice in this respect [20]. Interrogation units are still quite expensive but can be coupled and uncoupled when adopting a periodic monitoring maintenance strategy. An additional advantage of the measured strain field is that it can be directly related to the stress field. Such a system will also be able to measure quasi-static deformation as occurs in case of shrinkage, creep, thermal expansion and very slowly applied dynamic loads.

10.2 Elimination of Environmental Influences

It is well known that environmental changes like temperature variations may have an significant influence on features of the dynamic characteristics such as natural frequencies [4, 5]. So they may mask the influence of damage completely. A second cause of inherent variance is due to estimation errors while applying system identification algorithms to the measured response data [9].

When monitored over a short period of time, in which the rather slowly varying environmental influences remain constant, a structure behaves like a linear time-invariant system. However, over longer time spans, the dynamic features change in a nonlinear way because of the nonlinear relationships between environmental parameters (like temperature) and stiffness of structural materials or boundary conditions. Moreover, due to the large thermal inertia of most structures, there can be a time delay between environmental changes and adaptation of dynamic features. To connect changes of dynamic features, e.g. natural frequencies, mode shapes and/or modal strains, to damage, it is of paramount importance to account for this environmental variability. Therefore, global prediction models should be derived from measurements over a long time span, preferentially covering the complete range of possible environmental parameter values.

A possible approach for constructing the global prediction model is measuring the environmental factors that influence the damage-sensitive features, and identifying a black-box input model with these environmental factors as inputs and the corresponding features as outputs [8]. However, a major difficulty with this input-output approach is to determine which environmental (or even operational) influences should be measured, and where the corresponding sensors should be placed. This can be overcome by employing output-only system identification methods, for which measurement of the environmental parameters is not necessary [6, 7].

10.3 Model-Based Damage Identification Based on Modal Parameters

This is the most widespread model-based method. By a permanently (or periodically) installed monitoring system, modal parameters are identified before and after an earthquake (Fig. 10.1). It is assumed that the influence of varying environmental circumstances is filtered from the modal parameters.

In a linear FE-model, representing as close as possible the actual structure, a damage pattern is pursued that reproduces the observed changes in modal parameters. Underlying assumption is that, even after damage, the structure behaves linearly during the small vibration operational state. Damage is simulated by stiffness reductions in the FE-model. Classical FE-updating techniques are used to minimize the differences between observed and simulated alterations of modal parameters. As usually a restricted number of sensors are used in the monitoring system and the frequency interval of the ambient excitation is limited, only a scarce number of modal parameters is at the disposal for updating. Parametrization of damage is mandatory to avoid ill-conditioning of the updating problem.

The method will be illustrated by a few relevant examples.

10.3.1 Damage Identification of the Z24 Bridge

Although the damage was not due to seismic excitation but artificially introduced, this example illustrates perfectly the methodology.

The Z24 bridge was located in the canton Bern near Solothurn, Switzerland. The bridge was part of the road connection between the villages of Koppigen and Utzenstorf, over-passing the highway A1 between Bern and Zürich. It was a post-

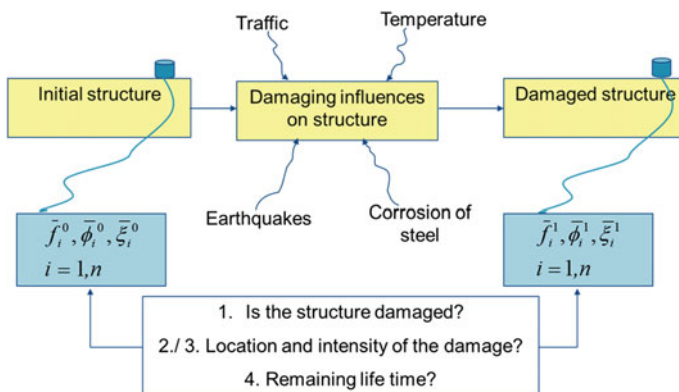


Fig. 10.1 Scheme of damage assessment based on modal parameters

tensioned two-cell concrete box girder bridge with a main span of 30 m and two side-spans of 14 m. Both abutments consist of three concrete columns connected with hinges to the girder. Both intermediate supports are concrete piers clamped into the girder. All supports are rotated with respect to the longitudinal axis which yields a skew bridge. The bridge, which dated from 1963, was demolished in 1998 because a new railway, adjacent to the highway, required a new bridge with a larger side-span.

In the framework of the Brite EuRam Program CT96 0277 SIMCES [21], the bridge was progressively damaged in a number of damage scenarios, before complete demolition. Before and after each applied damage scenario, the bridge was subjected to a full forced and ambient vibration test. A vibration monitoring system was installed on the bridge before and during the progressive damage test, for a total duration of one year, with the aim of quantifying the influence of the temperature on the bridge dynamics. Both the monitoring data and the vibration data from the full vibration tests have been used by many researchers as a benchmark for operational modal analysis algorithms and for algorithms for structural health monitoring and damage identification. A literature review of the benchmark results is provided by Reynders and De Roeck [22].

The damage scenario that is studied here is the settlement of the foundation of one of the supporting piers (at 44 m). It was simulated by lowering the pier by 95 mm (Fig. 10.2), thereby inducing cracks in the box girder. The crack pattern is shown in Fig. 10.3.

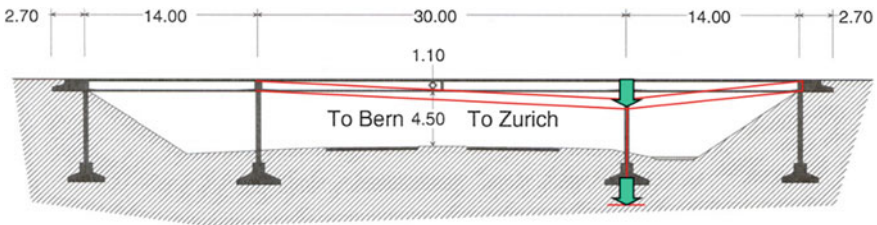


Fig. 10.2 Z24 bridge: damage introduced by settlement

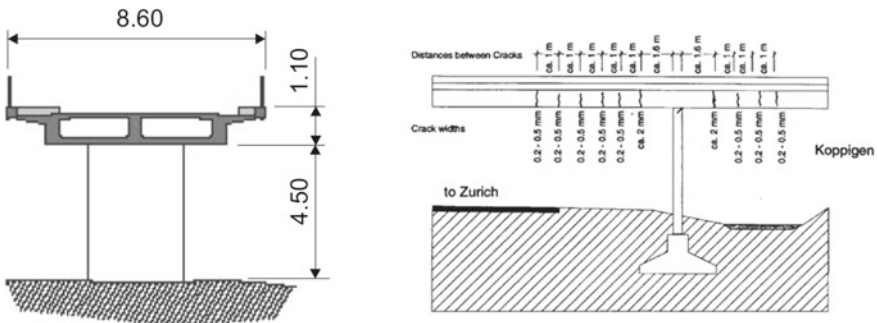


Fig. 10.3 Z24 bridge: cross section and crack pattern due to settlement

Accelerometers are placed on the bridge deck along 3 parallel measurement lines: at the centerline and along both sidelines (Fig. 10.4). 9 measurement setups are used to measure the mode shapes.

The first 5 identified modes are used for the updating. The natural frequencies are given in Table 10.1. The mode shapes are plotted in Fig. 10.5.

The first and the fifth are pure bending modes, the third and fourth are coupled bending and torsional modes, due to the skewness of the bridge and the second is a transversal mode. The settlement of the pier causes a change in mode shapes 3–5, due to the induced cracks in the bridge girder. It is the aim to detect, localize and quantify the damage pattern by adjusting the stiffness of the bridge girder.

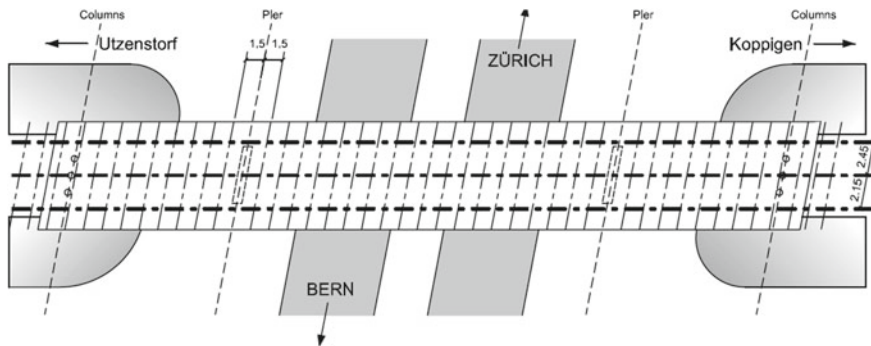


Fig. 10.4 Z24 bridge: top view of measurement grid

Table 10.1 Experimental, initial and updated natural frequencies and MAC values for the undamaged and damaged bridge Z24

Mode	Undamaged			Damaged		
	Experiment	Initial	Updated	Experiment	Reference	Updated
		FE model			FE model	
	<i>Eigen frequencies [Hz]</i>			<i>Eigen frequencies [Hz]</i>		
1	3.89	3.73	3.87	3.67	3.87	3.65
2	5.02	5.14	5.03	4.95	5.03	4.86
3	9.80	9.64	9.72	9.21	9.72	9.12
4	10.30	10.25	10.31	9.69	10.31	9.72
5	12.67	12.52	12.81	12.03	12.81	12.16
		<i>MAC values [%]</i>			<i>MAC values [%]</i>	
1		99.95	99.95		99.85	99.89
2		99.80	99.82		97.16	97.39
3		94.42	98.99		89.02	98.17
4		96.85	99.44		84.66	93.30
5		96.18	96.61		86.61	97.56

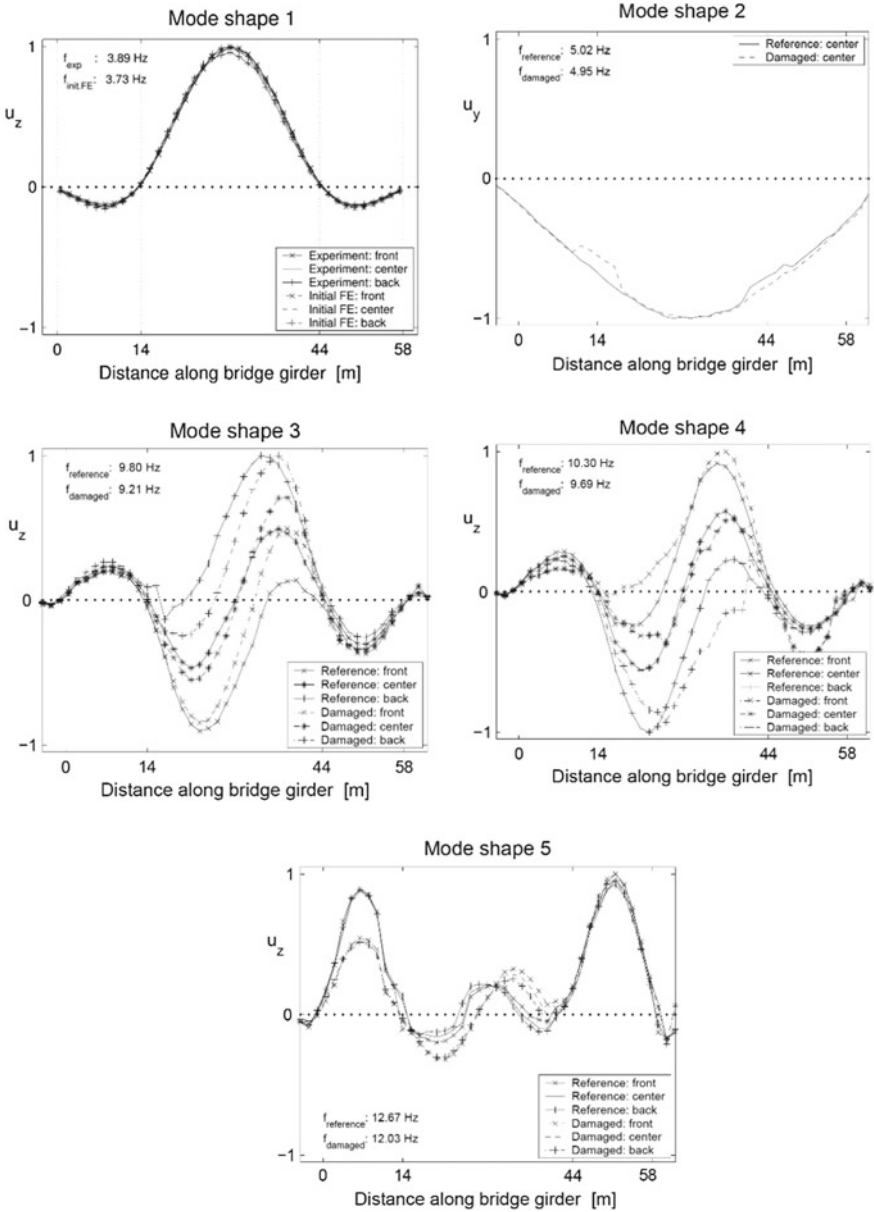


Fig. 10.5 Experimental natural frequencies and mode shapes of the bridge Z24 before and after the settlement of the pier. In the plots the front- and backline are shifted such that the measurement points on the three lines coincide

Model updating is used for the undamaged and the damaged state. 82 beam elements are used to model the girder (Fig. 10.6). The principal axes of the piers are rotated to model the skewness of the bridge. The width of the piers is taken into account by means of specific constraint equations. Mass elements are used for the cross girders and foundations. The concrete is considered to be homogeneous, with an initial value for the Young's modulus of $E_0 = 37.5$ GPa and $G_0 = 16$ GPa for the shear modulus. In order to account for the influence of the soil, springs are included at the pier and column foundations, at the end abutments and around the columns.

In the model updating it is important to reduce as much as possible the number of updating parameters. Choosing too many parameters probably leads to an ill-conditioned problem. In general, the more experimental modal parameters are available, the more updating parameters can be selected. A piecewise linear damage function is used to approximate the stiffness distribution along the beam [23]. This function expresses the relative changes in Young's modulus (as a measure for the bending stiffness) and shear modulus (as a measure for the torsional stiffness) along the bridge. The bridge girder is subdivided into 8 damage elements: 4 damage elements in the mid-span and 2 damage elements in each side-span (Fig. 10.7). Two (identical) piecewise linear damage functions are used for identifying the bending and the torsional stiffness distribution, respectively.

The four vertical modes (bending and bending-torsion) and the transversal mode of the undamaged bridge are used to update the initial FE model to the reference undamaged state of the bridge. The latter mode is included in the process in order to identify the stiffness of the soil springs. The objective function in the (first) reference updating process contains 5 frequency residuals and 492 mode shape residuals.

For the second updating process, the identification of the damaged zone, only the 4 bending modes are used, measured on the bridge after the pier settlement. The transversal mode is not used since the soil springs are not updated in this process. The objective function in this second updating process contains 4 frequency residuals and 451 mode shape residuals.

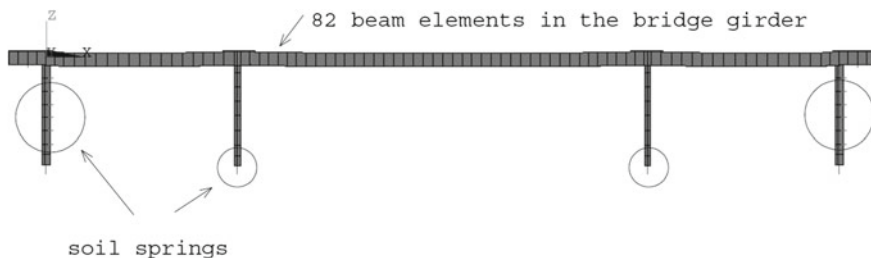


Fig. 10.6 FE model of the bridge Z24. 82 beam elements are used to model the girder. The soil springs at the supports are indicated

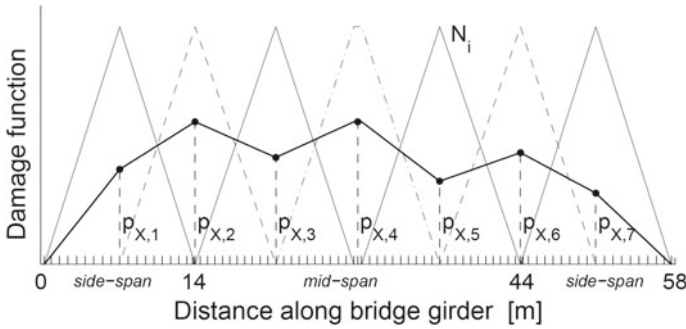


Fig. 10.7 Piecewise linear damage function used to identify the distribution of both sets of correction factors and for the reference and damaged state of the bridge Z24. The bridge girder is subdivided into 8 damage elements. The mesh of finite elements is also plotted on the horizontal axis

In both processes a weighting factor $w = 1/10$ is applied to the mode shape residuals. Looking for the optimum of the objective function (the minimization of the residuals) is in fact a least squares problem that is solved by the trust region Gauss-Newton method.

The stiffness distribution of the bridge girder for bending as well as for torsion is plotted in Fig. 10.8. The initial and the updated values for the reference and damaged state are shown.

In the damaged state a decrease in the girder stiffness above the pier at 44 m is clearly visible. This decrease is due to the lowering of the pier, which induced cracks in the beam girder at that location (Fig. 10.3). The bending and the torsional stiffness are reduced with a maximum of 35 and 24% respectively, located in the expected cracked zone (Fig. 10.8).

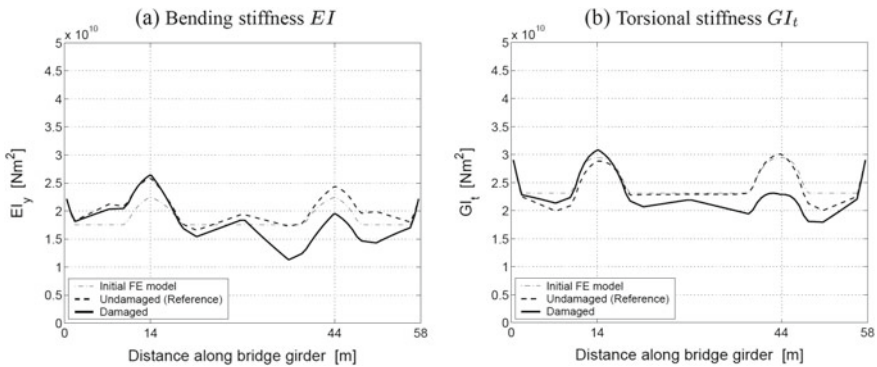


Fig. 10.8 Identified parameters of the bridge Z24: **a** bending stiffness distribution; **b** torsional stiffness distribution

Table 10.1 lists the initial and updated modal data for the undamaged as well as for the damaged bridge. In the former all the five modes are used in the updating process, whereas in the latter only the bending modes (nos. 1, 3, 4, 5) are used. By updating the initial FE model to the reference state, the numerical and experimental natural frequencies correspond much better and a clear improvement for the MAC values can be observed. In particular, the correction of the soil spring stiffness reduces the discrepancy in natural frequency for the transversal mode. For the damaged bridge, the correlation between the numerical and experimental natural frequencies is also improved very well with the updated FE model. The updated numerical mode shapes correspond clearly better with the experimental mode shapes. The MAC value for the 4th mode shape, however, remains under 95%, which is partially due to the bad quality of the experimental data of this mode shape.

10.3.2 Earthquake Induced Damage of a Building: Simulated Case

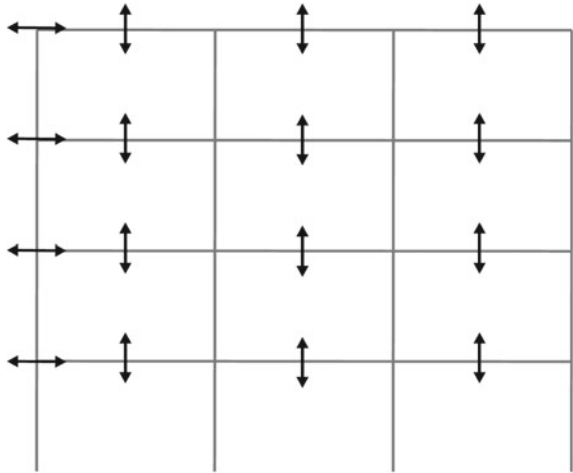
The second example relates to a simulated case of the effect of moderate earthquake. The considered structure is a ‘good’ quality typical existing building in the region to the north of the Marmara Sea in Turkey with a beam side-sway failure mechanism [13]. The building is chosen such that its geometrical, material and limit state properties are within the confidence intervals of the ‘good’ building classification for the Marmara region. The building considered is located in Bolu and is a moment resisting reinforced concrete frame system that represents a typical residential building in the Marmara region isolated from other buildings at both sides. The drawings of the building are taken from the curated depository of Turkish building data on the Kocaeli and Duzce Earthquakes of 1999 maintained by Purdue University, University of Michigan and University of Texas at Austin [24].

The building is a four story structure with three bays. The floor system is flat slab with beams. The building has a typical story height of 2.85 m and considered as regular in elevation. The dimensions of the columns are typically 0.5 m \times 0.25 m and the dimensions of the beams are 0.25 m \times 0.5 m. The concrete design strength is 16 MPa. The building does not have a basement and is fixed at the foundations. The building was under construction when the 1999 Mw = 7.4 Kocaeli and Mw = 7.1 Duzce earthquakes hit the region. After the 1999 earthquakes, it is reported that the reinforced concrete frame was moderately damaged.

The structure is modeled by ANSYS and is idealized as a two-dimensional frame taking into account the mass of the slabs in the transverse direction in the FE model. Eight beam elements per beams and 6 beam elements for columns are generated for the FE model. The locations of the virtual measurements are shown in Fig. 10.9.

Typically, in modeling the response of reinforced concrete structures to earthquake loading, it is assumed that the joint regions are rigid and the damage is limited to flexural yielding of beams, columns, slabs and walls. If the beam-column joint

Fig. 10.9 The location of the response points of the reinforced concrete frame



regions are adequately designed, and if the reinforced concrete frame is designed appropriately according to the weak beam–strong column philosophy, then the plastic hinges will form in beams close to the face of the columns. In this study, a damage scenario is considered such that the joint region is assumed to be adequately detailed with closely spaced stirrups and the frame is assumed to be designed according to the weak beam–strong column philosophy. Consequently, the joints are assumed to remain rigid during seismic excitations and the plastic hinges are expected to occur in the beams close to the beam–column joint regions spreading towards the point of contra flexure in the beams.

For this type of scenario, the stiffnesses of the beam elements in the FE model close to the beam–column joint regions are decreased. It is reasonable to assume that the stiffness at this cracked region is constant. This is primarily due to the fact that the reinforcement layout will not change along the cracked zone length provided this zone does not extend beyond the quarter span point. Figure 10.10 shows the elements of the reinforced concrete frame to which damage is simulated by reducing their stiffnesses.

To assume a realistic damage scenario, non-linear dynamic analysis is carried out. In order to ensure that the structure does not significantly yield, very strong ground motions should not be used for the dynamic analysis since the method proposed in this study is limited to structures which are damaged during an earthquake but that behave linear during an ambient vibration survey after the earthquake. Therefore, the Bolu record of the 1999 Duzce earthquake in Turkey is scaled down by a factor of 0.7 as the original record has significantly high PGA and PGV. For the non-linear dynamic analysis, beam elements are modeled as non-linear frame elements with lumped plasticity where the plastic hinges are defined at both ends of the beams.

The hinge pattern of the 4 story frame that is generated at the end of the nonlinear dynamic analysis is plotted in Fig. 10.11. The plastic hinges that have reached a

Fig. 10.10 The material numbers for the damaged elements in the FE model of the reinforced concrete frame. Materials numbers 2–25 represent the damaged elements whose stiffnesses will be updated. Material number 1 corresponds to the undamaged elements

5	9 13	17 21	25
4	8 12	16 20	24
3	7 11	15 19	23
2	6 10	14 18	22

deformation level between yield point B and IO (Immediate Occupancy) are assumed to have yielded lightly. The plastic hinges between the levels IO and CP (Collapse Prevention) are accepted to have yielded moderately and the hinges beyond the CP level are assumed to have collapsed.

The FE model is used to generate natural frequencies and mode shape components at the (virtual) measurement locations (Fig. 10.9). Noise is added to these results. In this study, the parametrization of the damage in the FE model is not performed by adopting damage functions (like in the case of the Z24 bridge) but by assuming that stiffness deteriorations can (only) happen at the beam-column joints. Model updating is performed by taking relative bending stiffness reductions of 24 elements as updating parameters (Fig. 10.10).

In the here used CLM [13], several start values for the updating variables are considered. The local optimization processes are coupled so that better solutions than multistart local optimization consisting of independent runs are obtained. This is achieved by minimizing the average cost function of the local minimizers subjected to pairwise synchronization constraints. An augmented Lagrangian which contains the synchronization constraints both as soft and hard constraints is used and a network is derived in which the local minimizers communicate and exchange information through the synchronization constraints.

Table 10.2 shows the actual and detected damage states by the model as well as the actual and predicted stiffness reduction factors. The table shows that all the damage states and the stiffness reduction factors are predicted quite accurately by the model, even in the case of noise. The FE model updating scheme used can successfully accomplish the first three levels of damage identification, namely detection, localization and quantification.

Fig. 10.11 The resultant plastic hinge patterns for the reinforced concrete frame structure at the end of the non-linear dynamic analysis

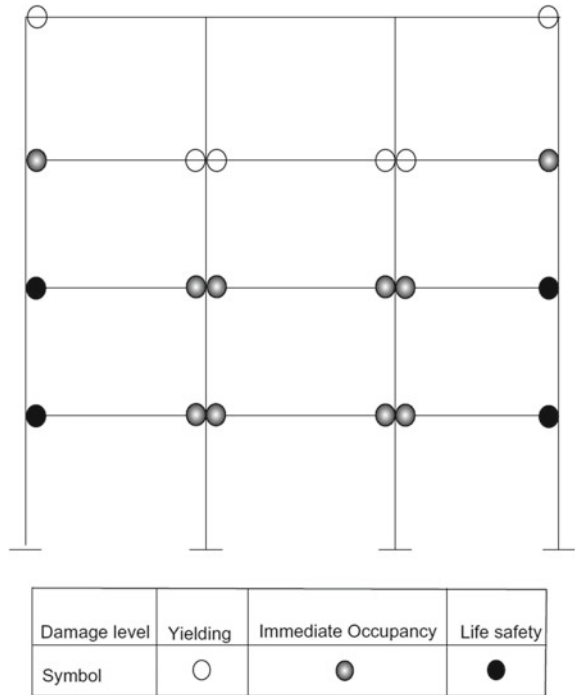


Figure 10.12 shows the relative natural frequency differences between the numerical and the simulated experimental modes in the presence of moderate noise, respectively. The results show that the relative differences in the natural frequencies are considerably improved after the FE model updating.

In [13] the ‘Coupled Local Minimizers’ technique used for FE model updating is compared with other optimization techniques in terms of accuracy, condition number of the Jacobian and the CPU time.

10.3.3 Earthquake Induced Damage of a Building: Laboratory Experiment

A 7-story building slice was tested on UCSD-NEES shake table in the period October 2005–January 2006 [25, 26]. The building was shaken by four earthquakes, introducing progressive damage. Both weak (ambient and white noise excitation) and strong motion (four earthquakes) response data are available for the four damage states of the structure. Objective was to verify the seismic performance of medium rise R/C building designed for lateral forces significantly smaller than those currently specified in building codes in the USA.

Table 10.2 Stiffness reduction factors predicted for the 24 damaged elements in the presence of random noise with normal distribution and 0.5% standard deviation applied to the natural frequencies; 2% standard deviation relative to the maximum amplitude applied to the mode shapes

Material no.	Damage + noise	FEM update	Detected damage	Actual damage
	a	a	Yes/No	Yes/No
1	0	NA	NA	NA
2	0.90	0.90	Yes	Yes
3	0.80	0.79	Yes	Yes
4	0.65	0.66	Yes	Yes
5	0.30	0.30	Yes	Yes
6	0.60	0.59	Yes	Yes
7	0.45	0.41	Yes	Yes
8	0.20	0.31	Yes	Yes
9	0	≈ 0	No	No
10	0.50	0.45	Yes	Yes
11	0.55	0.57	Yes	Yes
12	0	≈ 0	No	No
13	0.10	0.09	Yes	Yes
14	0.55	0.55	Yes	Yes
15	0.40	0.45	Yes	Yes
16	0	≈ 0	No	No
17	0	≈ 0	No	No
18	0.65	0.67	Yes	Yes
19	0.60	0.57	Yes	Yes
20	0.10	0.17	Yes	Yes
21	0.15	0.17	Yes	Yes
22	0.85	0.85	Yes	Yes
23	0.75	0.74	Yes	Yes
24	0.60	0.63	Yes	Yes
25	0.30	0.29	Yes	Yes

The building slice consists of a web (shear) wall, a back/flange wall for transversal stability, and an auxiliary post-tensioned column for torsional stability (Fig. 10.13).

A total of 68 dynamic shake table tests were applied on the test structure, including:

- Low amplitude ambient vibration and low white noise base excitation to identify the modal parameters of the test structure at different damage states.
- Free vibration.
- Seismic base excitation: four historic seismic tests were selected to damage the structure progressively.

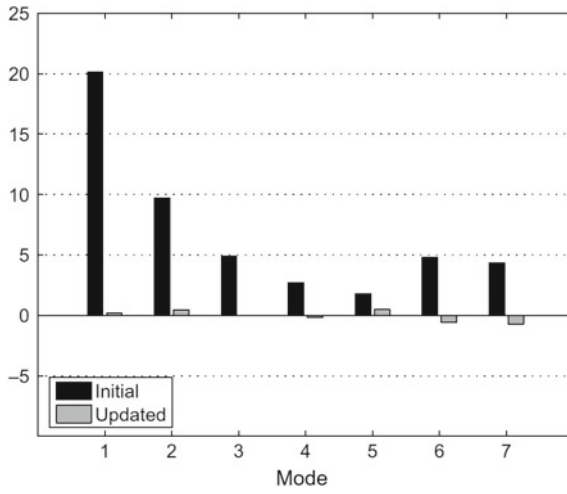


Fig. 10.12 Relative natural frequency differences (in%) between numerical and simulated experimental modes in the presence of moderate noise using the CLM algorithm

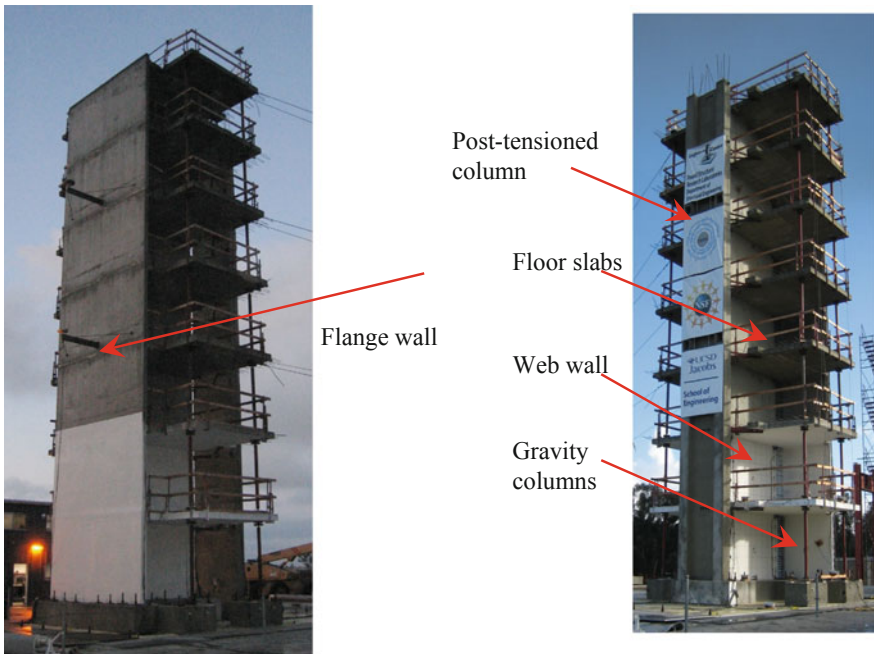


Fig. 10.13 7-story building: components of the building slice

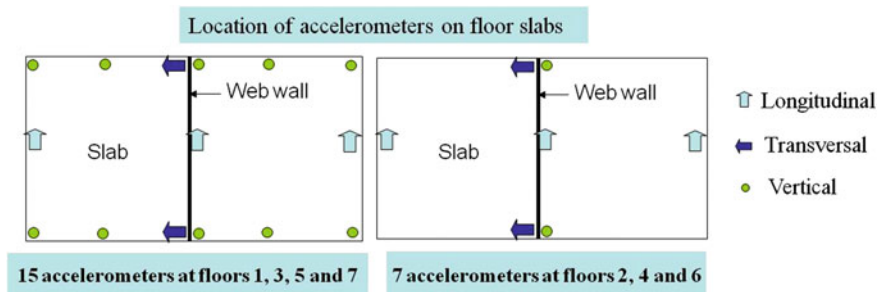


Fig. 10.14 7-story building: layout of accelerometers

Figure 10.14 shows the layout of the accelerometers used for the modal identification.

A three-dimensional linear elastic FE model is considered [25, 26]. For the updating process, the parametrization comprised the division of the building in substructures of which the effective stiffness values are the updating parameters. A first calibration has been performed to adapt an initial FE model to a reference model that reproduces as good as possible the initially measured modal parameters. The seventeen substructures used in the calibration of the initial FE model to the reference FE model during the damage identification are defined by ten substructures along the web wall (six along the first three stories, every half story each, and four along the higher stories, every story each) as shown in Fig. 10.15, and seven substructures consisting each of a floor slab. Table 10.3 shows the results of this calibration step.

In the case of damage identification, once the reference model is obtained, 10 updating parameters (corresponding to 10 substructures) are updated from the reference FE model (at the undamaged/baseline state S_0) to four damage states. These 10 substructures represent the web wall, six along the first three stories (two per story) and four along the higher stories (one per story) as shown in Fig. 10.15. The values of the stiffness parameters of the remaining substructures are kept fixed at the corresponding values in the reference FE model. For each of the considered states of the building, the natural frequencies and mode shapes of the first three bending vibration modes are used in the objective function for damage identification, resulting in a residual vector with 42 components (i.e., three natural frequencies and three vibration mode shapes with $14 - 1 = 13$ components each).

In Fig. 10.16 the damage factors (relative to the reference FE model or reference state) obtained at different damage states are presented in a bar plot in Fig. 10.5. These factors, expressing the relative decrease in stiffness, indicate that: (1) the severity of structural damage increases as the building is exposed to stronger earthquake excitations and (2) the extent of damage decreases rapidly along the height of the building (damage concentrated in the two bottom stories), except for a false alarm in the fourth story at state S_4 .

10.4 Non-Linear System (Damage) Identification

In many cases, first a calibration of a FE model is performed using modal parameters derived from ambient vibration measurements. In a next step this calibrated model is used as a base for a non-linear FE analysis to predict the response (including damage) due to a known seismic input.

In [27] a methodology is proposed to update directly mechanics-based nonlinear finite element (FE) models of civil structures subjected to unknown input excitation. The proposed framework uses spatially-sparse recorded output response time histories of the structure during an earthquake event to jointly estimate unknown time-invariant model parameters of a non-linear FE model and unknown input base excitations using a recursive Bayesian estimation approach. The unscented Kalman filter (UKF), which circumvents the computation of FE response sensitivities with respect to the unknown model parameters and unknown input excitations by using a deterministic sampling approach, is employed as estimation tool.

The use of measurement data obtained from arrays of heterogeneous sensors, including accelerometers, displacement sensors, and strain gauges is investigated in [27]. Based on the estimated FE model parameters and input excitations, the updated nonlinear FE model can be interrogated to detect, localize, classify, and assess damage in the structure. Numerically simulated response data of a three-dimensional 4-story 2-by-1 bay steel frame structure with six unknown model parameters subjected to unknown bi-directional horizontal seismic excitation, and a threedimen-

Fig. 10.15 7-story building:
FE mesh and substructures

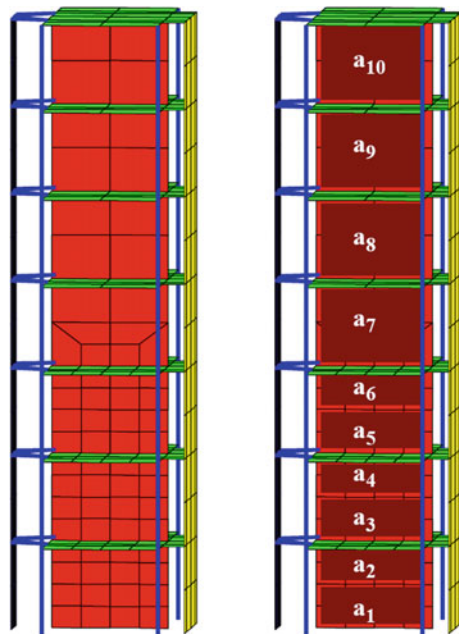


Table 10.3 Measured and effective moduli of elasticity of structural components at different sub-structures of initial and reference FE models

Substructure	Effective moduli of elasticity (GPa)		
	Initial FE model	Reference FE model based on ambient vibration data	Reference FE model based on white noise test data
Web wall, 1st story (bot.)	24.5	17.1	22.0
Web wall, 1st story (top)	24.5	21.6	17.5
Web wall, 2nd story (bot.)	26.0	27.4	21.1
Web wall, 2nd story (top)	26.0	25.9	20.8
Web wall, 3rd story (bot.)	34.8	35.3	35.1
Web wall, 3rd story (top)	34.8	37.5	41.8
Web wall, 4th story	30.2	33.9	42.4
Web wall, 5th story	28.9	28.4	36.9
Web wall, 6th story	32.1	34.4	18.2
Web wall, 7th story	33.5	34.6	40.7
Slab, 1st floor	24.5	22.9	23.3
Slab, 2nd floor	26.0	24.6	23.6
Slab, 3rd floor	34.8	35.6	28.7
Slab, 4th floor	30.2	26.2	34.1
Slab, 5 th floor	28.9	25.5	30.3
Slab, 6th floor	32.1	28.0	27.9
Slab, 7th floor	33.5	28.9	23.9
Base spring	1.56 GN m/rad	Fixed	1.81 GN m/rad

sional 5-story 2-by-1 bay reinforced concrete frame structure with nine unknown model parameters subjected to unknown bi-directional horizontal seismic excitation are used to illustrate and validate the proposed methodology.

10.5 Wave-Based Methods

The wave method for structural health monitoring aims to detect changes in stiffness of a structure, possibly caused by damage during an extreme event or by deterioration over time, by monitoring changes in the velocity of wave propagation through the

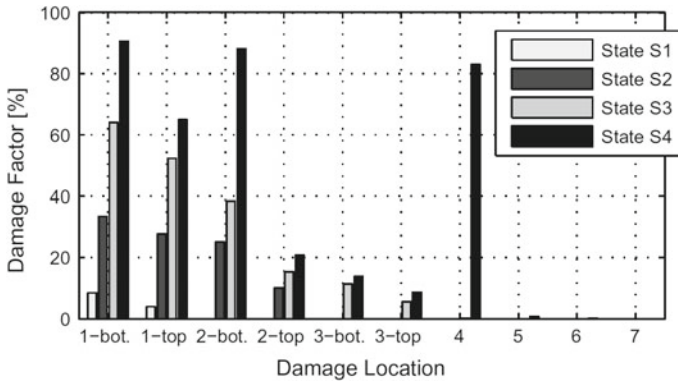


Fig. 10.16 Identified damage factors at various substructures for damage identification (based on ambient vibration data)

structure [24]. It is a relatively recent method first introduced as a concept in the late 1990s for buildings with vertically propagating waves, followed by proof of concept studies in the early 2000s on full-scale damaged buildings, and by in-depth studies providing better understanding of its capabilities and limitations and addressing its challenges. The underlying idea is that after damage has occurred, shear wave velocity of propagation within the damaged zone is reduced. This reduction can be detected by analyzing changes in wave propagation time with respect to undamaged or nominal situation.

The data used in the study [24] are those of a full-scale slice of the 7-story reinforced-concrete (RC) building (Fig. 10.13). In the past, the wave velocity was identified from cross-correlation or pulse time shifts, which is meaningful only for lightly dispersed wave propagation. These methods may be appropriate for frame structures, which deform as a whole predominantly in shear, but their accuracy decreases for structures that deform also in bending, such as moment frames with shear walls. Recently, a solution for this problem was proposed, which involves fitting a model that accounts for such dispersion [28].

In [24], that algorithm is applied to extreme conditions, i.e., highly dispersed wave propagation and damaged structure. The building slice (Fig. 10.13) is modeled as a linear uniform, cantilever Timoshenko beam (TB), stress free at the top and excited by horizontal motion at the base. The model longitudinal wave velocity, c_L , was identified using recorded acceleration response at base and top for three types of excitations: ambient, white noise, and earthquake. The detected changes in c_L were compared with those in the fundamental frequency of vibration f_1 . The main findings of this controlled experiment study, in which the effects of soil-structure interaction are small, are as follows:

- The simple uniform Timoshenko beam, with large shear stiffness, captured well the wave dispersion in the test structure in the band analyzed (0–15 Hz).

- Changes in c_L consistent with the level of observed damage could be detected for all states and types of test data.
- The identified c_L as well as the changes in c_L were amplitude dependent, consistent with previous observations for wave velocities and f_1 .
- The changes in c_L are comparable to those in f_1 for the smaller amplitude (ambient and white noise) tests, suggesting comparable sensitivity to damage of both parameters for smaller amplitude response. For the larger amplitude earthquake tests, however, the change in f_1 is significantly larger than the change in c_L .

Localization of damage would require the development of layered beam models and subsequent fitting.

In [29] a novel on-line system identification method for shear beam building models, based on a wave propagation approach, is developed as an alternative solution to modal analysis methods for the health assessment of multi-story buildings. System identification for layered shear beam models has been reformulated as a real-time parameter identification problem by using an on-line adaptive observer. An important advantage of the proposed model is that it allows buildings to be treated as a discrete shear beams, where wave propagation effects can be studied using a seismic action that excites its basement. The model allows the estimation of displacements and velocities, as well as the unknown shear wave velocities and damping coefficients in real-time. The adaptive observer design is based only on acceleration measurements, does not need a coordinate transformation, and uses the normalized recursive least squares method with forgetting factor and a parameter projection scheme to achieve stronger convergence. Moreover, the proposed identification scheme employs a novel parameterization based on linear integral filters, which eliminates constant disturbances and attenuates measurement noise. The algorithm efficiency is demonstrated through experimental results on a reduced scale five-story building. It is claimed that adaptive observers for civil structures are system identification methods able to operate on real-time, in contrast to other methods like modal analysis. Moreover, it can be designed as a multistep approach: after starting with a very reduced number of sensors, if changes on the wave propagation times or their associated parameters are detected, a more precise analysis can be performed with additional sensors, or with repositioning those that are available, that will locate the damage. At the end, the use of both methodologies, modal analysis and wave propagation, could provide more confidence in the SHM results, in particular when both indicate presence of damage.

10.6 Conclusions

In this chapter, model-based methods for damage identification after seismic events are presented. At the expense of a numerical model, they can provide more information about the health state of the structure than non-model methods.

The most used model-based methods are based on the differences in modal parameters before and after an earthquake. Hypothesis behind the use of modal properties is that the structure operates in a linear way during the small amplitude (ambient) dynamic test. For damaged structures it means that it is assumed that existing cracks don't grow during the dynamic test. In recent papers the uncertainties in modeling and measuring are taken into account, leading to a Bayesian identification approach. By minimizing the differences of modal parameters with predictions from a numerical FE model, damage can be localized and quantified. Essential is a kind of parametrization of the damage. This assumes some engineering judgment of the anticipated damage pattern and how it affects the stiffness of the structure. Three examples are given, demonstrating three different ways of damage representation. The availability of optical fiber strain sensors will enrich the objective functions of the minimization problem, probably allowing a more accurate assessment of the occurred damage.

Very promising are methods that try to identify non-linear structural parameters from the time histories of responses registered during an earthquake event. They also allow an estimation of the seismic input.

Under investigation are wave-based methods although there general and practical applicability asks for further research and validation.

References

1. Peeters B, De Roeck G (1999) Reference-based stochastic subspace identification for output only modal analysis. *Mech Syst Signal Process* 13(6):855–878
2. Reynders E (2012) System identification methods for (operational) modal analysis: review and comparison. *Arch Comput Methods Eng* 19(1):51–124
3. Reynders E, Houbrechts J, De Roeck G (2012) Fully automated (operational) modal analysis. *Mech Syst Signal Process* 29:228–250
4. Peeters B, De Roeck G (2001) One-year monitoring of the Z24-bridge: environmental effects versus damage events. *Earthq Eng Struct Dynam* 30(2):149–171
5. Deraemaeker A, Reynders E, De Roeck G, Kullaa J (2008) Vibration based structural health monitoring using output-only measurements under changing environment. *Mech Syst Signal Process* 22(1):34–56
6. Reynders E, Wursten G, De Roeck G (2014) Output-only structural health monitoring in changing environmental conditions by means of nonlinear system identification. *Struct Health Monit* 13(1):82–93
7. Reynders E, Wursten G, De Roeck G (2012, October) Output-only structural health monitoring by vibration measurements under changing weather conditions. In: Strauss A, Frangopol DM, Bergmeister K (eds) *Proceedings of IALCCE 2012, 3rd international symposium on life-cycle civil engineering*, Vienna, Austria, pp 185–191. Taylor & Francis
8. Reynders E, De Roeck G (2013) Robust structural health monitoring in changing environmental conditions with uncertain data. In: *Proceedings of the 11th international conference on structural safety and reliability: ICOSSAR 2013*, New York, NY, USA, 16–20 June 2013
9. Reynders E, Pintelon R, De Roeck G (2008) Uncertainty bounds on modal parameters obtained from stochastic subspace identification. *Mech Syst Signal Process* 22(4):948–969
10. Simoen E, De Roeck G, Lombaert G (2015) Dealing with uncertainty in model updating for damage assessment: a review. *Mech Syst Signal Process* 56–57:123–149

11. Shoorehdeli MA, Teshnehlab M, Sedigh AK, Khanesar MA (2009) Identification using ANFIS with intelligent hybrid stable learning algorithm approaches and stability analysis of training methods. *Appl Soft Comput* 9(2):833–850
12. McCall J (2005) Genetic algorithms for modelling and optimization. *J Comput Appl Math* 184(1):205–222
13. Bakir PG, Reynders E, De Roeck G (2008) An improved finite element model updating method by the global optimization technique ‘coupled local minimizers’. *Comput Struct* 86(11–12):1339–1352
14. Boscato G, Russo S, Ceravolo R, Fragonara LZ (2015) Global sensitivity-based model updating for heritage structures. *Comput-Aided Civ Infrastruct Eng* 30:620–635
15. D’Ambrisi A, Mariani V, Mezzi M (2012) Seismic assessment of a historical masonry tower with nonlinear static and dynamic analyses tuned on ambient vibration tests. *Eng Struct* 36:210–219
16. Ji X, Fenves GL, Kajiwaru K, Nakashima M (2011) Seismic damage detection of a full-scale shaking table test structure. *J Struct Eng* 137(1):14–21
17. Luco N, Mori Y, Funahashi Y, Cornell AC, Nakashima M (2003) Evaluation of predictors of non-linear seismic demands using ‘fishbone’ models of SMRF buildings. *Earthq Eng Struct Dyn* 32(14):2267–2288
18. Ebrahimian H, Astroza R, Conte JP, Papadimitriou C (2018) Bayesian optimal estimation for output-only nonlinear system and damage identification of civil structures. *Struct Control Health Monit* 25(4):e2128
19. Loh CH, Mao CH, Huang JR, Pan TC (2011) System identification of degrading hysteresis of reinforced concrete frames. *Earthq Eng Struct Dynam* 40(6):623–640
20. Anastasopoulos D, Moretti P, Geernaert T, De Pauw B, Nawrot U, De Roeck G, Berghmans F, Reynders E (2017) Identification of modal strains using sub-microstrain FBG data and a novel wavelength-shift detection algorithm. *Mech Syst Signal Process* 86A:58–74
21. De Roeck G (2003) The state-of-the-art of damage detection by vibration monitoring: the SIMCES experience. *J Struct Control* 10:127–143
22. Reynders E, De Roeck G (2009) Continuous vibration monitoring and progressive damage testing on the Z24 bridge. In: Boller C, Chang FK, Fujino Y (eds) *Encyclopedia of structural health monitoring*. Wiley, New York, NY, pp 2149–2158
23. Teughels A, Maeck J, De Roeck G (2002) Damage assessment by FE model updating using damage functions. *Comput Struct* 80(25):1869–1879
24. Ebrahimian M, Todorovska MI, Falborski T (2017) Wave method for structural health monitoring: testing using full-scale shake table experiment data. *J Struct Eng* 143(4)
25. Moaveni B, Conte JP (2009) Uncertainty and sensitivity analysis of damage identification results obtained using finite element model updating. *Comput-Aided Civ Infrastruct Eng* 24:320–334
26. Moaveni B, He X, Conte JP, Restrepo JI (2010) Damage identification study of a seven-story full-scale building slice tested on the UCSD-NEES shake table. *Struct Saf* 32:347–356
27. Astroza R, Hamed E, Yong L, Conte JP (2017) Bayesian nonlinear structural FE model and seismic input identification for damage assessment of civil structures. *Mech Syst Signal Process* 93:661–687
28. Rahmani M, Ebrahimian M, Todorovska MI (2015) Time-wave velocity analysis for early earthquake damage detection in buildings: application to a damaged full-scale RC building. *Earthq Eng Struct Dyn* 44(4):619–636
29. Morales-Valdez J, Alvarez-Icaza L, Concha A (2018) On-line adaptive observer for buildings based on wave propagation approach. *J Vib Control* 24(16):3758–3778
30. Reynders E, Teughels A, De Roeck G (2010) Finite element model updating and structural damage identification using OMAX data. *Mech Syst Signal Process* 24(5):1306–1323

Part III

Monitoring Tools

Chapter 11

An Optical Technique for Measuring Transient and Residual Interstory Drift as Seismic Structural Health Monitoring (S²HM) Observables



David B. McCallen and Floriana Petrone

Abstract Building interstory drift (ID), which is a measure of the relative displacement between two successive floors in a vibrating building, is a key response parameter utilized in both seismic design and post-earthquake damage assessments. To this point in time, there has been no accepted methodology or sensor technology for reliable and accurate direct measurements of building drift. Indirect measurement of drift, through signal processing and double integration of accelerometer data, is fraught with challenges, particularly when inelasticity-induced permanent drifts occur. In this paper, recent developments toward a new optically-based technique for measurement of both transient interstory drift (TID(t)) and residual interstory drift (RID) are described. The ability of a newly designed laser-based optical sensor system to directly measure interstory drift is demonstrated through experimental and model-based evaluations. This sensor technology has progressed to the point where practical application is feasible as an enabling S²HM technology.

Keywords SHM · Seismic monitoring · Interstory drift · Damage detection · Optical sensor development · Structural damage

11.1 Introduction

Traditional techniques for measuring structural system response under vibrations rely on strong motion accelerometer instrumentation [20]. A number of research works and practical applications have demonstrated the capability of accelerometer-based systems to provide data for structural vibration monitoring and modal identification [9, 13, 18]. However, for evaluating the performance of a building after major seis-

D. B. McCallen (✉)

Department of Civil and Environmental Engineering, University of Nevada,
1664 North Virginia St, Reno, NV, USA
e-mail: dmccallen@unr.edu

D. B. McCallen · F. Petrone

Energy Geosciences Division, Lawrence Berkeley National Laboratory,
1 Cyclotron Road, Berkeley, CA, USA

© Springer Nature Switzerland AG 2019

M. P. Limongelli and M. Çelebi (eds.), *Seismic Structural Health Monitoring*, Springer Tracts in Civil Engineering, https://doi.org/10.1007/978-3-030-13976-6_11

263

mic events, structural performance parameters such as peak interstory drift (PID) and residual interstory drift (RID) become key measures to assess structural damage and inform decisions on continuity of operations and safety of occupancy. Determining interstory drift from recorded acceleration response histories requires significant data processing and is subject to a number of technical challenges. Historically, ID has been computed by double integration of acceleration time histories to obtain floor absolute displacements, which in turn are differenced to obtain the relative displacement between two adjacent floors. Signal processing for baseline correction and bandpass filtering can be “delicate and sometimes subjective” [22], and the dynamic rotations of the accelerometer instrument, which are not typically measured/known, may be necessary to reliably compute displacements from acceleration records if rigid body rotations occur [23, 24].

Optical techniques for measuring building geometry based on photogrammetry have also been investigated and, under controlled laboratory conditions, have experimentally demonstrated an ability to achieve positional accuracy on the order of 0.5 cm with consumer grade single-lens-reflex cameras [7]. However, limitations for practical applications have been identified in the precision of the camera, the quality of the photos, the functionality of the photo-processing software as well as the lack of a formal method for assessing the accuracy of geometric measurements [8]. The demonstration of such methods in a more cluttered post-earthquake environment needs to be evaluated to understand the full potential for assessing for example residual drift in a damaged building.

More recently, research works have examined the potential of Micro Electro Mechanical Systems (MEMS) to detect structural damage. Hou et al. [11] have proposed an optimal layout of MEMS inclinometers to maximize the measurement accuracy in structures exhibiting elastic and inelastic deformations, but with experimental testing limited to single structural components under static loading conditions. Inclinometers typically rely on a constant gravity field for their measurement principle and imposition of earthquake accelerations in three dimensions can in fact disrupt rotation measurements. Hsu et al. [12] have developed MEMS seismometers to identify damage in building structures, but with the limitation of having the same post-processing criticalities highlighted for classical acceleration-based monitoring systems.

In the early development of the optical sensor described herein, the authors explored another optical technique based on the use of high-quality CCD cameras to directly measure building drift displacements but the repeatability and accuracy was less than expected.

In this context, it would be highly desirable to have a practical method for directly measuring interstory drift to validate computational models of existing buildings, to assess the attainment or exceedance of limit states, and to inform immediate post-earthquake damage assessments and decisions on emergency response. Critical facilities such as hospitals, emergency response centers and data/financial centers would benefit substantially from rapid data on potential damage levels, as well as potential damage locations, immediately after a major earthquake.

Rapid advancements in sensor technologies and agile communications are creating new opportunities for transformational approaches to S²HM. Driven by applications in many diverse fields (e.g. robotic machine control, autonomous vehicles etc.), optically-based sensor systems have undergone significant advancement in the past decade. Optically-based systems can have inherent advantages, including the extremely short latency of the underlying physics and the ability to perform high resolution measurements. Together, these features can result in very broad frequency band and high-fidelity measurements. In addition, the revolution underway in wireless communications and the Internet of Things (IOT) is providing an entirely new paradigm for command and control of sensor systems and for expedient exfiltration of data. Early research studies have investigated the potential of employing optical sensors and lasers to measure the dynamic response of structural systems [6, 25]. These works have also highlighted the need to account for rotations associated with structural member deformations that can have a significant impact on laser light propagation in determining interstory drift [21, 22].

In this paper a newly developed optical sensor for monitoring building earthquake response is described and the performance of the sensor is demonstrated through the data obtained from a comprehensive, multi-testbed, experimental campaign. This technology provides, for the first time, a means for obtaining direct, broad-band, high fidelity measurements of building interstory drift. The developed sensor technology can also readily be incorporated into advanced building monitoring frameworks such as described in Celebi et al. [3] and Celebi [4].

A number of existing seismic design standards utilize interstory drift to define building limit states, to establish limits on PID, which is the maximum TID(t) obtained over the duration of the earthquake, and to measure potential building damage states after a major earthquake event, as summarized in Table 11.1. Despite the prevalent use of drift as a key response parameter and damage observable, there remarkably has been no robust and reliable technique developed to directly measure drift displacements.

Table 11.1 International codes and standards utilizing interstory drift as a performance or damage observable

Specification	Standard
Definition of system limit states in terms of PID	ASCE 43-05
Definition of system maximum allowable Interstory drift in terms of PID	Eurocode EN1998-1 New Zealand standard NZS-1170.5 Tall building initiative TBI 2.01
Definition of system damage states in terms of RID	FEMA P58-1 Tall building initiative TBI 2.01

PID = Maximum TID(t) over the duration of the earthquake event, RID = TID(t) as $t \rightarrow \infty$

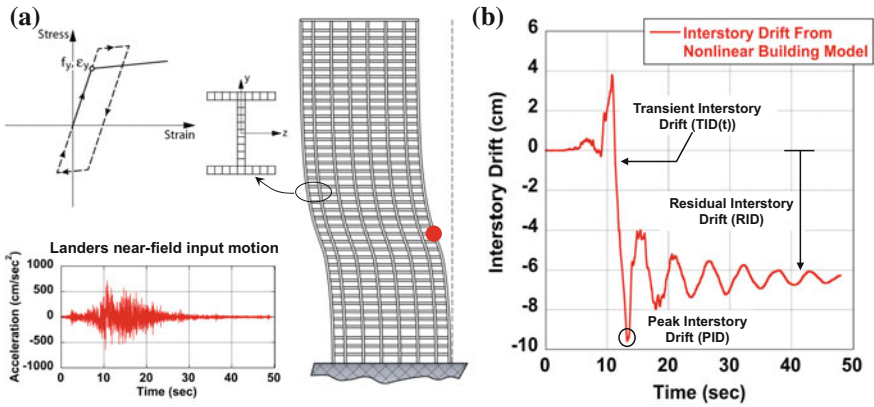


Fig. 11.1 Interstory drift from a representative nonlinear building model. **a** Deformed shape of a 40-story building FEM [14] subjected to Landers input motion [5]; **b** graphical representation of TID(t), PID and RID

11.2 Optically-Based Measurements for Interstory Drift

A graphical representation of TID(t), PID and RID is provided in Fig. 11.1, where a synthetic interstory drift waveform obtained from a 40-story nonlinear steel frame building model subjected to strong near-field motions is shown. The 40-story building was designed for UBC zone 3 and is characterized by a story height of 4 m in all intermediate floors, and 5.5 m in the first and top floor (Fig. 11.1a). The detailed building model utilizing finite deformation, fiber beam elements with elasto-plastic kinematic hardening [14] was subjected to near-fault Landers earthquake motions [5]. As evident in Fig. 11.1b, the interstory drift waveform at approximately one-third of the building height resulted in a significant PID (about 2.5% drift ratio) as well as in a substantial RID (about 1.5% drift ratio) as a result of building system yielding and inelastic deformation.

Although existing codes and standards only refer to PID and RID, the most effective system for drift measurement should be capable of measuring PID, RID and TID(t). In fact, for structures with potential cyclic degrading response features, e.g. reinforced concrete undergoing inelastic action associated with many cycles, it would be desirable to define a drift damage measure that includes aspects of the duration of loading and number of cycles at a given amplitude of drift, which can only be expressed by TID(t) [2, 10].

A new *Discrete Diode Position Sensor* (DDPS) has recently been developed to allow full broad-band measurements of interstory drift [15]. This technology utilizes a carefully configured geometric array of light-sensitive photodiodes to track the instantaneous position of an incident laser beam, as shown in Fig. 11.2c. The prototype DDPS adopted 92 diodes arranged in a staggered rectangular array configured such that the laser beam is always incident on one or more diodes. A sampling rate of

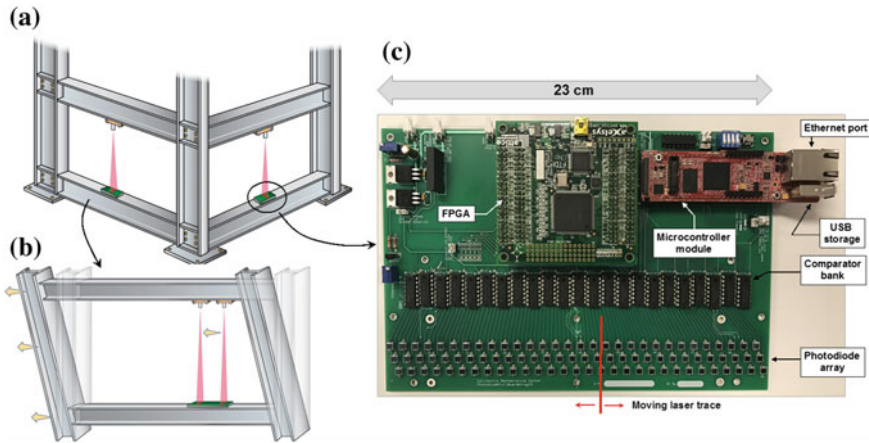


Fig. 11.2 Discrete Diode Position Sensor (DDPS) technology. **a** DDPS mounting for in-plane drift measurement; **b** translation of an incident laser line source on a DDPS during in-plane drift; **c** board mounted DDPS with moving laser trace illustrated

384 times per second is used, which corresponds to a Nyquist frequency of 192 Hz. To increase the position localization accuracy, the three linear arrays of diodes are staggered so that the active areas of the diodes overlap by $D/3$, where D is the nominal width of the diode active area.

As the laser line trace moves back and forth with in-plane motion, the position of the laser is theoretically determined to within $D/6$, and the readout of the sensor is a quantized set of displacements that increment by $D/3$. The width of the active area of the diodes adopted in this study is approximately 0.29 cm, which would yield a theoretical measurement error of approximately 0.05 cm. However, experimental tests on the as-built DDPS indicated that the realized position error is closer to 0.10 cm [15] due to slight positioning errors of the individual diodes, effective diode areas resulting from some dimensional variability, and the finite dimension of the diffracted laser trace.

As a building undergoes earthquake excitation, the laser beam translates back and forth across the photodiodes, which individually generate a voltage when hit by incident laser light, see Fig. 11.2a and b. The laser beam is diffracted through an optic to create a line projection as opposed to a point projection on the diode array. The resulting line trace is illustrated schematically in Fig. 11.2c, but in practice the line trace is much wider so that the laser will not move off the diode array when transverse displacements occur in a building undergoing vibration in three dimensions [15]. By rapidly sampling the photodiode voltages across the entire photodiode array using a Field Programmable Gate Array (FPGA), the instantaneous position of incidence of the laser line source on the sensor is determined and translated into a direct measurement of story drift displacement.

The next section of this article summarizes the results of a three-phase experimental campaign aimed at establishing DDPS dynamic performance.

11.3 Sensor Testbeds and Experimental Evaluation of DDPS Performance

Three experimental testbeds have been utilized in the DDPS development activities.

11.3.1 Testbed #1: DDPS Inherent Measurement Performance

The first testbed consisted of an automatically controlled precision motion table that could impart representative interstory drift motions to evaluate the inherent measurement performance of a DDPS as indicated in Fig. 11.3. This testbed allowed the evaluation of the fundamental ability and resolution of the DDPS to measure TID(t), PID, and RID. The experimental process consisted of imposing representative building drifts on the testbed and comparing DDPS measurements to the ground truth of imposed drifts. For example, for the synthetic drift in Fig. 11.1b, the imposed drift versus the DDPS measurement of the imposed drift and the resulting DDPS error are shown in Fig. 11.4a and b, respectively.

As illustrated in Fig. 11.4a and b, the DDPS very accurately measured all the key features of the entire imposed interstory drift waveform, with the sensor exhibiting a drift displacement measurement error of approximately 0.1 cm. This experimental

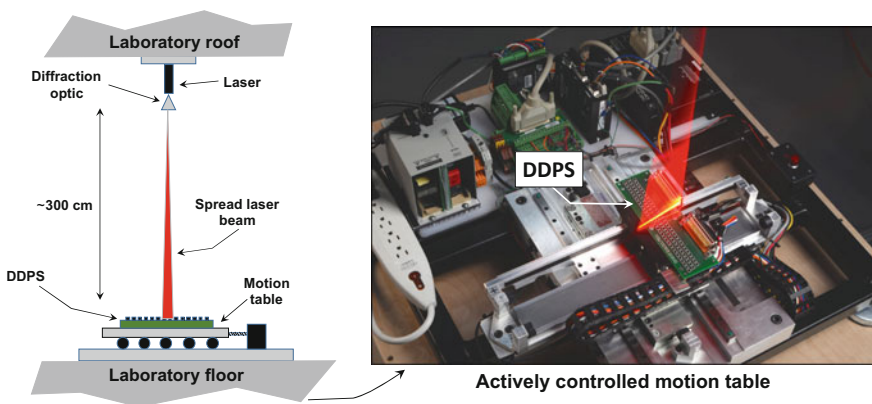


Fig. 11.3 Sensor testbed #1: automatically controlled motion table for generating representative ceiling-to-floor drift displacements

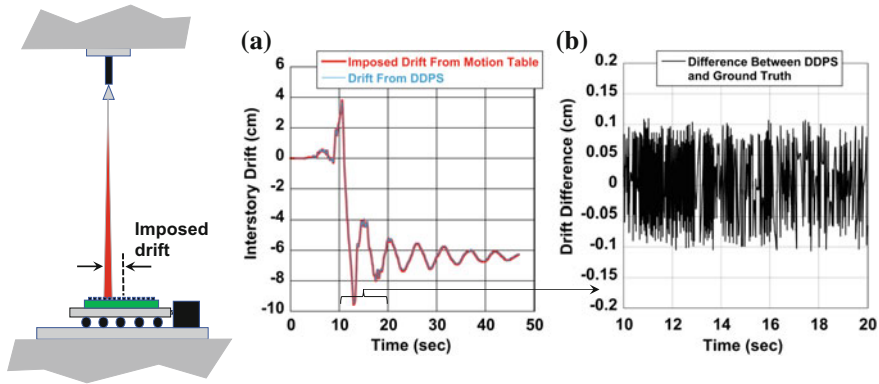


Fig. 11.4 Testbed #1 data on DDPS measurements. **a** Imposed motion versus DDPS measurements; **b** DDPS error

set-up provided the first data on DDPS performance and established that the accuracy of the DDPS met the sensor design objectives.

11.3.2 Testbed #2: DDPS Performance on a Laboratory Planar Frame

The second testbed consisted of a laboratory scale two-story moment frame with an automatically controlled stepper motor for imposing specified earthquake motions at the base of the frame, as shown in Fig. 11.5. Ground truth drift was acquired by tensioned wires connected to an adjacent diagnostic tower with string potentiometers for measuring wire extension and contraction, thus providing a direct measure of absolute story displacements. The objective of this experimental set-up was to evaluate the DDPS under more realistic structural dynamic conditions and include the additional challenge of developing a correction to account for the local structural member rotations at the mounting point of the laser. As documented in McCallen et al. [15], the local rotation of the structural members where the laser is mounted can have a substantial effect on the observed measurement of interstory drift. From the deformed shape of a frame subject to horizontal forces (Fig. 11.5), it is noted that the actual drift at each time step $\Delta_{Drift}(t)$ is computed as $\Delta_{Drift}(t) = \Delta_{Observed}(t) + \Delta_{Rotation}(t)$, where $\Delta_{Observed}(t)$ is the drift measured directly by the horizontal DDPS and $\Delta_{Rotation}(t)$ is the laser trace translation caused by the local rotation at the laser mounting point. $\Delta_{Rotation}(t)$ can be calculated as $\Delta_{Rotation}(t) = \Theta_{Laser}(t) \cdot H$, where $\Theta_{Laser}(t)$ is the local rotation at the laser mount location and H the distance between the laser and the horizontal DDPS. The unknown $\Theta_{Laser}(t)$ is then derived based on the measurements provided by a horizontal laser beam impinging onto the vertically mounted DDPS, as $\Theta_{Laser}(t) = \Delta_{Vertical}(t) / W$, where $\Delta_{Vertical}(t)$ is the vertical translation

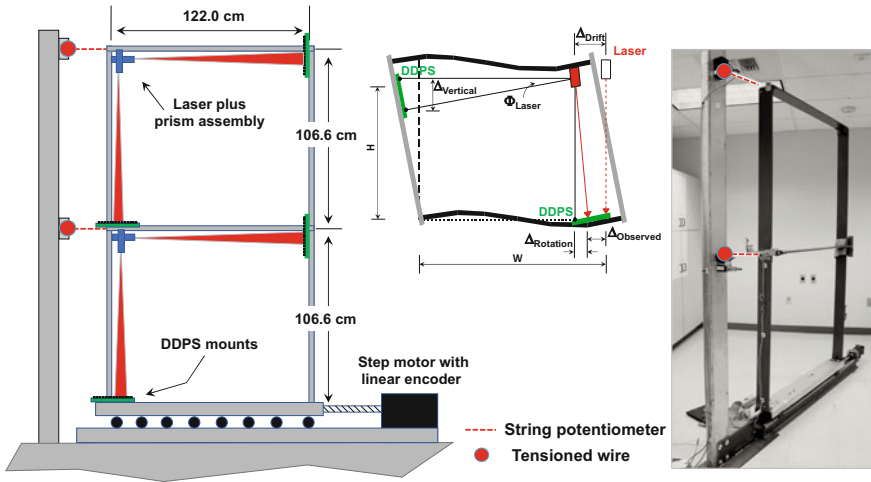


Fig. 11.5 Sensor testbed #2: scale model two story moment frame with an automatically controlled stepper motor for imposing earthquake motion

of the horizontal laser beam measured on the vertical DDPS and W is the distance between the location of the horizontally propagating laser and the vertical DDPS. Therefore, for a typical mounting configuration, such as that illustrated in Fig. 11.5, the deployment of a horizontal laser and vertical DDPS, in addition to the vertical laser and horizontal DDPS, allows calculating the local rotation of the vertical laser and appropriately correcting the drift measured by the vertical laser on the horizontal DDPS.

The experimental frame was subjected to ground motions from actual earthquake records and the story displacements were measured by the string potentiometers (taken as ground truth) and DDPS at each floor level. For applied El Centro earthquake input motion (PEER database [17]), the frame displacement drift waveforms are shown in Fig. 11.6a.

For Testbed #2, the DDPS error was $\sim 0.15\text{--}0.2$ cm (Fig. 11.6b). Based on a simple error analysis that accounts for both the error in the direct drift measurement on the horizontal DDPS and the error in the laser rotation measurement on the vertical DDPS, the maximum error is expected to be on the order of twice the error from a single sensor measurement. The observed peak sensor errors of $\sim 0.18\text{--}0.2$ cm were therefore in theoretical agreement with the expected maximum sensor error. Throughout the two-story frame experimental testing, it was confirmed that the DDPS error was essentially independent of drift amplitude, which was theoretically to be expected, and the DDPS hardware was robust against any adverse effects of the imposed shaking and vibration on the sensor components. Overall, the DDPS exhibited an ability to accurately measure the transient drift waveforms in terms of both frequency content and amplitude.

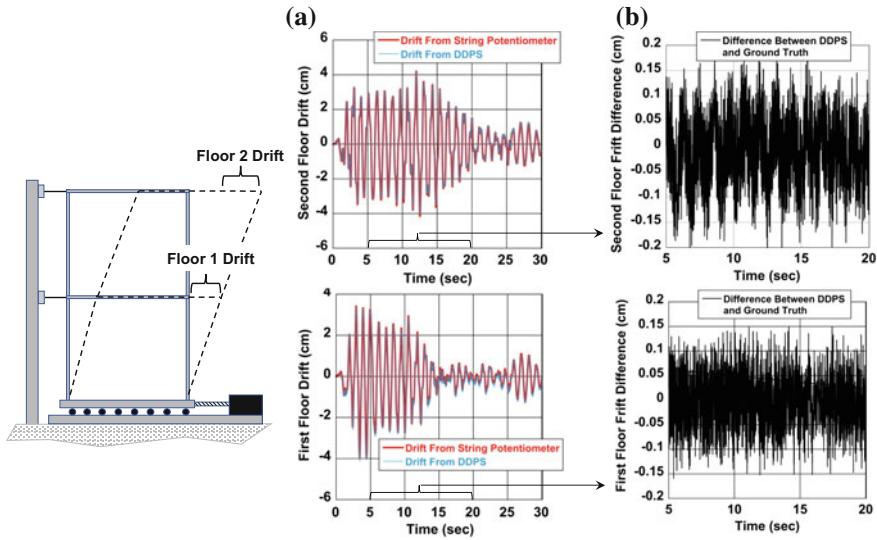


Fig. 11.6 Testbed #2 data on DDPS measurements. **a** DDPS versus ground truth; **b** DDPS error

11.3.3 Testbed #3: DDPS Performance on a Scaled 3D Steel Frame Under Bidirectional Excitation

The third testbed consisted of a significantly larger and more representative 1/3 scale steel frame structure mounted on a large hydraulic shake table at the University of Nevada, Reno Earthquake Engineering Research Laboratory (Fig. 11.7). The test set-up included a full suite of tensioned wire diagnostics to measure ground truth drift displacements at all three floor levels as well as accelerometers at each floor level. The test frame was subjected to bi-axial earthquake motions from representative measured earthquake records.

The objective of this testing set-up was to validate a second generation, single-board, DDPS design and demonstrate sensor performance at a scale more representative of actual building field conditions. For the Nevada experiments a large suite of tests were executed starting with scaled-down, low amplitude motions and progressing to increasingly higher motions until the earthquake input motions were scaled by up to 250%. This allowed evaluation of DDPS hardware performance under very strong shaking at larger optical distance ranges (laser-to-sensor) than previous laboratory structure experiments.

Representative data from the Nevada shake table experiments are shown in Fig. 11.8a for imposed El Centro earthquake ground motions scaled by 250%. As with previous tests, the drift measurements from the DDPS system deployed on the frame exhibited excellent agreement with ground truth drift and the DDPS peak error was on the order of 0.2 cm (Fig. 11.8b). It should be noted that in these larger-scale experiments the tensioned wires had a much longer span than in previous tests and

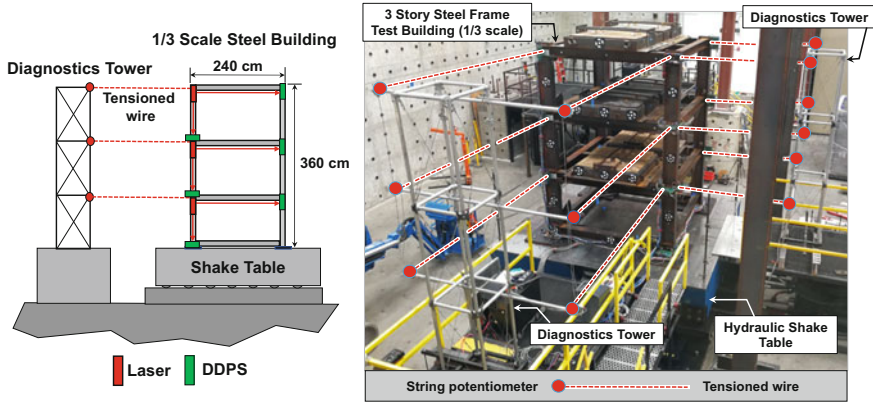


Fig. 11.7 Sensor testbed #3: 1/3 scale three story steel frame mounted on a hydraulic shake table

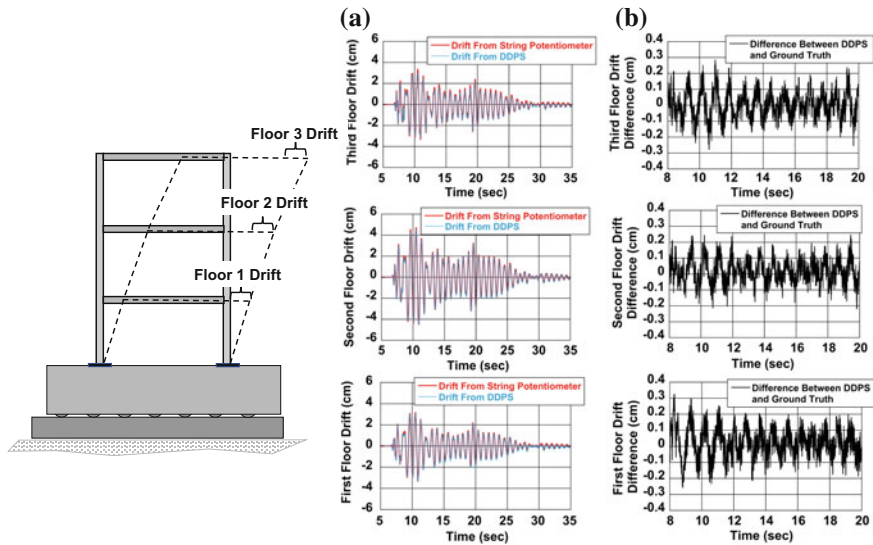


Fig. 11.8 Testbed #3 data on DDPS measurements. **a** DDPS versus ground truth and **b** DDPS error

some error in the ground truth measurements due to wire dynamic vibration could be expected. In the Nevada experiments the DDPS worked flawlessly throughout the entire test sequence under the very strong shaking associated with 250% ground motions. This provided significant performance data on the ruggedness of the DDPS board design.

The integrated set of experiments performed over the past two years on the three testbeds have provided significant data to validate the performance of a DDPS system for drift measurements. Looking forward to deployment on full-scale structures, it is instructive to evaluate how the drift displacements measured on the three testbeds

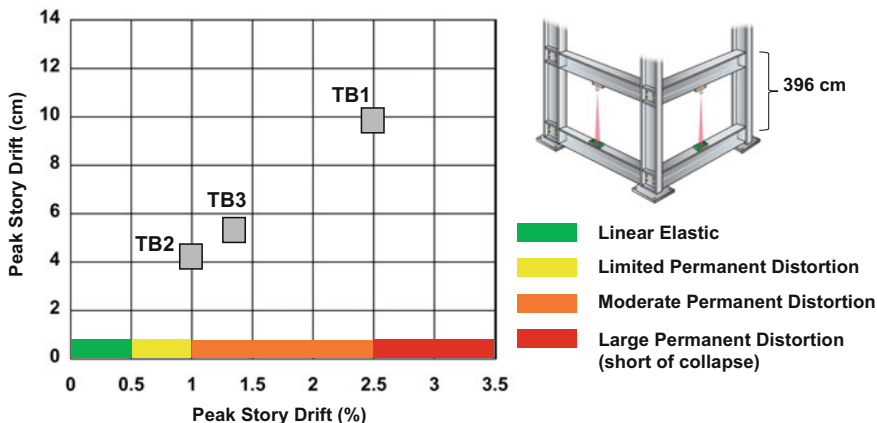


Fig. 11.9 Drift defined limit states for a representative steel moment frame (from ASCE/SEI 43-05 [1]) and drifts measured on each the three DDPS experimental testbeds (TB1, TB2, TB3)

compare to representative drifts that could be achieved on an actual full-scale building undergoing strong earthquake motions.

Figure 11.9 illustrates the drift for a representative steel moment frame with a story height of 366 cm (12 ft) and includes representation of limit states in accordance with the maximum drift limits provided in the ASCE/SEI 43-05 [1] for nuclear facilities. Standard 43-05 provides four drift-defined states for steel moment frames, which describe four regimes of system response ranging from linear elastic to large permanent distortion short of collapse as indicated in Fig. 11.9. The peak drifts measured in the experiments performed on each of the three testbeds are also indicated in Fig. 11.9 (TB1 = Testbed #1, TB2 = Testbed #2, TB3 = Testbed #3). The experimentally measured drifts from the scaled experiments are commensurate with the drift that would be achieved in a full-scale structure when significant inelastic behavior is occurring. This supports the fact that a DDPS can measure representative large drift displacements in a full-scale structure, and it should be noted that the range of the DDPS, defined by the length of the diode array (i.e. the 23 cm length in Fig. 11.2), can be adjusted to the maximum drift that might be achieved in a particular structure.

11.4 Model-Based Simulations of Sensor System Performance

As an integral part of the DDPS development, finite element models (FEMs) have been employed throughout the sensor design and testing process in order to build validated confidence in the ability of simulation models to predict deployed sensor system performance. Ultimately, confidence in a simulation-based tool for sensor

system design will be a key capability for appropriately designing sensor systems for specific structure configurations and is thus an important element of the overall technology base.

To help explore model-based predictions, computational models of testbed #2 and testbed #3 structures were constructed in the *OpenSees* [16] program environment. The test structures were modeled with combinations of beam elements with fiber cross-sections as well as shell elements for testbed #3. Rayleigh damping was employed to represent the system damping for both testbed structures. Damping coefficients were estimated from the dynamic response of the test structures during experiments, from applying a displacement and suddenly releasing the frame and observing the ring-down as well as through application of optimization of model-based predictions for imposed earthquake shaking [19].

In each modeling instance, the developed FEM was subjected to the earthquake motions imparted to the structure through the base motion generated by the automatically controlled excitation system. The displacements and rotations at the sensor and laser mounting locations were extracted from the FEMs as indicated in Fig. 11.10a and b and post-processed to predict what the sensor system should have measured for each event.

Model-based predictions of sensor measurements for the structures in both testbed #2 and testbed #3 experiments are shown in Fig. 11.10c and d. In these comparisons two features of the FEMs are being tested. First the ability of the model to accurately represent the actual structural response. Secondly, the ability, based on kinematic representation of DDPS system measurements, to translate model-based predictions of structure displacements and rotations into reliable estimates of sensor system performance.

As shown in Fig. 11.10c and d, the FEMs proved to be an effective tool for predicting the expected sensor measurements in both structures. These results exhibit sufficient accuracy to provide confidence in carefully constructed FEMs to predict sensor performance. Having a predictive tool will be important for designing sensor system layouts and extending the sensor designs to other structural configurations including shear wall structures, braced frames, hybrid systems etc. and is thus a key element of the overall technology base.

11.5 Conclusions

In the work presented herein, a new optical sensor for directly measuring transient and residual interstory building drift was described. The capabilities of the DDPS have been successfully demonstrated through extensive experimental testing and through model-based prediction of sensor performance. Exploiting the attributes of optical physics, the sensor is very broad band and can accurately measure time-varying transient drift ($TID(t)$), peak interstory drift (PID), as well as permanent residual drift (RID) associated with inelastic building response. Thus, the sensor can measure

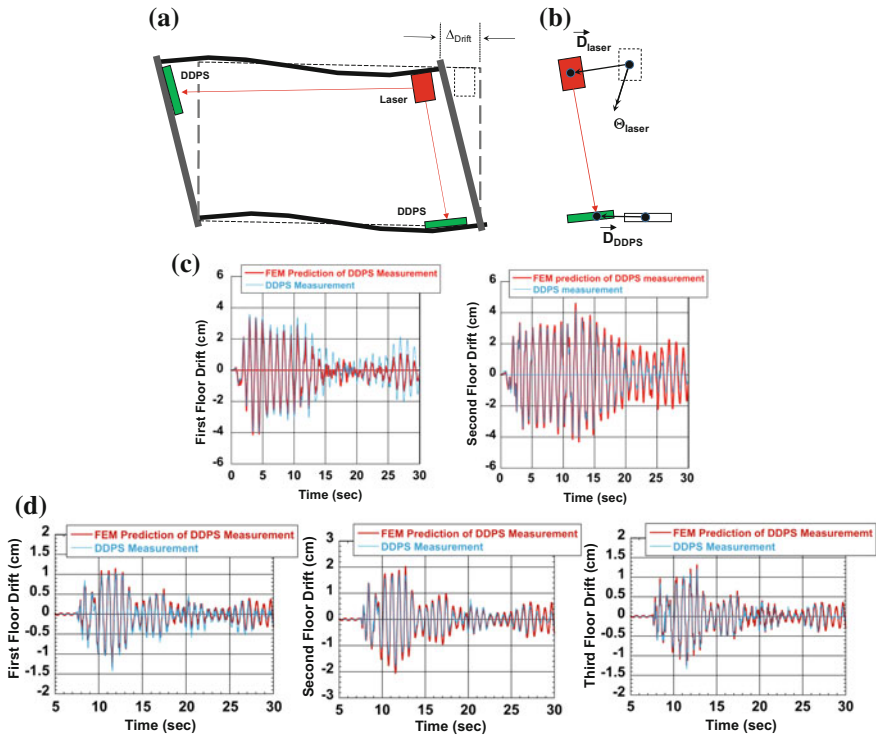


Fig. 11.10 FEM predictions of DDPS measurements. **a** Frame deformed shape from the FEM; **b** extracting displacements and rotations from the FEM at laser and DDPS locations to predict DDPS measurements. Comparison of FEM predictions of sensor measurements with actual DDPS measurements for **c** testbed #2 frame and **d** testbed #3 frame

the full breadth of drift components that are utilized in existing building design codes and standards.

The DDPS system is rapidly approaching readiness for practical application. Figure 11.11 illustrates the evolution of the DDPS technology: the first generation of the DDPS (GEN1) consisted of an assembly of interconnected components and was utilized on Testbed #1 and Testbed #2 (Fig. 11.11a). The second generation of the DDPS (GEN2), included all components integrated on a single circuit board and was utilized on Testbed #3 (Fig. 11.11b). A third generation of the sensor (GEN3), characterized by a simpler and much more compact integrated sensor with a single diode array is undergoing final development at the University of Nevada, Reno (Fig. 11.11c). By modifying the character of the incident laser beam, a single array of diodes can be used and early tests indicate drift displacement measurements with higher accuracy—on the order of 0.05 cm. With this advancement in accuracy, the DDPS is moving towards an ability to measure wind-induced drift in tall buildings, which would provide a secondary function for system identification of as-built structures under ambient vibrations.

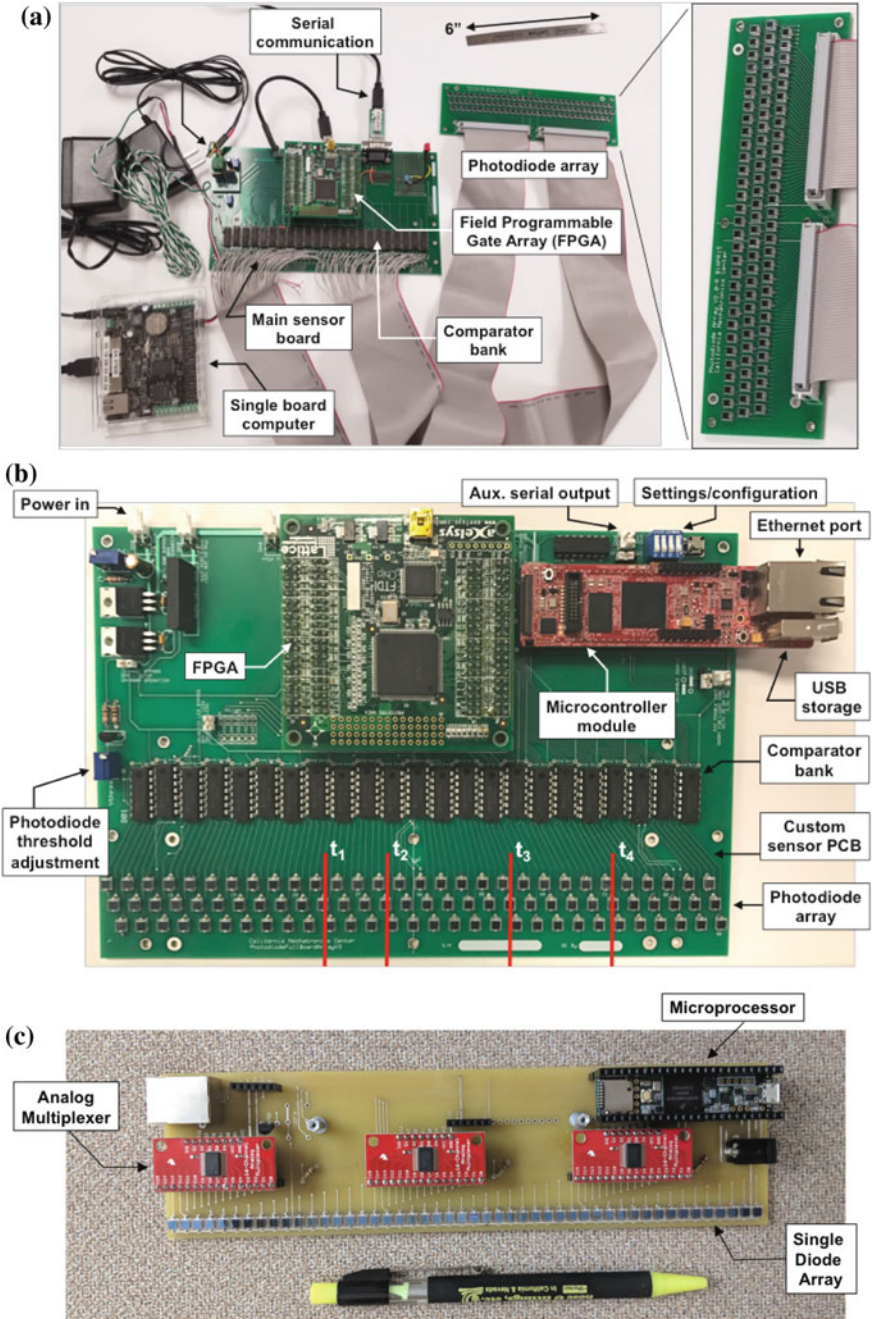


Fig. 11.11 Evolution of DDPS technology. a GEN1, interconnected components; b GEN2, integrated sensor on a single board; c GEN3, compact integrated sensor with single diode array

Final value engineering, to minimize system cost, robustness and packaging/form factor, is underway to achieve the most reliable and cost-effective deployable product. Additionally, the development of deployment “kits” for laser, sensor and mounting hardware, along with mounting guidance to expediently mount the laser and sensor systems on structures, will be required for effective and practical mounting. Improved techniques for addressing local member rotations have recently been identified through model-based simulations [19] and will be experimentally validated. Improved hardware and mounting techniques provide an opportunity to eliminate the need for correction for the local laser rotation, and would be a significant improvement for practical application. Future experimental work will validate the practical mounting concepts.

The DDPS systems can utilize traditional wired connectivity to exfiltrate drift data, but wireless communication nodes that would exfiltrate data across radio frequency (RF) links are under consideration. RF exfiltration to a central hub for access by the IOT would significantly simplify and economize sensor system mounting strategies.

Finally, the first pilot deployment of a DDPS system is being planned on a major building structure in support of S²HM objectives for the facility. The experimental campaign performed to-date has provided significant experience, but undoubtedly the first full-scale deployment will provide additional insight and lessons-learned.

Acknowledgements The work presented in this paper was supported in part by the U.S. Department of Energy (DOE) Office of Nuclear Safety. This support and the encouragement of Dr. Alan Levin of the Office of Nuclear Safety Research Program is greatly appreciated. The DDPS GEN1 and GEN2 sensors were fabricated at California State University Chico by engineers Jason Coates and Nicholas Repanich. The contributions of Professor Ian Buckle and Dr. Suiwen Wu in designing and conducting the University of Nevada shake table experiments are gratefully acknowledged.

References

1. American Society of Civil Engineers (ASCE) (2005) Seismic design criteria for structures, systems, and components in nuclear facilities. ASCE/SEI 43-05, Reston, VA
2. Bommer JJ, Magenes G, Hancock J, Penazzo P (2004) The influence of strong-motion duration on the seismic response of masonry structures. *Bull Earthq Eng* 2(1):1–26
3. Celebi M, Sanli A, Sinclair M, Gallant S, Radulescu D (2004) Real-time seismic monitoring needs of a building owner—and the solution: a cooperative effort. *Earthq Spectra* 20(2):333–346
4. Celebi M (2008) Real-time monitoring of drift for occupancy resumption. In: 14th world conference on earthquake engineering, Beijing China
5. Chen X (1995) Near-field ground motion from the landers earthquake. Report No. EERL 95-02, California Institute of Technology, Earthquake Engineering Research Laboratory, Pasadena, California, USA
6. Chen WM, Bennett KD, Feng J, Wang YP, Huang SL (1998) Laser technique for measuring three dimensional interstory drift. In: *Proceedings of the society for photonics and optics*, vol 3555, pp 305–310
7. Dai F, Dong S, Kamat VR, Lu M (2011) Photogrammetry assisted measurement of interstory drift for rapid post-disaster building damage reconnaissance. *J Nondestruct Eval* 30:201
8. Dai F, Lu M (2010) Assessing the accuracy of applying photogrammetry to take geometric measurements on building products. *J Constr Eng Manage* 136(2):242–250

9. Doebling SW, Farrar CR, Prime MB, Shevitz DW (1996) Damage identification and health monitoring of structural and mechanical systems from changes in their vibration characteristics: a literature review. Los Alamos National Laboratory, Los Alamos, NM
10. Hancock J, Bommer JJ (2006) A state-of-knowledge review of the influence of strong-motion duration on structural damage. *Earthq Spectra* 22(3):827–845
11. Hou S, Zeng CS, Zhang HB, Ou JP (2018) Monitoring interstory drift in buildings under seismic loading using MEMS inclinometers. *Constr Build Mater* 185:453–467
12. Hsu TY, Yin RC, Wu YM (2018) Evaluating post-earthquake building safety using economical MEMS seismometers. *Sensors* 18(5)
13. Lynch JP, Partridge A, Law KH, Kenny TW, Kiremidjian AS, Carryer E (2003) Design of piezoresistive MEMS-based accelerometer for integration with wireless sensing unit for structural monitoring. *J Aerosp Eng* 16(3):108–114
14. McCallen D, Larsen S (2003) NEVADA—a simulation environment for regional estimation of ground motion and structural response. Report UCRL-ID-152115, Lawrence Livermore National Laboratory
15. McCallen D, Petrone F, Coates J, Repanich N (2017) A laser-based optical sensor for broadband measurements of building earthquake drift. *Earthq Spectra* 33(4):1573–1598
16. *OpenSees* v 2.5.0 [Computer software]. Berkeley, CA, Pacific Earthquake Engineering Research Center, University of California
17. Pacific Earthquake Engineering Research Center Ground Motion Database (PEER). <https://ngawest2.berkeley.edu/>
18. Pakzad SN, Fenves GL, Kim S, Culler DE (2008) Design and implementation of scalable wireless sensor network for structural monitoring. *J Infrastruct Syst* 14(1):89–101
19. Petrone F, McCallen D, Buckle I, Wu S (2018) Direct measurement of building transient and residual drift using an optical sensor system. *Eng Struct* 176:115–126
20. Sabato A, Niezrecki C, Fortino G (2017) Wireless MEMS-based accelerometer sensor boards for structural vibration monitoring: a review. *IEEE Sens J* 17(2):226–235
21. Skolnik DA, Kaiser WJ, Wallace JW (2008) Instrumentation for structural health monitoring: measuring interstory drift. In: Proceedings of the 14th world conference on earthquake engineering, 12–17 Oct, Beijing China
22. Skolnik DA, Wallace JW (2010) Critical assessment of interstory drift measurements. *J Struct Eng* 136:1574–1584
23. Trifunac MD, Ivanovic SS, Todorovska MI (2001) Apparent periods of a building II: time-frequency analysis. *J Struct Eng* 127:527–537
24. Trifunac MD, Todorovska MI (2001) A note on the usable dynamic range of accelerographs recording translation. *J Soil Dyn Earthq Eng* 21:275–286
25. Yun F, Yong Z, Weimin C, Rong S, Shanglian H, Bennett KD (1999) Five dimensional interstory drift measurement with cross hair laser. *Acta Photonica Sinica* 28:1006–1009

Chapter 12

Hardware and Software Solutions for Seismic SHM of Hospitals



Carlo Rainieri, Danilo Gargaro and Giovanni Fabbrocino

Abstract Health facilities are strategic infrastructures at urban and territorial scale, particularly in the case of hazardous environmental events, such as earthquakes. Nevertheless, damage to structural as well as non-structural members, equipment and installations may affect their functionality. This is the reason why a scientific and technical effort is needed not only to improve structural performance, but also to deploy effective solutions and strategies aimed at quickly assessing the performance and health state of health facilities. The present paper provides an overview of hardware and software solutions for seismic Structural Health Monitoring (SHM) of health facilities. Attention is particularly focused on data processing and modal based damage detection procedures for timely detection of earthquake-induced damage. Moreover, the role of vibration measurements for seismic characterization and monitoring of non-structural components is discussed with reference to a real case study. Data from a permanent monitoring system are collected and manipulated to simulate the effect of damage. Such data are used to assess the anomaly detection performance of the system and validate the promising applicative perspectives of the described hardware/software architecture.

Keywords Health facilities · Seismic structural health monitoring · Hospital building · Modal based damage detection · Seismic damage indicators · Medical equipment

12.1 Introduction

Recent developments of knowledge on seismic hazard provide a clear image of the areas exposed to medium or high hazard worldwide, but also point out the relevance

C. Rainieri (✉) · G. Fabbrocino
Di. B. T. Department, University of Molise, Via F. de Sanctis, 86100
Campobasso, Italy
e-mail: carlo.rainieri@unimol.it

D. Gargaro
S2X s. r. l, Contrada Cese, 86100 Campobasso, Italy

© Springer Nature Switzerland AG 2019
M. P. Limongelli and M. Çelebi (eds.), *Seismic Structural Health Monitoring*, Springer
Tracts in Civil Engineering, https://doi.org/10.1007/978-3-030-13976-6_12

of the protection and safety management of existing structures. This is of paramount importance in the case of health facilities, whose structural design is often made according to out-dated codes or even in the absence of any consideration of seismic loads. Recent National and International codes are increasingly focusing the attention on such structures through the release of detailed rules concerning expected performance of new as well as existing hospital buildings in the case of refurbishment and/or structural upgrading interventions [23].

Hospitals and other health facilities are very complex systems since they perform a large number of functions supported by sophisticated equipment and technological distribution systems, thus resulting in a high vulnerability in seismic areas. The seismic vulnerability concerns structural, non-structural and administrative/operational aspects [23, 40]. As a result, a “safe hospital” can be defined as a facility whose services remain accessible and functioning at maximum capacity and in the same infrastructure during and immediately after the impact of a natural hazard [23]. After the event the structure should have been able to resist the force of the natural disaster, and equipment and furnishing should have remained undamaged, vital connections (water, electricity, medical gases, and so on) in service and the personnel able to provide medical assistance even in emergency conditions. However, existing hospitals often experience service interruption after an earthquake, mainly because of functional breakdown [11, 22, 35, 40].

Prompt detection of structural damage and/or of fault of equipment and installations after a ground motion therefore represents the main targets in the development of “smart health facilities” (SHFs), that is to say, health facilities equipped with integrated seismic Structural Health Monitoring (SHM) systems able to assess the health state of structural as well as non-structural components.

Assessing the performance and health state of equipment and installation is relevant also to detect the possible indirect losses associated to the loss of functions. For instance, a number of post-earthquake surveys allowed recognizing that damage to critical equipment and installations, such as tanks, lifeline services and so on, often causes severe downtime and indirect losses (medical gas leakage, for instance, can cause fire, explosions, and injuries). Thus, a thorough assessment of health facilities requires an integrated performance and health state assessment based the results of continuous monitoring of structural as well as non-structural components.

Seismic vulnerability assessment plays a primary role in the definition of the expected performance of the analyzed structure. It can be carried out according to qualitative or quantitative methods [17, 38]. In the context of seismic vulnerability assessment of hospitals, the former are usually used to analyze large stocks of structures and to prioritize interventions; on the contrary, the latter are used for individual buildings and require more detailed surveys and analyses. Among the qualitative methods, score assignment methods and, in particular, rapid visual screening (RVS) procedures are often adopted. Such methods suffer the subjectivity of the expert judgement [19, 24, 28]. Effective monitoring strategies can overcome this drawback: in fact, relevant parameters related to the system response and environmental factors are continuously recorded and processed in order to get relevant information about the health state of the system in operational conditions as well as after extreme events

such as earthquakes. Collecting measured data as well as information obtained from automated processing of those data supports the formulation of a more objective judgement about the overall health conditions and performance of the health facility, including equipment and other non-structural components. In other words, the implementation of effective SHM strategies allows setting a platform able to assist the management of the hospital in prompt and effective decision making about the need for maintenance of structure and equipment under operational conditions, as well as to support emergency management in the case of seismic events.

Since a high percentage of public spending [20] is for specialized healthcare personnel and sophisticated and costly equipment, hospitals must remain fully operational in the case of an earthquake. The implementation of effective seismic SHM strategies for hospitals, therefore, further remarks how this goal can be more effectively accomplished taking into account that functions and resilience of the system as a whole depend also on the ability of inspectors and managers to integrate theoretical evaluations with field measurements and their effective physical interpretation [1, 2]. The combination of effective SHM strategies with control and early warning systems can also contribute to enhance the global safety of hospitals against hazardous events [32].

The continuous monitoring of structural and non-structural components for seismic SHM purposes requires the definition of a sustainable monitoring strategy in terms of design of the measurement chain and implementation of distributed data processing and data reduction procedures [12]. In the following, an overview of hardware and software solutions for seismic SHM of health facilities is reported along with the definition of five criteria for a sustainable implementation of SHFs in earthquake prone areas. The expected performance of the SHF are associated to the integration into a single platform of different subsystems in the hospital as well as to the need for synthetic, intelligible information and scenarios to support decision making. Attention is therefore focused also on selected data processing and modal based damage detection procedures to support timely detection of earthquake-induced damage. Simulated damage is considered to assess the damage detection performance of the installed monitoring system and validate the promising applicative perspectives of the proposed hardware/software architecture. Moreover, the role of vibration measurements for seismic qualification and monitoring of non-structural components is discussed with reference to a real case study.

12.2 Design of Seismic SHM Systems for Health Facilities

The recent advances in civionics [15] encourage the development of smart structures, able to provide information about their health state in an automated way. Seismic protection of health facilities can take advantage of these new technologies. Risk reduction requires, first of all, a comprehensive assessment of the risk of the health facility starting from the identification of the hazard in the geographic area where it is located. However, the identification of vulnerabilities [40] is even more criti-

cal. In fact, design of the seismic SHM system heavily depends on the appropriate identification of the factors determining the seismic vulnerability of the investigated hospital. The most relevant factors determining a high seismic vulnerability of health facilities are:

- the large number of functions accomplished in hospitals, ranging from healthcare to office and administration, laboratory, warehouse and so on; they make the hospital a very complex system;
- the high level of occupancy and the presence of expensive medical equipment, potentially dangerous gases, and life support equipment requiring continuous power supply;
- the significant dependence on public services and infrastructures (power supply, water, clinical gases, oxygen, fuel, communications), and critical supplies (medicines, splints, bandages, and so on);
- the presence of heavy medical equipment (X-ray machines, backup generators, autoclaves and other pieces of specialized equipment) which are sensitive to vibrations and can be damaged by intense ground motions;
- the presence of hazardous materials, which can be the cause of indirect losses or contamination in the case of leakage.

The above-mentioned vulnerability factors dictate the distinction between structural and non-structural safety issues on one hand, and issues based on functional capacity on the other hand. Monitoring the structural response to hazards is the primary objective of seismic SHM. The remote assessment of the structural safety can take advantage of measurement of the structural response under operational conditions in order to identify incipient damage and eventual degradation phenomena, and assess the impact of earthquakes on structural integrity and functional capacity. Vibration based damage detection techniques able to identify and locate structural damage [8] can be profitably applied to this aim.

When non-structural elements, whose collapse may endanger occupants and equipment of the hospital, are of concern, checks of the stability of non-structural elements (supports, anchors...) as well as of the conditions of expensive medical equipment are additional monitoring objectives during and after an earthquake. Measuring and analyzing their performance provide relevant information to reduce downtime for functionality checks of equipment and networks after the impact of an earthquake. In fact, through appropriate monitoring strategies failures can be automatically and remotely detected.

Remote assessment of the performance and health state of structural as well as non-structural components allows the optimization of emergency management procedures, too. In fact, economic and human resources can be devoted to the maintenance of damaged systems only. Moreover, the organization of medical assistance in the early earthquake aftershock can take advantage of the knowledge of the conditions of relevant medical equipment and installations. Effective data processing procedures and information and communication technologies, therefore, play a fundamental role not only in the prompt definition of appropriate maintenance actions, but also in the

coordination of personnel after an earthquake. In addition, the combination of monitoring plans with basic early warning and control strategies can further enhance the overall safety of the health facility. The information coming from sensors can be used, for instance, to activate strategies for the immediate shutdown of elevators and other critical systems in the event of a potentially damaging earthquake, or to close valves in the case of damage to distribution systems (see, for instance: [42, 29]).

The previous discussion remarks how an effective reduction of the overall vulnerability of health facilities requires the development of integrated monitoring strategies concerning structural as well as non-structural components. An effective seismic SHM of hospitals cannot skip the installation of an appropriate number of sensors, of different types and performance, and, above all, the implementation of efficient and fully automated data processing procedures. The latter acquire sensor output, process data and eventually provide an alarm. Distributed data acquisition and parallel computation, data reduction and storage become critical in the implementation of seismic SHM systems for hospitals due to the need of acquiring data from a large number of heterogeneous sensors. Five criteria can be therefore identified for the sustainable design and implementation of seismic SHM systems for health facilities: Accuracy, Budget compliance, Computational burden, Durability, Ease of use. Their impact on the selection of hardware components, technologies and data processing procedures is discussed in detail in the following sections.

12.2.1 Accuracy

Sensor heterogeneity requires not only an appropriate design of the architecture of the system for data acquisition and storage, but also the selection of appropriate data processing procedures able to extract relevant information from the raw data which, otherwise, would provide limited value to the end-user. The extraction of relevant information from raw measurements is possible through a proper choice of the sensors and the measurement chain, which must be able to resolve the response of the monitored subsystems. The different nature of structural and non-structural components implies that there is not a unique sensor able to fit the needs of every application, as summarised in Table 12.1. The physical quantities of interest and the monitoring objectives are responsible for the final sensor choice. Those might depend also on the nature of the component and the expected vulnerability issues. For instance, if global assessment methods based on a number of accelerometers deployed on the structure and vibration based damage detection algorithms can provide relevant information about the health state of the structure, non-structural elements might require very different sensors and data processing strategies. As an example, connections and anchorages of tanks and large medical devices (CAT scanners, X-ray machines) can be more effectively monitored by strain gauges; FBG sensors are usually appropriate to monitor settlements of distribution systems; pressure sensors are frequently applied to detect losses in tanks and distribution systems, while medical equipment sensitive to vibrations require acceleration measurements but the employed sensors

Table 12.1 Monitoring objectives and recommended sensors

Item	Monitoring objective	Sensors
Structural safety	Overall structural performance and health assessment	High sensitivity, seismic accelerometers
	Structural detailing (connections, joints...)	Strain gauges, displacement transducers, fiber optic sensors
	Foundations (vulnerability to floods, differential settlement, liquefaction)	Fiber optic sensors
Non-structural safety	Connections and anchorages	Strain gauges, displacement transducers
	Large medical devices (CAT scanners, X-ray machines), medical equipment sensitive to vibrations	Accelerometers, displacement transducers
	Settlements of distribution systems	Fiber optic sensors
	Losses in tanks and distribution systems	Pressure sensors
	Antennas and lightning rods	Anemometers, corrosion sensors, accelerometers
	HVAC, pipes, connection, valves	Humidity sensors, fiber optic sensors, temperature sensors, pressure sensors, accelerometers
Safety based on functional capacity	Fire protection systems	Pressure sensors
	Alarm activation/deactivation	Accelerometers, displacement transducers
	Elevators	Seismic switches
	Valve shut off	Seismic switches
Hazard	Seismic hazard	Accelerometers, seismometers

usually show very different technical features with respect to the accelerometers commonly used to monitor the structural response.

12.2.2 Budget Compliance

Modular and wireless architectures for data acquisition and transmission are recommended to develop seismic SHM systems for hospitals able to fulfill budget con-

straints. In fact, consistent savings are usually associated to a relevant reduction in the use of cables; moreover, additional sensors and measurement nodes can be progressively added according to budget availability and rational prioritization, thus ensuring the scalability of the data acquisition systems over time.

The adoption of modular architectures requires the design of a versatile monitoring system, with distributed computational capabilities and a master-slave organization of servers to account for the specific needs of the different subsystems forming the health facility. As the number of sensors increases over time, the adoption of modular architectures and wireless sensing units leads also to a minimization of the impact of the monitoring system on the functions in the hospital.

12.2.3 Computational Burden

The need for a rapid response from the monitoring system after an earthquake implies that data must be collected, stored, assessed for validity and processed within a short time. Taking into account the number and variety of the installed sensors, the use of modular or even wireless architectures might be advantageous. In fact, they allow grouping sensors into clusters characterized by different data acquisition and processing settings. The main drawback is the need for strategies ensuring simultaneous sampling when this is critical, such as, for instance, in modal based damage detection. In addition to the modular architecture, an efficient data management is ensured by the implementation of relational databases that can simplify data storage, data mining and data fusion.

Automated modal identification techniques [30, 31] perform an effective data reduction and provide the synthetic information needed by vibration based damage identification techniques for health assessment of structures [8]. The collection, in the same database, of synthetic data correlated to the structural health and performance on one hand, and of data and information coming from different sensors and related to different physical variables on the other hand, allows exploiting the opportunities of advanced data mining and data fusion procedures—for instance, for removal of environmental effects on damage sensitive features [16].

On the analogy with monitoring of the structural response, appropriate sensors and analysis tools make possible the prompt fault detection of critical equipment and installations. Medical devices, tanks, adduction systems, power supply systems and backup generators, heat, ventilation and air conditioning (HVAC) systems significantly affect the in-service conditions of health facilities. Advanced techniques for machine condition monitoring and fault diagnosis [41] can process the acquired data and provide objective information about the functionality of equipment and installations, thus supporting the definition of priorities in maintenance interventions.

12.2.4 Durability

Service life of the SHM system depends on robustness of the equipment and it can take advantage of some redundancy and the adoption of distributed sensing and computing architectures. If possible, redundant schemes should be adopted for data transmission to make the SHM system more robust in the case of strong motions. However, this should be accompanied by local data processing procedures able to reduce the amount of data to be transmitted, in particular in the post-earthquake phase.

A database working as a collector of data and information from the peripheral nodes also plays a primary role to ensure durability. The adopted architecture, in fact, must prevent downtime when individual components are in need of replacement because they are out of order or obsolete. The setting of different databases for either raw data or synthetic information collection is a possible strategy to simplify the replacement of components without changes in the overall architecture of the monitoring system. Exploiting the opportunities related to the use of databases, only local settings are required when hardware components are added or replaced, thus ensuring the durability of the SHM system with minor maintenance efforts.

12.2.5 Ease of Use

The seismic SHM system must provide information about the conditions of the different subsystems of the health facility that can be readily understood by the technicians and managers who have in charge the operational maintenance or the coordination of rescue operations in the case of an emergency. As an example of the impact of intelligible information on the overall safety, checking the variations of selected damage features in a few minutes after the earthquake can help the staff involved in the emergency management in rapidly identifying and implementing the most appropriate interventions (for instance, replacement of components in distribution systems) to keep the hospital fully operational. The continuous monitoring of the health state and performance of hospitals, including equipment and installations, and the return of intelligible information to the management can also support the formulation of disaster mitigation plans and the prioritization of investments for safety of people and goods.

12.3 Data Processing for Seismic SHM of Hospitals

A number of past destructive earthquakes have highlighted how structural damage as well as fault of medical equipment and installations can jeopardize the functionality of the hospital at a time of large demand of medical assistance. Among these events,

one of the most relevant is the San Fernando Valley earthquake, a 6.6 magnitude event occurred in California in 1971. It resulted in the collapse of several hospital buildings in the area struck by the ground motion.

Following the earthquake, the United States Geological Survey (USGS) issued a large structural monitoring program focused on medical buildings across the national territory (<https://earthquake.usgs.gov/monitoring/nsmp/buildings/va.php>). They have been instrumented by dense arrays of seismic sensors to resolve the structural response to strong ground shakings as well as under operational conditions.

On the analogy with the American experience, a number of hospitals are currently monitored in Italy under a survey program issued by the Italian Civil Protection (http://www.protezionecivile.gov.it/jcms/en/osservatorio.wp?request_locale=en). When a significant earthquake occurs, the installed monitoring system records the accelerations at the ground and on the structure. The data are immediately sent to the central server in Rome, in order to automatically process them and obtain a synthetic report with the maximum measured values, some descriptive parameters related to the incoming earthquake, and indication of possible presence of structural damage. Hospitals that are permanently monitored in the framework of the Seismic Observatory of Structures program are instrumented by accelerometers distributed at every floor of the building and on the ground. A simplified sensor layout is also adopted in some cases, with measurements of the input ground motion and of the structural response at the top floor only.

The above-mentioned case studies remark the relevant role of vibration-based SHM and damage detection methods [9] as valuable tools to remotely assess the structural integrity of hospital buildings in a quantitative manner. A comprehensive review of vibration-based SHM and damage detection techniques is out of the scope of the present study. The interested reader can refer to the literature for more details [8, 9]. However, it is worth pointing out here that a variety of damage detection techniques and damage sensitive features have been developed over the years based on vibration data, and their effectiveness is influenced also by the type of structure under consideration, the sensor layout and the adopted damage features. This implies, in particular, that the appropriate selection of the damage indicators and the corresponding threshold values represents a critical aspect in the development of the SHM system, since the success or failure of the algorithm in detecting the presence of damage depends on those choices. This section therefore describes the SHM techniques that are commonly used to monitor hospital buildings in earthquake prone areas. While vibration-based damage detection techniques can be classified in two main groups, model-based methods and data-driven methods, model-based methods are not herein considered. In fact, they require a preliminary numerical model of the structure in the reference condition and it must be optimized in terms of correlation with the corresponding experimental estimates of the modal parameters. As a result, model-based methods are typically time consuming, computationally expensive, and might suffer from divergence or non-uniqueness of the solution [21]. On the contrary, data-driven methods rely on the measured data only and, as a result, they fit the requirements of continuous, automated and near real-time SHM.

An alternative strategy for damage detection is based on the computation of the interstory drift ratio [14, 36]. This is a demand parameter commonly used in the design of new structures as well as to assess the seismic performance of existing buildings. In particular, the most recent seismic codes (see, for instance, [10]) define four performance levels (Operational, Immediate occupancy, Life safety, and Collapse prevention) of buildings under seismic loads. These levels refer to limit drift values, which can vary depending on the type of structure. As a result, comparing the drift ratios obtained from the measured accelerations with the limit values associated to the different performance levels the damage state of the monitored structure after an earthquake can be rapidly assessed. The main drawbacks of the method are related to the need of monitoring the structural response at every floor, and to the assumption that the lateral deformation is dominated by shear. In addition, the computation of floor displacements by double integration of acceleration waveforms poses additional challenges in terms of reliability of monitoring results [37]. Despite these caveats, double integration still represents one of the most frequently used approaches to obtain displacements and, therefore, interstory drifts [37].

Careful data processing is needed in the computation of velocities and displacements by integration of acceleration data in order to minimize the errors [3, 4]. In fact, velocity $v(t)$ and displacement $d(t)$ are obtained from the acceleration $a(t)$ as follows:

$$v(t) = v(0) + \int_0^t a(\tau) d\tau \quad (1)$$

$$d(t) = d(0) + v(0) \cdot t + \int_0^t \left(\int_0^t a(\tau) d\tau \right) dz \quad (2)$$

where $v(0)$ and $d(0)$ are the initial velocity and displacement, respectively; if these are null the displacement response is given by:

$$d(t) = \int_0^t \left(\int_0^t a(\tau) d\tau \right) dz \quad (3)$$

As a consequence, if the initial conditions in terms of displacement and velocity are not null results are biased [25]. However, the influence of not exactly zero initial conditions, such as those associated to ambient vibrations, can be neglected when the response to large amplitude input ground motions is analyzed [33].

Additional sources of error also come from the offset or the noise present in the raw data. For this reason data have to be high-pass filtered, and the same filter has to be applied to all measurement channels to preserve data synchronization.

Time domain integration by the trapezoidal rule is frequently applied in the practice. However, recent studies have shown that other approaches in the literature are more accurate, while time domain integration by the trapezoidal rule is still acceptable for low frequencies—relative to the sampling frequency—[3, 4].

The modal parameters are also frequently used as damage sensitive features. Since they depend on the physical properties (mass, stiffness and damping) of the structure, and assuming that damage causes a change in the mass or stiffness properties of the monitored structure, tracking the variations of the modal parameters over time represents a valuable tool to detect anomalies in the structural response. In particular, if a reference set of modal parameters is available for the healthy condition of the structure, estimating the modal parameters after an earthquake and comparing them to the baseline condition allows detecting possible earthquake-induced damage.

Experimental tests on shaking tables have shown that natural frequencies are very sensitive to earthquake-induced damage, but they are of limited value when locating damage is necessary. On the contrary, mode shapes can support the identification of damage location, but significant changes in the mode shapes are observed only for severe damage conditions [39].

Modal-based damage detection is increasingly applied for seismic SHM because of the recent development of reliable and accurate automated output-only modal identification procedures. However, there are still some drawbacks that prevent its extensive application. They are mainly related to the sensitivity of the modal parameters to environmental and operational variables. Temperature, traffic, humidity are frequently recognized as the causes of fluctuations of the modal parameters. Thus, the influence of environmental and operational variables on the modal parameter estimates has to be compensated in order to increase the reliability of modal based damage detection [34].

12.4 Seismic SHM of Hospitals: Notes from a Field Experience

The potentialities of modal based SHM in ensuring timely detection of earthquake-induced damage are herein discussed with reference to a real case study. Two nearby reinforced concrete structures belonging to the main hospital in Campobasso (Southern Italy) are permanently monitored [12]. The vibration response is continuously recorded and analyzed in order to track the evolution of the modal parameters over time. Reliability of modal tracking and seismic SHM based on modal-based damage detection are discussed by analyzing the response of the structure in operational conditions as well as after seismic events. In the latter case, simulated damage is considered to assess the damage detection performance of the installed monitoring system.

The SHM system installed on the Campobasso's main hospital takes advantage of an innovative procedure for the automated analysis of the operational vibration response of the monitored structure and the extraction of the modal parameters [31]. The algorithm, called ARES[®] (acronym for Automated modal paRameter Extraction System) is able to provide accurate and precise modal parameter estimates without statically set thresholds and parameters. The key feature of the algorithm is, therefore, the absence of analysis parameters that have to be tuned at each new monitoring

application. Reliability and accuracy of the algorithm have been demonstrated by a number of tests on simulated datasets, obtaining a success rate larger than 99% [31]. However, as mentioned in the previous section, environmental and operational variables might have a significant influence on the collected estimates. It has been shown that the change of natural frequencies due to environmental factors like the temperature is often of the same order of magnitude of the variation caused by damage [27]. Thus, the environmental influence on reliability and robustness of SHM has to be considered.

The non-linear relationship with the mechanical properties of materials and the boundary conditions, and the typically large thermal inertia of structures make direct modeling of the environmental influence on the dynamic response of a structure difficult or even impossible. Black-box models are therefore frequently applied to map the changes of the modal properties with a set of monitored environmental and operational variables. When measuring these variables is impossible, alternative data processing methods not requiring the explicit measure of the environmental variables can be applied. These methods are effective in removing the environmental effects on the modal property estimates as long as their variations due to damage are in some way orthogonal or uncorrelated to those caused by the environmental variability [7]. An extensive review of the methods for compensation of the environmental and operational effects on modal properties for SHM purposes can be found elsewhere [34].

In the present application the influence of environmental factors on natural frequency estimates is not removed. In fact, its compensation often requires the availability of large datasets of modal properties referring to the healthy state of the structure [18]. Moreover, with the aim of developing an SHM strategy readily available to detect earthquake-induced damage, a complete characterization of the environmental influence is omitted, while limited data collected before and after an earthquake are considered and analyzed for anomaly detection.

Assuming that there is only one dominant environmental variable (for instance, the temperature), the proposed SHM strategy is based on 2-means clustering applied to the first two principal components obtained from the simultaneous analysis of pre-event data and post-event data. Possible earthquake-induced damage is detected by measuring the distance between the identified centroids. In order to quantify the sensitivity to damage of the SHM strategy, seismic damage has been simulated by a localized drop in the sequence of natural frequency estimates, and a threshold for damage detection has been defined according to the results of sensitivity analyses.

12.4.1 Structural Monitoring of Campobasso's Main Hospital

The vibration-based SHM system installed at the Campobasso's main hospital is briefly illustrated, and some results of automated identification of the modal param-



Fig. 12.1 View of the monitored hospital buildings in Campobasso (Southern Italy)

eters are presented to highlight the influence of temperature and weak earthquakes on the fundamental natural frequencies.

The main hospital in Campobasso consists of a number of reinforced concrete buildings designed and built according to out-dated seismic design codes. The vibration-based SHM system has been installed on two joint buildings hosting the inpatient wards. They have overall dimensions of about $78\text{ m} \times 14\text{ m}$ in plan and 30 m in elevation. The two buildings are denoted as Block V and Block VI, respectively (Fig. 12.1), and they are separated by a small structural joint.

The vibration response of the structure is continuously recorded by sixteen force-balance accelerometers installed at two upper levels along two orthogonal directions. Observability of translational as well as torsional modes is ensured by the location of the sensors at opposite corners of the block plans. The accelerometers are wired to a centralized data acquisition system. Data are sampled at 100 Hz and stored into a local MySQL database. ARES ensures a continuous tracking of the fundamental

modal parameters of the structure. The monitoring system started operating on March 24th, 2016, and the first four modes are continuously monitored over time.

The following mode shapes characterize the fundamental modes of the structure:

- the first mode consists in global bending of the two blocks in the transverse direction;
- the second mode consists in global bending of the two blocks in the longitudinal direction;
- the third mode is a global torsion involving the two blocks;
- torsion with counter rotating blocks characterizes the fourth mode.

The small structural joint that divides the two nearby blocks significantly influences the modal parameters. Inspecting the natural frequency time series in Fig. 12.2 systematic swings occurring every day can be recognized; the natural frequencies decrease in the night and gradually increase in the morning until the maximum value typically occurring in the early afternoon.

The primary influence of temperature on the observed variations of the natural frequency estimates can be recognized by comparing the time history of the fundamental frequency with the local temperature in Campobasso (Fig. 12.3).

Direct sun radiation along the predominant longitudinal extension, and the very small joint in between the two blocks are probably responsible for the increase of the fundamental frequencies with the temperature. In fact, when the temperature increases the thermal expansion causes a decrease in the distance between the two blocks, and the interlocking yields some stiffness increase in the longitudinal direction.

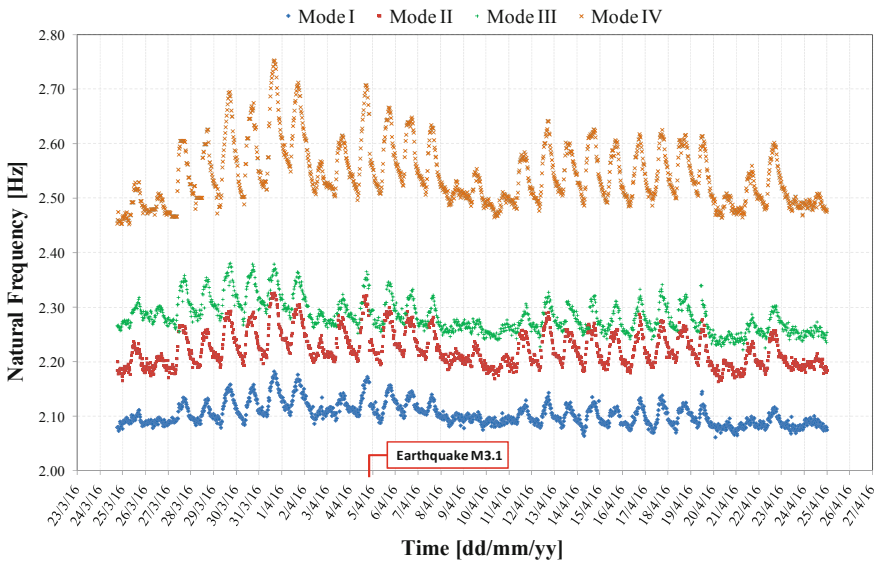


Fig. 12.2 Sample tracking of the fundamental natural frequencies the hospital building

The SHM system has also collected the structural responses to a number of earthquakes occurred since the beginning of monitoring. Some of these events caused a sudden drop of natural frequencies at the time of the event as a result of amplitude dependent changes of the contribution of non-structural components to the global stiffness of the structure, while the original pattern was soon recovered after the event. As an example, the $M_w = 3.1$ earthquake, occurred on April 4th, 2016 (<http://cnt.rm.ingv.it/event/6564571>) caused peak accelerations of 0.015 and 0.0075 g on top of the structure in the longitudinal and transverse direction, respectively, and a visible drop in the sequences of estimated natural frequencies at the time of the event (Fig. 12.4).

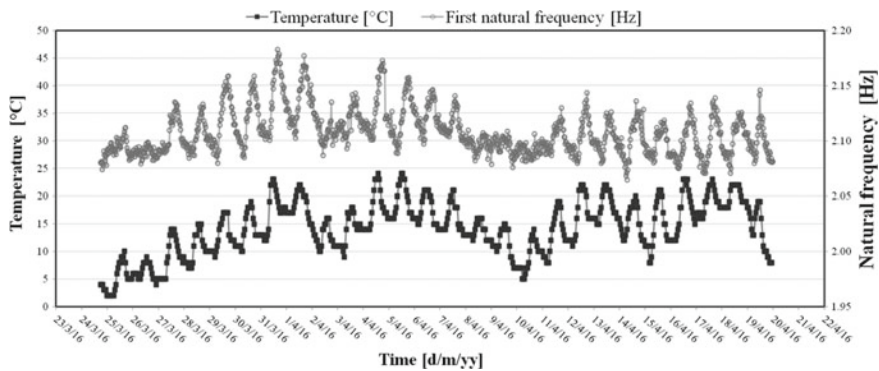


Fig. 12.3 Comparison between the fundamental frequency and local temperature

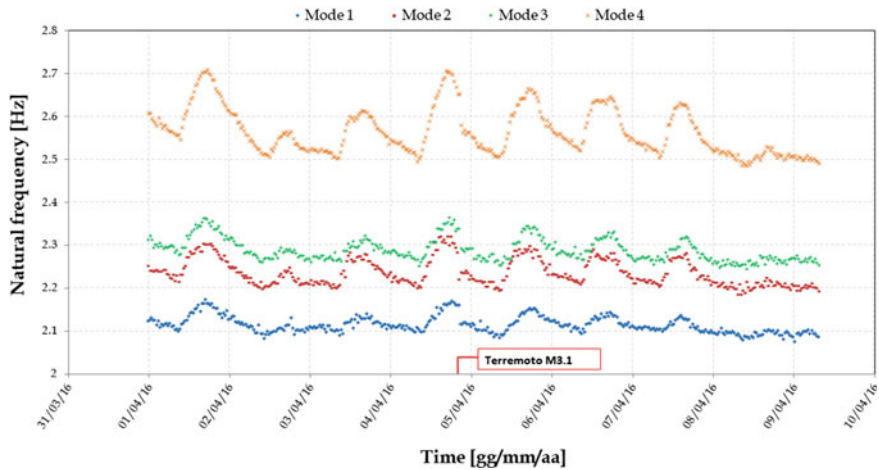


Fig. 12.4 Earthquake induced drop of the fundamental natural frequencies

12.4.2 Detection of Earthquake-Induced Damage

Analyzing the distribution of data in the space spanned by the first two principal components can provide an effective means to detect anomalies in the structural response when the natural frequency variability depends on a single environmental factor and the damage induced variations are in some way orthogonal or uncorrelated to those caused by the environmental variables. In fact, in the presence of a single dominant environmental factor, which is responsible for most of the variability of natural frequencies in operational conditions, the second principal component accounts for the damage induced variability of the estimates. Assuming that the environmental variability remains the same after the seismic event and that the earthquake-induced damage causes a permanent drop in the natural frequency time series, damage of increasing magnitude yields a separation of the data in two clusters. The distance between the centroids, which depends on both the dominant environmental factor and the damage, can be used as damage sensitive feature, and anomalies can be detected by the definition of an appropriate threshold. In order to demonstrate the damage detection capability of the proposed strategy, earthquake induced damage is simulated and applied to monitoring data collected on April 2017 and referring to normal operational conditions. These data also showed a clear influence of temperature on natural frequencies.

Figures 12.5, 12.6, 12.7 compare the identified clusters and the actual clusters of data (pre-event and post-event data of equal consistency) in the space of the first two principal components; different simulated damage levels are considered.

As expected, 2-means clustering yielded two clusters even in the absence of damage. However, it is interesting to note that the separation between the clusters as well as the distance between the identified centroids increase at increasing damage levels.

The illustrated method seems to ensure reliable detection of earthquake-induced damage even in the presence of limited amount of data (one month of monitoring data in the present case) and of relevant temperature influence, provided that a minimum frequency changes in the order of 3% occurs.

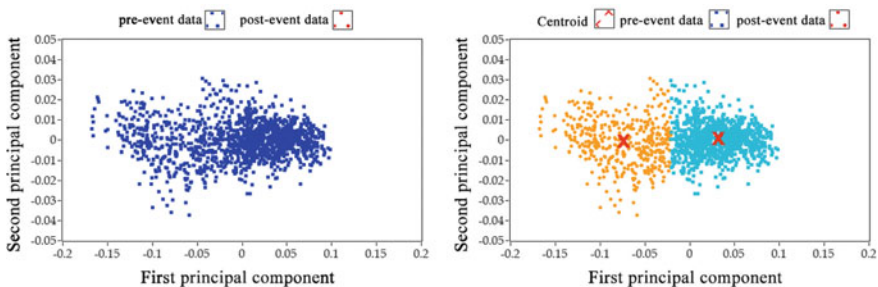


Fig. 12.5 Pre- and post-event data and clustering results corresponding to different simulated damage levels and equal amount of data in the two groups: no damage

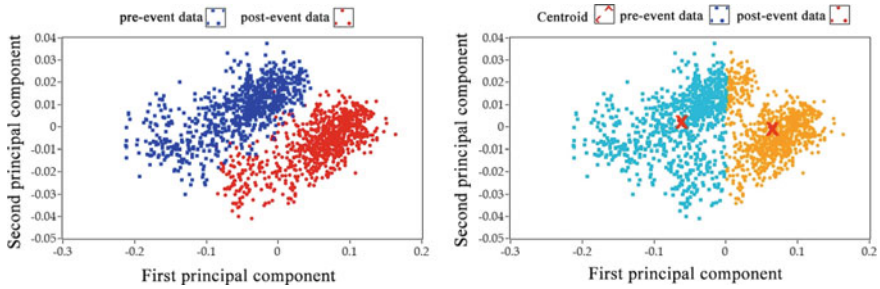


Fig. 12.6 Pre- and post-event data and clustering results corresponding to different simulated damage levels and equal amount of data in the two groups: 2% natural frequency variation

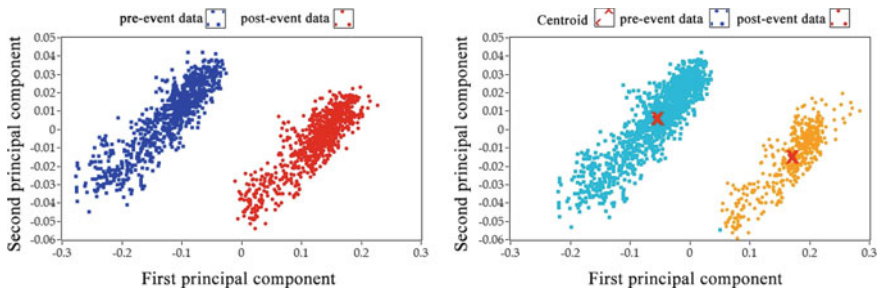


Fig. 12.7 Pre- and post-event data and clustering results corresponding to different simulated damage levels and equal amount of data in the two groups: 5% natural frequency variation

12.4.3 Dynamic Testing of Equipment

The seismic response in terms of acceleration at a floor of the structure becomes the input ground motion for equipment and furniture standing at that floor. If they are rigidly connected to the structure, the seismic force on the non-structural element depends on its elevation z with respect to the structural height H and on the ratio between the fundamental frequency of the structure and that of the considered non-structural element [6]. Thus, experimental modal testing of equipment represents a fundamental step in view of its seismic qualification and vulnerability assessment.

In the framework of the monitoring program for the Campobasso's main hospital, dynamic tests have been carried out on two drug dispensers placed, respectively, at the first and the fifth floor of the structure. The objectives of the tests were the identification of the dynamic properties of the dispensers and the evaluation of the dynamic interaction with the structure in view of equipment monitoring.

For each dispenser, output-only modal identification tests have been carried out [13]. Four piezoelectric accelerometers recorded the vibration response of the dispenser. The modal parameters have been estimated by means of well-established methods, such as the Frequency Domain Decomposition (FDD) [5] and the Covariance Driven Stochastic Subspace Identification [26].

The fundamental modes of the dispensers have been clearly identified. In view of seismic assessment, it is worth noting that the fundamental frequency of the Busterspid is about 6 Hz, quite higher than the fundamental frequency of the blocks.

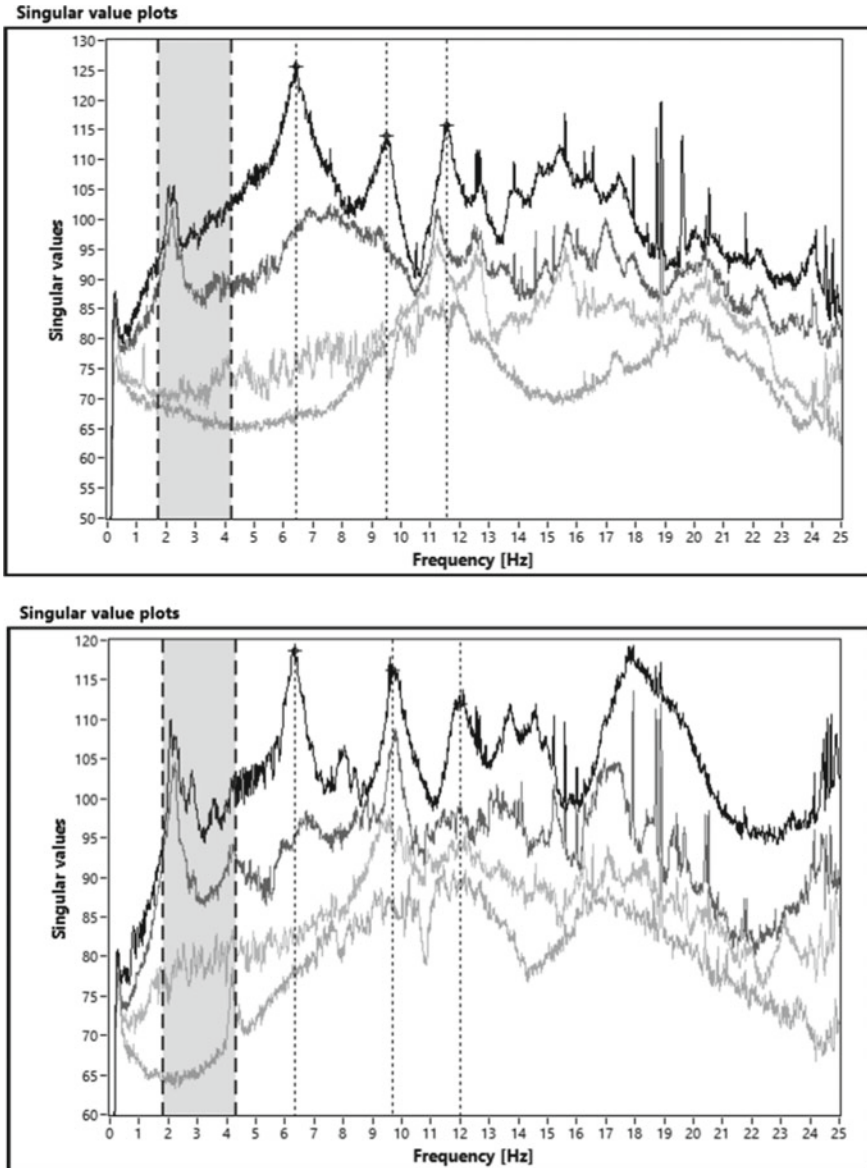


Fig. 12.8 Singular value plots: dispenser at the first floor (top) and at the fifth floor (bottom), structural frequency bandwidth is greyed

However, the singular value plots obtained from the FDD method (Fig. 12.8) put in evidence some effects of the input represented by the dynamic response of the structure in operational conditions. In fact, some peaks can be observed around 2 Hz, corresponding to the fundamental frequencies of the blocks (see also Fig. 12.4). Dynamic interaction effects are more evident for the dispenser located at the fifth floor than for the one at the first floor. Thus, dynamic interaction effects resulted in spurious frequencies in the vibration response of the dispensers. The implementation of modal-based damage detection strategies for medical equipment has to take into account this phenomenon, which might affect the reliability of results. Thus, robust modal identification and monitoring procedures, able to discard spurious frequencies, are needed.

12.5 Conclusions

The present study has remarked the importance of an appropriate design of the seismic SHM system for health facilities, defining hardware as well as data processing requirements to properly analyze the response of the different subsystems (structure, equipment, installations and so on) forming the hospital, taking into account the critical nature and interdependence of the various subsystems. The integration of different sensors and automated analysis procedures allows the assessment of the short-term impact due to earthquakes as well as the long-term deterioration due to physical aging and routine operation. Anomalies can be detected by continuous processing of the incoming data. At the same time, the adoption of local data processing procedures, such as the automated dynamic identification of the structure, leads to a significant data reduction which is relevant not only for data transmission in critical conditions but also to reduce the costs related to data storage.

A seismic SHM strategy able to detect earthquake induced damage in the presence of a single dominant environmental variable affecting the modal parameter estimates has been also presented. It is based on 2-means cluster analysis of data in the space of the first two principal components. Simulating earthquake induced damage by a frequency drop at the time of the event, in agreement with experimental observations, the method is able to detect damage provided that it causes a minimum frequency shift in the order of 3%.

Finally, it is worth pointing out that the implementation of modal-based damage detection strategies for medical equipment has to take into account dynamic interaction effects with the hosting structure because they can affect the reliability of output-only modal identification results.

Acknowledgements The present work has been carried out in the framework of a broader research project issued by ASREM—Molise Region Health Authority, on safety and structural health monitoring of the regional health facilities. Authors also acknowledge the support of the ReLuis-DPC Executive Project 2014–2018.

References

1. Applied Technology Council (2002) ATC 51-1, Recommended U.S.—Italy collaborative procedures for earthquake emergency response planning for hospitals in Italy, Redwood City, USA
2. Applied Technology Council (2003) ATC 51-2, Recommended U.S.—Italy collaborative guidelines for bracing and anchoring non-structural components in Italian hospitals, Redwood City, USA
3. Brandt A (2011) *Noise and vibration analysis—signal analysis and experimental procedures*. Wiley, Chichester, UK
4. Brandt A, Brincker R (2014) Integrating time signals in frequency domain—comparison with time domain integration. *Measurement* 58:511–519
5. Brincker R, Zhang L, Andersen P (2001) Modal identification of output-only systems using frequency domain decomposition. *Smart Mater Struct* 10:441–445
6. De Sortis A, Gregolo S, Di Pasquale G, Papa S, Dolce M, Rettore GF (2009) Linee guida per la riduzione della vulnerabilità di elementi non strutturali arredi e impianti. Presidenza del Consiglio dei Ministri, Dipartimento della Protezione Civile, Roma (in Italian)
7. Deraemaeker A, Reynders E, De Roeck G, Kullaa J (2008) Vibration-based structural health monitoring using output-only measurements under changing environment. *Mech Syst Signal Process* 22:34–56
8. Doebling SW, Farrar CR, Prime MB, Shevitz DW (1996) Damage identification and health monitoring of structural and mechanical systems from changes in their vibration characteristics: a literature review. Technical report LA-13070-MS, UC-900, Los Alamos National Laboratory, New Mexico 87545, USA
9. Farrar C, Worden K (2013) *Structural health monitoring—a machine learning perspective*. Wiley, Chichester, UK
10. Federal Emergency Management Agency (2003) FEMA 450—NEHRP Recommended provisions and commentary for seismic regulations for new buildings and other structures, Washington, USA
11. Federal Emergency Management Agency (2007) FEMA 577—Design guide for improving hospital safety in earthquakes, floods, and high winds: providing protection to people and buildings, Washington, USA
12. Gargaro D (2018) *Analisi modale output-only e monitoraggio strutturale per la caratterizzazione dinamica di componenti strutturali e non strutturali in complessi ospedalieri*. Tesi di Dottorato in Bioscienze e Territorio, indirizzo Territoriale, Università del Molise, XXX Ciclo (in Italian)
13. Gargaro D, Rainieri C, Fabbrocino G (2017) A step towards the implementation of a smart health facility: vibration-based identification and monitoring of structures and equipment. In: *Proceedings of the 16-th world conference on earthquake engineering 16WCEE 2017*. Paper no. 1469
14. Hou S, Zeng C, Zhang H, Ou J (2018) Monitoring interstory drift in buildings under seismic loading using MEMS inclinometers. *Constr Build Mater* 185:453–467
15. Klowak C, Rivera E, Mufti A (2005) Implementation of civionics in a second generation steel-free bridge deck. In: *Proceedings of SPIE—the international society for optical engineering, Nondestructive evaluation and health monitoring of aerospace materials, composites, and civil infrastructure IV*, vol 5767. <https://doi.org/10.1117/12.604903>
16. Lämsä V, Kullaa J (2008) Data normalization with partially measured environmental or operational variables. In: *Proceedings of the 4-th European workshop on structural health monitoring*, Cracow, Poland
17. Lang K (2002) *Seismic vulnerability of existing buildings*. Institute of Structural Engineering, Swiss Federal Institute of Technology, Zurich, Switzerland

18. Magalhães F, Cunha A, Caetano E (2012) Vibration based structural health monitoring of an arch bridge: from automated OMA to damage detection. *Mech Syst Signal Process* 28:212–228
19. Miniati R, Iasio C (2012) Methodology for rapid seismic risk assessment of health structures: case study of the hospital system in Florence, Italy. *Int J Disaster Risk Reduct* 2:16–24. <https://doi.org/10.1016/j.ijdr.2012.07.001>
20. Ministero della Salute (2003) Raccomandazioni per il miglioramento della sicurezza sismica e della funzionalità degli ospedali, Rome, Italy (in Italian)
21. Mottershead JE, Friswell MI (1993) Model updating in structural dynamics: a survey. *J Sound Vib* 167:347–375
22. Myrtle RC, Masri SF, Nigbor RL, Caffrey JP (2005) Classification and prioritization of essential systems in hospitals under extreme events. *Earthq Spectra* 21:779–802
23. PAHO (2008a) Hospital safety index—guide for evaluators. Washington, USA
24. PAHO (2008b) Hospital safety index: evaluation forms for safe hospitals. Pan American Health Organization, Washington, USA, Series Hospitals Safe from Disasters 2, pp 34. ISBN 9789275132579
25. Park KT, Kim SH, Park HS, Lee KW (2004) The determination of bridge displacement using measured acceleration. *Eng Struct* 27:371–378
26. Peeters B (2000) System identification and damage detection in civil engineering. Ph.D. thesis, Katholieke Universiteit Leuven, Leuven, Belgium
27. Peeters B, De Roeck G (2001) One-year monitoring of the Z24-Bridge: environmental effects versus damage events. *Earthq Eng Struct Dyn* 30:149–171
28. Perrone D, Aiello MA, Pecce MR, Rossi F (2015) Rapid visual screening for seismic evaluation of RC hospital buildings. *Structures* 3:57–70
29. Ptilakis K, Karapetrou S, Bindi D, Manakou M, Petrovic B, Roumelioti Z, Boxberger T, Parolai S (2016) Structural monitoring and earthquake early warning systems for the AHEPA hospital in Thessaloniki. *Bull Earthq Eng*. <https://doi.org/10.1007/s10518-016-9916-5>
30. Rainieri C, Fabbrocino G (2010) Automated output-only dynamic identification of civil engineering structures. *Mech Syst Signal Process* 24:678–695
31. Rainieri C, Fabbrocino G (2015) Development and validation of an automated operational modal analysis algorithm for vibration-based monitoring and tensile load estimation. *Mech Syst Signal Process* 60–61:512–534
32. Rainieri C, Fabbrocino G, Cosenza E (2010) Integrated seismic early warning and structural health monitoring of critical civil infrastructures in seismically prone areas. *Struct Health Monit An Int J* 10:291–308
33. Rainieri C, Gargaro D, Fabbrocino G, Maddaloni G, Di Sarno L, Prota A, Manfredi G (2018) Shaking table tests for the experimental verification of the effectiveness of an automated modal parameter monitoring system for existing bridges in seismic areas. *Struct Control Health Monit* 25. <https://doi.org/10.1002/stc.2165>
34. Rainieri C, Magalhaes F, Gargaro D, Fabbrocino G, Cunha A (2018) Predicting the variability of natural frequencies and its causes by second-order blind identification. *Struct Health Monit*. <https://doi.org/10.1177/1475921718758629>
35. Schultz CH, Koenig KL, Lewis RJ (2003) Implications of hospital evacuation after the Northridge, California, earthquake. *N Eng J Med* 348:1349–1355
36. Shan J, Yang HTY, Shi W, Bridges D, Hansma PK (2013) Structural damage diagnosis using interstory drift-based acceleration feedback with test validation. *J Eng Mech* 139:1185–1196
37. Skolnik DA, Wallace JW (2010) Critical assessment of interstory drift measurements. *J Struct Eng* 136:1574–1584
38. Trendafiloski GS (2003) GIS-oriented method for development of probabilistic earthquake scenarios. Institute of Earthquake Engineering and Engineering Seismology, Skopje, Macedonia
39. Ulusoy HS, Kalkan E, Banga K (2013) Real-time seismic monitoring of veterans affairs hospital buildings. In: Proceedings of the SPIE smart structures conference, San Diego, CA, USA

40. WHO—regional office for Europe (2006) Health facility seismic vulnerability evaluation—a handbook, Copenhagen, Denmark
41. Widodo A, Yang B-S (2007) Support vector machine in machine condition monitoring and fault diagnosis. *Mech Syst Signal Process* 21:2560–2574
42. Wu S, Cheng MH, Beck JL, Heaton TH (2016) An engineering application of earthquake early warning: ePAD-based decision framework for elevator control. *ASCE J Struct Eng* 142(1):04015092-1–04015092-10

Part IV
Applications of S²HM Around the World

Chapter 13

S²HM in Some European Countries



Maria Pina Limongelli, Mauro Dolce, Daniele Spina, Philippe Guéguen, Mickael Langlais, David Wolinieck, Emeline Maufroy, Christos Z. Karakostas, Vassilios A. Lekidis, Konstantinos Morfidis, Thomas Salonikios, Emmanouil Rovithis, Konstantia Makra, Maria Giovanna Masciotta and Paulo B. Lourenço

Abstract This paper compiles and describes the national initiatives and projects on Seismic Structural Health Monitoring (S²HM) active in a number of European countries. Sensors networks and typical layouts, data processing techniques and policies adopted for the management of alerts are described for the different national programs. The different policies adopted for the access to data are also described. Applications to buildings, bridges or cultural heritage constructions are used to describe in detail the seismic SHM systems installed in Italy, France, Greece and Portugal.

Keywords Seismic monitoring · Condition assessment · Sensors networks · Data processing · Alerts

13.1 Introduction

S²HM in seismic prone regions is a powerful tool in support of emergency management, and real-time performance assessment of structures. Data provided by the

M. P. Limongelli (✉)

Politecnico di Milano, Department Architecture, Built Environment and Construction Engineering, Piazza Leonardo da Vinci 32, 20133 Milan, Italy
e-mail: mariagiuseppina.limongelli@polimi.it

M. Dolce · D. Spina

Department of Civil Protection, Via Vitorchiano 2, 00189 Rome, Italy

P. Guéguen · M. Langlais · D. Wolinieck · E. Maufroy

Institute of Earth Science, Université Grenoble Alpes, Université Savoie Mont Blanc, CNRS, IRD, IFSTTAR, CS40700, 38058 Grenoble Cedex 9, France

C. Z. Karakostas · V. A. Lekidis · K. Morfidis · T. Salonikios · E. Rovithis · K. Makra

Institute of Engineering Seismology and Earthquake Engineering, Research Division of Earthquake Planning and Protection Organization (EPPO-ITSAK), Dassyliou Str., GR55535 Pylaia, Thessaloniki, Greece

M. G. Masciotta · P. B. Lourenço

Department of Civil Engineering, ISE, University of Minho, Campus de Azurém, 4800-058 Guimarães, Portugal

© Springer Nature Switzerland AG 2019

M. P. Limongelli and M. Çelebi (eds.), *Seismic Structural Health Monitoring*, Springer Tracts in Civil Engineering, https://doi.org/10.1007/978-3-030-13976-6_13

303

sensors installed on the structures can provide valuable information to the scientific and engineering community, allowing improvement of the understanding of the response of structures to earthquakes and the verification of algorithms for performance assessment. As a byproduct, information about the structural behavior provided by S²HM data support the updating the technical codes for constructions in seismic prone regions. In the past decades S²HM systems have been installed in several European countries in the framework of seismic risk prevention and mitigation policies. Monitoring systems operated by national services with civil protection functions are usually connected with a central server that processes data in real time. Indicators computed from data are used to assess the structural conditions and to trigger the deployment of further temporary monitoring system or to manage the permanent storage of data in case of exceedance of some pre-defined thresholds.

13.2 S²HM in Italy: The Italian Seismic Observatory of Structures

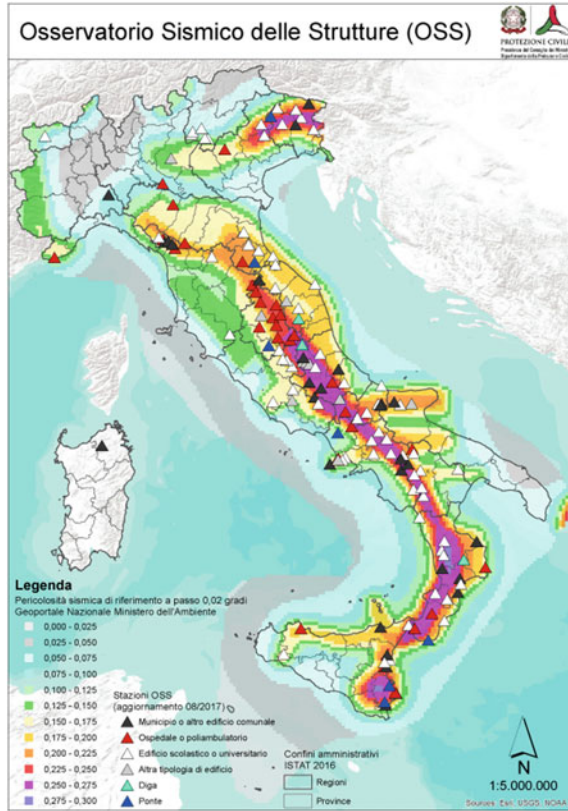
In the framework of the national seismic risk prevention and mitigation policy, the Italian Department of Civil Protection (DPC) is engaged in numerous initiatives and projects related to the topic of S²HM. These include promotion or direct participation to experimental campaigns aimed at the study of seismic strengthening techniques [1, 2] and/or development of methods, based on dynamic measurements, for the rapid evaluation of the vulnerability of existing strategic buildings [3].

However, the most important project of DPC in this field is definitely the development and the management of the Osservatorio Sismico delle Structure (OSS) [4]. The OSS is a network of permanent seismic monitoring systems installed in 152 public buildings, 7 bridges and 3 dams, whose primary civil protection scope is to provide quasi-real-time remote information on the damage state of the monitored structures in case of an earthquake. With reference to buildings, 46% of the monitoring systems are installed in schools, 20% in hospitals, 19% in town halls. The remaining 11% are installed in churches, libraries, sports buildings and others. From the structural point of view, slightly less than two thirds of the sample consists of reinforced concrete buildings, a quarter of masonry buildings, while the remainder are a mixed construction or other structural types, such as steel or wood buildings.

The map of the distribution of the monitored structures is shown in Fig. 13.1. They are distributed according to the level of seismic hazard, but, in any case, at least one monitored structure per region is present.

It took about twenty years for the OSS to reach its current inventory. The first systems were installed in 1999, while the last one was activated in July 2018. During this time very important sets of data have been collected, for example during the earthquakes of L'Aquila in 2009 [5], of Northern Tuscany in 2011 [6] and, significantly, during the seismic sequence that affected Central Italy from 24 August 2016 to 18 January 2017.

Fig. 13.1 Geographical distribution of the structures of OSS in the Italian territory



Each of the civil structures belonging to OSS is equipped with a number of Force-Balance Accelerometers (FBA) for measuring and recording the seismic dynamic response of that structure to both weak and strong earthquakes. The working range of accelerometers is set according to local seismic hazard. Typically either ± 0.5 g or ± 1.0 g range is chosen for accelerometers on the ground and, correspondingly, either ± 1.0 g or ± 2.0 g range for accelerometers on the structure, to account for structural dynamic amplification. All systems acquire continuous data and store it in a temporary memory. When at least 70% of the signals exceeds a predetermined amplitude threshold, generally 0.001 g, the data are copied to a permanent memory and immediately sent to the DPC server through a dedicated internet connection. The typical sample rates for digitizing is 200 and 250 Hz. Regarding the number and position of the sensors installed, for buildings it is possible to identify some general criteria underlying the choices made in the system design. For bridges and dams the design of the accelerometers' layout is performed ad hoc for each specific case. In Fig. 13.2a and b, a general view of the “Santa Chiara” arch masonry bridge (Noto—Sicily) is shown and the sensor layout is presented on the right side of the same figure. The sensor layout (represented as red arrows in Fig. 13.2c and d) has

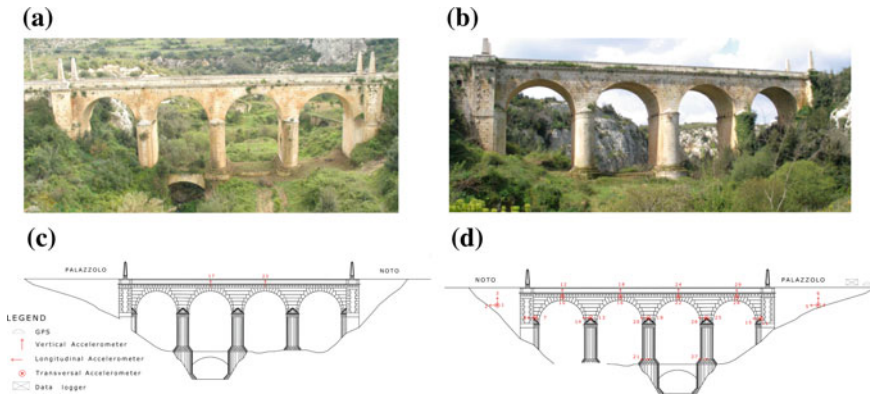


Fig. 13.2 Santa Chiara bridge: general view (a and b)—sensor layout (c and d)

been designed for monitoring both the lateral vibration of the piers and the vertical and lateral vibrations of the arches.

In the case of buildings, two different types of monitoring systems can be fundamentally distinguished: the “complete” and the “simplified” system. The complete systems, deployed in 129 buildings, consists of a three-axis accelerometer installed at the ground level plus several uniaxial accelerometers per floor, sufficient to completely describe its seismic behavior, according to some rational reasonable kinematic assumptions. In the case of regular reinforced concrete buildings, as the one shown in Fig. 13.3 on the left side, the rigid floor assumption allows to measure only three components of acceleration per floor (black arrows in the figure). For complex buildings (e.g. the one in Fig. 13.3 on the right), more components for floor are needed in order to properly represent the dynamic behavior.

The analog signals of all the sensors are transmitted via cable to a central data logger with a 24-bit converter installed in the building, which provides for their conversion into digital. If certain acceleration thresholds are exceeded, data are stored in a fixed memory and transmitted via internet to the server in the headquarters of the DPC.

The installation of complete monitoring systems is always joined to surveys aimed to collect data on the geometry and mechanical characteristics of the structure. These data, together with the identified modal parameters, are used to build and calibrate a Finite Element Model (FEM) of the structure.

In the 22 buildings equipped with simplified systems, only the top floor is instrumented together with a three-axis accelerometer installed on the ground for measuring the seismic excitation. Moreover, the number and position of the sensors is usually decided under the assumption of rigid floors. Each sensor is included in an Independent Device (ID) equipped with a 24-bit independent Analogical to Digital converter, a solid-state drive for data storage and a GPS receiver to get the Coordinate Universal time (UTC). The signals recorded by different ID, synchronized with the

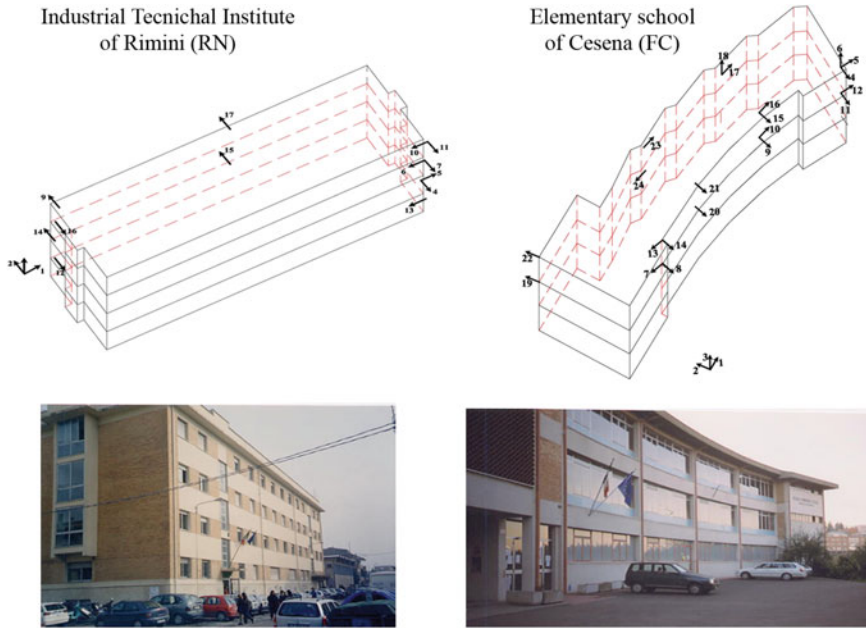


Fig. 13.3 Sensor system configuration and general view of a regular RC building (Industrial Technical Institute of Rimini, on the left side) and of an irregular one (Elementary school of Cesena, on the right side)

UTC and therefore also with each other, are sent to a master ID using a WiFi network that, using a 4G router, sends data to the Central Server of DPC.

A recent development of OSS in building monitoring is represented by the system installed on the town hall of Recanati on July 2018. This is a sort of hybrid system between a complete and a simplified one. The town hall of Recanati is a clay brick masonry building built in 1898 in order to commemorate the hundredth anniversary of the great Italian poet Giacomo Leopardi's birth. As seen in Fig. 13.4 it is a complex building, both from a geometrical and structural point of view, considering both the C-shape floor and the presence of different types of vaults. Moreover, the town hall is not completely structurally independent because of the connection with the adjacent San Domenico Church.

The hallmark in this building is that, as for simplified system, only the top floor is instrumented, but, as for complete system, this floor is monitored in detail, in order to describe its deformability with accuracy. A three-axis ground sensor for measuring the seismic input is deployed at the base of the building. This sensor configuration is shown in Fig. 13.5.

Each two-axis accelerometer (slave sensors) is equipped with an integrated 24-bit Digital Analog converter. The three-axis accelerometer deployed on the ground (master sensor) receives the digital signals from the slave sensors through Ethernet cables and transmits all data to the central server through a 4G router.

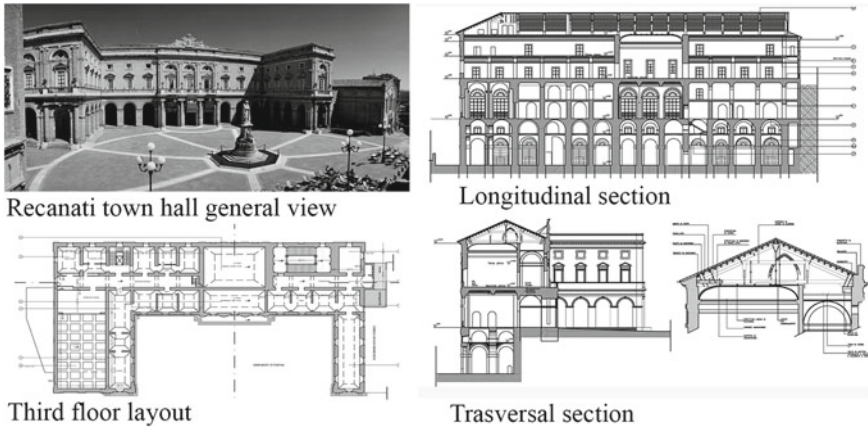
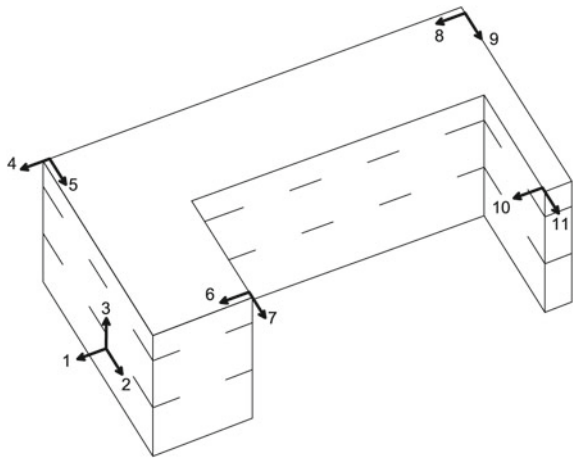


Fig. 13.4 Recanati town hall: a general view, the third floor layout, longitudinal and transversal sections

Fig. 13.5 Recanati town hall: layout of the sensor deployment



Before deploying the permanent monitoring network a detailed equivalent linear model of the building [3] has been obtained by recording ambient vibrations through a temporary network of sensors installed at all the floors of the building. During seismic events, this model allows to retrieve approximate information about the dynamic response at the unmonitored floors using the signals recorded by the permanent network at the ground and at the top floor.

13.2.1 Data Analysis and Dissemination

Seismic data, recorded and sent to the DPC central server by the monitoring systems installed on structures involved in an earthquake, are immediately and automatically processed in order to perform a quick and rough damage assessment.

The analysis is carried out by a Matlab script called RADOSS (Rapid Assessment Data of OSS). RADOSS is continuously connected to the web server of the Italian Institute of Geophysics and Volcanology (INGV) in order to receive, as soon as available, the magnitude and the epicentral geographic coordinates of the last earthquake. Immediately after receiving this information, if the local or moment magnitude is equal to or greater than 3.0, RADOSS looks for the presence of recordings in the server which, for trigger time and geographical position, are compatible with the parameters of the reported earthquake.

Automatic data processing involves the calculation of the PGA in the three spatial directions, the maximum structural accelerations along to the two main horizontal axes of the structure and the estimation of a performance parameter that can be used for damage assessment.

For buildings the damage parameter is the maximum inter-story drift (MIDR); for RC beam bridges is the drift ratio related to failure; for masonry arch bridges is the maximum vertical deflection. All these dimensionless parameters are computed in terms of displacements obtained through double numerical integration and high pass filtering of the recorded accelerations. The latter processing hampers the detection of residual displacements related to plastic behavior and this has to be accounted for when performing damage assessment.

At the end of the processing, the relative summary report, related to all the involved structures, together with the recorded data, are uploaded on the OSS website (www.mot1.it/OSSdownload). As an example, referring to the Amatrice earthquake of 24 August 2016 (MI = 6.0), Fig. 13.6 shows the map of the monitoring systems that recorded the event (left) together with the MIDR estimated by RADOSS for the eight building closest to the epicenter (right).

In addition to the automatic data processing described above, a more accurate damage assessment can be carried out, if it is considered appropriate, through the

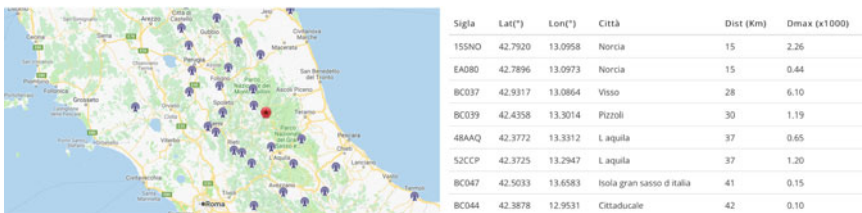


Fig. 13.6 Amatrice earthquake of 24 August 2016 (MI = 6.0): map of the monitoring systems that recorded the event (left) together with the MIDR estimated by RADOSS for the eight structures closest to the epicenter (right)

use of the MuDi (Multilevel Damage Identification) software platform [7]. This platform has been designed for the OSS in the framework of a multi-year Research Project between DPC and ReLUIIS, a network of university laboratories of seismic engineering. The word “Multilevel” refers to the classification of damage proposed by Rytter [8]: detection, localization, quantification and post-damage structural safety estimation. MuDi performs damage identification up to quantification. A set of modal parameters is identified in a reference condition and used as baseline. After a seismic event the modal parameters are identified from ambient vibrations using classical operational modal analysis techniques and used by the MuDi platform to apply in sequence several methods of Damage detection and localization. Quantification of damage is carried out using the new set of modal parameters to update a finite element model of the structure. Model updating is performed by minimizing the euclidean distance between the experimental modal parameters and the those computed by the finite element model. It is important to underline that in this final step, the information about the location of damage is used since the updating of the model is restricted to the mechanical characteristics of the structure at the damaged location.

Data recorded by the OSS are available on request and can be used for scientific purposes. In the following are reported some examples. The first one concerns data recorded on the Zingone Bridge (Fig. 13.7), a fixed arch reinforced concrete bridge located in Mercato Saraceno (Forli, Italy) featuring a reinforced concrete of 54.9 m length with a rise of 15.6 m.

Thirty-two seismic sensors were installed by the OSS to record the seismic behavior of the bridge: 26 sensors were placed on the structure and 6 sensors were located at two reference free field sites near the bridge (Fig. 13.8). Responses are recorded in the vertical, longitudinal, and transversal direction of the bridge.

In reference Limongelli [9] earthquake data recorded during the San Leo-Novafeltria earthquake (August 1, 2000) on the Zingone bridge were used to check



Fig. 13.7 The Zingone bridge

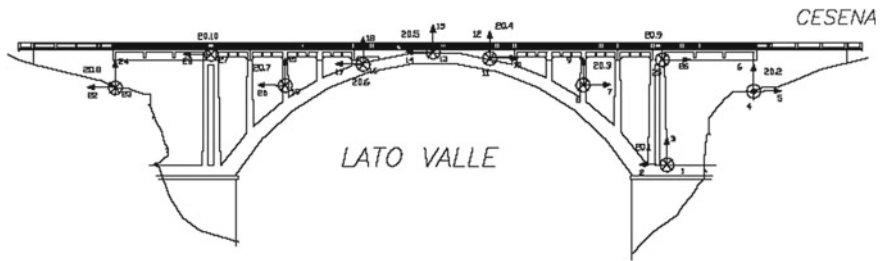


Fig. 13.8 Zingone bridge: sensors location (courtesy of Servizio Sismico Italiano)

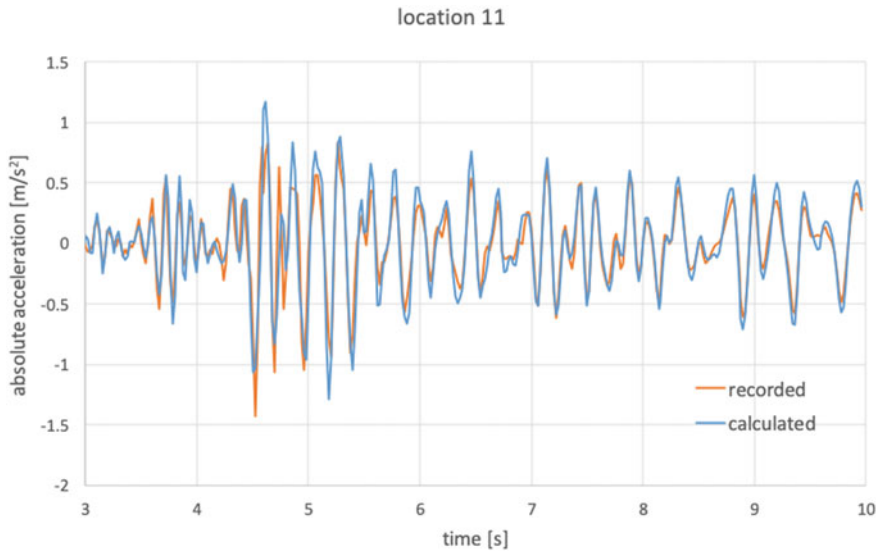


Fig. 13.9 Zingone bridge: comparison of recorded and calculated accelerations

a technique to reconstruct seismic responses at locations not equipped with sensors. The technique is used, jointly with a criterion based on modal filtering [10], to optimally locate a limited number of recording sensors for the computation of responses at locations not equipped with sensors. As an example of results in Fig. 13.9 is reported the comparison between the recorded accelerations and the accelerations calculated using responses of a limited number of sensors at the optimal locations.

The second example is the Norcia School, a four-storey reinforced concrete building, with a rectangular plan 60 m in length and 13 m in width. This building, since 2002, is monitored by the OSS with the network of accelerometers shown in Fig. 13.10. In 2010, was strengthened with dissipative braces in the longitudinal and transversal directions and in August 2016 was struck by the Central Italy earthquake. Between 2002 and 2017 several earthquakes have been recorded by the

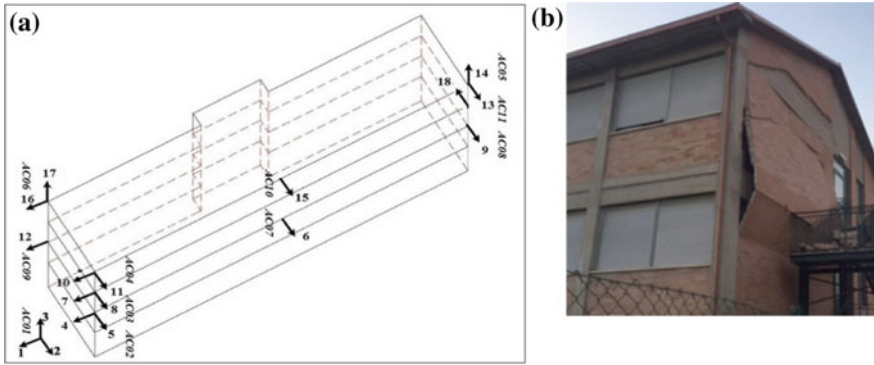


Fig. 13.10 Norcia school. **a** Sensor's layout; **b** damages after August 2016 earthquake



(a) August 24, 2016

(b) November 3, 2016

Fig. 13.11 Damages to non structural elements during the earthquakes in 2016

OSS sensors. In Figs. 13.10b and 13.11a, b are reported some of the damages to nonstructural elements after the 2016 earthquakes.

The analyses of the evolution of the first modal frequencies (Fig. 13.12) allows to clearly detect both the effect of the seismic upgrading through the dissipative braces (increase of modal frequencies between 2008 and 2013) and the evolution of damage induced by the sequence of seismic events starting from August 2016 to January 2017. The higher values identified during the last three seismic events (February to June 2017) are likely to depend on their lower intensity.

A further example is relevant to the Cusumano bridge (Fig. 13.13), located near Prioro Gargallo, in Sicily. Data recorded by the OSS enabled the calibration of a numerical model of the bridge. This model has been used to apply a pre-posterior Bayesian analyses for the computation of the Value of the Information retrieved by the network of sensors for the seismic emergency management of the bridge [12].

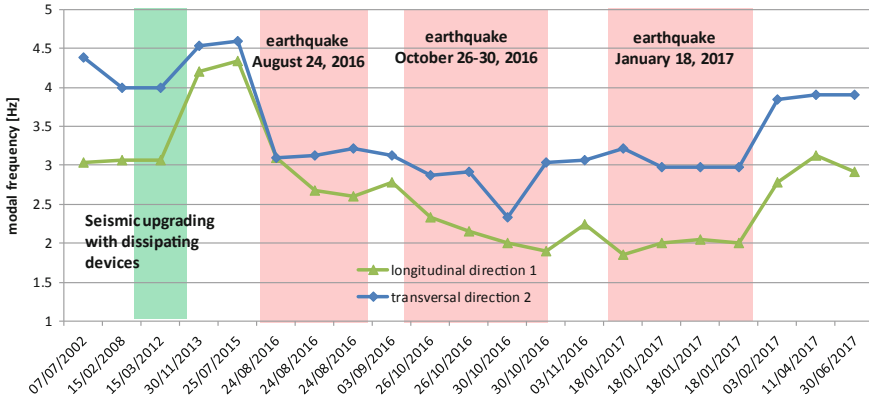


Fig. 13.12 Evolution of modal frequencies in the longitudinal and transversal directions [11]



Fig. 13.13 West side elevation of the Cusumano bridge

13.3 S²HM in France: The French National Building Array Program

The seismic hazard map of France clearly indicates relatively high (Antilles, Alps, Provence and Pyrenees) and moderate (Rhine Rift Valley, Ardennes and Armorican Massif) seismic prone areas.

The French National Building Array Programme consists in five reinforced concrete buildings, equipped permanently with accelerometric sensors, in mainland France and in the Lesser Antilles near the Caribbean subduction zone. Three are

towers comprising more than 15 levels, one is a long building and the other is a seismic isolated building.

The RAP/RESIF permanent accelerometric network (<http://rap.resif.fr>) encompasses all French academic and public research institutes related to the definition and management of seismic risk [13]. It measures the seismic ground motion permanently in seismic areas as well as in certain exposed urban areas where ground motion prediction is essential.

The national permanent instrumentation program for buildings (NBAP: National Building Array Program) in France was launched ten years ago by RAP/RESIF to install permanent instruments in buildings and to record their response to seismic loading. This type of activity is not innovative in itself since at the end of the 1950s, California began its own program initiated by seismologists (Californian Strong Motion Instrumentation Program), comprising around a hundred instrumented buildings. This project has recorded a number of major earthquakes (San Fernando, Whittier Narrows, Loma Prieta, etc.) and has influenced certain construction practices and regulations. Other highly seismic countries have followed California's example (Japan, Taiwan, ...) but unlike these networks, RAP/RESIF decided to make the data freely available based on the Californian model. RAP decision to publish these data is essential to generate added value, to check the quality of the data (currently this is the most efficient solution available) and to initiate collaborative projects with European and/or international academic partners.

13.3.1 Description of the Buildings

Five buildings are instrumented in France (Fig. 13.14). Although their constructions are different, they each represent a category of construction and design type typically found in France. As for the free-field stations, RAP chooses to deploy sensitive systems with large dynamics to enable the recording of low to high amplitude signals (± 1 g full scale). They can be used to analyze the dynamic behaviour of the structures during local and/or regional earthquakes, to understand the relationships between their dynamics and design type, to analyze the relations between ground motion and structure deformation, to observe soil-structure interaction and to understand the non-linear phenomena that develop within the structure, in the foundation and/or at the soil-structure interface.

Grenoble City Hall (Codes OGH1 to OGH6) has 18 accelerometric acquisition channels at the top and at the bottom of the structure (Fig. 13.14a). It was the first building to be equipped with permanent instruments in France in 2004. It is located in a deep sedimentary valley of the Alps, near seismic sources. The building is 44 m long, 13 m wide and 52 m high [14]. Its main structural system is a concrete frame comprising pillars and beams bearing slabs, except for one pre-stressed concrete platform, which forms the third floor. The inter-storey height is 3.2 m from the third floor up, 4.8 m for the first floor and 8 m for the second. It is a reinforced concrete construction, its lateral stiffness being ensured mainly by the lift shaft and staircase

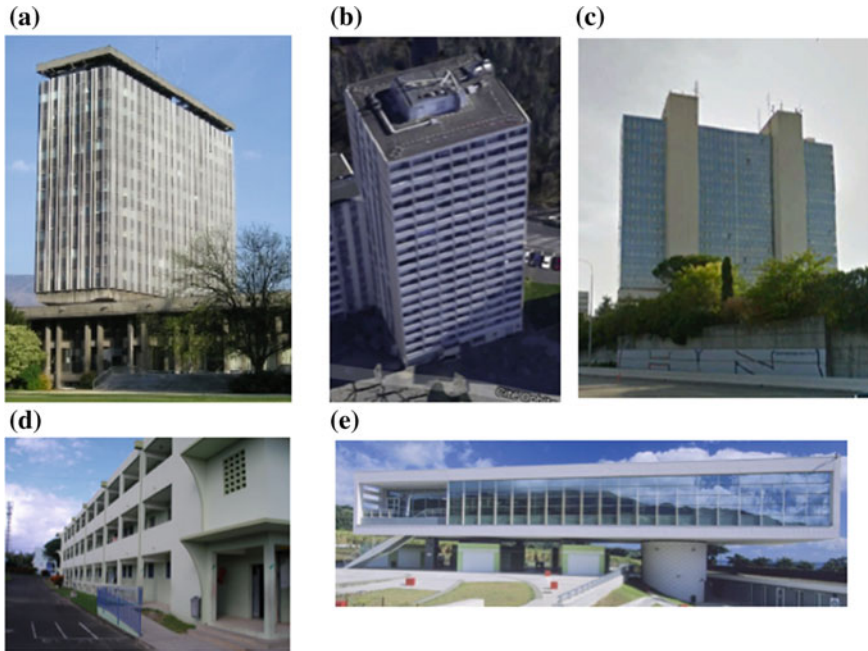


Fig. 13.14 View of the buildings instrumented by RAP/RESIF. **a** Grenoble City Hall (Alps region), **b** Ophite tower (Lourdes, Pyrenean region), **c** Nice Préfecture (South-East region), **d** Basse-Pointe school (French lesser Antilles), **e** Earth and science discovery centre (French Lesser Antilles)

walls on either side of the main tower. The Grenoble City Hall building is resting on a superficial soil layer, 15–20 m thick, of peat and soft clay, lying on a layer of sand and gravel. The building foundations are made from pillars anchored in the stiff layer of sand and gravel, at an approximate depth of 15 m. Operation and maintenance of the network was entrusted to the Earth Science Institute (ISTerre) of Grenoble Alpes University/CNRS/IFSTTAR in November 2004. Initially, the data were in trigger mode, but following updating in 2010, the data are now recorded continuously and transmitted in real time to the national accelerometric data archiving centre (RAP-DC), which is part of the national seismology data center (RESIF-DC). The instrumentation program was partly funded by the city of Grenoble.

In February 2005, the **Earth and science discovery centre in Martinique** (Codes CGCP and CGLR) was equipped with two 3-component accelerometric stations [15]. This building, located near an active seismic zone, comprises a seismic isolation system on rubber bearing: the two stations are located on the two faces of the bearing Fig. 13.15e. It was built in 2004 in the form of a hollow, upper parallelepiped block, whose reinforced concrete walls make up the outer framework of the structure (50 m × 18 m). The slab of the upper block is made from reinforced concrete, 1.2 m thick. It lies on rubber bearings on three reinforced concrete pillars (H = 7.90 m, X = 1.00 m, Y = 2.50 m) at one end, and on a hollow, circular column made from

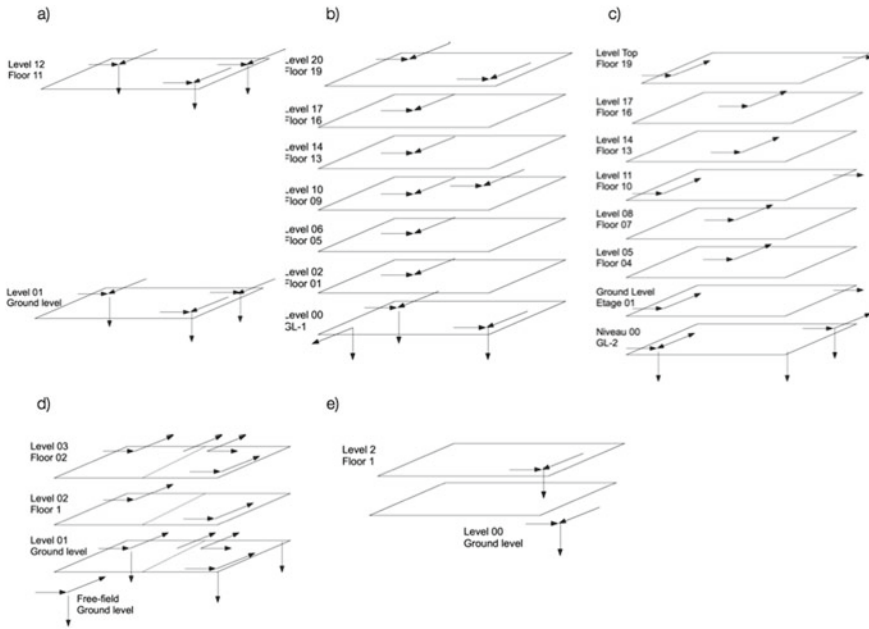


Fig. 13.15 Position of the sensors in the buildings instrumented by RAP/RESIF. **a** Grenoble City Hall (Alps region), **b** Ophite tower (Lourdes, Pyrenean region), **c** Nice Préfecture (South-East region), **d** Basse-Pointe school (French lesser Antilles), **e** Earth and science discovery centre (French Lesser Antilles)

reinforced concrete containing the stairwell, at the other end. The external diameter of the column is 7.70 m for an internal diameter of 6.30 m. The pillars and column lie on stiff ground (EC8 type A) on superficial foundations, interconnected by a system of girders. The data are triggered and later sent to the national accelerometric data archiving centre (RAP-DC part of the RESIF-DC). The network is operated and maintained by the volcanological and seismological observatory of Martinique (OVSM/IPGP), a partner of the RAP network. The instrumentation was funded by Martinique regional council.

In October 2008, **Ophite tower** (code PYTO) in Lourdes [16] was instrumented with 24 accelerometric channels spread out from the top to the bottom of the structure (Fig. 13.15b). Located near an active seismic area, it lies on a rocky formation (Ophite) from which the building is named. It was the second building to be equipped permanently in mainland France. It was built from 1970s reinforced concrete (year of construction: 1972), with shear walls resisting system. It is a residential building and classed B by regulation EC8. Comprising 20 levels (basement + ground floor + 18 upper floors), it rises 50 m above the ground, with ground dimensions of 24 m (L) by 19 m (T). It has a terrace roof. It is regular on the ground floor and upper levels. From the beginning, the data have been recorded continuously and transmitted in real time to the national accelerometric data archiving centre (RAP-DC part of the

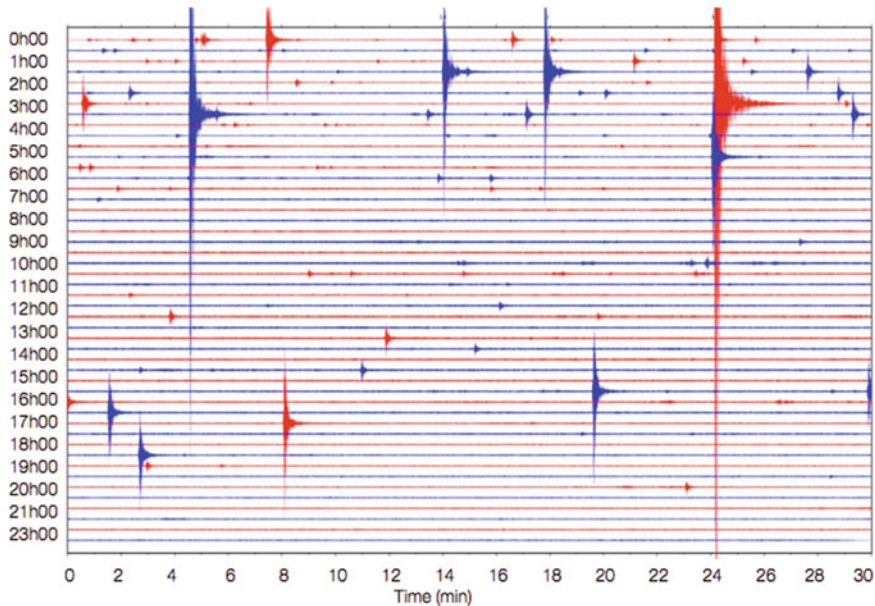


Fig. 13.16 24-hours recording at the bottom of Ophite tower during a seismic sequence in 2012

RESIF-DC). The earth sciences institute and Observatory Midi-Pyrénées (OMP) in Toulouse, is a partner of RAP operates and maintains the network. The operation was partly funded by the Pyrenees regional agency for development (DDT). Figure 13.16 shows an example of 24-hours continuous recording by a sensor at the bottom of PYTO during a nearby seismic events sequence.

The **Nice Préfecture tower** (code NCAD) was equipped in September 2010 with 24 accelerometric channels spread between the top and bottom (Fig. 13.15c). This building, with 22 floors, is built over a sedimentary fill, near a seismic area [17]. It comprises two twin towers, separated by a 10 cm thick joint. Only the western tower is instrumented in the vertical direction since the two towers are similar. Its resistance is mainly provided by reinforced concrete walls and partly by its external glass frontage. Located on a thick alluvial area, its foundations are deep, but no other information is available concerning their composition. Data recording has always been continuous with real time transmission to the national accelerometric data archiving centre (RAP-DC part of the RESIF-DC). The network is operated and maintained by Nice Sophia Antipolis University and CEREMA of Nice, partners of RAP.

Basse-Pointe school (Code CGBP) was equipped in January 2011 with 24 accelerometric channels spread along the main dimensions of the building (Fig. 13.15d). It is located near a very active seismic zone, specifically the one that caused the Mw 7.4 earthquake in 2007. The building was constructed in the 1970s. It has a concrete frame structure, oriented along its transversal direction. Its longitudinal stiffness is mainly due to the stairwells located at its ends. The instrumented part

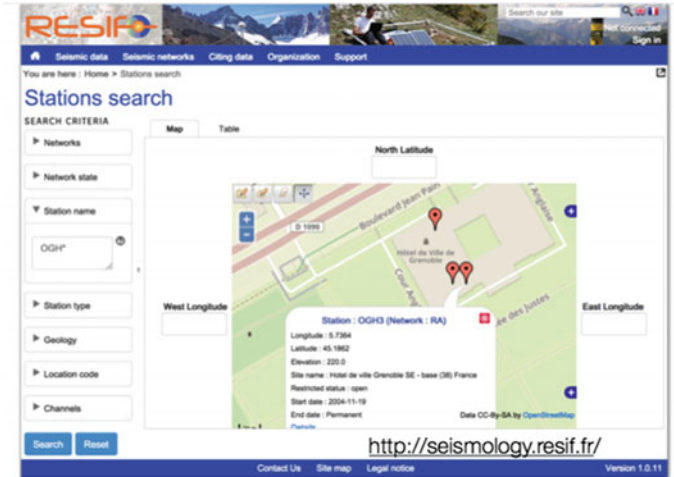
comprises two blocks, separated by a 4–5 cm thick construction joint. The building is used for teaching and therefore corresponds to EC8 regulation Type III. Its dimensions are regular at ground level, measuring 57 m \times 9 m with a height of 10 m (2 floors). All the floors are identical. We have no information on the foundations that are likely continuous superficial. Data has always been recorded continuously and transmitted in real time to the national accelerometric data archiving centre (RAP-DC part of RESIF-DC). The network is operated by the Institute of Earth Science (ISTerre) and jointly maintained by the volcanological and seismological observatory of Martinique (OVSM/IPGP). The building was instrumented in partnership with BRGM (RAP partner) with funding from Martinique regional council.

13.3.2 Data Policy

When the network was created, RAP/RESIF decided to make all the recorded data, including data from buildings, available to the scientific community. These data include (1) metadata describing the stations and acquisition channels (i.e., sensor position, orientation, instrumental response, etc.), (2) wave shapes in miniSeed format, which is standard for sharing seismological data, and (3) information on station operation and data continuity. Triggered data corresponding to the largest earthquake events are also available. RAP national data center (RAP-DC) has been managing the data since 2000 and in 2012, it was integrated to the national RESIF-DC seismological data center hosted at Grenoble Alpes University. Data in Matlab format, segmented by seismic events, can also be obtained from the authors.

All these data are accessed via various services, which are described on the RESIF data distribution portal (<http://seismology.resif.fr>) in the Data Access section (Fig. 13.17). In this portal, the position of the sensor in the building, the description of the acquisition and sensors and additional information (metadata) are available, relevant for processing and interpreting data. This portal also describes a number of solutions according to the type of data retrieved (wave form, metadata in txt or xml format, etc.) and data quality (real-time data or validated data), as well as downloading tools (e.g., via web-services developed by the Federation of Digital Seismograph Networks, FDSN, or by the Arclink system developed by EIDA for Europe). The EIDA system enables the interconnection of major European data center via the Arclink system developed during the European projects NERIES and NERA, to which RAP/RESIF also contributes. In Fig. 13.17, an example of link provided through the GUI for web-service request is given.

Each station transfers its data in real time directly to the RAP-DC via a SEEDLINK protocol on a ring buffer. The data are then pushed to the RESIF-DC after verification and a first level quality control. Some data quality (such as noise level) is processed automatically and can be viewed on-line on the RESIF portal. Figure 13.18 shows an example of data continuity from the PYTO station after this quality check.



<http://ws.resif.fr/fdsnws/dataselect/1/query?network=RA&station=CGBP&quality=B&starttime=2017-06-01T22:44:00&endtime=2017-07-01T22:44:10&nodata=404>

Fig. 13.17 Screenshot of the RESIF web portal to access data, and example of the web-service request that enables downloading a continuous window of data from the Basse Pointe school building (Code CGBP) between 01/06/2017 and 01/07/2017

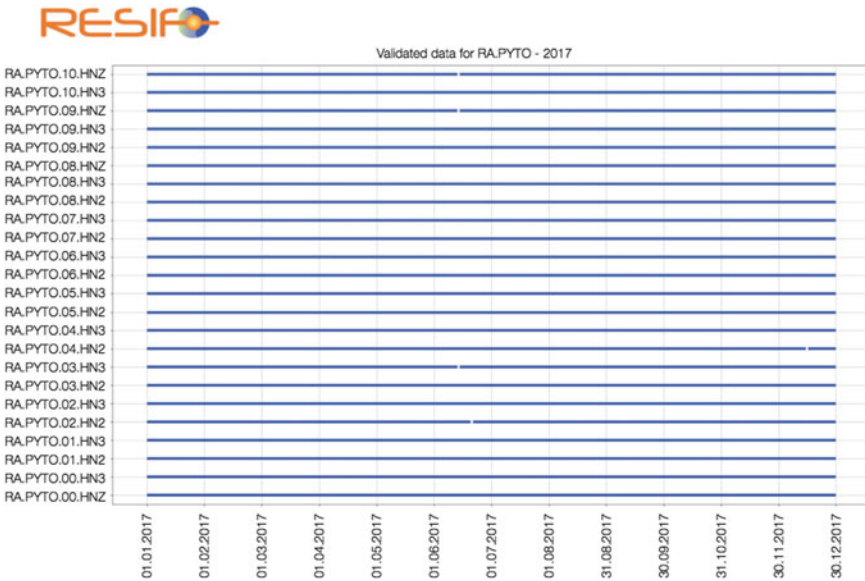


Fig. 13.18 Example of data continuity from the 24 acquisition channels of the PYTO building for 2017

13.3.3 Results at a Glance

Added to the information provided in case of a significant earthquake, many scientific publications have been published using these data. These applications include (see Fig. 13.19):

- (a) analysis of the seismic response of structures to moderate-to-strong earthquakes (in the Antilles) enabling better understanding of the specific behavior of these structures and their operation with respect to French regulations (e.g., [14, 15]);

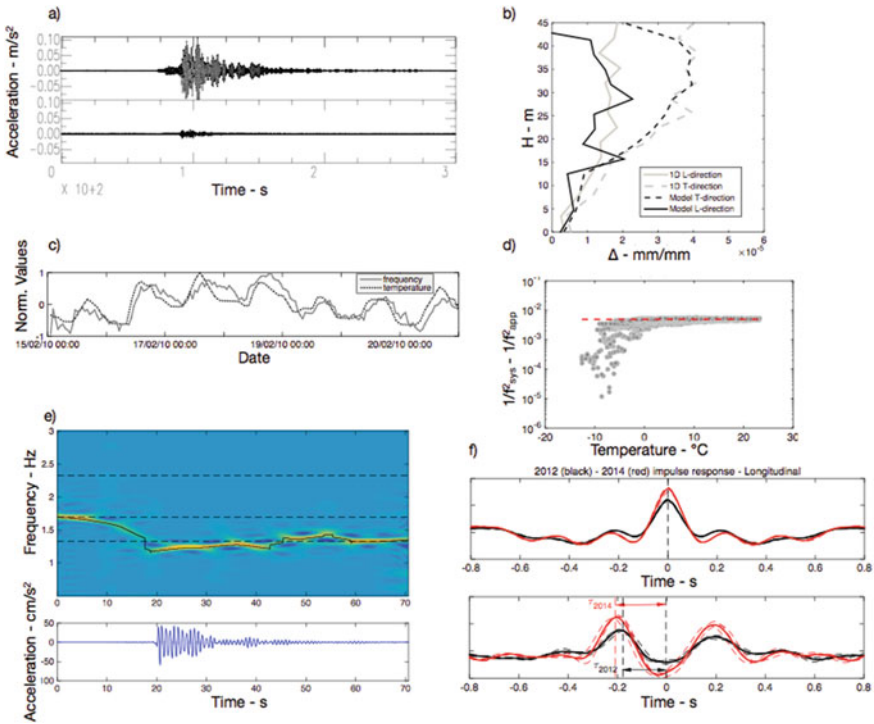


Fig. 13.19 Example of result using data provided by the French National Building Array Program (see references listed in the text). **a** Top and bottom accelerometric data at the Grenoble City-Hall building during the Mw 4.6 2005 earthquake. **b** Structural drift observed during earthquake shown in **a** sued for calibrating numerical modeling for seismic vulnerability assessment. **c** One-week variation of the resonance frequency of the Ophite tower correlated to air temperature. **d** Variation of the soil-structure interaction at the Grenoble City Hall building during extreme low air temperature in France. Soil-structure is computed as the difference between the resonance frequency of the soil-structure system and the apparent structural frequency computed using accelerometric data. **e** Time-frequency distribution representing the variation of the resonance frequency of the Earth and science discovery centre in Martinique base-isolated building during the Mw 7.3 2007 Martinique earthquake. **f** Pulse propagation between the bottom and the top of the Grenoble City-Hall building during two moderate earthquakes (2012 and 2014) by seismic interferometry by deconvolution method, that shows slight variation of the velocity

- (b) validation of structure vulnerability assessment methods using an experimental approach (e.g., [14, 18]);
- (c) time monitoring of frequency and damping under changing atmospheric conditions (temperature, humidity, etc.) and in the event of an earthquake to understand the physical processes involved (e.g., [16, 19–21]);
- (d) analysis of soil-structure interaction under seismic loading or ambient vibrations, and its evolution over time (e.g., [19]);
- (e) development of a modal analysis method applied operationally to detect changes in elastic properties (e.g., [22, 23]);
- (f) detection and location of changes using seismic interferometry methods by deconvolution and modal approach (e.g., [24]).

Some of the important outcomes of these works relate to (Fig. 13.19): (1) the physical significance of the variation of frequency and damping, information that can be used to characterize the health of the structure; (2) the non-linear behaviour of a building on rubber bearings suffering a magnitude 7.4 earthquake; (3) the development of combined experimental/empirical/numerical methods to characterize the physical vulnerability of structures.

13.4 S²HM in Greece—The ITSAK Experience

The Institute of Engineering Seismology and Earthquake Engineering (www.itsak.gr) is a research center established in Thessaloniki in 1984, which was merged in 2011 with the Earthquake Planning and Protection Organization, becoming its research unit ITSAK-EPPO. Since its establishment, ITSAK has been particularly active in monitoring the seismic response of structures (S²HM), mainly during the aftershock sequence of major earthquake events. Due to space limitations, a concise description of the Institute's various efforts focused especially on the S²HM field is presented, together with some important conclusions for each instrumentation case. The interested reader can find more detailed information in the cited literature. In the majority of the cases presented herein, unless otherwise stated, high-resolution (>19-bit) special accelerometer arrays with several uniaxial sensors have been used, with common-trigger and common-time capabilities and a 200 sps sampling frequency. ITSAK has also performed several other investigations based on the ambient vibration (operational) response of instrumented structures that are not presented herein. The authors welcome the interested readers to contact ITSAK for more information on their research efforts in the field of SHM/S²HM.

13.4.1 Instrumented Buildings

OTE Building, Ano Liosia, Athens. On September 7, 1999 at 11:56 GMT a M5.9 earthquake, struck Athens, Greece. A few days after the main event, ITSAK instrumented (with a 19-bit special accelerometer array) the National Telecommunications (OTE) building (Fig. 13.20a) in the municipality of Ano Liosia, near (≈ 10 km) the epicentral area, and recorded its response to several aftershocks for almost three weeks. The R/C building consists of two statically independent parts, separated by a 0.03 m expansion joint (Fig. 13.20b). A network of six sensors was used, recording responses with a sampling rate of 100 sps, aiming, among others, at investigating the possible pounding between the two parts (Fig. 13.20b).

Two of the most intense recorded aftershocks (of the order of 20–40 mg) were used to identify the dynamic properties of the building, using a custom software developed by the Department of Mechanical and Industrial Engineering of the University of Thessaly, Greece. In Table 13.1 the identified eigenperiods (T) and critical damping ratios (ζ) for the two first translational (in each direction) modes are presented for one of the more intense aftershocks (event AX017), based on either a one-input/one-output identification scheme (first value in each cell) or a one-input/multiple output scheme (second value, in parentheses) [25].

The experimental results were used to properly calibrate the finite element model of the building (Fig. 13.20c). The soil compliance was modeled through Winkler springs, with values of the spring constants corresponding to a dynamic behavior (i.e. almost an order of magnitude bigger than the static value). The values of the Winkler springs constants, recovered through a parametric investigation, allowed to

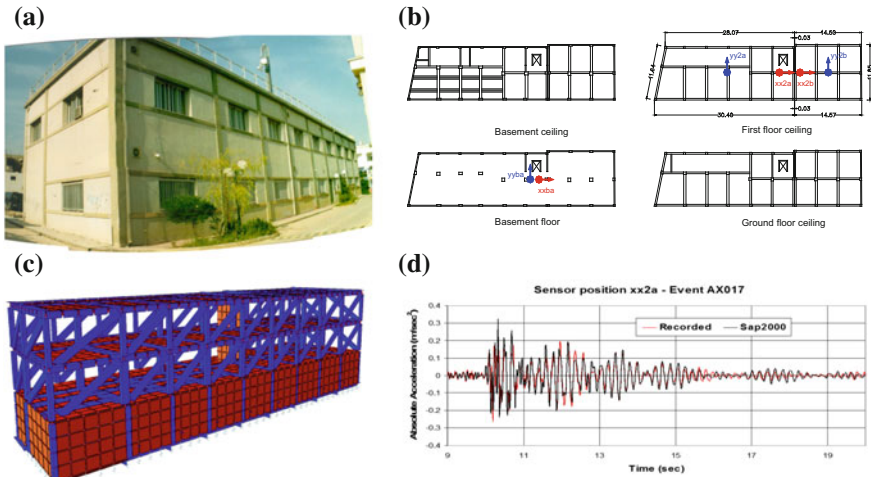


Fig. 13.20 a OTE building at Ano Liosia, b instrumentation layout, c F.E. model, d predicted versus recorded response (updated model, longitudinal direction)

Table 13.1 Identified modal parameters of OTE building at Ano Liosia—event AX017

Mode	Building ‘a’				Building ‘b’			
	x-dir		y-dir		x-dir		y-dir	
	T (s)	ζ (%)						
1	0.1929 (0.1930)	4.9477 (5.0006)	0.3788 (0.3780)	6.9907 (6.7572)	0.3174 (0.3174)	5.0969 (5.1765)	0.4279 (0.4288)	5.6406 (5.5666)
2	0.0654 (0.0631)	3.7182 (4.4715)	0.1232 (0.1229)	3.3103 (2.8524)	0.1065 (0.1071)	6.3247 (7.1213)	0.1371 (0.1375)	4.8965 (5.8503)

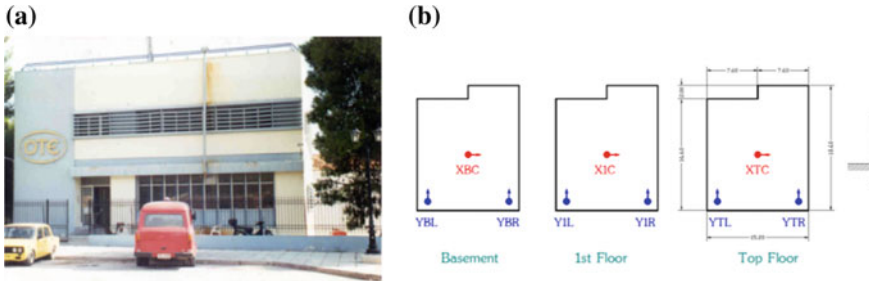


Fig. 13.21 a OTE building at Thrakonakedones, b instrumentation layout

obtain a good match between recorded and calculated accelerations, especially in the longitudinal direction. In Fig. 13.20d is reported the comparison at the location of one of the sensors. For either parts of the building, the peak relative displacement computed from recorded accelerations exhibited values far lower than the dimension of the existing expansion joint. This is a strong indication that no pounding took place, at least for the examined events. A further indication towards this conclusion is the fact that the calibrated analytical model, in which no pounding simulation capabilities were provided, accurately described the recorded response.

OTE Building, Thrakomakedones, Athens. For two weeks after the Ano Liosia earthquake, ITSAK monitored the seismic behavior of a respective (OTE) building (Fig. 13.21a) in the municipality of Thrakomakedones, also in the meizoseismal area. Damage due to the mainshock was limited to cracking at some of the interior infill brick walls, whereas the R/C load bearing system was unharmed. The same structural array was used, with nine sensors and a 200 sps sampling rate (Fig. 13.21b). The selection of the particular configuration of the sensors aimed at the detection of the higher modes of the building, as well as at the detection of possible differentiations between the recordings of the two parallel sensors YBL and YBR at the basement [26].

During the monitoring period 21 aftershocks were recorded. Several of them were used to assess the dynamic characteristics of the building. It was found that the modal properties depend on the intensity of the earthquake. Specifically, the higher the intensity of the event, the higher the values identified for the period and the

Table 13.2 Identified modal parameters of OTE building at Thrakomakedones for different intensity events

Mode	Event BA007 (lower intensity)		Event BB010 (higher intensity)	
	T (s)	ζ (%)	T (s)	ζ (%)
1 (x-dir)	0.2253	2.928	0.2845	5.069
2 (y-dir)	0.1605	3.780	0.1831	5.105

critical damping ratio. In Table 13.2, the corresponding results for a lower intensity event (BA007, peak base accelerations x-dir 2.02 mg and y-dir 3.41 mg) and a higher intensity one (BB010, peak base accelerations x-dir 35.10 mg and y-dir 40.13 mg) are presented.

This shift is reversible, i.e. independent of the chronological order of the events. It must be noted that during the monitoring period, the building exhibited a virtually linear behavior during the aftershocks (i.e. no further damage to the infill walls was observed). This shift to longer periods for higher intensity excitations may be attributed to the formation of microcrackings, as well as to the activation of various extra friction mechanisms in the structure (e.g. between the infill walls and the surrounding R/C structural frames). These are reversible phenomena that occur during excitations exceeding a certain intensity threshold, and which disappear at the end of the excitation.

As in the case of Ano Liosia, the identified dynamic parameters were used to update a Finite Element (F.E.) model of the building. An additional finding was the observable difference between the recordings at the two parallel sensors YBL and YBR deployed at the basement level. Given the small dimensions of the building, a possible cause may be a soil-structure interaction effect between the torsional response of the building superstructure and its foundation. This explanation was partly confirmed by the analytical investigations carried out on the calibrated F.E. model of the building. A detailed presentation of the experimental and analytical investigations of the two buildings can be found in Karakostas et al. [25] and Karakostas et al. [26].

Municipality Building, Korinthos. The Municipality building in the city of Korinthos (Fig. 13.22a) was instrumented by ITSAK for six months in 2003. The load bearing system of the building consists of R/C shear frames (i.e. with no shear walls, apart from those at the basement perimeter). A 19-bit Kinematics K2[®] special array was used, together with 8 uniaxial FBA-11 accelerometers and a 200 sps sampling rate. The instrumentation scheme, presented in Fig. 13.22b, aimed at the determination of the main translational modes of the building. During the monitoring period, only one low intensity event was recorded (peak base accelerations 1.38 and 1.44 mg).

The two fundamental periods were identified through the use of the relative PSD spectra of the recorded responses, yielding values of $T_x = 0.19$ s and $T_y = 0.22$ s [27]. For a quick cross-check between experimental and analytical results which can be performed even on site, the following empirical relation (proposed by the Greek National Seismic Code, EAK2000, §3.5.2) can be used:

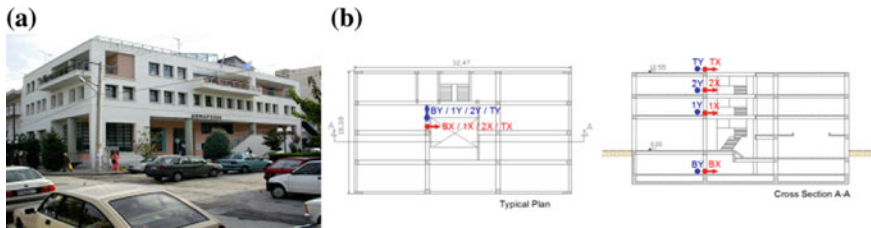
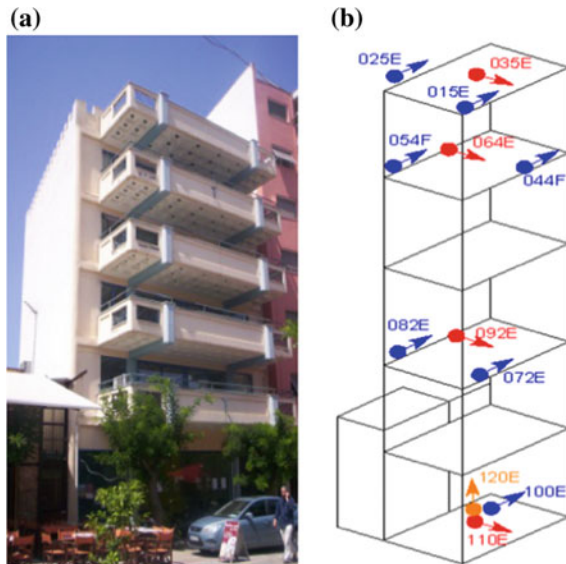


Fig. 13.22 a Municipality building at Korinthos, b instrumentation layout

Fig. 13.23 a The Technical Chamber of Greece building at Patras, b instrumentation layout



$$T = 0.09 HL^{-1/2} \{H / (H + \rho L)\}^{1/2} \tag{13.1}$$

where H is the height of the building, L the length of the building along the assumed (x or y) direction and ρ the ratio of the area of the shear walls along the same direction to the total area of shear walls and columns (equal to 0 in case of shear frame systems, as in the present case). For the Korinthos Municipality building, Eq. (13.1) yields values of the periods equal to $T_x = 0.20$ s and $T_y = 0.26$ s, i.e. in fairly good agreement with those evaluated experimentally.

Technical Chamber of Greece Building, Patras. After a M6.5 mainshock on June 6, 2008 at a distance of approximately 35 km southeast of the city of Patras, ITSAK researchers instrumented the five-story R/C building of the Technical Chamber of Greece (Fig. 13.23a). A 19-bit special array was used, together with 12 uniaxial accelerometers and a 200 sps sampling rate (Fig. 13.23b).

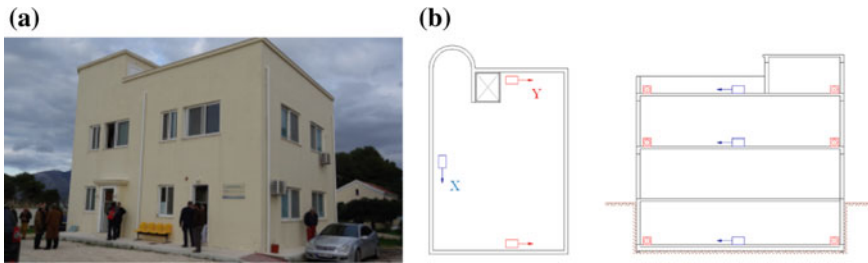


Fig. 13.24 **a** The instrumented administrative building of Lixouri Hospital, **b** instrumentation layout

During its instrumentation, the building was subjected to an earthquake on 26/9/2003, which allowed the estimation of its dynamic characteristics (fundamental modes) through a PSD-based methodology [28].

Administration Building of Lixouri Hospital, Cephalonia Island. In 2014, the island of Cephalonia, Greece was struck by two major earthquakes: a M6.1 on 26/1/2014 and a M6.0 on 3/2/2014. During these events ($PGA = 0.54$ and 0.68 g respectively at Lixouri) the administrative building of the hospital in the town of Lixouri (Fig. 13.24) (designed according to the 2003 Seismic code for a design $PGA = 0.36$ g) behaved exceptionally well. Essentially no damage to neither its load bearing structural system nor the infill walls' bricks and plaster occurred. For this reason it was decided to monitor the building. On February 5, 2014 ITSAK instrumented it with a special 24-bit accelerometer array with 9 uniaxial sensors.

The response of the building—recorded during various aftershocks (82 events were recorded)—was used to assess its actual dynamic characteristics (eigenvalues, eigenmodes, damping ratios). These were then used to calibrate finite element models of the structure that were developed in order to reliably represent its actual dynamic behavior. The updated F.E. models were used to compute the maximum story drifts during the two aforementioned major events through time-history analyses, and to explain the lack of any damage to the building. The ratios of the peak values at the top and basement of the building were also used to validate the corresponding values of the spectral amplification factors (β) adopted by the Greek Seismic Code (EAK/2003) for the specific soil type at the site and building's period. The experimentally mean computed amplifications were higher than the ones of the Code, with the latter, however, in general lying within the mean-1 Standard Deviation range of the recorded amplifications. A detailed presentation of the research results is presented in Karakostas et al. [29].

Municipality Building, Lefkada Island. The building of Municipality of the town of Lefkas (Fig. 13.25) was instrumented in 2012 by ITSAK with a special 24-bit resolution accelerometer array comprising twelve uniaxial accelerometers. Since its installation, several earthquakes have been recorded by the special array, and a major (M6.1, on 26-1-2014) earthquake excitation was used to evaluate the dynamic response of the building.

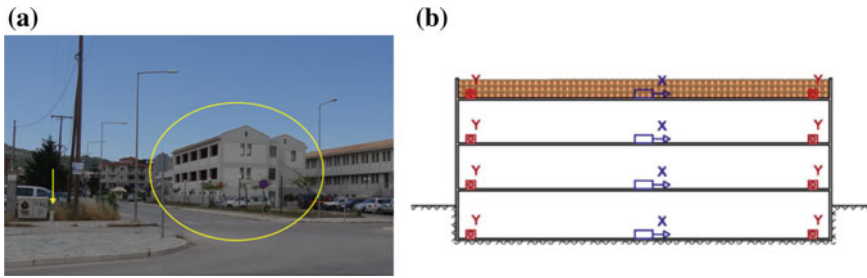


Fig. 13.25 **a** Lefkada Municipality building (yellow ellipse) and location of the free-field accelerometer (yellow arrow), **b** instrumentation layout



Fig. 13.26 **a** The municipal gymnasium building (Bing Maps Image) and **b** the steel water tank located in the broader urban area of Kalochori, west of Thessaloniki. The locations of the accelerometric stations are also shown

Also, at a distance of around 40 m from the building, a free-field triaxial sensor was installed in 2013. Its recordings were compared to those of the special array at the basement of the instrumented building, and an investigation of the SSI effects was conducted, in order to justify the discrepancies (both in the time and frequency domain) observed between recordings at the free-field site and the base of the building [30].

Kalochori Accelerometric Network (KAN). Two buildings and one steel water tank have been instrumented since 2014 in the urban area of Kalochori, near Thessaloniki, as part of the Kalochori Accelerometric Network [31]. The instrumentation refers to a pair of triaxial accelerometric stations; one installed on top of the structure and one on the ground surface at a close distance from the structure’s base (Fig. 13.26).

A set of 78 earthquakes has been recorded by KAN between 01/16/2014 and 12/31/2016, allowing the investigation of possible urban effects on ground motion and the evaluation of dynamic response features of the instrumented structures including

soil-structure interaction [32]. The complete set of KAN stations data and earthquakes recordings are available through the Web-GIS portal: <http://apollo.itsak.gr/apollo-portal/ApolloPro.aspx> while the DOI linked to the above data is <https://doi.org/10.6084/m9.figshare.5044804>.

13.4.2 Instrumented Bridges

Chalkis Cable-Stayed Bridge. In 1994 ITSAK instrumented the 395 m long Cable-Stayed section of the bridge at Evripos Channel, Greece (Fig. 13.27a), with a permanent accelerometer network of 42 sensors supported by three interconnected 12-bit recording units (Fig. 13.27b). In 2012 the system was upgraded with a new 36-channel, 24-bit recording station that also allowed real time telemetry over Ethernet.

Several earthquake events were recorded by the system, which were used for the experimental assessment of the dynamic characteristics of the bridge [33, 34]. A methodology for updating the F.E. model of the bridge based on its recorded seismic response is presented by Papadimitriou et al. [35]. In Lekidis et al. [36] is presented a study on the effect of local soil on the variation of the ground motions at the bridge's supports and on the structure's response. The investigation is based on recordings from both the permanent accelerometer array and an additional geodetic system. Finally, several investigations of the dynamic response of the bridge under the asynchronous ground motions recorded by the accelerometer array are presented in Karakostas et al. [37], Papadopoulos et al. [38], Lekidis et al. [39] and Sextos et al. [40].

Kavala and Polymylos bridges at Egnatia Motorway. Egnatia Motorway is a 670 km long highway, that crosses Northern Greece in the E–W direction. ITSAK, in collaboration with the Bridge Maintenance Dpt. of Egnatia Odos S.A., instrumented two R/C bridges, namely the 2nd Kavala Bypass Ravine Bridge and the 9th Ravine Bridge on the Veria—Polymylos section (Fig. 13.28). Both bridges have two, almost identical, statically independent lanes, one for each traffic direction. For both bridges only one lane was instrumented.

Several ambient noise measurements as well as earthquake excitations were recorded, and they were used for the identification of the dynamic characteristics

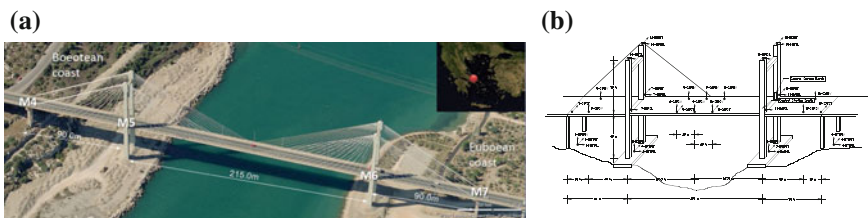


Fig. 13.27 a The Cable-Stayed section of the Evripos Channel bridge, b instrumentation layout

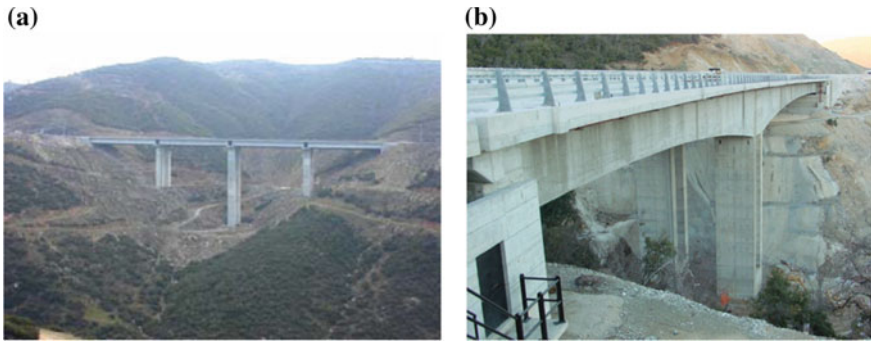


Fig. 13.28 Instrumented bridges by ITSAC and Egnatia Odos S.A. **a** the Kavala bridge, **b** the Polymylos bridge

of the bridges [41, 42], as well as the updating of F.E. models [43, 44]. Methodologies for the computation of vulnerability curves for the two bridges are presented in Karakostas et al. [45] and Makarios et al. [46]. It has to be noted that the Bridge Maintenance Dpt. of Egnatia Odos S.A. monitors several other bridges along the Egnatia motorway with a custom-developed bridge management system [47].

13.5 Seismic SHM and Testing for Cultural Heritage in Portugal

In the last years, the employment of Structural Health Monitoring (SHM) tools in support of the dynamic characterization and condition assessment of the existing built environment has earned a wide consent in Portugal, especially when dealing with strategic structures and infrastructures systems. The great interest that SHM has received from both the scientific and professional sectors is essentially due to the unquestionable advantages that vibration-based structural monitoring procedures offer in terms of modal feature extraction, characterization of the global structural behaviour, rapid condition screening, identification of anomalies and damage mechanisms, evaluation of operational and environmental effects, assessment of strengthening needs, validation of structural interventions and calibration of realistic numerical models for structural analyses. Yet, the possibility to continuously track the structural health of the system under observation without resorting to any invasive technique has further encouraged the application of SHM to historical constructions and monuments, despite the numerous challenges associated with such complex and unconventional artefacts. Trying to cover emblematic examples of SHM over the Portuguese territory, the following applications can be mentioned: Pedro e Inês footbridge [48], Braga Stadium suspension roof [49], Foz Tua centenary railway bridge [50], Infante

D. Henrique bridge [51], Mogadouro clock tower [52], Jeronimos church [53], Saint Torcato church [54], Baixo Sabor arch dam [55], Foz Côa church [56].

SHM systems also result particularly attractive for advanced seismic protection of critical structures located in earthquake-prone areas, given their potential for real-time structural assessment and early warning of seismic damage. Strong ground motions can trigger major damages and collapses, but repeated earth-shakings of small or medium intensity can cause cumulative damages which are often not directly detectable by visual inspections. Hence, the employment of reliable SHM tools in the early post-earthquake phase is fundamental to spot damages that lie unseen beneath the surface of the structure and to track the evolution of ongoing mechanisms in order to safely manage rescue operations and support civil protection activities. The added value that SHM-weighted information can bring to both stages of event preparedness and event response is doubled in case of ancient constructions, as none of them meet earthquake design requirements nor comply with any particular design code.

Ranked as one of the oldest countries in the world, Portugal features a large number of age-old structures which are all potentially exposed to both inland and offshore earthquakes, being the country located near the Eurasia-Africa plate boundary, opposite the Atlantic Ocean. One of the largest ever recorded earthquakes to impact Europe was indeed the 1755 Lisbon Earthquake, which also triggered an enormous tsunami in the North Atlantic Ocean. After such a destructive event, Lisbon metropolitan area was rebuilt according to anti-seismic provisions and great efforts have been made since then to reduce the seismic risk of building stock across the territory. Nevertheless, built heritage still represents an important part of this building stock. The well-known seismic vulnerability of existing historical constructions, combined with all the uncertainties that still arise on their actual structural behaviour, continues to promote investigations aimed at improving SHM-based condition assessment procedures, while shedding light on the seismic response of such systems. The following sections discuss the operational framework adopted in Portugal for the rapid condition screening of heritage structures in the context of seismic risk prevention. Because of space limitations, only a concise description of a few emblematic examples is presented hereafter.

13.5.1 Operational Framework for Rapid Condition Screening of Heritage Structures

Due to the seismotectonic characteristics of the region, the seismic hazard maps of mainland Portugal forecast two scenarios [57]: severe magnitude events at long distances with offshore epicentres (Type 1 seismic action) and moderate magnitude events at short distances with inland epicentres (Type 2 seismic action). In either case, apart from the Lisbon and Algarve regions, the seismicity of the Portuguese continent is rather low when compared to the rest of Europe (Fig. 13.29), being the reference PGA lower than 0.125 g in great part of the Country. Nevertheless, repeated mod-

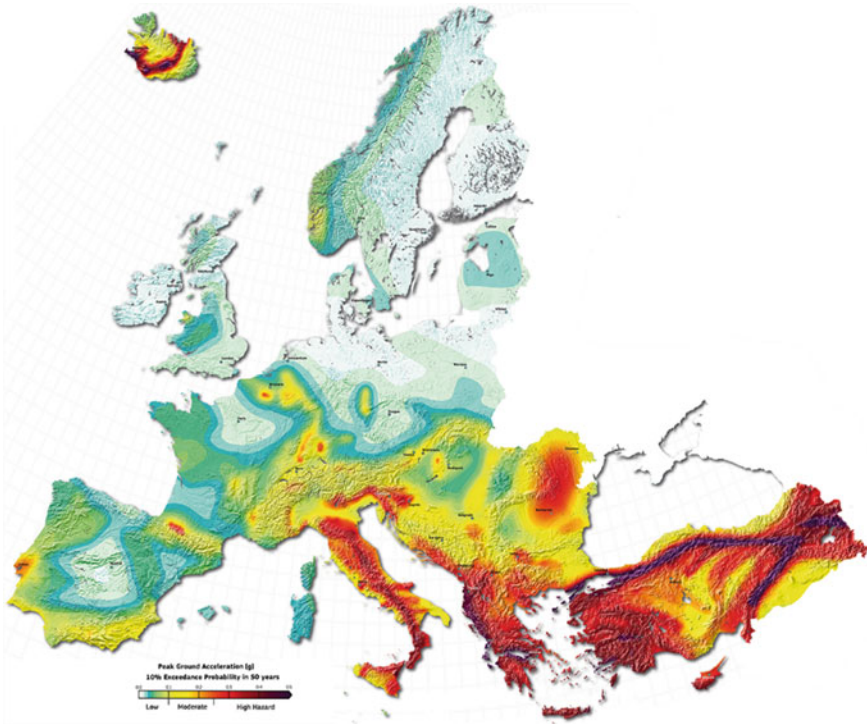


Fig. 13.29 Europe seismic hazard map. Source www.seismo.ethz.ch

erate earthquakes can be particularly harmful to centuries-old constructions, being cause of cumulative damages which can further increase their structural vulnerability. Depending on their specific structural characteristics, buildings can experience a considerable degree of loss for low input intensities and vice versa. Indeed, the seismic risk is determined by the combination of hazard, vulnerability and exposure.

In the context of heritage preservation and seismic risk reduction, the University of Minho is engaged in various monitoring activities and investigations aimed at improving SHM-based condition assessment procedures, while shedding light on the seismic behaviour of non-conventional historic structures. Three relevant examples will be presented herein with the purpose of giving a brief insight into the *modus operandi* adopted for tracking the dynamic behaviour of heritage buildings over time and assessing their health conditions in pre- and post-seismic scenarios.

In most cases, a simplified layout consisting of two tri-axial force-balance accelerometers, one installed at the ground level and another on top of the structure, is adopted for permanent monitoring systems. Although a higher density of sensors would be preferable to fully describe the dynamic behaviour of complex heritage buildings, this number of accelerometers is considered sufficient enough for

a rapid and low-cost global assessment of the structural conditions, enabling also to account for the amplification of the structural response in case of seismic event.

The installed accelerometers typically feature a dynamic range of ± 1.0 g, a sensitivity of 10 V/g and a temperature range between -20 °C and 70 °C, where the operating ranges are set according to the local seismic hazard and environmental conditions. Each sensor is connected by cable to a strong motion recorder provided with an integrated 16-bit or 24-bit ADC (Analog-to-Digital Converter). The recorder at the ground level is the master recorder, while the recorder at the top level is the slave recorder. Both recorders have the same capabilities but work independently. Still, they communicate through an enhanced interconnection network which enables synchronization and allows to set a common trigger. The system is conceived in such a way that, if more recorders are added, the same network can be easily extended to the new apparatus. Whenever the amplitude level of the monitored structure exceeds a predefined threshold value, the recorders are activated and the dynamic response at the instrumented locations is measured. To comply with the acquisition time length requirements, the total duration of the dynamic recordings is never lower than 1000–2000 times the structure's fundamental period (meaning around 9–17 min for a building with $T_1 = 0.5$ s). Moreover, depending on the frequency content of the monitored structure, the sampling rate for the signal acquisition may vary between 100 and 200 Hz. To detect frequency shifts and separate the influence of environmental conditions, monthly and seasonal programmed events are also recorded. Indeed, subtle changes caused by damage in masonry structures may be often masked by changes due to varying ambient conditions. It is worth noting that changes in the frequency-temperature relationships of the principal vibration modes of the structure may also take place after the occurrence of seismic events. Hence, it is common practice in Portugal to couple SHM with the analysis of the environmental variability for a thorough assessment of the system's behaviour.

Any heritage structure is the result of different building phases, construction techniques and changes which have followed over time up to the present state. Therefore, before deploying the SHM system, historical analyses, surveys and preliminary in situ diagnostic investigations are carried out to collect meaningful information about the geometrical and mechanical properties of the structure under observation as well as about possible local defects and vulnerabilities. Then, this information is combined with the results from ambient vibration tests (AVTs), allowing to set tailored acquisition parameters for the permanent monitoring system and to calibrate a reference FE model for assessing and comparing the seismic performance of the monitored structure in case of earthquake.

13.5.2 Instrumented Buildings and Data Analysis

Noteworthy examples of heritage monumental structures currently monitored by the University of Minho are the Clock tower of Mogadouro, the Church of Saint Torcato and the Church of Jerónimos Monastery in Lisbon. After a first phase of data

collection, including historical information, geometrical and topographic surveys, in situ diagnostic investigations and AVTs, simplified SHM systems consisting of a limited number of accelerometers have been installed in the three monuments along with temperature/humidity sensors plus crack meters and tilt meters at critical locations. Data are acquired periodically for programmed and triggered events.

Built in the XVI century to serve the neighboring church as a bell tower, the *Mogadouro clock tower* is a historic granite masonry structure with a rectangular cross section of $4.7 \times 4.7 \text{ m}^2$ and a height of 20.4 m (Fig. 13.30). The walls feature 1 m thickness, being their central part made of rubble stones with thick mortar joints and the corners built of large granite units with dry joints. Although located in a region with low seismic hazard, the tower's vulnerability before consolidation works was high. Thus, in 2006 the structure was equipped with a low-cost permanent monitoring system composed of three piezoelectric accelerometers placed at opposite corners at about mid height of the tower (Fig. 13.30). This sensor layout was chosen based on the outcome of previous AVTs in order to ensure the tracking of the first five vibration modes, including the torsional mode. The accelerometers are connected by coaxial cables to a USB data acquisition card with 24-bit resolution, provided with anti-aliasing filters, which is connected to a laptop with an uninterruptible power supply device. LabView software is used to record and acquire the signals through an ad hoc Virtual Instrument (VI). Besides triggered events, the VI is programmed to acquire 10 min of ambient vibrations in the 3 channels every hour. In parallel, a combined sensor connected to the laptop through a serial cable records ambient temperature and relative air humidity.

Saint Torcato church is a Neo-Manueline temple located in the homonymous village, North of Portugal. The church is characterized by a Latin cross longitudinal

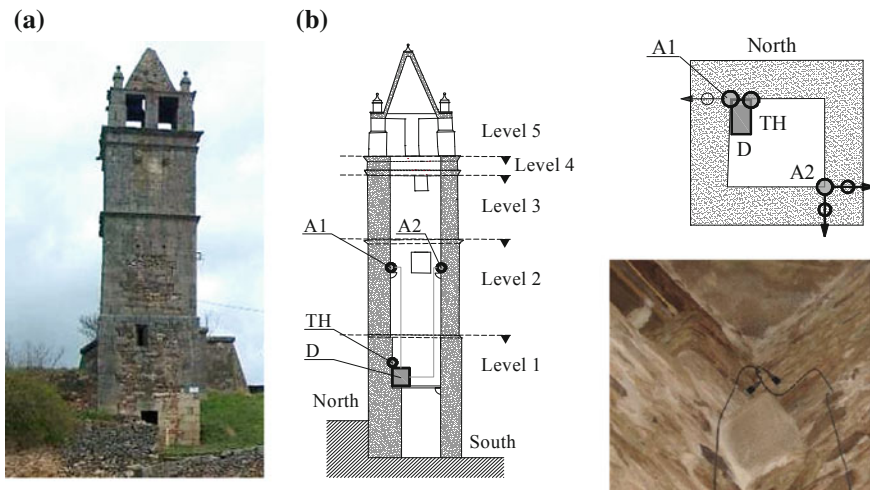


Fig. 13.30 Mogadouro clock tower: **a** view of the structure; **b** SHM sensors deployment

plan with a central nave of nearly 58 m length and a transept of about 37 m length, both covered with a barrel vault. The crossing between longitudinal nave and transept is capped with a dome. Two spired towers with rectangular section frame the façade (Fig. 13.3a–b). The construction of the church started in 1825 and stretched over nearly two centuries, involving several building phases and different materials. Towers and nave are made of three-leaf walls consisting of outer regular granite masonry blocks with thin mortar joints and inner rubble core, whereas apse and main altar are built by reinforced concrete walls covered with granite veneer [54]. The church is located in a region with low seismic hazard, but the stratigraphy of the soil beneath together with the structural damage that the fabric suffered over time increase its vulnerability against horizontal actions. The temple stands on a slope which is levelled by a landfills bank, thus the steady bedrock layer is very close to the foundation in the apsis and transept areas, but it goes deeper and deeper while proceeding towards the front of the temple. Here the soil is mostly composed of sands and non-cohesive layers, whose poor mechanical characteristics get worse when approaching the area below the western tower. This caused differential settlements in the strata underlying towers and façade, leading to separation movements of the towers and a severe V-cracking pattern in the façade (Fig. 13.31c–d).

After a long-term static and dynamic monitoring, strengthening works were carried out in 2014–2015 aiming at eliminating differential soil settlements and restraining the towers leaning. The Church appears now in sound state, however since 2014 a simple permanent SHM system for quick condition screening has been installed on top of the western tower, namely the one exhibiting higher tilting (Fig. 13.32). The system consists of one strong motion recorder with 16-bit ADC and one tri-axial force balance accelerometer with a dynamic range of ± 1 g and a sensitivity of 10 V/g. The vibration response of the structure is recorded for both triggered and programmed events. As the mode shapes of interest of the church are those associated with the towers' movements, whose frequencies fall within the range 2–3 Hz according to the former AVTs [52], signals are acquired for 600 s with a sampling frequency of 100 Hz.

The Church of “*Santa Maria de Belém*” is a limestone masonry structure built during the XVI century and located inside the majestic Monastery of Jerónimos in Lisbon, one of the regions with the highest seismic hazard in Portugal. The church features a cruciform shape with a single nave of 70 m length crossed by a transept of 40 m width, and an average height of 24 m. A single bell tower of 50 m height rises in the corner between south and west façades. Two rows of slender octagonal columns with a free height of 16 m and a radius ranging from 1.04 to 1.88 m provide support to the barrel vault of the longitudinal limb, allowing to reduce the large free span of the nave (Fig. 13.33). The seismic performance of the structure during the strong earthquake of 1755 was impressive. No severe damage was registered in that occasion in the whole compound. On the contrary, the subsequent shake of 1756 caused the collapse of one of the columns supporting the vaults of the church (with subsequent ruin of the nave) and also the partial collapse of the vault of the higher choir [53, 58]. Following these events, during the XIX century changes were made in the structure of the two towers and in the roof. The effect of these changes on the seismic performance

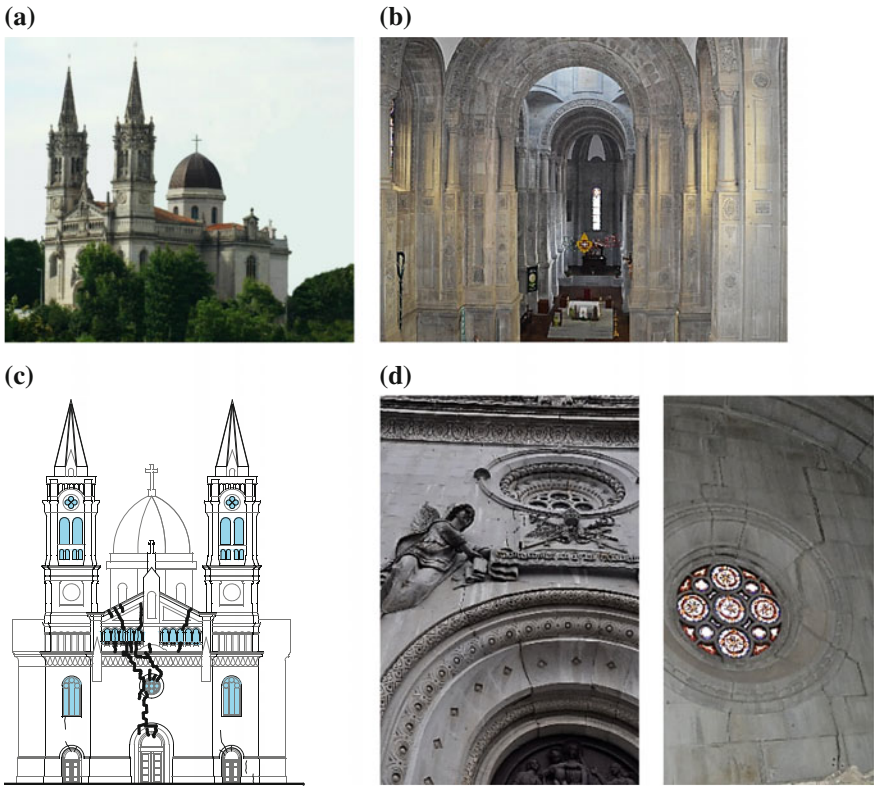


Fig. 13.31 Saint Torcato church: **a** exterior view of the building; **b** interior of the church; **c** and **d** damage pattern before consolidation

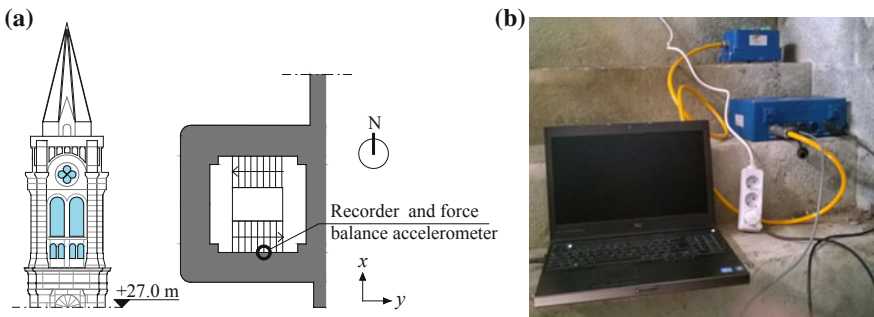


Fig. 13.32 SHM system of Saint Torcato church: **a** location of the devices; **b** setting of accelerometer and strong motion recorder on top of the western tower

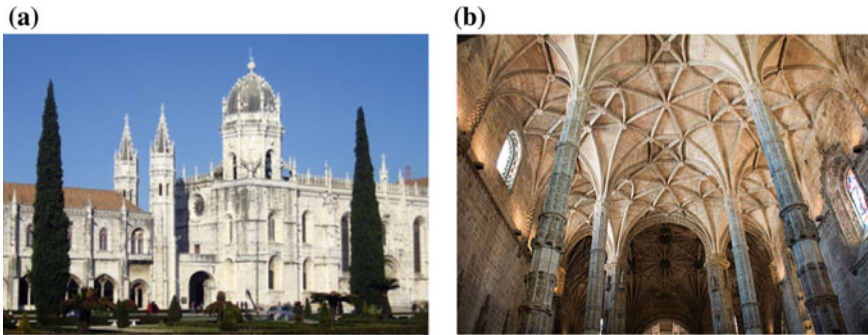


Fig. 13.33 Church of Jerónimos Monastery: **a** exterior view; **b** nave ribbed vault

of the structure remained an open issue [58]. Hence, several studies and numerical simulations have been performed in the last decades to investigate the structural behaviour of this church [58, 59]. In addition, to keep under control the health state of the monument and mitigate the seismic risk, a simplified monitoring system has been installed in the church since 2005. The type and location of sensors have been chosen according to the features to be extracted and in conformity with the directions of IGESPAR, former IPPAR (Portuguese Authority for the Architectural Heritage), with the purpose of minimizing the visual impact of the systems in the church [53].

The SHM system is composed of two strong motion recorders and two tri-axial force balance accelerometers (Fig. 13.34a–b), one (A1) located at the base of the structure near the chancel and connected to the master recorder, and the other one (A2) installed on the nave extrados and connected to the slave recorder. The recorders are mutually interconnected and synchronized for both triggered and programmed events. A predefined amplitude threshold of 0.5 mg is set in all 3 directions for the sensor at the base. As for the sensor at the nave extrados, thresholds of 1 mg and 5 mg are assigned in x (longitudinal) and y/z (transversal/vertical) directions, respectively. Anytime the amplitude level of the signals exceeds the predefined thresholds, data are recorded and stored to a permanent memory. Besides, monthly and seasonal programmed events of 10 min are registered to follow frequency trends over time and separate possible environmental fluctuations. According to the results of previous Operational Modal Analysis (OMA), the sampling rate adopted for digitizing the signals is 100 Hz for all events. On 12 February 2007 at 10:35 a.m., a moderate earthquake of magnitude $M_w = 6.1$ and with epicentre offshore Southwest Iberia occurred. The Monastery felt the ground shaking and its response was acquired by the strong motion recorders installed in the church (Fig. 13.34c–d). No severe damage took place, but a slight drop in the modal frequencies as well as a change of the frequency-temperature correlation were observed after the occurrence of the seismic event.

The data recorded by the SHM systems installed on the monitored heritage structures are automatically processed in order to perform a rapid condition screening

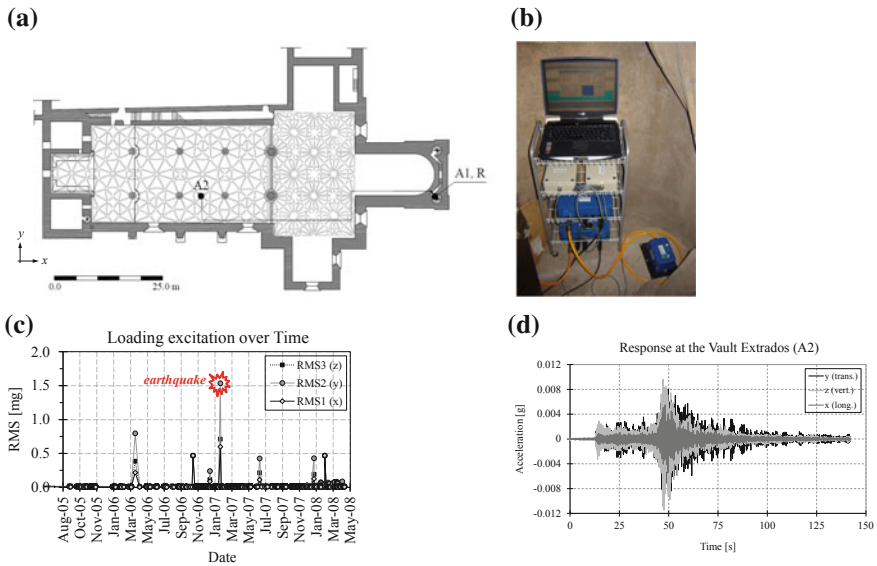


Fig. 13.34 SHM system of the Church of Jerónimos Monastery: **a** sensors location; **b** battery of recorders and accelerometer at the base level; **c** ambient excitation before, during and after the earthquake of 12/02/2007; **d** response of the church at the vault extrados during the seismic event

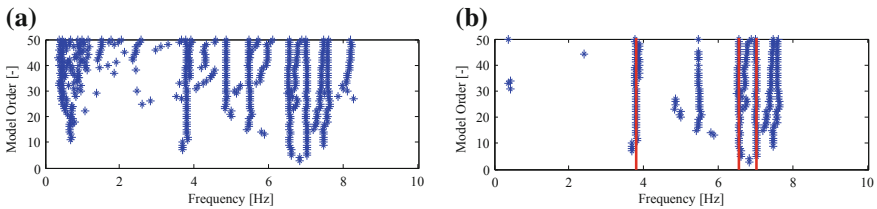


Fig. 13.35 Modal feature estimation: comparison between **a** full and **b** automatically cleared stabilization diagrams. The eigenfrequencies relevant to the stable modes are plotted as vertical lines on top of the cleared diagrams

of the system’s health. The automatic procedure is carried out through a MatLab algorithm based on the Stochastic Subspace Identification method (SSI-data driven) [60] as fulcrum for the feature extraction process. Control parameters and threshold values are established beforehand to avoid unrealistic estimations. Particular attention is given to the choice of the model order since the selection of small system orders can hinder the identification of weakly excited modes, but the choice of inappropriate large system orders can result in the appearance of many spurious modes. As an example, Fig. 13.35 shows the stabilization diagrams obtained for the chosen model order from the automated modal parameter estimation of the Church of Santa Maria de Belém.

The stable poles (physical modes) characterized by nearly identical frequencies, damping coefficients and mode shapes, are sorted from mathematical poles (spurious modes), which tend to exhibit lack of coherence between these quantities, according to a clustering analysis [53]. The clusters corresponding to the final physical modes are selected based on the fulfilment of two criteria, i.e. the Frequency Assurance Criterion (FAC) and the Modal Assurance Criterion (MAC):

$$FAC = \left| \frac{f_{i+1} - f_i}{f_i} \right|_k \leq FAC_{thr} \quad k = [1, 2, \dots, n] \quad (13.2)$$

$$\min(MAC_{i,i+1})_k \geq MAC_{thr} \quad k = [1, 2, \dots, n] \quad (13.3)$$

It is worth noting that when the dynamic monitoring system relies only on one measurement position, the MAC criterion is exploited as a relative modal amplitude comparison of the pole-weighted mode shape component identified in each iteration.

The characteristic values of each physical mode are computed by averaging frequency and damping values obtained iteratively per each model order. Finally, the whole routine is looped in order to estimate the characteristic values of each mode throughout the monitoring period along with their 95% confidence intervals. In this regard, dealing with a large number of data, a normal distribution is assumed and the two-sided confidence limits around each predicted value \hat{y} are evaluated as follows:

$$[\hat{y} - 1.96\sigma_y, \hat{y} + 1.96\sigma_y] \quad (13.4)$$

where σ_y is the estimated standard deviation of \hat{y} and 1.96 is found from a statistical t-distribution table. The definition of such confidence intervals provides an unbiased criterion to identify the occurrence of damage if the predicted values of new observations do not lie within the estimated confidence limits.

The control values required for the automated modal analysis are defined using as reference parameters the results from preliminary ambient vibration tests. The datasets not matching the sorting criteria imposed by the control values are discarded during the process. Before starting the procedure, a preliminary pre-processing task is performed, including decimation, de-trending and band-pass filtering of the collected signals. This operation reduces the total number of data points in the signals and increases the accuracy of the identification in the frequency range of interest. Acquisition and data processing parameters adopted for the automated modal identification relevant to the presented case studies are summarized in Table 13.3.

Besides the extraction of modal features, the spectral acceleration of the building in the three spatial directions are usually calculated and global damage-sensitive parameters are estimated to carry out a first rough damage assessment. If the estimated frequency shifts do exceed the confidence limits established around each predicted value, more accurate analyses are carried out for locating and quantifying the damage. This might include either modal-based inverse approaches such as Vibration-based Damage Identification Methods (VBDIMs) or model-based inverse approaches like the Finite Element Model Updating (FEMU).

Table 13.3 Acquisition and data processing parameters for the automated modal identification

Parameters	Description	Value(s)		
		Mogadouro tower	Saint Torcato church	Jeronimos church
Acquisition parameters	Sampling rate (Hz)	100	100	100
	Signal duration (s)	600	600	600
	Sampling interval (h)	1 (programmed events)	2 (programmed events)	1 (programmed events)
Processing parameters	State-space model order	50	50	50
	Decimation factor	5	5	5
	Frequency range	2.0–8.0	2.0–3.0	3.0–8.0
	Damping range (%)	0.5–3.0	0.1–5.0	0.1–5.0
	FAC threshold	0.04	0.05/0.05/0.03/0.00	0.06
	MAC threshold	0.95	0.90	0.90
	Freq. control vector	[2.5 2.7 7.1]	[2.13 2.58 2.82 2.95]	[3.7 5.2 6.6 7.3]

13.6 Conclusions

In this paper a summary of the seismic SHM applications to civil structures in different European countries is reported.

Several examples of instrumented buildings, bridges and cultural heritage constructions are shown. In Italy, France and Greece national programs supported by local public bodies are organized for civil protection activities. Data recorded by the monitoring systems are used for condition assessment, damage detection and emergency management and constitute the base for the scientific community to improve the understanding of the structural behavior during strong motions and sequences of events with variable intensity. Data recorded under low intensity ambient vibration are also used to calibrate and update finite element models for long term-assessment of the structural conditions and damage detection connected with a rapid condition screening of the system health.

Acknowledgements This work was partially funded by the Italian Civil Protection Department within project DPC-RELUIS 2017–2018. RESIF is a national research infrastructure managed by the RESIF Consortium, composed of 18 research institutions and universities in France. RESIF is also supported by a public grant, supervised by the French national research agency (ANR) as part

of the “Investissements d’Avenir” programme (reference: ANR-11-EQPX-0040) and the French Ministry for an Ecological and Solidary Transition. RAP national building array programme was launched thanks to funding from the environment ministry, Martinique regional council, Grenoble city council and the Pyrenees regional agency for development (DDT65). During its research efforts, ITSAK have collaborated with various scientists from the Civil Engineering Dpts. of the Aristotle University, the Dpt. of Mechanical and Industrial Engineering, University of Thessaly, Volos, as well as the Municipality of Delta, Thessaloniki, the EL.PE. Oil Company and the Bridge Maintenance Dpt. of Egnatia Odos S.A. Their particular contributions are noted in the respective literature. Many thanks are also due to the Institute’s technical and IT staff, for their invaluable contribution in the instrumentation efforts and the proper maintenance of the electronic equipment.

References

1. Dolce M, Ponzo FC, Goretti A, Moroni C, Giordano F, De Canio G, Marnetto R (2008) 3D dynamic test on 2/3 scale masonry buildings retrofitted with different systems. In: Proceeding of 14th world conference on earthquake engineering, Beijing, China, 12–17 Oct 2008
2. Valente C, Spina D, Nicoletti M (2006) Dynamic testing and modal identification. In: Mazzolani FM (ed) Seismic upgrading of RC buildings by advanced techniques. Monza, pp 29–101
3. Mori F, Acunzo G, Fiorini N, Pagliaroli A, Spina D, Dolce M (2015) The SMAV (Seismic Model from Ambient Vibrations) methodology for the evaluation of the structural operativity of the buildings (in Italian). In: Proceedings of the XVI Congresso Nazionale “L’ingegneria Sismica in Italia” (ANIDIS2015), L’Aquila, Italy
4. Dolce M, Nicoletti M, De Sortis A, Marchesini S, Spina D, Talanas F (2017) Osservatorio sismico delle strutture: the Italian structural seismic monitoring network. *Bull Earthq Eng* 15:621–641
5. Spina D, Lamonaca BG, Nicoletti M, Dolce M (2011) Structural monitoring by Italian department of civil protection and the case of 2009 Abruzzo seismic sequence. *Bull Earthq Eng* 9:325–346
6. Ceravolo R, Matta E, Quattrone A, Zanotti Fragonara L (2017) Amplitude dependence of equivalent modal parameters in monitored buildings during earthquake swarms. *Earthq Eng Struct Dyn* 46(14):2399–2417
7. Acunzo G, Gabriele S, Spina D, Valente C (2014) MuDI: a multilevel damage identification platform. In: Proceedings of the twelfth international conference on computational structures technology, paper 10.123 from CCP: 106. ISBN 978-1-905088-61-4
8. Rytter T (1993) Vibration based inspection of civil engineering structure. PhD dissertation, Department of Building Technology and Structure Engineering, Aalborg University, Denmark
9. Limongelli MP (2004) Modeling of unknown seismic responses of a partially instrumented bridge structure. In: 13th world conference on earthquake engineering, Vancouver, Canada, 1–6 Agosto 2004
10. Limongelli MP (2003) Optimal location of sensors for reconstruction of seismic responses through spline function interpolation. *Earthq Eng Struct Dyn* 32:1055–1074
11. Papathoma-Köhle M (2016) Vulnerability curves vs. vulnerability indicators: application of an indicator-based methodology for debris-flow hazards. *Nat Hazards Earth Syst Sci* 16:1771–1790
12. Giordano PF, Miraglia S, Limongelli MP (2018) The value of information for the seismic emergency management of a highway bridge. In: Innovative industry workshop. COST action TU1402, Lisbon, Apr 2018
13. Péquegnat C, Guéguen P, Hatzfeld D, Langlais M (2008) The French accelerometric network (RAP) and national data centre (RAP-NDC). *Seismol Res Lett* 79(1), 79–89. <https://doi.org/10.1785/gssrl.79.1.79>

14. Michel C, Guéguen P, El Arem S, Mazars J, Kotronis P (2010) Full scale dynamic response of a RC building under weak seismic motions using earthquake recordings, ambient vibrations and modelling. *Earthq Eng Struct Dyn* 39:419–441
15. Guéguen P (2012) Experimental analysis of the seismic response of an isolated building according to different levels of shaking: example of the Martinique earthquake (2007/11/29) Mw 7.3. *Bull Earthq Eng* 10(4):1285–1298
16. Mikael A, Guéguen P, Bard P-Y, Roux P, Langlais M (2013) Long-term frequency and damping wandering in buildings analysed using the random decrement technique (RDT). *Bull Seism Soc Am* 103(1):236–246
17. Fernández-Lorenzo G (2016) From accelerometric records to the dynamic behavior of existing buildings. PhD dissertation, Université de Nice Sophia Antipolis
18. Guéguen P (ed) (2013) Seismic vulnerability of structures. Civil engineering and geomechanics series. Wiley, Hoboken, USA and ISTE, London, UK, 368 pp
19. Guéguen P, Langlais M, Garambois S, Voisin C, Douste-Bacqué I (2017) How sensitive are site effects and building response to extreme cold temperature? The case of the Grenoble's (France) City Hall building. *Bull Earthq Eng* 15(3):889–906
20. Larose E, Carrière S, Voisin C, Bottelin P, Baillet L, Guéguen P, Walter F, Jongmans D, Guillier B, Garambois S, Gimbert F, Massey C (2015) Environmental seismology: what can we learn on earth surface processes with ambient noise?. *J Appl Geophys* 116:62–74
21. Michel C, Guéguen P (2010) Time–frequency analysis of small frequency variations in civil engineering structures under weak and strong motions using a reassignment method. *Struct Heal Monit* 9(2):159–171
22. Brossault MB, Roux P, Guéguen P (2018) The fluctuation–dissipation theorem used as a proxy for damping variations in real engineering structures. *Eng Struct* 167:65–73
23. Nasser F, Li Z, Guéguen P, Martin N (2016) Frequency and damping ratio assessment of high-rise buildings using an automatic model-based approach applied to real-world ambient *vibration recordings*. *Mech Syst Signal Process* 75:196–208
24. Michel C, Guéguen P (2018) Interpretation of the velocity measured in buildings by seismic interferometry based on Timoshenko beam theory under weak and moderate motion. *Soil Dyn Earthq Eng* 104:131–142
25. Karakostas CZ, Lekidis VA, Pavlidou M, Papadimitriou K (2002) Analytical and experimental investigation of the dynamic behaviour of R/C buildings during the Athens (7-9-99) after-shock sequence. In: Proceedings of the 12th European conference on earthquake engineering (12ECEE), paper no. 270, London, 9–13 Sept
26. Karakostas CZ, Lekidis VA, Papadimitriou K (2003) Seismic response of instrumented R/C buildings during the Athens (7-9-99) aftershock sequence. In: Proceedings of the fib-symposium on concrete structures in seismic regions (FIB2003), paper no. 113, Athens, Greece, 6–9 May
27. Makarios T, Salonikios T, Karakostas C, Lekidis V, Sous I, Anastasiadis A (2006) Assessment of dynamic characteristics of a R/C building through a seismic excitation recording. In: 15th national reinforced concrete conference, Vol B', Alexandroupolis, Greece, 25–27 Oct, pp 396–409 (in Greek)
28. Makarios T, Salonikios T, Lekidis V, Karakostas C, Demosthenous M (2009) Identification of eigen-periods & mode-shapes of vibration of a five-storey building by its response during the post-earthquake sequence of the Achaia-Ilia earthquake. In: 16th national reinforced concrete conference, Pafos, Cyprus, 21–23 Oct (in Greek)
29. Karakostas C, Lekidis V, Morfidis K, Salonikos T (2016) Investigation of the dynamic response of an instrumented building during the Cephalonia 2014 seismic sequence. In: Proceedings of the 17th national reinforced concrete conference, paper no. 35, Thessaloniki, Greece, 10–12 Nov (in Greek)
30. Karakostas C, Rovithis E, Morfidis K, Chatzistefanou GA, Lekidis V, Theodoulidis N, Makarios T (2018) Investigation of the dynamic response and SSI effects of the instrumented municipality building in Lefkas, Greece. In: Proceedings of the 16th European conference on earthquake engineering, paper no. 11461, Thessaloniki, Greece, 18–21 June

31. Rovithis E, Makra K, Kirtas E, Manesis C, Bliziotis D, Konstantinidou K (2018) Field monitoring of strong ground motion in urban areas: the Kalochori accelerometric network (KAN), database and Web-GIS portal. *Earthq Spectra*, 34(2), pp 471–501
32. Kirtas E, Rovithis E, Makra K, Papaevangelou I (2018) Dynamic response characteristics of an instrumented steel water tank in Kalochori, N. Greece. In: *Proceedings of the 16th European conference on earthquake engineering*, paper no. 11167, Thessaloniki, Greece, 18–21 June
33. Lekidis VA, Karakostas CZ, Talaslidis DG (1998) Dynamic characteristics of the cable-stayed bridge on Evripos channel, Greece. In: *Proceedings of the 11th European conference on earthquake engineering*, CNIT, Paris, France, 6–11 Sept
34. Lekidis VA, Karakostas CZ, Talaslidis DG (2001) Instrumentation, measurements and numerical analysis of bridges: an example of the cable-stayed bridge on Evripos channel, Greece. In: Erdik M et al (eds) *Proceedings of the advanced NATO workshop on strong motion instrumentation for civil engineering structures*, Istanbul, Turkey. Kluwer Academic Publishers, pp 481–493
35. Papadimitriou C, Karamanos SA, Christodoulou K, Pavlidou M, Lekidis VA, Karakostas CZ (2002) Model updating of bridges using vibration measurements. In: *Proceedings of the 12th European conference on earthquake engineering (12ECEEE)*, paper no. 485, London, 9–13 Sept
36. Lekidis V, Tsakiri M, Makra K, Karakostas C, Klimis N, Sous I (2005) Evaluation of dynamic response and local soil effects of the Evripos cable-stayed bridge using multi-sensor monitoring systems. *Eng Geol* 79:43–59
37. Karakostas C, Sextos A, Lekidis V, Papadopoulos S (2011) Investigation of the dynamic response of the Evripos cable-stayed bridge in Greece under asynchronous ground motion records. In: *Proceedings of computational methods in structural dynamics and earthquake engineering (COMPDYN2011)*, paper no. 486, Corfu, Greece, 25–28 May
38. Papadopoulos S, Lekidis V, Sextos A, Karakostas C (2013) Assessment of EC8 procedures for the asynchronous excitation of bridges based on numerical analyses and recorded data. In: *Proceedings of computational methods in structural dynamics and earthquake engineering (COMPDYN2013)*, paper no. 1498, Kos, Greece, 12–14 June 2013
39. Lekidis V, Papadopoulos S, Karakostas C, Sextos A (2013) Monitored incoherency patterns of seismic ground motion and dynamic response of a long cable-stayed bridge. In: Papadrakakis M, Fragiadakis M, Plevris V (eds) *Postconference book computational methods in earthquake engineering*, Vol 2, Chapter 2 in *Computational methods in applied sciences*, Vol 30, pp 33–48
40. Sextos A, Karakostas C, Lekidis V, Papadopoulos S (2015) Multiple support seismic excitation of the Evripos bridge based on free-field and on-structure recordings. *Struct Infrastruct Eng* 11(11):1510–1523. <https://doi.org/10.1080/15732479.2014.977302>
41. Lekidis VA, Karakostas CZ, Christodoulou K, Karamanos S, Papadimitriou K, Panetsos P (2004) Investigation of dynamic response and model updating of instrumented R/C bridges. In: *Proceedings of the 13th world conference on earthquake engineering (13WCCEE)*, Vancouver, 1–6 Aug
42. Ntsios E, Karakostas C, Lekidis V, Panetsos P, Nikolaou I, Papadimitriou C, Salonikios Th (2009) Structural identification of Egnatia Odos bridges based on ambient and earthquake induced vibrations. *Bull Earthq Eng* 7(2):485–501
43. Karamanos SA, Papadimitriou C, Christodoulou K, Karakostas CZ, Lekidis VA, Panetsos P (2004) Multi-objective framework for model updating with application to a four-span concrete bridge. In: Boller C, Staszewski WJ (eds) *Proceedings of 2nd European workshop on structural health monitoring*, Munich, 7–9 July. DEStech Publications, pp 195–202
44. Pavlidou M, Christodoulou K, Gkaras V, Karamanos SA, Papadimitriou C, Perdikaris P, Lekidis VA, Karakostas CZ (2002) Model updating of bridges using vibration measurements. In: *Proceedings of the 1st European workshop on structural health monitoring (SHM2002)*, Paris, 10–12 July, pp 1107–1114
45. Karakostas C, Makarios T, Lekidis V, Kappos A (2006) Evaluation of vulnerability curves for bridges—a case study. In: *Proceedings of the 1st European conference on earthquake engineering and seismology*, paper no. 1435, Geneva, 3–8 Sept

46. Makarios T, Lekidis V, Kappos A, Karakostas C, Mochonas J (2007) Development of seismic vulnerability curves for a bridge with elastomeric bearings. In: Proceedings of computational methods in structural dynamics and earthquake engineering (COMPDYN2007), paper no. 1516, Rethymno, Greece, 13–16 June
47. Panetsos P, Lambropoulos S, Papadimitriou C, Karamanos S, Lekidis V, Karakostas C (2006) Bridge health monitoring for Egnatia Odos bridge management system. In: Proceedings of the 3rd European workshop on structural health monitoring, Granada, Spain, 5–7 July
48. Caetano E, Cunha A, Magalhães F, Moutinho C (2010) Studies for controlling human-induced vibration of the Pedro e Inês footbridge, Portugal. Part 1: assessment of dynamic behaviour. *Eng Struct* 32:1069–1081
49. Martins N, Caetano E, Diord S, Magalhães F, Cunha A (2014) Dynamic monitoring of a stadium suspension roof: wind and temperature influence on modal parameters and structural response. *Eng Struct* 59:80–94
50. Magalhães F, Pacheco J, Cunha A (2016) Illustrating the relevance of SHM in a case study: the Foz Tua centenary railway bridge. In: 8th European workshop on structural health monitoring, Bilbao, Spain, 5–8 July
51. Magalhães F, Cunha A, Caetano E (2012) Vibration based structural health monitoring of an arch bridge: from automated OMA to damage detection. *Mech Syst Signal Process* 28:212–228
52. Ramos LF, Marques L, Lourenço PB, De Roeck G, Campos-Costa A, Roque J (2010) Monitoring historical masonry structures with operational modal analysis: two case studies. *Mech Syst Signal Process* 24(5):1291–1305
53. Masciotta M-G, Roque JCA, Ramos LF, Lourenço PB (2016) A multidisciplinary approach to assess the health state of heritage structures: the case study of the Church of Monastery of Jerónimos in Lisbon. *Constr Build Mater* 116:169–187
54. Masciotta M-G, Ramos LF, Lourenço PB (2017) The importance of structural monitoring as a diagnosis and control tool in the restoration process of heritage structures: a case study in Portugal. *J Cult Herit* 27:36–47
55. Pereira S, Magalhães F, Gomes J, Cunha A, Lemos JV (2017) Installation and results from the first 6 months of operation of the dynamic monitoring system of Baixo Sabor arch dam. *Procedia Eng* 199:2166–2171
56. Mesquita E, Arêde A, Pinto N, Antunes P, Varum H (2018) Long-term monitoring of a damaged historic structure using a wireless sensor network. *Eng Struct* 161:108–117
57. Iacovino C, Ditommaso R, Ponzo FC, Limongelli MP (2019) Preliminary analysis of the dynamic behaviour of several structures subjected to the 2016 Central Italy earthquake. Submitted to SEMC 2019. Cape Town, Sept 2019
58. Lourenço PB, Krakowiak KJ, Fernandes FM, Ramos LF (2007) Failure analysis of Monastery of Jerónimos, Lisbon: how to learn from sophisticated numerical models. *Eng Fail Anal* 14:280–300
59. Oliveira DV, Ramos LF, Lourenço PB, Roque JCA (2005) Structural monitoring of the Monastery of Jerónimos. In: International conference on the 250th anniversary of the 1755 Lisbon earthquake, Lisbon, pp 466–473
60. Peeters B, De Roeck G (1999) Reference-based stochastic subspace identification for output-only modal analysis. *Mech Syst Signal Process* 13(6):855–878
61. Paquette J, Bruneau M (2006) Pseudo-dynamic testing of unreinforced masonry building with flexible diaphragm and comparison with existing procedures. *Constr Build Mater* 20(4):220–228

Chapter 14

S²HM Practice and Lessons Learned from the 2011 Tohoku Earthquake in Japan



Toshihide Kashima and Yoshiaki Hisada

Abstract During the 2011 Tohoku earthquake, a vast number of buildings suffered violent shaking that has never been experienced in the past. Strong motion data of the 2011 Tohoku Earthquake were obtained in many buildings, and many meaningful analytical results have been reported. We introduce several findings obtained through the analysis of the strong motion data recorded in buildings such as; change in dynamic characteristics of damaged buildings, amplitude-dependence of dynamic characteristics, and long period long duration strong motion and response of tall buildings. In addition, we report the application of the real-time S²HM (real-time building damage assessment system) to emergency management in high-rise buildings during the Tohoku earthquake.

Keywords Strong motion data · 2011 Tohoku earthquake · Real-time S²HM · Real-time building damage assessment system · Emergency management

14.1 Introduction

The history of strong motion observation for building structures in Japan has reached 60 years. We have accumulated valuable strong motion structural response data with many earthquakes so far. In particular, during the 2011 Tohoku earthquake and its aftershocks, a large quantity of high-quality strong motion data were recorded, and facilitated important research on the dynamic characteristics of buildings. A number of findings applicable to S²HM (Seismic Structural Health Monitoring) have also been obtained. On the other hand, recently, S²HM has been applied to the damage assessments of a building immediately after earthquakes, for utilizing the

T. Kashima (✉)

IISEE, Building Research Institute (BRI), 1 Tachihara, Tsukuba, Ibaraki 305-0802, Japan
e-mail: kashima@kenken.go.jp

Y. Hisada

Department of Urban Design and Planning, Kogakuin University, 1-24-2 Nishishinjuku,
Shinjuku, Tokyo 163-8677, Japan
e-mail: hisada@cc.kogakuin.ac.jp

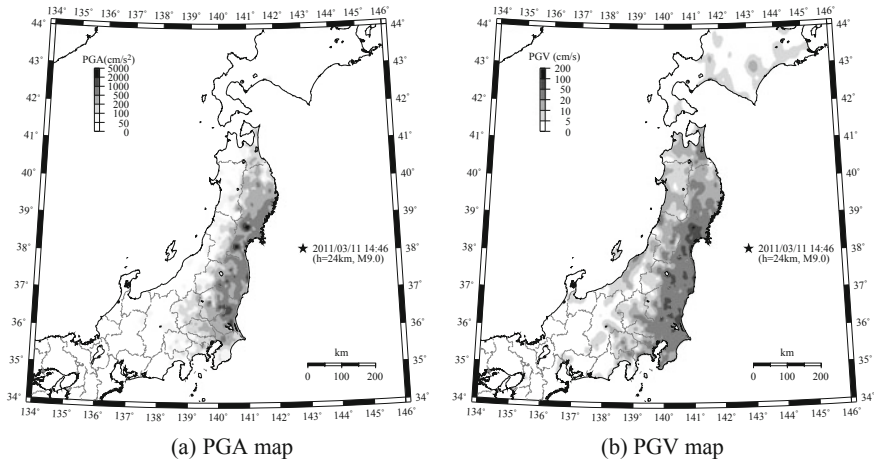


Fig. 14.1 Peak ground acceleration (PGA) and peak ground acceleration (PGV) maps of the 2011 Tohoku earthquake

emergency/crisis management and improving the resilience performance. This paper introduces some of these recent findings on building seismic response, and the application to the real-time damage assessment system.

14.2 Lessons Learned from the 2011 Tohoku Earthquake

In Japan, strong motion instruments are deployed in about five hundred of buildings [1]. Hence, during the 2011 Tohoku earthquake, strong motion responses of a large number of buildings were recorded. This chapter introduces findings related to building seismic responses based on the analyses of the strong motion data acquired by the strong motion network of the Building Research Institute (BRI), Japan.

14.2.1 Ground Motions

On March 11, 2011, a large earthquake with a moment magnitude (M_w) 9.0 occurred off the Pacific coast of the north-eastern Japan. The earthquake, hereinafter referred to as the 2011 Tohoku Earthquake, brought about monstrous tsunami and widespread damage to the eastern Japan. Figure 14.1 illustrates the location of the epicentre as an asterisk, and ground acceleration (PGA) and peak ground acceleration (PGV) distributions of the Tohoku Earthquake. The northern Pacific side of Japan widely suffered severe shaking, and PGA exceeded 1 G in several areas.



(a) External appearance before the 2011 Tohoku Earthquake

(b) Damage detail

Fig. 14.2 Damaged building of Tohoku University

14.2.2 Damaged Buildings

Earthquake damages to several buildings having strong motion instruments were reported so far. Among them, a building of Tohoku University suffered the severest damage. The building was a nine-story steel-framed reinforced concrete building located in Sendai City, 177 km from the epicentre. External appearance of the building before the 2011 Tohoku Earthquake is shown in Fig. 14.2a. Multi-storey shear walls of the building suffered bending fractures at the third-floor level and the exterior columns were severely crushed as shown in Fig. 14.2b [2].

Two tri-axial acceleration sensors were deployed on the first and ninth floors of the building by BRI. The strong motion data clearly captured the destruction process [3]. Figure 14.3a and b indicate acceleration waveforms recorded in the building during the 2011 Tohoku Earthquake. Figure 14.3c and d show building displacements (relative displacements of the ninth floor to the first floor). The natural periods and damping ratios of the building are plotted in Fig. 14.3e and f. The natural periods and damping ratios represent those of the first vibration mode identified in every 10 s by the method of searching optimal parameters of a single-degree-of-freedom system using the strong motion data [4].

In Fig. 14.3a and b, thick lines and thin lines indicate acceleration waveforms on the first floor and ninth floor, respectively. Two notable wave groups at the times of 40 s and 80 or 90 s can be recognised on the waveforms. Earthquake motions and building responses of the second wave group seem to be more severe than those of the first wave group. The natural periods were 0.65 s in the initial stage, and then increased to 1 s at the time of 50 s after the first wave group arrival. When the second wave group arrived around 80 s, the natural periods in the both of horizontal directions were extended to over 1 s. Especially in the N282°E direction (282 degrees clockwise from the north, corresponding to the short-side direction of the building),

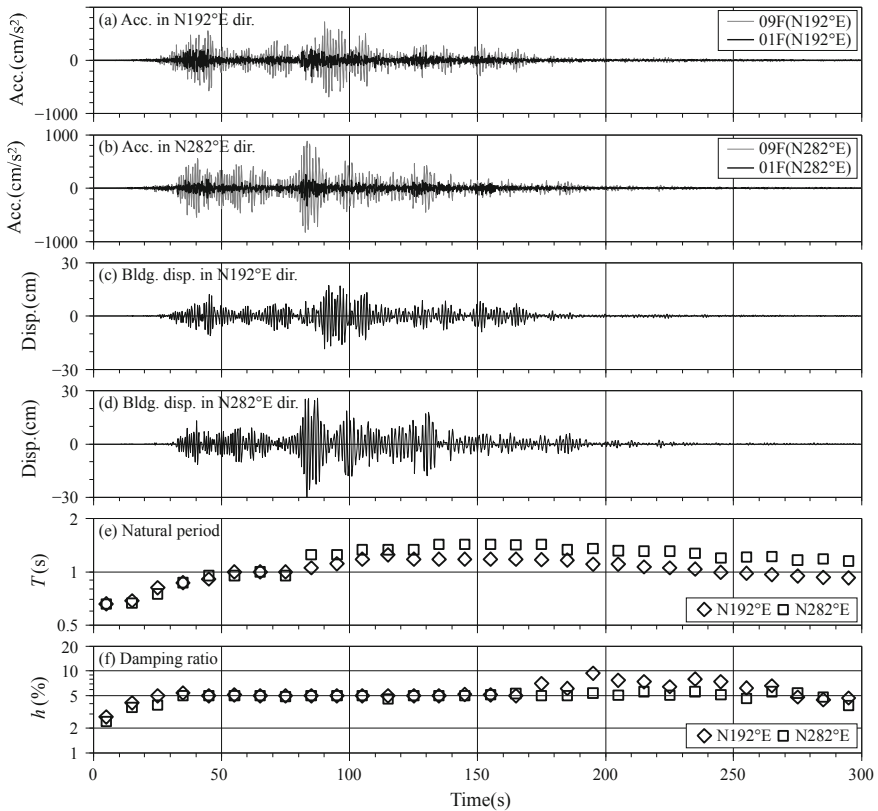


Fig. 14.3 Accelerations, building displacements, natural periods and damping ratios of the damaged building of Tohoku University

the increase of the natural period is notable. During the time window of 130–180 s, the natural periods in the N282°E direction are increased to that of the initial natural period.

14.2.3 Response to Long-Period Long-Duration Earthquake Motion

A 256 m tall, 52-story steel-framed super high-rise building, a 52-storey steel-framed building in Osaka suffered unexpectedly prolonged shaking during the 2011 Tohoku Earthquake even though it was 770 km away from the epicentre. Five tri-axial acceleration sensors on the first floor, 18th floor, 38th floor, and (two on the) 52nd floor of the building were installed by instrumentation program of BRI only a few weeks

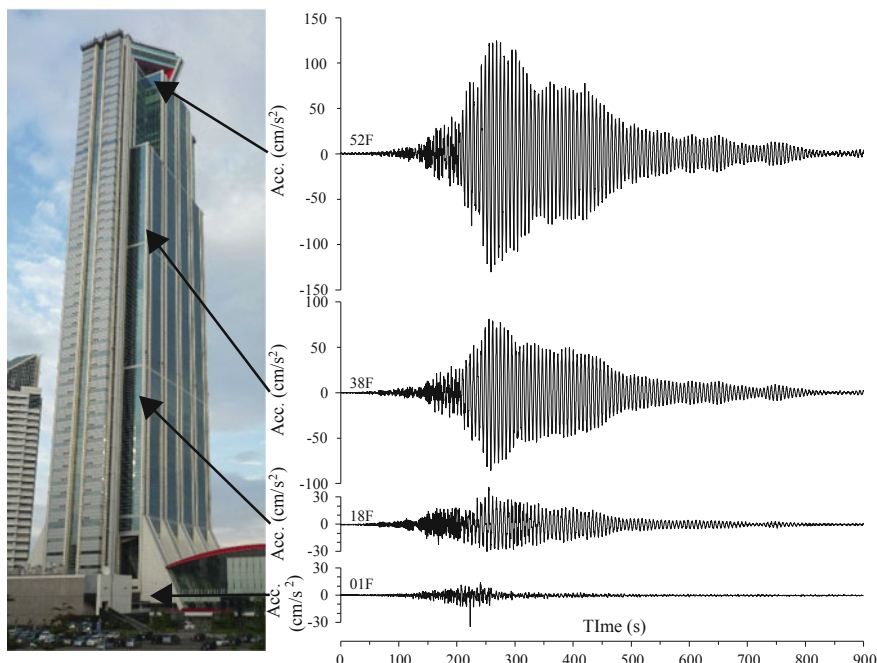


Fig. 14.4 Acceleration time histories recorded in a super high-rise building in Osaka City

before the earthquake. On the 52nd floor, two sensors are placed in the north and south sides to investigate torsional movement.

Acceleration waveforms in the N229°E direction (corresponding to the short-side direction of the building) on the all floors are shown in Fig. 14.4. The acceleration data on the first floor has spike-like noises affected by the collision of lift cables, therefore the maximum accelerations by the earthquake motion might be smaller than 20 cm/s^2 . In contrast, the maximum acceleration on the 52nd floor was extremely large exceeding 130 cm/s^2 . The maximum horizontal displacement of the 52nd floor is estimated to exceed 130 cm.

The predominant periods matched the natural periods of the building, consequently the resonance and the low damping ratios of the building enormously magnified building response. Subsequently, the shaking continued for more than 800 s mainly in the N229°E direction. There was no structural damage to the building, but facility equipment and non-structural elements were considerably damaged [5]. Since accelerations at the central monitoring room on the first floor were small, the building managers did not realize such serious situation on upper floors, and could not respond appropriately [6]. A S²HM system can quickly identify the locations of possible severity by the effect of strong shaking.

14.2.4 Change in Dynamic Characteristics of Buildings During the 2011 Tohoku Earthquake

Kashima et al. [7] discussed the dynamic characteristics of 27 reinforced concrete (RC) and steel-framed reinforced concrete (SRC) buildings based on strong motion data recorded during the 2011 Tohoku Earthquake. Changes in the fundamental natural periods and damping ratios of the buildings were investigated through a comparison of these values in the initial, main and coda parts of the strong motion data. Figure 14.5a and b show the natural periods and damping ratios, respectively. In each figures, hollow triangles, solid circles, and hollow inverted triangles indicate the values in the initial, main and coda parts, respectively.

In some of the buildings, i.e. the building 1, 3, 7, 8 and 9, significant changes in the natural periods of the main and coda parts from the initial part were detected. The building 1 is the seriously damaged one introduced in Sect. 14.3.2, and the buildings 3, 7, 8 and 9 were slightly damaged. The damping ratios tended to increase in the main part, although the ratios varied widely.

14.3 Influence Factors in the Dynamic Characteristics of Buildings

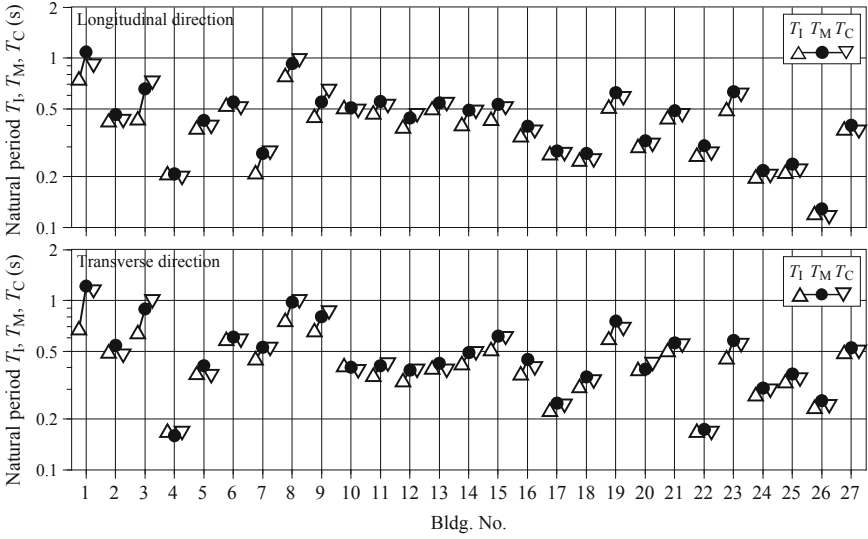
Not only structural damage, but also various factors influence the dynamic characteristics of buildings. Some examples that are clarified from the analysis of strong motion data are introduced.

14.3.1 Target Building

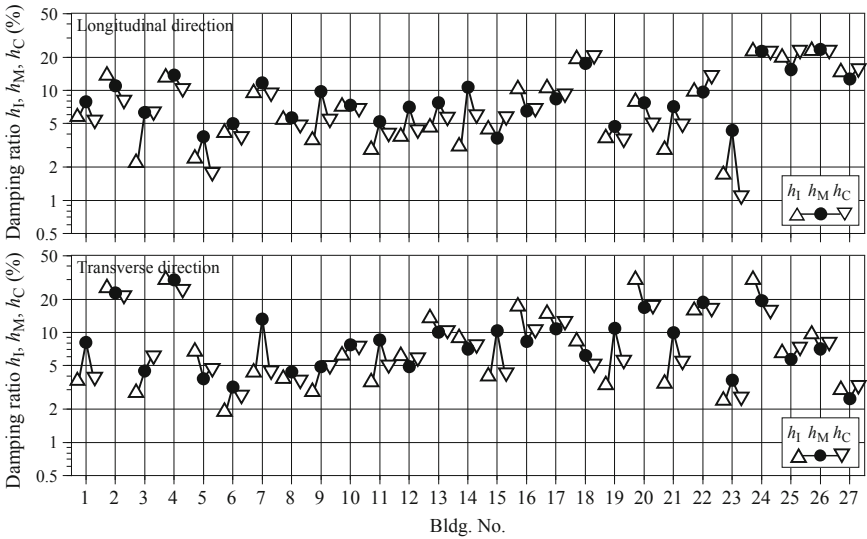
The annex building of BRI is an eight storeyed SRC building located in Tsukuba City, Japan. Acceleration sensors were densely placed in and around the building at the time of its completion in 1998 as shown in Fig. 14.6. More than 1700 strong motion data, including that of the 2011 Tohoku Earthquake, were accumulated for 20 years. Using the strong motion data obtained in this building, influence factors in the dynamic characteristics are discussed.

14.3.2 Change in Dynamic Characteristics with Time

Figure 14.7 shows change in natural periods and damping ratios of the annex building with time. Solid circles (●) and hollow triangles (△) represent the values in NS and EW directions, respectively. Looking at the natural period in Fig. 14.7a, the natural



(a) Natural periods



(b) Damping ratios

Fig. 14.5 Natural periods (T_1, T_M and T_C in a) and damping ratios (h_1, h_M and h_C in b) identified using the initial, main and coda parts of strong motion data in 27 RC/SRC buildings

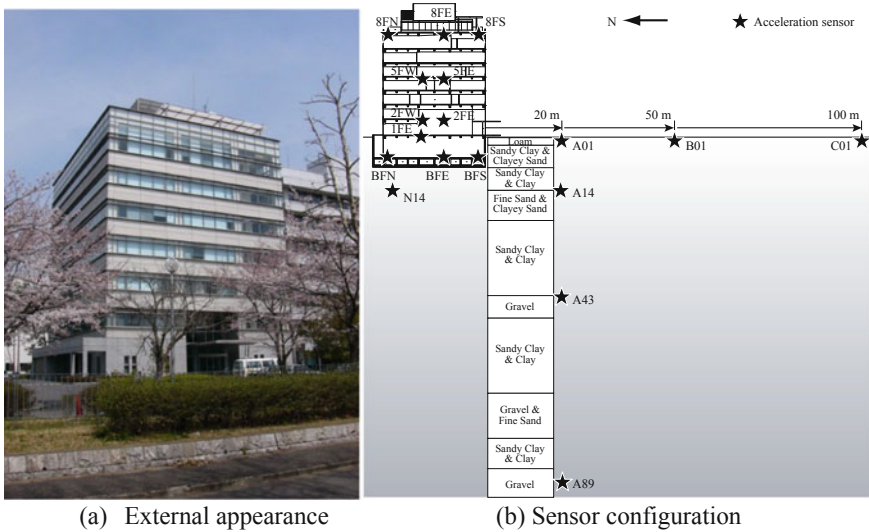


Fig. 14.6 External appearance and sensor configuration of the BRI annex building

periods, which were a little over 0.5 s just after the completion in 1998, gradually increased thereafter, and reached about 0.7 s in 2006. The natural periods seem to be stable for a while (2006–2010) but has extended to about 1 s at the time of the 2011 Tohoku Earthquake. The damping ratios varies widely, and it is difficult to find a trend due to time passage.

14.3.3 Amplitude Dependence of Dynamic Characteristics

Next, let's look at the amplitude dependence of dynamic characteristics of the annex building. As the value representing the response amplitude, the maximum displacement angle, the ratio of the maximum relative displacement to the building height, is adopted. The relationship of the natural periods and the damping ratios to the maximum displacement angles is shown in Fig. 14.8. Upper plots (Fig. 14.8a and b) and lower plots (Fig. 14.8c and d) correspond to the natural period and damping ratios, respectively. The left plots (Fig. 14.8a and c) and right plots (Fig. 14.8b and d) represent the values in North-South and East-West directions, respectively. In each plot, solid circles (●) and hollow circles (○) indicate the values before and after the 2011 Tohoku Earthquake, respectively. Looking at the natural period, it is clearly shown that the natural period increases as the maximum displacement angle increases. The same trend is observed both before and after the 2011 Tohoku Earthquake, but the value before the earthquake varies.

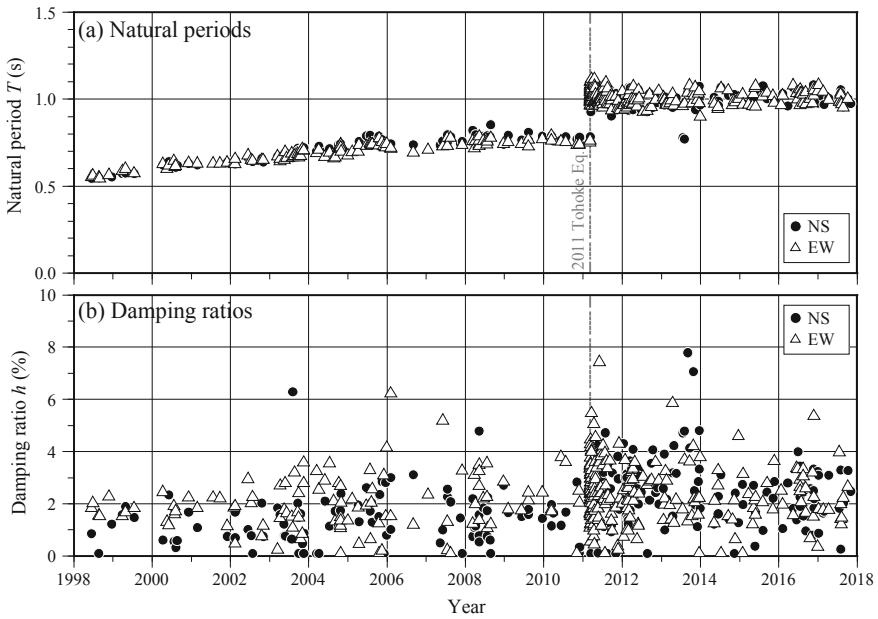


Fig. 14.7 Change in natural periods and damping ratios of a 8-storey SRC building with time

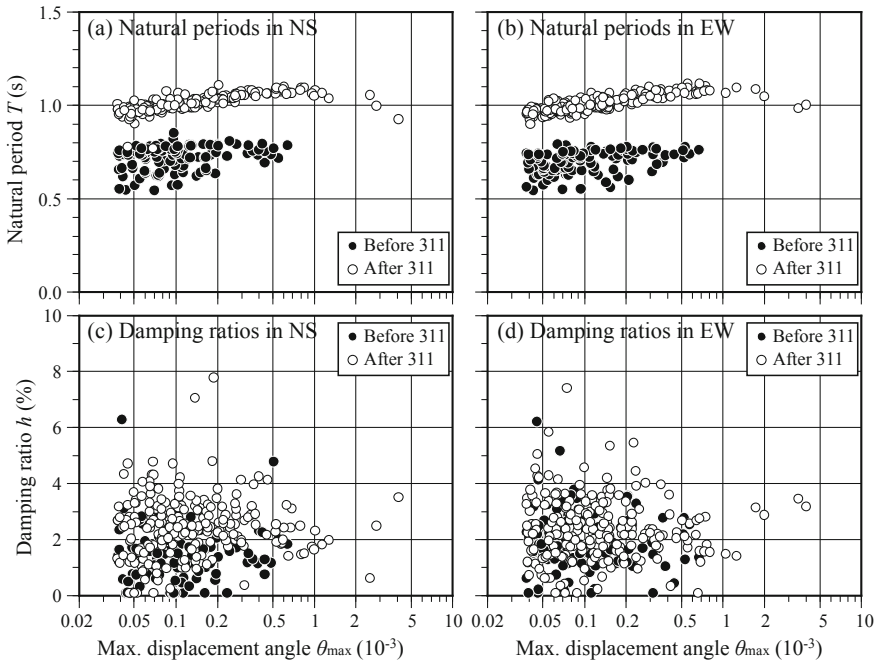


Fig. 14.8 Relation of natural periods and damping ratios to maximum displacement angle

14.4 Damage of High-Rise Buildings and Applications of S²HM to Emergency Management During the 2011 Tohoku Earthquake

We first show typical damage of high-rise buildings in the Shinjuku area, Tokyo, during the 2011 Tohoku Earthquake, and next introduce applications of S²HM to the real-time assessment of building damage immediately after the earthquake.

14.4.1 *Recorded Strong Motions and Damage of a High-Rise Building in Tokyo During the 2011 Tohoku Earthquake*

Figure 14.9 shows the picture of the Kogakuin University campus and the adjacent STEC office buildings, which are located in Shinjuku, Tokyo, the locations of acceleration sensors on a plan, the accelerations and displacements at the 1st and 29th floors recorded during the 2011 Tohoku earthquake [8, 9]. The maximum acceleration and displacement are 2.32 m/s^2 and 0.37 m , respectively, at the top floor. Figure 14.10 shows the main damage in the university building. There were no serious structural damage, but the non-structural damages comprised falling of ceiling panels, toppling of an un-anchored bookshelf, deformation of the partition, move and fall of unstable objects, and tangles of the main cables of an elevator.

Similar damage has been reported in other high-rise buildings in the Shinjuku area. Shindo et al. [10] conducted a questionnaire survey on damage and emergency response for the high-rise buildings in the area, and obtained the similar results from 16 buildings and 23 tenants. That is, there was no structural damage to any building, but a lot of damage to non-structural elements are reported: fall of exterior panels (4 buildings), and peeling/falling of ceiling panels (13 buildings), interior panels (9 buildings), deformation of doors and failure of opening (6 buildings), deformation of partitions (2 buildings), breaking of sprinkler head and leaking water (2 buildings). All the elevators were stopped temporarily, and several people were trapped in elevator cages. Severe damage to elevators were also reported, such as tangles/cutting of main and control cables (4 buildings), falls of panels/counterweight inside an elevator hoistway (2 buildings), and deformation of elevator door (1 building), which caused the elevators to become unusable for a few months. One person was injured by catching a finger in a heavy fire door.

As for the emergency management, no buildings were installed the real-time S²HM, and thus, it took several hours to understand the overall damage of the buildings. Even though the emergency managers did not announce the evacuation from the buildings, 8 out of 23 tenants evacuated voluntarily, because some of them judged the buildings were dangerous, and the others followed the emergency manual for the case of fire. Consequently, thousands of people evacuated from the buildings,

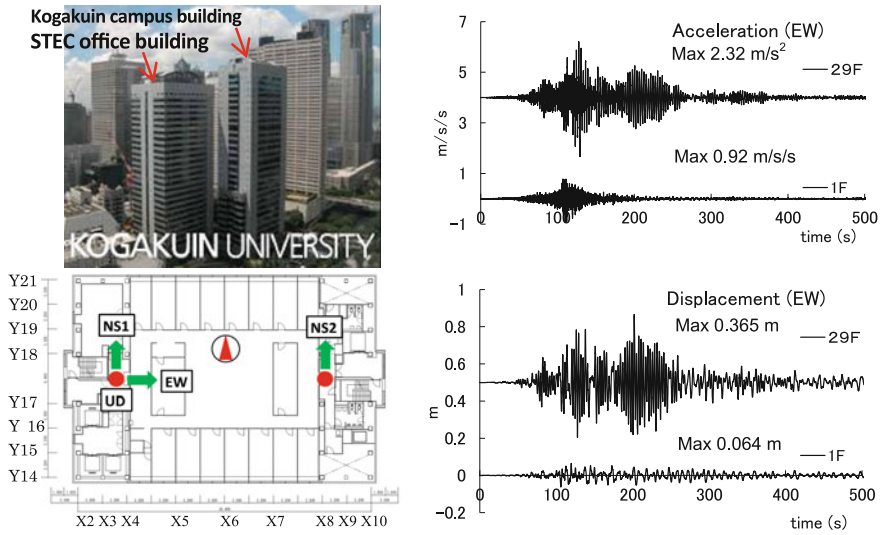


Fig. 14.9 Picture (upper left), locations of acceleration sensors on a plan (lower left), accelerations (upper right), and displacements (lower right) of the Kogakuin University campus building

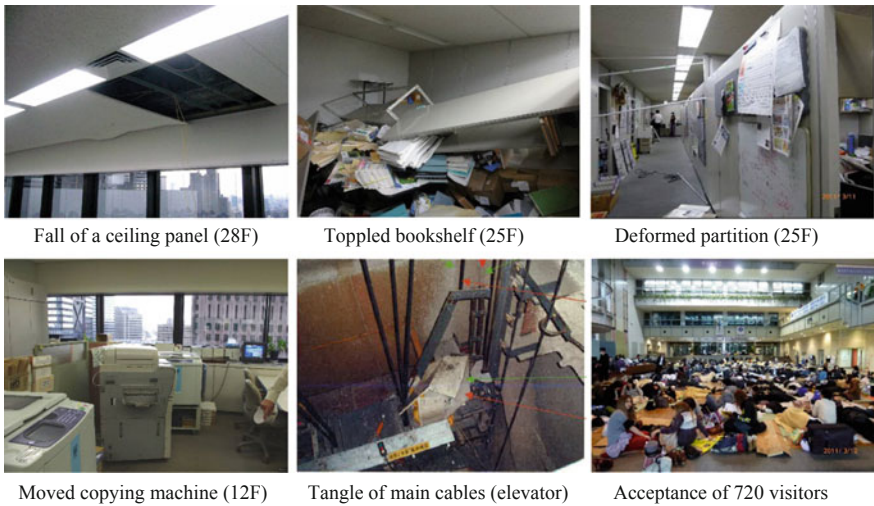


Fig. 14.10 Damage in the Shinjuku campus building of Kogakuin University during the 311 earthquake

combined with those who evacuated from the Shinjuku station, made the area much more congested.

14.4.2 Earthquake Early Warning and Real-Time Damage Assessment Systems, and Emergency Management During the 2011 Tohoku Earthquake

The systems of EEW (Earthquake Early Warning) and RDA (Real-time Damage Assessment, or Real-time Strong Motion Monitoring) were operated in the Kogakuin University building [11–13]. The monitor of EEW had been installed at the EOC (Emergency Operation Centre) on the first basement floor, but RDA was used for experimental purposes, at the time of the 2011 Tohoku earthquake.

Figure 14.11 is a screen of EEW, which shows about 45 s after the start time of the earthquake just before the P wave arrival, and S wave was expected to arrive after 43 s. Furthermore, the long-period ground motion was estimated to arrive 100 s later by considering the surface waves with about half of S-wave velocity. The estimated magnitude and the JMA seismic intensity were 7.3 and 3 at the Shinjuku area, respectively. Although the final magnitude by the EEW system rose to 8.2, the intensity remained only 3. Later, the real magnitude was 9 and the seismic intensity was found to be 5 in Tokyo. Since the assumed intensity was small, this information was not used for emergency response. The author (Hisada) was watching this screen in real time at the 25th floor at the time [14].

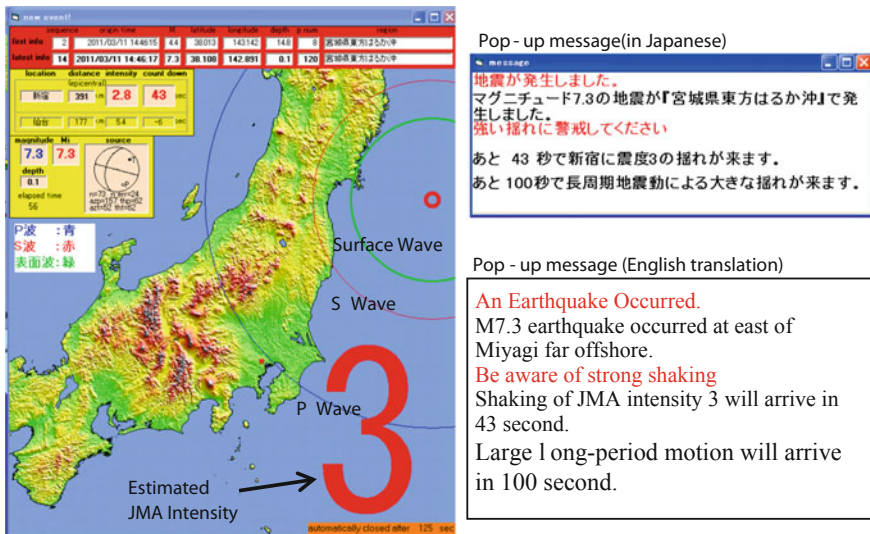


Fig. 14.11 PC screen of EEW at Kogakuin University during the 311 Tohoku earthquake

Figure 14.12 shows the result of RDA in the Kogakuin and STEC buildings during the Earthquake. The inter-drift angles indicated no structural damage, but the estimated intensities suggested possible interior damage from middle to upper floors. Since this system was at the testing stage, it was not used directly at EOC. Immediately after the strong shaking, the manager of the centre announced by following the emergency manual, “Please calm down because this building is earthquake proof and safe”, “All the elevator are stopped, they cannot be used for a while. Please use stairs if necessary”, and, “Please wait for a while, we are currently grasping the current situation”, and so on. If the system had been used, it would be possible to identify the possible floors of the severe damage, and could announce to members of the floors, such as, “Please investigate the interior damage, and check possible injured people”. Fortunately, since the building was minor damage, the facility manager could check all the floors, and finally could confirm that there is no hazard in the building in about two hours. All the public transportations stopped, so tens of thousands had to stay around the Shinjuku station for one night. Consequently, the university could provide the staying spaces to 720 people, as shown in Fig. 14.13. After this earthquake, the building managers understood the effectiveness of RDA, and installed it officially at EOC.

We show the other example of the application of EEW and S²HM to emergency management to a high-rise buildings during the Tohoku earthquake, which was provided by Hakusan Corporation. The building is a steel office building of 40-stories, built in 1970, in the Minato ward of Tokyo, and EEW and S²HM have been installed at EOC since 2008 and 2009, respectively. Figure 14.13 shows the PC screen of EEW started immediately after the earthquake before the arrival of P-wave, and the security manager of EOC realized an unprecedented earthquake (M8.2 on the

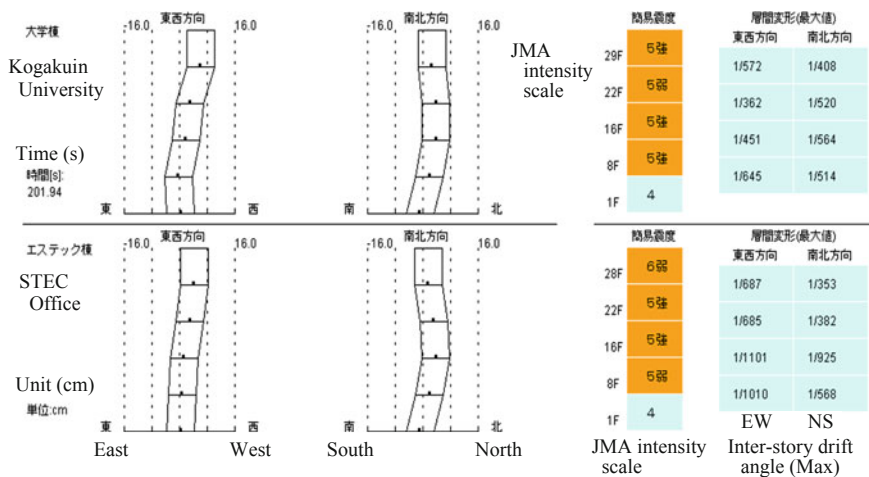


Fig. 14.12 Real-time damage assessment system of the Kogakuin University and STEC office buildings during the 311 earthquake

screen) occurred, and strong motions were arriving. Even though the estimated shaking level was not large (2.9 on the screen), they could prepare for the coming ground motions by contacting the facility members. After the actual strong shake came, RDA indicated that there was no possibility of serious damage in the building, and thus, they could announce the safety of the building and no need for evacuating.

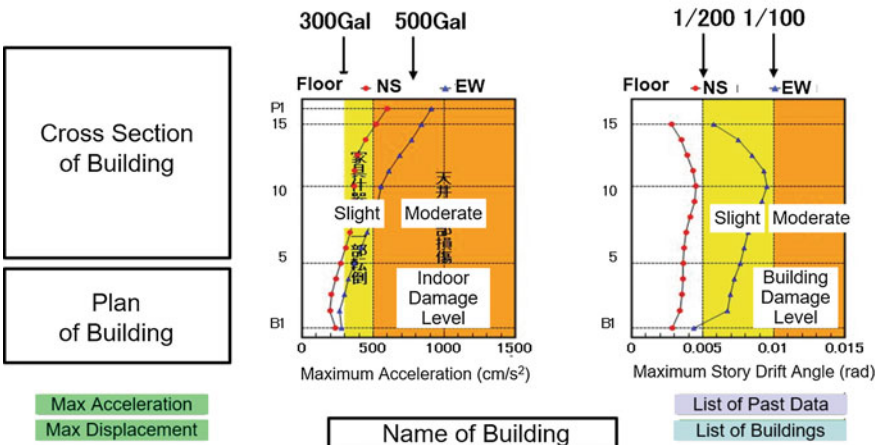
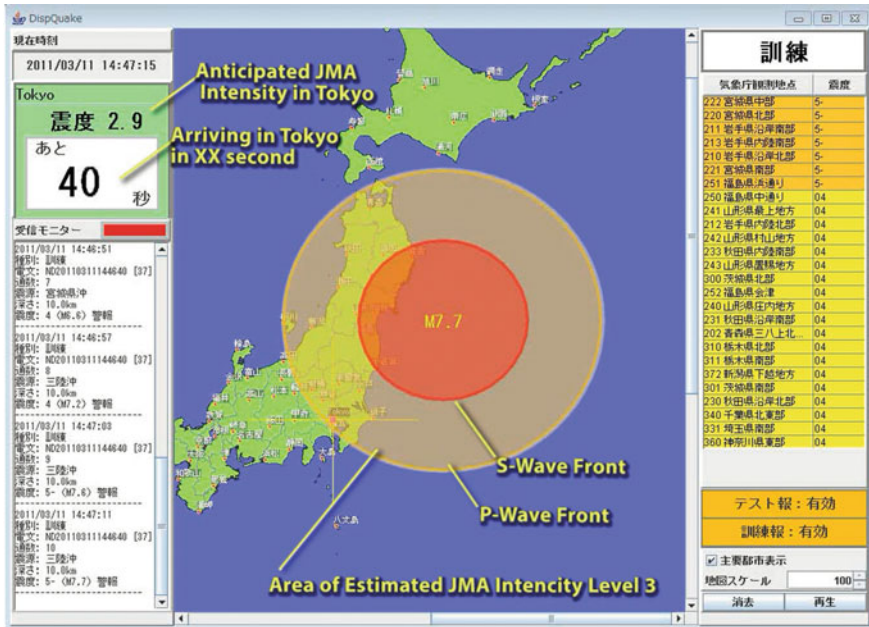


Fig. 14.13 EEW (top) of a high-rise office building during the 311 earthquake, and an example of result of RDA (bottom) provided by Hakusan Corporation (DispQuake and VissQ-Pro)

They distributed the printed results to all the building tenants during the on-site floor checking, and convinced them the safety of the building. Figure 14.13 shows the example of the result report for printing (Note that the figure is not the real report, because the building owner did not allow it to open to public).

After the 2011 Tohoku Earthquake, the Tokyo Metropolitan Government issued an ordinance, in which all the buildings in the city center have to keep people inside the building as much as possible for a couple of days after a big earthquake, in order to avoid the great confusion by large crowd and traffic jams. In addition, large-scale not only public but also private buildings are now expected to accept anyone whenever possible. Therefore, large-scale buildings, especially high-rise buildings, are being expected not only the higher seismic performance to keep building functionality, but also respond to the needs of effective emergency/crisis management immediately following an earthquake. Therefore, S²HM/RDA and its application to the quick damage assessment and emergency management is gaining importance.

14.5 Conclusions

In this paper, we reported the lessons learned from the 2011 Tohoku Earthquake for ground motions, damaged buildings, response of high-rise buildings to the long-period long-duration earthquake motion, and investigated the change in dynamic characteristics of buildings during the earthquake. In addition, we showed the case study of a high-rise building in Tokyo for the damage, and the applications of S²HM to emergency management in the building during the earthquake. In recent years, many researches on dynamic characteristics of buildings of various sizes and structures have been conducted as a consequence of the accumulation of strong motion data of various buildings. Such findings may be useful to improve the S²HM technology.

Acknowledgements Parts of this research were supported by the Disaster Mitigation Research Centre of Kogakuin University, and Private University Research Branding Project of MEXT (Ministry of Education, Culture, Sports, Science and Technology).

References

1. Tobita J et al (2014) Database of earthquake response observation of buildings in Japan. In *AII Journal of Technology and Design* No.48:901–904 Oct (in Japanese)
2. Tsoggerel T, Motosaka M (2011) Investigation of dynamic behavior of a 9-story building during the 2011 off the Pacific Coast Tohoku earthquake. In: *Proceeding of the 8th annual meeting of Japan association for earthquake engineering*, pp 44–45
3. Kashima T, Koyama S, Okawa I, Iiba M (2012) Strong motion records in buildings from the 2011 Great East Japan earthquake. In: *15th world conference on earthquake engineering*, Lisbon, Portugal, 24–28 Sept

4. Kashima T, Kitagawa Y (2006) Dynamic characteristics of buildings estimated from strong motion records. In: Proceedings of the 8th U.S. national conference on earthquake engineering, San Francisco, USA, 18–22 Apr
5. Osaka City (2011) Verification results on the safety of the Sakishima Government Building. <http://www.pref.osaka.lg.jp/otemaemachi/saseibi/bousaitai.html>
6. Japan Meteorological Agency (2012) Report on information of long period ground motion (in Japanese). http://www.data.jma.go.jp/svd/eqev/data/study-panel/tyoshuki_kentokai/hokoku/siryou.pdf
7. Kashima T, Koyama S, Iiba M, Okawa I (2014) Change in dynamic characteristics of RC/SRC buildings during the 2011 Great East Japan earthquake. In: Proceedings of the 10th U.S. national conference on earthquake engineering, Anchorage, USA, 21–25 July
8. Çelebi M, Hisada Y, Omrani R, Ghahari F, Taciroglu E (2016) Responses of two tall buildings in Tokyo, Japan, before, during, and after the M9.0 Tohoku earthquake of 11 March 2011. *Earthq Spectra* 32:463–495
9. Hisada Y, Yamashita T, Murakami M, Kubo T, Arata T, Shindo J, Aizawa K (2012) Seismic response and damage of high-rise buildings in Tokyo, Japan, during the 2011 Tohoku earthquake. In: 15th world conference on earthquake engineering, Lisbon, Portugal, 24–28 Sept
10. Shindo J, Hiramoto T, Murakami M, Hisada Y (2012) Questionnaire survey on behaviour of businesses, etc., around Shinjuku station during the Great East Japan earthquake. *J Jpn Assoc Earthq Eng* 12(4):288–307 (in Japanese)
11. Hisada Y, Murakami M, Kubo T (2010) Disaster mitigation activities of a high-rise building in the Shinjuku station area by collaborating with local government and communities. In: Proceedings of 7th international conference on urban earthquake engineering (7CUEE) & 5th international conference on earthquake engineering (5ICEE), Tokyo, Japan
12. Kubo T, Hisada Y, Horiuchi S, Yamamoto S (2009) Application of long-period ground motion prediction using earthquake early warning system to elevator emergency operation control system of a high-rise building. *J Jpn Assoc Earthq Eng* 9(2):31–50 (in Japanese)
13. Kubo T, Hisada Y, Murakami M, Kosuge F, Hamano K (2011) Application of an earthquake early warning system and a real-time strong motion monitoring system in emergency response in a high-rise building. *Soil Dyn Earthq Eng* 31(2):231–239
14. Hisada (2011) <http://kouzou.cc.kogakuin.ac.jp/Open/2011-3-11/video/> (accessed on 2019-02-20)

Chapter 15

Building Structural Health Monitoring Under Earthquake and Blasting Loading: The Chilean Experience



R. Boroschek, P. Villalpando and E. Peña

Abstract Near real-time structural health monitoring (SHM) has been used in Chile since mid-2009. Chile is located in one of the most active seismic zones in the world so initially SHM was driven mainly by research demands to evaluate the earthquake response of structures. In addition, one of the main industries of Chile is mining, which has operational characteristics that include strong vibrations generated by blasting and heavy machinery operations. This article presents research and professional experiences on building monitoring under environmental, earthquake and blasting vibration conditions. A low-cost monitoring system is used to monitor most of the structures. To identify modal characteristics, different techniques are used such as Stochastic Subspace Identification (SSI), Multivariable Output Error State Space (MOESP), and symbolic data analysis. Currently, more than 20 structures are being monitored by the procedures described in this article. A typical system consists of sensors, a local and a remote processing system, a robust data server and several communications media. The system provides information such as maximum response values, instrumental intensity, acceleration, velocity, displacement and modal parameters and, in parallel with numerical models, expected demands on structural member. All of this information is processed in near-real-time to obtain an indication of system changes that could be related with the damage.

Keywords System identification · Shm · Modal tracking · Monitoring · Blasting · Earthquakes · Low-cost sensors · Seismic isolation

R. Boroschek (✉)
Department of Civil Engineering, Universidad de Chile, Santiago, Chile
e-mail: rborosch@ing.uchile.cl

P. Villalpando · E. Peña
RBA, Luis Thayer Ojeda 1027 Of. 1002, Santiago, Chile
e-mail: pastor.villalpando@rba-global.com

E. Peña
e-mail: emilio.pena@rba-global.com

15.1 Introduction

Chile is located in one of the highest seismic zones in the world. In addition, one of its main industries is mining that has among its characteristics strong vibrations generated by blasting and heavy machinery operations. The recent Magnitude 8.8 earthquake, that occurred in Central South Chile in 2010, affected more than 8 million people and more than 10,000 structures (not including low rise housing) [4, 8, 15]. The inspection of the structures took more than 4 months and the human and technical resources were not sufficient for in depth evaluation for rapid recovery.

The economic and technological development has allowed an important access to cheap and robust internet connections and sensors. These characteristics together with the increased speed of data processing computers allows the system to record, analyze and report the state of health under extreme events in near real time. The appropriate instrumentation, processing and communication systems can provide users with the needed information to capture the response of structures to take appropriate actions.

Real time monitoring is been used in several buildings around the world [3, 12, 14], bridges [9, 16] and other structures [11]. Researchers use different procedures for the characterization of the signals i.e. [23], for the system identification i.e. [21] and for the presentations of the results to the stakeholders.

Chile has mandatory seismic monitoring of its dams, but this instrumentation is in general not online. Other structures are not mandatorily instrumented. The first real-time monitoring system was installed in 2009 by the University of Chile [3]. Other structures are monitored but not in real time [5, 7, 17] or are real-time but with temporary deployment [13, 19].

In this work, we present examples of near real-time monitoring experiences developed in Chile using low-cost accelerometers. The sensors installed measure vibrations during service, earthquakes and blasting. The recorded accelerations are processed locally and remotely in order to obtain characteristics of the structure, and an algorithm performs tracking and detects variations of these properties for extended periods of time.

15.2 Monitoring

The implemented monitoring systems are divided into the following main areas.

Local Recording Network: The local monitoring network consists of accelerometers and one or several interconnected dedicated recording and communication systems. The accelerometers are low cost digital 16 bits MEMs. The overall sensitivity of the 16-bit sensor is 1 mg, and the maximum acceleration is 8g. The sampling rate could be set between 125 and 1000 Hz. Communication is performed using local internet providers or cellular data, with 3G or 4G systems.

Structural Health Monitoring Software: A locally installed software was developed to detect events and preprocess data to discriminate between noise and desired events

and communicate data to a robust server. At the remote server, data is analyzed based on structure requirements. A typical analysis includes the following: maximum responses (peak record acceleration, peak velocities and peak displacements), motion duration, power spectrum, linear and nonlinear response spectrum, Arias Intensity, instrumental intensity, perception levels [1] and modal properties.

System identification is performed using stochastics subspace identification [21], MOESP [25, 26], symbolic data analysis and distance metrics [23] among others, which depends on the structure complexity, sensor layout, environmental effects and noise levels.

To evaluate variations of the response or the modal properties with time, tracking algorithms have been implemented based on different distance metrics. The most common one is the frequency and MAC distances i.e. [24].

Based on building design information and models, recorded vibrations and derived data (peak values, modal parameters, etc.) are compared with predefined limits to establish normal responses. In case a predefined level is surpassed, an alert or alarm is generated to stakeholders for action.

Communication and Alerting System: The system can warn the stakeholder about a threshold that has been exceeded. The information can be sent by text message (SMS), e-mail, twitter, or it can be uploaded to a website. This option provides the users with a rapid alert in order to take action.

Strong Motion Alert: Taking advantage of the accelerometers deployed over structures or at ground level, the system can detect strong motion produced by earthquakes and blasting. This information can be sent to a website, and an automatic report can be sent indicating the occurrence of an event.

System State of Health: To ensure good operating conditions, the system permanently sends information about the sensors and computer state. This information allows the timely reaction of the maintenance crew to allow the system to continue running properly. The health parameters that are evaluated are the acquisition system, energy supply, backup battery, communication system, and software operation.

15.3 Identification and Monitoring System Experience

This paper presents three examples of the system applied to building structures with continuous data and triggered motion from environmental and event-based excitations. They are present from the most basic sensor arrangement to a complex sensor and alerting system.



Fig. 15.1 Office building

15.3.1 Building 1, Office Building

The first building is a 25-story office building. This building is made out of reinforced concrete, and its structural system corresponds to a dual system (Fig. 15.1). The building is instrumented with a single triaxial sensor located at the twenty-fourth floor. This setup is an example of the simplest instrumentation that we have implemented, and it shows some of the relevant information that could be obtained from this very limited and cost-effective system.

15.3.1.1 Continuous Data

A typical environmental record is shown in Fig. 15.2. The continuous usage vibration allows the identification and tracking of modal properties in near-real time. Typical acceleration amplitudes of $0.0015g$ are sufficient to identify the modal response. This level of excitation is not always attained so a reliable identification is not necessarily obtained.

The signal is analyzed continuously using the SSI algorithm [20].

The results of several model orders are arranged in a stability diagram. By measuring the distance between each pole and modal shape, it is possible to select stable columns. These stable columns represent real modal properties [2]. In Fig. 15.3, the stable columns are plotted against the superimposition to the power spectral density of the horizontal channels used in the identification. From the stable columns, the properties of each mode are selected from a cluster analysis, as presented in Fig. 15.4.

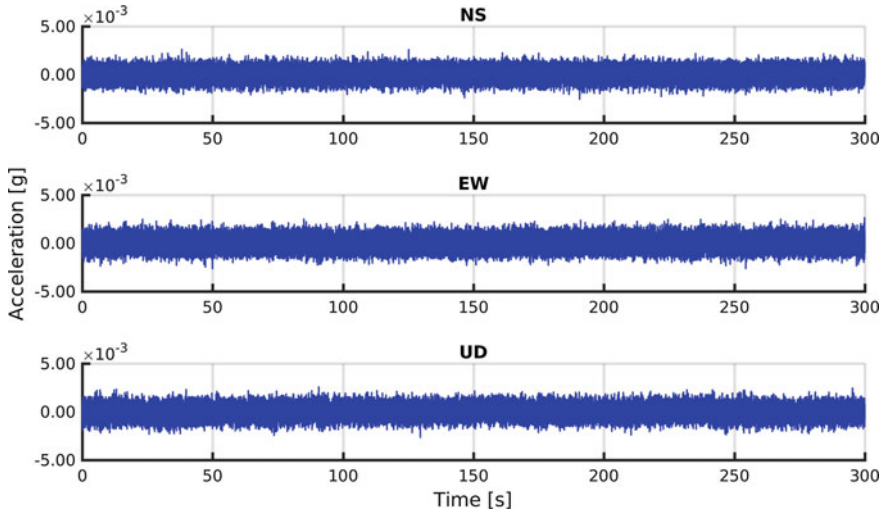


Fig. 15.2 Continuous data. Office building

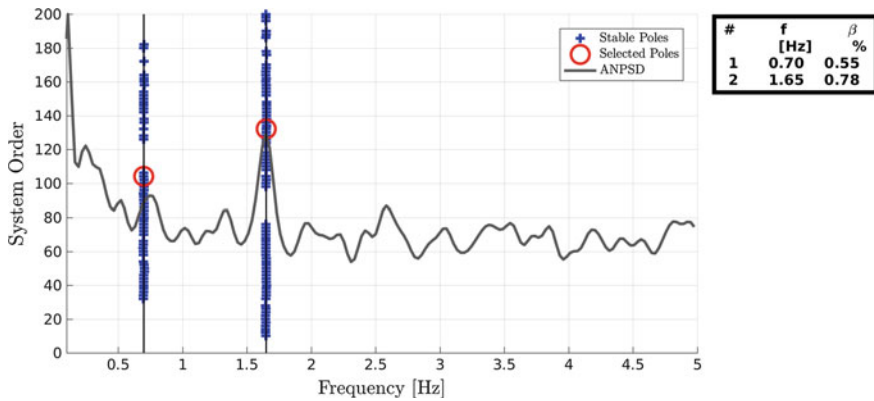


Fig. 15.3 Stability diagram using data from a low-cost accelerometer. Office building

As the data are continuously recorded and stored, this procedure is performed every 5–15 min. The continuously identified data from the low-cost sensors are presented in Fig. 15.5. The figure obtained is rather noisy, due to the low signal-to-noise ratio. The identification is clearer during working hours and gives no results during the weekends and nights. In the same figure, the histogram of the identified frequencies is presented from which the permanent frequencies are easily distinguished. Using this information together with a distance metric based on frequency and mode, the properties can be tracked (Fig. 15.6). The tracking using a low-cost sensor is possible only during the workday because the amplitude of the vibration increases with the building usage. This issue does not pose a problem because the

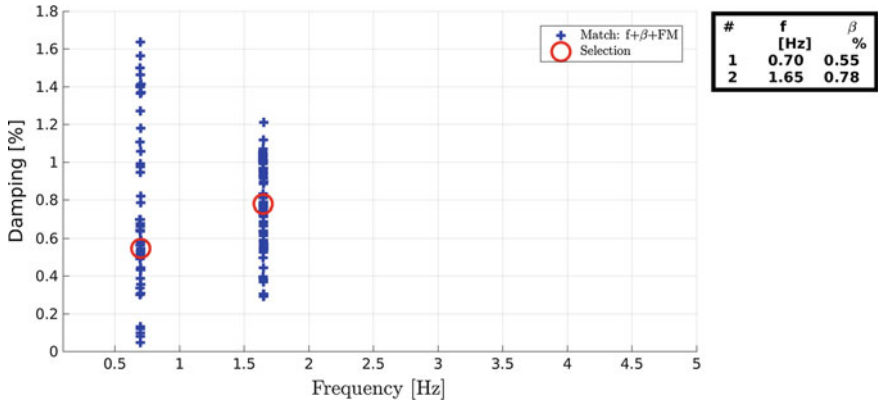


Fig. 15.4 Frequency-damping cluster using data from a low-cost accelerometer. Office building

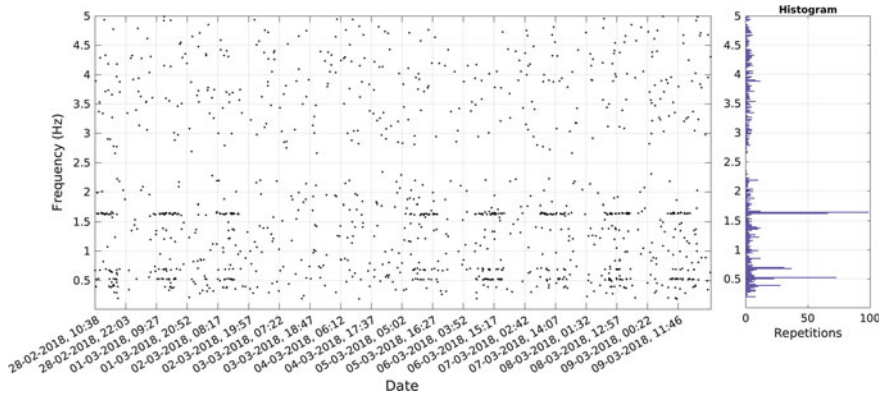


Fig. 15.5 Continuous data identification with a low-cost accelerometer. Office building

data from environmental vibration is used as a reference to identify a change of state after each earthquake event that affects the structure. A more sensitive sensor is required if environmental vibrations are used as the main state-change reference detector.

To validate the values obtained from the low-cost accelerometers; this information is compared in Table 15.1 with data from high-accuracy sensors in the horizontal direction. The frequency difference is very small, so it can be concluded that the low-cost sensor provides consistent results and a reliable source of information for this structure.

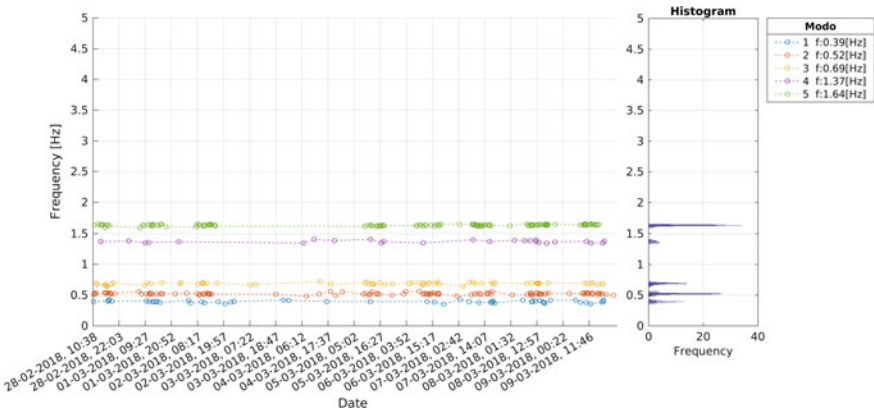


Fig. 15.6 Horizontal direction mode tracking with a low-cost accelerometer

Table 15.1 Horizontal direction frequency summary, environmental measurements

Mode	High-accuracy sensor		Low-cost sensor							
	Freq. [Hz]	Damp. [%]	Frequency [Hz]				Damping [%]			
			Mean	Min	Max	Diff. [%]	Mean	Min	Max	Diff. [%]
1	0.39	1.3–1.5	0.39	0.38	0.41	0	2.6	0.4	7.5	85.7
2	0.52	0.6–0.7	0.52	0.5	0.56	0	1.9	0.1	6.0	192.3
3	0.69	0.7–1.1	0.69	0.66	0.73	0	1.5	0.1	4.1	66.7
4	1.37	0.9–1.1	1.37	1.34	1.39	0	0.8	0.2	2.0	20.0
5	1.64	0.4–0.6	1.64	1.62	1.65	1.2	0.7	0.1	2.1	40.0
6	2.64	0.5–0.7								

15.3.1.2 Earthquake Data

More than 36 earthquakes have been recorded with the MEM accelerometer from the period of April 2013 to March 2018. Magnitudes for the earthquakes range from 4.4 to 8.4, with a maximum structural acceleration of 10%g.

The typical analysis procedure for a seismic event is presented for the earthquake of the 16th of September 2015, which reached 0.09g at the 24th floor (Fig. 15.7). The acceleration records are integrated to obtain velocity and displacements (Fig. 15.8). In this case, the earthquake maximum displacements are around 26.8 mm in the bandwidth from 0.45 to 50 Hz. As is shown in these figures, the resolution is adequate to properly characterize the velocities and displacements.

The short-time Fourier transform or spectrogram of the north-south acceleration component is shown in Fig. 15.9. Due to the low damping of this structure, it is possible to identify the predominant periods from the response decay. In Fig. 15.9,

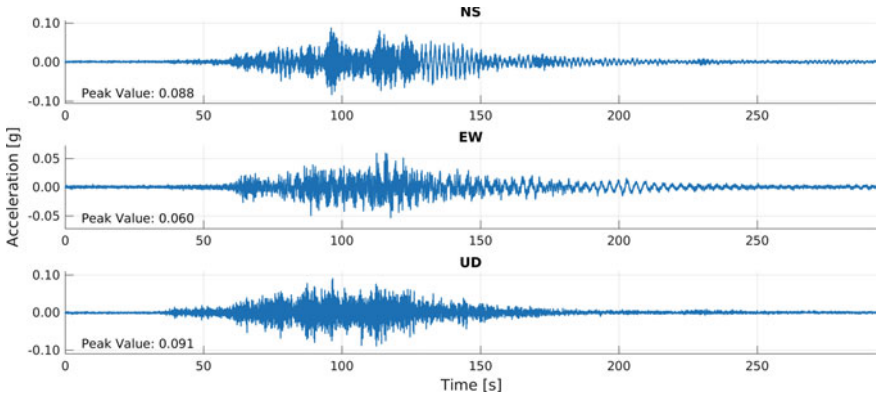


Fig. 15.7 Three channels acceleration record

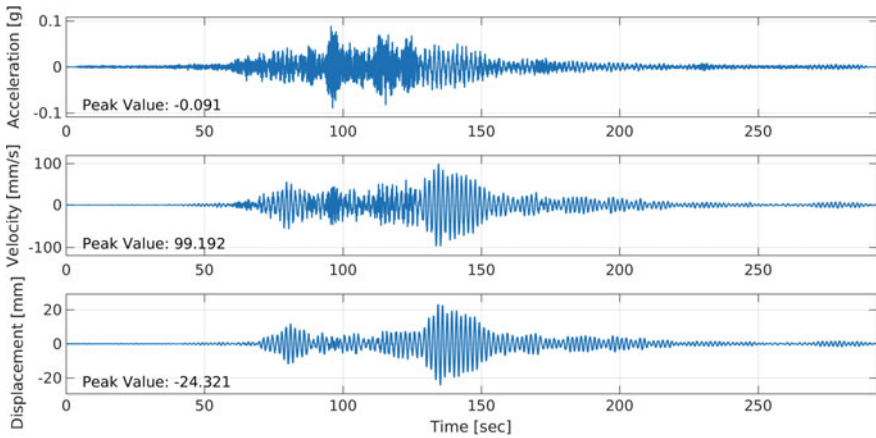


Fig. 15.8 Integrated earthquake motion data from low-cost accelerometers, north-south direction. Low- and high-frequency filter 0.45 and 50 [Hz]. Office building

the first and second natural frequencies (0.39 and 0.52 Hz, respectively) start to become predominant at a time of 60 s during the records until 250 s. Mode 3, with a frequency of 1.67 Hz, is also excited, and its response lasts until a time of 140 s. Other modes are also present.

The SSI algorithm is used to obtain the predominant modal properties from this earthquake record. Despite the clearly nonwhite-noise nature of the recording, the algorithm, without any modification, gives excellent results, as shown in Fig. 15.10.

The parametric identification can be programed to be performed automatically and to track for ambient vibrations and earthquake motion (Figs. 15.6 and 15.11). The identification from the continuous ambient monitoring and the earthquake motions allows the characterization of the modal properties under different environmental and amplitude responses. This approach allows the setting of limits to establish alert

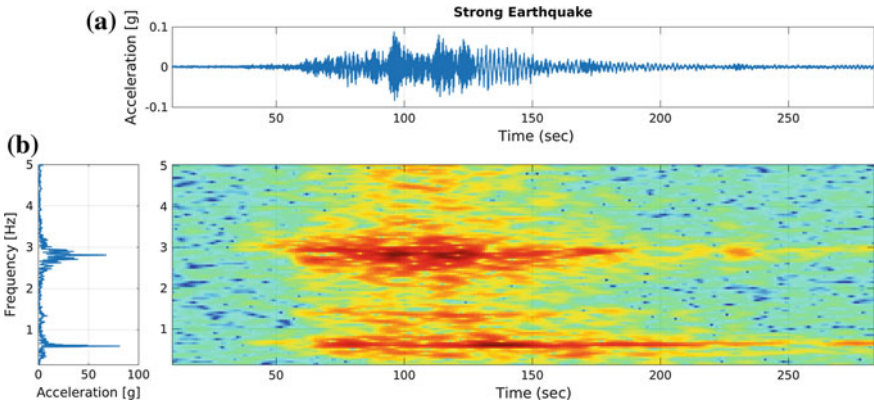


Fig. 15.9 Horizontal direction spectrogram of a strong earthquake, data from a low-cost sensor

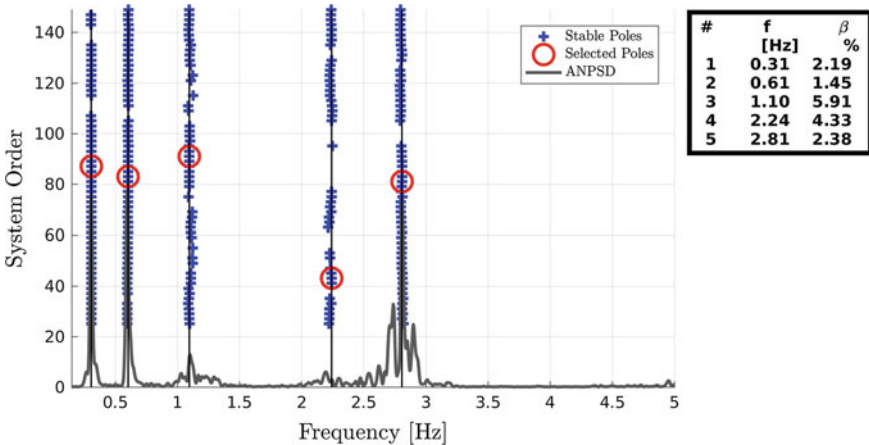


Fig. 15.10 Stability diagram using data from a low-cost accelerometer

and alarm thresholds. Typical limits based only on period have been recommended in the literature when the environmental changes are considered. For temperature and rain, the typical period changes are in the order of 1 to 6% [6, 22]. Earthquakes that do not produce damage increase the frequency variations up to 10% and with minor damage below 30% [10, 18].

For tracking modal properties, we use a distance algorithm based on frequencies. Modes shapes are not used because of the low number of recording channels and clearly separated frequencies. Figure 15.11 shows the frequencies identified for a set of 36 earthquake events. The frequency variations observed depends on the intensity of the motion due to the nonlinearity of the system and robustness of the identification algorithm. In this case, tracking allows the system to identified predominant modes from spurious or earthquake forced frequencies. Not all of the frequencies

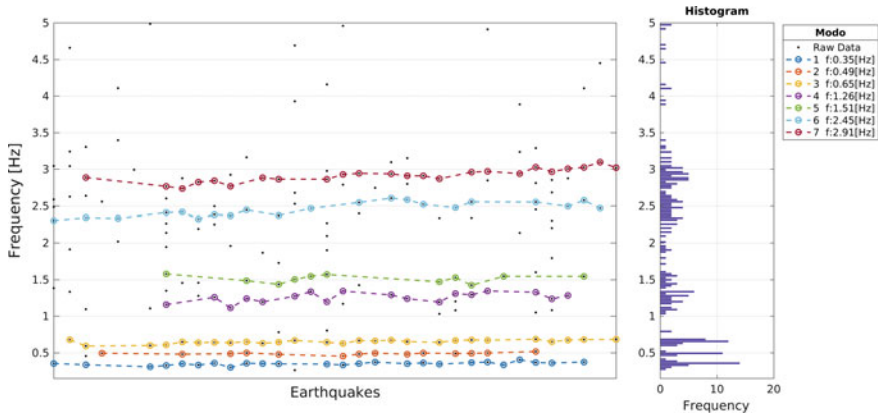


Fig. 15.11 Tracking of properties in the horizontal direction from earthquake data using a low-cost accelerometer

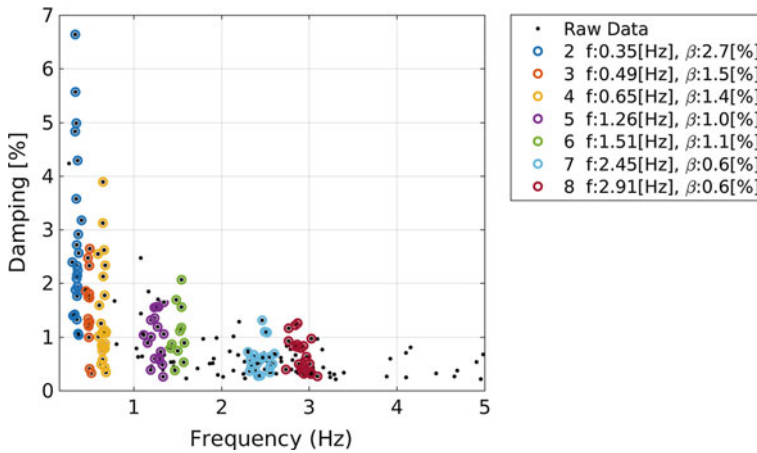


Fig. 15.12 Identified damping during earthquakes. Office building

are identified on all events; this is highly dependable on the earthquake frequency content and the response level. In Fig. 15.12, we show the identified damping. The figure shows larger fluctuations than those for the value of the frequency, as expected, due to the limitations in the sensing system and identification procedure indicating the low reliability of this information.

Table 15.2 shows the summary of horizontal direction acceleration from 36 earthquake measurements.

Table 15.2 Horizontal direction frequency summary and earthquake measurements

Mode	Frequency [Hz]				Damping [%]			
	Average	Min	Max	Variation [%]	Average	Min	Max	Variation [%]
1	0.35	0.31	0.37	17.14	2.6	1	5.1	157.7
2	0.49	0.45	0.52	14.29	1.5	0.7	2.2	100.0
3	0.65	0.6	0.68	12.31	1.5	0.5	2.9	160.0

15.3.1.3 State of Health Assessment

From the ambient vibrations the reference modal base line is determined as a function of temperature and building occupancy changes (determine indirectly using the time of the day). This information is also validated and reference with properties identify from previous earthquake. The base line allows the system to identify changes in frequency after each new earthquake event, activating an alert in case of crossing a predefined limit. Additionally, any acceleration over a threshold, jointly defined by the stakeholders and operators of the system forces the system to send an e-mail to a list of email addresses defined for the project. With these information the user could request an inspection of the building. For example in the September 16th of 2015, 8.4 Mw earthquake, the accelerometer reached around 0.09 [%g] and no sensible period change. With the notification the owner did not took any special action. In particular, in this earthquake there were not detrimental effects, like structural or non-structural damage. Also, no large variations in the identified frequencies were measured during the next 3 h. Immediately after the main event there were 4 other smaller earthquakes. Three of them, with low acceleration levels, were used to evaluate the building health by comparing its frequencies to the identified frequencies of minor earthquake events, which occurred before the event under evaluation. In this case, we observed a 2.8% variation in the first mode frequency between the average value for between pre and post events (without removing usage and environmental perturbations). As the storage capacity in computers is relatively low cost, now the system also stores raw ambient data to compare the building state before and after each event to determine changes that could indicate a damage situation.

15.3.2 Building 2, Base Isolated Building

Several isolated buildings are monitored in Chile to evaluate their structural safety. Isolated buildings consist of structures with a flexible interface that uncouples the response of the superstructure from the ground. This flexible interface allows the upper structure to reduce its response but presents large displacements. Known Chilean earthquakes demand could generate displacements in the range of 30–75 cm. In order to allow for these large displacements, a gap is created around the building

perimeter. If this gap is filled or closed during the operation of the building, an impact can occur. The monitoring system allows for the quick detection of the full closure of the gap, by monitoring the low-amplitude predominant period of the system or the occurrence of an impact during small events. The impact is identified from the recordings by high-frequency and high-amplitude acceleration signals.

A typical monitoring and identification procedure is presented for a high technology building. The building structure is essentially a concrete perimeter wall with interior gravity columns, with plan dimensions of 65 by 50 m. The building is supported on 104 lead rubber isolators. The typical rubber diameter is 70 cm, and the lead plug diameter is 12.7 cm. This isolator is highly nonlinear, especially at low levels of vibrations; this creates an additional challenge for the identification process. The recording system consists of 12 recording channels: 6 of them are below the isolation interface and 6 above. These records are processed online in less than three minutes after the earthquake. Processed data and reports are sent to a selected group of users to inform them as to the state of the system.

15.3.2.1 Earthquake Data

From August 2014 to August 2017, 34 earthquake events were already recorded and informed. To show the nonlinear behavior of the system, the spectrogram of the above isolator acceleration relative to ground motion, NS component, is presented in Fig. 15.13. This figure shows the predominant frequency at the start and end of the earthquake between 2.7 and 2.8 Hz. During the strong phase, the predominant frequency is reduced to values below 2 Hz, and at the end of the vibration, the predominant frequency recovers.

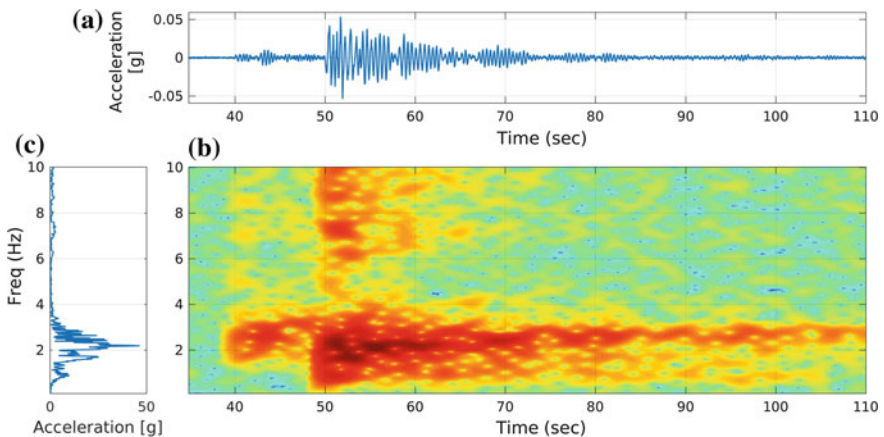


Fig. 15.13 Ground motion earthquake spectrogram. Base isolated building

We analyze a 20 s window during the strong-phase response using the SSI method. The stability diagram is shown in Fig. 15.14, and the frequency-damping clusters are shown in Fig. 15.15. Despite the nonstationarity of the signal and the nonlinearity of the system, the method is able to extract some indication of the predominant frequencies of the response. Later, these values are used as references for a combined SSI spectrogram system identification method as show in Fig. 15.16. In this figure, the response of the system to four earthquake events is presented consecutively. Events are ordered in terms of increasing response amplitude. The identification presents several possible modes. Using the maximum value from the spectrogram as reference, the closest corresponding identified frequency is selected. Finally, to avoid outliers, a moving average method is used to select the representative frequencies for each window, see Fig. 15.17a, b.

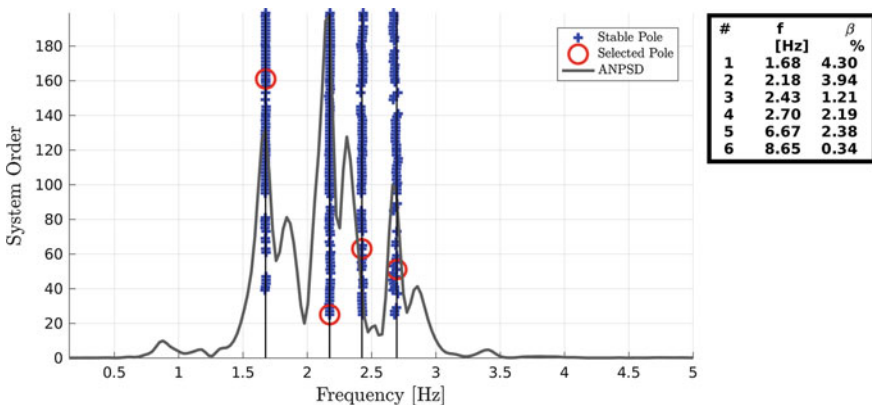


Fig. 15.14 Stability diagram from earthquake record. Base isolated building

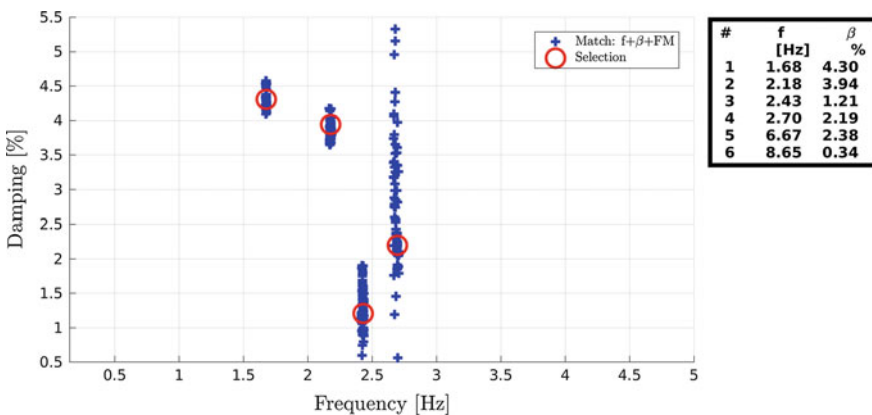


Fig. 15.15 Frequency-damping cluster from earthquake record. Base isolated building

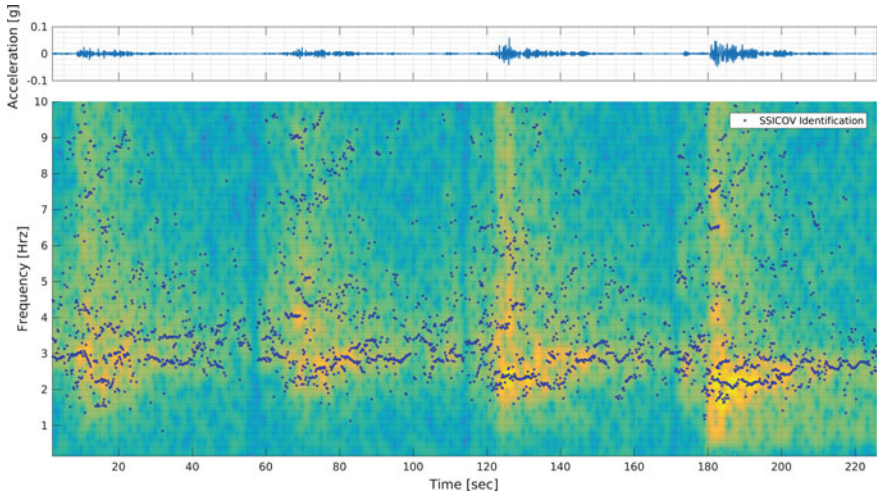


Fig. 15.16 Top: concatenated recorded earthquakes. Below: spectrogram and identified frequencies from SSI procedure. Base isolated building

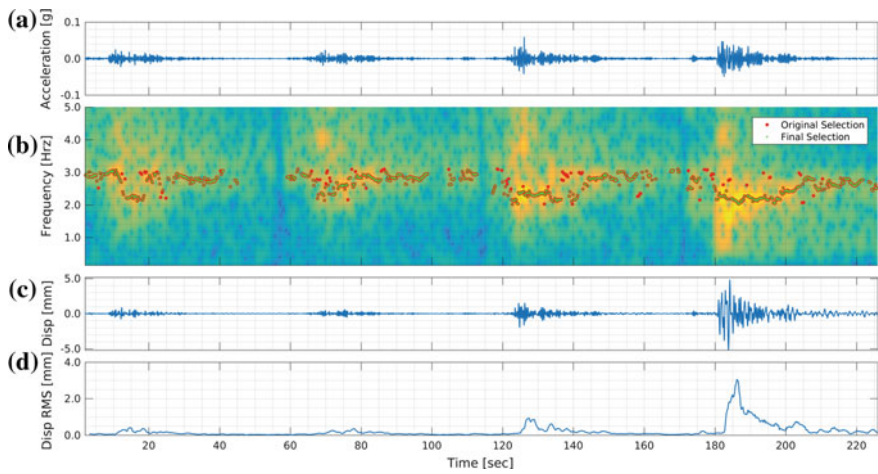


Fig. 15.17 Spectrogram and SSI identification results for the earthquakes after smoothing. Base isolated Building **a** Sequentially arranged acceleration records. **b** Spectrogram of acceleration signals in the back ground with dots indicating SSI identified frequencies. **c** Displacement. **d** Displacement RMS

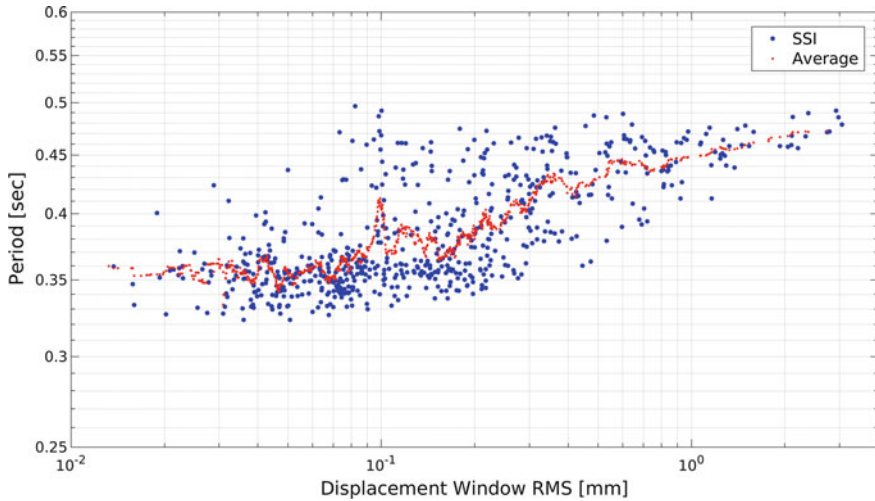


Fig. 15.18 Identified period-displacement relationship from earthquake records. Based isolated building

The accelerations are integrated twice to obtain the isolation relative displacements, as shown in Fig. 15.17c. At this stage, the permanent displacements typically observed in the isolation system are purposefully not preserved. Figure 15.17d presents the root mean square displacement value (RMS) for a 4 s moving overlapping window, the same as the one used for the spectrogram and SSI. With this information, we now create the period-displacement relation for the earthquake selection, shown in Fig. 15.18 in logarithmic scale. The figure presents the values obtained and a mean value relation. As expected the increase in displacement is consistent with an increase in the period. This chart is used to characterize and define the alert and alarm for the system.

15.3.2.2 State of Health Assessment

The state of health assessment is based on the determination of the maximum relative displacement on each bearing and the period change. This data is sent after each event by e-mail to the building owner or administrator to inform them if the design displacement allowance was reached or exceeded. For the moment this situation has not arrived because the earthquakes that have occurred have not produced large demands on system.

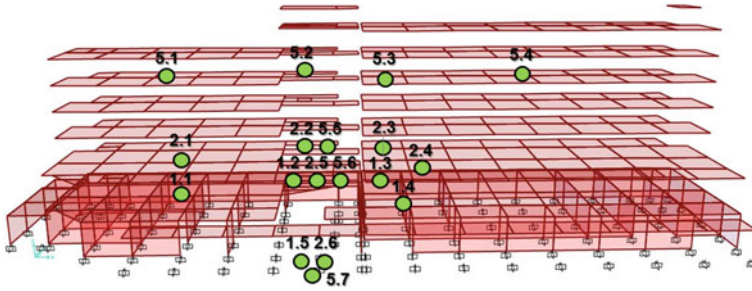


Fig. 15.19 Schematic of steel building with triaxial sensor locations (green circles) (color figure online)

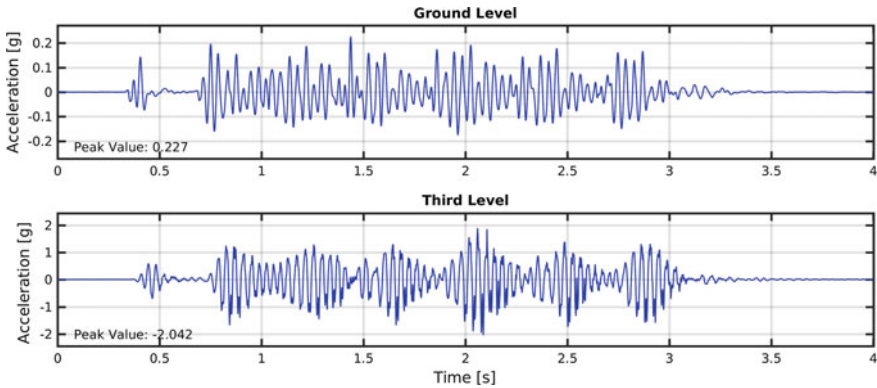


Fig. 15.20 Acceleration measured in the building during blasting. Vertical directions ground and third level

15.3.3 Building 3, Steel Building

A 7-story steel office and hotel building with one basement floor is located in a mining area and subjected to blasting vibrations every other day (Fig. 15.19). Blasting has occurred at distance from 40 to 1200 m from the building. The recorded acceleration caused by blasting inside this building has reached values up to 2g, and the ground acceleration has reached up to 0.22g (Fig. 15.20). The structure is located at high altitude in the Andes and has extreme weather conditions with 20 °C daily temperature variations and varying snow accumulations of 1–2 m on the roof.

15.3.3.1 Blasting and Earthquake Data

For safety requirements, the building is being monitored to help detect damage. Monitoring consists of continuous modal tracking with a high-sensitivity sensor system using ambient vibrations and a complementary strong motion blast-monitoring

system, identical to the one used on the other buildings. A total of 40 channels of acceleration are used. Blasts are monitored with low-cost accelerometers which are integrated to obtain velocity and displacements in near real time. The parameters are evaluated by a fully automatic system before and after a blasting sequence has occurred to detect possible state changes.

Several numerical models of the structure were developed considering different environmental and usage conditions. These models also include uncertainties in geometrical, mechanical and mass characteristics of the structure, and they were calibrated using densely instrumented ambient vibration monitoring campaigns.

The sensor data and the models are part of a real-time monitoring system. After every blast or earthquake, the local network sends information from the recorded data and identified modal properties. These data are processed in a fast server that establishes modal parameter changes or response modifications that will indicate the possibility of damage. The ground recorded acceleration is applied to the numerical models that are run in parallel. These models evaluate the possibility of overstress in critical elements and their location. The structure is fully characterized, and elements on the structure are properly identified. Using this information, a ground crew reviews the locations and performs repairs, if necessary, after every blast. The system has been in use for more than a year and has performed more than 398 blast and earthquake evaluations in real time.

Blasts are performed with three possible objectives: presplitting, main material removal and secondary material removal. The blast is fully designed for each objective and consists of charge bore holes arranged in lines. The blast sequence can be designed and controlled with precision. To limit the damage in the structure, several tests were performed to develop a predictive model to limit the damage on the structure. The model depends on blasting material, volume of the blast, number of boreholes, number of blast lines, distance to the building and building period and damping.

Some of the blast sequences are shown in Figs. 15.21, 15.22, and 15.23. Presplitting (Fig. 15.21) is applied to create a controlled failure plane to allow the main blasting. The objective of this approach is to reduce and attenuate damages and to control stability of the blasting pit walls. The main purpose of the blasting is the fragmentation of the rock in appropriated sizes. Figure 15.22 shows spectrograms of recorded signals at ground level during a main blast sequence, which consists of 6 lines. The maximum acceleration of the ground is in the order of 0.15g. From a different blast sequence Fig. 15.23 presents ground and structural responses at the third floor with accelerations of 0.25g and 2.0g, respectively. The typical predominant frequency is close to 30 Hz, but the energy is spread up to 100 Hz.

The blast of each borehole was designed so that the response of the building from each pit blast has nearly decayed before the next one arrives to avoid superimposing responses and to limit the damage in the building. The building response is amplified up to a frequency of 120 Hz.

The objective of the monitoring system is to identify a change of state due to earthquakes or blasting. The SSI algorithm is used in the continuous data to detect changes in the modal properties before and after blasting. One case is shown in

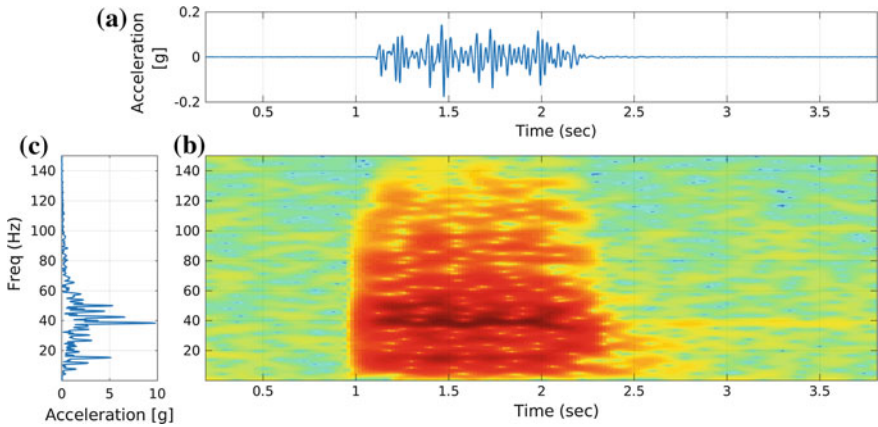


Fig. 15.21 Presplitting ground motion acceleration example during mining blasting

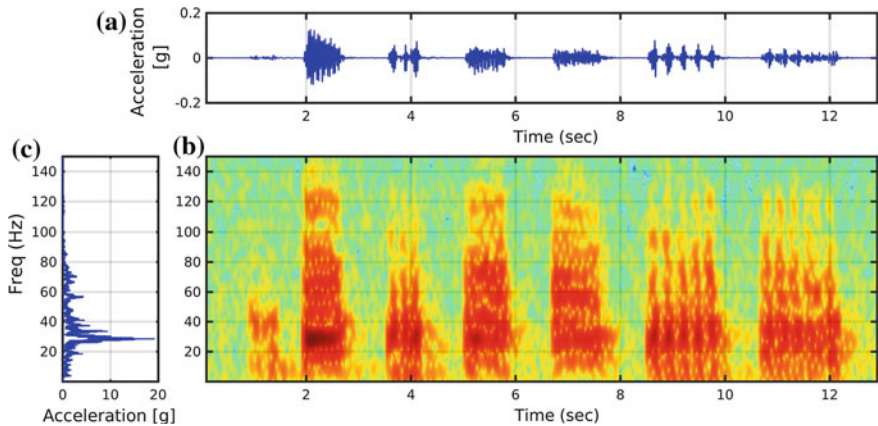


Fig. 15.22 Blasting sequence example

Fig. 15.24, where modal properties from environmental vibrations are compared to the ones obtained after blasting. In this figure, the blast time is depicted by a vertical red line. A change of state is alerted if pre-established variations are detected in the system. Softening or stiffening of the system can occur due to snow and boundary condition modification. The numerical models are used to identify the most possible location of damage so that a crew can visually inspect and in some cases repair the building. The entire process, consisting of data recording, cleansing, conditioning, system identification, change of state detection, and computer model evaluation, takes from 20 to 40 min after the blast has been reported to the stakeholders. The process is fully automatic without any human intervention.

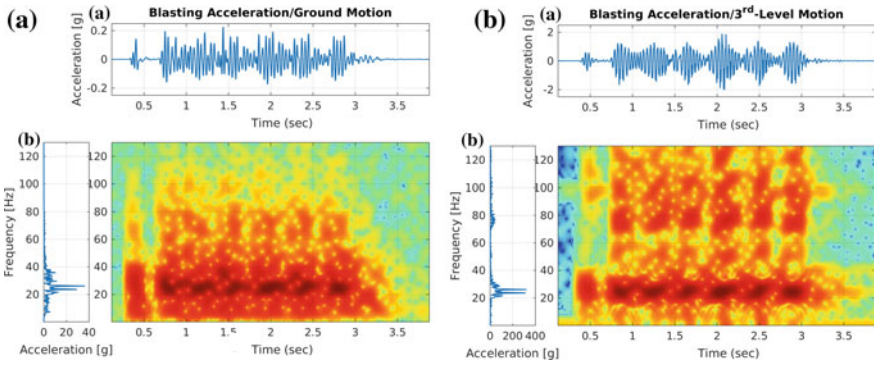


Fig. 15.23 Spectrogram comparison, ground and third floor. Data are from a low-cost accelerometer (up-down)

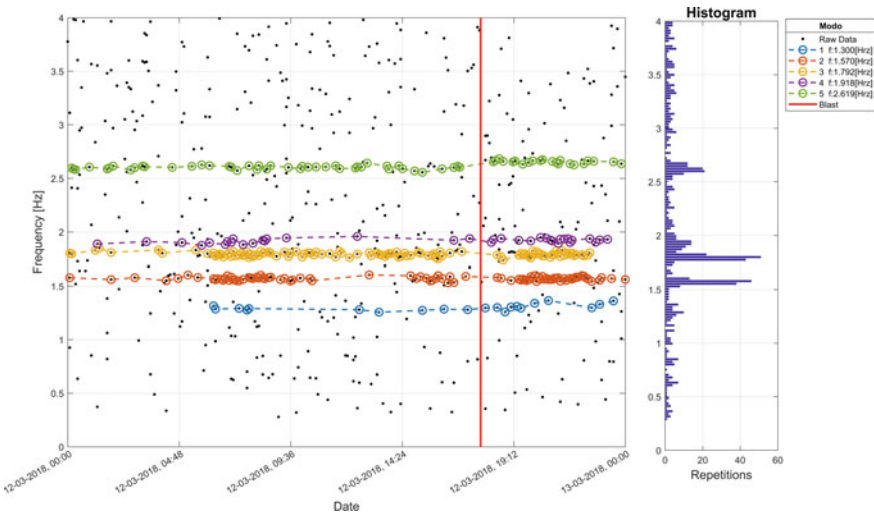


Fig. 15.24 Tracking of modal properties in the horizontal direction. Data are from a low-cost accelerometer. Red line separates before-after blasting (color figure online)

This project has been monitoring the building during an entire year. During this period, the project has achieved good performance over both natural and manmade extreme load conditions, such as earthquakes, snow and blasting. The modal tracking of the identified and selected modes during a 7-month period is shown in Fig. 15.25. The frequency variations observed in this figure are related to environmental conditions and repairs during this period.

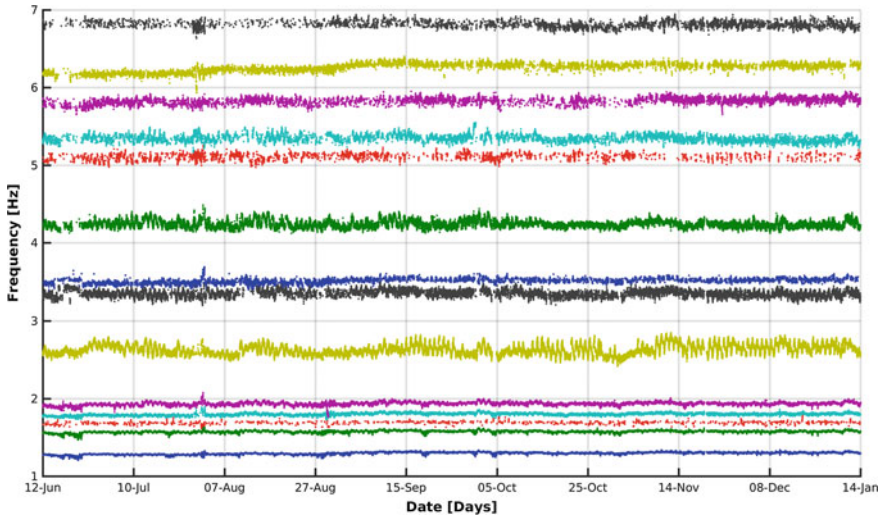


Fig. 15.25 Modal tracking with the high-sensitivity system

15.3.3.2 State of Health Assessment

The system is permanently evaluating changes in state using the identified modes with the information acquired during the day, sending reports once a day to the building owner, building manager, blasting engineer, and the structural engineer in charge, with data and its variation over the last 24 h. In addition, after each blasting the system sends a report with an evaluation on the change of state comparing some time before the event and a few minutes after it. This is send by email providing the stakeholders with information to define the safe return to the building. Beside the change of state, the data is use to run finite element models to evaluate the stress and deformations in each element in the model, sending an alert that indicates if there is an element exceeding defined limits. With this information, when the indicator shows an element that needs to be verified, the local engineer in charge sends a team to check the integrity of the element that is in warning condition. In this particular case, for each blast during a year, the system indicated sections to be verified and the inspection team reported. All this information was in their phones as e-mail in less than 40 min after the beginning of the blasting sequence. This system provided the owner with a tool for health assessment and the possibility of fast response.

15.4 Conclusions

Chile is located in a high seismic area. This condition controls the design of most structures. Early and systematic damage detection from earthquakes and other

extreme loads was recognized as necessary after the extensive destruction that occurred due to the 2010 Mw 8.8 earthquake. The necessity to instrument structures requires reliable and low-cost instrumentation in order to cover a large number of critical structures. Several dams have been instrumented, but just a few other structures have been, because of the cost of the instrumentation, continuous data processing and system maintenance. A new system, based on low-cost accelerometers, has been installed to evaluate the response of critical infrastructure. In this chapter, we evaluate its performance using examples such as an office building, a base-isolated high-tech building and a multipurpose mining structure. The low-cost instrumentation is compared with high-sensitivity and expensive instrumentation. The low-cost instruments are able to properly monitor ambient vibrations above $0.0015g$, from which semicontinuous modal properties can be tracked. Perceivable earthquake events occurred frequently in Chile, and in general, they are not damaging. These earthquakes are used to evaluate the structural characteristics under larger loads than those of environmental excitations and to characterize the initial nonlinear elastic behavior of the system. From the low-cost system, several response characteristics can be derived such as response spectra, acceleration, velocity and displacements and modal properties.

The low-cost sensor implementation allows the user to deploy a set of sensors en masse for a detailed representation of the building motion. For the office building, a single triaxial sensor is used to track predominant frequencies from ambient and earthquake vibrations. Detection of frequency changes using a simple distance metric is used to inform the necessity for inspection. A more extensive instrumentation is used for the base-isolated structure, where modal tracking of predominant low-amplitude vibrations is used together with earthquake displacement and recorded high acceleration from impact to detect obstructions on the building gaps. A much more intensive instrumentation, link with a family of computer models, for the mining building is used to detect changes and locate possible elements that have been damaged due to earthquakes or blasting.

All of these examples have been in operation twenty-four hours a day for several years, providing a secure monitoring and alert system to the stakeholders.

In all the cases shown in this chapter, the main purpose of monitoring was to provide a quick and reliable information to the stakeholders about the levels of response, to inform changes to the state of health and to contribute to keep a safe work place without the need of a complex inspection after each event. Additionally, the system is integrated with social networks and contributes to the information about earthquakes intensities and their locations.

Acknowledgements We want to thank to CORFO Chile for their economic support and the owners of the buildings who allowed us to install our sensors and to measure the response of the buildings with our system.

References

1. Aguilar R, Apostoliti C, Boroschek R, Cardoni A, Cares D, Cimellaro G, Galdo D (2017 Dec 5–8) Monitoring human emotions during earthquakes. In: The 8 international conference on structural health monitoring of intelligent infrastructure
2. Bakir P (2011) Automation of the stabilization diagrams for subspace based system identification. *Expert Syst Appl* 38:14390–14397
3. Boroschek RL (2013) Structural health monitoring performance during the 2010 gigantic Chile earthquake. *Earthq Health Monit Civ Struct*, 197–216
4. Boroschek RL, Contreras V, Kwak DY, Stewart J (2012) Strong ground motion attributes of the 2010 Mw 8.8 Maule, Chile, earthquake. *Earthq Spectra* 28:S19–S38
5. Boroschek R, Moroni MO, Sarrazin M (2003) Dynamic characteristics of a long span seismic isolated bridge. *Eng Struct* 25(12):1479–1490
6. Boroschek R, Tamayo F, Aguilar R (2014 July 8–11) Evaluation of the environmental effects on a medium rise building. In: EWSHM-7th European workshop on structural health monitoring
7. Boroschek R, Yañez F (2000) Experimental verification of basic analytical assumptions used in the analysis of structural wall buildings. *Eng Struct* 22(6):657–669
8. Bray J, Rollins K, Hutchinson T, Verdugo R, Ledezma C, Mylonakis G, Olson S (2012) Effects of ground failure on buildings, ports, and industrial facilities. *Earthq Spectra*, S97–S118
9. Brownjohn JM, Magalhaes F, Caetano E, Cunha A (2010) Ambient vibration re-testing and operational modal analysis of the Humber Bridge. *Eng Struct* 32(8):2003–2018
10. Carreño R, Boroschek R (2011) Modal parameter variations due to earthquakes of different intensities. *Civ Eng Top* 4:321–333
11. Catbas N, Kijewski-Correa T, Aktan E (2013) Structural identification of constructed systems: approaches, methods, and technologies for effective practice of St-Id. American Society of Civil Engineers
12. Celebi M, Sanli A, Sinclair M, Gallant S, Radulescu D (2004) Real-time seismic monitoring needs of a building owner—and the solution: a cooperative effort. *Earthq Spectra* 20:333–346
13. Celebi M, Sereci M, Boroschek R, Carreño R, Bonelli P (2013) Identifying the dynamic characteristics of a dual core-wall and frame building in Chile using aftershocks of the 27 February 2010 (Mw = 8.8) Maule, Chile, Earthquake. *Earthq Spectra* 29(4):1233–1254
14. Kaya Y, Safak E (2013) Real-time structural health monitoring and damage detection. *Top Dyn Civ Struct* 4:11–19
15. Ledezma C, Hutchinson T, Ashford S, Moss R, Arduino P, Bray J, Frost D (2012) Effects of ground failure on bridges, roads, and railroads. *Earthq Spectra* 28:S119–S143
16. Magalhaes F, Cunha A, Caetano E (2008) Dynamic monitoring of a long span arch bridge. *Eng Struct* 30(11):3034–3044
17. Moroni MO, Boroschek R, Sarrazin M (2005) Dynamic characteristics of Chilean bridges with seismic protection. *J Bridge Eng* 10(2):124–132
18. Muria-Vila D, Camargo J, Aldama B, Rodriguez G, Aguilar L, Ayala M (2013 Dec 9–11) Structural health monitoring of an instrumented building in Mexico with accelerometers and GPS sensors. In: The 6th international conference on structural health monitoring of intelligent infrastructure
19. Nuñez T, Boroschek R, Larrain A (2011) Validation of a construction process using a structural health monitoring network. *Journal of Performance of Constructed Facilities* 27(3):270–282
20. Peeters B, De Roeck G (1999) Reference-based stochastic subspace identification for output-only modal analysis. *Mech Syst Signal Process* 13(6):855–878
21. Peeters B, Ventura C (2003) Comparative study of modal analysis techniques for bridge dynamic characteristics. *Mech Syst Signal Process* 17(5):965–988
22. Rahmani T, Hao Y, Todorovska M, Boroschek R (2017 Jan 9–13) Structural health monitoring of torre central by the wave method. In: 16th world conference on earthquake engineering
23. Santos JP, Cremona C, Orcesi A, Silveira P, Calado L (2015) Static-based early-damage detection using symbolic data analysis and unsupervised learning methods. *Front Struct Civ Eng* 9(1):1–16

24. Torres W, Almazan JL, Sandoval C, Boroschek R (2017) Operational modal analysis and FE model updating of the Metropolitan Cathedral of Santiago, Chile. *Eng Struct* 143:169–188
25. Verhaegen M, Dewilde P (1992a) Subspace model identification. Part 1. The output-error state-space model identification class of algorithms. *Int J Control* 56(5):1187–1210
26. Verhaegen M, Dewilde P (1992b) Subspace model identification. Part 2. Analysis of the elementary output-error state-space model identification algorithm. *Int J Control* 56(5):1211–1241

Chapter 16

Developments in Seismic Instrumentation and Health Monitoring of Structures in New Zealand



S. R. Uma and S. Beskhyroun

Abstract New Zealand is one of the seismically active countries on the planet and its tectonic setting has featured many active faults. Strong motion monitoring has been carried out for about 40 years in New Zealand and recorded data on ground shaking as well as structural response. While the ground motion monitoring has been growing in scale over the years, just over a decade ago, a nationally significant structural monitoring program was established to record seismic response of typical structures that are representative of New Zealand building inventory. Monitoring with permanent instrumentation and continuous recording of data enable to perform short-term damage detection after an event as well as long-term effects in the health of the structure. The chapter will further discuss on the damage detection methods that were proposed and adopted using the records from instrumented structures in New Zealand. It will include a description around the new computational tools for damage identification and long-term dynamic monitoring. The toolkits provide functions for automated dynamic parameters and response amplitudes monitoring. The potential of these toolkits is illustrated using data collected by the continuous dynamic monitoring system installed on a full scale reinforced concrete bridge in Wellington, New Zealand.

Keywords Seismic instrumentation of structures · Structural health monitoring · Damage detection · Structural dynamics · Modal parameters

16.1 Introduction

The tectonic setting of New Zealand includes the boundary of the Australian and Pacific plates. Many active faults in the country have generated a high rate of “small

S. R. Uma (✉)

Department of Risk and Society, GNS Science, P O Box 30368, Lower Hutt, New Zealand
e-mail: s.uma@gns.cri.nz

S. Beskhyroun

Auckland University of Technology, 34 Saint Paul Street, Auckland, New Zealand
e-mail: sherif.beskhyroun@aut.ac.nz

© Springer Nature Switzerland AG 2019

M. P. Limongelli and M. Çelebi (eds.), *Seismic Structural Health Monitoring*, Springer Tracts in Civil Engineering, https://doi.org/10.1007/978-3-030-13976-6_16

385

to moderate” earthquakes ($M < 7$), many “large” earthquakes ($M 7-7.9$) and one “great” earthquake ($M 8$) in historical time and such events continue to contribute to relative motion of the plates. A southeast-dipping subduction zone lies at the far south-western end of the country (“Fiordland subduction zone”). It is linked to a major northwest-dipping subduction zone in the eastern North Island (“Hikurangi subduction Zone”) by a 1000 km long zone of right-lateral oblique slip faults (“Axial tectonic belt”). The faults of the axial tectonic belt in the area between the Fiordland and Hikurangi subduction zones accommodate the relative plate motion as indicated in Fig. 16.1.

Most of the seismically active countries in the world have established monitoring networks to study ground motion characteristics. However, only a few countries have taken initiatives to establish an integrated monitoring network with instruments not only on the ground but also in the built structures. New Zealand is one of the countries to have such an integrated monitoring network that offer several benefits to science, engineering community and the public. The purpose of such a network is to measure the response of various kinds of structures and soils to strong ground shaking caused

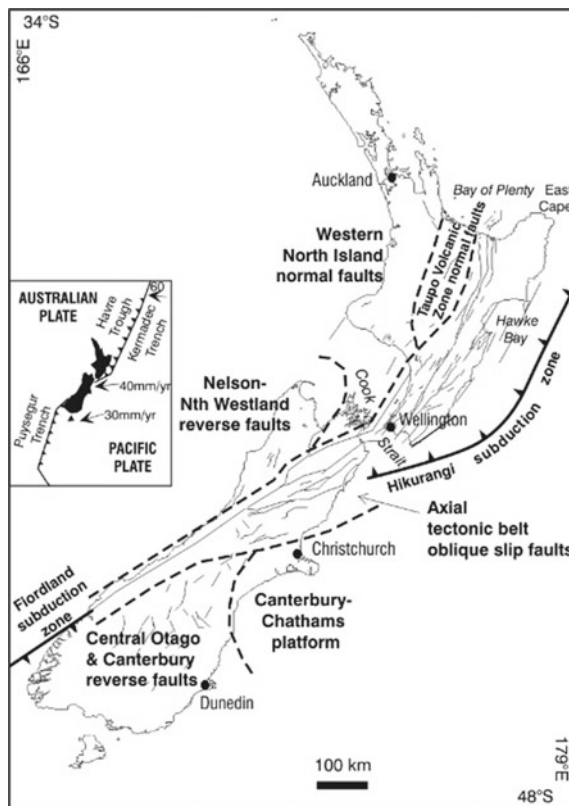


Fig. 16.1 Tectonic setting of New Zealand

by earthquakes in New Zealand. The recorded data from the ground instruments are useful in various applications including (a) the development of ground motion hazard model; and (b) the studies of microzonation. Similarly, monitoring of the structural response with sensors and their recorded data can be used in many applications including (a) validation of the assumptions of design standards and verification of structural models [1]; (b) development of new methods of design and devices to achieve better performance objectives; (c) comparison of the predicted damage in the instrumented structure with the observed damage after an earthquake; and (d) performing ‘health checks’ by analyzing the data collected from a structure over a period of time and by evaluating the change in their dynamic characteristics to understand the suitability of the structure for its intended functionality.

16.2 Seismic Monitoring Network in New Zealand

Monitoring and data collection of various hazards using instrumentation provide a fundamental step to strengthen the underlying assumptions of scientific and engineering research by increasing their quality, applicability and confidence limits. In New Zealand, seismic instrumentation network operation was begun in 1960s. In the early years, a combination of film recorders and scratch plate accelerographs were used. However, gradually the use of digital accelerographs increased in 1990s, many of them were used for structural arrays in buildings, bridges, dams and power-stations including an offshore gas platform [2]. This is a significant milestone in the history of structural response monitoring in New Zealand.

Over time, the need for establishing a dedicated platform to monitor various hazards and collect data for the benefit of New Zealand Inc. became more pronounced. Based on this need, a ‘GeoNet’ project (<https://www.geonet.org.nz/>) was conceived with new funding support from Earthquake Commission (EQC, New Zealand) to establish a modern monitoring network that can provide national coverage for hazard detection, emergency response and data collection. There are several components in ‘GeoNet’ system that contribute to the collection and utilization of recorded data. These include national scale, regional scale networks with sensors on the ground and a structural array network where select structures are instrumented to monitor their dynamic response during earthquakes. Distribution of accelerometers, broad band sensors and instrumented buildings are shown in Fig. 16.2. Distribution of several other types of monitoring networks can be obtained from the link: <https://www.geonet.org.nz/data/network/sensor/search>.

16.2.1 Ground Motion Monitoring

Over time, the scale of monitoring has increased through expanding network and quality of data has improved with advancement in instruments. Currently, the national

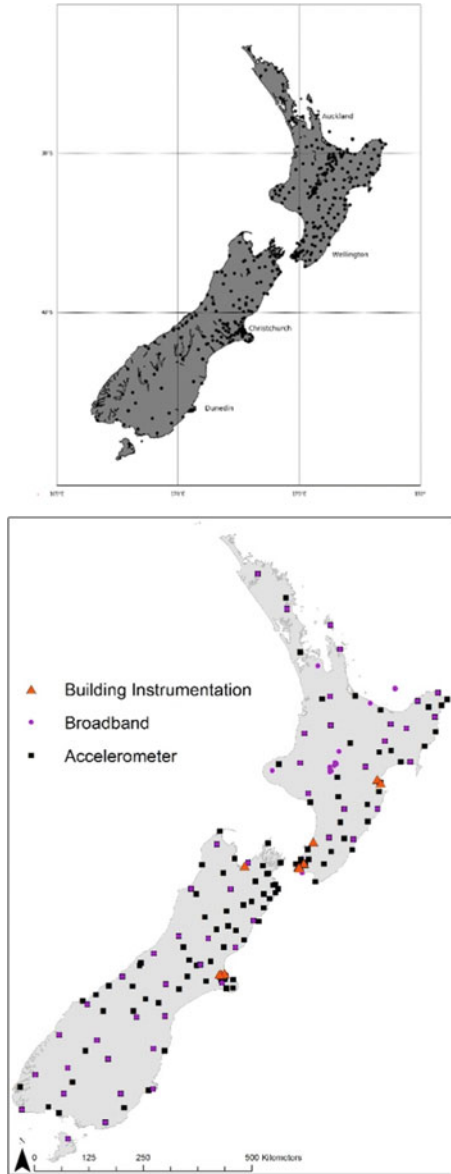


Fig. 16.2 Locations of sensors throughout the country

scale network comprises ‘national strong-motion network’, ‘national seismograph network’ giving total of over 500 recording locations. The six component (3D broadband and 3D strong-motion) seismograph recording sites are located throughout the country (at about 100 km spacing) to provide uniform and data collection capability for the study of New Zealand and international tectonic problems.

A combination of strong motion recorders and weak motion sensors record ground motion data in New Zealand towns and cities, including data for near-fault ground motions. The network configuration supports continuous monitoring, remote access to data and to manage functional status of the instrument via standard internet protocol (IP) networks.

16.2.2 Structural Response Monitoring

In New Zealand, for many years GNS Science has been responsible for monitoring earthquake responses of structures (both publicly and privately owned), but on a very small scale [3, 4]. Within the new and improved funding structure provided to GeoNet, a dedicated stream of structural monitoring project was initiated [5]. The project adopted the scheme for long-term monitoring by which continuous response data from ambient vibration as well as from the real events are recorded. Sometimes, data recorded from the instruments installed temporarily for a short and definitive period to monitor the aftershock effects also aid in understanding the dynamic characteristics of the structure.

16.2.2.1 New Zealand Building Instrumentation Program

The building instrumentation program is currently sitting with ‘GeoNet’ so that the infrastructure that are established for geological hazards monitoring can be used where possible. Differences in operating requirements for monitoring geological hazards and recording of structural responses leave room for variations in data management structure and end-user products.

The building instrumentation program has a broader objective of building safer structures and to minimize economic loss and Earthquake Commission of New Zealand supported with funding to commission this program. To achieve the broader objective, it is important to verify the assumptions in the design standards with an improved understanding of dynamic behavior of structures through instrumentation. The structures are selected from high seismic risk areas inclusive of different types of buildings and a few bridges. Currently 14 buildings, 3 bridges are instrumented and responses are archived.

Figure 16.3 shows a typical schematic representation of the components of the seismic instrumentation deployed within a building. The sensors used are triaxial accelerometers with CUSP-M series models supplied by Canterbury Seismic Instruments (CSI) Ltd. They are distributed at various levels of the building and connected

through ethernet cable to the CUSP-M central recording unit. The CUSP-M models have evolved over time and the models include CUSP-Ms, CUSP-Me versions. The full-scale range is ± 5 g but because of gravity the vertical sensors are $+4/-6$ g. The sensitivity ranges from ~ 10 to $80 \mu\text{g}$ (10^{-6} g) among these models. Some of the CUSP-Me sensors can measure around $10 \mu\text{g}$ which could be considered closer to ambient vibration range (Personal communication with CSI Ltd). The GPS receiver provides accurate timing (no less than 1 ms). Often one of the sensors is mounted in an enclosure at a short distance from the building to record “free-field” motions. The data recorded by the central acquisition unit gets transferred through dedicated internet protocol (IP) connection and archived at GeoNet data centre. As many of the buildings are owned by private parties, the current data policy requires the end-user to submit a request form to the data centre manager (info@geonet.org.nz) to get access to the raw data (https://www.geonet.org.nz/data/types/structural_arrays). The end-users are expected to perform the necessary correction procedures on the raw data.

16.2.3 Learning from Recent Earthquake Events

Recently, moderate to strong earthquakes have occurred with epicenter closer to populated region. Darfield earthquake in 2010 (Public ID: 3366146), Christchurch earthquake in 2011 (Public ID: 3468575), Cook-Strait earthquake in 2013 (Public ID: 2013p543824) and Lake Grassmere earthquake in 2013 (Public ID: 2013p613797); and Kaikoura earthquake in 2016 (Public ID: 2016p858000) were large enough in magnitude to record significant responses in instrumented struc-

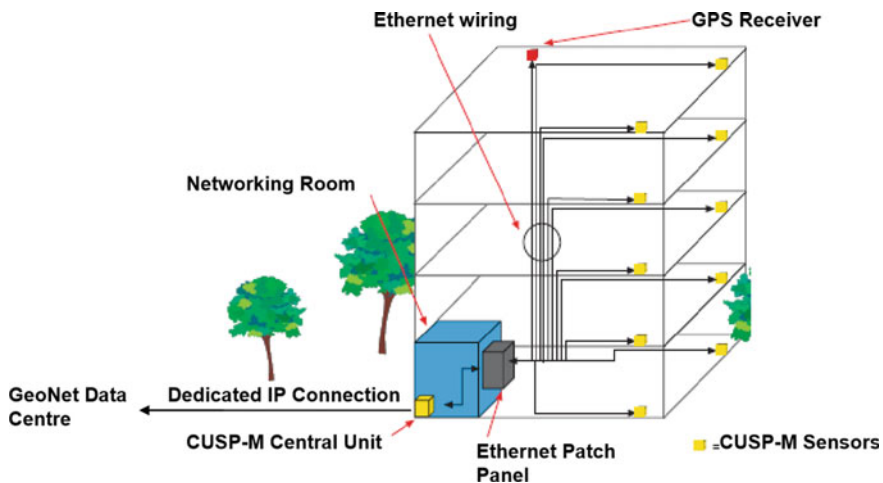


Fig. 16.3 Typical configuration of instrumentation in a building. *Courtesy* CSI Ltd

tures that were subjected to shaking. Several studies were undertaken to understand their dynamic characteristics in terms of their vibration period and real responses were compared with design recommendations [6–8]. The extensive and dense array of instruments enable understanding the floor level responses and the inter-storey drift parameters which are the key design variables used in current design practice (NZS 1170.5:2004) and the recorded responses are desirable predictors for building damage [9]. A few studies were also dedicated to exploring the soil-structure interaction effects from the recorded response [1, 8].

16.3 Long Term Structural Health Monitoring

Utilization of a sensor network system integrated within the structure can greatly enhance the inspection process through rapid in situ data collection and processing [10–12]. However, these sensor networks typically produce such large and complex sets of data that it becomes difficult to process using on-hand database management tools or traditional data processing applications [13–17]. The challenges include capture, storage, search, sharing, transfer, analysis and visualization. The main objective of this research is to design and develop new computational tools for structural modal identification and long-term dynamic monitoring. The automated data analysis program presented in this study was recently developed by the second author to analyse the large sets of data that have been previously recorded by GeoNet SHM system in the past few years. The data analysis program was not part of the GeoNet SHM system. The newly developed data analysis program is intended to be utilized not only for the analysis of previously recorded data but can also be integrated in the GeoNet SHM system for real time (or near real time) analysis of the data. The toolkit presented here is developed in the MATLAB [18] environment as it permits the easy development of graphical interfaces and provides powerful tools for automated data processing; a characteristic that is essential in the context of continuous monitoring. The developed system consists of two independent toolkits: the Modal Parameters Identification Toolkit (MPIT) (Fig. 16.4), which is used for structural dynamic identification [19], and the Automated Data Analysis Toolkit (ADAT) (Fig. 16.5), which is used for data management and processing of large data sets.

The MPIT is mainly used for identification of dynamic characteristics such as natural frequencies, mode shapes and damping ratios [20–22]. In this toolbox, frequency domain based and time domain-based system identification techniques are implemented. System identification techniques also include output only as well as input-output methods. Three frequency domain based techniques: the Peak Picking (PP) method [23], the Frequency Domain Decomposition (FDD) method [24] and the Enhanced Frequency Domain Decomposition (EFDD) method [25] as well as five time domain based techniques: Stochastic Subspace Identification (SSI) [26, 27], the Auto Regressive eXogenous (ARX), the Auto Regressive Moving Average eXogenous (ARMAX), the Observer/Kalman filter Identification (ERA/OKID)

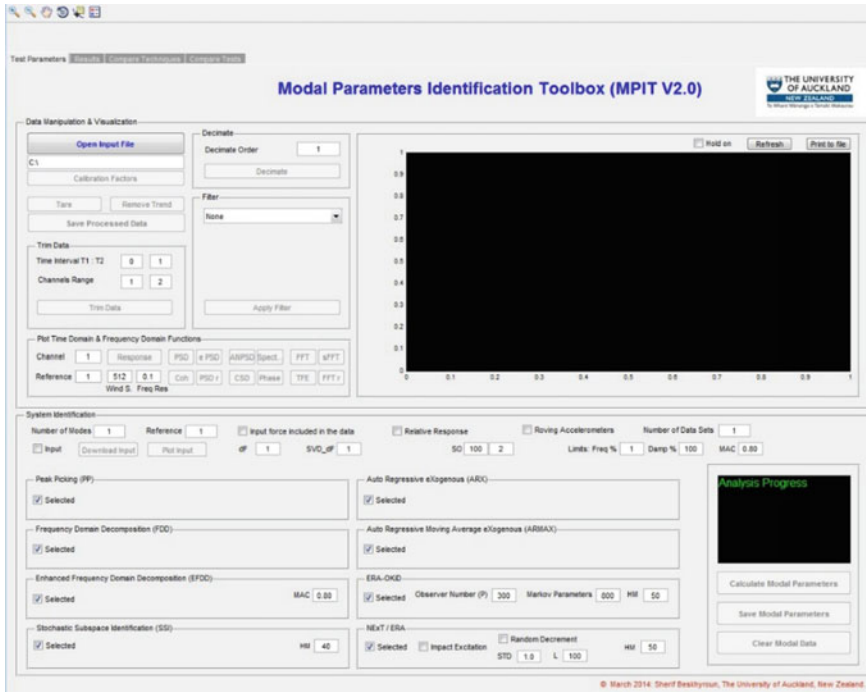


Fig. 16.4 Modal parameters identification toolkit (MPIT)

[28–30], and the Eigen Realization Algorithm combined with the Natural Excitation Technique (NExT/ERA) method [31, 32] are adopted in the toolbox. It was decided to use a number of time domain and frequency domain based modal identification techniques to ensure the reliability of the identified modal parameters and improve the identification of true modes.

The toolbox offers extensive functionalities for the visualization and processing of the data, the determination and visualization of the structure’s modal parameters, comparison of the identified modal parameters from different modal parameters identification techniques and comparison of modal parameters obtained from a particular technique using data from different data sets. The intention is to develop an automated toolbox for estimating modal parameters and providing functions to compare the system identification results from various available techniques and also to compare modal parameters produced by a specific system identification technique using different data sets.

The ADAT is used for automated dynamic monitoring, excluding any user interaction. This toolkit can divide and process large data sets automatically. Available tools in this toolkit include functions for communications with servers, data downloads, changing the format of the raw data, dividing continuous data to user specified intervals, running data analysis and saving the results. The toolkit also provides functions

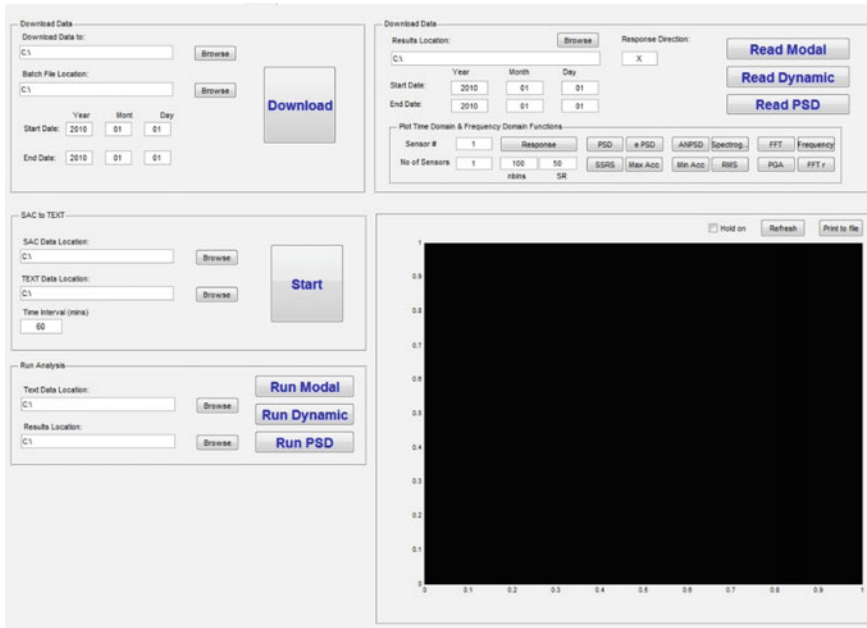


Fig. 16.5 Automated data analysis toolkit (ADAT)

for data visualization and comparison. ADAT consists of four main panels; “Download Data”, “SAC to Text”, “Run Analysis” and “Download Results”, as shown in Fig. 16.5. The “Download Data” panel is used to collect and transfer raw data from a remote server to a local computer in a user specified time frame. In the “SAC to Text” panel, the format of the raw data is changed to text format, divided to a selected interval and then saved in a new folder location. The “Run Analysis” panel includes functions for running modal analysis, identification of dynamic features and estimation of power spectral density (PSD) using recorded data intervals. The “Run Modal” function in this panel runs selected system identification techniques in the MPIT toolbox. Previously saved results from any structure in a specific time frame can be downloaded and visualized using several available functions in the “Download Results” panel.

The potential of the developed system is illustrated using data collected from a bridge by a continuous dynamic monitoring system for nearly one year. Ambient vibration data were continuously recorded using 16 tri-axial accelerometers at a rate of 50 samples per second for several years. Acceleration data between 1st of January and 31st of December 2013 were considered in this study as two major earthquakes and several aftershocks were recorded during this period.

Firstly, peak values, Root Mean Square (RMS) and Square Root of Sum of Squares (SRSS) accelerations are detected automatically, enabling the statistical treatment of the response time series. Secondly, a succession of PSD lines is produced to form

a spectrogram of hourly distribution of frequency components. Then, an automated modal parameters identification procedure is implemented to extract dynamic characteristics from successive hourly data sets.

16.4 Structure and Instrumentation

16.4.1 *Thorndon Bridge*

The Thorndon Bridge constructed between 1967 and 1972 is a twin 1.35 km long elevated concrete bridge along the original offshore of the Wellington Harbor in Wellington, New Zealand. The bridge carries State Highway one (SH1) over the main trunk railway, the Inter Islander Ferry Terminal and also two significant access roads into Wellington city; Aotea Quay and Thorndon Quay [33]. This superstructure consists of simply supported precast concrete I girders spanning between pier caps. Two superstructure expansion joints, which can rotate in plan, were provided per span to enable the piers to respond independently to the seismic loads in transverse direction. The northbound and southbound of the bridge are 11.5 m wide and carry three of 3.5 m traffic lanes in addition to 0.5 m shoulders.

The Thorndon Bridge is located in a high seismicity area because the Wellington Fault, the significant earthquake source in New Zealand, passes under the bridge. Therefore, it has recently been instrumented with strong motion accelerometers for condition monitoring. This project is a part of GeoNet Structures Instrumentation Program (www.geonet.org.nz) to install multiple seismic instruments in various representative commercial and residential buildings and bridges located in areas with high seismic hazard throughout the New Zealand.

16.4.2 *Instrumentation*

The bridge was instrumented with 16 tri-axial accelerometers in North and South bounds. In each bound, seven accelerometers were located on the superstructure on two adjacent piers and two adjacent spans and one accelerometer at the ground level. The accelerometer zones in the two bounds were approximately 400 m apart. The accelerometer locations in Zone I and II are shown in Fig. 16.6a and b, respectively. As indicated in these figures, in each zone, seven accelerometers were installed on the superstructure on two adjacent piers and two adjacent spans and one accelerometer at the ground level on the concrete base slab of the control cabinet. Accelerometers 1–8 were located on piers 25 and 26, Spans 24–25 and 25–26 in Zone I and accelerometers 9–16 on piers 13 and 14, Spans 13–14 and 14–15 in Zone II.

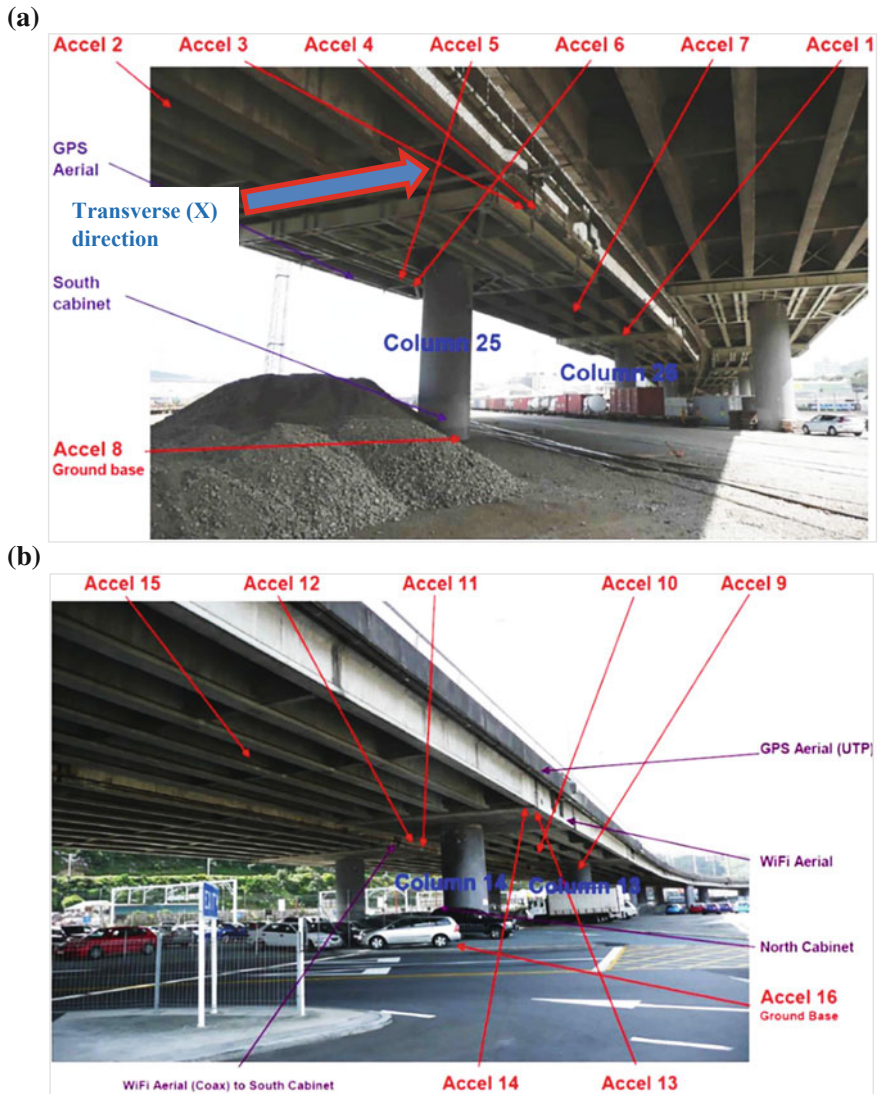


Fig. 16.6 Sensor locations on the Thorndon bridge: a Zone I, b Zone II

16.4.3 Strong Earthquakes Recorded During Monitoring Period Between 1st of January and 31st of December 2013

16.4.3.1 Seddon Earthquake

The M_L 6.5 Seddon earthquake struck at 5:09:30 pm on 21 July 2013 (05:09 UTC) at a depth of 13 km and was centered around 55 km south of Wellington, according to GeoNet (www.geonet.org.nz). The quake caused moderate damage in Wellington and nearby cities. Only minor injuries were reported, and several aftershocks occurred after the earthquake.

The earthquake was preceded by a series of foreshocks and generated a series of aftershocks. Table 16.1 lists all foreshocks and aftershocks of M_L 5.4 and above that occurred in the region between 19 July 2013 and 29 July 2013 (www.geonet.org.nz).

16.4.3.2 Lake Grassmere Earthquake

The M_L 6.6 Lake Grassmere earthquake occurred at 2:31:05 pm (NZST) on Friday 16 August 2013 (www.geonet.org.nz). The epicenter was located about 10 km south-east of Seddon city, under Lake Grassmere, with a focal depth of 8 km. The earthquake caused significant damage buildings in Seddon and it was widely felt in both the North and South Islands of New Zealand. The earthquake generated a significant series of aftershocks, the largest was M_L 6.0. Table 16.2 lists of all aftershocks M_L 5.0 and above that occurred in the region between 16 August 2013 and 17 August 2013 (www.geonet.org.nz). A summary of the vertical and horizontal peak ground acceleration records from Seddon and Lake Grassmere earthquakes are shown in Fig. 16.7a and b, respectively (www.geonet.org.nz).

Table 16.1 Summary of strong earthquake events recorded between 19 July 2013 and 2 August 2013

Date (NZST)	Time (NZST)	Magnitude (M_L)	Epicenter	Depth (km)
19 July 2013	9:06:39 am	5.7	30 km east of Seddon	17
21 July 2013	7:17:10 am	5.8	30 km east of Seddon	20
21 July 2013	5:09:30 pm	6.5	25 km east of Seddon	13
29 July 2013	1:07:14 am	5.4	20 km east of Seddon	12

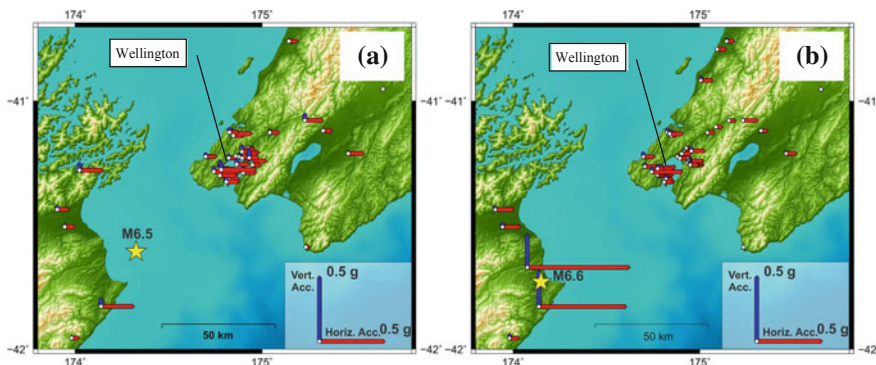


Fig. 16.7 a Seddon earthquake, b Lake Grassmere earthquake (www.geonet.org.nz)

16.4.3.3 Recorded Data

Acceleration data between 1st of January and 31st of December 2013 were considered in this study as two major earthquakes and several aftershocks were recorded during this period. Given the high sampling rate (50 Hz), the large number of recording channels (48 channels) and the long monitoring period considered in this study (365 days), the SHM system produced a very large amount of monitoring data that could be very challenging to manage, process and analyze. In the considered mon-

Table 16.2 Summary of strong earthquake events recorded between 16 August 2013 and 17 August 2013

Date (NZST)	Time (NZST)	Magnitude (M_L)	Epicenter	Depth (km)
16 August 2013	2:31:05 pm	6.6	10 km south east of Seddon	8
16 August 2013	2:37:27 pm	5.4	5 km south east of Seddon	9
16 August 2013	2:45:27 pm	5.4	10 km south east of Seddon	6
16 August 2013	3:09:08 pm	5.5	10 km south of Seddon	8
16 August 2013	3:51:35 pm	5.6	10 km east of Seddon	19
16 August 2013	5:31:16 pm	6.0	15 km east of Seddon	14
16 August 2013	6:55:58 pm	5.5	20 km east of Seddon	20
17 August 2013	8:58:39 pm	5.5	10 km south of Seddon	20

itoring period, the SHM system produced more than 26,280 ($365 \text{ days} \times 24 \text{ h} \times 3 \text{ directions}$) hourly interval files with around 952 GB of total data size. The developed toolkit in this study was successfully utilized to divide the data to hourly intervals and then process each interval and report the results in a fully automated way.

16.5 Results and Discussion

In this section, firstly the histogram of vibration intensity parameters including peak accelerations, RMS and SRSS of vibration measurements are automatically computed using the monitoring toolbox providing statistical treatment of the time-series response. Then, a succession of PSD lines is produced using the toolbox to form a spectrogram of hourly distribution of frequency components. Then, an automated procedure for modal parameter identification is implemented to extract dynamic characteristics of the bridge from successive hourly datasets. Subsequently, a small window of recorded data during large-amplitude earthquakes is analysed using the toolbox to provide a precise examination on the bridge performance during the strong, medium and weak ground motions.

16.5.1 *Dynamic Characteristics of the Bridge*

The toolbox also performs automated frequency-domain analysis of acquired data, evaluating the PSD spectra at different sensors. Several time-frequency distribution methods have been developed for structural health monitoring applications [11, 34–37], however it was decided to use PSD analysis in this part of the current investigation to reduce the computational demand and to achieve higher resolution of the frequency data. PSD is calculated for each hour of data producing one line of frequency domain representation of the data at the time of the recorded data. By plotting sequences of the PSD spectral estimates of every hour of data, spectrogram plots are obtained, as shown in Figs. 16.8 and 16.9. From spectrogram plots, the frequency component distribution is easily captured, allowing the observation of the time variation of natural frequencies, as well as the identification of different intensity periods. Figure 16.8 depicts the PSD distribution of vertical acceleration data obtained from accelerometer 2, which is located in the mid span of the bridge deck, in the period between 1st of January to 31st of December 2013. A drop of 0.05 Hz in the natural frequency of the first vertical mode has been observed immediately after the Cook Strait earthquake (21st of July 2013) indicating a very minor but permanent alteration of the bridge dynamic performance due to this earthquake. No further drop or change in the natural frequency was noticed after the second major earthquake; Lake Grassmere earthquake which occurred on 16 August 2013. To confirm that the observed shift in frequency is not due any alteration in the sensor orientation or

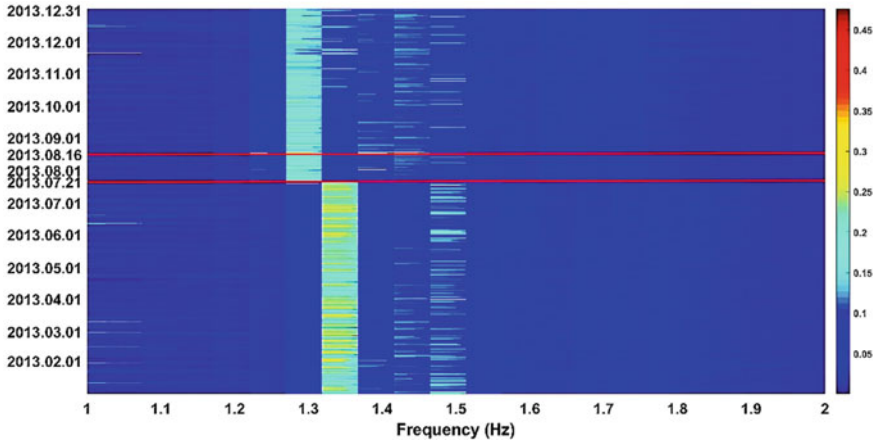


Fig. 16.8 PSD of acceleration recorded by accelerometer 2 in the transverse (X) direction from 1 January to 31 December 2013

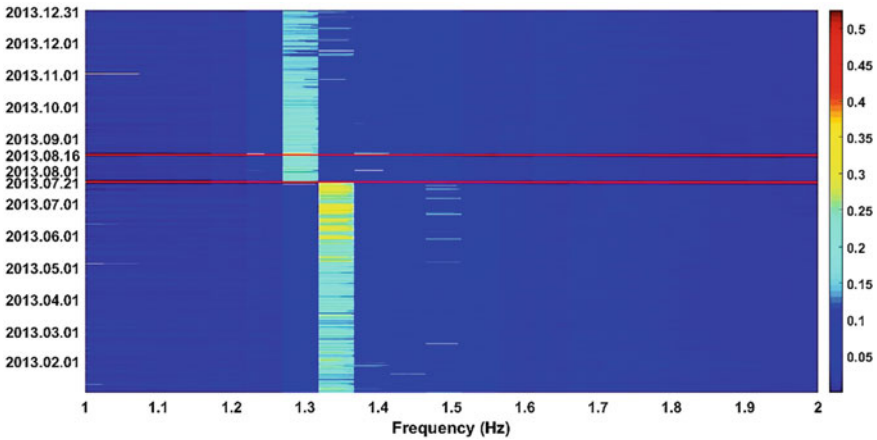


Fig. 16.9 PSD of acceleration recorded by accelerometer 4 in the transverse (X) direction from 1 January to 31 December 2013

performance, the PSD spectrograms at other sensors were estimated. As clearly seen in Fig. 16.9, the same shift in frequency after the strong earthquakes was also found.

16.5.2 *Vibration Intensity of the Bridge*

The vibration intensity is a good indicator for the stress level of a structure subjected to dynamic loads. Increasing vibration intensities of individual structural members

under similar operational loads can be an indicator of fatigue-relevant damage mechanisms. Acceleration data from the tested bridge in this study has been recorded continuously at a rate of 50 samples per second since August 2012. Raw data was divided to hourly intervals and peak acceleration, RMS and SRSS values were determined for every hour interval. Several other vibration parameters are also estimated by the developed data analysis program. The historical results of these parameters can be used to establish a reliable threshold values for the monitored structure to track any gradual degradation of the structure's conditions.

Figure 16.10a and b show the peak positive and negative acceleration values in transverse direction recorded by accelerometer 6 installed on the pier of the bridge over one year monitoring period. As is obvious from the figure, the accelerometer recorded two strong ground motions in 2013; Cook Strait Earthquake and Lake Grassmere Earthquake. The first ground motion with peaks of around $-0.21g$ to $0.20g$. The second earthquake with peaks of around $-0.07g$ to $0.09g$ occurred at 2:30 pm on 16 August 2013, with a magnitude of 6.6. Figures 16.11a and b show a histogram of the peak acceleration values reported at accelerometer 6 in the vertical direction for the monitoring periods between January–June 2013 and July–December 2013, respectively. The July–December 2013 period includes data during and after the two major earthquakes; Cook Strait and Lake Grassmere. The intention here is to compare the vibration intensities before and after the two major earthquakes including several strong aftershocks. As clearly indicated in Fig. 16.11a and b, no significant change in the peak acceleration distribution was observed before and after the earthquakes. The acceleration peaks histogram comprises two close to normal distribution sections. The peak acceleration in the first section ranges from 0 to 0.15 m/s^2 and is centered around 0.08 m/s^2 which indicates very light traffic volume, likely during night hours and outside rush hours. In the second section, peak acceleration values are higher compared to the first part indicating heavier traffic loads during rush hours. Very similar distribution is observed for the two monitoring periods. RMS data before and after the earthquakes are shown in Fig. 16.12a and b, respectively. Similar distribution and amplitudes of RMS data can be clearly observed in the two monitoring periods. Similarity in the peak and RMS acceleration data indicates with good confidence that the bridge performance has not been altered after the earthquakes. SRSS histogram of recorded vibration datasets is also provided to assess different dynamic parameters of the structure. The histogram of SRSS vertical accelerations recorded by accelerometers 6 for the two monitoring periods are depicted in Fig. 16.13a and b, respectively. As clearly shown in these figures, similar distributions of SRSS values before and after the earthquakes are found. According to the analysis results obtained using the new toolkit, it can be concluded that the vibration intensities of the bridge have not been changed due to the seismic loading of the strong earthquakes. The feasibility of using vibration intensity indicators such as peak acceleration, RMS and SRSS to monitor structures' conditions and detect small damage levels needs further investigation.

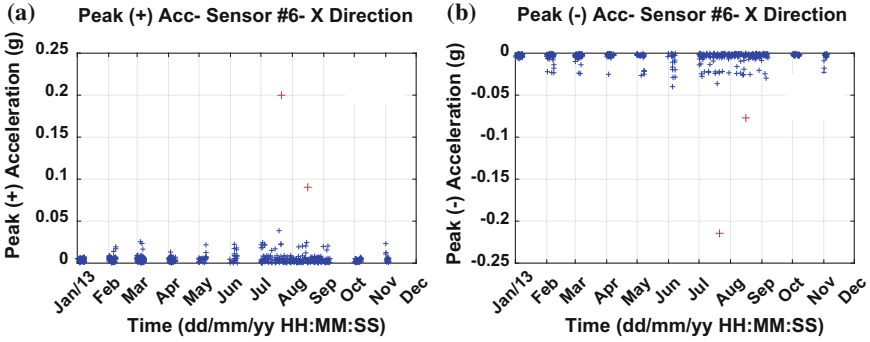


Fig. 16.10 Maximum negative and positive accelerations recorded by accelerometer 6 in the transverse (X) direction during one-year monitoring period

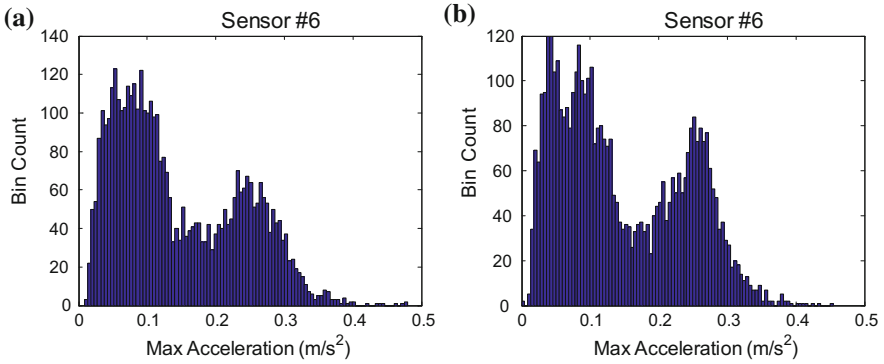


Fig. 16.11 Histogram of maximum vertical acceleration recorded by accelerometer 6 from: **a** 1 January to 30 June 2013, **b** 1 July to 31 December 2013

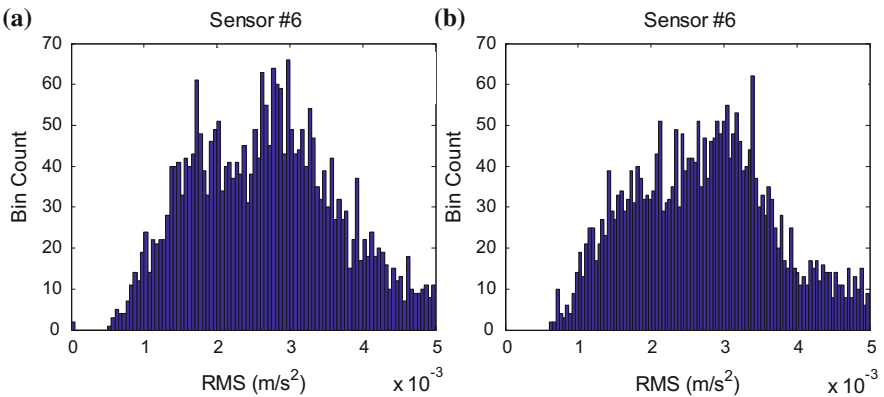


Fig. 16.12 Histogram of RMS of vertical acceleration recorded by accelerometer 6 from: **a** 1 January to 30 June 2013, **b** 1 July to 31 December 2013

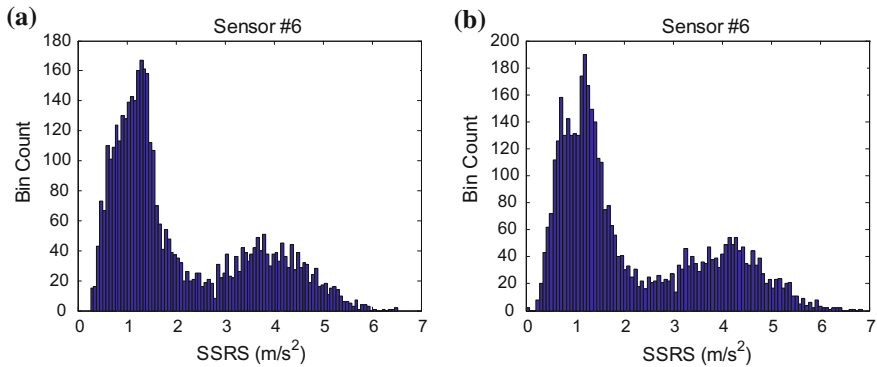


Fig. 16.13 Histogram of SRSS of vertical acceleration recorded by accelerometer 6 from: **a** 1 January to 30 June 2013, **b** 1 July to 31 December 2013

16.5.3 Earthquake-Induced Vibration Data

In this section, the dynamic performance of the bridge during various levels of shaking intensity is investigated. For this purpose, three sets of vibration data recorded with considerable difference in peak acceleration values are considered. These sets include high-amplitude vibration induced by the Cook Strait Earthquake (peak response acceleration = $0.21g$), moderate-amplitude vibration induced by the Lake Grassmere Earthquake (peak response acceleration = $0.09g$), and low-amplitude vibration induced by an aftershock occurred after the second earthquake (peak response acceleration = $0.02g$).

A thorough time-frequency analysis can be carried out on the recorded structural response during earthquakes, however a simple spectrogram of the time-frequency distribution of the data was presented here due to the limited size of the chapter. The spectrogram of acceleration data recorded by accelerometer 1 in the X direction is calculated using the MPIT toolbox and shown in Fig. 16.14. As indicated in this figure, the natural frequency of the bridge is found at 1.3 Hz before and after the strong shaking (0–9.5 s and 12–30 s) but during the strong ground motion the natural frequency dropped to 0.97 Hz (the dark colour points). This drop in frequency can be attributed to cracks opening in concrete, soil structure interaction, sliding of supports. The spectrogram of acceleration recorded by accelerometer 1 in X direction during moderate-amplitude earthquake is shown in Fig. 16.15. The results show that the bridge's natural frequency dropped to the same previous value of 0.97 Hz, which clearly indicates that the drop in frequency is related to the structure's stiffness and boundary conditions not to the earthquake characteristics. It is quite beneficial to understand the dynamic performance of structures at various level of shaking for con-

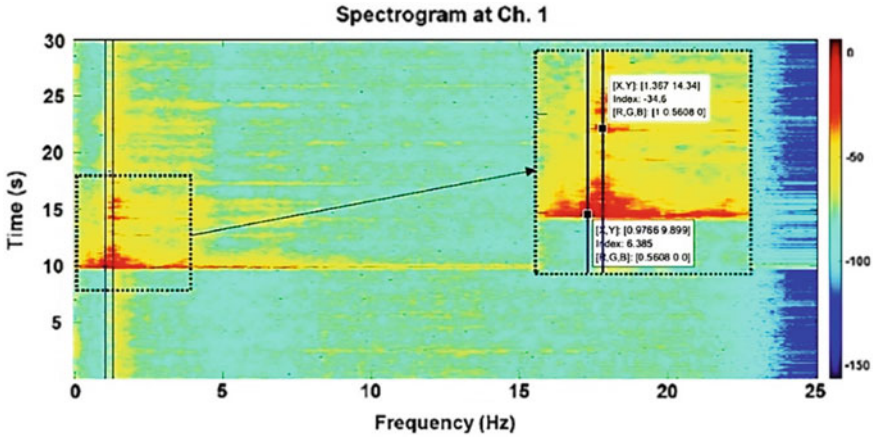


Fig. 16.14 Spectrogram of acceleration data recorded by accelerometer 1 in the transverse (X) direction during a high-amplitude Earthquake

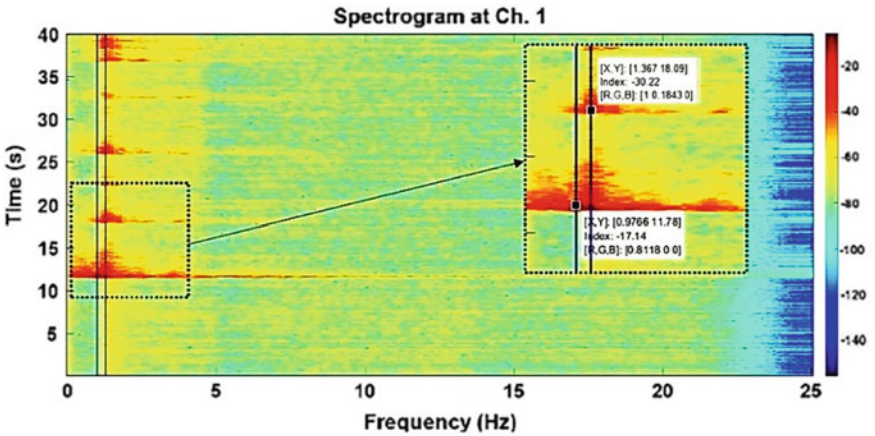


Fig. 16.15 Spectrogram of acceleration data recorded by accelerometer 1 in the transverse (X) direction during a moderate-amplitude Earthquake

dition monitoring and design. To confirm the previous findings, the spectrogram of a low-magnitude vibrations was calculated, as shown in Fig. 16.16. As depicted in this figure, there is no drop in natural frequency of the bridge during this low-magnitude aftershock and the bridge behaves at a constant frequency of around 1.3 Hz.

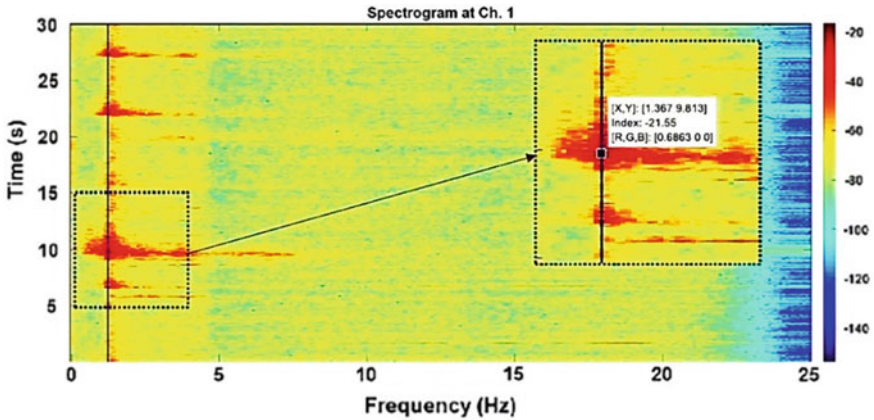


Fig. 16.16 Spectrogram of acceleration data recorded by accelerometer 1 in the transverse (X) direction during a low-amplitude aftershock

16.6 Conclusions

New Zealand experiences high level of seismic activities over various parts of the country. The strong-motion monitoring program features dense array of sensors on the ground as well as a dedicated structural response monitoring program. The GeoNet building instrumentation program has offered several benefits to the end-users through its continuous monitoring and recording of data, particularly by capturing the response from the ground shaking during an unexpected earthquake.

This chapter further contributes on the development of computational tools for monitoring and damage assessment of structures. The toolkits provide functions for automated dynamic parameters and response amplitudes monitoring and it has been developed to integrate long term continuous structural monitoring systems. The application of this toolkit in the context of long-term monitoring has been demonstrated using acceleration data recorded over one year from a full-scale concrete bridge located in Wellington, New Zealand. The test bridge was subjected to two major earthquakes of magnitude M_L 6.5 and 6.6 and several aftershocks during the monitoring period. The dynamic performance of the bridge was evaluated before and after the earthquakes utilizing the developed toolkit. A very small drop in the natural frequency of the first vertical mode was observed after the first earthquake but with no major change in the overall dynamic performance of the bridge.

The developed toolkit in this study was successfully utilized to manage, analyze and report the results from very large sets of recorded data from a continuous SHM system in a fully automated way. The effectiveness of the toolkit in running computationally extensive analysis has also been demonstrated.

This investigation illustrates the potential of this package in terms of automated processing of large amount of data enabling the accurate characterization of the

time variation of natural frequencies and dynamic performance indicators over long periods of continuous monitoring.

Acknowledgements The authors gratefully acknowledge contributions from the GeoNet project and its sponsors EQC and GNS Science for supporting the structural monitoring programme. Authors are grateful to GeoNet staff in providing support and clarifications in preparation of the manuscript. Special thanks to Niusha Navabian, a Ph.D. candidate at Auckland University of Technology, for her assistance in the data analysis.

References

1. Butt F, Omenzetter P (2014) Seismic response trends evaluation and finite element model calibration of an instrumented RC building considering soil-structure interaction and non-structural components. *J Eng Struct* 65:111–123. <https://doi.org/10.1016/j.engstruct.2014.01.045>
2. Cousins WJ (1993) Highlights of 30 years of strong-motion recording in New Zealand. *Bull NZ Soc Earthq Eng* 26(4):375–389
3. Cousins WJ (2001) Status and developments in strong-motion recording in New Zealand. In: COSMOS: Workshop on strong-motion instrumentation of buildings. Emeryville, California
4. Deam BL, Cousins WJ (2002) Strong-motion instrumentation of buildings in New Zealand. In: New Zealand society of earthquake engineering conference proceedings. Paper 2.3
5. Uma SR, King A, Cousins WJ, Gledhill K (2011) The GeoNet building instrumentation programme. *Bull NZ Soc Earthq Eng* 44(1):53–63
6. Thomson EM, Bradley BA (2014) Preliminary analysis of instrumented Wellington building responses in the July/August 2013 Seddon/Lake Grassmere earthquakes. In: New Zealand society of earthquake engineering conference, Rotorua, New Zealand
7. Chandramohan R, Ma Q, Wotherspoon LM, Bradley BA, Nayyerloo M, Uma SR, Stephens MT (2017) Response of instrumented buildings under the 2016 Kaikoura earthquake. *Bulletin of the New Zealand Society for Earthquake Engineering*, 50(2): 237-252
8. Zhao JX, Uma SR (2011) A preliminary analysis on the response of an instrumented building during the 2010 Darfield earthquake: significant effects of soil-structure interaction and non-linear response. Paper 68. Ninth Pacific Conference on Earthquake Engineering. Auckland, New Zealand
9. Ma Q, Beskhyroun S, Simkin G, Wotherspoon LM, Ingham J, Gebreyohannes A, Sharpe R (2014) Experimental evaluation of inter-storey drifts during the Cook Strait earthquake sequence. In: New Zealand society of earthquake engineering conference, Rotorua, New Zealand
10. Beskhyroun S, Wegner LD, Sparling BF (2012) New methodology for the application of vibration-based damage detection techniques. *Struct Control Health Monit* 19(8):632–649. <https://doi.org/10.1002/stc.456>
11. Nakata N, Snieder R, Kuroda S, Ito S, Aizawa T, Kunimi T (2013) Monitoring a building using deconvolution interferometry. I: earthquake-data analysis. *Bull Seismol Soc Am* 103(3):1662–1678. <https://doi.org/10.1785/0120120291>
12. Ou J, Li H (2010) Structural health monitoring in mainland China: review and future trends. *Struct Health Monit* 9(3):219–231. <https://doi.org/10.1177/1475921710365269>
13. Abdelgawad A, Yelamarthi K (2017) Internet of Things (IoT) platform for structure health monitoring. *Wirel Commun Mob Comput* 10. <https://doi.org/10.1155/2017/6560797>
14. Brownjohn JM, De Stefano A, Xu Y-L, Wenzel H, Aktan AE (2011) Vibration-based monitoring of civil infrastructure: challenges and successes. *J Civ Struct Health Monit* 1(3–4):79–95. <https://doi.org/10.1007/s13349-011-0009-5>

15. McDonald C (2010) *n.* 882 N. Fair Oaks Ave Pasadena, CA 91103 United States: CGM Engineering, Inc
16. Li J, Deng J, Xie W (2015) Damage detection with streamlined structural health monitoring data. *Sensors* 15(4):8832–8851. <https://doi.org/10.3390/s150408832>
17. Yang J, Lam H, Hu J (2015) Ambient vibration test, modal identification and structural model updating following Bayesian framework. *Int J Struct Stab Dyn* 15(07):1540024. <https://doi.org/10.1142/S0219455415400246>
18. MATLAB (2017) User's manual. The Mathworks, Inc
19. Beskhyroun S (2011) Graphical interface toolbox for modal analysis. In: Ninth Pacific conference on earthquake engineering
20. Beard SJ, Kumar A, Qing X, Chan HL, Zhang C, Ooi TK (2005) Practical issues in real- world implementation of structural health monitoring systems. Acellent Technologies Inc, Sunnyvale, CA
21. Chopra AK (1995) Dynamics of structures, vol 3. Prentice Hall, New Jersey
22. Döhler M, Andersen P, Mevel L (2012) Operational modal analysis using a fast stochastic subspace identification method. In: Topics in modal analysis I, vol 5. Springer, Berlin, pp 19–24
23. Bendat JS, Piersol AG (2011) Random data: analysis and measurement procedures, vol 729. Wiley, New York
24. Brincker R, Zhang L, Andersen P (2000) Modal identification from ambient responses using frequency domain decomposition. In: Proceedings of the 18th international modal analysis conference (IMAC), USA
25. Jacobsen N-J, Andersen P, Brincker R (2007) Using EFDD as a robust technique to deterministic excitation in operational modal analysis. In: Proceedings of the 2nd international operational modal analysis conference (IOMAC), Copenhagen, Denmark
26. Katayama T (2005) Subspace methods for system identification. Springer, Berlin
27. Van Overschee P, Moor BD (1996) Subspace identification for linear systems. Kluwer Academic Publishers
28. Juang J-N (1994) Applied system identification. Prentice-Hall, Englewood Cliffs, NJ
29. Juang J-N, Phan M, Horta LG, Longman RW (1993) Identification of observer Kalman filter Markov parameters: theory and experiments. *J Guid Control Dyn* 16(2):320–329
30. Phan M, Horta LG, Juang J-N, Longman RW (1993) Linear system identification via an asymptotically stable observer. *J Optimiz Theory Appl* 79(1):59–86
31. James GH, Carne TG, Lauffer JP (1993) The natural excitation technique for modal parameter extraction from operating wind turbines. Report No SAND92-1666, UC-261. National Laboratories, Sandia
32. Juang JN, Pappa RS (1985) An Eigensystem realization algorithm for modal parameter identification and model reduction. *J Guid Control Dyn* 8(5):620–627
33. Wood J (2014) Strong motion records from the Thorndon Overbridge in the 2013 Cook Strait and Lake Grassmere earthquakes. In: Proceedings of the annual conference of the New Zealand Society of Earthquake Engineering (NZSEE2014)
34. Astorga A, Guéguen P, Kashima T (2018) Nonlinear elasticity observed in buildings during a long sequence of earthquakes. *Bull Seismol Soc Am* 108(3A):1185–1198. <https://doi.org/10.1785/0120170289>
35. Michel C, Gueguen P (2010) Time-frequency analysis of small frequency variations in civil engineering structures under weak and strong motions using a reassignment method. *J Struct Health Monit*. <https://doi.org/10.1177/1475921709352146>
36. Beskhyroun S, Ma Q, Wotherspoon LM (2017) Development of monitoring system for damage assessment of buildings after earthquakes. In: 16th World Conference on Earthquake engineering, Santiago, Chile
37. Navabian N, Bozorgnasab M, Taghipour R, Yazdanpanah O (2016) Damage identification in plate-like structure using mode shape derivatives. *Arch Appl Mech* 86(5):819–830. <https://doi.org/10.1007/s00419-015-1064-x>

Chapter 17

Seismic Monitoring of Seismically Isolated Bridges and Buildings in Japan—Case Studies and Lessons Learned



Yozo Fujino, Dionysius M. Siringoringo, Masaru Kikuchi, Kazuhiko Kasai and Toshihide Kashima

Abstract Monitoring of seismic response of structures has been widely employed for decades in Japan. From the structural point of view, the objectives of seismic monitoring are mainly to verify designed load assumption, evaluate seismic response and structure performance during large earthquake, detecting possible damages due to earthquake and monitoring for verification of structural retrofit. Seismic monitoring is very important for large, important structures and structures with specific features and innovative technologies such as seismic isolation or response control systems. This paper describes several case-studies and lessons learned of seismic monitoring on seismically isolated bridges and buildings in Japan.

Keywords Seismic monitoring · Seismically isolated structures · Base-isolated bridges · Base-isolated buildings · Seismic records

Y. Fujino (✉) · D. M. Siringoringo
Institute of Advanced Sciences (IAS), Yokohama National University, Yokohama, Japan
e-mail: fujino@ynu.ac.jp

D. M. Siringoringo
e-mail: dion@ynu.ac.jp

M. Kikuchi
Faculty of Engineering, Hokkaido University, Sapporo, Japan
e-mail: mkiku@eng.hokudai.ac.jp

K. Kasai
Institute of Innovative Research (IIR), Tokyo Institute of Technology, Tokyo, Japan
e-mail: kasai.k.ac@m.titech.ac.jp

T. Kashima
Building Research Institute, Tsukuba, Japan
e-mail: kashima@kenken.go.jp

17.1 Introduction

Japan has more than thirty years of experience in designing and constructing base-isolated structures. Construction has increased significantly especially since the 1995 Hyogoken-Nanbu (Kobe) earthquake. Many new developments and refinements have been made in the material, device, design, and construction of these structures. The size, height, and fundamental natural period of newly built base-isolated buildings and bridges increase steadily with time, indicating that base-isolation in Japan is reaching maturity.

Technical development on the application of seismic isolation design to highway bridges was initiated in 1986 by Public Works Research Institute (PWRI) together with several private companies. Results of extensive research were summarized in the draft manual for seismic isolation design method of highway bridge which was made available in 1992. The design manual includes the design method for isolators and unseating prevention devices. As for the building, the first design recommendations for seismically isolated buildings was issued by the Architectural Institute of Japan (AIJ) in 1989.

In the field of structure response and seismic monitoring, Japan has more than sixty-year history since the domestic development of accelerometers. The development of a strong motion instrument in Japan began after the 1948 Fukui Earthquake, which was a large damaging inland earthquake. In 1953, the SMAC accelerometer was developed by the Strong Motion Accelerometer Committee. "SMAC" stands for the name of the Committee. The SMAC accelerometer is an analog device that can record triaxial accelerations up to 1 g. Twenty-five SMACs were installed in buildings in 1956, marking the start of earthquake-induced response monitoring of structures in Japan. For monitoring ground motions, the sensors are installed at more than 5000 locations, covering the entire geographic area of Japan. The recorded data are publicly available from the National Research Institute for Earth Sciences and Disaster Resilience (NIED) [22], Japan Meteorological Agency (JMA), and local governments.

Many of long-span and important bridges in Japan are instrumented and monitored regularly after their construction completion. Initially, monitoring system put more emphasis on structural evaluation against extreme events such as large earthquake and typhoon. Monitoring data are utilized to verify design assumptions, update specifications, and facilitate the efficacy of vibration control system. For buildings, more than 80 buildings are instrumented in major cities throughout Japan, where one-third of them are located in Tokyo and its outskirts. Their data are publicly available from the Building Research Institute (BRI). Note that many other buildings are also instrumented, but the response data are typically made unavailable to the public by the building owners.

The protective technologies of base-isolation as well as vibration-control have not often been validated through response to actual earthquakes. During large earthquakes such as the 1995 Kobe and 2011 Tohoku earthquakes, however, many of the bridges and buildings using the seismic isolation technologies experienced the

strong shaking. This provides an opportunity to evaluate performance of seismically-isolated structures. In this chapter, monitoring experiences of seismically-isolated bridges and buildings in Japan are described along with lessons learned from the monitoring experiences with several case studies.

17.2 Seismic Monitoring of Seismically-Isolated Short and Medium Span Bridges

There are important characteristics of design method for seismically-isolated bridges in Japan that are uniquely different from other countries. While seismic force reduction can be achieved considerably by lengthening natural period of the bridge, the main purpose of seismic isolation of bridges in Japan is the improvement of damping and distribution of seismic force without attaining excessive elongation of natural period. There are several reasons behind this objective, the first is the fact that many highway bridges are built on comparatively soft soil and considering that large earthquakes occur quite frequently in Japan, if excessive elongation of natural period is attained, then large superstructure displacement and possible damaging contact with abutments or adjacent girders could be resulted. To avoid such cases, expansion joints should be enlarged but this would create noise problem, vehicle-induced vibration and extra maintenance. Therefore, excessive elongation of natural period is undesirable. Instead, improvement of damping performance and distribution of seismic force to substructure become the key factors. This design principle, commonly called '*menshin*' is different from application of seismic isolation system of bridges in other countries.

The first seismically-isolated bridge in Japan is the Miyagawa bridge. The bridge girder is a three-span continuous non-composite steel with length of 105.8 m. Located in Haruno-cho, Shizuoka prefecture, the bridge was open in March, 1991 and was one of eight bridges selected from the whole country as the pilot construction project of base-isolation system. Lead Rubber Bearing (LRB) was adopted as a seismic isolation device. To examine the earthquake response characteristic of the seismic isolation bridge, strong-motion seismographs (accelerometers) were installed at the Miyagawa bridge at the pier cap, girder and free-field. On April 25, 1992, an earthquake with magnitude of 4.9 on the JMA (Japan Meteorological Agency) scale with epicenter in Shizuoka was recorded. This was first seismic records from monitoring system of seismically-isolated bridge in Japan. Analysis of the records help confirming some important aspects adopted in the design of base-isolated bridge [13].

In the following section we will describe in detailed case studies of seismic monitoring of two short-medium span bridges. The objective is to analyze the dynamic behavior of base-isolated bridges and to quantify the performance of isolation bearings in actual earthquakes, using recordings at instrumented the bridges.

17.2.1 *Matsunohama Viaduct*

Matsunohama viaduct is an elevated bridge located on the Hanshin Expressway bay shore route in Kansai area, west of Japan. The bridge was opened in 1994. Some of the spans of this elevated expressway are supported by base isolation bearings and this was the first application of base-isolated bridge on the Hanshin Expressway. The viaduct is a 4-span continuous steel box girder bridge with the bridge length of 211.5 m and the curvilinear radius of 560 m. Matsunohama viaduct has two base isolated bridges Bridge A and Bridge B. The design was performed based on the 1990 JRA design specifications for highway bridges. The design of seismic isolation bearings was made according to the 1992 Manual (Draft) of Seismic Isolation Design of Highway Bridges.

Bridge A is a four-span continuous bridge having equal spans of 45 m with 13 non-composite steel girders supported on laminated natural rubber bearing (NRB) at the inner piers (P-21 to P-23) and on Teflon sliding bearings at the end piers (P-20 and P-24). The bearings can move in the longitudinal direction of the bridge only and are restrained by steel stoppers in the transverse direction. Bridge B is also a four-span continuous bridge having a total length of 211.5 m. The two middle spans are 60 m, and the side spans are 46.5 and 45 m; with two non-composite steel box girders supported by lead rubber bearing (LRB) at the inner piers (P-29, P-31, and P-32) and by pivot roller bearings at the end piers (P-28 and P-33). Bearings can move only in the longitudinal direction with two side stoppers installed with 5-mm clearance to prevent movement in the transverse direction. Pier P-23 of Bridge A and P-32 of Bridge B are instrumented with strong motion accelerometers, as shown in Fig. 17.1.

Monitoring system was installed on the bridge with the main objective to confirm the performance of base-isolation system under seismic excitation. This objective is set as the bridge is one of the first seismically-isolated bridges in Japan and therefore the accuracy of design procedure and model for the bridge need to be verified with recorded responses. The monitoring system was installed and operated by the bridge operator Hanshin Expressway. The system consists of triaxial accelerations at four locations: free field, pile cap, pier cap, and girder; connected by wired network system. Figure 17.1 illustrates locations of the sensors and measuring direction. The accelerometers frequency bandwidth of 0.05–35 Hz and operate at sampling frequency 100 Hz. Monitoring system operates under an event-based recording system where sensors start the recording when a ground motion exceeds a preset trigger level. All data is stored temporarily in a local storage system and then collected by staff of bridge operator for analysis. Analysis of the records was conducted in a research collaboration between bridge operator and the University of Tokyo, former institution of the authors. Data analysis was conducted by the authors and the results were communicated to inform the bridge operator about condition of the bridge and performance of isolation system.

About one year after opening, the bridge was hit by the 1995 Kobe earthquake. The bridge is located about 35 km east-south-east from the epicenter of. Maximum

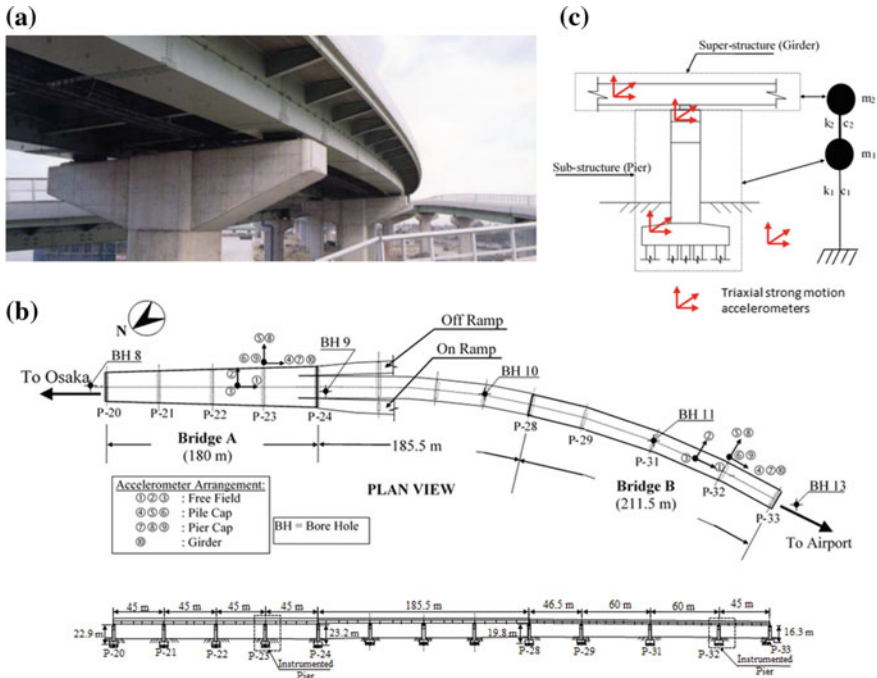


Fig. 17.1 **a** Matsunohama viaduct, **b** General dimension of viaduct and layout and strong motion Instrumentation system for Matsunohama Viaduct and **c** Pier-girder detailed 2-D model and location of sensors

accelerations recorded in the longitudinal direction during the main shock and four aftershocks of the January 17, 1995, Kobe earthquake are listed in Table 17.1.

A procedure for system identification of the bridge is described in detailed by Chaudhary et al. [2]. Since the main objective is on the performance of seismic-isolation system, the analysis was focused on the bridge longitudinal direction where the dominant motions were observed. A two-step system identification method was developed to identify structural parameters from strong-motion records. The first step identifies complex modal parameters of a non-classically damped base-isolated bridge-pier-pile-foundation system. The second step identifies the structural parameters that correspond to the identified modal parameters. The study showed that it is possible to capture the overall behavior of the bridges with simple equivalent linear, 2-DOF lumped mass models [2]. Flowchart of the system identification system is shown in Fig. 17.2.

Figure 17.3 shows the comparison of the measured and identified structural model's Fourier amplitude spectra and acceleration time histories during the main shock for Bridge A. The frequency and damping ratio were identified with an average variation of 0.2 and 2.9%, respectively. The figure demonstrates that the seismic isolation system performed satisfactorily because it effectively decoupled the super-

Table 17.1 Maximum observed accelerations at Matsunohama Viaduct in 1995 Kobe earthquake (m/s^2)

Earthquake 1995 Kobe	Free-field	Bridge A Pile cap	Pier cap	Girder	Free-field	Bridge B Pile cap	Pier cap	Girder
Mainshock	1.49	1.12	2.26	2.24	1.36	0.91	2.01	1.72
Aftershock 1	0.20	0.13	0.22	0.22	0.20	0.14	0.16	0.11
Aftershock 2	0.13	0.09	0.40	0.15	0.18	0.11	0.28	0.10
Aftershock 3	0.05	0.03	0.09	0.09	0.04	0.03	0.03	0.05
Aftershock 4	0.20	0.16	0.27	0.28	0.13	0.17	0.17	0.21

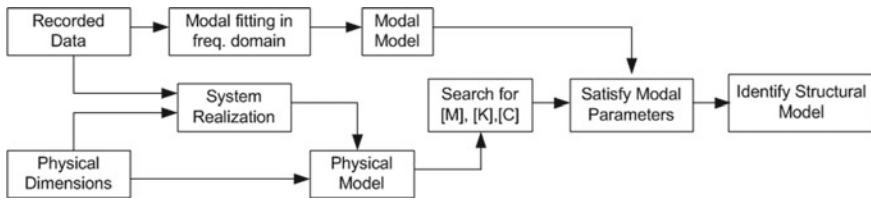


Fig. 17.2 Flowchart of two-step system identification method used in analysis

structure from the substructure, such that spectra of the girder contains only the dominant superstructure frequency and filters out other frequencies.

Identified modal frequencies and damping ratios show dependency on the amplitude of ground accelerations as shown in Fig. 17.4 for the 1995 Kobe main shock and four aftershocks. The following trends are observed from the figure:

- Natural frequencies decrease with increasing earthquake intensity for both bridges. Decrease in the first modal frequency is due to decrease in bearing stiffness with increasing amplitude, and reduction in the second modal frequency is due to reduction in stiffness of the substructure. The second modal frequency is quite high for Bridge B due to stiffer piers.
- Damping ratio of the first mode, which is associated with the isolator, is larger in Bridge B compared to Bridge A. This difference is due to the properties of the isolation system employed in both bridges. Bridge B, being isolated with LRBs, naturally exhibited more damping than the NRBs used in Bridge A.
- Damping ratio shows an increase with increasing earthquake excitation for both modes in Bridge A and the first mode in Bridge B, whereas the damping ratio decreases in the second mode of Bridge B with increasing earthquake excitation. This decrease may be due to increased energy dissipation in the first mode, which is associated with LRBs.

Performance of the isolation bearings was evaluated further by comparing the identified structural parameters namely stiffness and damping coefficient of the bearings with the equivalent linearized experimental values, as shown in Fig. 17.5. The identified bearing stiffness was found larger than the experimental values, especially during the low-level excitation of aftershocks. This discrepancy is attributed to the contribution of friction in metal bearings. Comparison of the identified and experimentally determined damping coefficient for Bridge B is shown in Fig. 17.5c. The two values of damping coefficient are nearly the same during the main shock. Whereas during the aftershocks, the damping coefficient in LRBs is zero during the experiment because no hysteresis loop formed at this low level of excitation and all the contribution comes from friction damping in the pivot roller bearings. Note that damping of Bridge A is not studied because the NRB in this case is not designed to dissipate energy but to distribute horizontal inertia force.

17.2.2 Yamaage Bridge

Yamaage bridge is a 6-span continuous prestressed concrete twin cell box girder with the bridge length of 244.8 m located on the National Highway Route No. 294 of Karasuyama Tochigi prefecture. Completed in May 1993, the bridge is the first one in Japan that utilizes high damping rubber (HDR) bearings as isolation system. The HDR is a special type of rubber interspersed by thin steel plates to achieve desired flexibility and damping characteristics. Two bearings are used at each sub-structure. To prevent excessive movement in the transverse direction, one pin-type transverse

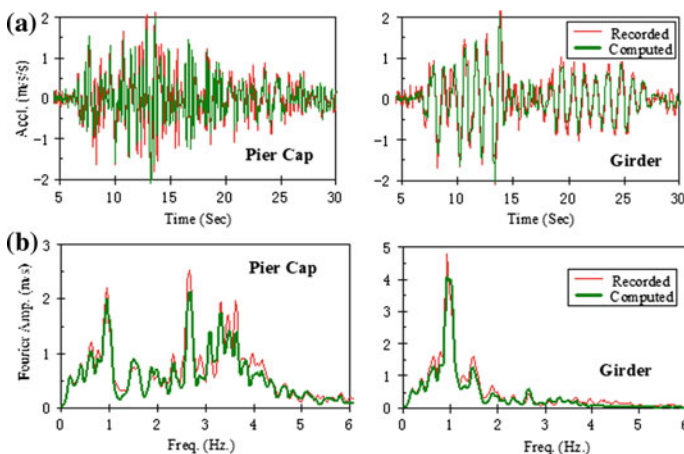


Fig. 17.3 Recorded accelerations of Matsunohama Viaducts during 1995 Kobe earthquake main-shock and the computed responses from 2DOF two-step system identification

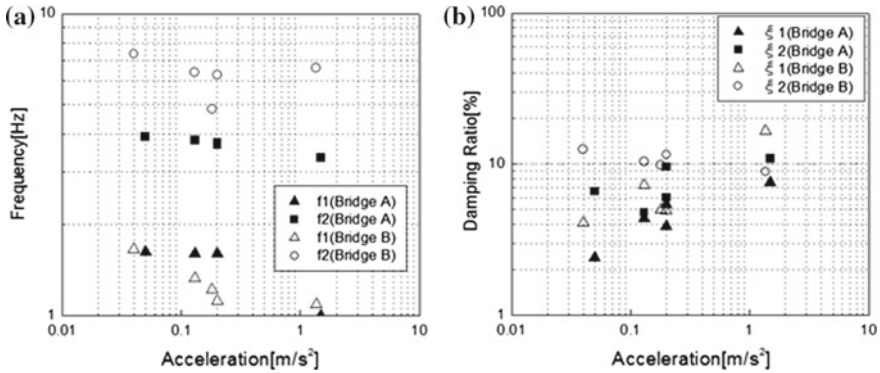


Fig. 17.4 Variation of modal parameters with earthquake intensity: **a** frequency; **b** damping ratio

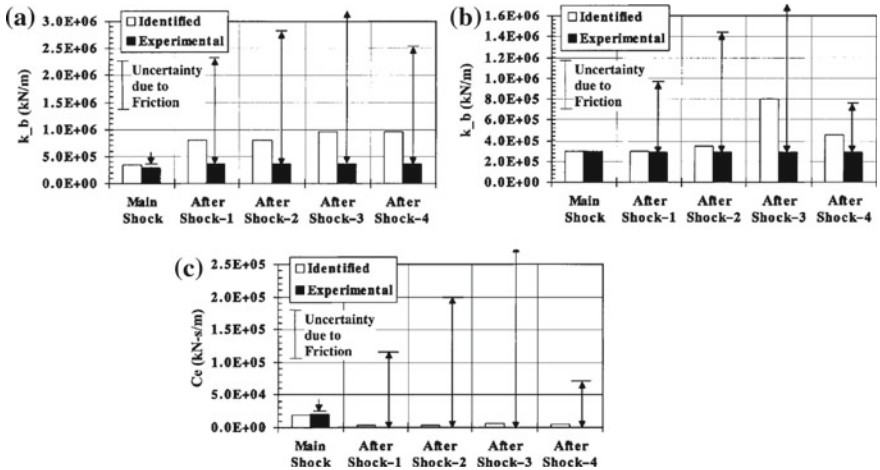


Fig. 17.5 Comparison of identified and experimental bearing stiffness: **a** Bridge A; **b** Bridge B and **c** identified and experimental bearing damping for Bridge B

side stopper with a clearance of ± 10 mm is placed between the two seismic isolation bearings at each sub-structure.

In order to verify the practicality of the seismic isolation design in parallel to the research and development, the Ministry of Land, Infrastructure, Transport and Tourism (formerly Ministry of Construction) of Japan, conducted pilot construction program of the five seismically-isolated (menshin) bridges, where Yamaage bridge is one of them. Within this framework and objective, the bridge is instrumented with triaxial strong motion accelerometers measuring along bridge's longitudinal axis, transverse axis and vertical; and placed on three locations, namely, free field, pier cap and girder (Fig. 17.6).

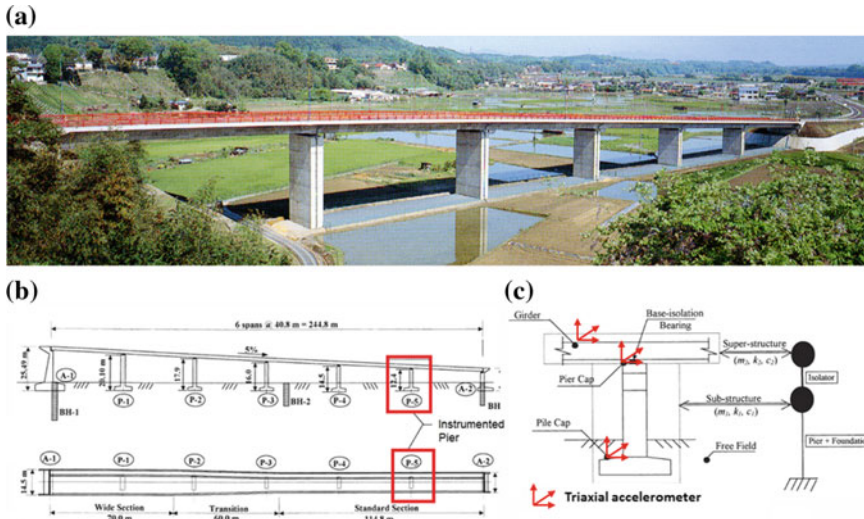


Fig. 17.6 a Photo of Yamaage Bridge, b general layout and c strong motion instrumentation

Table 17.2 Maximum observed acceleration at Yamaage Bridge (m/s^2); and identified frequency and damping

Earthquake Date	Free-field	Pier cap	Girder	f_1 (Hz)	f_2 (Hz)	ξ_1 (%)	ξ_2 (%)
EQ1 1994-10-04	0.089	0.365	0.115	1.47	9.76	3.49	5.22
EQ2 1996-02-17	0.291	0.682	0.322	1.50	9.57	4.34	8.27
EQ3 1997-02-20	0.100	0.355	0.075	1.70	9.92	3.33	7.35
EQ4 1997-05-12	0.122	0.268	0.130	1.50	9.81	3.70	7.28

Similar to the monitoring system in Matsunohama bridge, the strong motion accelerometers were connected by wired network system with frequency bandwidth of 0.05–35 Hz and operate at sampling frequency 100 Hz. Monitoring system operates under an event-based recording system where sensors start the recording when a ground motion exceeds a preset trigger level. All data is stored temporarily by a local storage system and then collected by staff of bridge operator for analysis.

Table 17.2 presents the maximum acceleration recorded at these locations, in the longitudinal direction, during four earthquakes. Records in the longitudinal direction are selected as the bridge is isolated in this direction. The transfer functions of the accelerations (Fig. 17.7) reveal that most of the spectral energy is clustered around two distinct frequencies (about 1.5 and 10 Hz).

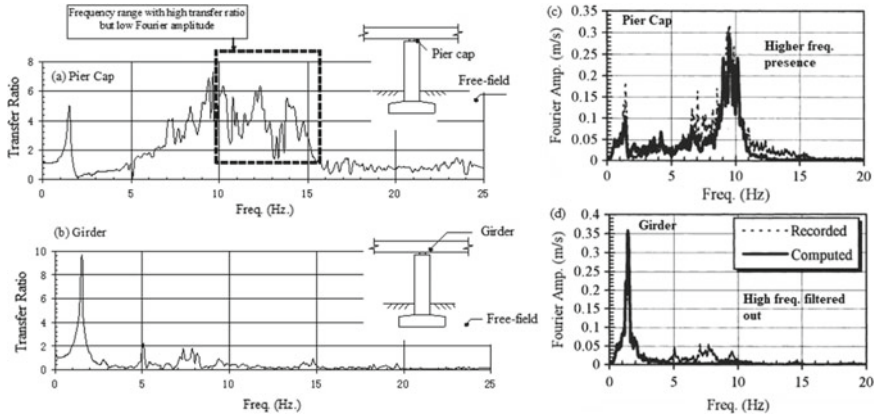


Fig. 17.7 Recorded transfer function with respect to free field (Earthquake 1 in Table 17.2). **a** Pier cap, **b** Girder. Comparison of frequency contents in **c** pier cap and **d** girder records

Modal parameters were identified via a two-step system identification explained by the flowchart in Fig. 17.2, with free field motion as the input and responses at pier cap and girder as the outputs [3, 4]. The structure was modeled as two degree-of-freedom non-classically damped system; and the resulted modal parameters, structural parameter and responses show satisfactory match with the recorded values of the parameters (Fig. 17.7). Note that spectrum of girder contains only the dominant super-structure’s frequency while other frequencies of the pier cap record have been essentially filtered out. This indicates that the seismic isolation system performed satisfactorily as it lengthened the natural period of the superstructure and effectively decoupled the super-structure from the sub-structure.

The bearing stiffness and damping coefficient of HDR were identified from system identification and the results are shown in Fig. 17.8. The identified bearing stiffness and damping coefficient are found to be larger than the experimental values during all earthquakes, which is due to the contribution of friction in the transverse side-stoppers used at each sub-structure. In fact, friction in the side-stopper contributed significantly to the stiffness and damping of super-structure. Another reason for the discrepancies is the substantial different behavior of the HDR bearings at small strains observed during the strongest earthquake (0.5–1.5%) and the weakest earthquake (0.07–0.2%) for different bearings. The bearings were tested at a strain of more than 50% and their equivalent stiffness for the recorded strain levels is computed by curve fitting an analytical expression to the recorded experimental load–displacement curves. HDR bearings are known to possess a highly non-linear behavior at low strain levels (<2%) and the analytical expressions based on the results of testing at high strain levels might not have been able to capture their true behavior at low strains.

Performance of instrumented seismic-isolated bridges, supported by LRB, HDR and NRB, during actual earthquake is investigated in this section. Major conclusions are as follows:

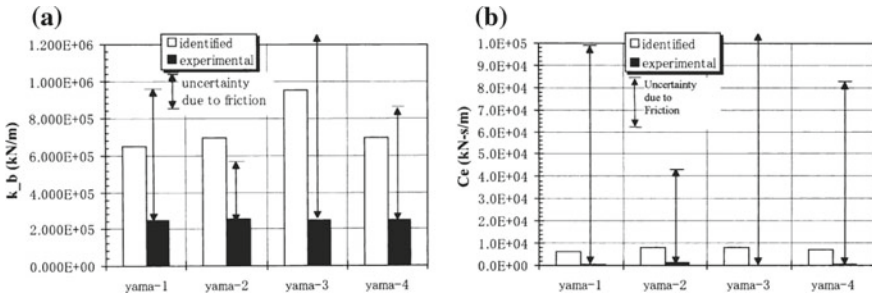


Fig. 17.8 Comparison of experimental and identified HDR bearing parameters **a** Stiffness, **b** Damping coefficient

- The isolated girders are found to behave rigid body in longitudinal direction and flexible beam for transverse direction, which indicates the seismic isolation effect to isolate girder and pier is present in all bridges.
- The performance of isolation bearings identified from actual earthquake agree reasonably with predicted performance based on loading test conducted prior to installation within the possible range of modeling uncertainties, i.e., the effect of friction.
- Friction force introduced by minor structural elements can affect the dynamic behavior of superstructure and increase the modeling uncertainty considerably, which may degrade the seismic isolation effects. This effect is found particularly prominent for smaller earthquakes. Although contribution of these minor details is usually neglected in current design and analysis, careful treatment is essential to achieve the design performance.

17.3 Seismic Monitoring of Seismically-Isolated Long-Span Bridges

Long-span bridges are more flexible than the short and medium span bridges. In design of long-span bridge, seismic load is usually considered to be lower compared to the wind load. However, inertia load caused by superstructure can be significantly large due to heavy weight of long span girder. Therefore, reductions of seismic load by further lengthening the natural periods are commonly explored. This can be achieved by isolating girder from tower using specially-designed tower-girder connection system. However, it should be noted while isolation minimizes the seismic load, unexpected excessive displacement due to flexibility could be resulted. Therefore, treatment of excessive motion should be well considered for long-span isolated bridge.

Strategies for lengthening natural period of long-span bridge using tower-girder connection can be found in some long-span cable-stayed bridges in Japan. Meiko

Triton cable-stayed bridge in Nagoya, for example, utilizes elastic cable connecting the main tower and girder in longitudinal direction to elongate the natural period to about 2–3 s. Tsurumi-Tsubasa cable-stayed bridge in Yokohama adopts an elastic restriction cables system between tower and girder, and vane type oil damper to control the motion [19]. Another example is Higashi-Kobe cable-stayed bridge where concept of all-free movable supports in the longitudinal direction at all bearing supports at towers and piers was adopted to lengthen the natural period. To improve the safety and increase damping, a vane type oil damper was installed at the girder end [30].

During the 1995 Kobe earthquake, the Higashi-Kobe bridge suffered damage such as failure of the link shoes or wind shoes, damage to the expansion joints, and compression buckling of the steel bridge pier at the girder end. Seismic monitoring on the bridge successfully recorded the bridge responses during the earthquake and analysis of the seismic records was conducted to explain the bridge response and cause of the damage [5]. Seismic monitoring systems are also employed at other long-span bridges such as Yokohama-Bay bridge, Tsurumi-Tsubasa Bridge, Rainbow Bridge [24, 25], to name a few. In the following section, case study of long-term seismic monitoring of Yokohama-Bay bridge, a seismically-isolated long-span cable-stayed bridge is described in detail.

17.3.1 Seismic Monitoring of Yokohama-Bay Cable-Stayed Bridge

Yokohama-Bay Bridge located at the entrance of Yokohama harbor is a part of the Yokohama-Tokyo bay-shore expressway (Fig. 17.9). It is a continuous three-span cable-stayed bridge with the main girder consisting of a double-deck steel truss-box. The central span is 460 m with side spans of 200 m each. The upper and lower deck have 6 and 2 lanes, respectively, with the upper deck being part of the Yokohama Expressway Bay shore route and the lower deck a part of the national route. The lower deck was added later and completed before 2004 Chuetsu-Niigata earthquake. The bridge has two H-shaped towers of 172 m height and 29.25 m width with a welded monolithic section. Construction was completed in 1988 and the bridge was opened in September 1989 [16].

Considering seismicity of the area, possible recurrence of a large earthquake such as the 1923 Great Kanto Earthquake, the weak ground condition, and the high center of gravity of the bridge; special seismic isolation design system Link-Bearing Connections (LBC) was adopted (Fig. 17.9). The system consists of 10-m-long end-links at the end-piers (P1 and P4) and 2-m-long tower-links at the towers (P2 and P3) and accommodates girder longitudinal motion. The LBC system maintains long fundamental period of mode in longitudinal (bridge axis) direction and allows the girder to be suspended from towers and piers. By lengthening the natural period, the structure experiences smaller acceleration thus minimizes the effect of inertia force

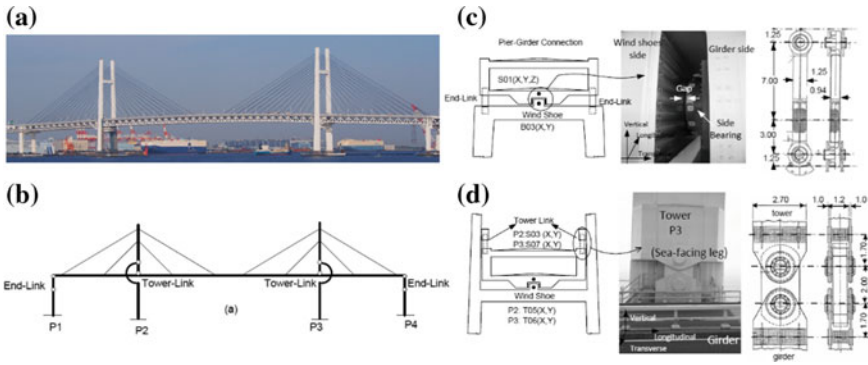


Fig. 17.9 **a** Yokohama-Bay Bridge, **b** characteristics of pier–girder and tower–girder link-bearing connections (LBC) and location of sensors on the connections, **c** detail figure of end-link, **d** detail figure of tower-link. Photos by D. M. Siringoringo

of superstructure on substructure during an earthquake. However, larger displacement is expected, hence, shorter LBCs at the tower was placed to restrict excessive longitudinal displacement during large earthquake.

The original design model describes LBCs as longitudinal hinge connections, and they are expected to function as such in any level of earthquake. This implies that relative displacement between pier and girder will have to be sufficiently large to ensure that high-frequency components of pier and tower’s seismic-induced vibration are not transferred to the girder. When such a condition is satisfied, inertia force from girder on the piers and towers is minimized, and the amount of moment force on the substructures can be significantly reduced. This will create an isolation effect commonly found in seismic-isolated bridges. The fundamental longitudinal mode that captures such link behavior is noted as the longitudinal slip mode. The finite-element model generates such a mode with period of 7.7 s.

In transverse direction, the girder is suspended over the piers and towers. Girder transverse movements are restricted by wind shoes located at the pier–girder and tower–girder connections. A small gap exists between wind shoes and girder to accommodate small relative motion. Part of girder connections that face wind shoes are covered by side bearings with Teflon polytetrafluoroethylene (PTFE) surface, whereas the surfaces of wind shoes are made of stainless steel. Both side bearings and wind shoes are designed to resist maximum transverse load of 27,654 and 48,346 kN for pier–girder and tower–girder connections, respectively [27].

17.3.1.1 Structural Monitoring System and Recorded Seismic Responses

Considering the bridge is located in a seismically high-risk area and its importance as a major transportation link, the Metropolitan Expressway installed a structural monitoring system and recorded seismic responses of the bridge regularly. Two types of accelerometers are used, namely, servo type accelerometers SA-355CT (triaxial) and SA-255CT (biaxial) produced by manufacturer Tokyo Sokushin. These accelerometers have the maximum amplitude capability 20 m/s^2 , sensitivity $2 \text{ m/s}^2/\text{V}$ and linearity 0.03% of the full-scale. All sensors have frequency bandwidth of $0.05\text{--}35 \text{ Hz}$ and operate at sampling frequency 100 Hz . The sensors are connected through a wired network system and responses are recorded every time accelerations exceed the preset trigger level. The monitoring system is operated and maintained by Tokyo Metropolitan Expressway Public Corporation. Strong motion data are stored in a local storage at first and then subsequently converted to binary data file for further analysis. The processing and analysis of the strong motion data are systematically conducted in a collaboration research project between Metropolitan Expressway and university. Results of analysis are discussed with the bridge operator, Metropolitan Expressway, as feedbacks and recommendation on bridge condition from monitoring system and whenever necessary action is needed.

Figure 17.10 shows the 85 channels of permanently deployed sensors measuring acceleration responses at 36 locations in three directions including piers, towers and girder. For end-piers and towers, accelerometers were installed on the pile cap, pier cap, and between tower and girder. Using the response from these sensors one can observe the behavior of link-bearings connecting the girder with the towers and with the end-piers.

The monitoring system was deployed after the bridge was opened and about 104 earthquakes have been recorded by the monitoring system from January 1990 until April 2011 [26]. About half of the earthquakes are of significant level (JMA intensity

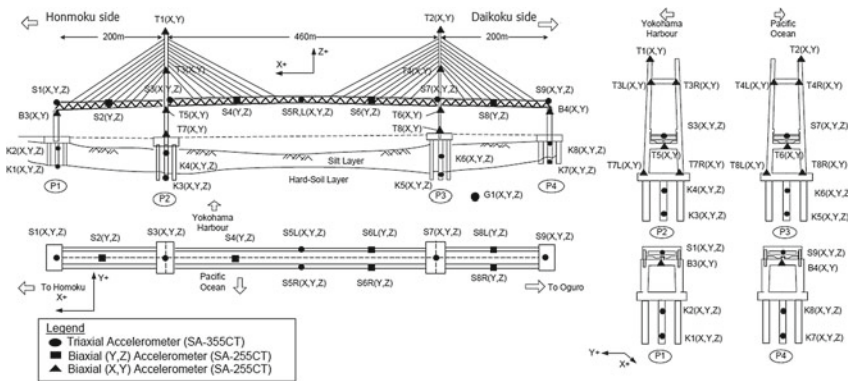


Fig. 17.10 Layout of seismic monitoring system on Yokohama-Bay Bridge

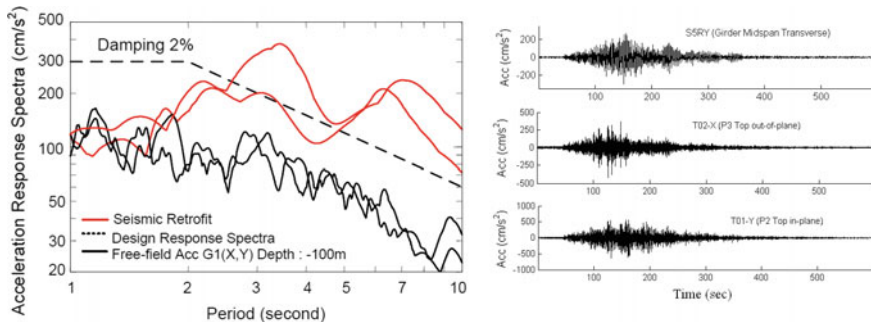


Fig. 17.11 Acceleration response spectra at the free-field and the largest accelerations at the girder and top of the tower due to the 2011 Great East-Japan Earthquake, the largest ground motion ever recorded on the Yokohama-Bay Bridge

> 3) or Peak Ground Acceleration (PGA) equal or more than equivalent to 0.08 m/s^2 . The largest ground motion ever recorded at the bridge is due to 2011 Great East Japan (Tohoku) earthquake. Figure 17.11 shows the response spectra of free-field ground motions, along with the original design response spectrum for the hard rock layer and two seismic retrofit ground motions in 2005. As shown in the figure, acceleration spectra of the 2011 Great East Japan earthquake main shock are smaller than both the original design and the retrofit.

Seismic records of the bridge have been studied extensively. The study of seismic records from long-term monitoring system was divided into three categories: (1) earthquakes before 2004, which is before addition of new traffic lane on the lower deck [24], (2) earthquakes due to 2004 Chuetsu-Niigata and after, the 2004 Chuetsu Niigata earthquake generated main-shock and series of aftershocks [25], and (3) earthquakes due to 2011 Great East-Japan earthquake and aftershocks [27].

Data analysis were conducted by employing multi-input multi-output (MIMO) system identification based on the System Realization using Information Matrix (SRIM) [9] algorithm that utilizes correlations between input-output data to estimate modal parameters of dynamical system through a realization process. To implement the identification, one needs to select a set of input-output data. In this study responses from triaxial accelerometers located at the bottom of the end-pier (P1: sensor K2) and the towers (P2: sensor K4 and P3: sensor K6) were selected as inputs. These responses were utilized instead of the free-field responses (G1) to minimize the effect of soil-structure interaction and to realize the multi-input multi-output system. As the outputs, 41 channels that include girder (23 channels), pier P1 (two channels), tower P2 (eight channels) and tower P3 (eight channels) were selected. Since the inputs and outputs data are derived from multiaxial accelerations, the identification yields in three-dimensional mode shapes. Detailed explanation on implementation of system identification is provided in Siringoringo et al. [27].

Frequency characteristics were obtained from spectra analysis and the results are confirmed by system identification. Mostly, the system identification and spectra

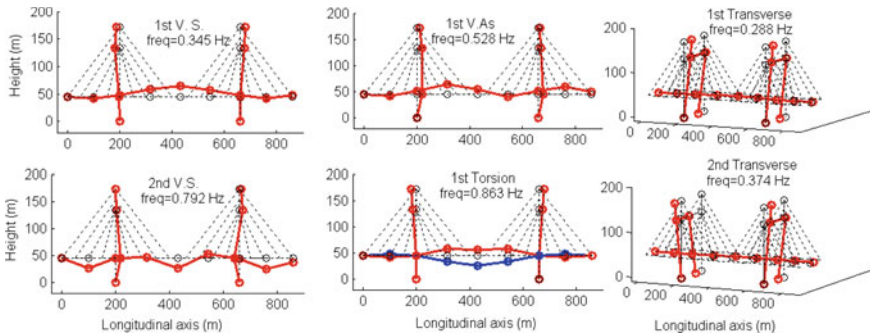


Fig. 17.12 Example of mode-shapes of Yokahama-Bay bridge identified from seismic response due to 2004 Chuetsu-Niigata earthquake

analysis were adequate to provide quick observation of bridge response for small and moderate earthquakes. Time-frequency analysis by wavelet transform was conducted for larger earthquake considering possible nonlinearity (Siringoringo et al. 2013). Dense sensor configuration allows identification of significant number of modes typically 14 modes between 0.1 and 2.5 Hz. In addition, dense sensor configuration also allows for modal identification with higher spatial mode-shapes, which is important for structural assessment using performance indicator associated with mode-shapes. Figure 17.12 illustrates some of typical mode-shapes identified from 2004 Chuetsu-Niigata earthquake.

Comparisons of the results from earthquakes before 2004, after 2004, and during 2011 Great East-Japan earthquake show that generally natural frequencies decrease with the increase of excitation amplitude [24, 25, 27]. The frequencies identified from earthquakes on 2004 and after, were lower compared to the corresponding results from earthquakes before 2004. These changes are significant and imply that the structural properties may have changed. Considering that the Chuetsu-Niigata earthquake occurred when the construction of additional deck has been completed, the decrease may indicate that the new deck contributes largely as added mass rather than added stiffness to the whole structure system [25]. For the earthquake series related to the 2011 Great East-Japan, it was observed that natural frequencies generally decrease with the increase of excitation amplitude. Damping ratio estimates show large variation within 0.5–6%. In some cases, such as earthquakes before 2004, the results indicate that damping ratios of lower modes increase with the increase of earthquake amplitude, which might be due to the results of greater energy dissipation caused by friction in bearings that occurs during large earthquake.

17.3.1.2 Observed Performance of Link-Bearing Connection

The actual performance of the LBC is studied by observing modal parameters of the first longitudinal mode identified from earthquake records. Due to nonlinear behavior

of LBC the motion associated with LBC is excited only by earthquakes and not measurable during ambient measurement. Investigation of the LBC is performed by observing the relative modal displacement between girder and both towers and end-piers using an index (φ) that denotes the normalized longitudinal modal displacement of girder, tower and pier at each of LBC location. In the case of slip mode, the value of index (φ) is nearly or larger than one whereas for the stick mode it is closer to zero.

Results for earthquakes from 1990 to 1997, the 2004 Chuetsu-Niigata and after show three typical first longitudinal modes. The first mode, identified at around 0.11–0.15 Hz, is a typical first mode with the hinge-hinge assumption of end-piers as predicted from the finite element model. The second and third modes were identified at higher frequencies between 0.18 and 0.24 Hz. The second mode exhibits a mixed mechanism in which by judging from the small relative modal displacement, one of the end-pier cap remains fixed or closely connected with the girder, while the other has developed the fully hinged mechanism. The third mode exhibits even smaller relative modal displacement between pier cap and girder. In this mode, both end-piers cap remained fixed or closely connected to the girder. In the case of records from 2011 Great East-Japan earthquakes and aftershocks, observation shows that the index is nearly equal to one suggesting the occurrence of slip mode.

Based on the results of seismic monitoring between 1990 and 2005, the possibility that LBC may not function properly during a large earthquake was recognized. In such a case, excessive moment at the bottom of end-pier could be ensued and the LBCs could fail causing girder to uplift. As a feedback of monitoring, the seismic retrofit of the bridge conducted in 2005 included a fail-safe design by connecting the girder to footing using prestressed cables to prevent uplift of the girder-end in case of LBC failure (Fig. 17.13c).

Another interesting finding from the records of 2011 Great East-Japan earthquake is the indication of tower-girder transverse pounding. The tower transverse acceleration records are characterized by many periodic spikes resembling impulses, espe-

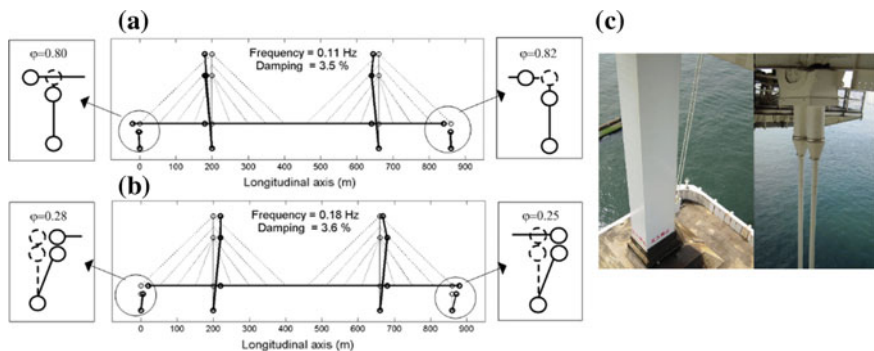


Fig. 17.13 Example of the first longitudinal mode with **a** slip-slip condition and **b** stick-stick condition [25]. **c** Photos of a fail-safe design system using pre-stressed cable

cially during the largest excitation. Visual inspection performed afterwards; indicate the occurrence of transverse pounding between girder and tower and the tower-girder connections. Despite its occurrence, transverse pounding did not cause structural damage during the earthquake. The pounding process is studied using simplified model of two-side contact problem between the nodes that correspond to tower and girder at wind shoes locations. In the model, the values of spring constant that represent the contact stiffness between pier or tower and the girder are determined by adjusting the value of modal parameters identified from seismic response with that of bridge model. The simplified structural model can reasonably simulate the pounding mechanism and its effect on the structure such as the maximum impact force experienced by tower and wind shoes Siringoringo et al. [29].

17.4 Seismic Monitoring of Seismically-Isolated Buildings

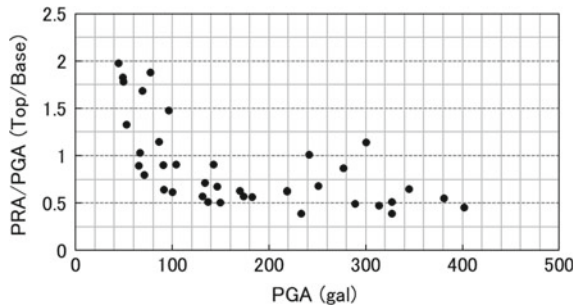
Currently, more than 80 buildings in major cities throughout Japan are instrumented with structural monitoring system, where one-third of them are located in Tokyo and its outskirts. For monitoring building responses, the sensors are installed on different story levels, typically including its top and base. During the 2011 Great East Japan (Tohoku) earthquake, many of the buildings using the technologies experienced the strongest shaking ever recorded. The Japan Society of Seismic Isolation (JSSI) made significant efforts to obtain the permissions from building owners and/or related engineers regarding the release of the privately-owned response records. Accordingly, including the records publicly available, the JSSI obtained and analyzed the records of 20 base-isolated buildings, 11 vibration-controlled buildings, along with 9 undamped buildings for comparison purposes [8, 10]. The JSSI also conducted survey of the damage and performance of 327 base-isolated buildings and 130 vibration-controlled buildings. More than 40% of the base-isolated buildings had scratch plates to show trajectories of building motion during the shaking.

In Miyagi prefecture where the seismic intensity scaled by the Japan Meteorological Agency (JMA) [7] was at the highest level of 7, the largest isolator displacement of 41.5 cm, and the average was about 20 cm. Near Tokyo (Kanto area), the intensity was at least 5- (referred to as '5 lower'), where the largest isolator displacement was 18 cm and the average about 5 cm.

During the 2016 Kumamoto earthquake the seismic intensity 7 was observed twice in succession within the 28-h period, and the largest isolator displacement of 46 cm was reported [20, 21]. It is also the largest in the history of base-isolation technology. The value was obtained from the scratch plate, and no sensors were installed in the base-isolated buildings. The responses recorded during the 2011 Tohoku earthquake, therefore, are significant, and they will be discussed in the subsequent sections.

Table 17.3 summarizes the recorded responses of twenty different base-isolated buildings mentioned above [8, 9]. The most northern buildings are located in Miyagi prefecture and the most southern in Kanagawa prefecture. The buildings range in height from 2 stories to 21 stories, and about 60% of the buildings use natural

Fig. 17.14 Acceleration magnification ratio (PRA/PGA) versus PGA for the twenty base-isolated buildings in both x- and y-directions (see Table 17.3)



rubber bearings with dampers, which is consistent with the nationwide trend in Japan. Note also that about 40% of the buildings use high damping rubber bearing or lead rubber bearing, without utilizing externally attached dampers. Because of the wide geographical area, the peak ground acceleration (PGA) varies from 44.5 to 402 cm/s^2 , and building top accelerations range from 57 to 344 cm/s^2 . The maximum displacement at the isolation level, typically calculated from the accelerations and their double integrations, ranged from 2.9 to 18.0 cm.

Figure 17.14 shows the peak roof acceleration (PRA) recorded at building top normalized to the PGA, hereby referred to as the acceleration magnification ratio (PRA/PGA). It is calculated for each horizontal direction and is plotted against the PGA. Remarkably, PRA/PGA and PGA are strongly correlated, and PRA/PGA becomes smaller for the larger PGA. The hysteretic characteristic of the isolation system is typically a softening type, in which larger excitation results in more deformation, less equivalent stiffness and more energy dissipation, leading to a high damping system. In such a case, better control of accelerations occurs, reducing the value of PRA/PGA. The specific values are given in Table 17.3, where they appear to have less dependency on building height.

Note that creating the base-isolation system means adding one floor to the building and its effect on the cost is small for buildings having many floors. By this reason, there are many tall base-isolated buildings in Japan, and the following section discusses the 20-story base-isolated building (Table 17.3) as an example of tall base-isolated buildings.

17.4.1 Responses of 20-Story Base-Isolated Building

Figure 17.15 shows the elevations of the 20-story base-isolated building in the campus of Tokyo Institute of Technology. The foundation and 1st floor of this building are RC structure. The other stories are of hybrid structure having steel beams and concrete-filled-tube (CFT) columns. The so-called Mega-Braces (Υ -500 \times 160 \times 19–32 mm) are installed on the both sides of building because the horizontal stiffness of the superstructure is needed for maintaining the seismic isolation effects.

Table 17.3 Twenty base-isolated buildings and their responses during the 2011 Tohoku Earthquake

Stories	Prefecture	Isolator	Damper	PGA _X (cm/s ²)	PGA _Y (cm/s ²)	PRA _X (cm/s ²)	PRA _Y (cm/s ²)	PRA _X /PGA _X	PRA _Y /PGA _Y	U _{iso} (cm)
2	Tokyo	Natural rubber	Oil damper Steel damper	109	143	124	125	1.14	0.87	4
3	Miyagi	High damping rubber	-	301	241	344	244	1.14	1.01	11.5
3	Chiba	Natural rubber	Viscous damper	150	134	75	96	0.50	0.71	7.8
4	Kanagawa	Synthetic rubber sliders	-	97	77	143	145	1.48	1.88	4.2
5	Miyagi	High damping rubber	-	327	345	167	224	0.51	0.65	11.2
5	Chiba	High damping rubber Lead rubber	-	143	170	130	107	0.91	0.63	2.9
6	Miyagi	High damping rubber	-	381	277	209	240	0.55	0.87	18.0
6	Tokyo	Lead rubber	-	137	132	70	75	0.51	0.57	7.6

(continued)

Table 17.3 (continued)

Stories	Prefecture	Isolator	Damper	PGA _X (cm/s ²)	PGA _Y (cm/s ²)	PRA _X (cm/s ²)	PRA _Y (cm/s ²)	PRA _X /PGA _X	PRA _Y /PGA _Y	U _{iso} (cm)
7	Ibaraki	Natural rubber Lead rubber	-	327	233	126	91	0.39	0.39	5.9
7	Kanagawa	High damping rubber	Oil damper	147	87	99	100	0.67	1.15	6.8
7	Kanagawa	Natural rubber	Passive oil damper	66	71	68	57	1.03	0.80	12.0
8	Chiba	High damping rubber	-	174	219	99	137	0.57	0.63	4.7
9	Miyagi	Natural rubber	Lead damper Steel damper	251	289	170	142	0.68	0.149	16.8
10	Tokyo	Natural rubber	Viscous wall	219	183	137	104	0.62	0.57	3.0
11	Tokyo	Natural rubber Lead rubber	Oil damper	91	104	82	94	0.90	0.90	5.1

(continued)

Table 17.3 (continued)

Stories	Prefecture	Isolator	Damper	PGA _X (cm/s ²)	PGA _Y (cm/s ²)	PRA _X (cm/s ²)	PRA _Y (cm/s ²)	PRA _X /PGA _X	PRA _Y /PGA _Y	U _{ISO} (cm)
12	Tokyo	Natural rubber Lead rubber	Oil damper Rotational friction damper	100	91	62	59	0.62	0.64	6.5
13	Tokyo	Natural rubber sliders	Semi-active Oil damper Passive oil damper	65	53	59	70	0.90	1.32	12.1
14	Kanagawa	Natural rubber Sliders	Oil Damper	49	45	90	88	1.83	1.98	9.5
20	Kanagawa	Natural rubber	Oil damper Steel damper	49	69	88	116	1.78	1.68	9.1
21	Ibaraki	Natural rubber	Lead damper Steel damper	314	402	149	181	0.47	0.45	14.0

Notes The stories indicates the number of stories above ground level, and not necessarily the story above the isolator. In some cases, isolator is a few stories above of below ground level

PGA Peak Ground Acc, PRA Peak Roof Acc, U_{ISO} Peak vector isolator displacement

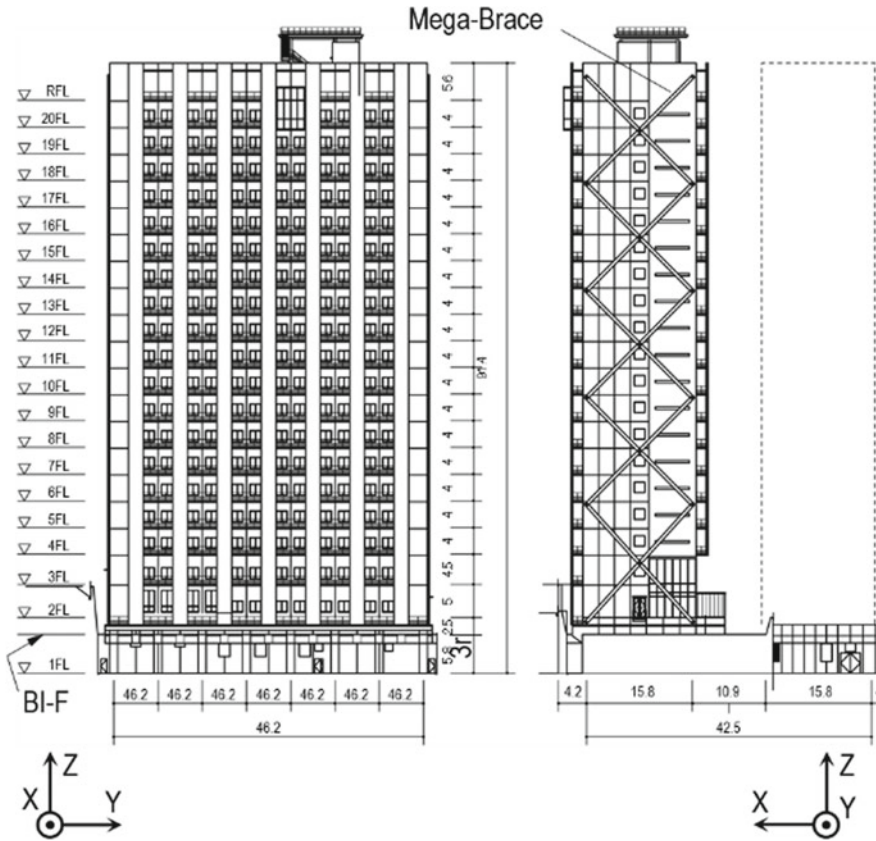


Fig. 17.15 20-story building in the campus of Tokyo Institute of Technology isolated at mezzanine level

At the mezzanine level, four 1200 mm diameter rubber bearings with uplifting capability (Fig. 17.16a) are used at the corners of the floor. Twelve sets of 1100 mm diameter rubber bearing and steel damper (Fig. 17.16b) are used along the Y-direction perimeters. Two steel dampers (Fig. 17.16c) and two oil dampers (Fig. 17.16d) are used along the X-direction perimeters.

As shown in Fig. 17.17, the building has 45 sensors including accelerometers, displacement transducers, and strain gages. Total of 27 accelerometers are located on the 1st, mezzanine (base-isolation), 2nd, 7th, 14th, and 20th floors, respectively. Their floor locations and directions are shown in Fig. 17.17a. In order to measure the story drift of the isolated floor directly (Fig. 17.17b), the displacement sensors for long (Fig. 17.18a) and short (Fig. 17.18b) stroke are installed.

As shown also in Fig. 17.18a, the trace recorder is fixed to the bottom of the superstructure and stainless steel board is fixed to the top of the substructure. Strain gages are installed to measure axial forces in the total of four cross sections of the

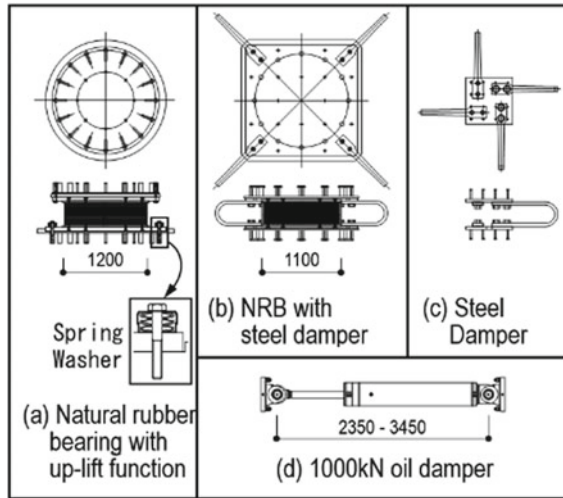


Fig. 17.16 Isolators and dampers used at mezzanine level of 20-story building: (a) Four units of 1200 mm diameter natural rubber bearing with uplifting capability, (b) Twelve units of 1100 mm diameter of natural rubber bearing with steel damper, (c) two units of steel dampers and (d) two units of 1000 kN oil dampers

columns and the Mega-Braces (Fig. 17.17a). The force and deformation of one oil damper is measured by using strain gages and displacement transducers, respectively (Fig. 17.18d). Possible up-lift responses noted earlier for the corner bearings (Fig. 17.17b) are measured also by the displacement sensors of short stroke (Fig. 17.18c).

Output voltage of accelerometers, displacement transducers and strain gages are A/D converted by the data loggers installed at each instrumented floor, transmitted to data servers through a LAN, and recorded continuously. The clock on data server is set using a GPS signal data on each data logger via the LAN. It is a continuous system in operation at sampling rate of 100 Hz. The data is also written on a separate file, when the acceleration exceeds 0.01g. The accelerometer is of servo-type made by Tokimec (product: TA-25E-05-10), and has recordable range of $\pm 4g$, tolerance of $10^{-6}g$, and frequency range up to 200 Hz (± 3 dB).

Including the sensors mentioned above, the university currently maintains 162 sensors in different buildings and grounds of the campus, and monitors both earthquake and wind responses. The recorded data is publicly available.

The accelerometers in the building recorded the responses during the 2011 Tohoku earthquake, where the PGAs were 51.4 and 67.1 cm/s^2 , in the X- and Y-directions, respectively. The responses of the base-isolation system and the building are discussed below [17, 18]:

Figure 17.19 shows hysteretic response of the isolation level computed using the acceleration data and the calculated inertial mass of the structure. The absolute accelerations of each floor were calculated by the acceleration records of the 2nd,

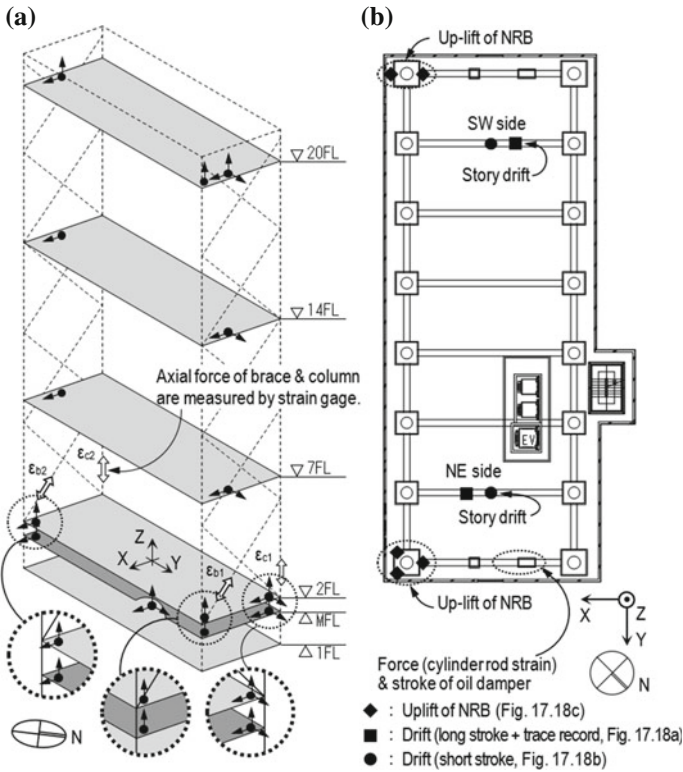


Fig. 17.17 Sensors installed into the building: **a** Accelerometers and strain gages, **b** Details of isolated floor

7th, 14th, and 20th floors and linear interpolation. The relative displacements above and below the isolation plane were obtained by the displacement transducers. Double integration of the accelerations at the same locations appears to give almost the same results.

The hysteresis curves clearly show the linear and bilinear nature of the response caused by the steel damper. The envelope curves are in excellent agreement with the design curves, therefore the steel damper has functioned as expected. Although the linear stiffness before large deformation is the same as design curve of steel damper (Fig. 17.19a and e), its declines slightly (Fig. 17.19d and h) after the large deformation.

Figure 17.20a shows the relative displacement above and below the isolators, and Fig. 17.20b and c show the results of the autoregressive with exogenous inputs (ARX) method [6] using the accelerations of the ground and 20th floor. The function ARX contained in the “system identification tool box” of MATLAB is used by using $n_a = 20$, $n_b = 5$, and $n_k = 1$, respectively, where n_a and n_b are the orders of the ARX model, and n_k is the delay. Note that, before processing, the time history records

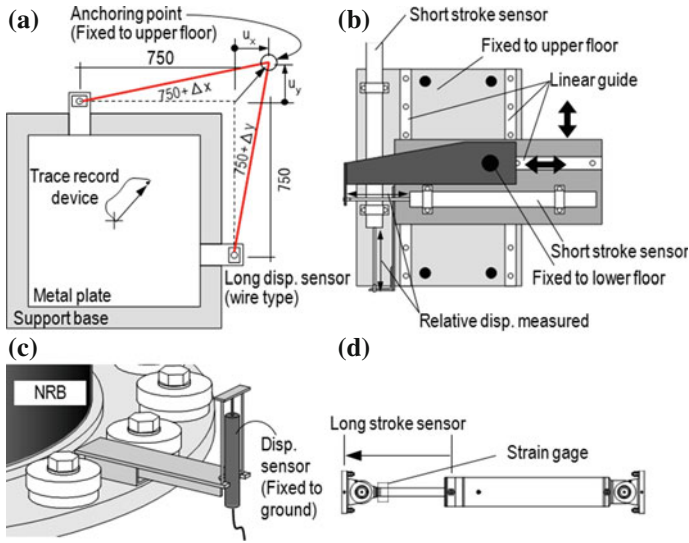


Fig. 17.18 Details of measurement system: **a** Story drift measured by long stroke sensor and trace recorder, **b** Story drift measurement by small stroke sensor, **c** Uplift measurement for natural rubber bearing (NRB), **d** Stroke and force measurement for oil damper

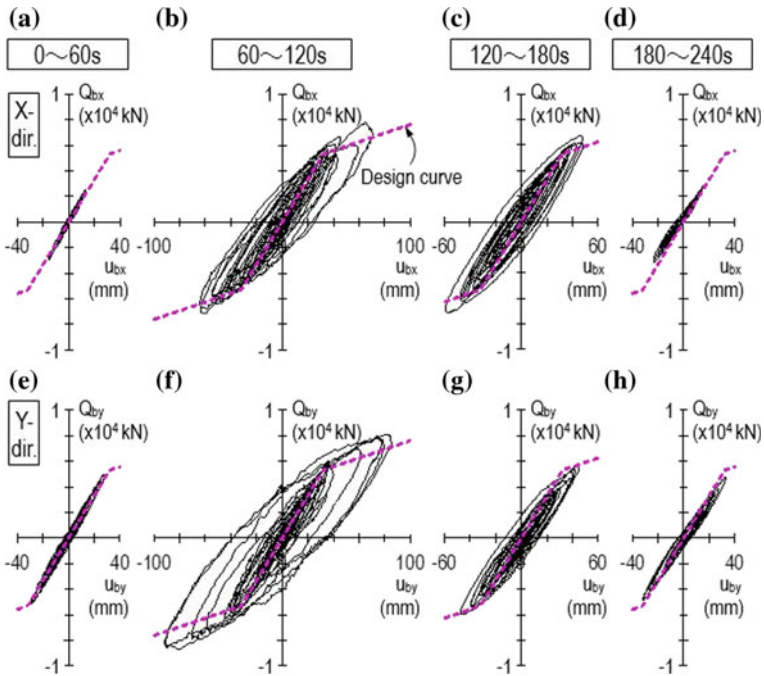


Fig. 17.19 Story shear force versus story drift at the mezzanine (isolation) level

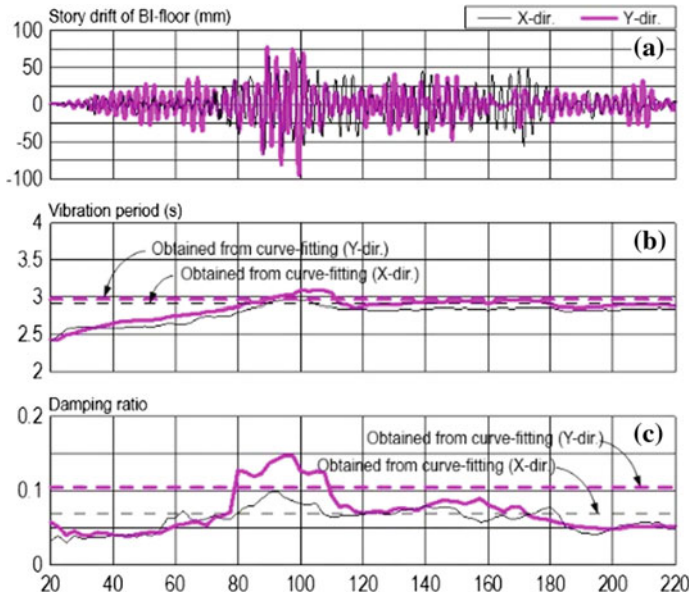


Fig. 17.20 Histories of displacements, vibration periods, and damping ratios

were modified by filtering out the frequency contents outside the range of 0.1 Hz and 3 Hz.

As shown by Fig. 17.20a, the maximum displacement excursions between 80 and 110 s, the first mode vibration periods of the whole isolated building reach the peaks of about 3.0 and 3.1 s, and the damping ratios about 0.10 and 0.15 in the X- and Y-directions, respectively. These changes of the dynamic properties are due to the bilinear characteristics of the isolation system. Figure 17.20a also show that the peak damping ratios are about 1.4 times those obtained from the basic system identification method to fit the linear transfer function to the spectral ratio between the floor accelerations and base accelerations during the entire duration of the shaking.

Using the first to the third modal properties obtained from the basic system identification method and the monitored base accelerations as the input, time-history responses were obtained by superposing the modal responses. The results agreed well with the monitored responses, except for the localized errors in simulating the phase difference between the damped isolation system and most stories [17, 18]. Combining this with separate analytical studies varying building height [11], the modal properties obtained by this practical approach may be considered accurate enough, unless the deformation of the isolation system is very large, producing highly non-proportional damping.

The approach therefore is used to evaluate the vibration periods and damping ratios for the smaller shaking that lead to increased stiffness and thus less deformation of the isolators relative to those of the superstructure. Figure 17.21 summarize the vibration

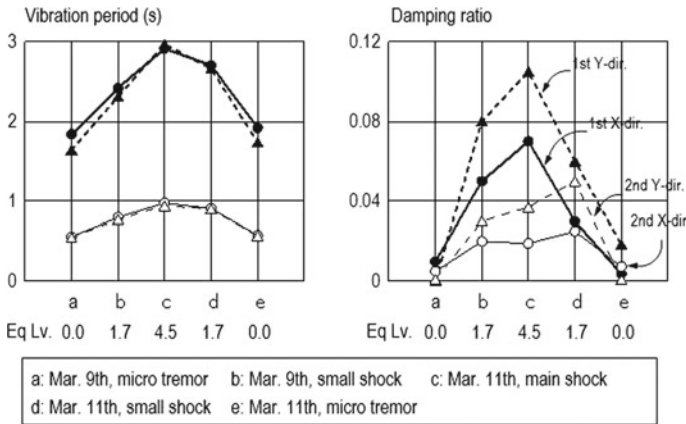


Fig. 17.21 Vibration periods and damping ratios at five different shakings

periods and damping ratios for the following five different shakings: (a) microtremor on March 9, (b) small shock on March 9, (c) the main shock on March 11 (the Tohoku earthquake), (d) aftershock on March 11, and (e) microtremor on March 11. Clearly, the isolation system becomes more effective by producing longer vibration period and larger damping at the larger earthquake (Fig. 17.21). The vibration periods and damping ratios at the shaking (c) is about 1.7 times and 7–10 times those at (a), respectively.

Figure 17.22 contrasts envelopes of the story deformations and accelerations between shakings (b) and (c) mentioned above. The PGA of the shaking (b) is about 0.02 times the PGA of the shaking (c), where deformation mode of the former shows less deformation of the isolation system relative to the superstructure, since the steel dampers remain elastic and maintains high stiffness. This results in almost no energy dissipation by the dampers and consequently more than twice acceleration magnification ratio (PRA/PGA) compared with the shaking (c), which is inconformity with the trend observed earlier from Fig. 17.14.

Another notable work on the seismic response of isolated building during the 2011 Great East Japan (Tohoku) earthquake is the analysis of responses of an asymmetric base-isolated building, where effect of isolation on servicability performance is critical [28].

17.5 Seismic Retrofit of National Museum of Western Art Tokyo Using Base-Isolation System

Seismic isolation is applied not only to new structure but also for retrofit of existing structure. Application of base-isolation to seismic retrofit of National Museum of Western Art (NMWA) in Tokyo is an excellent example of such concept. The building

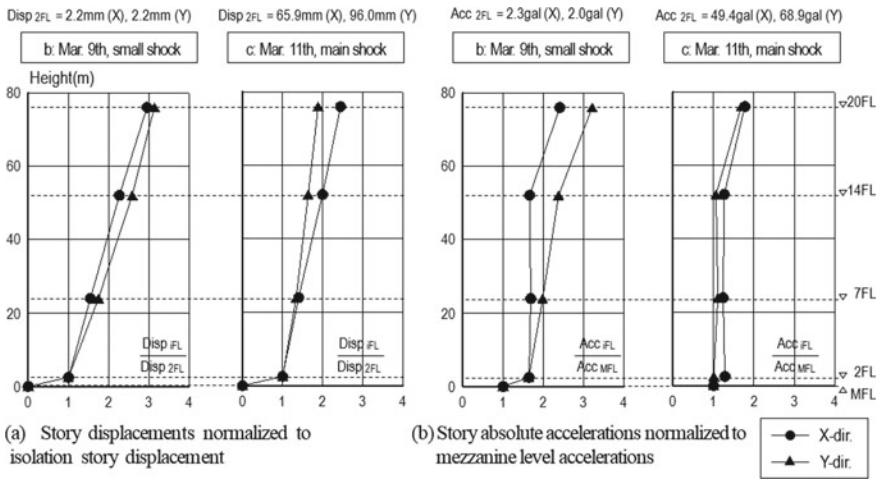


Fig. 17.22 Envelopes of story displacements and accelerations

was originally constructed in 1959 and upgraded in 1998 with a seismic isolation system composed of 49 high-damping rubber bearings (HDRs) (Fig. 17.23). The main building is one of the renowned works of the French architect, Le Corbusier and constructed by Shimizu Corporation under supervision of Junzo Sakakura, Kunio Maekawa and Takamasa Yoshizaka as the former ministry of education of Japan. It is designated as the UNESCO world heritage in 2016. The building is made of reinforced concrete, has three floors above ground, one floor below ground and one penthouse space with gross floor space is 4399 m².

The upgrade of the NMWA was the first retrofit project in Japan to use seismic isolation. Design analyses for the upgrade utilized the hysteresis model for the HDRs developed by Kikuchi and Aiken [14]. The isolation system is composed of 49 KL401-type HDRs manufactured by Bridgestone Corporation, Japan. There are two

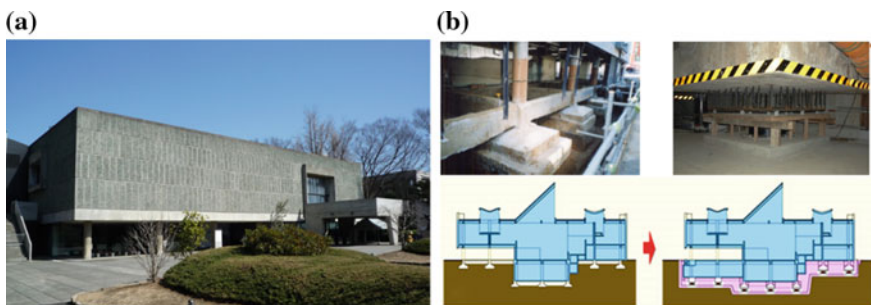


Fig. 17.23 a View of NMWA main building, b Seismic isolation building upgrade. Photos courtesy of Mr. Kazuyuki Morihiro, and illustration provided by Shimizu Corporation

different sizes of HDRs used in the building; 47 are 600 mm in diameter with a total rubber thickness of 200 mm, while the other 2 are 650 mm in diameter and 198 mm thick. Design criteria of isolation system are summarized in Table 17.4.

The advisory committee for the retrofit project recommended to monitor seismic behavior of the building to verify effectiveness of the seismic isolation system. In response to the recommendations, the Building Research Institute of Japan (BRI) set up a strong motion instrument in 1999 [1, 12].

The instrument consists of six triaxial sensors deployed were in and around the building (Fig. 17.24) and a digital recording system. Two sensors (BFW and BFE) were placed at the east and west corners on the mat foundation. Two other sensors (1FW and 1FE) were fixed to the foundation of the superstructure at their corresponding corners. Another sensor (RF) was on the top floor girder, and the last one (GL) was placed outside on the ground. The specifications of the instrument are listed in Table 17.5. The recording system works such that when a ground motion is sensed the sensors are triggered, start recording and store the data in a local storage system. Afterwards, a staff of BRI will collect the data via telephone line. The processing and analysis of the strong motion data are systematically conducted in BRI.

In the study by Kashima et al. [12] earthquake records were carefully examined and a clear dependence of natural frequency on the amplitude of relative displacement

Table 17.4 Isolation system design criteria in seismic retrofit of NMWA

Horizontal period	2.0 s for moderate earthquake intensity 2.5–3.0 s for severe earthquake intensity
Vertical period	Less than 0.1 s
Compressive stress in isolators	Less than 10 MPa
Horizontal deformation capacity	400 mm

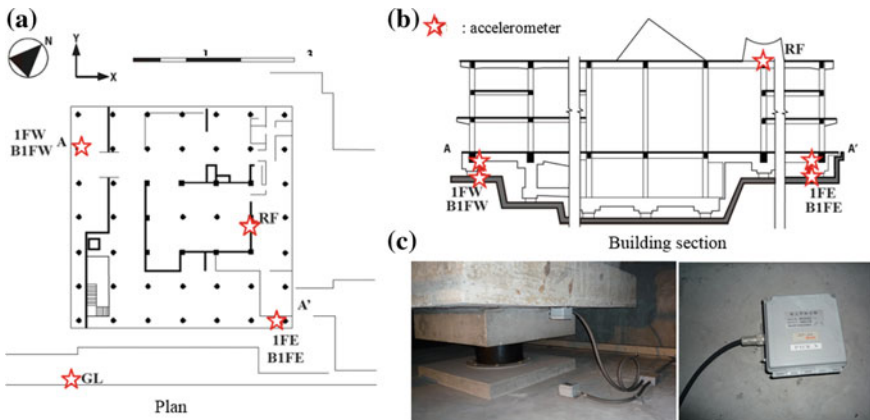


Fig. 17.24 Strong ground motion accelerometer locations: **a** plan, **b** building section, **c** location of accelerometers below and above isolation

ment was found. The natural frequencies were about 2 Hz for the records with relative displacements less than 0.5 mm (0.25% isolator shear strain) and fell to about 1 Hz for the records with about 10 mm relative displacement (5% shear strain). The dependency of the natural frequency on the relative displacement amplitude appeared to be caused by the non-linear force-deformation relationship of the HDR isolation system.

17.5.1 *Seismic Response of the Building During 2011 Great East Japan (Tohoku) Earthquake*

During the 2011 Tohoku earthquake on March 11, 2011 two strong ground motion were recorded on the building, are the responses observed in the building during the main shock (JMA seismic intensity 5 or lower) and aftershock (JMA seismic intensity 4) of the 2011 Tohoku earthquake on March 11, 2011 [7].

Figure 17.25 shows the response acceleration time histories recorded during the main shock, which compares the acceleration time histories observed above and below the isolation level. It is clear that low-frequency components are very strong in the time histories above the isolation level. The peak response accelerations observed during the main shock and aftershock are shown in Fig. 17.25c and d, where the values observed on the ground (GL) and at the foundation (B1FW), the peak response acceleration decreased considerably. The accelerometer at B1FW is not isolated from ground motion because it is located below the isolation level. Therefore, this reduction seems to be caused by input loss due to the geometry of the foundation structure. Figure 17.25 also shows less amplification of response accelerations from lower to upper levels in the building.

The 5% damped response spectra for the main shock are shown in Fig. 17.26. The left figure shows the spectra of B1FW below the isolation level, and the right figure shows that of 1FW above the isolation level. By comparing the two spectra, the peak response periods of the horizontal components (X- and Y-directions) increased from 0.3–0.5 to 1.0–1.5 s. There was, however, no change in the response spectra for the vertical component (Z-direction).

Table 17.5 Specifications of the strong motion instrument

Sensor type	Displacement-feedback accelerometer
Acceleration range	$\pm 2097 \text{ cm/s}^2$
Frequency range	DC to 30 Hz
A-D converter	24-bit, Sigma-Delta conversion
Dynamic range	114 dB
Sampling frequency	100 Hz
Recording	Event trigger recording

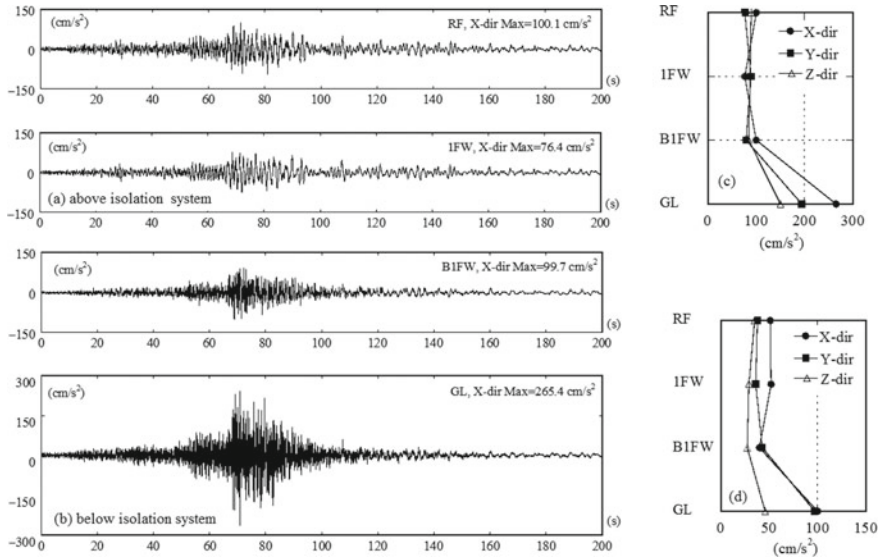


Fig. 17.25 Response acceleration time histories observed during main shock of 2011 Tohoku earthquake **a** above isolation system, **b** below isolation system. Peak response accelerations for **c** main shock and **d** aftershock

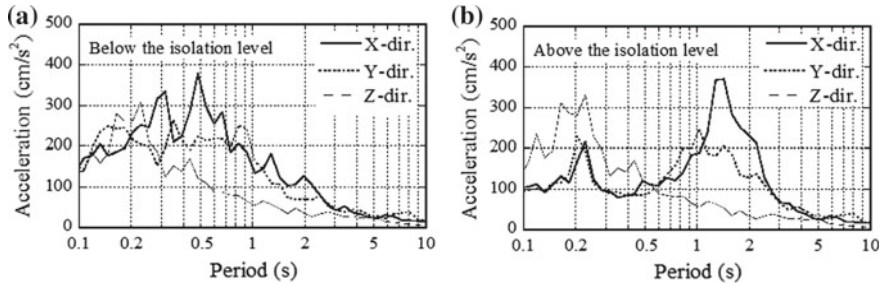


Fig. 17.26 5% damped response spectra for main shock of 2011 Tohoku earthquake: **a** below isolation system level, **b** above isolation system level

Figure 17.27a shows the relative displacement time histories and the orbit at the isolation level, which were obtained by double-integrating the observed accelerations at B1FW and 1FW. The building moved 3–4 cm during the earthquake. A photo of the berm and gravel is also shown in Fig. 17.27b. The gravel was moved by the berm due to the horizontal motion of the building. However, no exhibits were damaged, and there was no structural damage during the earthquake.

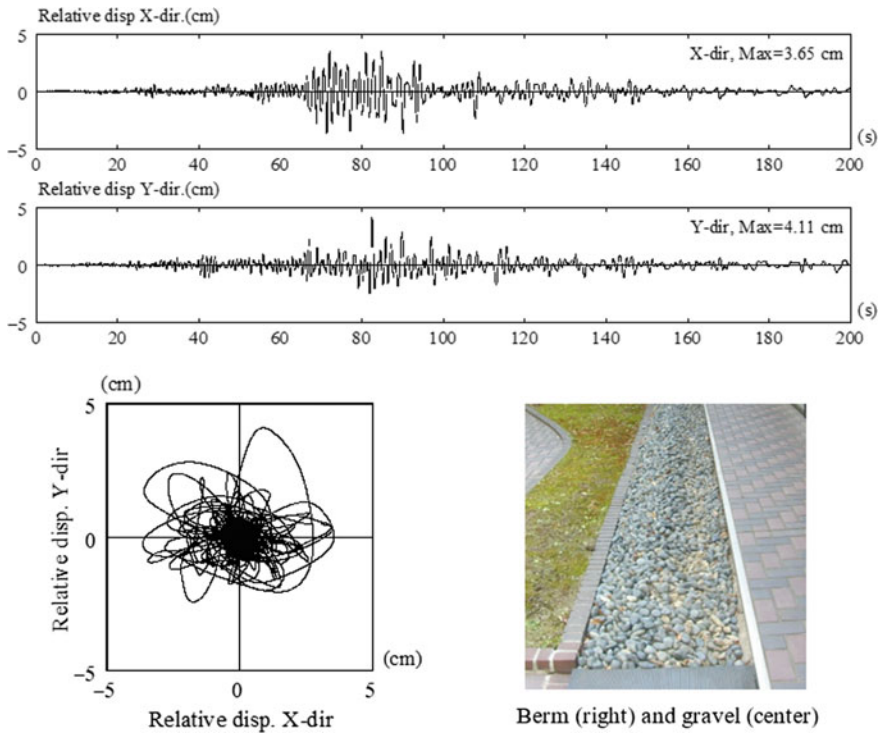


Fig. 17.27 (a) shows the relative displacement time histories and the orbit at the isolation level, which were obtained from time integration of the observed accelerations at B1FW and 1FW. The building moved 3–4 cm during the earthquake. A photo of the berm and gravel is also shown in (b)

17.5.2 Analytical Hysteresis Model

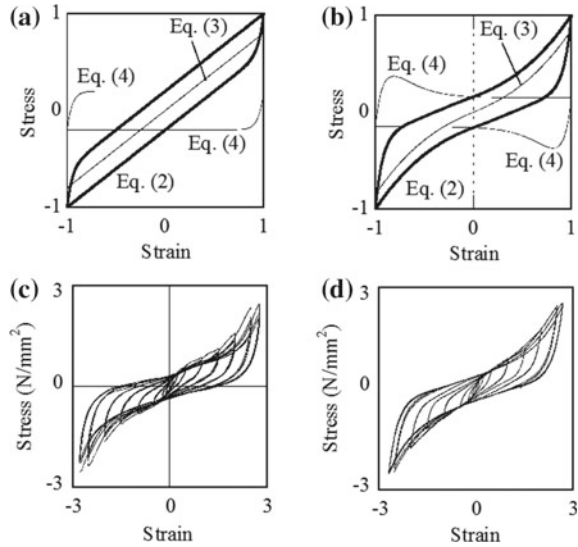
The hysteresis model used for the upgrade design analyses is now described. The relationship between horizontal force F and deformation X for the first loading is defined by Eq. (17.1):

$$F = \frac{G_{eq} A_r}{H_r} X \tag{17.1}$$

where G_{eq} is the equivalent shear modulus as a function of shear strain, A_r is the bearing shear area, and H_r is the total height of rubber in the bearing.

The relationship between F and X for the unloading of the skeleton curve can be expressed by the combination of an elastic component of force, F_1 , and hysteretic component, F_2 , and is given by Eqs. (17.2–17.4). These equations were obtained by evaluating a large number of experimental results [14]. Figure 17.28a and b show

Fig. 17.28 Normalized hysteresis loops **a** low shear strain level, **b** high shear strain level; and KL401-type HDR bearing hysteresis loops **c** experimental, **d** analytical



typical hysteresis loops given by Eqs. (17.2–17.4). The shape of these hysteresis loops is typical of those of elastomeric seismic isolation bearings.

$$F = F_1 + F_2 \tag{17.2}$$

$$F_1 = \frac{1}{2}(1 - u)F_m \{x \pm |x|^n\} \tag{17.3}$$

$$F_2 = \pm uF_m \{1 - 2e^{-a(1\pm x)} + b(1 \pm x)e^{-c(1\pm x)}\} \tag{17.4}$$

where F_m is the peak force on the skeleton curve, x is the normalized displacement ($x = X/X_m$), and X_m is the peak displacement on the skeleton curve. In Eq. (17.3), the parameter n specifies the stiffening, and parameter u is the ratio of force at zero displacement F_u to F_m ($u = F_u/F_m$). The parameters a and b are calculated from Eqs. (17.5) and (17.6), which are derived assuming that the analytical and experimental hysteresis loop areas are equal:

$$\frac{1 - e^{-2a}}{a} = \frac{2u - \pi h_{eq}}{2u} \tag{17.5}$$

$$b = c^2 \left[\frac{\pi h_{eq}}{u} - \left\{ 2 + \frac{2}{a}(e^{-2a} - 1) \right\} \right] \tag{17.6}$$

where h_{eq} is the equivalent viscous damping ratio, and parameter c is a pre-selected constant that specifies the shape of the hysteresis loop.

Equation (17.5) cannot be solved in closed form for parameter a ; thus, must be solved numerically. All the parameters that control the shape of the hysteresis loop

Table 17.6 Design equations for high-damping rubber (KL401-type) for NMWA Building

$G_{eq} = 0.8023 \gamma^{-0.4524}$	(0.0005 < γ < 1.0)
$= 2.118 - 2.328\gamma + 1.204\gamma^2 - 0.1916\gamma^3$	(1.0 < γ < 2.7)
$h_{eq} = 0.1379 + 0.05446\gamma - 0.02992\gamma^2$	
$+ 0.002588\gamma^3$	(0.0005 < γ < 2.7)
$u = 0.3301 - 0.04032\gamma - 0.009868\gamma^2$	(0.0005 < γ < 2.7)
$n = 1.0$	(0.0005 < γ < 1.0)
$= 7.095 - 7.962\gamma + 2.599\gamma^2$	(1.0 < γ < 2.7)
$c = 6.0$ (const.)	(0.0005 < γ < 2.7)

are updated using Eqs. (17.5) and (17.6) when load reversal from the skeleton curve occurs.

The above formulae were derived for application to steady-state hysteresis behavior for HDR bearings. The Masing rule [23] is applied to fully define the force under randomly varying displacement conditions for earthquake response analyses.

The empirical formulae used are summarized in Table 17.6. Figure 17.28c and d shows typical hysteresis loops for a KL401-type HDR isolation bearing. The analytical hysteresis model could accurately predict the force-displacement relationship into the range of large shear strain level.

17.5.3 Analytical Structural Model

The seismic response analyses were conducted using a nonlinear structural analysis program IDAC developed by Shimizu Corporation, which is a successor program of DAC3N used for the retrofit design of the building [15]. The three-dimensional model of the building used for the retrofit design was used for the analyses (Fig. 17.29a). Each isolator was modeled as a multi-shear spring model (Fig. 17.29b) to capture horizontal bi-directional shear behavior [31]. Stiffness proportional damping was assumed for the superstructure only. A h_{eq} of 3% of critical was assumed for the fundamental period of the fixed-base superstructure. Step-by-step direct time integration was carried out assuming constant average acceleration and a time increment of 0.01 s.

17.5.4 Seismic Response Analyses

A scaled isolation bearing has been installed since the building was retrofitted in 1998 (Fig. 17.30). A diagnostic test was conducted to evaluate G_{eq} and h_{eq} in November 2011, 13 years after the bearings were manufactured. The test results indicate that

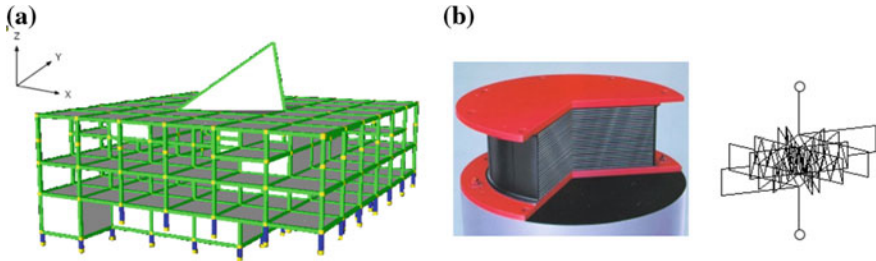


Fig. 17.29 **a** Three-dimensional building frame model for seismic response analyses, **b** seismic isolation bearing model (Illustration provided by Bridgestone Corporation)



Fig. 17.30 Scaled test specimen for diagnosis

G_{eq} had increased by 14.7%, and h_{eq} had decreased by 10.6% since the bearings were inspected at the time of shipping in 1997 due to aging.

In general, a high-damping rubber bearing’s G_{eq} and h_{eq} depend on temperature. The manufacturer proposed the following equations to evaluate temperature-related variations for KL401-type HDRs. We used the average temperature, 6.4 °C, which was observed at the JMA in Tokyo on March 10 and 11, 2011, for temperature (°C) T in Eqs. (17.7) and (17.8).

$$\frac{G_{eq}(T)}{G_{eq}(20\text{ }^\circ\text{C})} = 1.13 - 8.81 \times 10^{-3}T + 1.68 \times 10^{-4}T^2 - 2.20 \times 10^{-6}T^3 \quad (17.7)$$

$$\frac{h_{eq}(T)}{h_{eq}(20\text{ }^\circ\text{C})} = 1.06 - 3.24 \times 10^{-3}T + 2.65 \times 10^{-5}T^2 - 1.25 \times 10^{-6}T^3 \quad (17.8)$$

Equations (17.7) and (17.8) predict that G_{eq} will be 8.03% higher and h_{eq} will be 4.02% higher at 6.4 °C than the standard values.

We considered the aging and temperature effects on the elastomeric isolation bearings’ G_{eq} and h_{eq} in the analyses. We examined four different cases. The cases were based on the following assumptions:

Table 17.7 Rate of change

Case	G_{eq} [%]	h_{eq} [%]
1	100	100
2	114.7	89.4
3	108.0	104.0
4	123.9	93.0

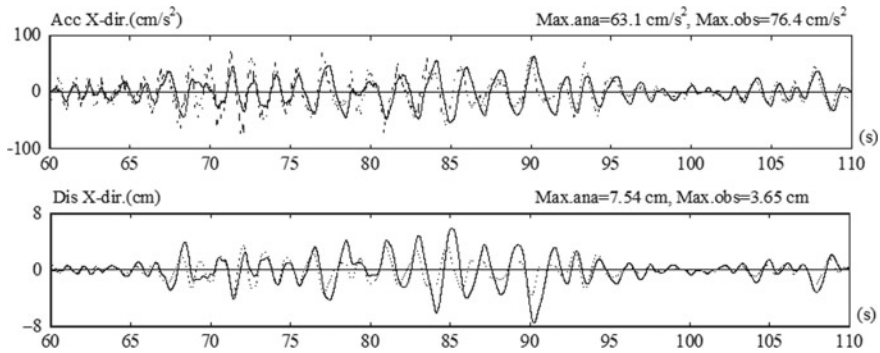


Fig. 17.31 Response acceleration and displacement time histories (Case 1, X-dir.) (dotted line: observed, bold line analysis)

Case 1: no change, values as used during design

Case 2: consider changes due to aging

Case 3: consider changes due to temperature

Case 4: consider aging and temperature changes

The rate of change of the G_{eq} and h_{eq} for each case are summarized in Table 17.7. Figure 17.31 shows the time histories of X-direction response acceleration on the first floor and relative displacement of the isolation story obtained in Case 1, and Fig. 17.32 shows those obtained in Case 4. To quantify the agreement between the observed and analytical responses in each case, the following equations are introduced.

$$\text{Acceleration: } D_{acc} = \frac{\sum |a_{obs} - a_{ana}|}{N} \tag{9}$$

$$\text{Relative displacement: } D_{dis} = \frac{\sum |d_{obs} - d_{ana}|}{N} \tag{10}$$

where N is the total amount of response data points ($N = 5000$).

Figure 17.33 describes the comparison between recorded response acceleration and relative displacement and the predicted values in the X-direction. The best predictions were for Case 4. This shows that the effects of aging and temperature on the HDR mechanical properties should be considered when predicting the seismic response behavior of an isolated building if such information is available.

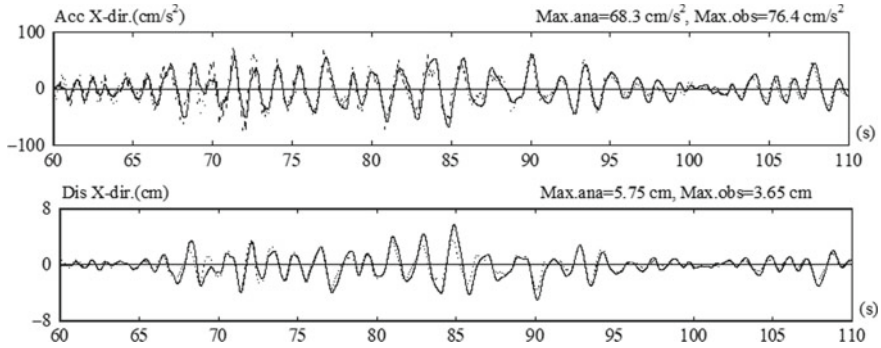


Fig. 17.32 Response acceleration and displacement time histories (Case 4, X-dir.) (dotted line: observed, bold line analysis)

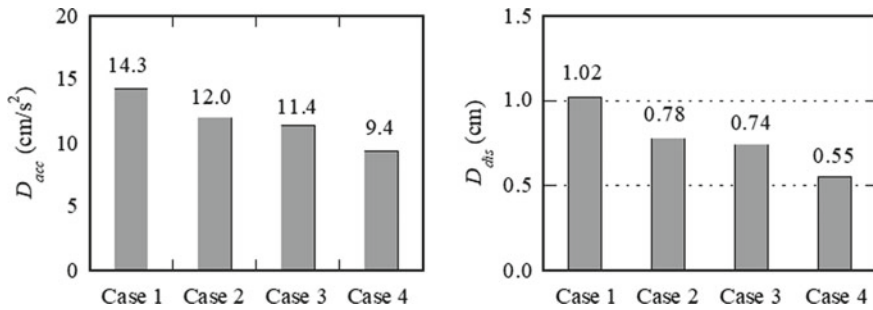


Fig. 17.33 Comparison between recorded and predicted responses

17.6 Conclusions

Monitoring experiences of seismically-isolated bridges and buildings in Japan are described along with lessons learned from the monitoring experiences with several case studies.

Generally, the structural monitoring systems for seismic isolated bridges and buildings were installed with the original objective to confirm the performance of the isolation system under various level of seismic excitations. Since the isolation technique is considered new and advanced, accuracy of design procedure and model for the bridge need to be verified with recorded responses. For seismic isolated bridges, the main target of monitoring is pier or pylon and girder responses. Performance of isolation is evaluated by comparing responses of pier and girder through response analysis and system identification. The system generally consists of triaxial accelerations at four locations: free field, pile cap, pier cap, and girder; connected by wired network system. For long-span bridges, larger number of sensors were employed along the girder and tower but one of important monitoring target is the girder-tower and girder-pier connections that utilize the isolation system. For seismically isolated

building the main target of monitoring is also performance of isolation. Typically, sensors are placed below and above isolator layer and at the top of the building. Based on analysis of building responses, one can evaluate performance of isolation in reducing the seismic response by comparing the response amplification factor between upper stories and ground motion.

The structural monitoring system usually installed and operated by operator or owner of the structures. In the case of bridges, highway operators usually oversee monitoring, data collecting, storing and maintenance of the sensors. However, not all bridge operators have human resources to conduct detailed analysis of the recorded data so some of them work together with other parties such as university or research institute to analysis the data in a framework of research collaboration. In the case of buildings, owner of the building such as university in the example presented here, oversee the monitoring and maintenance of the sensors directly.

Typically, the monitoring system operates under an event-based recording system where the sensors start recording when a ground motion exceeds a preset trigger level. All data is stored temporarily by a local storage system and later are collected for analysis. Wired networks of sensors are generally employed. Maintenance of wired networks of sensors is not an easy task, especially for monitoring system of long-span bridges. Durability of sensors and connection system is also an issue. In the case of Yokohama-Bay bridge, for example, the wired networks of sensors have worked successfully for over 30 years now. However, we need to consider the appropriate expected duration of monitoring system and the amount of initial investment amid the fast development of advanced sensing technology and the objectives of structural monitoring. Recently, some researchers in Japan have been developing and testing the implementation of wireless sensors for seismic monitoring of isolated bridges. In the future the wireless monitoring system may offer reasonable alternative to wired one, once the reliability issues associated with transmission, synchronization and power consumption have been fully resolved.

Lessons learned from structural analysis of recorded seismic isolated bridges in Japan are explained in detailed in this chapter. On the short-medium span bridges, based on seismic records it was observed that isolation performed satisfactorily during large earthquake such as 1995 Kobe earthquake. Performance of the isolation bearings was evaluated further by comparing the identified stiffness and damping coefficient with the equivalent linearized experimental values. Some uncertainties due to friction force was found and this was caused by minor structural elements that can affect the dynamic behavior of superstructure. On long-span bridge, application of link-bearing connection on Yokohama-Bay bridge was effective in decoupling the response of girder and pylon and reducing the seismic load caused by large weight of the girder. Long-term seismic monitoring of the bridge revealed some unwanted structural modes associated with link-bearing motion and fail-safe countermeasure was implemented during seismic retrofit. This is evident that structural monitoring can be very useful to provide a feedback for improvement of structure performance.

Response control effectiveness of the base-isolated building is discussed by summarizing the monitored responses of twenty base-isolated buildings shaken by the 2011 Tohoku earthquake. The buildings range from 2-story to 21-story. Accelera-

tions of the superstructure are controlled better at the greater level of shaking due to softening and more energy dissipation by the isolation system. As an example of many tall base-isolated buildings constructed in Japan, the monitored responses and isolation effectiveness of the 20-story building are discussed. Base-isolation system as seismic retrofit is also discussed with National Museum of Western Art in Tokyo as an example. Based on evaluation of the building responses during the 2011 Tohoku earthquake, it can be concluded that the isolation system performed well during the main shock and aftershock.

From several case-studies described in this chapter we can conclude that seismic monitoring of seismically-isolated structures is effective to verify design assumptions, evaluate seismic response and structure performance during large earthquake, detecting possible damages due to earthquake and verification of structural retrofit.

References

1. BRI (1999) Strong Motion Network. <http://smo.kenken.go.jp/smn>. Building Research Institute (BRI), Japan
2. Chaudhary MTA, Abe M, Fujino Y, Yoshida J (2000) System identification of two base-isolated bridges using seismic records. *J Struct Eng (ASCE)* 126(10):1187–1195
3. Chaudhary MTA, Abé M, Fujino Y (2001) Performance evaluation of base-isolated Yamaguchi bridge with high damping rubber bearings using recorded seismic data. *Eng Struct* 23(8):902–910
4. Chaudhary MTA, Abé M, Fujino Y (2002) Investigation of atypical seismic response of a base-isolated bridge. *Eng Struct* 24(7):945–953
5. Ganey T, Yamazaki F, Ishizaki H, Kitazawa M (1998) Response analysis of the Higashi-Kobe bridge and surrounding soil in the 1995 Hyogoken-Nanbu earthquake. *Earthquake Eng Struct Dyn* 27(6):557–576
6. Isermann R, Münchhoff M (2011) Identification of dynamic systems, an introduction with applications. Springer, New York
7. JMA, Earthquake Information (2018) Retrieved from: http://www.data.jma.go.jp/svd/eqev/data/seis_st/. Japan Meteorological Agency (JMA)
8. JSSI (2012) Report of response-controlled buildings investigation committee. Japan Society of Seismic Isolation, January 26, Tokyo, Japan
9. Juang JN (1997) System realization using information matrix. *J Guidance, Control, Dyn*, 20(3):492–500
10. Kasai K, Mita A, Kitamura H, Matsuda K, Morgan T, Taylor A (2013) Performance of seismic protection technologies during the 2011 Tohoku-Oki earthquake. *Earthq Spectra. Special Issue on the 2011 Tohoku-Oki Earthquake and Tsunami*, pp 265–294
11. Kasai K, Chimamphant S, Matsuda K (2016) Performance curves for base-isolated buildings reflecting effect of superstructure vibration period. *J Struct Construct Eng AIJ* 81(720):239–249 (in Japanese)
12. Kashima T, Koyama S, Iiba M, Okawa I (2008) Dynamic behavior of a museum building retrofitted using base isolation system. In: *Proceedings of 14th world conference on earthquake engineering*, Beijing, China, 12–17 Oct
13. Kawashima K, Nagashima H, Masumoto S, Hara K (1994) Response analysis of Miyagawa bridge based on a measured acceleration record. *J Struct Eng (JSCE)* 40:203–227
14. Kikuchi M, Aiken ID (1997) An analytical hysteresis model for elastomeric seismic isolation bearings. *Earthq Eng Struct Dyn* 26:215–231

15. Kikuchi M, Watanabe K (2004) Computer program for three-dimensional nonlinear dynamic response analysis of seismically-isolated buildings. In: Proceedings of 13th world conference on earthquake engineering, Vancouver, Canada, 1–6 Aug
16. Maeda K, Otsuka A, Takano H (1991) The design and construction of Yokohama Bay Bridge. In: Ito M et al (eds) Cable-stayed bridges recent developments and their futures. Elsevier, Amsterdam, pp 377–395
17. Matsuda K, Kasai K (2014) Study on dynamic behavior of high-rise base-isolated building based on its responses recorded during the 2011 Tohoku-Oki earthquake. *J Struct Construct Eng AIJ* 79(704):1445–1455 (in Japanese)
18. Matsuda K, Kasai K (2015) Dynamic responses of high-rise base-isolated building during the 2011 Great East Japan earthquake. International Association for Bridge and Structural Engineering (IABSE 2015), CD-ROM, Nara, Japan
19. Metropolitan Expressway Public Corporation (MPEC) (1994) Construction report of Tsurumi Tsubasa Bridge
20. Morita K (2017) Behavior of seismically isolated buildings and users' comment. *J Jpn Struct Consult*, No. 142 (in Japanese)
21. Morita K, Takayama M (2018) Performance of seismically isolated building in the 2016 Kumamoto earthquake. Engineering Faculty Report, Fukuoka University No. 100, 95–109 (in Japanese)
22. NIED, Strong motion seismograph networks. Retrieved from: <http://www.kyoshin.bosai.go.jp/>. National Research Institute for Earth Sciences and Disaster Resilience (NIED), Japan
23. Rosenblueth E, Herrera I (1964) On a kind of hysteretic damping. *J Eng Mech Div ASCE* 90:37–48
24. Siringoringo DM, Fujino Y (2006) Observed dynamic performance of the Yokohama-Bay Bridge from system identification using seismic records. *Struct Control Health Monit* 13(1):226–244
25. Siringoringo DM, Fujino Y (2008) System identification applied to long-span cable-supported bridges using seismic records. *Earthq Eng Struct Dyn* 37(3):361–386
26. Siringoringo DM, Fujino Y (2017) Over-twenty-years seismic monitoring of a cable-supported bridge: lessons learned on structural assessments. Proc of 16th world conference on earthquake, 16WCEE 2017, Santiago, Chile, 2017
27. Siringoringo DM, Fujino Y, Namikawa K (2013) Seismic response analyses of the Yokohama Bay cable-stayed bridge in the 2011 Great East Japan Earthquake. *J Bridge Eng (ASCE)* 19(8):A4014006
28. Siringoringo DM, Fujino Y (2015) Seismic response analyses of an asymmetric base-isolated building during the 2011 Great East Japan (Tohoku) Earthquake. *Struct Contr Health Monit* 22(1):71–90
29. Siringoringo DM, Takamoto G, Fujino Y (2015) Analysis of tower-girder transfer pounding on the Yokohama-bay cable-stayed bridge during 2011 Great East Japan Earthquake. In: IABSE symposium report (vol 104, No 1, pp 1–8). International Association for Bridge and Structural Engineering
30. Unjoh S (2014) Menshin (seismic isolation) bridges in Japan. Technical Note of PWRI, No. 4288
31. Wada A, Hirose K (1989) Building frames subjected to 2D earthquake motion. Research & practice proceedings, structures congress '89, ASCE, 388–397, San Francisco, USA, 1–5 May